Integrating chemical and biological approaches to target NAMPT with ADC technology in cancer

Dissertation

Zur Erlangung des akademischen Grades

Doctor rerum naturalium (Dr. rer. nat.)

Vorgelegt von

Pablo Ruedas Batuecas

Fachbereich Biologie

Fakultät für Mathematik, Informatik und Naturwissenschaften

Universität Hamburg

September 2023

The work described herein was carried out between September 2019 and February 2023 at Heidelberg Pharma Research GmbH, Dept. of Chemistry and Dept. of Biochemistry and cell biology under the supervision of Prof. Dr. Andreas Pahl, Dr. Torsten Hechler, Dr. Werner Simon, Dr. Hendrik Gruß and Anikó Pálfi.

Disputation date: 24/11/2023

- **Referee:**

  Prof. Dr. Dr. Andreas Guse

  Department of Biology from the faculty of mathematics, informatics and natural sciences.

  University of Hamburg

- **Referee:**

  Prof. Dr. Andreas Pahl

  Heidelberg Pharma Research AG

To all those who fought cancer

And now see us from the stars

Mamá esto va por ti

Acknowledgements

Dear Reader,

Welcome to the culmination of my doctoral journey, an endeavour that has been shaped by a myriad of experiences, both enriching and challenging. As I open the pages of my dissertation, I extend a sincere invitation for you to join me on this intellectual voyage. Within these chapters, you will find the culmination of years of dedicated research, tireless exploration, and the pursuit of knowledge in the realm of cancer research through the usage of NAMPT inhibitors as ADC payloads.

The path I have traversed has not been without its trials and tribulations. Along the way, I have encountered obstacles that tested my resolve and demanded resilience. However, it is through these difficulties that I have grown both personally and academically. Every setback has served as a valuable lesson, driving me to refine my approach, reassess my methods, and embrace the invaluable support of those around me.

With deep gratitude, I would like to acknowledge the invaluable contributions of my supervisors, Dr. Werner Simon, Anikó Pálfi, Dr. Hendrik Gruß, Dr. Torsten Hechler and Prof. Dr. Andreas Pahl, whose guidance and expertise have been instrumental in shaping the trajectory of my research. Their unwavering support and insightful feedback have propelled me forward, even during moments of uncertainty.

I would also like to express my heartfelt appreciation to my friends and family, whose unwavering belief in me has been a constant source of inspiration. Their encouragement, patience, and understanding have provided the necessary foundation upon which I built my academic pursuits.

I would like to express my total gratitude to my dear friend, Cesar. His unwavering support, attentive listening, and invaluable advice have served as a guiding light during the darkest of days. In those moments of life when the shadows seemed insurmountable, his presence provided solace and renewed hope. Cesar, your friendship is an immeasurable source of strength throughout this journey, and for that, I am eternally grateful.

Additionally, I cannot overlook the significance of the fellow companions who accompanied me while pursuing on their own individual PhD journeys. To Dani, Ele, and Ale, I extend my deepest appreciation. Your presence, camaraderie, and unwavering support have made this voyage all the more meaningful. You are not merely friends; you have become an extension of my family, and I am profoundly grateful for the bond we share.

This dissertation is a testament to the collective effort and support of those who have walked beside me on this journey, and this include the whole HDP team. I am humbled by the opportunity to share this work with you and invite you to engage with the ideas, discoveries, and reflections that have emerged from this transformative process.

Warmest regards,

Pablo Ruedas Batuecas

Table of contents

Declaration on oath

German:

Hiermit erkläre ich an Eides statt, dass ich die vorliegende Dissertationsschrift selbst verfasst und keine anderen als die angegebenen Quellen und Hilfsmittel benutzt habe.

English:

I hereby declare on oath that I have written the present dissertation independently and have not used further resources and aids than those stated in the dissertation.

Ort, Datum | City, date — Unterschrift | Signatur

Ladenburg, 08.09.2023

Declaration of correspondence between printed and digital versions

German:

Ich versichere, dass dieses gebundene Exemplar der Dissertation und das in elektronischer Form eingereichte Dissertationsexemplar (über den Docata-Upload) und das bei der Fakultät (zuständiges Studienbüro bzw. Promotionsbüro Physik) zur Archivierung eingereichte gedruckte gebundene Exemplar der Dissertationsschrift identisch sind.

English:

The undersigned declare that this bound copy of the dissertation, the dissertation submitted in electronic form (via the Docata upload), and the printed bound copy of the dissertation submitted to the faculty (responsible Academic Office or the Doctoral Office Physics) for archiving are identical.

Ort, Datum | City, date — Unterschrift | Signature

Ladenburg, 08.09.2023

Abstract

Cancer is a large group of diseases and has become a major societal problem; it is the second leading cause of mortality in EU countries after cardiovascular diseases and a leading cause of death worldwide. Current chemo- and radiotherapeutic approaches lack selectivity and efficacy, leading to low quality of life and poor outcomes in patients. In recent years, targeted therapy using antibody-drug conjugates (ADCs) has become an increasingly important treatment option. ADCs are hybrid molecules that use an antibody to deliver a cytotoxic drug specifically to tumour sites to reduce the systemic toxicity associated with traditional chemotherapy. Currently, 11 ADCs have been approved by the FDA, more than 50% of which use potent microtubule metabolism-disrupting agents, such as auristatins or maytansines. They have shown outstanding results in clinical trials over a variety of malignancies from liquid to solid tumours. However, their use is limited due to the mode of action of the cytotoxic payload, since only actively dividing tumour cells can be targeted, leaving dormant or non-dividing tumour cells untouched. Therefore, this thesis focuses on NAMPT inhibitors as promising novel payload candidates with a novel mode of action (MoA) due to their high potency in affecting cellular energetics by depleting intracellular NAD^+ levels, a biological feature essential for both dividing and non-dividing cells.

First, the *in vitro* efficacy of published NAMPT inhibitors on $CD19^+$ and $HER2^+$ human cancer cell lines, both as free payloads and ADCs, was explored. Optimisation of the free payload and linker-payloads for ADC delivery was initially chemically guided, based on the pharmacophores identified on the inhibitor molecule. Despite the promising results of the free inhibitors, ADCs loaded with these NAMPT inhibitor linker-payloads showed poor *in vitro* efficacy.

Accordingly, the effects of NAMPT inhibitors on cellular endocytosis processes were investigated in more detail. The aim was to determine the feasibility of ADC-target complex internalisation when using CD19 or HER2 surface receptors as targets for ADCs loaded with NAMPT inhibitors as payloads. Initial findings suggested that ADC-surface receptor complex internalisation is inefficient in $CD19^+$ cell lines when targeted with NAMPT inhibitors, prompting the exploration of alternative targets. CD30 was identified as an optimal tumour-associated antigen for NAMPT inhibitor-ADCs due to the efficacy of ADCs in depleting cellular NAD^+ levels, which was supported by promising *in vitro* results. However, the ADCs based on such NAMPT inhibitors lacked full-blown cytotoxicity, even in $CD30^+$ cell lines. Biochemical exploration subsequently revealed that the hydrophobic nature of these NAMPT inhibitors is counterproductive for their use as ADC payloads due to excessive cytoplasmic clearance through passive diffusion, resulting in cellular escape.

To increase efficacy, a computationally aided lead optimisation campaign for NAMPT inhibitors was performed, leading to a payload showing significantly higher hydrophilicity. This resulted in full-blown cytotoxicity of the corresponding ADC with EC_{50} values in the picomolar range on a $CD30^+$ cell line *in vitro,* as well as promising 80-day survival in mouse xenograft models *in vivo*. However, lysosomal *in vitro* stability assays showed instability of the new NAMPT inhibitors, as demonstrated by more than 50% lysosomal hydrolysis of the delivered NAMPT inhibitor. The resulting lower intracellular payload concentration limited its applicability to L540, a $CD30^+$ cell line particularly sensitive to NAMPT inhibition. The cause of this sensitivity was demonstrated through q-RT-PCR experiments, which showed significantly lower expression of the NAMPT enzyme in L540 cells compared to other cell lines tested *in vitro*. In the latter, free NAMPT inhibitors had a cytotoxic effect, whereas ADCs loaded with NAMPT inhibitors as payloads were ineffective due to lysosomal hydrolysis.

Finally, a new family of NAMPT inhibitors resistant to lysosomal conditions was designed through computationally assisted virtual screening of a 3000-compound database generated by reaction-based compound enumeration methods and using the first lead candidate as the initial molecule. This set the basis for new NAMPT inhibitors optimised for ADC delivery targeting different tumour-associated antigens, such as CD30, CD19, and HER2 aiming to target not only liquid but solid cancer. The investigation of these new and highly efficacious ADC payloads holds promise to enable the development

of ADCs with a new mode of action targeting non-dividing cancer cells for improved treatment of various types of malignancies, with potent efficacy values at the same time as safety in *in vivo* models.

Abstract in German

Krebs ist eine große Gruppe von Krankheiten und hat sich zu einem großen gesellschaftlichen Problem entwickelt; er ist in den EU-Ländern die zweithäufigste Todesursache nach Herz-Kreislauf-Erkrankungen und eine der häufigsten Todesursachen weltweit. Den derzeitigen chemo- und strahlentherapeutischen Ansätzen mangelt es an Selektivität und Wirksamkeit, was zu geringer Lebensqualität und schlechten Behandlungsergebnissen bei den Patienten führt. In den letzten Jahren hat sich die gezielte Therapie mit Antikörper-Wirkstoff-Konjugaten (ADCs) zu einer immer wichtigeren Behandlungsoption entwickelt. Bei ADCs handelt es sich um Hybridmoleküle, die einen Antikörper verwenden, um ein zytotoxisches Molekül spezifisch zu dem Tumor zu bringen und so die mit der herkömmlichen Chemotherapie verbundene systemische Toxizität zu verringern. Derzeit sind 11 ADCs von der FDA zugelassen, von denen mehr als 50% potente Wirkstoffe verwenden, die den Mikrotubuli-Stoffwechsel unterbrechen, wie z. B. Auristatine oder Maytansinoide. Sie haben in klinischen Studien bei einer Vielzahl bösartiger Erkrankungen - von hämatologischen bis zu soliden Tumoren - hervorragende Ergebnisse gezeigt. Ihr Einsatz ist jedoch aufgrund der Wirkungsweise der zytotoxischen Nutzlast begrenzt, da nur sich aktiv teilende Tumorzellen angegriffen werden können, während ruhende oder sich nicht teilende Tumorzellen unversehrt bleiben. Daher konzentriert sich diese Arbeit auf NAMPT-Inhibitoren als vielversprechende neue Nutzlastkandidaten mit einer neuartigen Wirkungsweise (MoA) aufgrund ihrer hohen Potenz bei der Beeinflussung der zellulären Energetik durch Verarmung des intrazellulären NAD^+-Spiegels, einer biologischen Eigenschaft, die sowohl für sich teilende als auch für sich nicht teilende Zellen wesentlich ist.

Zunächst wurde die *In-vitro*-Wirksamkeit veröffentlichter NAMPT-Inhibitoren auf $CD19^+$- und $HER2^+$-Zelllinien menschlicher Krebszellen sowohl als freie Wirkstoffe als auch als ADCs untersucht. Die Optimierung der freien Wirkstoffe und der Linker-Payloads für die ADC-Verabreichung wurde zunächst auf der Grundlage der auf dem Inhibitormolekül identifizierten Pharmakophoren chemisch gesteuert. Trotz der vielversprechenden Ergebnisse der freien Inhibitoren zeigten ADCs, die mit diesen NAMPT-Inhibitor-Linker-Payloads beladen waren, eine schlechte In-vitro-Wirksamkeit.

Daher wurden die Auswirkungen von NAMPT-Inhibitoren auf zelluläre Endozytoseprozesse genauer untersucht. Ziel war es, die Internalisierung von ADC-Zielkomplexen zu bestimmen, wenn CD19 oder HER2 Oberflächenrezeptoren als Ziel für ADCs verwendet werden, die mit NAMPT-Inhibitoren als Nutzlast beladen sind. Erste Ergebnisse deuteten darauf hin, dass die Internalisierung von ADC-Oberflächenrezeptorkomplexen in $CD19^+$-Zelllinien ineffizient ist, wenn sie mit NAMPT-Inhibitoren behandelt werden, was die Erforschung alternativer Oberflächenmoleküle veranlasste. CD30 wurde als optimales tumorassoziiertes Antigen für NAMPT-Inhibitor-ADCs identifiziert, da die ADCs den zellulären NAD^+-Spiegel wirksam senken, was durch vielversprechende In-vitro-Ergebnisse bestätigt wurde. Den auf solchen NAMPT-Inhibitoren basierenden ADCs mangelte es jedoch an vollständiger Zytotoxizität, selbst bei $CD30^+$-Zelllinien. Biochemische Untersuchungen ergaben, dass die hydrophobe Beschaffenheit dieser NAMPT-Inhibitoren für ihre Verwendung als ADC-Nutzlast kontraproduktiv ist, da sie durch passive Diffusion übermäßig aus dem Zytoplasma entfernt werden, was zu einem Entweichen aus den Zellen führt.

Zur Steigerung der Wirksamkeit wurde eine rechnergestützte Lead-Optimierungskampagne für NAMPT-Inhibitoren durchgeführt, die zu einer Nutzlast mit deutlich höherer Hydrophilie führte. Dies führte *in vitro* zu einer ausgeprägten Zytotoxizität des entsprechenden ADCs mit EC50-Werten im pikomolaren Bereich bei einer $CD30^+$-Zelllinie, sowie *in vivo* zu einer vielversprechenden 80-tägigen Überlebenszeit in Maus-Xenograft-Modellen. Lysosomale In-vitro-Stabilitätstests zeigten jedoch eine Instabilität der neuen NAMPT-Inhibitoren, was durch eine mehr als 50% lysosomale Hydrolyse des verabreichten NAMPT-Inhibitors belegt wurde. Die daraus resultierende niedrigere intrazelluläre

Nutzlastkonzentration schränkte die Anwendbarkeit auf L540-Zellen ein, eine $CD30^+$-Zelllinie, die besonders empfindlich auf NAMPT-Inhibition reagiert. Die Ursache für diese Empfindlichkeit wurde durch q-RT-PCR-Experimente nachgewiesen, die eine deutlich geringere Expression des NAMPT-Enzyms in L540-Zellen im Vergleich zu anderen *in vitro* getesteten Zelllinien zeigten. Bei Letzteren hatten freie NAMPT-Inhibitoren eine zytotoxische Wirkung, während ADCs, die mit NAMPT-Inhibitoren als Nutzlast beladen waren, aufgrund der lysosomalen Hydrolyse unwirksam waren.

Schließlich wurde eine neue Familie von NAMPT-Inhibitoren, die gegen lysosomale Bedingungen resistent sind, durch ein rechnergestütztes virtuelles Screening einer Datenbank mit 3000 Verbindungen entwickelt, die durch reaktionsbasierte Aufzählungsmethoden generiert wurde, wobei der erste Lead-Kandidat als Ausgangsmolekül diente. Dies bildete die Grundlage für neue NAMPT-Inhibitoren, die für die ADC-Verabreichung optimiert wurden und auf verschiedene tumorassoziierte Antigene wie CD30, CD19 und HER2 abzielen, um nicht nur flüssigen, sondern auch festen Krebs zu bekämpfen. Die Untersuchung dieser neuen und hochwirksamen ADC-Nutzlasten verspricht die Entwicklung von ADCs mit einer neuen Wirkungsweise, die auf sich nicht teilende Krebszellen abzielt, für eine verbesserte Behandlung verschiedener Arten von bösartigen Erkrankungen, mit starken Wirksamkeitswerten bei gleichzeitiger Sicherheit in In-vivo-Modellen.

0. Abbreviations

Scientific terms:

- 5'-7-methylguanosin cap (m^7G cap)
- Absorption, distribution, metabolism and excretion (ADME)
- Amanitin-based ADCs (ATACs)
- Antibody dependent cellular cytotoxicity (ADCC)
- Antibody dependent cellular phagocytosis (ADCP)
- Aqueous (Aq)
- Biolayer interferometry (BLI)
- Brentuximab (Brt)
- Bromodeoxyuridine (BrdU)
- Catalogue product reference (Ref)
- Complement dependent cytotoxicity (CDC)
- Density functional theory (DFT)
- Drug-antibody ratio (DAR)
- Deruxtecan (Dxd)
- Electro spray ionisation (ESI)
- Electron (e^-)
- Equivalent (eq)
- European bioinformatics institute (EBI)
- Foetal bovine serum (FBS)
- Flash Chromatography (FC)
- Food and Drug Administration (FDA)
- Formylglycine generating enzyme (FGE)
- Forward (Fwd)
- Fragment antigen-binding (Fab)
- Fragment crystallisable region (FC region)
- hBCE19 (anti-CD19)
- Heavy chain (HC)
- High DAR (hD)
- High performance liquid chromatography (HPLC)
- Intra venous (IV)
- Light chain (LC)
- Maximum tolerated dose (MTD)
- Micro-RNA (MIR)
- Mode of action (MOA)
- Monoclonal antibodies (mAbs)
- Multiple reaction monitoring (MRM)
- Natural Killer cells (NK)
- NAMPT inhibitor (NAMPTi)
- New England Biolab (NEB)

0. Abbreviations

- Overnight (ON)
- Over weekend (OW)
- Patient derived xenograft (PDX)
- Pharmacokinetics (PK)
- Polarisable continuum model (PCM)
- Reactive oxygen species (ROS)
- Reverse (Re)
- Reversed phase (RP)
- Room temperature (RT)
- Severe combined immunodeficiency (SCID)
- Size exclusion chromatography (SEC)
- Sodium dodecyl sulphate–polyacrylamide gel electrophoresis (SDS-Page)
- Solution (Sol)
- Thin layer chromatography (TLC)
- TNF-R associated factor (TRAF)
- Trastuzumab (T)
- Tumour necrosis factor receptor superfamily member 8 (TNFRSF8)
- Ultra-performance liquid chromatography (UPLC)
- Variable region (VR)

Solvents:

- Acetonitrile (ACN)
- Chloroform ($CHCl_3$)
- Dichloromethane (DCM)
- Dimethyl sulphide (DMS)
- Dimethyl sulfoxide (DMSO)
- Dulbecco's phosphate buffered saline (dPBS)
- Ethanol (EtOH)
- Ethyl acetate (EtOAc)
- Hexane (Hex)
- Methanol (MeOH)
- Methyl-tertbutyl ether (MTBE)
- Tetrahydrofurane (THF)

Reagents and chemical groups:

- (3-(4,5-dimethylthiazol-2-yl)-2,5-diphenyltetrazoliumbromid) (MTT)
- 1,8-diazabicyclo[5.4.0]undec-7-ene (DBU)
- 1-ethyl-3-carbodiimide hydrochloride (EDCl)
- 2-(Trimethylsilyl)ethoxymethyl (SEM)
- 4-(2-hydroxyethyl)-1-piperazineethanesulfonic acid (Hepes)
- 7-azabenzotriazol-1-yloxy)tripyrrolidinophosphonium hexafluorophosphate (PyAOP)

0. Abbreviations

- Acetic acid (AcCOOH)
- Acetyl (Ac)
- Alcohol dehydrogenase (ADH)
- Bovine serum albumin (BSA)
- Dehydroascorbic acid (dhAA)
- Dibenzocyclooctyne (DBCO)
- Diciclohexyl carbodiimide (DCC)
- Diethyl azodicarboxylate (DEAD)
- Di-isopropyl-ethyl-amine (DIPEA)
- Di-methylaminopyridine (DMAP)
- Hexafluorophosphate azabenzotriazole tetramethyl uronium (HATU)
- Hydroxy benzotriazole (HOBt)
- N,N'-diisopropylcarbodiimide (DIC)
- Maleimide (Mal)
- NAD^+ kinase (NADK)
- N-hydroxysuccinimide (NHS)
- Nicotin amide (NAM)
- Nicotinamide mononucleotide adenylyltransferase (NMNAT)
- Nicotinamide riboside kinase 1 (NMRK1)
- Nicotinate phosphoribosyl transferase (NAPRT)
- Nicotine adenine dinucleotide (NAD^+)
- Nicotine amide riboside (NR)
- Nicotine mononucleotide (NMN)
- Nicotine-adenine mononucleotide (NAMN)
- Nicotinic acid (NA)
- Nicotinic acid adenine dinucleotide (NAAD)
- N-methylimidazole (NMI)
- N-methylmorpholine (NMM)
- N-methylmorpholine oxide (NMO)
- N-β-maleimidopropyl-oxysuccinimide ester (BMPS)
- N-ε-malemidocaproyl-oxysuccinimide ester (EMCS)
- *P*-aminobenzyl (PAB)
- Phenazine ethosulfate (PES)
- Phenol (PhOH)
- Phenylmethylsulfonyl fluoride (PMSF)
- *p*-nitrophenol carbonyl (PNP)
- Phosphoribosyl pyrophosphate (PRPP)
- Pyrrolobenzodiazepin (PBD)
- Poli-ADP ribose polymerase (PARP)
- Polyethylene glycol (PEG)
- Polyethylenimine (PEI)
- Quinolinate phosphoribosyltransferase (QPRT)

0. Abbreviations

- Quinolinic acid (QA)
- Tert-butyl-oxi-carbamate (Boc)
- Tri-ethyl amine (Et_3N or TEA)
- Tri-fluoroacetic Acid (TFA)
- Tri-phenylphosphine (PPh_3)
- Tris(2-carboxyethyl)phosphin-hydrochlorid (TCEP)
- γ-amino butyric acid (GABA)

Amino acid codes:

Amino acid	*One-letter code*	*Three-letter code*
Alanine	A	Ala
Arginine	R	Arg
Aspartic acid	D	Asp
Cysteine	C	Cys
Glutamic acid	E	Glu
Glutamine	Q	Gln
Glycine	G	Gly
Histidine	H	His
Isoleucine	I	Ile
Leucine	L	Leu
Lysine	K	Lys
Methionine	M	Met
Phenylalanine	F	Phe
Proline	P	Pro
Serine	S	Ser
Threonine	T	Thr
Tryptophane	W	Trp
Tyrosine	Y	Tyr
Valine	V	Val

1. Introduction

1.1. Cancer, a polygenic and multifactorial group of diseases

Cancer is a group of diseases characterised by the uncontrolled growth and spread of abnormal cells. It is a complex and multifaceted condition that can affect almost any part of the body and is the leading cause of death worldwide, accounting for nearly 10 million deaths in 2020, or nearly one in six deaths. It is therefore essential to deepen our understanding of this altered health state in order to develop better tools for detecting, preventing, and curing cancer.[1]

Notably, cancer is not a "modern" condition; it was already considered a "mysterious curse" 3,000 years ago, dating back to ancient Egypt. It was not until 1914 that Theodor Boveri first proposed that cancer may be caused by abnormal segregation of chromosomes during cell division, marking the beginning of the modern understanding of cancer as a polygenic and multifactorial group of diseases.[2]

The 20th century saw numerous biological milestones, including the discovery of the structure of DNA in 1953,[3] the identification of regulatory genes such as p53 in 1979,[4–6] and the development of PCR technology in 1983,[7] all of which contributed to a deeper understanding of cancer. These advancements led to the "hallmarks of cancer", first proposed by Hanahan and Weinberg in 2000 and updated in subsequent years, which describe the fundamental biological traits that enable cancer cells to grow, survive, and spread.[8]

1. Introduction

Figure 1. The hallmarks of cancer.[8,9] Red ovals denote core tumoral characteristics; blue ovals denote enabling characteristics, with permission from publisher for using the image in accordance with license number 5530710114206 and 5530701378201.

The hallmarks of cancer can be divided into two groups: enabling characteristics and core characteristics (Figure **1**). Enabling characteristics are the conditions that allow normal cells to transition into cancer cells, which leads to the development of the core characteristics describing the cancer phenotype. Cancer is generally believed to be enabled by sustained genomic and epigenomic instability combined with a pro-inflammatory microenvironment, allowing the selection of tumour cells through clonogenic growth. However, several dramatic events must occur for a preneoplastic cell to evolve into a tumour: disruption of mechanisms that prevent mutations (such as MDR proteins), dysregulation of enzymes that act as "antioxidants" (such as superoxide dismutase and catalase), DNA damage detection and repair machinery ultimately leading to block sustained cell death (including p53) and loss of resistance to transformation (controlled by the balanced expression of proto-oncogenes and tumour-suppressor genes). The loss of these mechanisms, which help to maintain homeostasis, repair, and regeneration in normal cells, leads to preneoplastic cells exhibiting increased cellular plasticity, stem cell characteristics and ultimately acquiring the continuous proliferative trait, characteristic of neoplastic cells.[10]

The core characteristics of tumour cells then progressively develop, driven by an evolutionary transformation characterised by a mutator phenotype that includes resistance to cell death, evasion of immune surveillance, angiogenesis, tissue invasion, and metastasis. These hallmarks allow cancer cells to evade normal cellular controls and establish themselves as a malignant tumour. Despite the extensive knowledge available, cancer remains difficult to treat for several reasons. One challenge is the genetic and molecular diversity of cancer cells, which makes it difficult to develop a universal cancer treatment. Additionally, cancer cells often develop resistance to classical therapies, such as chemotherapy and radiation, which limits

their effectiveness and leads to local and metastatic failures, ultimately resulting in patient death.[9,10]

Historically, the most effective approach for cancer treatment has been surgical removal of the tumour and surrounding affected tissues for solid tumours (such as carcinomas) and bone marrow transplantation for liquid tumours (such as leukaemia). However, this approach can have drawbacks for the patient, such as loss of function in a particular part of the body or a high risk of infection for patients undergoing bone marrow transplantation due to immunosuppression. Additionally, depending on the size, location, and type of tumour, it may be difficult for the surgeon to completely remove it, increasing the risk of cancer recurrence.[10–13]

In response, adjuvant chemotherapy and radiotherapy are often used, but classical chemotherapeutic agents (e.g., cisplatin) have limited effectiveness and can cause significant side effects and systemic toxicities, leading to a lower quality of life for patients. Despite their ability to target rapidly dividing cells, such as tumour cells, these therapies are often unable to eliminate dormant populations of cells, which can lead to local and metastatic failures.[10,12,14]

In light of these limitations, this research focuses on developing new-generation therapies, such as immunotherapies and targeted therapies, that aim to improve specificity and effectiveness against non-dividing cells, reduce side effects, and improve the quality of life and life expectancy of patients. These approaches are discussed in further detail in the following chapters.[15]

1.2. Immunotherapy and small molecules for targeted active treatment of cancer

This section provides an overview and comparison of the main new-generation therapeutic technologies for targeted cancer treatment: small molecules and immunotherapeutic agents. Personalised medicine has revolutionised the field of translational medicine, moving away from a “one size fits all” approach to cancer treatment. Instead, treatment is now based on an understanding of the underlying biological mechanisms of the disease and is increasingly tailored to the unique molecular characteristics of a patient’s tumour. While oncology still operates within broad disease categories, there is a trend towards treatment plans that are specific to the characteristics of an individual’s tumour, with the potential to improve patient outcomes and quality of life.[16]

Targeted drugs can be broadly classified into two categories: small molecules (such as cancer overexpressed enzyme inhibitors and DNA-repairing and/or -remodelling enzyme inhibitors) and macromolecules (such as monoclonal antibodies, nucleic acids, and antibody-drug conjugates). Small molecule drugs, typically defined as therapeutics weighing 50–1500 Daltons (Da), have several advantages over macromolecules.[16] One advantage is their superior pharmacokinetic profile, as their small size allows for better diffusion and permeability into tissues, including the ability to pass the blood-brain barrier, which makes them more effective at reaching their target in the body. Moreover, small molecules have a more predictable pharmacokinetic and pharmacodynamic profile, which makes them easier to dose and predict their effects in a clinical setting. Small molecules also typically have a higher affinity for their targets, making them more potent at inhibiting the function of target proteins.[15] From a chemical perspective, small molecules are more amenable to structure-activity relationship

(SAR) analysis, which can aid in the design and optimisation of new small molecule therapeutics. Finally, small molecules are easier and more cost-effective to synthesise and manufacture, and they tend to have a longer shelf life than macromolecules, which are more prone to degradation.[15]

The development of small molecule anticancer drugs is a promising area of scientific and therapeutic research, with the number of FDA-approved compounds reaching 90 by 2022. These drugs typically target enzymes that are mutated or overexpressed in cancer cells, among which kinase inhibitors are the most common. Kinases are enzymes that catalyse the transfer of a phosphate group from ATP to protein residues containing hydroxyl groups. They play a key role in many cell signalling pathways, particularly those related to proliferation and survival, which are often altered in cancer cells. Examples of targeted kinases include ALK, c-Met, and the EGFR family, including receptors such as Erbb2. Small molecule drugs targeting these kinases have been effective in treating a variety of solid tumours, such as non-small cell lung cancer (NSCLC), breast cancer (including triple negative), hepatic tumours, and liquid tumours such as B-cell lymphomas.[15]

Compared to traditional chemotherapy, small molecule drugs have been shown to be more effective at lower doses in the nanomolar range.[15] However, cancer cells often adapt to these treatments, leading to resistance after an average of 12 months. Point mutations in the binding pockets or moieties targeted by the inhibitors are a common mechanism of resistance. While newer generations of inhibitors are being developed to overcome resistance mechanisms, they may lack selectivity for tumour-specific isoforms of enzymes and can cause systemic toxicities by targeting non-tumour cells. This has been observed in clinical trials with the second-generation EGFR inhibitors afatinib and dacomitinib, which caused severe rash and diarrhoea and had to be limited in their clinical doses.[15]

Tumours are complex environments that contain a variety of cell types. In solid tumours, the development of new blood vessels (angiogenesis) is critical for providing the tumour with the nutrients and oxygen required to grow. A key family of receptors involved in angiogenesis is the vascular endothelial growth factor receptor (VEGFR) family. The premise behind the development of VEGFR inhibitors is to “starve” the tumour. However, most antiangiogenic small molecule drugs have only modestly improved survival rates in clinical trials. One reason for this is that the tumour vasculature tends to normalise, meaning that the inhibitors have an effect on the immature blood vessels in the tumour rather than targeting the mature, functional vasculature, as it lacks the receptors targeted by the inhibitors. As a consequence, antiangiogenic treatment is often effective only when combined with chemotherapy. Additionally, vascular remodelling is controlled by multiple signalling pathways, so inhibiting only one pathway may be compensated for by others.[15]

Another target for small molecule anticancer drugs is the fusion protein BCR-Abl, which is generated by the Philadelphia chromosome or the 9-22 translocation. BCR-Abl is present in nearly all cases of chronic myeloid leukaemia and in 20% of acute lymphocytic leukaemia cases. The first approved small molecule anticancer drug, imatinib, specifically inhibits BCR-Abl. The main difference between this example and others is that BCR-Abl is a cancer-specific protein, so off-target effects are not common.[17]

In addition to targeting cytoplasmic enzymes, small molecule drugs can also target DNA-remodelling enzymes that affect the epigenome and chromatin compaction in tumours.

1. Introduction

Histone deacetylases (HDACs) are key epigenetic regulators that remove acetyl groups from N-acetylated lysine residues of histones and non-histone residues. Aberrant upregulation of HDACs is reported in various types of cancer and can disrupt the balance between oncogenes and tumour suppressor genes, leading to cell proliferation, apoptosis, differentiation, migration, and cancer angiogenesis. The sirtuin family (Sirt 1-7) is an important family of HDACs. Specific inhibitors of sirtuins, such as sirtinol and cambinol, have been developed. However, HDAC inhibitors are largely restricted to haematological malignancies.[15] Another approach is to inhibit the production of cofactors for the enzyme, such as NAD^+ for sirtuins. NAMPT inhibitors, which block the rate-limiting enzyme in the NAD^+ salvage production pathway, can deplete NAD^+ in cells and enhance the effectiveness of small molecule drugs. However, this strategy may also affect healthy cells, so alternative delivery systems must be considered to improve their specificity. Other families of small molecule drug inhibitors target proteasomes or DNA repair mechanisms like PARPs.[18,19]

Overall, the landscape of small molecule anticancer drugs is broad and diverse. However, nearly all small molecule drugs still encounter significant challenges after a period of clinical use, such as drug resistance. Additionally, serious problems occur due to the lack of selectivity, meaning that these drugs may also kill healthy cells if the target is not cancer-specific. Problems have also been reported with their metabolic stability in the case of quick metabolisation, which limits their effectiveness. Despite efforts to optimise these compounds to make them more target-specific, problems can still persist with off-target effects. Finally, delivery to the target cell is a major challenge for small molecule anticancer drugs, as they are typically administered intravenously. However, due to their charge, solubility, and drug size, some molecules have limited delivery.[15]

In oncology, targeted therapies using macromolecules, such as monoclonal antibodies (mAbs), have been found to be a promising approach in cancer treatment. Unlike small molecule therapies, mAbs require a selective and very specific interaction with cell surface proteins before exerting their effects. In addition, in some cases, interaction with the target is not sufficient, as the mAbs must be internalised and exert their effects intracellularly.[20] This added layer of selectivity makes them more specific and less prone to off-target toxicity, but also more challenging to apply.

These targeted therapies can be classified into two groups based on their mode of action: cytotoxic drugs, which aim to destroy tumour cells, and immune-stimulating agents, which aim to enhance the patient's immune response towards cancer. Monoclonal antibodies (mAbs) have become a popular approach for targeted therapy in oncology due to their outstanding affinities for specific targets. Additionally, targeting surface receptors in an immunocompetent patient leads to the activation of various antibody effector mechanisms, such as antibody-dependent cellular cytotoxicity (ADCC). In this case, targeted cells become opsonised by monoclonal antibodies. Effector cells are then recruited to exert cell death by lysis induced by the cytotoxic granules released from NK cells. Antibodies act as bridges that bind to the target cells through their FAB portion and link the effector cells via their Fc portions. Other mAbs trigger what is called complement-dependent cytotoxicity (CDC), whereby the antibody interacts with the C1q complement element, releasing the classical complement activation cascade that leads to cell lysis. Finally, the last effector mechanism is antibody-dependant cellular phagocytosis (ADCP). Here, a similar bridging effect as the one described for ADCC occurs, with the difference that macrophages are linked to the target cells through the

interaction of their HLA-1 receptors and Fc portion of the mAb, leading to the phagocytosis of the cancer cells.[20,21]

Checkpoint inhibitors target proteins that inhibit the immune system's ability to attack cancer cells, such as PD-1, PD-L1, and CTLA-4. These therapies have been found to be promising in the treatment of various cancer types, including unresectable triple negative breast cancer. However, they also have significant side effects, such as dermatological toxicity, pneumonitis, and severe endocrinopathies. To further improve clinical results, it is crucial to identify patient populations that are likeliest to benefit from these therapies and to develop new combination strategies with other treatments.[22,23]

Conversely, immunotherapy based on mAbs has its limitations, as cells can adapt their physiological pathways and rely on alternative pathways, leading to a clonal selection of resistant tumour cells. An alternative solution is the combination of antibodies with potent cytotoxic compounds to produce ADCs. The development of mAb technology has opened the door for the use of mAbs as guiding agents for these potent compounds, resulting in new treatment options. In all cases, the principle is similar: The antibody targets a specific protein on the surface of cancer cells, and the attached compound is delivered directly to the cancer cell, unfolding its cytotoxic potential.

In the following, several mAb-based therapy forms are described:

Antibody-drug conjugates (ADCs): ADCs are monoclonal antibodies that are linked to cytotoxic drugs, thus allowing for more targeted chemotherapy. Early examples of ADCs include brentuximab vedotin (Adcetris) and gemtuzumab ozogamicin (Mylotarg).[24]

Antibody-targeted radioimmunotherapy: This treatment combines monoclonal antibodies with radioactive isotopes, delivering radiation directly to the cancer cell. Examples of radio immunotherapies include ibritumomab tiuxetan (Zevalin) and iodine-131 tositumomab (Bexxar).[25]

Antibody-directed enzyme prodrug therapy (ADEPT): ADEPTs are carrying an enzyme that converts a prodrug, which is an inactive form of a drug to its active form. The enzyme is conjugated to an antitumour antibody that ensures localisation in the tumour. A nontoxic prodrug is then given, which is selectively converted to a cytotoxic drug in the tumour, enable killing of the cancer cell.[26]

Antibody-targeted photodynamic therapy: This treatment combines monoclonal antibodies with a photosensitising agent that is activated by a specific wavelength of light. Upon tumour binding, the photosensitising agent is activated by light, which leads to the destruction of the cancer cell. An example of this type of therapy is Tookad Soluble.[27,28]

This new group of targeted therapies arrives as a combination of two worlds: a macromolecule (mAb) to deliver with pinpoint accuracy a small molecule with high cytotoxic activity. Such a combination can help improve the dosing of the therapeutic molecule, since it is delivered specifically to the target cell. Due to the nature of these molecules, the possibility of off-target toxicity and the adaptation of tumours to the therapeutic agent can be significantly reduced.

1. Introduction

1.3. Magic bullets against cancer; ADCs for targeted therapy

Antibody-drug conjugates (ADCs) are complex and advanced molecules that deliver anticancer drugs with high precision and specificity. The concept behind ADCs is rooted in the idea of the magic bullet first proposed by Nobel laureate Paul Ehrlich over a century ago.

As shown in Figure **2**, the basic structure of an ADC consists of a monoclonal antibody (mAb) that recognises tumour-associated antigens and a potent cytotoxic agent that is attached to the mAb via a chemical linker. This technology combines the advanced targeting and pharmacokinetic properties of mAbs with the potent cytotoxic potency of the payload, resulting in enhanced anti-tumour activity, with reduced off-target toxicities in patients.

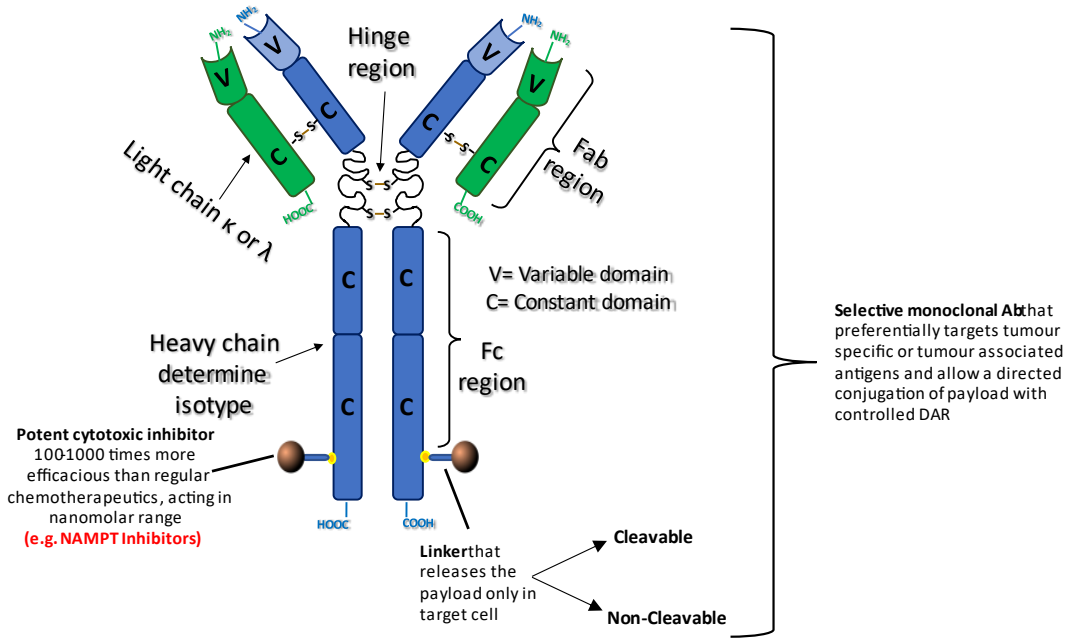

Figure 2. Structure of an IgG I DAR2 thiomab ADC

1.3.1. Monoclonal antibodies

Monoclonal antibodies (mAbs) are the guiding moieties used to build antibody-drug conjugates (ADCs). The first generation of ADCs in the 1970s and 1990s were based on murine or chimeric antibodies, which were plagued with numerous immunogenicity issues.[29,30] Therefore, all mAbs used in ADC technology today are human or at least humanised with the exception of Brentuximab vedotin that uses a chimeric monoclonal antibody. Regarding the isotype variant of immunoglobulin, any variant can theoretically be conjugated to a payload, but isotype G (IgG) is mainly used due to its long half-life in circulation, while its monomeric structure allows for good penetration into tissues and low propensity to aggregation. Additionally, its monomeric structure makes it ideal for genetic engineering, and it can recruit other immune cells through interaction with Fcγ receptors on immune cell surfaces. Among the four isoforms of IgG, the most commonly used is type 1, followed by type 4, whereas only IgG types 1 and 3 are able to activate effector functions, such as ADCC, ADCP, or CDC. The hinge region of IgG1, linking the Fab (fragment antigen binding) region to the Fc (fragment

crystallisable) region, is highly solvent exposed and therefore highly accessible by enzymes, making it optimal to be used for payloads with enzymatic cleavable linkers.[31–33]

In addition to the structural characteristics required for an ADC, the target of the antibody must be expressed abundantly on the surface of (cancer) cells and show a differential expression pattern with significantly higher abundance in cancer cells than in normal tissue to avoid on-target off-tumour toxicity. Furthermore, the binding of the mAb should be sufficient to ensure accumulation and durable retention at the tumour site without compromising the delivery of the antibodies through solid tumours, as vascularisation is reported to be significantly lower in solid tumours; therefore, covering the whole tumour mass relies heavily on diffusion, meaning that overly strong binding to target cells in the surroundings of the vasculature leads to low concentration of mAb in the tumour mass.[34]

To ensure optimal performance of the ADC, the conjugate must be internalised upon binding to the target. However, in contrast to unconjugated mAb, no requirement of antibody effector activity is necessary because ADCs are designed to exert their cytotoxic activity mainly through the selective release of cytotoxic payload.[35]

To reduce the effector activity of the mAb, a common strategy is to reduce the FcγRIIa receptor interaction with the Fc region on the antibody, also known as Fc silencing. Fc silencing can be achieved through single point mutations in the mAb backbone; examples include the LALA (Leu234Ala, Leu235Ala) and D265C mutations (EU numbering), both proven to reduce Fc recognition.[36] This has been reported to result in reduced cytokine release as well as reduced antibody-dependent cell cytotoxicity (ADCC) and antibody-dependent cellular phagocytosis (ADCP) *in vivo*, as well as limited off-target toxicity in target negative cells. The reasons for this relate to the fact that payload conjugation to ADC increases aggregation, and this is especially true when highly hydrophobic payloads are conjugated. It is reported that mAb or ADC aggregates dramatically increase plasma clearance through the activation of FCγ receptors on immune cells, leading to the internalisation of the ADC into target-negative cells, which causes off-target toxicity at the same time as reducing the half-life time of the therapeutics, thereby reducing their efficacy in target positive cells. The Fc silencing induced by these mutations is demonstrated to reduce FCγ receptor mediated off-target cytotoxicity, improving the therapeutical window.[36–38] Additionally, the D265C mutation incorporates a new thiomab™ cysteine into the Fc part, allowing site-specific thiomab™ conjugation with a low DAR (maximum 2) or a high DAR interchain conjugation with a maximum DAR of 10. The thiomab™ strategy will be introduced more in detail in the linker section (**1.3.2**). Finally, due to its location in the antibody tertiary structure, position 265C is not directly exposed to external media, meaning that a lower percentage of non-specific payload release by retro-Michael reaction has been reported. The Michael reaction for maleimide-cysteine conjugation will be introduced in the following section.[39]

1.3.2. Linker

A crucial component of an ADC is the linker, a chemical moiety that enables targeted drug delivery by minimising premature payload release in plasma, hence promoting selective release (ideally only in the target cell). Additionally, linkers can modulate the physicochemical properties of the ADC, thereby playing a significant role in aggregation and solubility.[32]

1. Introduction

From a structural perspective, linkers are divided into three sections: a) a mAb selective conjugation handle, b) a linkage moiety that defines the nature of the linker, and c) a payload conjugation handle, which is usually a chemically activated group. Cleavable linkers aim to release the cytotoxic payload without any remaining moiety from the linker. A variety of modern linkers also contain a *p*-aminobenzoic (PAB) moiety that, upon linker cleavage, performs a 1–6 elimination as a self-immolative mechanism, releasing the free payload.[40]

Linkers are broadly classified into two groups, namely cleavable and non-cleavable (Figure **3**).

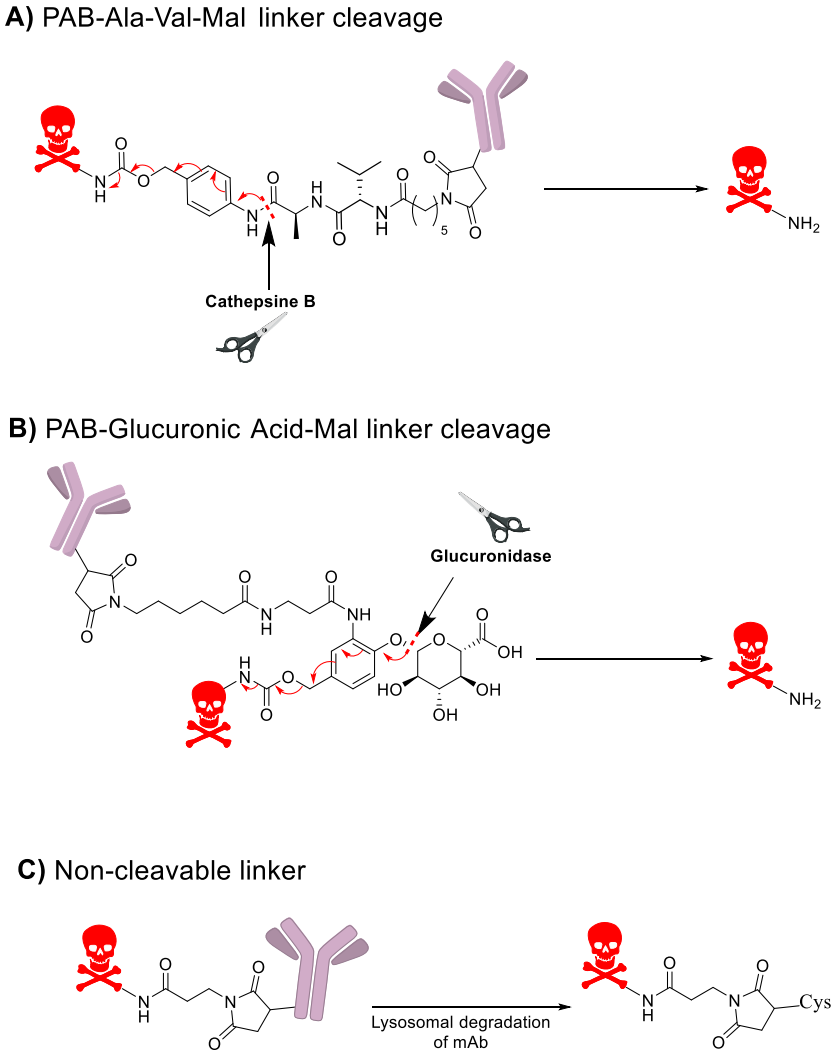

Figure 3. ADC models with different types of linkers used in this research and their cleavage mechanisms; the red skull represents the cytotoxic payload. A) Peptidase-cleavable linker B) Glucuronidase-cleavable linker C) Non-cleavable linkers that require lysosomal total degradation of mAb.

Non-cleavable linkers

ADCs developed with non-cleavable linkers rely on lysosomal proteolytic degradation of the monoclonal antibody (mAb) to release the cysteine-adduct of the payload. As a result, the lysosomal residence time is significantly longer than with cleavable linkers; therefore, the payload must be stable under lysosomal conditions and remain cytotoxic as cysteine adduct.

Hence, ADCs that use non-cleavable linkers may have amplified plasma stability towards unspecific cleavage, leading to better performance *in vivo.*[41] Non-cleavable linkers are further divided into two groups: thioether or maleimidocaproyl constructs.[40,42]

Cleavable linkers

Cleavable linkers, as their name suggests, release the payload by means of an active mechanism, such as an enzyme or a change in pH. Most cleavable linkers are selectively cleaved upon internalisation of the ADC in the lysosome or endolysosome. One of the most common mechanisms of cleavage is induced by peptidases, such as cathepsin B, which are selectively located in the endolysosome and catalyse the hydrolysis of dipeptides, such as Val-Ala, Val-Cit, and Phe-Lys.[43–45] Generally, this type of linker is very stable in circulation and presents a fast cleavage inside a cell. From a physicochemical point of view, they do not contribute substantially to the hydrophilicity of the payload. This could be problematic in the case of hydrophobic payloads, as they can modify the hydrophilic surface of the mAb significantly, leading to aggregation due to stabilisation of hydrophobic ADC complexes by intermolecular hydrophobic interactions. Aggregation is not desired, since it significantly reduces the half-life of the ADC complexes, as will be explained in sections **1.5.2** and **3.1.1.3**. In contrast, another family of linkers that are more complex from a chemical point of view are the glucuronide-containing linkers, which significantly increase the solubility of the linker-payload compared to peptide linkers. From a safety point of view, they are less stable than dipeptide linkers, since glucuronidases can be found in the extracellular medium of tumours (tumour micro-environment), not just in the lysosome.[42] Additionally, the use of lysosomal phosphatase-cleavable linkers has been reported.[40]

Other types of cleavable linkers include chemically labile linkers, which have a less selective mechanism of cleavage than enzyme-cleavable linkers. One example is acid-labile linkers, which are cleaved in the acidic milieu of the tumour micro-environment, or endolysosome to break down hydrazine, acyl hydrazine, ketal, acetal, or carbonate linkages.[42]

Furthermore, disulphide-containing linkers take advantage of the high concentration of glutathione and a low molecular weight thiol found in the cytosol of tumour cells (1–10 mM) to selectively release their payload.[42]

1.3.3. Cytotoxic payloads

The cytotoxic payloads in ADCs are crucial to their efficacy; they need to be active in the sub-nanomolar range, given that only 0.001–0.01% of injected ADCs binds to tumour cells in humans.[46] This high potency requirement also allows the use of discontinued small toxic compounds with remarkable side effects. Additionally, these payloads must contain functional groups that allow for successful conjugation to the antibody component, and they should also be soluble and stable under physiological conditions.[47]

FDA-approved ADCs typically use potent microtubule inhibitors, such as auristatins (monomethyl auristatin-E, MMAE, and monomethyl auristatin-F, MMAF) and maytasines (DM1 and DM4), as their payloads. The mode of action of these inhibitors is based on inhibiting tubulin polymerisation and causing cell cycle arrest in actively dividing cells. MMAE, being membrane permeable, allows for “bystander killing”, or the killing of antigen-negative cells via diffusion of the payload from antigen-positive cells. Maytasines inhibit the assembly of

microtubules, thereby decreasing microtubule dynamic instability to cause mitotic arrest and eventually cell death.[47]

DNA-damaging agents are less extensively used. Their mode of action is based on direct targeting of the minor groove of DNA, such as duocarmycins that induce alkylation upon binding or calicheamicin derivatives that induce double-strand breaks. More potent derivatives like pyrrolobenzodiazepin dimers (PBD) and indolinobenzodiazepine pseudodimers (IGNs) have been presented, but they pose safety issues in use due to their high potency.[47]

Currently, new cytotoxic payloads are emerging that target vital cellular pathways, such as energetics or protein production. For example, NAMPT inhibitors are potent small molecules that target the main NAD synthetic pathway in cells, leading to intense energy scarcity in cells. Another example is α-amanitin, a selective inhibitor of RNA-polymerase II, which results in the shutdown of protein metabolism in cells. However, the use of both NAMPT inhibitors and α-amanitin has been limited due to their extremely high toxicity as free drugs.[32,48]

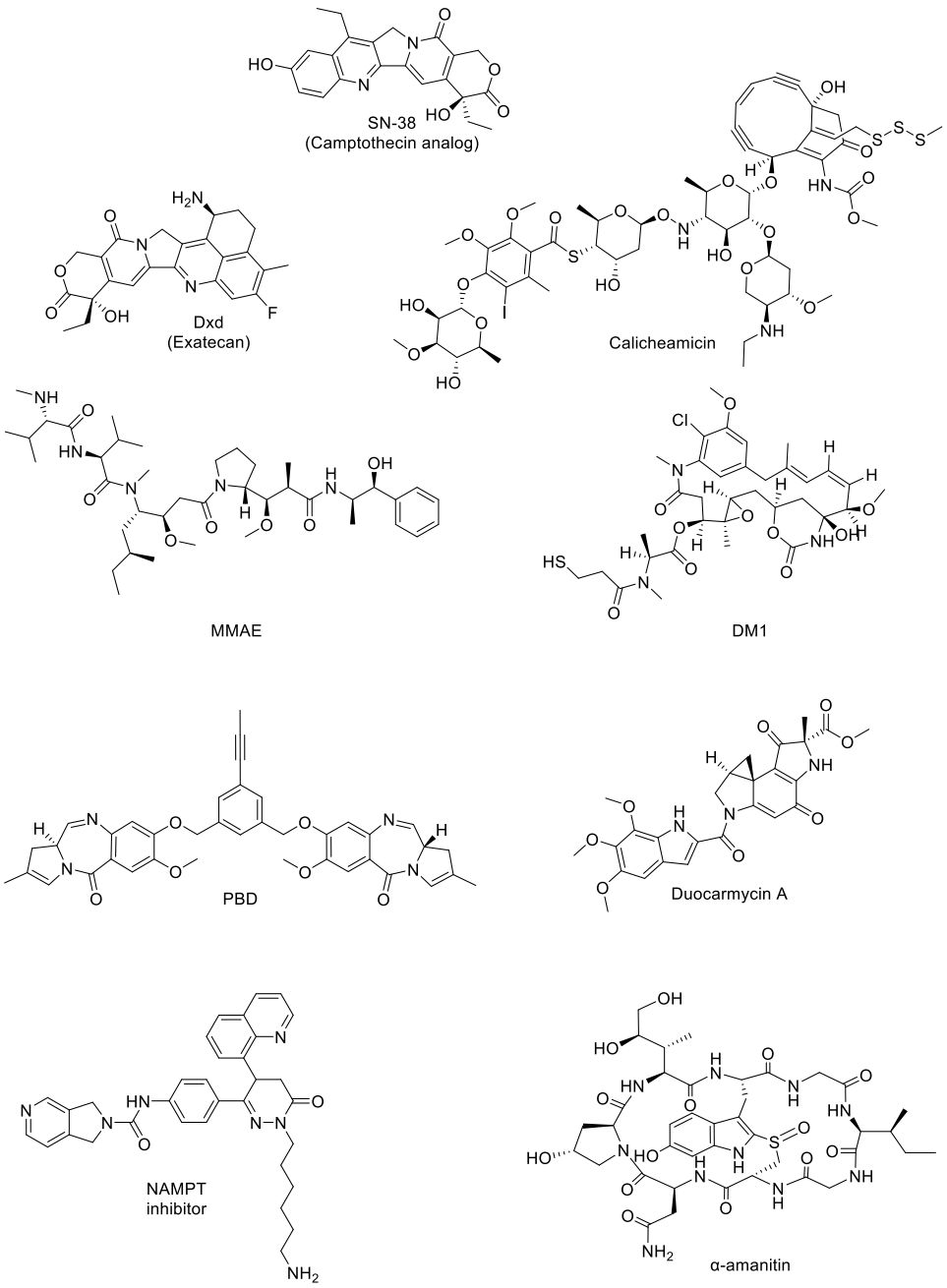

Figure 4. Different families of cytotoxic payloads used in ADC technology. **SN-38** (Camptothecin analogue) is a topoisomerase inhibitor; **Dxd** (Deruxtecan) is a topoisomerase inhibitor; **Calicheamicin** is a DNA destabilising agent; **Mono methyl auristatin E** (MMAE) is an antimitotic agent that inhibits tubulin polymerisation; **Mertansine maytansinoid** (DM1) is an antimitotic agent that inhibits the assembly of the microtubules by binding to tubulin; **Pyrrolobenzodiazepine dimer** (PBD) induces DNA crosslinking; **Duocarmycin A** is a DNA alkylating agent; **NAMPT inhibitor** is a cellular energy metabolism disruptor; and **α-amanitin** inhibits protein synthesis via blockage of RNA polymerase type II.[49–55]

1.3.4. Strategies for payload conjugation to mAbs

The success of an ADC is determined not only by the toxin but also by both the conjugation strategy and the conjugation site. These strategies can be broadly classified into two categories, namely chemical and enzymatic approaches (Figure **5**).

1. Introduction

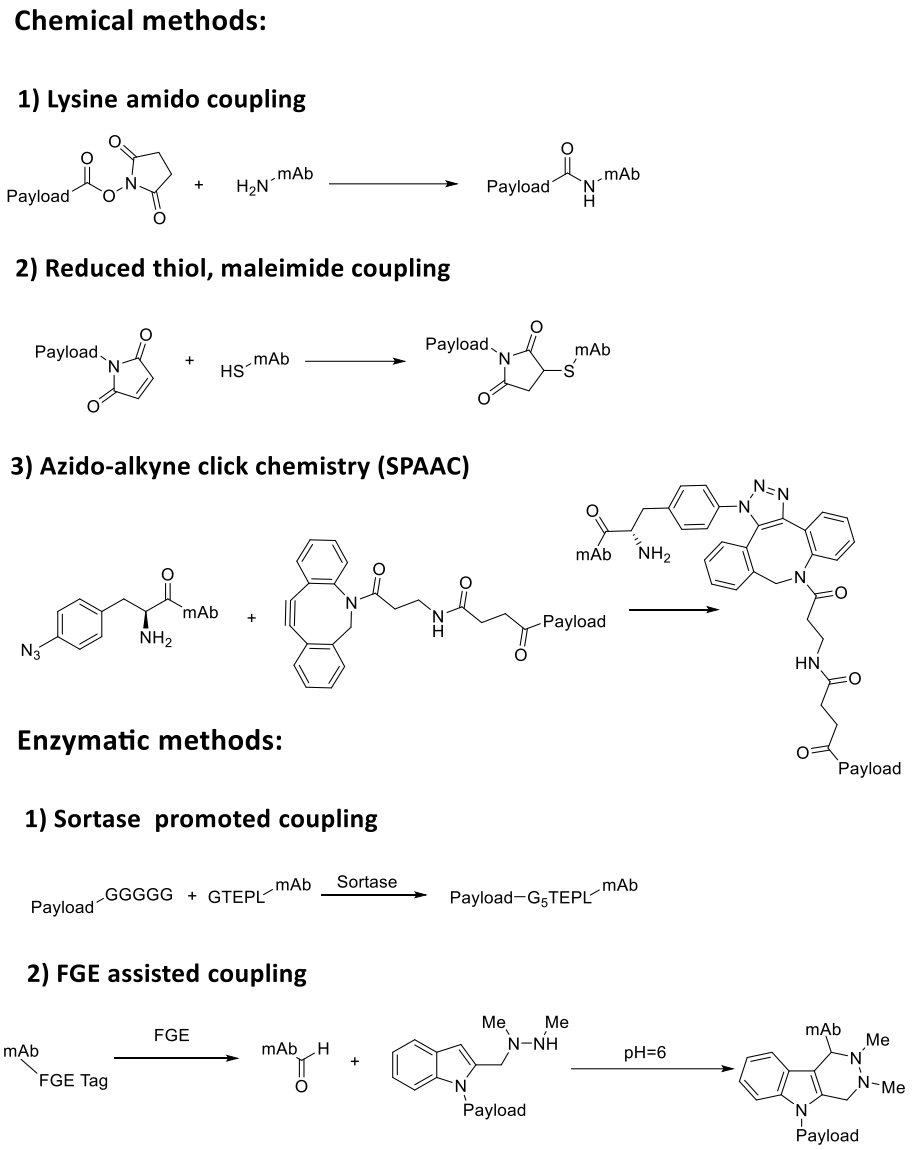

Figure 5. Examples of payload-mAb conjugation strategies. Chemical: 1) Coupling between the free amino terminus of lysins in the mAb and NHS activated carboxylic acid payloads; 2) Coupling between reduce thiols of solvent exposes cysteines in mAb and maleimide-bearing payloads; 3) Strain-promoted azido alkyne click reaction between unnatural azido-containing amino acids in mAb and dibenzocyclooctyne (DBCO) containing payload. Enzymatic methods: 1) Sortase-promoted coupling between a pentaglycine chain-bearing payload and a GTEPL tag-bearing mAb; 2) FGE-assisted coupling between an aldehyde-containing payload and an FGE tag bearing an mAb.

Chemical approaches involve direct coupling between surface-exposed lysine nucleophilic primary amino groups (Lys-conjugation) or with reduced thiol groups from disulphide-forming cysteines (Cys-conjugation). The most commonly used method for lys conjugation is amide coupling using carboxylic acid esters as linkers, typically activated in the form of NHS esters. For cys conjugation, interchain disulphide bridges must be reduced using mild reductive agents (e.g., TCEP or DTT) to ensure that the intrachain disulphide bonds remain unmodified. This allows for conjugation to payloads containing maleimide moieties (Michael addition), pyridine disulphides (disulphide bond formation with mAb), and α-halo amides (α-halo carbonyl alkylation).[32,40]

Maleimide conjugation is a very popular chemical strategy, as it is fast, chemo-selective, affords conjugates with good yields, and is versatile in terms of linkers. However, it can lead to

premature release of payload through de-conjugation of the thioether linkage by retro-Michael reaction. The maleimide-containing payload, in the presence of thiol-containing (macro)molecules in the blood, can then lead to off-site toxicity and insufficient efficacy.[32,40,56,57] To mitigate this issue, several methods have been published highlighting the solution to the retro-Michael reaction presented by the "self-hydrolising maleimide" reagents, which are able to undergo a fast hydrolysis post-conjugation to the corresponding succinamic acids (maleimide ring opening).[58–60] Other methods involve the use of distinct thiol reactive groups or modifying the maleimide scaffold to some exocyclic olefinic maleimides.[61–63]

While using native amino acids for linker-payload conjugation to the mAb has the advantage of minimal protein modification, it can lead to heterogeneous conjugates showing a heterogeneous mixture of drug antibody ratios (DAR), spanning typically from DAR 2 to 8 in the case of conjugation to reduced interchain cysteines in native IgG1. Heterogenous ADCs can have undesirable properties, such as increased toxicity, aggregate formation, and faster systemic clearance. This can be overcome by site-specific conjugation technologies, such as the use of genetically engineered cysteines in the antibody backbone, known as thiomab™, a technology first introduced by Genentech in 2008.[64] This enables the selection of the location of conjugation site in the mAb, which could have a major impact on properties of the ADC, such as stability and hydrophobicity.[32,35]

Enzymatic methods also aim for site-specific conjugations by engineering enzymatic recognition sequences in the mAb, including for transglutaminase, sortase, or formylglicine-generating enzyme (FGE). This strategy may require modified amino acids bearing enzyme recognition sequences, or the incorporation of handles for bio-orthogonal reactions (e.g., containing azido moieties), which can couple via click chemistry with payloads harnessing dibenzylcyclooctyne moieties to trigger strain-promoted azide-alkyne click (SPAAC) reaction. SPAAC-promoted conjugation of payloads to the mAb could lead directly to the connection of cytotoxic payload or to the incorporation of the aforementioned enzyme recognition sequences.[35]

Finally, site-specific conjugation can also be achieved by incorporating genetically encoded unnatural amino acids in the mAb backbone through techniques such as CRISPR/Cas technology. This may circumvent problems found with thiomab-introduced cysteines, where the positioning in the antibody must be chosen carefully to avoid unwanted disulfide pairing.[35] Additionally, encoding unnatural amino acids opens the door for new methods of site-specific coupling as well as enabling ADCs with improved pharmacokinetics, potency, and antigen binding properties. Although more than 50 unnatural amino acids have been incorporated into recombinant antibodies, the most commonly used are *p*-acetophenylalanine and *p*-azidophenylalanine. The side chains of these unnatural amino acids' new reactivity is provided, allowing the creation of stable conjugates through strategies such as the SPAAC reaction.[32,35,65]

In summary, various conjugation strategies can be used to conjugate linker-payloads to antibodies as a means of generating ADC. Chemical approaches are the most commonly used, with maleimide conjugation a popular choice. However, the use of native mAb amino acids can lead to heterogeneous conjugates with a range of drug-antibody ratios (DARs). Site-specific conjugation technologies, enzymatic methods, or the incorporation of unnatural amino acids can overcome this issue and enhance the properties of the ADC, including stability and hydrophobicity.

1.3.5. Mode of action

The mode of action of an ADC involves several steps, as illustrated in Figure **6**. The first is the binding of the mAb component of the ADC to a specific antigen on the surface of the cancer cells. This binding typically occurs through the Fab region of the antibody. The antigen binding site of the mAb is highly specific, allowing the ADC to selectively target cancer cells while leaving healthy cells unharmed in the case of tumour-specific antigens. Once the ADC-target complex is formed, it is internalised into the cell through endocytosis. The ADC is then released from the antigen and recycled in the endosome, leading to the release of the cytotoxic payload. The mechanism of release depends on the type of linker used. For non-cleavable linkers, the mAb component must be completely degraded. For cleavable linkers, selective chemical or enzymatic cleavage of the linker is required. After release, the cytotoxic payload diffuses to the cellular compartment in which its target is located, binds to it, and consequently induces cell death.[40]

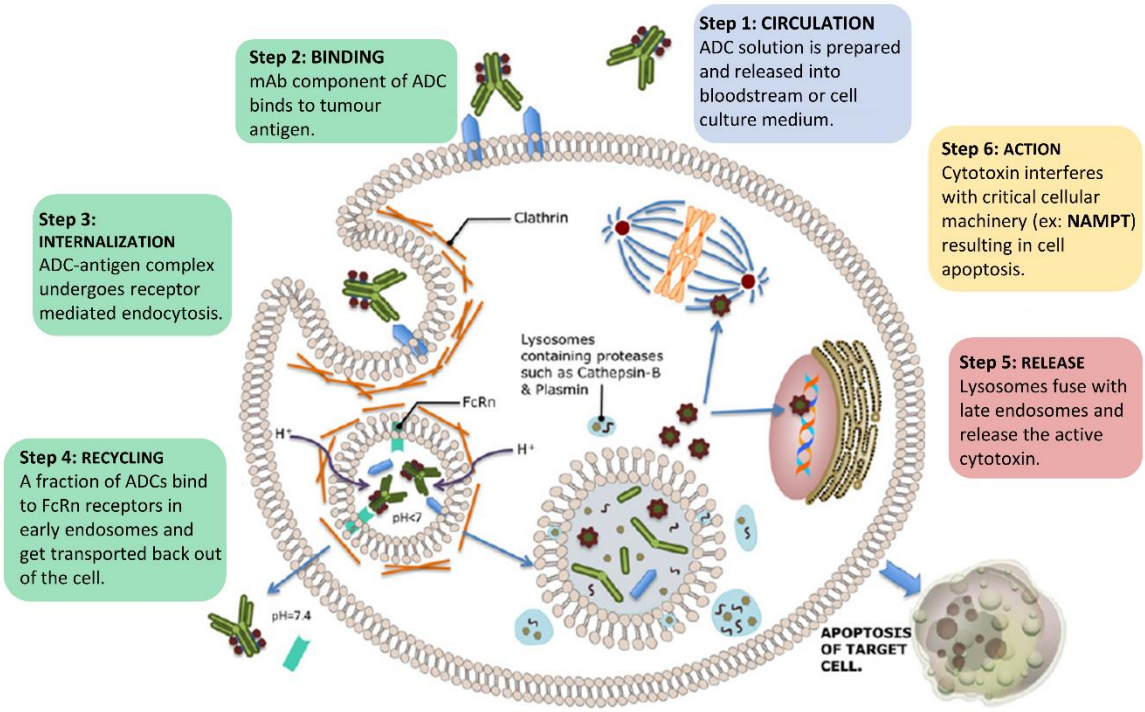

Figure 6. ADC metabolism in cell. Circulating ADCs bind their specific receptor on the surface of cancerous cells, which triggers the internalisation of the complex and recycling of the receptor in the endosome. Subsequently, the endolysosome is formed, and the payload is released. The final step involves the cytotoxin acting on its intracellular target, resulting in cell death. Figure adapted from Peters et al.[66]

1.3.6. Overview of FDA-approved ADCs

The importance of ADCs in cancer treatment is demonstrated by the increasing number of FDA-approved drugs, which currently stands at 11. However, this number had been 12 prior to the withdrawal of Blenrep from the market in November 2022 after the results of the DREAMM-3 phase III clinical study, which failed to meet the FDA criteria for accelerated approval.[67] Nonetheless, the use of ADCs has been steadily rising since 2000, with 5 out of 12 ADCs approved in the last 3 years. Furthermore, ADCs have been used to treat a wide range of malignancies, both haematological and solid. Additionally, over 80 ADCs are currently in various stages of clinical trials.[40,68]

Table 1. Summary of FDA-approved ADC descriptions.

	Mylotarg	Adcetris	Kadcyla	Beponsa	Polivy	Enhertu
Target	CD33	CD30	HER2	CD22	CD79b	HER2
Approval year	2000 (withdraw 2010 reapproved 2017)	2011	2013	2017	2019	2019
mAb isotype	IgG4	IgG1	IgG1	IgG4	IgG1	IgG1
Toxin	Calicheamicin	MMAE	DM1	Calicheamicin	MMAE	Dxd
Conj. site	Lysine	Cysteine	Lysine	Lysine	Cysteine	Cysteine
Release mechanism	Hydrazone + disulfide	Dipeptide	Non-cleavable	Hydrazone + disulfide	Dipeptide	Peptide
DAR	Av. 2-3	Av. 4	Av. 3.5	Av. 6-7	Av. 4	8
	Padcev	**Trodelvy**	**Blenrep**	**Zylonta**	**Tivdak**	**Elahere**
Target	Nectin-4	Trop-2	BCMA	CD19	TF	FOLR1
Approval year	2019	2020	2020 (withdraw 2022)	2021	2021	2022
mAb isotype	IgG1	IgG1	IgG1	IgG1	IgG1	IgG1
Toxin	MMAE	SN38	MMAF	PBD	MMAE	DM4
Conj. site	Cysteine	Cysteine	Cysteine	Cysteine	Cysteine	Lysine
Release mechanism	Dipeptide	Peptide	Non-cleavable	Peptide	Dipeptide	Reduction
DAR	Av. 4	8	Av. 4	Av. 2.3	Av. 4	3,4

1.3.7. ADCs past and present: Focus on payloads with new modes of action

As discussed in this chapter, ADC technology has a promising future, with 11 therapeutics already approved since 2000 and nearly 100 currently in clinical trials.[40] However, this success is the result of years of sustained development.

A brief look at the historical development of ADCs shows that initial attempts used murine-derived mAbs, with only limited success due to immunogenicity issues. This problem has been overcome by using humanised or fully human mAb. However, the cytotoxic compounds (e.g., doxorubicin or vinblastine) used in these initial versions, which were also employed as non-selective cancer therapeutics, did not provide the required potency when used in ADCs. This was attributed to the small percentage of linked cytotoxic agent delivered to the tumour. The use of more potent cytotoxic compounds, such as auristatin, maytasinoids, and PBDs, addressed this issue.[69]

Early super-toxic payloads, such as the EGFR inhibitor Icotinib, lacked specificity for tumours and attempted to limit side effects by targeting only actively dividing cells.[15] However, more recent understanding of the tumour micro-environment has highlighted the importance of considering the diversity of cell types and characteristics within the tumour, which includes

variable levels of surface target expression among different cellular populations or among cells in different metabolic states (e.g., tumour dormant cells, also called tumour non-dividing cells). Therefore, targeting a single surface target protein in a single cell population may lead to medium-long term resistance to treatment and ultimately to metastatic and loco-regional failure events.[24,47]

Therefore, to achieve maximum coverage of the tumour micro environment in solid tumours rather than targeting only actively dividing tumour cells, some strategies involve bystander killing: the killing of target negative cell populations in the tumour micro environment through diffusion of the cytotoxic payload released from ADC targeted cells.[70] However, to be effective, bystander killing requires more hydrophobic payloads to ensure a maximum diffusion rate between cell membranes.[70] That said, as seen with PBDs, this can lead to problems such as the accumulation of the payload in patient tissues, limiting their applicability to only a few treatment events due to high toxicity.[69]

In general, ADCs have shown better performance in liquid malignancies than in solid tumours. This is attributed to the difficulty of delivering macromolecules to solid tumours due to poor vascular supply and problems with crossing the endothelium, overcoming the tumour interstitial fluid pressure, diffusing through dense stroma, and passing through tight epithelial barriers. This implies that micro-distribution across the entire tumour does not always correlate with the drug dose or plasma concentration, which can lead to poor responses due to suboptimal concentrations of therapeutic agents in the tumour micro-environment of solid tumours.[69,71]

One of the main areas of research to improve the effectiveness of ADCs is the development of new cytotoxic payloads. Recent research has focused on compounds that target dormant cells or tumoral altered metabolic states, such as RNA polymerase II inhibition or NAD disruption. Examples of these innovative payloads are described in Table **2**.

Table 2. Innovative payloads used in ADCs

Therapeutic agent	Function	Mode of action
Bcl-xL inhibitors of AbbVie (Clezutoclax)	Inhibition of BCL-xL antiapoptotic factor	Cancer cells can acquire resistance to apoptosis by overexpression of Bcl-2 family members as BcL-xL. Inhibition of this factor induces apoptosis in cancer cells.
Thailanstatin and analogues	Spliceosome subunit inhibitor	Inhibition of mRNA splicing leads to an altered cellular proteome that induces apoptosis.
Amatoxin	RNA polymerase II inhibitor	Inhibition of protein biosynthesis.
FK866	NAMPT inhibitors	NAD metabolism disruption leading to cell death by energy scarcity.
Carmaphycins	Proteasome inhibitors	Interference with cell recycling dynamics leading to cell death.

Among these innovative payloads, amatoxins, Bcl-xL inhibitors, and NAMPT inhibitors present the most advanced development in their application as ADC payloads. All of them target vital enzymes for correct cellular function.

BcL-xL inhibitor (Clezutoclax) from AbbVie is currently in phase I trials as the ADC payload in the ADC Mirzotamab clezutoclax targeting CD276 (B7H3) in patients with relapsed and/or refractory solid tumours.[72] Clezutoclax represents the final stage of a year-long development process by AbbVie scientists, in contrast to initially developed small drugs against other members of the BCL superfamily, including anti BCL-2 Venetoclax. Clezutoclax is designed as an ADC payload to overcome patient platelet unspecific targeting, the main dose-limiting effect associated with these BCL superfamily inhibitors.[73]

Amatoxins are derived from a natural compound found in the green death cap mushroom (*Amanita phalloides*). They are challenging to synthesise: The process requires more than 30 steps, and the compound itself has a bicyclic structure consisting of a peptidic macrocycle of eight *L*-configured amino acids. The macrocycle is bridged by a tryptathionine, which is a tryptophan substituted with a cysteine residue in the 2-position of the indole moiety. Amatoxins are highly potent cytotoxins due to their tight binding to RNA polymerase II, allowing them to target all types of cells, including dormant cells. Additionally, they have high hydrophilic properties, making them completely water-soluble. This accounts for the safety profile *in vivo*, as they cannot enter cells through passive diffusion. However, an active transporter (OATP-1B3) is widely expressed on the surface of hepatocytes, which explains why the liver is the target organ for unspecific toxicity with non-derivatised amatoxins.[48,74]

Recently, new payloads with innovative modes of action have been reported that target dormant cells and altered metabolic states in tumours, such as NAD disruption. NAMPT inhibitors are one example of these new payloads. They bind with high specificity to the enzyme nicotinamide phosphoribosyl transferase (NAmPRTase or NAMPT), which is the rate-limiting enzyme in the NAD salvage synthetic route. These inhibitors are fully synthetic small molecule payloads, typically produced through a 10-step synthetic process, making them affordable and easily modifiable for different applications. While NAMPT inhibitors can act on nearly every cell type, they have been shown to be especially effective in tumour cells due to the energy dysregulation typical of this type of cell.[75] However, their potency and hydrophobic nature grants them free diffusion into cellular cytoplasm, and initial approaches of NAMPT inhibitors as small-molecule drugs for cancer treatment ended with dose-limiting side effects such as thrombocytopenia, gastrointestinal toxicity, and retinal toxicity. In response, the focus of this dissertation is to develop new ADCs loaded with NAMPT inhibitors to overcome these issues. The following sections of the introduction will describe NAD metabolism, the activity of NAMPT, and the panorama of NAMPT inhibitors.[74]

1.4. NAD^+: Cellular energetics' main actor and more

Nicotine adenine dinucleotide (NAD^+) is a vital coenzyme that is composed chemically of two nucleotides (nicotinamide and adenosine) joined through their phosphate groups, as shown in Figure **7**. It is conserved in every cell system throughout evolution.[76]

From the perspective of its function, NAD^+ is considered a multifaceted molecule. First, it has a major role in bioenergetic redox pathways, where it is reduced to NADH and acts as an electron transfer molecule in cellular energetics without being catabolised. Additionally, it plays a vital role in biosynthetic pathways and helps maintain redox stability in cells by neutralising the reactive oxygen species (ROS) generated during metabolism. When phosphorylated by NAD^+ kinase, it generates $NADP^+$. Secondly, NAD^+ acts not only as a coenzyme but also as a reactant; it is consumed in biological processes, as discussed in the following chapters. Therefore, the pathways involved in its regeneration are of major importance to the cell.[76,77]

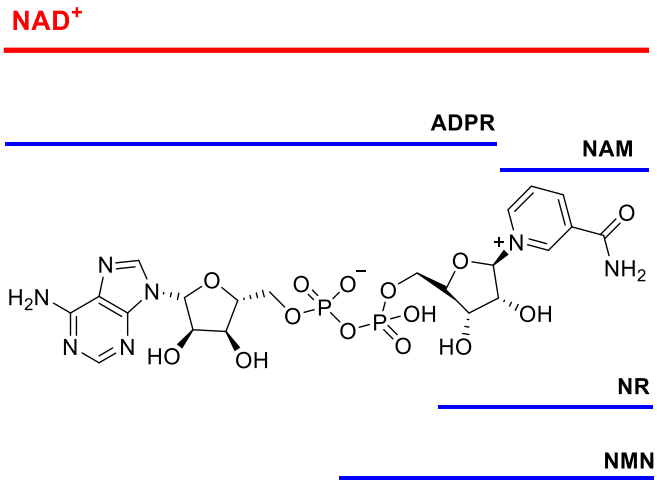

Figure 7. NAD^+ (nicotine adenine dinucleotide) structure with precursors, adapted from Cambronne et al.[78] Abbreviations of the various chemical moieties contained in the NAD^+ molecule: Adenosine diphosphate-ribose (ADPR), nicotinamide (NAM), nicotinamide ribose (NR), nicotine amide mononucleotide (NMN).

1.4.1. NAD^+ synthesis and compartmentalisation with focus on cancer

Four main routes are associated with NAD^+ synthesis, spanning a *de novo* synthetic route or recycling from some of the degradation intermediates, as shown in Figure **8**.

1) NAD^+ can be *de novo* synthetised by a cell from tryptophan. First, tryptophan is transformed through the five-step kynurenine pathway into quinolinic acid (QA), a direct precursor of NAD^+. The QA is then directly transformed into nicotine-adenine mononucleotide (NAMN) using quinolinate phosphoribosyltransferase (QPRT). NAMN can also be obtained through the Preiss-Handler route (explained below); it is transformed into nicotinic acid adenine dinucleotide (NAAD) by one of the three nicotinamide mononucleotide adenylyltransferases (NMNAT 1–3). The final step involves the amidation of NAAD by NAD synthase (NADS) yielding NAD^+. This *de novo* pathway is limited to certain cell types, specifically to hepatocytes in liver, kidney, and some immune cells. Due to the costly nature of this route in terms of energy and enzyme resources, it is an inadequate route to overall NAD^+ production.[76]

Elsewhere, the so-called "salvage pathways" or biosynthetic pathways recycle intermediaries from a degradative process, in this case NAD^+ degradation:

2) The Preiss-Handler route uses nicotinic acid (NA) as a precursor, which can be obtained not only as a degradation product but also from the diet as niacin or vitamin B3. Through the action of the nicotinate phosphoribosyl transferase (NAPRT), the rate-limiting enzyme of this route, NA is adenylated into NAMN, converging with the *de novo* pathway to yield NAD^+.[76]

3) Nicotine amide riboside (NR) can also be incorporated from diet, and it can be used to produce NAD^+ through phosphorylation of NR to nicotine mononucleotide (NMN) by nicotinamide riboside kinase 1 (NMRK1), followed by adenylation to afford NAD^+ by one of the NMNAT enzymes.[76]

4) The final salvage pathways for NAD^+ biosynthesis rely on nicotinamide (NAM) as their precursor, which is phosphorylated by the rate-limiting enzyme nicotinamide phosphoribosyl transferase (NAMPT) of this route to yield NMN. The synthesis then converges with the route of NR as starting compound, leading to the production of NAD^+ by adenylation of NMN by one of the NMNAT enzymes.[76]

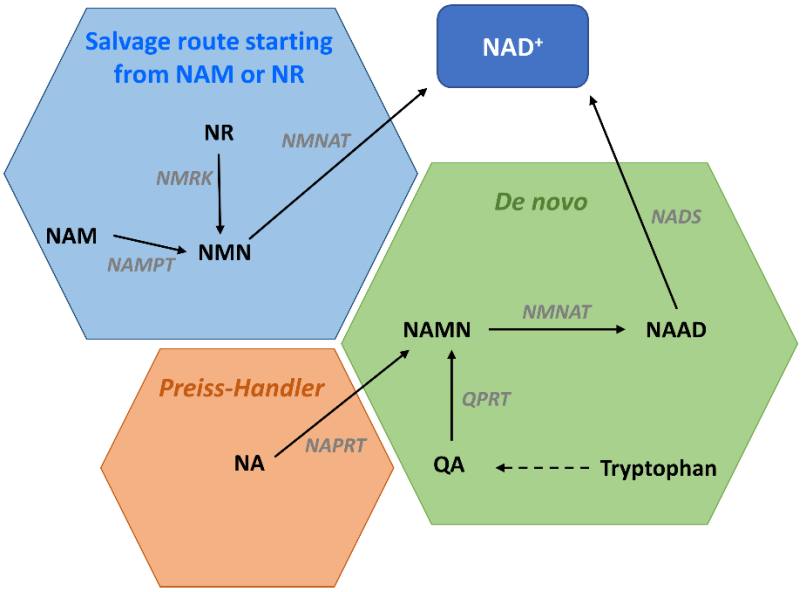

Figure 8. NAD biosynthetic pathways. De novo synthesis in green uses tryptophan as the starting compound. Salvage pathways in orange: Preiss-Handler route starts from nicotinic acid (NA) and converges in de novo pathway. In blue, the route uses nicotine amide (NAM) or nicotinamide riboside (NR) as the starting compound. Figure adapted from Cambronne et al.[78] Description of the enzyme abbreviations (in grey): Quinolinate phosphoribosyl transferase (QPRT), Nicotinamide mononucleotide adenylyltransferase (NMNAT), NAD^+ synthase (NADS), Nicotinic acid phosphoribosyl transferase (NAPRT), Nicotinamide riboside kinase (NMRK), and Nicotinamide phosphoribosyl transferase (NAMPT). Abbreviations of the molecular intermediates of the synthetic routes (in black and bold): Quinolinic acid (QA), Nicotinic acid (NA), Nicotinic acid mononucleotide (NAMN), Nicotinic acid adenine dinucleotide (NAAD), Nicotinamide (NAM), Nicotinamide mononucleotide (NMN), and Nicotin riboside (NR).

In highly proliferative cells, including cancer cells, the metabolism often focuses on supporting anabolic and glycolytic pathways at the expense of mitochondrial respiration. As a result, many tumours upregulate the expression of NAD^+ biosynthetic enzymes. It is important to note that two key enzymes, NAPRT and NAMPT, are frequently upregulated in cancer, albeit through different mechanisms. NAPRT is typically upregulated through gene amplification, whereas NAMPT is upregulated through epigenetic modification at the promoter level. As expected, the dynamism of epigenetic changes is significantly higher, making the latter more feasible and faster to occur than gene amplifications and mutations. Hence, the Preiss-Handler route is often detrimental in cancer due to the lower expression of NAPRT. This leads to the salvage pathway starting from NAM, with NAMPT as the rate-limiting enzyme, being the most upregulated and becoming the primary route for maintaining NAD^+ homeostasis in many tumours. The upregulation of NAD^+ synthetic pathways leads to an increase in cytoplasmic pools of this metabolite, promoting cell proliferation by supporting glycolysis and biomolecule synthesis through NADPH production. Nuclear NAD^+ pool concentrations also increase as the glycolytic enzyme GAPDH shuttles cytoplasmic NAMPT to the nucleus. These early subcellular changes in NAD^+ levels are common in most tumours and make targeting the NAD^+ pool a potential therapeutic approach in cancer treatment.[76,79]

1.4.2. NAD^+: Not only a bioenergetics regulator

In addition to its role in bioenergetics, NAD^+ can also act as a biological metabolite and is consumed as part of a variety of biological pathways:

1) Poly-ADP ribose polymerases (PARP) are a family of 18 enzymes, each encoded by different genes, which consume a significant proportion of cellular

NAD^+. Their main function is the transfer of ADP-ribose to the target proteins. PARP enzymes play several key roles, including the detection and repair of single-strand DNA breaks through the base excision repair mechanism carried out by PARP-1 and -2. Additionally, PARP enzymes are involved in cell proliferation. Most of their substrates are nuclear proteins involved in nucleic acid metabolism, such as modulation of the chromatin structure by poly-ADP ribosylation of DNA poly-nucleosomes leading to chromatin relaxation that facilitates DNA transcription. Another major role of PARPs is in DNA repair. This can be clearly observed by PARP expression upregulation upon radiation-induced DNA damage. PARPs also regulate cell death in response to extensive or irreparable DNA damage. In these situations, PARP enzymes undergo hyperactivation, leading to sustained consumption of NAD^+ and ultimately an energy crisis at the cellular level, resulting in programmed necrosis of the cell, thereby protecting the organism's genetic stability.[80]

2) Sirtuins belong to the class III protein deacetylases, which are the only histone deacetylases that are NAD^+ dependent. Although mammalian sirtuins have various non-histone protein substrates. They are highly conserved from bacteria to human. Sirtuins have major implications in the control of longevity and lifespan, as reported initially for SIR2 in yeast in 1999.[81] Mammals possess seven sirtuins, all of which possess the NAD binding and catalytic domain, also called the sirtuins core domain. Among them, one of the most prolific sirtuins is SIRT1, as it presents various functions as a chromatin state regulator through its deacetylase activity. From a metabolic point of view, it plays a crucial role in aging- and survival-related metabolic diseases like obesity or type 2 diabetes due to their effect on gluconeogenesis regulation upon fasting and control over insulin secretion in β-cells in the pancreas. Other important roles of sirtuins involve regulation of inflammation and tumour angiogenesis by suppression of HIF1α to protect the heart against age-related cardiac hypertrophy. Overall, sirtuins have localisations and roles that comprise the participation in the whole cellular metabolism.[81]

Additionally, Ramsey *et al.* found that NAMPT has a connection to the body's internal clock: The presence of SIRT1 in the NAMPT promoter sequence leads to an increase in NAMPT expression, which is regulated by the primary component of the circadian system. This results in the production of NAD^+, which activates enzymes that depend on NAD^+. SIRT1 then negatively impacts the component, leading to a decrease in NAMPT expression through a feedback loop that downregulate the expression of NAMPT. It is believed that this process is crucial for regulating metabolic patterns in relation to the circadian rhythm.[82]

3) Other NAD^+ consuming enzymes are the NAD^+ glycohydrolases, CD38 and SARM1, which play major roles in calcium metabolism.[76]

4) NAD^+ is also involved in the post-transcriptional 5'-capping of mRNA, which is in contrast to the canonical 5'-7-methylguanosin cap (m^7G cap) that promotes mRNA stabilisation. On the contrary, the NAD^+ capping leads to rapid

decomposition and therefore has a regulatory effect on gene expression through metabolite-directed mRNA turnover in mammals.[76,83]

1.4.3. NAMPT: A key regulator of intracellular NAD^+

The protein nicotinamide phosphoribosyltransferase (NAMPT) is a key enzyme that plays a crucial role in the most widely used salvage pathway for NAD^+ regeneration in cancer cells. This enzyme is found in a wide range of organisms, including mammals, insects, sponges, and prokaryotes, and is highly conserved across different species. NAMPT is a dimeric class of type II phosphoribosyl transferases with a molecular weight of about 52 kDa. Each monomer consists of a catalytical pocket domain that binds to its substrate NAM with a K_m value of around 1 µM. However, the enzyme is typically auto-phosphorylated at His247, resulting in a 1 x 10^3 fold increase in enzyme activity and an 1.6 x 10^4 fold enhanced affinity for NAM, leading to an effective K_m value of around 5 nM. In mammals, the two isoforms of NAMPT are intracellular and extracellular variant (iNAMPT and eNAMPT, respectively). This dissertation focuses on the intracellular form of NAMPT, which is responsible for the enzymatic reaction that transforms NAM into NAMN and is primarily found in the cytosol and nucleus, along with its possible presence in mitochondria.[77,79,84]

The extracellular isoform eNAMPT was initially associated with fully developed adipocytes, but evidence now suggests its location in the extracellular medium of the liver, cardiomyocytes, skeletal muscle, and brain cells.[77,85] The structure and enzymatic activity of eNAMPT in an extracellular environment is not well understood, with debates ongoing about the exact mechanism of eNAMPT secretion. However, evidence has shown that eNAMPT can be secreted by living cells in response to cellular stressors, nutritional changes, and inflammatory signals.[85] In addition to possible enzymatic activity, eNAMPT has been found to have cytokine-like properties linked to obesity, diabetes, and increased expression simultaneously to iNAMPT in cancer tissue.[85]

1.5. Inhibiting NAMPT: A historical overview, problems, and future perspectives with NAMPT inhibitors

Targeting NAMPT with specific inhibitors has shown promising results in various types of cancers, including solid tumours such as glioblastoma, chondrosarcoma, breast cancer, gastric cancer, and lung cancer, as well as liquid malignancies like T-cell leukaemia/lymphoma, Burkitt lymphoma, and multiple myeloma.[86–89]

In addition to the inhibition of the protein NAMPT, other approaches involve the control of NAMPT expression at the post-transcriptional level with microRNA interference, such as MIR-381.[90] However, the most promising path is the use of small molecule inhibitors that selectively bind to the NAM-binding site, including the tunnel cavity that extends to the NAM binding pocket (Figure **9**).[79]

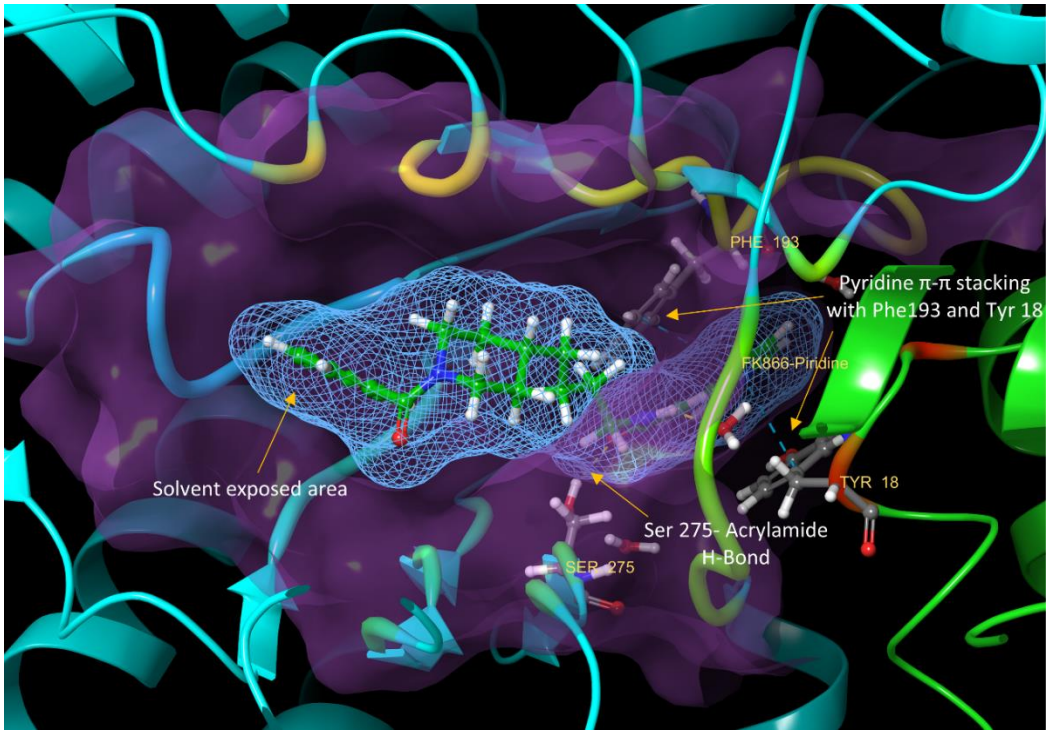

Figure 9. Crystal of NAMPT and inhibitor FK866 (PDB code: 2GVJ), including 3D render. The purple surface represents the NAMPT catalytic pocket; the blue grid surface represents the volume occupied by FK866 in the pocket. Cartoon ribbons represent the secondary structure elements of NAMPT, where the blue- and green-coloured structures represent each monomer of the active NAMPT dimer, and yellow represents the interaction areas between the two NAMPT monomers. It is noticeable how the aromatic tail of FK866 sticks out at the entry of the solvent-exposed area of the NAMPT pocket. The additional main stabilisation of intermolecular interactions is highlighted between Phe193 and Tyr18, as well as the hydrogen bond with Ser 275. Moreover, the tight fitting of FK866 in the NAD docking position at the end of the catalytic pocket is noteworthy.

1.5.1. Small molecule NAMPT inhibitors

Since 1997, various NAMPT inhibitors have been published and tested in clinical trials. Lead compounds for NAMPT inhibition are usually obtained through fragment-based screening, virtual screening, and high-throughput cellular screening. Figure **10** shows the primary NAMPT inhibitors and the year of publication. The following paragraphs provide an overview of the main NAMPT inhibitor lead compounds published to date, focusing solely on pure NAMPT small molecule inhibitors. ADC payloads will be covered in later sections; dual inhibitors are outside the scope of this dissertation.[91]

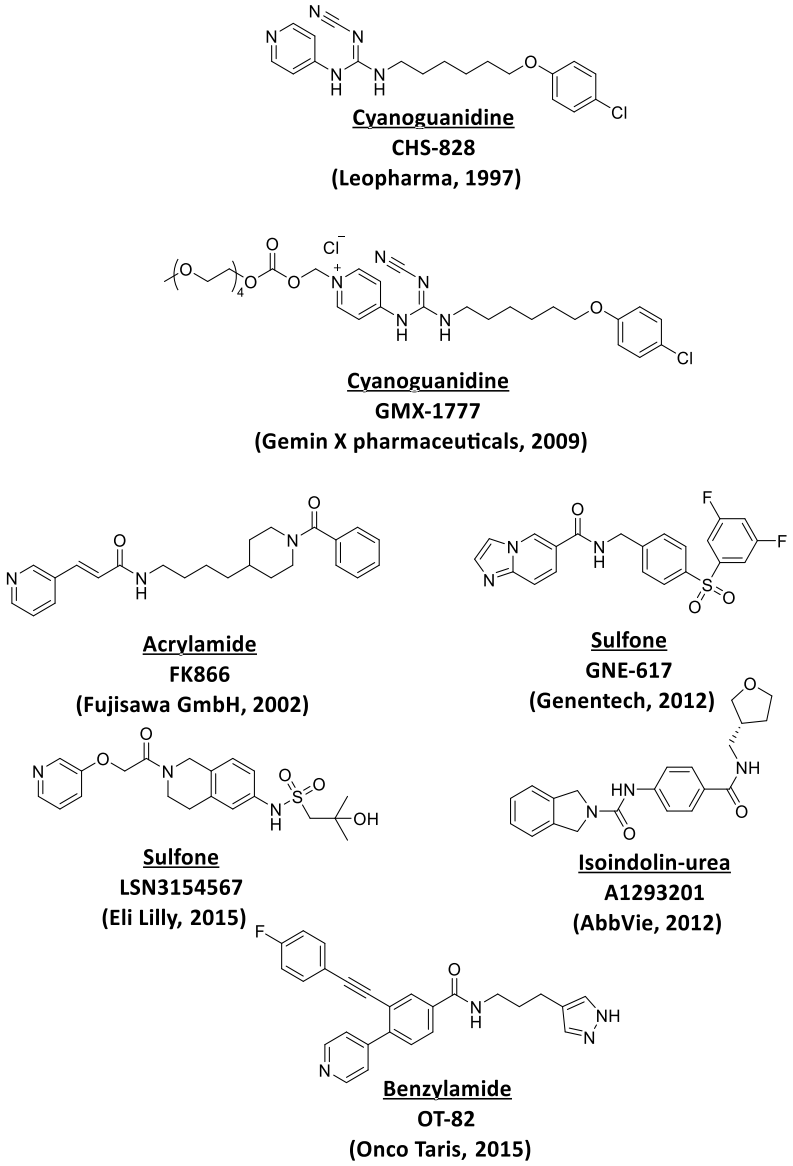

Figure 10. Families of NAMPT inhibitors used in small molecule treatment for cancer; their developers and years of publication are shown in brackets.[92–98]

Cyanoguanidines CHS828 and GMX1777

CHS828 is a small molecule with a pyridinyl cyanoguanidine NAM-mimicking component developed by Leo Pharma in 1997. Early tests in cells revealed strong efficacy against lung and breast cancer, and the efficacy in nude mice showed tumour regression in both types of cancer. Despite these promising results, CHS828's clinical trial in 2003 was impacted by solubility and pharmacokinetic issues, leading to its withdrawal in 2012 during phase I.[79,92,99]

A second-generation prodrug of CHS828 was created by Gemin X Pharmaceuticals, with GMX1777 the most promising candidate. GMX1777 had improved solubility, converting quickly into the active drug CHS828. Two clinical trials were initiated in 2007 and 2008 targeting patients with multiple myeloma or chronic lymphocytic leukaemia and metastatic melanoma, respectively. However, both trials were terminated in 2010 due to dose-limiting toxicities, such as thrombocytopenia and gastrointestinal symptoms, as well as a lack of tumour remission among patients treated with GMX1777.[79,93,100–102]

Acrylamide FK866

FK866 was first reported by Fujisawa GmbH in 2002. Also known as Daporinad or APO866, it is an example of an NAMPT inhibitor that includes a pyridinylacrylamide moiety as an NAM-mimicking group, connected to benzoyl-piperidyl residue by an aliphatic spacer. The benzoyl-piperidyl moiety is exposed to the solvent when binding to the NAMPT tunnel attached to the binding pocket.[103]

FK866 is reported to have IC_{50} values with efficiencies in the nM range for several tumour cell lines and in mouse and non-human primate *in vivo* models, including solid malignancies, such as ovarian, colorectal, prostate, liver, and brain cancer, as well as several liquid malignancies, including adult T-cell leukaemia and multiple myeloma.[86,104–108]

In 2007, three phase I/II clinical trials were initiated to treat B-cell chronic lymphocytic leukaemia, melanoma, and cutaneous T-cell lymphoma (NCT numbers: NCT00435084, NCT00432107, and NCT00431912, respectively) based on promising preclinical results. However, the trials were terminated due to the dose-limiting toxicity of thrombocytopenia and a lack of objective responses among the patients treated.[109]

The interaction between FK866 and NAMPT has been studied closely, and several co-crystal structures have been published (PDB IDs 2GVJ and 3G8E) demonstrating a clear and selective interaction between the enzyme and the inhibitor. Metabolic studies have shown that FK866 initially depletes intracellular NAD^+ pools, leading to cell death via selective autophagy and degradation of hydrogen peroxide catalase, a main cellular antioxidant. This increases production of reactive oxygen species (ROS), leading to potent mitochondrial depolarisation and depletion to caspase-dependent apoptosis after 96 hours of sustained NAD^+.[86,110]

Recently, new derivatives based on the structure of FK866 have been published with potential for ADC technology; these are discussed in more detail in Section **1.5.2**.[79]

Sulfone-based inhibitors Gne617 and LSN3154567

The NAMPT inhibitor Gne617 was introduced in 2012 by Genentech and Forma Therapeutics. It has a benzimidazole group as an NAD-mimicking moiety. Although Gne617 showed promise in terms of *in vitro* and *in vivo* efficacy in the nM range, as well as good ADME properties, preclinical studies revealed potent unintended effects, such as haematological, cardiac, and retinal toxicities in rats.[111,112]

In 2015, LSN3154567 was developed by Eli Lilly as a new orally bioavailable NAMPT inhibitor based on the structure of Gne617. To avoid haematological and retinal toxicities when co-administered with nicotinic acid, the polarity of the compound was increased, resulting in lower permeability of the blood-retinal barrier, while no retinal toxicity in rat and dog models were reported while still maintaining a nM range of IC_{50}.[96,113]

Isoindoline-urea A1293201

In 2012, AbbVie introduced A1293201, the lead compound of a series of new, active NAMPT inhibitors. It possesses an isoindoline-urea moiety rather than the common pyridine ring, making it a non-substrate inhibitor of NAMPT and opening up potential for new derivatives. Prior to A1293201's introduction, it was believed that phosphoribosylation of the

pyridinic sp2-hybridised atom was crucial for NAMPT interaction. However, A1293201 has shown nM range toxicities *in vitro* and *in vivo*, demonstrating that it is not necessary.[97,114]

A1293201 has demonstrated potent antitumour activity against various cancers, including non-small cell lung cancer, ovarian cancer, and glioblastoma.[114,115] However, there have been no reported clinical trials yet, possibly due to important retinal damage and haematological toxicities observed in preclinical zebrafish and mammalian models.[116]

Benzylamide OT-82

In 2015, Onco Taris introduced OT-82. Unlike other NAMPT inhibitors, OT-82 has a distinct structure, as shown in Figure **10**.[98,117] Preclinical studies have shown excellent results in acute lymphocytic leukaemia cells and patient-derived xenograft models (PDX).[118–120] Such positive results led to FDA approval for a clinical trial (NCT03921879) in acute lymphoid leukaemia patients, which was initiated in 2019 and is ongoing, with no updates disclosed.

NAMPT inhibitors are attracting growing interest as cancer therapeutic agents, as they feature a well-established mode of action; indeed, NAMPT inhibitors are potentially applicable to a wide range of malignancies. However, the toxicity of these inhibitors, including haematological, cardiac, and retinal toxicities, remains a challenge in clinical trials. The next section presents the latest strategies for using NAMPT inhibitors in targeted ADC therapies as a way to mitigate toxicity to healthy tissues.

1.5.2. NAMPT inhibitors as ADC payloads

With the goal of expanding the therapeutic window and safety of NAMPT inhibitors while reducing non-specific toxicities, pharmaceutical companies such as Seattle Genetics, Novartis, and Bayer are working on NAMPT inhibitor-linker payloads that can be conjugated to monoclonal antibodies for use as ADC payloads. The following section describes the strategies and leading NAMPT payloads developed by these companies.

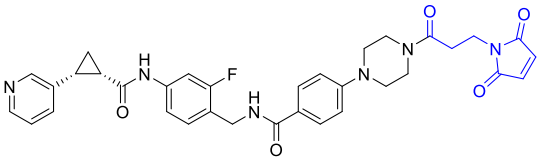

1) Novartis lead non-cleavable linker-payload

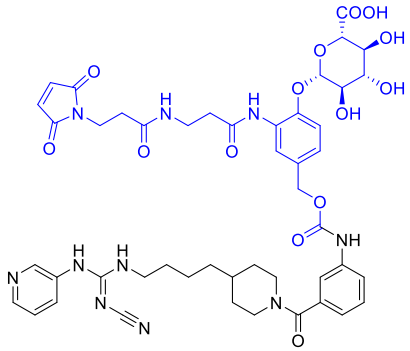

2) Seattle Genetics lead glucuronidase cleavable linker-payload

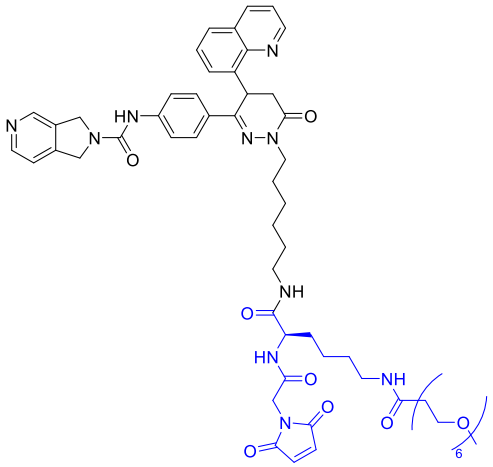

3) Bayer lead protease cleavable linker-payload

Figure 11. NAMPT inhibitor-linker lead compounds used in ADC technology: 1) Novartis lead candidate; 2) Seattle Genetics lead candidate; and 3) Bayer lead candidate. Linker moiety is lined in blue.[121,122]

In 2017, Novartis developed a lead candidate (as depicted in Figure **11**) for NAMPT inhibitors through virtual screening using the co-crystal structure of Fujisawa's lead inhibitor FK866 and NAMPT as a starting point (PDB code: 2GVJ). This highlighted the crucial role of π-π stacking interactions between the pyridyl ring of FK866 and the residues Tyr18 and Phe193 of NAMPT, which mimics the positioning of the biological ligand NAM. Despite efforts to improve the solubility of the free NAMPT inhibitor lined in black in the linker-payload 1 (Figure **11**), it remained poorly soluble but had a highly potent IC_{50} in the nM range, likely due to its good passive membrane permeability.[123]

Novartis has developed anti-c-Kit and anti-HER2 ADCs with a range of DAR from 2.3 to 4. The lead compound 1 (Figure **11**) was conjugated to a piperazine NH moiety using both cathepsin B cleavable and non-cleavable linkers, which were then Ab-conjugated through Michael reaction. Although the different payloads showed very good nM activities, aggregation was high, with the exception of those using non-cleavable linkers.[121] However, an isotype control ADC showed high nM toxicity in all cell lines, suggesting possible retro-Michael de-

conjugation of the payload lined in black in linker-payload 1 (Figure **11**). This hypothesis is supported by the lack of patent protection for the linker-payloads and ADCs, as well as the absence of further reports since 2018.[121]

In 2018, Seattle Genetics aimed to expand the therapeutic window for NAMPT inhibitors using ADC technology. The company presented analogues of FK866 and CHS-828 with amine, hydroxyl, or sulfhydryl groups as conjugation handles. Additionally, all presented inhibitors rely on the pyridine moiety as the NAM-mimicking group, varying the hydrogen bonding connectors. Furthermore, as reported in the co-crystal structure (PDB reference: 6E68), the compounds from Seattle Genetics present a clear advantage: The introduction of an aniline moiety as conjugation handle ensures hydrogen bond stabilisation interaction between NAMPT Glu376, which is located in the solvent-exposed area observed in Figure **9**, and the inhibitor offsetting any desolvation penalty for addition of a polar functional group.[124,125]

To minimise the aggregation problems, Seattle Genetics incorporated PEG chains (not shown in Figure **11**) and a glucuronic acid moiety in the linker, as observed in linker payload 2 (Figure **11**), which also activates drug release after cleavage by lysosomal or extracellular β-glucuronidases. The average DAR of the ADCs was 8, achieved by conjugation to the interchain cysteines of the mAb.[125]

Seattle Genetics targeted CD30, CD19, and CD123, showing *in vitro* activity only in the $CD30^+$ L540 cellular model. *In vivo* xenograft models showed tumour-delaying activity for the three targets, possibly due to release of the NAMPT inhibitor by extracellular glucuronidases. However, the lack of an unconjugated mAb control raised doubts over whether the reported effect was only related to the ADC or if an mAb-triggered effect was involved. In contrast to Novartis, Seattle Genetics included in its *in vivo* testing an isotype control, which showed no target specificity. The toxicological assay showed only mild haematological toxicities in rats and no cardiac or retinal toxicity, which were associated with NAMPT inhibitors when used as small molecule therapeutics. This underlines the potential benefits of ADC technology. Furthermore, due to the prolonged half-life of the ADC in circulation, a sustained inhibitor influx in targeted cells for at least 96 hours can be maintained, which is ideal for inducing NAD depletion in tumours.[125]

In 2019, Bayer introduced a series of NAMPT inhibitors optimised for ADC technology. These inhibitors exhibit single-digit nanomolar or sub-nanomolar potency and are based on a pyrrolopyridinyle moiety as the NAM-mimicking group. They are stabilised in the pocket by hydrogen bond interactions of the urea moiety with the enzyme resulting from crystallographic measurements. The inhibitors were linked to maleimide-containing linkers and conjugated to reduced cysteines in anti-C4.4a and anti-HER2 mAb by Michael reaction, resulting in ADCs with a DAR ranging from 2.2 to 7.8 with low aggregation. The ADCs were tested *in vitro*, exhibiting potency in the pM range in the leukaemia cell line THP-1, which is highly sensitive to NAMPT inhibitors. However, suspected off-target toxicities were also observed, since the isotype control showed *in vitro* activity in the nM range. *In vivo* studies of THP-1 xenograft leukaemia models in SCID mice using DAR 8 and 4 ADCs in multiple dosing only showed effective tumour growth inhibition for the higher DAR ADC. In the MDA-MB-453 breast cancer xenograft model in NOD-scid mice, employing a daily treatment for seven weeks, both ADCs showed good results in terms of tumour reduction without tumour regrowth after treatment end.[55,126]

1. Introduction

Cancer is a pressing medical concern requiring new effective treatments. Traditional cancer treatments and new metabolic therapies using small molecules lack sufficient selectivity. Targeted therapies with monoclonal antibodies (mAbs) are the best option for selective treatment of cancer patients, but some immunotherapies lack potency. This has led to the development of antibody-drug conjugates (ADCs) as a promising approach, with 11 approved constructs currently and many more in clinical trials.[40] The pressing need for more ADCs is clear, but the drawback of existing ADCs is their limited variability in the payload featuring a mode of action, which also affects non-dividing cells. NAMPT inhibition holds promise as a new mode of action, with several promising NAMPT inhibitor-loaded ADCs in development. However, the selectivity of these ADCs is low, with the added risk of toxicity. Additionally, the advanced NAMPT inhibitor ADCs from Bayer involve a complex and difficult synthesis, leading to potentially high costs-of-goods. In response, the aim of this PhD dissertation is to present new NAMPT inhibitor-loaded ADCs with a simple and accessible synthesis of the inhibitors and high potency and safety for patients.[55]

In order to achieve the production of ADCs loaded with NAMPT inhibitors, a chemically guided lead optimization of CHS-828 and FK866 analogues led to the discovery that hydrophobic NAMPT inhibitors were not effective as ADC payloads. Consequently, in the second chapter, an *in silico* guided lead optimization led to the discovery and synthesis of new families of highly effective, more hydrophilic NAMPT inhibitors. However, the specific cellular dynamics of ADCs impeded the stability of the cyanoguanidine group, which is widely used in NAMPT inhibitors. Therefore, in the last part of the thesis, the demonstration of lysosomal hydration of NAMPT inhibitors containing the cyanoguanidine group suggested that they were not a good option for use as ADC payloads. Finally, an *in silico* discovery campaign proposed urea-containing NAMPT inhibitors as a lysosomal proof alternative for the design of NAMPT inhibitors to be use as ADC payloads.

2. Objectives

The ADC technology represents a major advancement in cancer treatments, with 11 approved therapies and over 100 drugs in clinical trials. Its goal is to enhance the well-being of patients and their families by specifically targeting malignancies and reducing the systemic toxicity often associated with traditional chemotherapy and radiotherapy. Furthermore, the new generation of ADCs equipped with innovative payloads, such as amanitin or NAMPT inhibitors, not only target actively dividing cancer cells but also dormant tumour cells, addressing one of the major challenges in cancer therapy: metastatic cells that often arise from these dormant cell populations.[40,48]

The NAMPT inhibitor-loaded ADCs described in the literature thus far present some shortcomings, such as inconsistent *in vivo* results or complicated synthetic processes. This PhD dissertation aims to address the following question: What are the biological and chemical factors that impact the performance of NAMPT inhibitors, and can they be optimised to enhance the application of NAMPT inhibitors in ADCs? To achieve this, it is employed a multistep scientific approach aimed at functionally and synthetically optimising CHS-828, and FK866 analogues NAMPT inhibitors. This will lead to a deeper understanding of their cellular dynamics and the preferential properties of various cell types towards ADC-mediated NAMPT inhibition. Ultimately, the goal is to create new and effective ADCs for cancer treatment that broaden the therapeutic scope for both liquid and solid malignancies while minimising systemic toxicity.[55,121,122]

2. Objectives

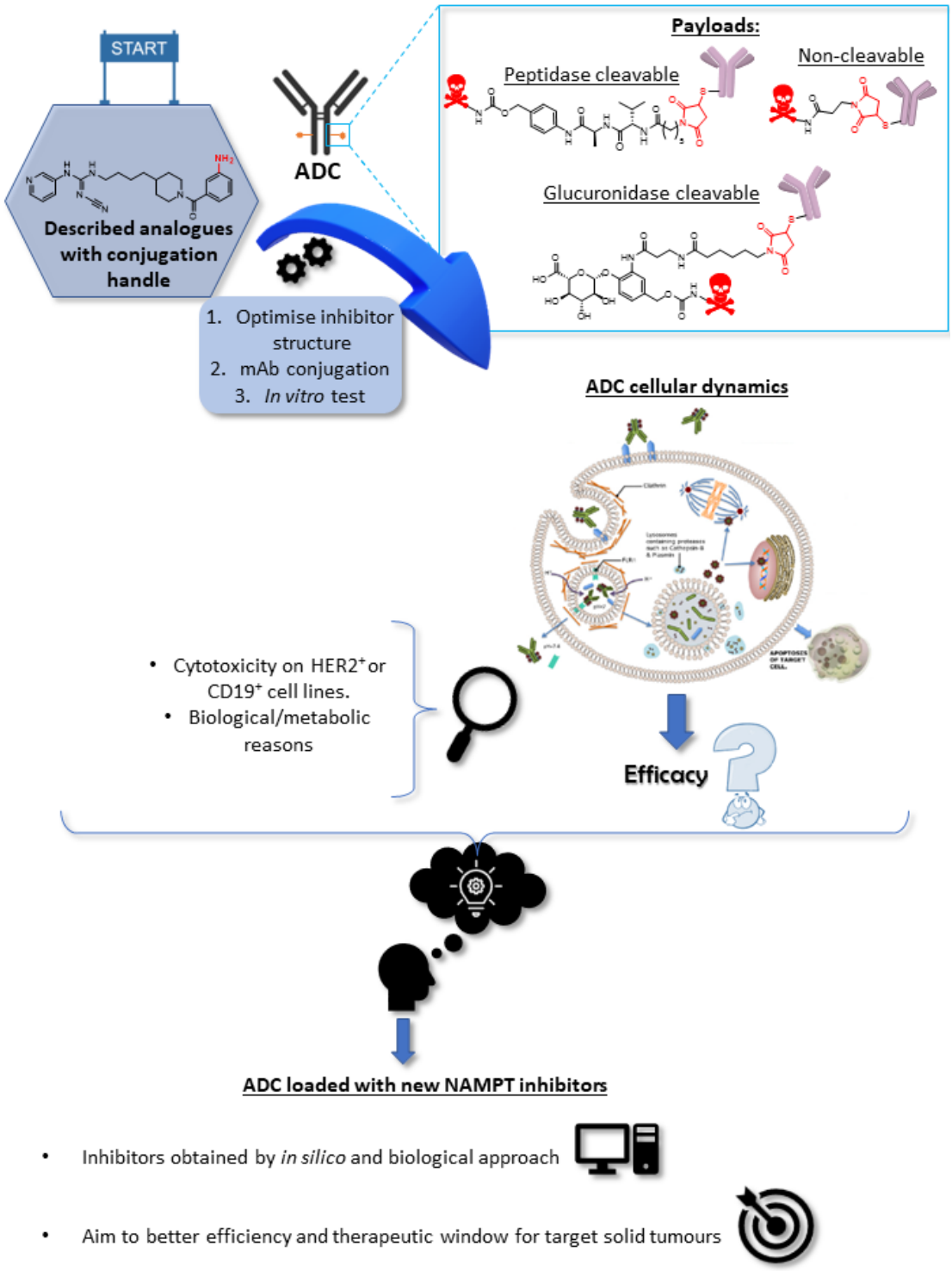

Figure 12. Graphical representation of the research objectives.

3. Results and Discussion

3.1. A chemical iterative approach to the generation of NAMPT inhibitors

3.1.1. Synthesis of FK866- and CHS828-derived standards and controls: Published inhibitors

3.1.1.1 Synthesis of cyanoguanidine **19**, containing a PhOH moiety as a conjugation handle, allowing linker attachment for mAb conjugation

All the NAMPT inhibitors presented in this thesis were based on the chemical skeletons of FK866 and CHS828 due to their ready commercial availabilities as standards and their high potencies. FK866 is an acrylamide-based NAMPT inhibitor described by Fujisawa GmbH in 2002.[103] This NAMPT inhibitor is characterised by the potent NAMPT inhibitory activity translated in nM range IC_{50} values in most NAMPT dependent cancer cell lines. [86,104–108] Additionally, due to the potency as free inhibitor reported for the Leo Pharma-described cyanoguanidine-containing NAMPT inhibitor CHS828, the FK866 characterising acrylamide moiety was modified in some of the presented NAMPT inhibitors by the CHS828 cyanoguanidine characteristic moiety. [79,92,99]

While FK866 and CHS828 perform outstandingly well as free inhibitors, they lack the chemical handle required to conjugate mAbs in order to generate ADCs. Typically, these handles are nucleophilic groups such as hydroxy or amino, which allows the establishment of stable ester or amide bonds between inhibitor (payload) and linker, respectively. This was envisioned to be solved by the phenol cyanoguanidine-containing payload **19** as described by Vogel *et al.*[127] Phenol **19** was reported to act as free NAMPT inhibitor in nM range, thus maintaining the cytotoxic activity of the parental compounds FK866 and CHS828.

In contrast to the synthetic approach published comprising a Mitsunobu reaction in the synthesis of intermediate amine **6**, amine **6** was synthetised in two steps from carboxylic acid **4** involving amide formation and amide reduction yielding amine **6** in moderate yields (Scheme **1A,** steps A and B). Further derivatisation with phenyl (*E*)-*N'*-cyano-*N*-(pyridin-3-yl)carbamimidate intermediate **1** afforded cyanoguanidine **7** at a satisfying yield of 55%. [128]

However, deprotection of Boc-protected cyanoguanidine **7** with hydrochloric acid in dioxane did not lead to the desired secondary amine **13** (Scheme **1a**). The highly acidic conditions of the Boc deprotection was likely to hamper the stability of the cyanoguanidine group. In fact, it has been reported that a pH of 2 or lower leads to the degradation of the cyanoguanidine group to guanyl urea intermediates, most probably via a carbodiimide intermediate.[129] Hence, the synthetic route was modified, and the Boc-protecting group was substituted against Cbz. Hydrogenolysis of the Cbz-protected cyanoguanidine analogue **12** provided secondary amine **13** at a very good yield of 85%.

The final published compound **19** was then obtained following the synthetic strategy described in the literature.[130] Briefly described, the piperidyl moiety of cyanoguanidine **13** was capped by reaction with 2,5-dioxopyrrolidin-1-yl 4-acetoxybenzoate to yield the desired inhibitor **19** after acetyl deprotection (Scheme **1a**, step f). Due to a very low yield in the

reduction step from amide **10** to amine **11**, the overall yield with the synthetic strategy described above was not satisfactory in synthesising enough material for *in vitro* testing. As reported,[131] reduction of the carbon oxidative state typically leads to several side products, which was most likely the reason for the low yield of amine **11**. Resulting in not enough inhibitor for linker attachment that allows the conjugation to a mAb to generate an ADC.

To improve the synthesis of compound **19**, a longer yet milder synthetic pathway involving the Gabriel synthesis for the amine formation (Scheme **1B**) avoided the harsh conditions for the reduction of an amide (Scheme **1A**). Starting with the acylation of secondary amine **22**, the obtained N-acyl alcohol **14** was converted to mesylate **15** in a good yield. Mesylate **15** as substrate for the Gabriel synthesis was then transformed in two steps to amine **17** via phthalimide **16** as intermediate and obtained in satisfying yields of 60% and 40%, respectively. Overall, the strategy shown in Scheme **1b** represents an improvement over the strategy in Scheme **1A**, allowing for a higher yield of inhibitor **19** and resulting in sufficient material for *in vitro* testing and linker attachment for the conjugation to an mAb.[132]

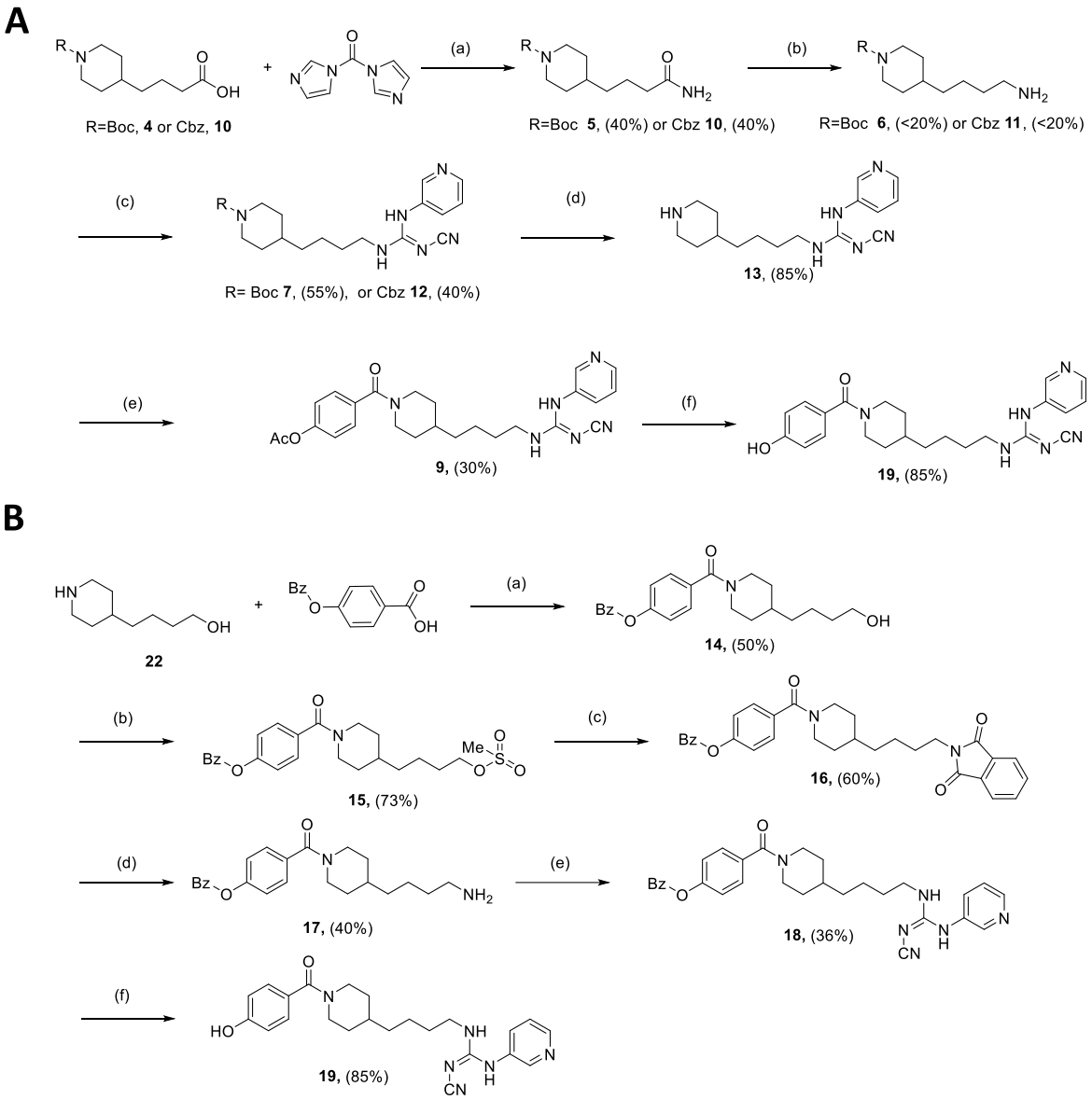

Scheme 1. Synthesis of NAMPT inhibitor **19**, **A)** Approach involving amide reduction. Reagents and conditions: (a) NH_4OH, EtOAc, r.t, overnight; (b) BH_3-THF, 73°C, overnight; (c) Phenyl (*E*)-*N*'-cyano-*N*-(pyridin-3-yl)carbamimidate intermediate **1**, Et_3N, CH_3CN, r.t., 1.5 d; (d) H_2, Pd/C, r.t., 3h; (e) NHS-*p*-acetoxy benzyl ester, DIPEA, DMF, r.t, overnight; (f) LiOH, MeOH, r.t; 2h **B)** Approach involving Gabriel synthesis. Reagents and conditions: (a) DCC/HOBt, DIPEA, DCM, r.t., 16h; (b) Methane sulfonyl chloride, Et_3N, DCM, r.t., 2h; (c) Potassium phthalimide, DMF, 50°C, overnight; (d) Hydrazine monohydrate, EtOH, r.t, 6h; (e) Phenyl N-cyano-N'-3-pyridinylcarbamimidate intermediate **1**, Et_3N, ACN, r.t., 48h; (f) H_2, Pd/C, EtOH/EtOAc (1:1), r.t., 3.5h.

3.1.1.2 Synthesis of Cathepsin B-cleavable linker-payload **27**

To allow the conjugation of inhibitor **19** to ADCs (Section **3.1.4.1**), the Mal-Val-Ala-PAB linker was connected by a benzyl ether bond to the inhibitor, following the synthetic route described in Scheme **2**. Starting with an SN_2 substitution of the bromide at the benzylic position of the linker in slightly basic conditions, intermediate **20** was obtained in a satisfying yield. The Boc-and silyl-protecting groups of intermediate **20** were then removed using TFA in the first step and ammonia solution in the second step, affording intermediate **21**. Finally, the maleimide (Mal) group for antibody conjugation was attached using the NHS activated ester BMPS, affording the final linker-payload **27** in a moderate yield of 40%. Importantly, the

maleimide group must be incorporated in the last step, since decomposition and oligomerisation are expected under the deprotection conditions that lead to intermediate **21**. This compound was then conjugated and tested *in vitro* (Section **3.1.4.1**).

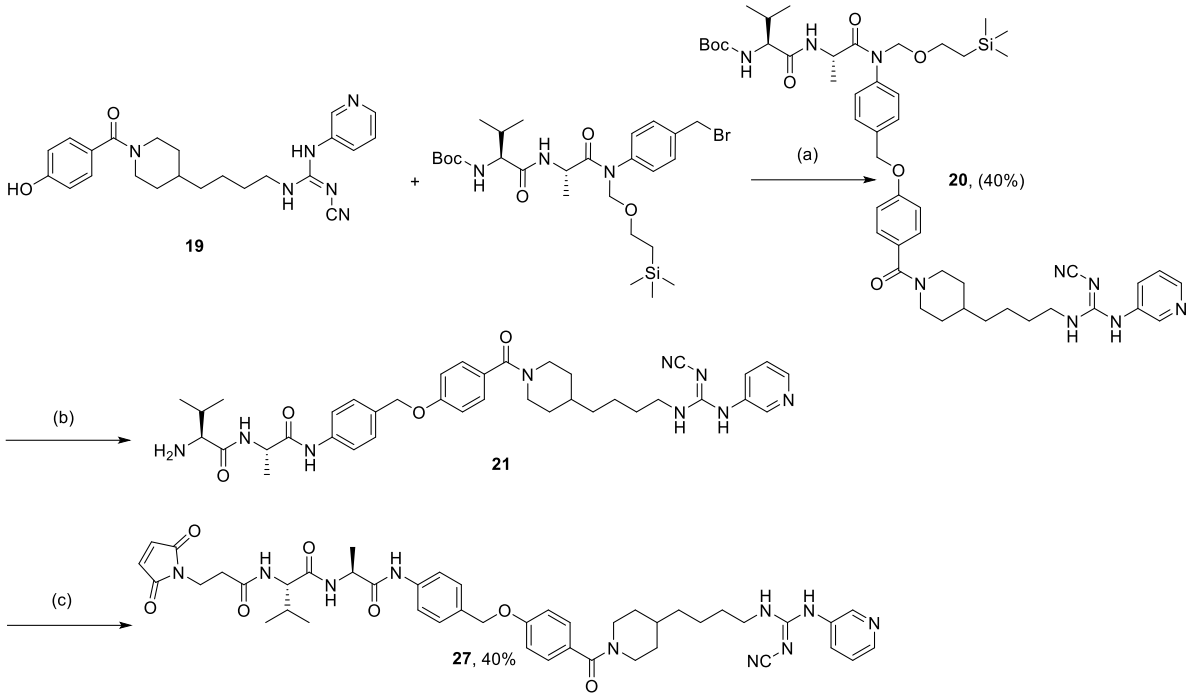

Scheme 2. Synthesis of linker-payload **27**. Reagents and conditions: (a) Cs_2CO_3, DMF, r.t.; overnight; (b) 1) TFA, 2) NH_4OH/ACN, pH = 10, r.t., 5 min; (c) BMPS, DIPEA, DMF, r.t., 4 h.

3.1.1.3 Synthesis of Inhibitor **36** and linker-payload **37:** Optimised alternatives described in literature to inhibitor **19**.

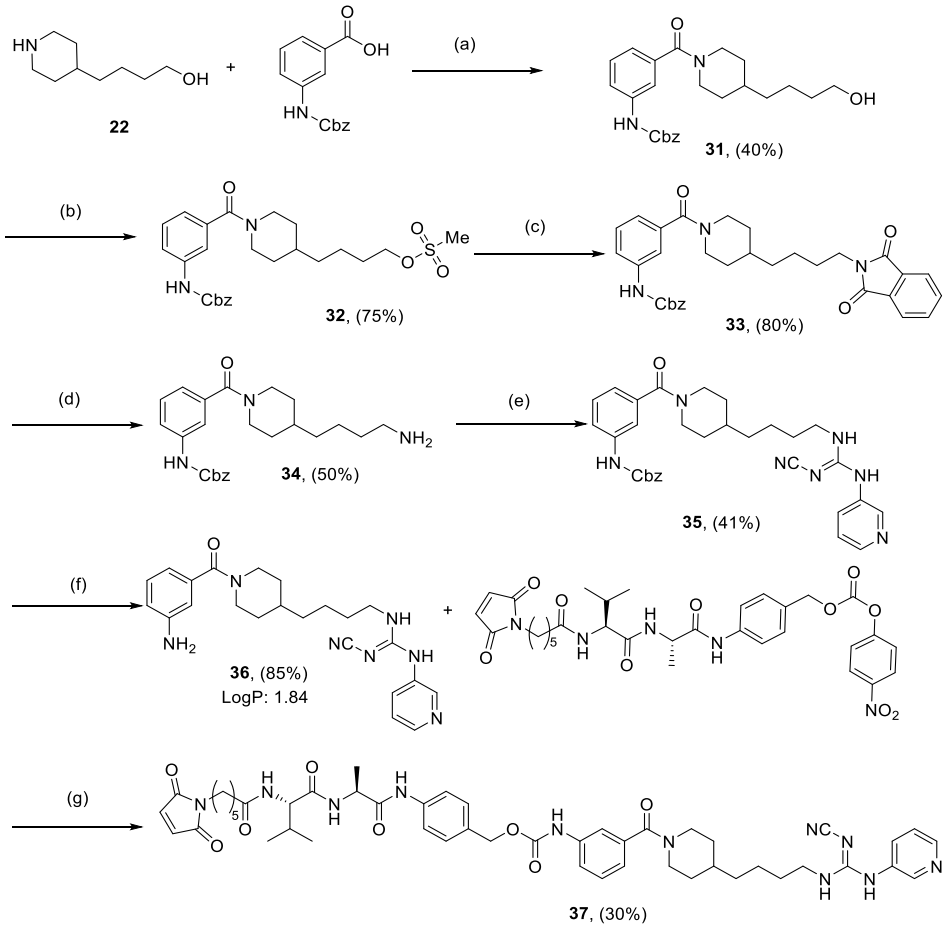

Scheme 3. Synthesis of payload **36** and linker-payload **37**. LogP for inhibitor **36** is provided. Reagents and conditions: (a) DCC/HOBt, DIPEA, DMF, r.t., overnight; (b) Methane sulfonyl chloride, Et_3N, DCM, r.t, 1h; (c) Potassium phthalimide, DMF, 50°C, overnight; (d) Hydrazine monohydrate, EtOH, r.t., overnight; (e) Et_3N, ACN, r.t., 48h; (f) H_2, Pd/C, EtOH/EtOAc (1:1), r.t., 3h; (g) PyAOP; DIPEA, DMF, r.t., overnight.

The above-described aniline **36** was selected as the second NAMPT inhibitor standard suitable for linker attachment. As reported in literature and confirmed in Section **3.1.4.1**, aniline **36** showed an improved cytotoxic profile compared to payload **19**.[122] Inhibitor **36** reveals in the cocrystal structure with NAMPT a hydrogen bond interaction between aniline handle and Glu 376.[122] Hence, a better binding to the enzyme concomitant with a better performance of inhibitor **36** was envisioned.

The synthetic route of primary amine **34** was performed in analogy to inhibitor **19**, involving a Gabriel synthesis as an amine-forming reaction affording phthalimide **33** with a high yield of 80 % (scheme **3**). The following hydrazinolysis step led to intermediate **34** with a yield of 50%. Then, the cyanoguanidine intermediate **35** was afforded by the reaction of amine **34** with phenyl (*E*)-*N*'-cyano-*N*-3-pyridinylcarbamimidate followed by hydrogenolytic removal of Cbz, leading to inhibitor **36** in a good yield of 85 %. As observed during the synthesis of inhibitor **19** in Section **3.1.1.1**, acid-cleavable protecting groups such as Boc were avoided, since cyanoguanidines are prone to being hydrated in acidic media.

As reported in Section **3.1.4.2**, *in vitro* testing of aniline inhibitor **36** reveals more efficient cytotoxicity in comparison to phenol-containing inhibitor **19**, probably due to the

enhanced interaction with NAMPT given the intermolecular hydrogen-bond interaction with the aniline already reported above.

One important parameter to quantify the hydrophobic character of a small molecule is the logP, defined as the logarithm in base 10 of the partition coefficient between octanol and water for a given compound and is considered a measure of lipophilicity. For example, higher positive values mean more lipophilicity, while smaller or negative values mean more hydrophilicity.[133,134] Hence, the calculated logP value for aniline inhibitor **36** provided in Scheme **3** shows a very hydrophobic compound. On the one hand, this has a major effect on ADC aggregate formation, which directly affects ADC half-life as well as *in* vivo tolerability. On the other hand, hydrophobic compounds present higher cellular membrane passive permeation, which can lead to a bystander effect but at the same time has a direct effect on the intracellular concentration of ADC deployed inhibitors and therefore ADC cytotoxic efficacy.[70] These ideas are further developed in chemical Sections **3.2.1** and **3.2.3** and biological Sections **3.2.6.2**, **3.2.7**, and **3.2.8**.

Next, linker-payload **37** was synthesised following a one-step reaction in which a Mal-Val-Ala-PAB-*p*-NO_2-phenyl-activated linker is pre-reacted with PyAOP. This was followed by conjugation to aniline **36** by carbamate bond formation, yielding linker-payload **37** in a low yield (Scheme **3**). The reason for this low yield may be the lower nucleophilic character of the aniline compared to aliphatic amines or phenols. Therefore, the synthesis was managed using PyAOP, an azabenzotriazole-derived phosphonium reagent, in an attempt to release HOAt to form a more reactive intermediate carbamate. Hence, PyAOP was not used in its default application as peptide bond-forming reagent but solely to release HATU. To ensure a sufficient amount of HATU, an improvement for the reaction might be the use of neat HATU instead of PyAOP as the amount of released HATU from PyAOP is uncertain.

3.1.1.4 Piperazyl inhibitor **43** as an alternative to piperidine inhibitors **19** and **36**

Since most of the NAMPT inhibitors described in the literature are optimised to be used as free inhibitors and not as ADC payloads, new families of NAMPT inhibitors are needed to be suitable as payloads for ADC technology. The published inhibitors **19** and **36** are cytotoxic as free inhibitors, whereas the corresponding ADCs showed no activity in *in vitro* cytotoxicity assays (Sections **3.1.4.1** and **3.1.4.2**). Additionally, payload synthesis and mAb conjugation were achieved with only moderate yields. Therefore, new inhibitors with both easier synthetic access and higher conjugation efficiency were explored.

Initially, Novartis published a very promising inhibitor using a substitution of the piperidyl- against a piperazyl-bridge, as depicted in Figure **11** lined in black.[121] This opens the possibility to use commercially available starting materials such as *Boc*-GABA-OH and increase the synthetic plasticity of the molecules, since piperazine can easily be modified with different aliphatic spacers, allowing a more convergent synthesis at the same time. Therefore, inhibitor **36** was adapted accordingly, resulting in inhibitor **43**. Additionally, as *Boc*-GABA is commercially available as intermediate, the Gabriel synthesis to form amine intermediate **39** is obsolete. Hence, the synthesis of compound **43** only involves six synthetic steps instead of eight, which were required to synthesise inhibitor **36**. As shown in Scheme **4**, the main steps in the synthesis of intermediate **43** compared to inhibitor **36** are the synthesis of amide **38** and amine **39**, where Cbz-protected piperazine intermediate **38** as core of the molecule was synthesised from

commercially available chemicals *Boc*-GABA-OH and *N*-Cbz-piperazine through a DCC/HOBt promoted condensation in a satisfying yield of 60 %. Then, the Boc-protected amide **38** was selectively deprotected with TFA, leading to aliphatic primary amine **39** at an excellent yield of 90%. Subsequently, the synthetic pathway proceeded in line with the synthetic route to access inhibitor **36**, specifically through a base catalysed substitution over phenyl N-cyano-N'-3-pyridinylcarbamimidate by amine **39** with subsequent release of phenol and cyanoguanidine group formation, leading to intermediate **40** with an acceptable yield of 50 %. Then, the Cbz group of intermediate **40** is deprotected by hydrogenolysis, leading to intermediate **41** in an excellent yield of 80 %. The aniline handle required for linker conjugation is then incorporated by condensation with carboxylic acid **30** promoted by HOBt/DCC pair, leading to Cbz-protected aniline intermediate **42** in an acceptable yield of 40 %. Finally, a hydrogenolysis step deprotects the aniline group, affording inhibitor **43** in a good yield of and was as confirmed by mass spectrometry.

However, no cytotoxicity was observed for the free inhibitor, raising the question of whether the module modification at the piperidyl-bridge described by Karpov *et al*.[121] strongly affects the activity of inhibitor **43** compared with **36**, see cytotoxicity test in Section **3.1.4.3**.

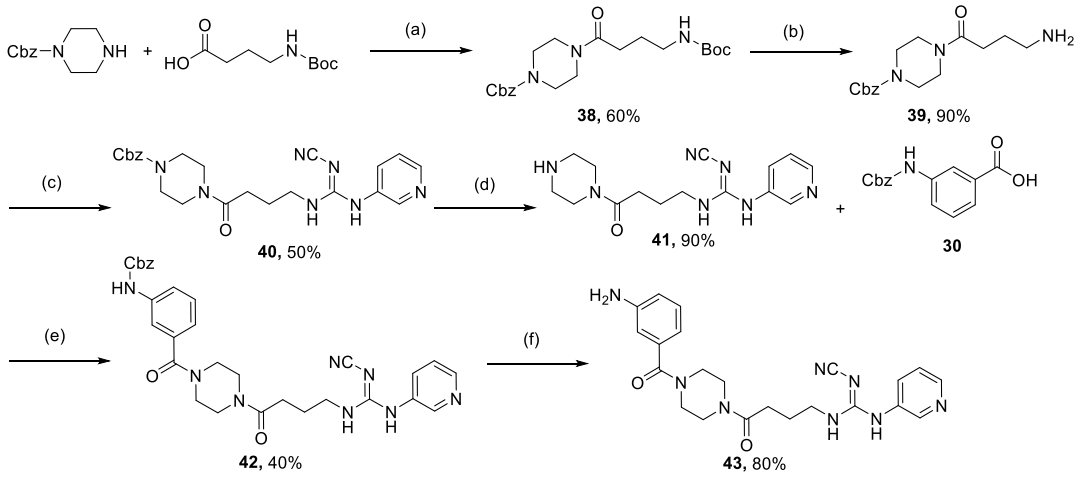

Scheme 4. Synthetic scheme of inhibitor **43**. Reagents and conditions: (a) DCC/HOBt, DIPEA, DCM(abs.), r.t., overnight; (b) TFA/DCM (1:10), r.t., 2 h; (c) 1) Phenyl *N*-cyano-*N*'-3-pyridinylcarbamimidate, Et_3N, 1,4-dioxane, r.t., 48 h; (d) H_2, Pd/C, EtOH/EtOAc (1:1), r.t., overnight; (e) DCC/HOBt, DIPEA; DCM(abs.), r.t., overnight; (f) H_2, Pd/C, EtOH/EtOAc (1:1), r.t, overnight.

3.1.2. Chemical modifications: Systematic evaluation of NAMPT inhibitors by pharmacophores and synthetic evaluation

Motivated by the suboptimal results from previous sections and to determine the pharmacophores controlling the cytotoxicity, NAMPT inhibitors were divided into five molecular sections to allow a systematic variation of the molecular sections of NAMPT inhibitors against the random variation performed in previous sections. This allowed, in sections **3.1.2** and **3.1.3.2,** the synthesis of new families of NAMPT inhibitors and their subsequent evaluation for differences in cytotoxic activity, linker conjugation yield, and solubility (Sections **3.1.4.3**, **3.1.4.4**, and **3.1.4.5**, respectively). This lead optimisation campaign based on a chemically iterative process contrasted with the computationally aided lead optimisation campaign explored in the second results and discussion chapter **3.2.15**, in which new families of NAMPT inhibitors were proposed based on virtual screening of docking pockets on NAMPT derived from X-ray diffraction data of NAMPT-inhibitor cocrystals.

3.1.2.1 Analogues of FK866: Synthesis of inhibitors without cyanoguanidine moiety

New families of FK866 analogue NAMPT inhibitors were obtained based on an experimental driven lead optimisation campaign exploring modifications of the inhibitors based on a five-section division of NAMPT inhibitors as observed in Figure **13**. The names of the sections were based on structural characteristics and/or non-covalent stabilisation interaction between the specified section on NAMPT inhibitor and NAMPT enzyme, in line with data from the cocrystal study of an NAMPT inhibitor and NAMPT reported by Neumann *et al.*[122]

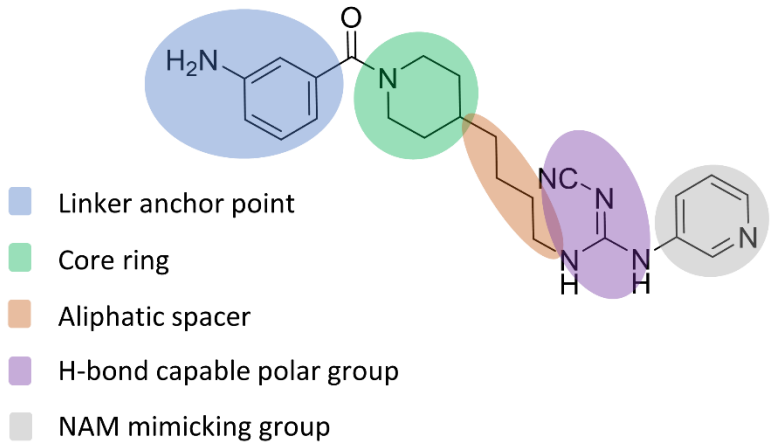

Figure 13. FK866 and CHS828 analogues divided into molecular sections.

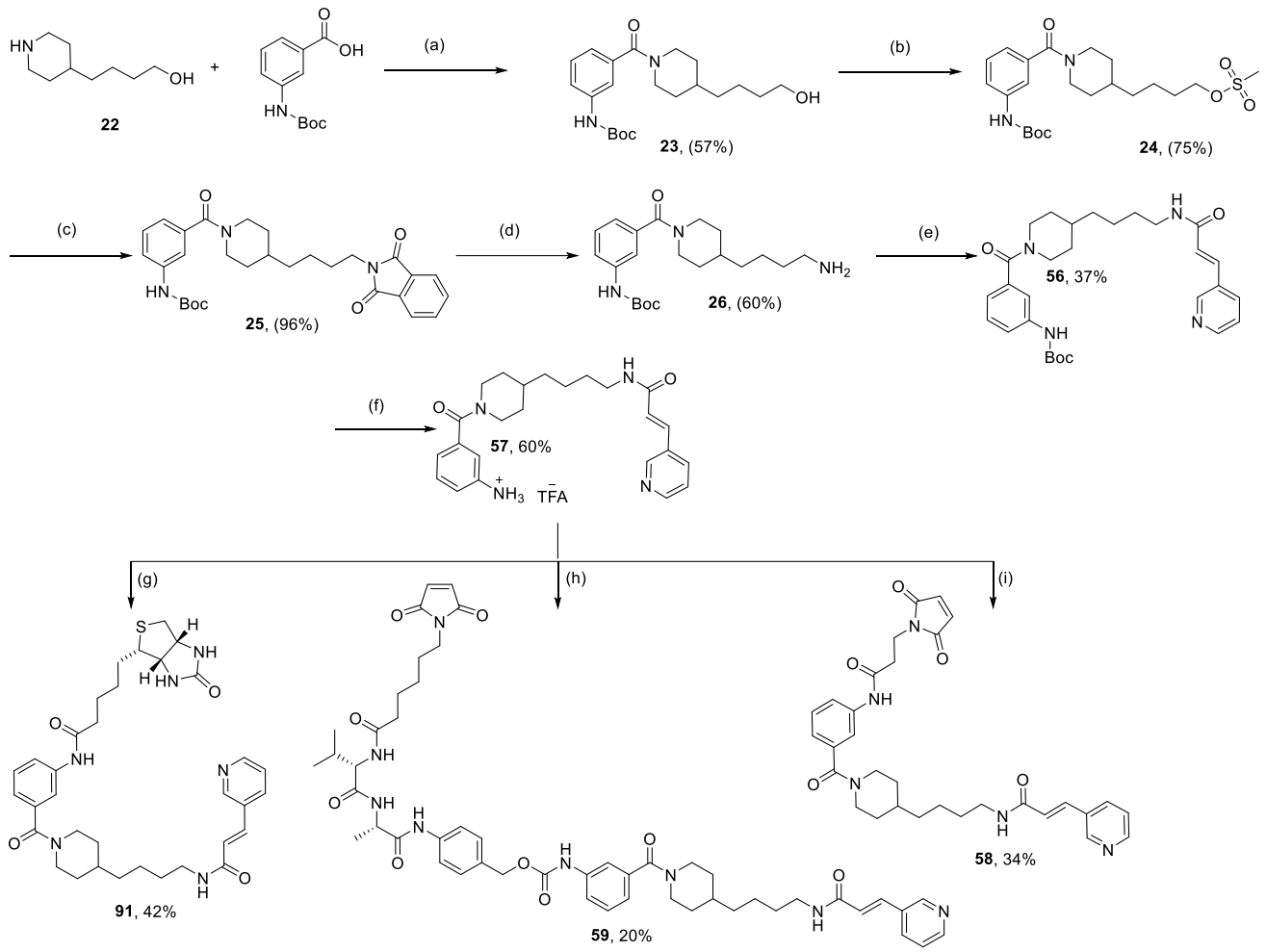

Scheme 5. Synthesis of payload **57**, linker-payloads **58** and **59**, and biotinylated inhibitor **91**. Reactions and conditions: (a) DCC/HOBt, DIPEA, DMF, r.t., overnight; (b) Methane sulfonyl chloride, Et_3N, DCM, r.t., 1h; (c) Potassium phthalimide, DMF, 50 °C, overnight; (d) Hydrazine monohydrate, EtOH, r.t., overnight; (e) DCC/HOBt, (*E*)-3-(3-pyridyl)-acrylic acid, DIPEA, r.t., overnight; (f) Neat TFA, r.t., 5min; (g) Biotin, HATU, DIPEA, r.t., 2 days; (h) *p*-nitro-phenyl-carbamate activated PAB-Ala-Val-pentyl-Mal linker, PyAOP, DIPEA, r.t., overnight; (i) 3-maleimidyl-propionic acid, PyAOP, DIPEA, r.t., overnight.

The first modified analogue **57** aimed to test the effect of modification at the level of a hydrogen-bond-capable polar group moiety. As discussed in Section **3.1.1.1**, it has been shown that the cyanoguanidine moiety may be hydrolysed to guanylurea during the synthesis due to its low stability under strong acidic conditions. Therefore, chemically stable groups are desired to allow invariant compounds towards biological acidic environment. At the same time, NAMPT inhibition performance in cells should be enhanced, aiming to produce active ADCs. Therefore, optimised inhibitors are highly needed.

Acrylamide inhibitor **57**, as described by Neumann *et al,*[122] was expected to show a good compromise between toxicity as free NAMPT inhibitor and chemical stability as it lacks the cyanoguanidine group. In addition, the molecule possesses a suitable aniline handle for linker conjugation.

The synthesis of inhibitor **57** was afforded by a convergent approach analogous to the synthesis of amine **34**, a precursor of inhibitor **36**. Briefly, 4-(4-piridyl)-butanol **22** condenses with *N*-Boc-3-amino benzoic acid aided by DCC/HOBt in order to afford amide **23** in an acceptable yield of 57 %. The mesylate **24** was then synthesised to have a good leaving group

in the two-step Gabriel synthesis involving the synthesis of phthalimide **25**, followed by hydrazinolysis, in order to synthesise amine **26** in a good yield of 60 %. Afterwards, two synthetic steps, involving a DCC/HOBt-mediated condensation of amine **26** with commercially available *E*-3-(3-pyridyl)-acrylic acid afforded amide **56** followed by Cbz-hydrogenolysis deprotection to obtain aniline **57** at a good yield of 60 % (Scheme **5**).

Additionally, linker-payloads **58** and **59** were synthesised as conjugable linker-payload versions of inhibitor **57** bearing non-cleavable and cleavable maleimide-containing linkers, respectively (Scheme **5)**.

Inhibitor **57** was also biotinylated to be used in binding experiments with the NAMPT enzyme (Section **3.1.5.1**) by direct condensation with biotin using HATU as coupling reagent affording biotinylated inhibitor **91** in an acceptable yield of 42% (Scheme **5**).

3.1.2.2 Optimisation of NAMTP inhibitors: Understanding the contribution to enzyme-binding by selective modification of inhibitors

To focus more specifically on the modifications of NAMPT inhibitors at the level of "linker anchor point" and "aliphatic spacer" (Figure **13**), inhibitor **57** was further modified.

A)

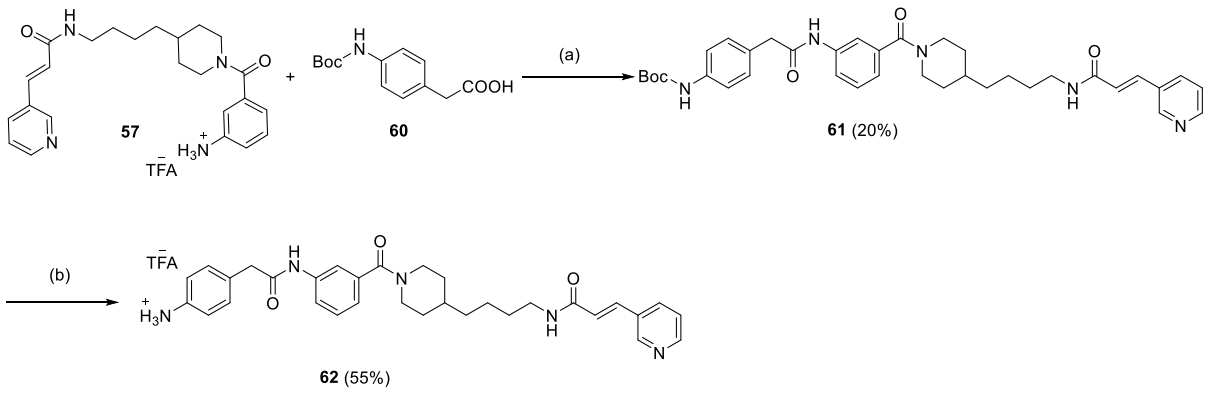

B)

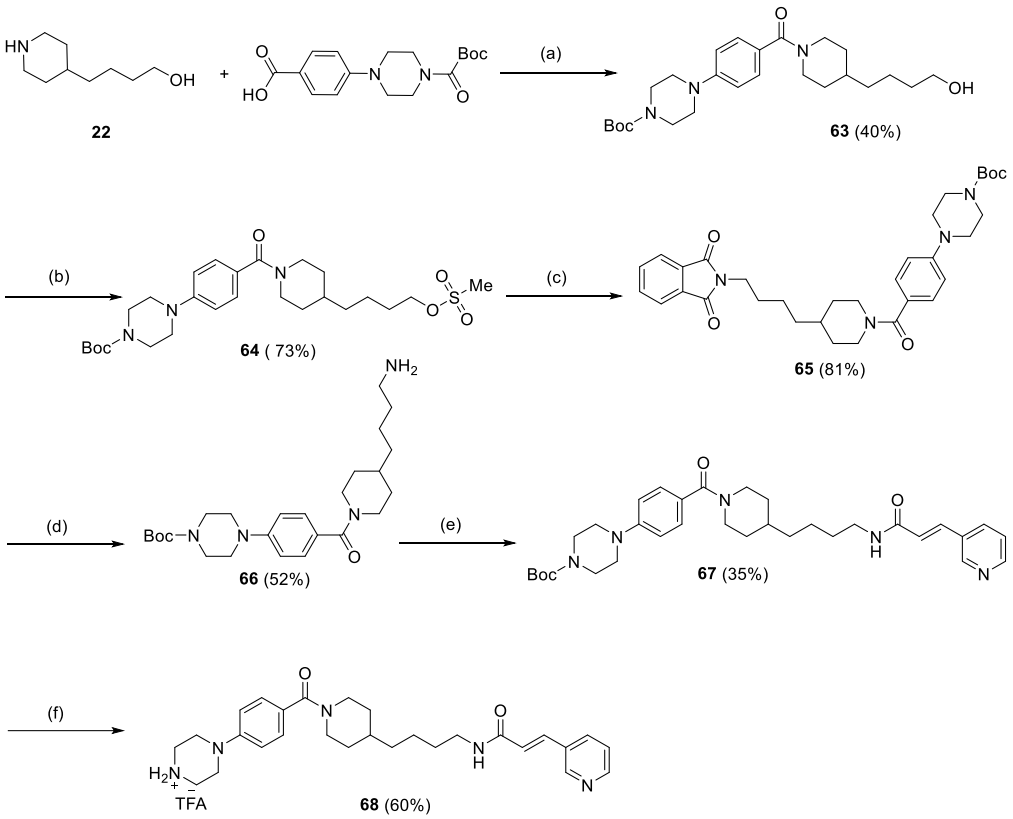

Scheme 6. A) Synthesis of inhibitor **62**. Reagents and conditions: (a) PyAOP, DIPEA, DMF (abs.), r.t., overnight; (b) Neat TFA, r.t., 5 min. **B)** Synthesis of inhibitor **68**. Reagents and conditions: (a) DCC/HOBt, DIPEA, DMF (abs.), r.t., overnight; (b) Methane sulfonyl chloride, DIPEA, r.t., 2h; (c) Potassium phthalimide, DMF (abs.), r.t., overnight; (d) Hydrazine monohydrate, EtOH, r.t., overnight; (e) (*E*)-3-(3-pyridyl)-acrylic acid, DCC/HOBt, DIPEA, r.t., overnight; (f) Neat TFA, r.t., 5 min.

Initially, the inhibitors aniline **62** and piperazine **68** were synthesised as analogues of acrylamide **57**, exploring with these new inhibitor modifications at level of "linker anchor point" (Scheme **6**). The synthetic approach for inhibitor **62** used acrylamide **57** as starting material for further derivatisation via incorporation of a 4-aminobenzyl ester unit (Scheme **6A**), while inhibitor **68** involved the Gabriel synthesis for aliphatic amine formation (Scheme **6B**).

On the one hand, inhibitor **62** was designed as a more lipophilic version of inhibitor **57** in which the aniline "linker anchor point" was elongated (Scheme **6A**), aiming to determine if increasing hydrophobicity as well as the length of the linker anchor point tail could allow better interaction with the catalytic pocket of NAMPT. On the other hand, inhibitor **68** was designed to be a more hydrophilic version compared to inhibitor acrylamide **57**. At the same time, inhibitor **68** featured a more reactive piperazyl moiety as a promising handle for linker attachment.

Pab-Val-Ala-Mal linker attachment (Figure **3A**) with *p*-nitro-phenol containing linkers mediated by HOAt released from PyAOP did not show conversion with inhibitor **62**, probably due to reduced reactivity of anilines as well as increased sterical hindrance induced by the accumulation of aromatic rings in the modified section of the molecule. Reactions of those linkers with inhibitor **68**, on the contrary, afforded cleavable linker-payload **69** and non-cleavable linker-payload **70** with excellent yields as a matter of the more reactive piperazine

moiety, bearing a secondary amine. The reason is that the aliphatic amine shows a much higher electron density over the nitrogen in comparison with the partial π-delocalisation of electrons typical of anilines. This leads to significantly better performance of piperazine towards the nucleophilic attack to the carbonyl group of the activated linker, allowing the syntheses with better yields than in any of the other aniline-containing inhibitors.[131] This was an improvement on previous inhibitors bearing a less reactive aniline handle for linker conjugation.

To investigate the modification of the "aliphatic spacer", inhibitor **85** was synthesised to address the effect by elongation of the "aliphatic spacer" length from four to six carbon atoms. The length of the aliphatic spacer has an impact on enzyme binding, with examples using 6-C aliphatic chain spacers instead of 4. Nevertheless, due to the specific interaction between a protein and its ligand (or inhibitor), the doubt was raised if the modification of inhibitor **57** with longer aliphatic chain spacer would negatively affect the binding to the NAMPT enzyme.[93]

The synthesis of inhibitor **85** started with a Sonogashira-Hagihara cross-coupling between commercially available *p*-bromopyridine and 5-hexin-1-ol to form alcohol **74**, followed by a complete reduction of the pyridyl residue and the triple bond by hydrogenation catalysed with PtO_2 affording amino alcohol **73** in a very good yield of 85 %. Then, inhibitor **85** was synthesised in eight more steps based on the Gabriel synthesis as described for inhibitor **57**.[135] Briefly, after an initial Boc protection of the piperidyl moiety on amino alcohol **73** in a good yield of 70 %, the mesylate of *Boc* protected intermediate **74** was as well obtained in a good yield of 73 %. The mesylate as good leaving group activates the molecule towards the nucleophilic substitution by potassium phthalimide affording the phthalimide intermediate **79** in good yield of 75 %. Then, amine **80** was obtained by hydrazinolysis of the phthalimide with a yield of 50%. Next, acrylamide **82** was afforded by DCC/HOBt promoted coupling with *E*-3-(3-pyridyl)-acrylic acid followed by Boc- deprotection using neat TFA leading to intermediate **83** in a very good yield of 80 %. The final two steps of the synthesis involved the functionalisation of the piperidyl end by condensation with 3-aminobenzoic acid in a coupling promoted by DCC/HOBt and lastly, the final inhibitor **85** was obtained by Boc-deprotection of intermediate **84** in a very good yield of 80%.

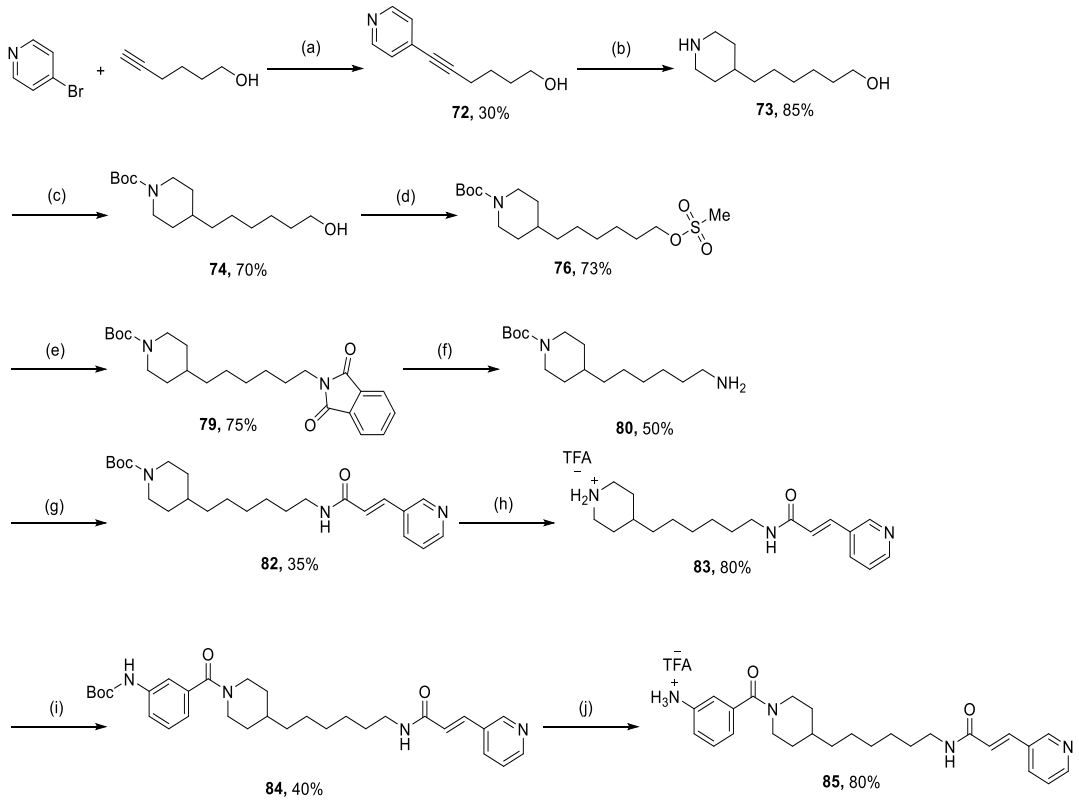

Scheme 7. Synthetic scheme of inhibitor **85**. Reagents and conditions: (a) $PdCl_2(PPh3)_2$ (cat), CuI (cat), Et_3N, reflux (95ºC), 30 min; (b) H_2, PtO_2, acetic acid, r.t., 3 d; (c) Boc anhydride, Et_3N, DCM, 0 to 20 ˚C, overnight; (d) methylene sulfonyl chloride, Et_3N, DCM (abs.), 0 ˚C to r.t, 1.5 h; (e) Potassium phthalimide, DMF (abs.), 50 ˚C, overnight; (f) hydrazine monohydrate, EtOH, r.t., overnight; (g) (*E*)-3-(3-pyridyl)-acrylic acid, DCC/HOBt, DIPEA, DCM (abs.), r.t., overnight; (h) neat TFA, r.t.; 5 min; (i) 3-aminobenzoic acid, DCC/HOBt, DIPEA, DCM (abs.), r.t., overnight; (j) neat TFA, r.t, 5 min.

3.1.3. Increase hydrophilicity of linker-payload

Aiming to increase the hydrophilicity of new linker-payloads compared to linker-payload **37**, new variants with PEG 4 and PEG 8 spacers between the linker and maleimide were synthesised and are described in this section. The expected outcome of applying linker-payloads with higher hydrophilicity was to enhance conjugation efficiency, translating into a more homogeneous DAR what aimed to reduce aggregate formation in aqueous media, and therefore avoiding lowering the applied ADC concentration *in vitro* and *in vivo*. The low availability of ADC due to aggregate formation during the 96 h of the cytotoxicity assay is therefore considered a possible explanation for the disappointing cytotoxicities of ADCs loaded with linker-payload **37** developed in Section **3.1.4.2**.

3.1.3.1 Increase of payload hydrophilicity by incorporation of PEG chains into linkers

The synthesis of linker-payloads **50** and **52** aimed to determine whether ADCs derived from these payloads presented improved conjugation efficiency and ADC stability that translated into a differential cytotoxic effect due to their more hydrophilic nature compared with linker-payload **37** (Scheme **8**).

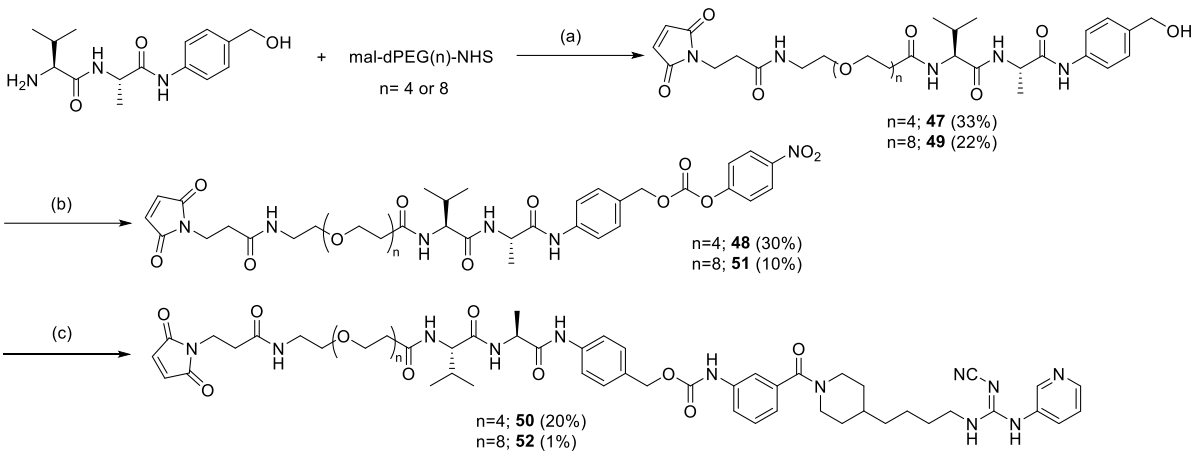

Scheme 8. Synthesis of linker-payload **50** (4 PEG units) and **52** (8 PEG units). Reagents and conditions: (a) DIPEA, DMF (abs.), r.t., 2.5 h; (b) Bis-(4-nitrophenyl)-carbonate, DIPEA, DMF (abs.), r.t., 3h; (c) **36**, HATU, DIPEA, DMF (abs.), r.t., 3 days.

Briefly, the synthesis of linker-payloads **50** and **52** were based on an approach where the initial linker H-Val-Ala-PAB-OH was PEGylated with commercially available NHS-PEG (4 or 8) activated esters, affording linkers **47** and **49** in moderate yields of 33% and 22%, respectively (Scheme **8**, step A). After activationof the PAB alcohol with bis-(*p*-nitrophenyl)-carbamate, a condensation with aniline **36** mediated by HOAt released from HATU gave linker-payload **50** with a moderate yield of 20 %, while only traces of linker-payload **52** were obtained. This low yield was probably related to the induction of the guanylation side reaction with the aniline by the employed HATU.[136] Moreover, anilines have low reactivity, as described in previous chapters.

Related to the poor result with T-DAR10-**50** reported in Section **3.1.4.4**, the synthesis of a new batch of linker-payload **52** was cancelled as equivalent results were expected due to chemical similarity.

3.1.3.2 Carboxylic acid incorporation to inhibitor **36** ("linker anchor point"): Synthesis of payload **92** and linker-payload **93**

Aiming to increase the hydrophilic character of NAMPT inhibitors, which may reduce diffusion through the cellular membrane, a carboxylic acid moiety was incorporated into inhibitor **92** (Scheme **9**). Inhibitor **92** is a modified version of inhibitor **36**, where the aromatic 3-amino group was substituted against the carboxylic acid moiety. The carboxylic acid residue was chosen as the "linker anchor point"-modification, as it has been demonstrated using inhibitors **62** and **68** that modifications at this point may affect the cytotoxic potency while still maintaining substantial activity of the free inhibitor. Although carboxylic acids are known to be reactive groups, the attachment of a linker to this moiety for ADC conjugation ensures that the carboxylic acid remains protected as an ester until released into cells, thus avoiding unintended side effects. Furthermore, it is reported that the "linker anchor point" remains exposed to the solvent upon NAMPT binding.[122] Therefore, if hydrophilic groups like carboxylic acid were introduced into the molecule, this position could allow less distortion of the electrostatic environment of the NAMPT catalytic pocket. Moreover, the pKa for the carboxylic acid moiety of inhibitor **92** was determined to be 3.67 by quantum mechanics density functional calculations (DFT, model used: B3LYP; Figure **14a**). Hence, it was expected that, even at lysosomal pH, that at least 50% of the cellular accumulated inhibitor was ionised, and at a

significantly lower LogP value than the aniline inhibitor **36**. Thus, inhibitor **92** was significantly more hydrophilic than inhibitor **36** and may therefore present a lower tendency to diffuse passively along cellular membranes. This may lead to a higher accumulation in the cell after ADC delivery. However, the probable ionised state of inhibitor **92** in a lysosomal medium could potentially impede its free diffusion into the cytoplasmic medium, resulting in a low cytoplasmic concentration of inhibitor available to inhibit NAMPT.

Inhibitor **92** was synthetised following a similar route as described for aniline **36**. Initially, the piperidinyl moiety of amino alcohol **22** was conjugated via DCC/HOBt-mediated coupling to Cbz-protected benzoic acid **81**, affording amide **86** at an acceptable 38% yield. Then, analogously to the synthesis of inhibitor **36** and aiming for a Gabriel synthesis of amines, the hydroxy moiety of intermediate **86** was activated through mesylate formation, affording intermediate **87** at a good yield of 80 %. Next, the two steps of the Gabriel synthesis of amines were then conducted starting with a substitution of the mesylate against phthalimide, followed by hydrazinolysis to afford amine **89** at an acceptable overall yield of 36% over both steps. Afterwards, cyanoguanidine **90** was afforded by SN_2 substitution of phenyl N-cyano-N'-3-pyridinylcarbamimidate **1** at an acceptable 40% yield. Finally, H_2 reduction of the Cbz group catalysed by Pd/C led to inhibitor **92** in a very good yield of 80 % (Scheme **9**). In contrast to the linker attachment to anilines or amines of previously synthesised inhibitors, the synthesis of linker-payload **93** involved a DIC/HOBt activation of the carboxylic acid moiety, followed by a reaction with the Mal-Val-Ala-PAB-OH linker to attach the linker via an ester bond.

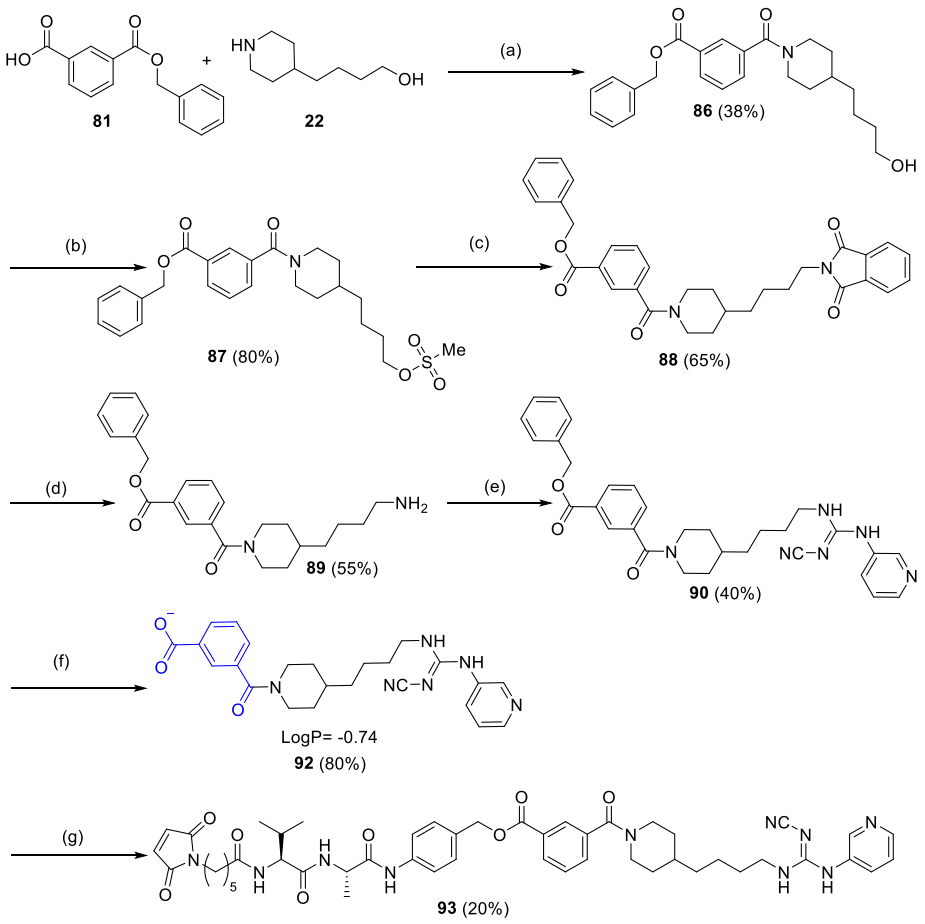

Scheme 9. Synthetic scheme of inhibitor and linker-payload **92** and **93**, respectively, with LogP data of **92**. Reagents and conditions: (a) DCC/HOBt, DIPEA, DCM (abs.), r.t., overnight; (b) methylene sulfonyl

chloride, Et_3N, DCM (abs.), r.t., 1.5 h; (c) Potassium phthalimide, DMF (abs.), 50 °C, overnight; (d) hydrazine monohydrate, EtOH, r.t., overnight; (e) Phenyl *N*-cyano-*N*'-3-pyridinylcarbamimidate, Et_3N, 1,4-dioxane, r.t., overnight; (f) H_2, Pd/C, EtOH/EtOAc (1:1), r.t., overnight; (g) Mal-Val-Ala-PAB-OH, DIC/HOBt, DIPEA, DMF (abs.), r.t., overnight.

As reported in the biology *in vitro* cytotoxic results (Section **3.1.4.5**), carboxylic acid **92** did not show cytotoxicity. This may be explained by the computational study of inhibitor **92**, which was docked to NAMPT with five grids (or computational simplifications of the catalytic pocket used for docking) generated from PDB published X-ray diffraction data[137–141], resembling the interaction between the catalytic pocket of the NAMPT enzyme and the inhibitor. As a result, high solvent exposure of the lipophilic regions of inhibitor **92** (symbolised by grey halos around the exposed atoms in the interaction diagram in Figure **14B**) was observed, particularly in its ionised form. This implies lower stability in the catalytic pocket due to impaired hydrophobic interaction in the solvated regions and therefore higher desolvation energy values for the ionised form of inhibitor **92** compared with inhibitor **36** (Figure **14C**), leading to average docking scores of -3 for inhibitor **92** (ionised) and -8 for inhibitor **36**. The significantly lower absolute value for inhibitor **92** implied poorer docking to the enzyme compared with inhibitor **36**. As reported in Section **3.1.4.5**, the free inhibitor **92** shows no cytotoxicity in Raji or Ramos cells. This result also applied to the ADC loaded with the corresponding linker payload **93**. Access to the docking software Maestro was granted after the synthesis of these compounds. Using the software, a significantly lower docking score (in absolute value) was calculated for the carboxylic acid inhibitor **92** conformers compared with the aniline inhibitor **36** conformers. The lower docking score was in agreement with the unexpectedly low cytotoxicity of linker-payload-**93**-loaded ADCs. Briefly, simulations showed that in order to gain stability with the ionised form of inhibitor **92**, the system tends to expose the carboxylic acid region to the solvent to increase the stabilisation by solvation. This could affect the lipophilic skeleton of the molecule, which exposes the aromatic ring to unfavourable interactions with water, which may be detrimental for docking with the enzyme. Additionally, since catalytic pockets are very narrow, this conformational change caused by the solvation of the carboxylate moiety could create several unfavourable collision points within the pocket.

New inhibitor design assisted by computational methods was explored in chapter **3.2**. This new NAMPT inhibitors relied on the unfavourable results for inhibitor **92**, assuming that success could be based on a balanced increase in hydrophilicity, thereby avoiding the possibility of charged conformers that could bias docking up to a point that makes it unfavourable.

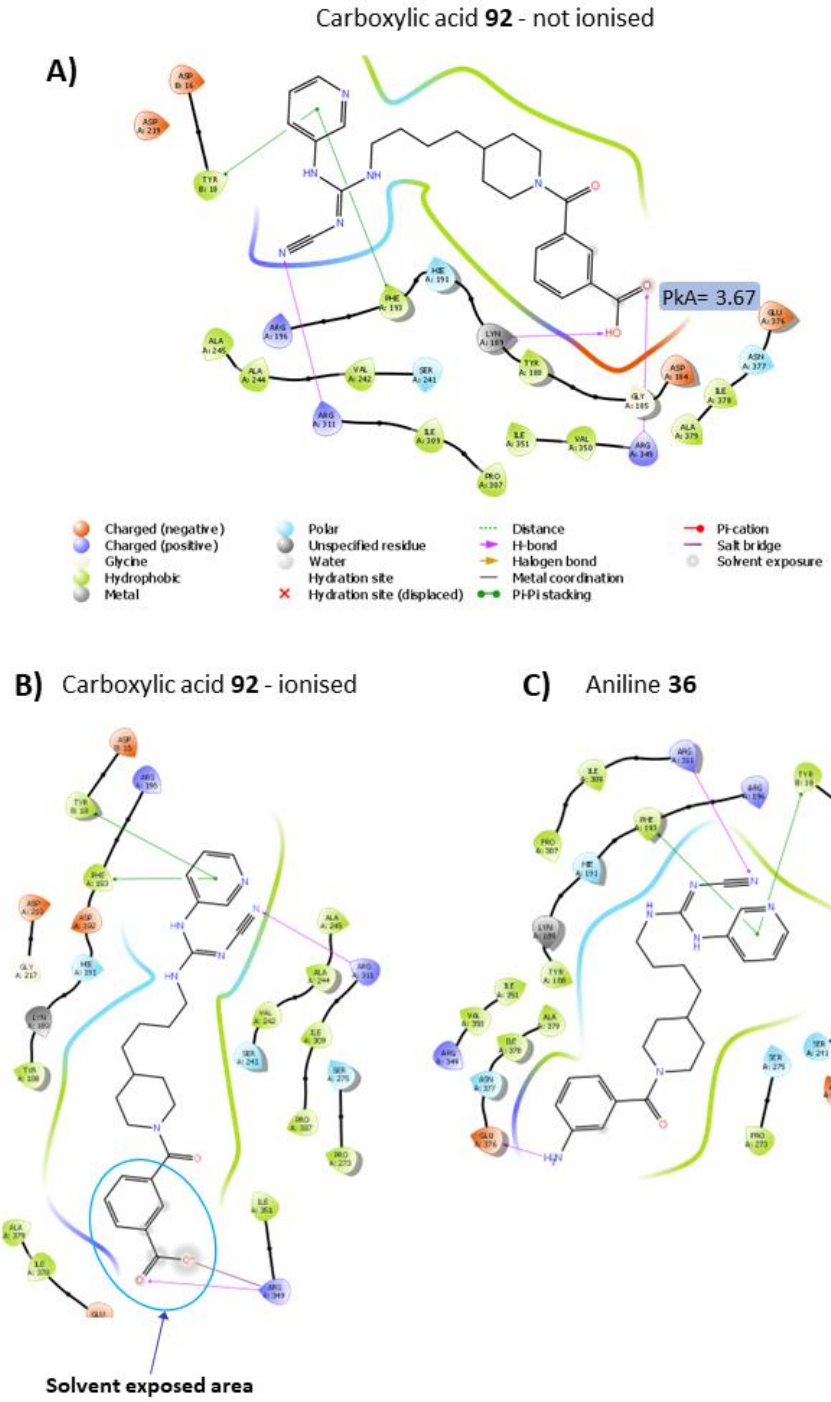

Figure 14. Interaction diagrams of NAMPT with A) Not-ionised carboxylic acid **92**, including pKa; B) Ionised conformer or carboxylic acid **92;** C) Interaction diagram of docking of aniline **36** as a control**.** It can be observed that the ionised form of carboxylic acid **92** stabilises the carboxylate by enhancing the solvent exposure of the linker conjugatable handle of the molecule, leading to increased solvent exposure of hydrophobic aromatic groups (blue oval), which is expected to be detrimental in favouring docking to the enzyme.

3.1.4. ADC production and target screening: *In vitro* cellular viability testing

3.1.4.1 Production and *in vitro* testing of trastuzumab-linker payload **27** ADCs (control)

To determine the reproducibility of the published data, payload **19** was tested directly as a free inhibitor on BT474 cells representing an Erbb2^{+} breast cancer cell line. The cell line was chosen as it is reported to have high sensitivity against NAMPT inhibitors. As expected, the EC_{50} values were in the low µM range (Figure **15**), as reported by Vogel *et al.*[127,142,143]

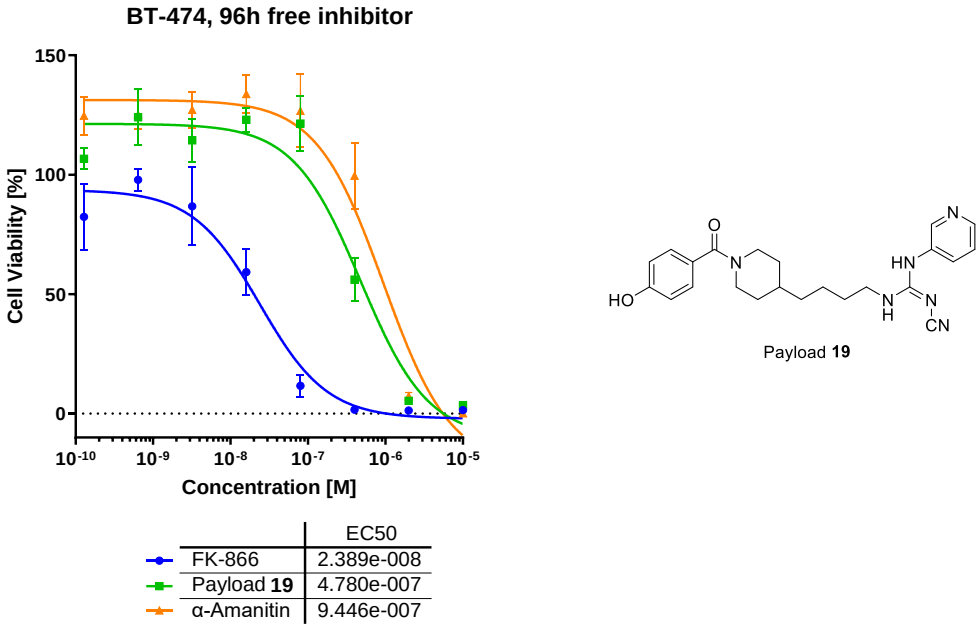

Figure 15. Cytotoxicity assay of free compound **19** compared with FK866 and α-amanitin on BT474 cells (EC_{50} in M)

Table 3. Cytotoxicity values for several Trastuzumab-**27** ADCs

ADC ID	DAR	Inhibitor	Cell line tested	ADC EC_{50}
Trastuzumab (T)-D265C-27	2	19	BT474, JIMT1	≈ $1*10^{-7}$ M
T-A118C-D265C DAR4-27	4	19	BT474, JIMT1, SKOV-3	≈ $1*10^{-7}$ M
T-D265C DAR10-27	10	19	BT474, JIMT1	≈ $1*10^{-7}$ M
T-D265C	0	--	BT474, SKBR-3	$1.9*10^{-7}$ M
T-D265C DAR2-amanitin (**positive control**)	2	α-amanitin	BT474, JIMT1, SKBR-3, HCC-38	≈ $1*10^{-10}$ M

Linker-payload **27** (based on payload 19) was conjugated to Trastuzumab-D265C or Trastuzumab-A118C-D265C to obtain ADCs with DARs of 2, 4, and 10. DAR values of 2 or 4 were achieved by site-specific conjugation to the engineered cysteines of the thiomabs™, whereas DAR10 ADCs were achieved by conjugating the payload to the native interchain cysteines (8 for

IgG1) and thiomab™ cysteines of single thiomab™ antibodies. In all cases, the quality analysis of the ADCs confirmed the expected DAR values as well as low aggregation of the ADCs (lower than 5%). The cytotoxicity results were summarised in Table **3** and showed that none of the tested ADCs exhibit significant cytotoxicity in contrast to the free inhibitor **19** (Figure **15**).

3.1.4.2 Production and *in vitro* testing of ADC loaded with linker-payload **37** (control)

Initially the free aniline inhibitor **36** was tested for cytotoxicity (Table **4**) in the Erbb2$^+$ cell lines BT474, HCC-38, JIMT-1, and SKBR-3. To broaden the scope of malignancies as well as to obtain a representative sample of different tumour models, the cytotoxicity of free inhibitor **36** was tested additionally on the CD19$^+$ cell lines MEC-1, MEC-2, NALM-6, Raji, and Ramos. CD19 is a well-characterised target for ADCs in blood malignancies. The selection criteria for the tested cell lines were the reported sensitivity to NAMPT inhibitors and/or the good performance in ADC dynamics (e.g., receptor targeting and internalisation, data not shown) reported by previous studies from HDP.[144,145] As described in Table **4**, the NAMPT inhibitor **36** showed activity only on the HER2$^+$ cells BT474 and HCC-38 as and the CD19$^+$ cells Ramos and Raji with EC_{50} values in the nM range.

Table 4. EC_{50} values for free inhibitor **36**

Cell line tested	EC_{50}
BT474	≈ $1.1*10^{-10}$ M
HCC-38	≈ $4.1*10^{-9}$ M
Ramos	$2.1*10^{-8}$ M
Raji	$1.2*10^{-8}$ M
JIMT-1, SKBR-3, MEC-1, MEC-2, NALM-6	> $1*10^{-5}$ M

Maleimide containing linker-payload **37** was conjugated initially to Trastuzumab (T-D265C) as well as to an anti-CD19 antibody (antiCD19-D265C). In brief, the strategy of Ab conjugation based on coupling to reduced cysteines was performed in a three-step process. Initially, interchain and thiomab™ cysteines were reduced by TCEP. After membrane dialysis purification, an optional re-oxidation of interchain cysteines promoted by dhAA was performed, which was skipped in cases where the production of high-DAR ADCs was aimed. A Michael-type reaction with the maleimide-containing linker-payload then afforded the ADCs.

As reported in Table **5**, no cytotoxicity was detected for the new constructs in contrast to the free inhibitor. Due to the good potency and chemical properties of inhibitor **36**, it was used as an NAMPT inhibitor control for comparing the advantageous properties of the newly designed NAMTP inhibitors.

Table 5. Cytotoxicity values for anti-CD19 ADCs loaded with linker-payload **37** (inhibitor **36)** in Ramos and Raji cells.

ADC	EC_{50}
antiCD19-D265C-DAR2-**37**	> 1 µM
antiCD19-D265C-interchain-DAR10-**37**	> 1 µM
antiCD19-D265C (control)	> 1 µM
antiCD19-D265C-DAR2-amanitin (control)	$1*10^{-10}$ M

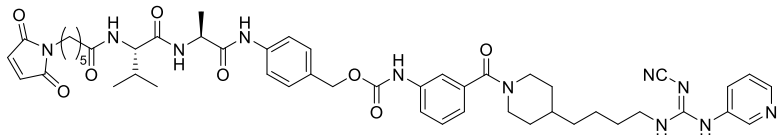

Linker-payload **37**

3.1.4.3 Understanding the biological effects of modification of FK866 analogues at different molecular levels *in vitro*

First, a single-dose cytotoxicity assay on BT474 cells was performed with on inhibitor **43** to understand the effects on cellular viability of the modifications applied at the "core ring" (see Figure **13**). As shown in Figure **16**, piperazyl inhibitor **43** showed no cytotoxicity (EC_{50} > $1*10^{-5}$ M) in contrast to inhibitor **36** (NAMPT inhibitor control) and α-amanitin (method control).

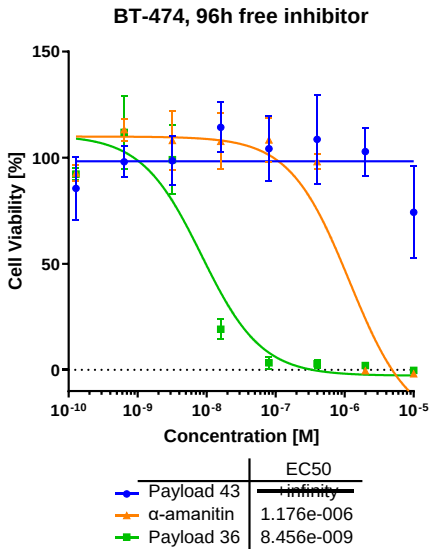

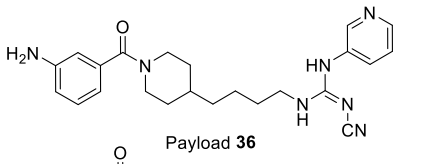

Payload **36**

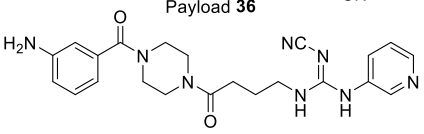

Payload **43**

Figure 16. Cytotoxicity assay of free compound **43** compared with compound **36** and α-amanitin on BT474 cells (EC_{50} in M).

Next, the effects of modifying the inhibitors at the H-bond capable polar group (see Figure **13**) were explored with acrylamide inhibitor **57** and linker-payloads **58** and **59** harnessing maleimide containing non-cleavable and cathepsin B cleavable linkers, respectively. Initially, linker-payloads **58** and **59** were conjugated through the maleimide moieties to reduced

cysteines in the Fc region of antiCD19-D265C (anti-CD19) monoclonal antibodies producing ADCs with an average DAR of 10. Then, the cytotoxicity of naked inhibitor **57** and the ADCs conjugated to linker-payload **58** were tested *in vitro* in Ramos and Raji cells (Figure **17**). The inhibitor **57** performed promisingly well as free inhibitor with cytotoxicity in the nM range (Figure **17 A** and **C**), which was in agreement with the literature data.[125] Disappointingly, none of the ADCs showed any cytotoxicity (Figure **17 B** and **D**).

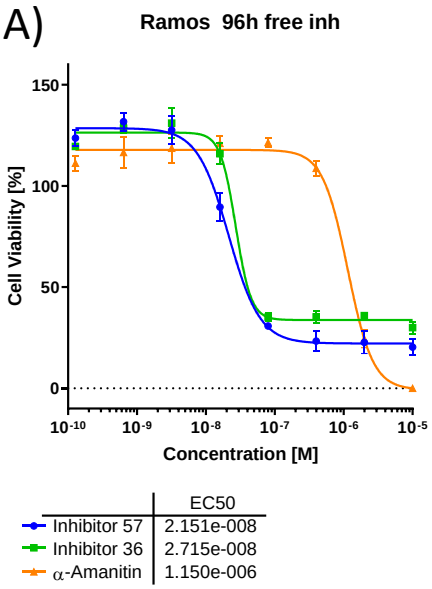

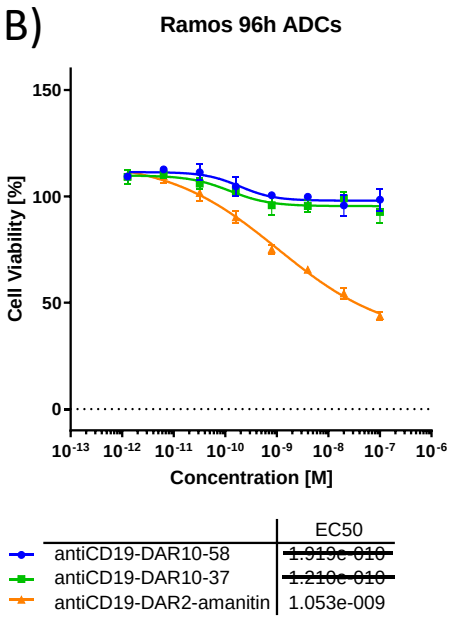

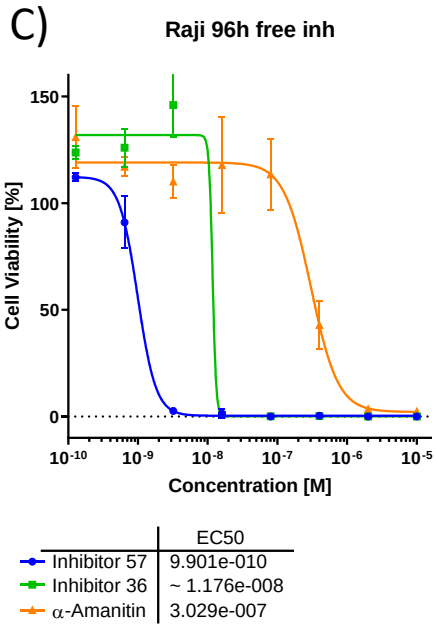

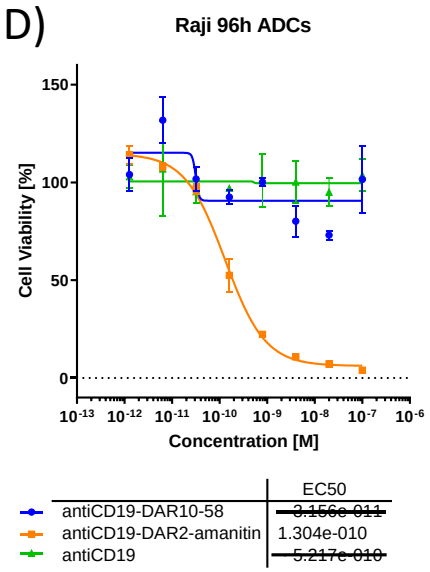

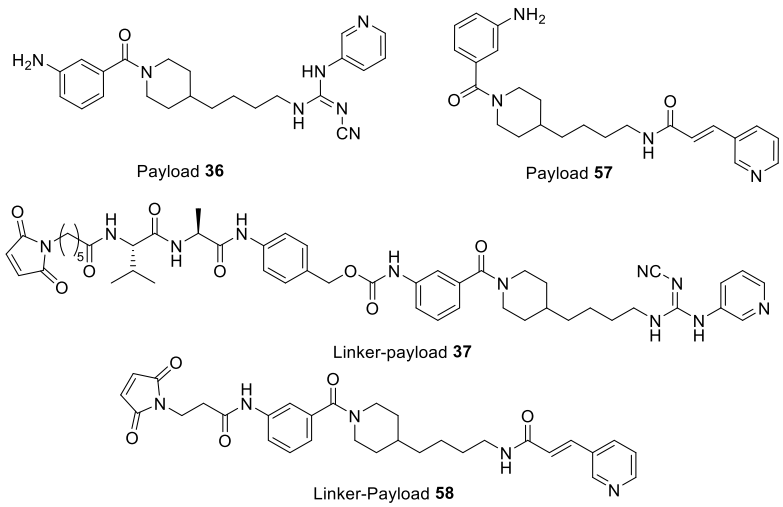

Figure 17. Cytotoxicity of new inhibitor **57** and ADCs, A) Free inhibitor on Ramos cells B) anti-CD19 ADCs on Ramos cells C) Free inhibitor on Raji cells D) anti-CD19 ADCs on Raji cells, α-amanitin and antiCD19-DAR2-amanitin are used as method positive control, antiCD19-DAR10-**37** and anti-CD19 Ab are used as negative controls (EC_{50} in M).

Next, modifications at the "linker anchor point" were evaluated in Raji and Ramos cells ($CD19^+$ cells), with inhibitor **62** showing an EC_{50} in a nM range (Figure **18A**) similarly to inhibitor **57** (purple line). However, the more hydrophilic piperazine inhibitor **68** showed EC_{50} values in high nM range in Raji and Ramos cells (Figure **18A**) indicating inhibitor **68** to be a slightly less toxic analogue than aniline **36**.

Afterwards, linker-payloads **69** and **70** based on inhibitors **62** and **68** were conjugated to fully reduced antiCD19-D265C in order to produce ADCs with an average DAR of 10. Disappointingly, no improved cytotoxicity with respect to the control antiCD19-DAR2-amanitin was observed when tested in Raji cells (Figure **18B**).

A)

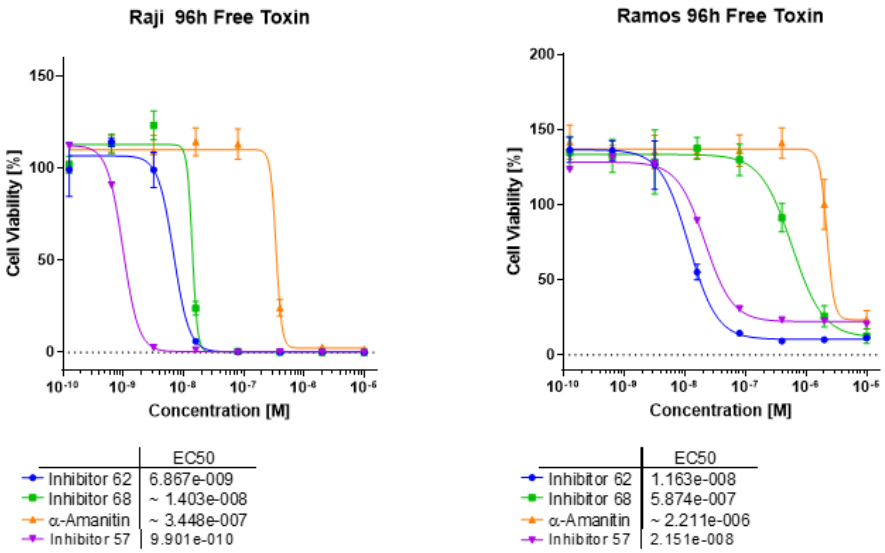
Raji 96h Free Toxin
Cell Viability [%]
Concentration [M]
EC50
Inhibitor 62 6.867e-009
Inhibitor 68 ~ 1.403e-008
α-Amanitin ~ 3.448e-007
Inhibitor 57 9.901e-010
Ramos 96h Free Toxin
Cell Viability [%]
Concentration [M]
EC50
Inhibitor 62 1.163e-008
Inhibitor 68 5.874e-007
α-Amanitin ~ 2.211e-006
Inhibitor 57 2.151e-008

B)

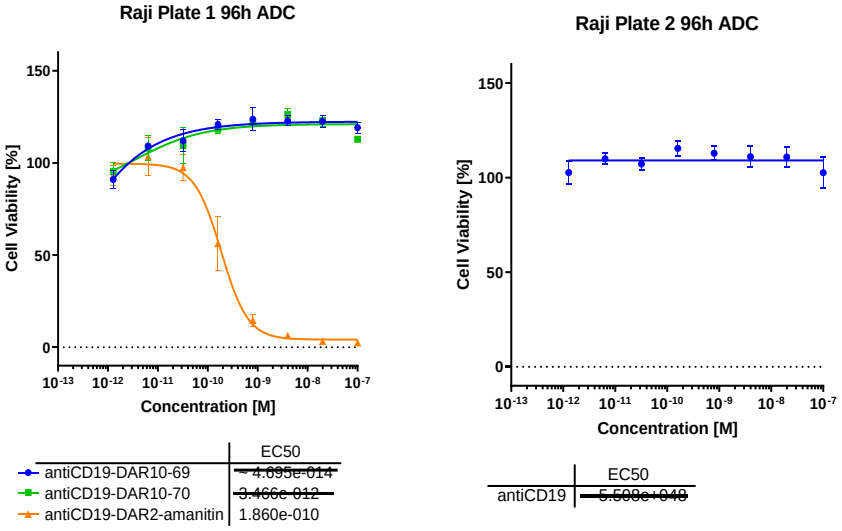
Raji Plate 1 96h ADC
Cell Viability [%]
Concentration [M]
EC50
antiCD19-DAR10-69 ~ 4.695e-014
antiCD19-DAR10-70 3.466e-012
antiCD19-DAR2-amanitin 1.860e-010
Raji Plate 2 96h ADC
Cell Viability [%]
Concentration [M]
EC50
antiCD19 5.598e+049

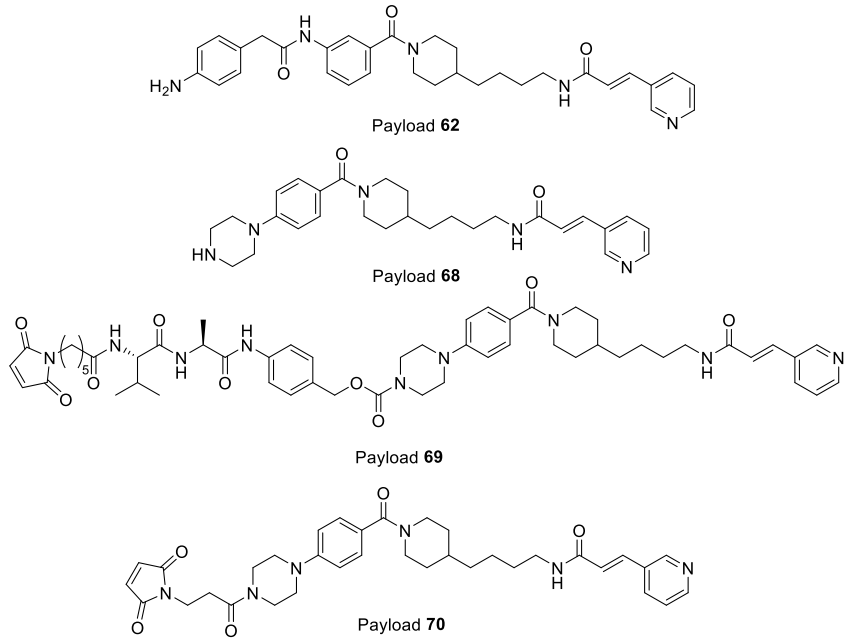

Figure 18. *A) Cytotoxicity assay of inhibitors **62** and **68** compared with α-amanitin and inhibitor **57** on Raji and Ramos cells; B) Cytotoxicity assay of ADC antiCD19-DAR10-**69** and **70** compared with antiCD19-DAR2-amanitin on Raji cells (EC_{50} in M).*

The effect of longer aliphatic spacers was tested with inhibitor **85** as a free inhibitor against Ramos cells. Four times less cytotoxicity was observed compared to the control inhibitor **36** (Figure **19**). Due to a lack of improved cytotoxicity in a more lipophilic molecule than inhibitor **36** (concomitant with a longer synthesis), no ADCs were produced with linker-payloads based on inhibitor **85**.

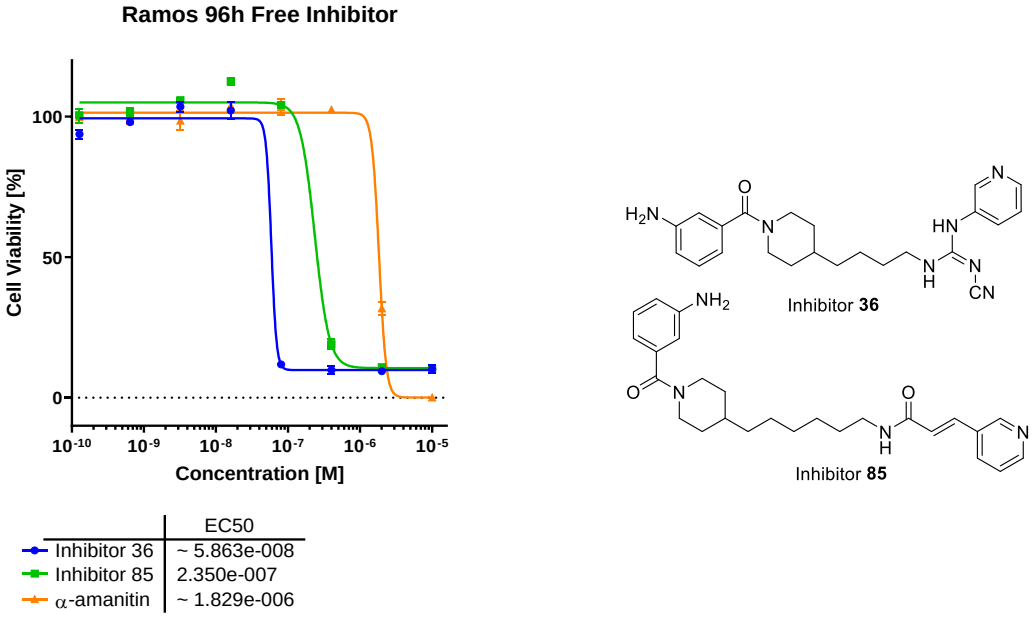

Figure 19. Cytotoxicity assay of inhibitor **85** compared with inhibitor **36** and α-amanitin on Ramos cells (EC_{50} in M).

3.1.4.4 Effects of increasing linker hydrophilicity on cellular viability

Next, the effects on cellular viability of ADCs loaded with more hydrophilic linker-payloads than the control linker-payload **37** were determined. The strategy followed first aimed to modify the cathepsin B cleavable linker by means of pegylation, resulting in PEG(4) linker-payload **50**.

After thiomab™ site-specific conjugation to T-D265C, T-DAR10-**50** was tested in a 96h cell viability assay on BT474 cells. The ADC showed poor cytotoxicity compared to the amanitin-based ADC (in orange), and the curve progression for T-DAR10-**50** was the same as for the naked antibody trastuzumab (Figure **20**).

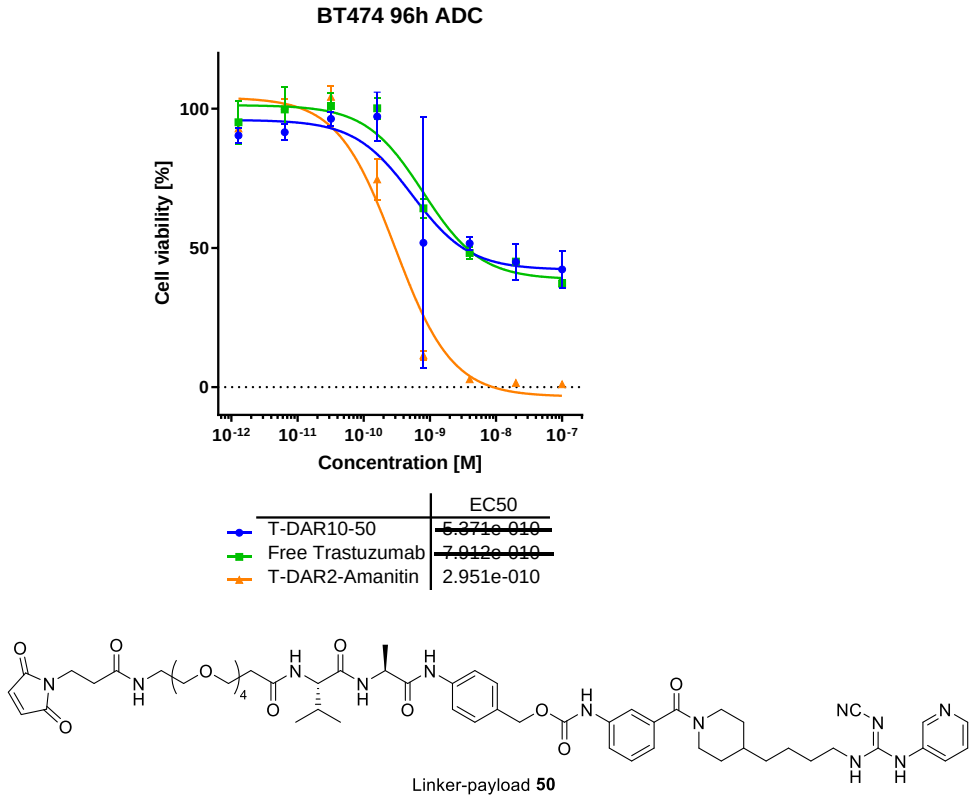

Figure 20. Cytotoxicity assay of T-DAR10-**50** ADC loaded with a PEG(4)-containing payload compared with naked antibody and T-DAR2-amanitin on BT474 cells (EC_{50} in M).

3.1.4.5 Carboxylic acid incorporation to aniline inhibitor **36** at "linker anchor point": *In vitro* efficacy evaluation

Inhibitor **92** containing a carboxylic acid at the linker anchor point was tested in a cell viability assay on Ramos and Raji cells, but no cytotoxicity was found (Figure **21**). This could be expected since the molecule is about 400 times more hydrophilic than aniline inhibitor **36** and therefore cannot pass the cellular membrane as a free toxin. However, only low activity in the nM range was observed for the ADC loaded with the corresponding linker-payload **93** (Figure **21**).

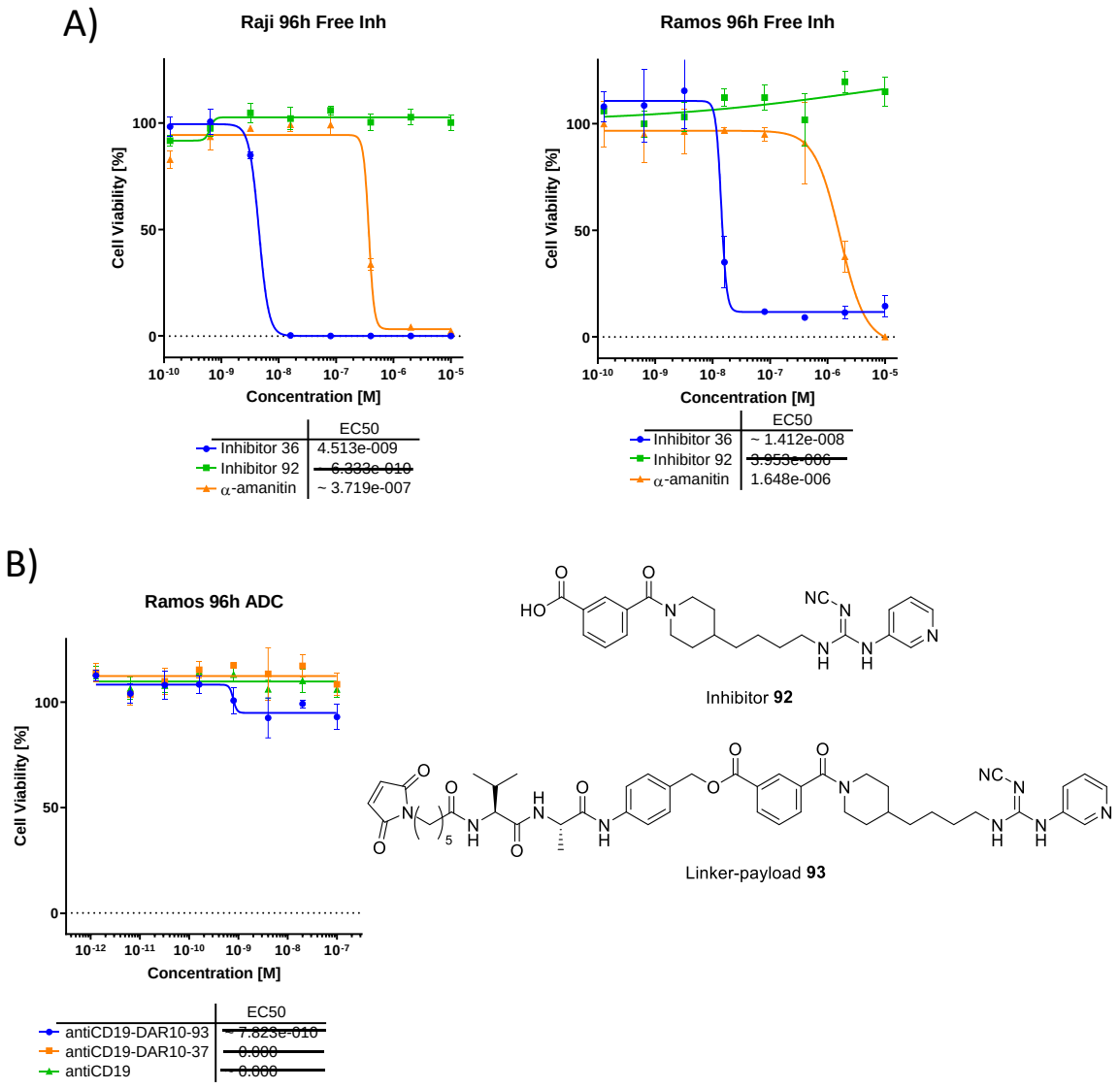

Figure 21. Cytotoxicity assay of (A) Inhibitor 92 compared with Inhibitor 36 and amanitin on Ramos and Raji cells and (B) of antiCD19-DAR10-93 with antiCD19-DAR10-37 and naked antibody antiCD19 on Ramos cells (EC_{50} in M).

3.1.5. Biochemical evaluation of NAMPT inhibitors: Cellular extract NAD measurement, NAMPT binding affinity by BLI, metabolic effects of NAMPT inhibitors on target receptor recyclability, and determination of NAMPT expression across NAMPT inhibitor-sensitive cell lines

3.1.5.1 Quantification of binding of biotinylated NAMPT inhibitors to NAMPT enzyme *in vitro* through biolayer light interferometry (BLI) measurement

The enzyme-inhibitor binding kinetics were determined by light interferometry through the measurement of the change in thickness in the biolayer generated over Octet® optic sensors. Sensors were coated with streptavidin, to ensure selective and strong binding to biotinylated NAMPT inhibitors. After binding to the streptavidin on the sensor, the binding of

the captured inhibitors to the recombinant NAMPT enzyme was assessed over time by changes in the thickness of the biolayer.

First, an evaluation of the binding kinetics of inhibitor **36** to NAMPT was accomplished with the biotinylated version **46**. The measurement revealed that the biotinylated inhibitor **46** binds to NAMPT with a linear dependency on the enzyme concentration and a K_D value in the nM range (Figure **22**).

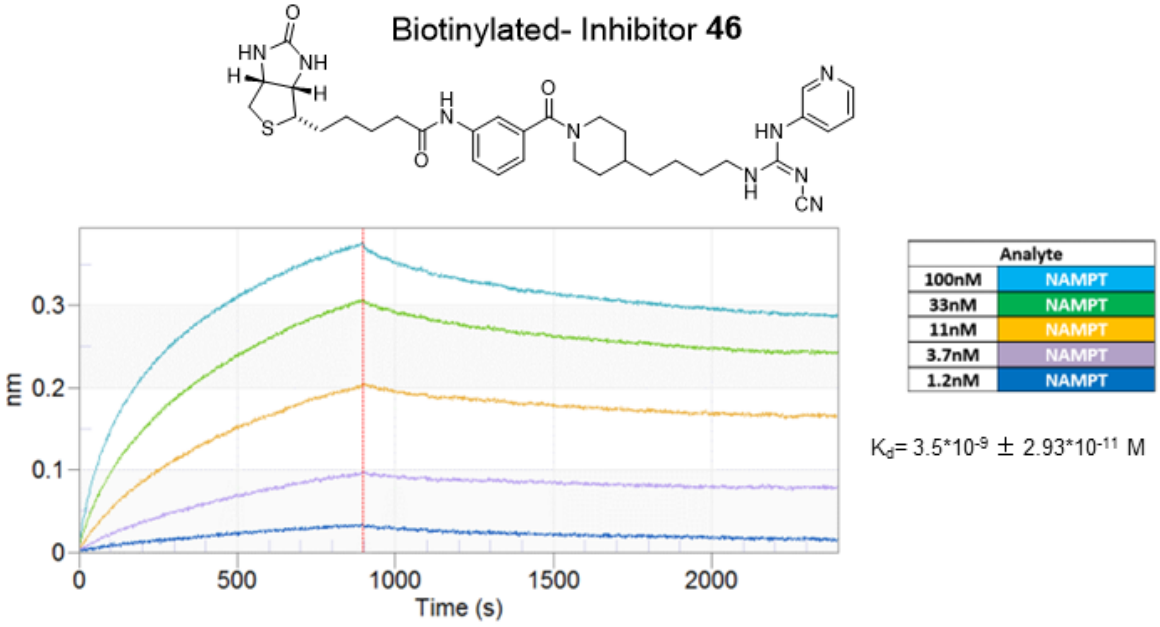

Figure 22. Biolayer light interferometry assay, binding of recombinant NAMPT (analyte) to biotinylated inhibitor **46** (100 nM).

Then, to determine whether a significant difference in enzyme binding existed between inhibitor **57,** which harnessed an acrylamide moiety as an H-bond capable polar group, and inhibitor **36,** which harnessed the cyanoguanidine moiety, a BLI experiment was performed with inhibitor **91**, the biotinylated analogue of inhibitor **57.**

As shown in Figure **23**, binding to the NAMPT enzyme in a linear concentration-dependent form was observed for biotinylated inhibitor **91**, with a K_D comparable to the one reported for biotinylated inhibitor **46**.

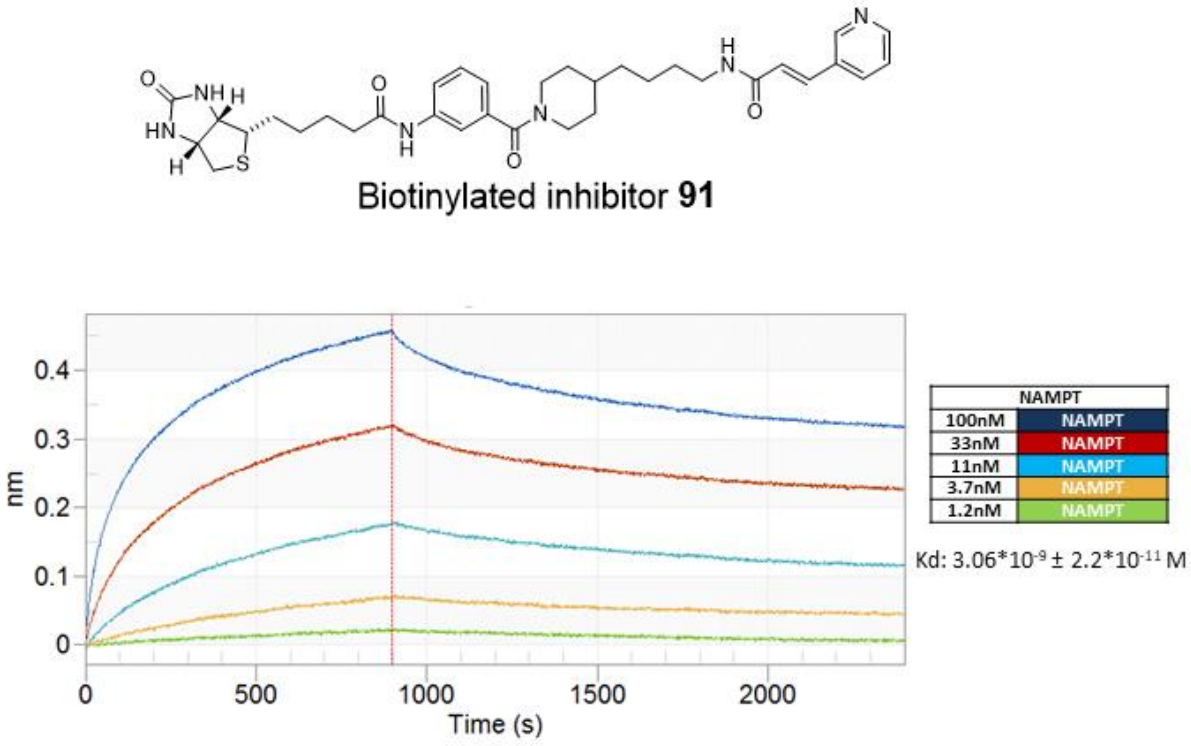

Figure 23. Binding of biotinylated inhibitor **91** (100 nM) to NAMPT, measured by light interferometry in Octet®.

3.1.6. [NAD⁺] determination in cell extracts by colorimetric enzymatic cycle assay: Assessing the effects of NAMPT inhibitor-loaded ADCs beyond cellular viability

To complement the *in vitro* cytotoxicity results and demonstrate partial NAD^+ depletion in situations where the threshold depletion required to induce cell death was not reached, the concentration of NAD^+ was determined in cell extracts.[125,146]

Results are based on determination of total NAD^+ content of cells treated with NAMPT inhibitor loaded ADCs or free NAMPT inhibitors, measured at three time points (24 h, 48 h, 72 h) with a colorimetric enzymatic cyclic assay based on alcohol dehydrogenase (ADH), and normalised to cell extract total protein concentration measured with commercial BCA kit.[86,147]

3.1.6.1 Comparison of NAD^+ depletion ability of free NAMPT inhibitors against anti-CD19, NAMPT inhibitor-loaded ADCs

Figure **24** shows that in Ramos cells after 48 h of treatment with free NAMPT inhibitors, a full depletion of [NAD^+] was achieved in accordance with the cell viability results (Figure **19**). In contrast to the free inhibitors, NAMPT inhibitor-loaded ADCs showed no cytotoxic activity. Nevertheless, a reduction of [NAD^+] of around 30% of the initial concentration was detected during the first 24–48h after ADC treatment, whereas [NAD^+] levels were fully recovered 72 hours after treatment. Additionally, cells treated with ADCs not only completely recovered [NAD^+] levels, but they also showed even higher [NAD^+] levels than the untreated control group after 72 h.

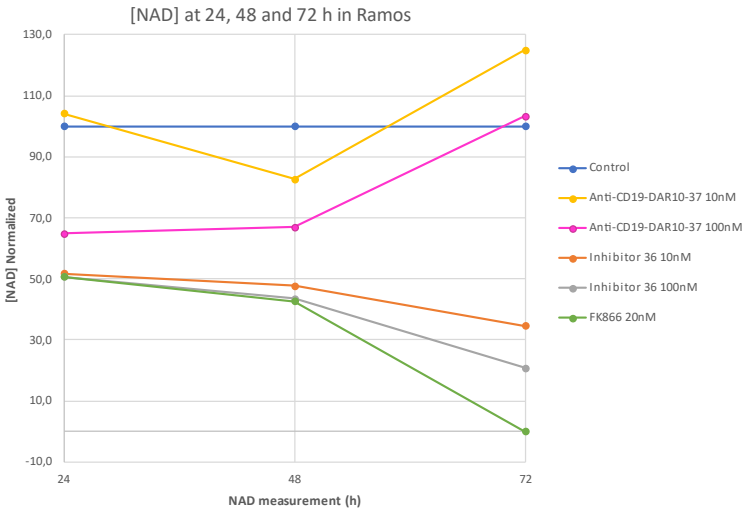

Figure 24. NAD^+ concentration in Ramos cells after single treatment with free inhibitor 36 or antiCD19-DAR10-37 at three time-points (24, 48, and 72 h). Control cells are untreated, and FK866-treated cells act as a positive control for NAD depletion. Free inhibitors maintain a stable [NAD^+] depletion for 72 h and correlate with in vitro data. ADC-treated groups show moderate [NAD^+] depletion during the initial 48 h; at 72 h, initial [NAD^+] is recovered.

3.1.7. Discussion of chemical iterative pharmacophore base NAMPT inhibitor design chapter

NAMPT is the rate-limiting enzyme of the salvage pathway for NAD^+ production starting from nicotinamide (NAM).[94] FK866 is one of the leading NAMPT inhibitor small molecules showing remarkable toxicity against a broad selection of tumours.[91,144] However, although NAMPT inhibition is a highly interesting mode of action (MOA) for the development of antibody drug conjugates (ADCs), FK866 cannot be easily used for ADC production, as it lacks a suitable handle for linker attachment except for the pyridine nitrogen.[148] Inhibitor **19**, which showed high nanomolar EC_{50} in all tested cell lines, was designed as a linkable variant of FK866.[130] However, in contrast to free inhibitor **19**, the ADCs thereof carrying the corresponding linker-payload **27** were lacking cytotoxicity. One possible explanation for this, lies in the complex dynamics of ADCs in cells, since the release of the inhibitor requires several steps, such as linker-cleavage, lysosomal release and localisation to the cell cytoplasm. This may lead to lower levels of inhibitor in the cytoplasm upon target mediated ADC uptake and degradation compared to the cellular uptake of extracellular free inhibitor by passive diffusion. To solve this problem, more potent inhibitors were needed as described by Neumann *et al.*[122]

As reported previously,[122] compound **36** showed increased cytotoxicity in a low nanomolar range in BT474 cells as compared to FK866. This could be explained by the better docking into the catalytic pocket of the enzyme mediated by the H-bond between the aniline moiety of the inhibitor and Glu-376 of the enzyme, as described earlier.[122] To test the hypothesis of the need for a more potent NAMPT inhibitor, compound **36** was evaluated as potential ADC payload. For this purpose, a standard cleavable Mal-Val-Ala-PAB linker was attached to the aniline group of the inhibitor **36**. To widen the target selection and make the outcome results less target-dependent but more inhibitor-dependent, the resulting linker-payload **37** was conjugated to a Trastuzumab-based thiomab™ as well as an anti-CD19 thiomab™. The rationale behind choosing CD19 as target was as follows: First, it has already been used and approved as an ADC target, with the FDA approval of the anti-CD19-PBD ADC

ZYNLONTA™ in 2021 showing the high interest in targeting CD19 in blood malignancies. Second, CD19 is typically expressed in haematological cancers. This type of malignancies comprises easier models for macromolecule therapy like ADC because they are better accessible compared to solid tumours, which usually have a low permeation rate.[149,150] In case of Trastuzumab it was selected as solid malignancy treatment option as HER2, which is trastuzumab target it is widely express in solid malignancies like breast cancer. Additionally, trastuzumab is one of the most studied mAb in literature as in HDP allowing easier implementation as ADC model.[151,152] Despite the promising cytotoxic results of the free inhibitor **36**, (Section **3.1.4.2**) the corresponding ADCs did not show cytotoxicity *in vitro.* Considering the tight binding to NAMPT with a nanomolar K_D as observed in the *in vitro* enzyme binding assay determined with biolayer light interferometry (BLI), it seems that despite the promising activity and potent enzyme binding of the aniline-inhibitor **36**, the compound concentration in the cytoplasm was not sufficient to achieve an effective inhibition of the enzyme after release from the ADC in lysosomes and transfer to the cytoplasm. This was in accordance with the results observed in the cell extract NAD^+ determination, where an initial NAD^+ depletion induced by the ADCs was not sufficient to maintain a sustained inhibition of NAMPT during the whole duration of the assay (72 h), explaining the observed lack of cytotoxicity. Remarkably, in contrast with the *in vitro* results, good *in vivo* results were reported in the published work of Neumann *et al,*[122] where glucuronidase cleavable linkers were used for their ADCs. This suggests that the *in vivo* toxicity reported for this inhibitor was not only related to the inhibitor itself but also to the linker and its biological cleavage mechanism. The linker-payload **37** features a cathepsin B-cleavable Val-Ala linker, which is known to be degraded in lysosomes, but stable in extracellular compartments. In contrast, in the work of Neumann *et al*,[122] a glucuronidase-triggered linker was used. This type of linker is reported to be significantly cleaved by the extracellular glucuronidase activity in the tumour micro-environment. [153] Therefore, the lack of *in vitro* activity but at the same time good *in vivo* activity showed by Neumann *et al*. may be related to an extracellular release of the inhibitor *in vivo*, with subsequent passive diffusion to the cytoplasm of surrounding cells in the tumour micro-environment without entering the lysosomal pathway. However, this may also cause the problem of unspecific release of potent cytotoxic compound in the organism lacking selective targeting.

In vitro cytotoxicity assays of the already published free inhibitors, as well as the ADCs thereof, were proving that the performance of the free inhibitor in cells did not transfer to ADC performance. Furthermore, it was found that cell viability assays, only give a limited view on NAMPT inhibitor performance. The effect of physicochemical properties – such as the permeability and solubility of the different inhibitors in cellular membranes, which theoretically may have a decisive role in the final efficacy of the inhibitor – was not considered. This can veil the real binding efficacy of the free inhibitor, as more lipophilic compounds were expected to gather in higher concentrations in the cytoplasm, showing a virtual higher efficacy. Therefore, it was mandatory to compare the *in vitro* cellular viability test with kinetic measurements by light interferometry in Octet® to determine the direct binding of the inhibitors to the NAMPT enzyme.

One good example illustrating this problem, was acrylamide-inhibitor **57**, which performed as a free inhibitor better than aniline-inhibitor **36** in Ramos and Raji cells. However, this was most likely due to a higher passive permeation through the membrane, resulting in a higher partition coefficient rather than a stronger binding to NAMPT. The biolayer

interferometry measurements showed strong binding to the enzyme but not significantly higher than the one reported for aniline-inhibitor **36** inhibitor. From a physicochemical viewpoint, LogP measurements showed that inhibitor **57** (LogP = 2.00) was 12 times more hydrophobic than inhibitor **36** (LogP = 1.84). This could be somehow disadvantageous, as inhibitor **57** is likely to be more permeable to cell membranes, so that the compound released from the ADC may have a faster clearance rate from the cytoplasm than inhibitor **36**. This also explains the increased cytotoxicity profile of acrylamide-inhibitor **57** compared with aniline-inhibitor **36** when applied as free inhibitors, as increased cellular permeation is expected by passive diffusion for the more hydrophobic inhibitor, in this case, acrylamide **57**. However, despite the fact that inhibitor **57** showed promising cytotoxicity as a free inhibitor, as an ADC payload it did not show cytotoxicity. The acrylamide modification of the H-bond polar group moiety may be an option for free NAMPT inhibitors, but not for ADC payloads, at least when applied alone.

Subsequently, the modification established with inhibitor **57** was maintained as it increased the cytotoxic potential of the free inhibitor, and the synthetic exploratory lead optimisation process was guided towards the "linker anchor point". As described above, inhibitor **36** showed improved cytotoxic performance compared with the initial phenol-inhibitor **19**, setting the linker anchor point due to its effect on performance as a promising moiety for modifications. To achieve a deeper understanding of the effect of "linker anchor point" modifications and to keep exploring the effect of cell membrane permeability, inhibitors **62** and **68** were tested, whereby inhibitor **62** was more hydrophobic and inhibitor **68** was more hydrophilic than acrylamide-inhibitor **57**. Despite an expected higher partition coefficient, analysis of the cytotoxic potential of inhibitor **62** did not show an improved cytotoxic profile of the free inhibitor compared to inhibitor **57**. Additionally, efforts to conjugate inhibitor **62** with the Mal-Val-Ala-PAB linker were unsuccessful. Inhibitor **68** showed acceptable cytotoxic potential as a free inhibitor despite the expected lower cellular permeability. Additionally, inhibitor **68** showed outstanding yields in the condensation with the linkers, both making the compound promising. Nevertheless, the ADCs produced with linker-payloads **69** and **70** (based on inhibitors **68**), harnessing cleavable and non-cleavable linkers, respectively, were not active in the tested cells.

Modification of acrylamide-inhibitor **57** at the "aliphatic chain spacer" level led to the design of inhibitor **85** with an extended 6-C aliphatic chain against the 4-C length spacer in acrylamide-inhibitor **57**. Despite the greater synthetic effort, inhibitor **85** showed significantly lower cytotoxicity as a free inhibitor, leading to the abandonment of the project to produce payloads with longer aliphatic chain spacers and leading the discussion towards the reasons behind the significantly different performance of NAMPT inhibitors when applied as free compounds or as ADC payloads.

As discussed above, it was clear that despite the modifications of NAMPT inhibitors driven by the effect of synthetic reasons on the potency of the inhibitors, a common factor underpins the surprising lack of activity of ADCs loaded with NAMPT inhibitors. One common feature of all the tested NAMPT inhibitors was the significantly higher **hydrophobicity** of these molecules compared with other ADC payloads (e.g., MMAF or amanitin). This allows NAMPT inhibitors to internalise by passive diffusion across cell membranes, but it could also lead to suboptimal cytoplasmatic concentrations when deployed inside the cell from the ADC due to the higher partition coefficient. Additionally, hydrophobic payloads increase the risk of ADC

aggregation in circulation, especially at a high DAR (8 or 10), which could lead to faster clearance *in vivo*, as mentioned in the introductory chapters.[32]

Like most proteins, antibodies are exposed to aqueous buffers and media to obtain a stable, solvated globular tertiary structure. Therefore, hydrophilic amino acids are presented outwards on the surface of their folded structure. This gives the protein an overall hydrophilic outer layer, while the inner structure of the protein is significantly less hydrophilic, allowing hydrophobic interactions that contribute to the overall stability of the folded protein.[154] Additionally, proteins are highly dynamic systems. Hence, when the surface of the protein is heavily modified (e.g., by conjugation of a hydrophobic payload), the stability can be compromised, causing the protein to adapt its tertiary structure to the modifications.[32] In turn, one possibility is that the dynamics of the antibody may cause the conjugated hydrophobic payloads to be partially trapped inside the tertiary structure of the mAb to gain stabilisation. This may lead to poor linker cleavage by cathepsin B due to steric hindrance of the linker cleavage site, ultimately preventing the release of the inhibitor from the ADC. Therefore, a more hydrophilic payloads could grant better solvent exposure and hence access to the cleavage point, leading in theory to better payload release in cells. Thus, a hydrophilic PEG(4) analogue of payload **37** was produced (linker-payload **50**). The conjugation of the PEG(4)-containing linker-payload to trastuzumab was significantly improved compared to linker-payload **37**. DAR10 ADCs with excellent yield and low payload precipitation during conjugation were produced, likely as a consequence of improved solvation of the linker-payload due to the pronounced hydrophilicity of the PEG(4) linker-payload. Disappointingly, the newly produced ADC showed no improvement of *in vitro* efficacy. According to the literature, PEG(8) linker-payloads significantly improve the hydrophilicity of ADC payloads.[155] However, due to a poor yield during the chemical synthesis of a PEG(8) linker-payload (linker-payload **52)**, generation of the corresponding ADCs was not possible. Due to the lack of cytotoxicity of the PEG(4) linker-payload ADC T-DAR10-**50** and the synthetic problems, the approach with PEG(8) was abandoned.

Ruling out the idea of increasing the hydrophilicity of the linker-payload by increasing the hydrophilicity of the linker, a carboxylic acid containing NAMPT inhibitor (inhibitor **92**) was developed aiming to increase hydrophilicity of the inhibitor itself. Disappointingly, inhibitor **92** showed a significant lack of activity *in vitro*, probably related to the low cellular permeation by passive diffusion expected. Disappointly this lack of activity also applied to the performance of the linker-payload deployed in the cellular lysosome. This lack of activity of the ADC *in vitro* was explained after computational analysis of carboxylic acid-inhibitor **92**, which showed that the pKa of the carboxylic acid moiety was predicted to be 3.67, this means that most of the inhibitor was in the carboxylate form even at lysosomal pH. Thus, the inhibitor would show extreme hydrophilicity in ionised form, leading first to block the just released payload in lysosomal compartments upon cathepsin B linker cleavage of the linker and second to an inefficient binding to NAMPT. Because as shown in *in silico* docking studies with the inhibitor and NAMPT (see Figure **14** in Section **3.1.3.2**) the stabilisation of the high-charge density of the carboxylate moiety upon binding to the enzyme requires the “linker anchor point” section of the inhibitor to be solvated, which in turn forced the hydrophobic residues of inhibitor **92** to be in contact with the solvent, which accounts for the unfavourable interactions that led to an inefficient docking between inhibitor **92** and NAMPT.

In summary, several different NAMPT inhibitors were designed, synthesised, and *in vitro* tested as free inhibitors and as payloads for ADCs without any significant cytotoxic effect being observed in any of the produced ADCs. This reinforced the current trend of relying on biological reasons through enzyme docking virtual screenings as the go-to procedure for designing novel molecules with balanced chemical and bioactive properties. An iterative synthetic base approach for lead optimisation did not afford NAMPT inhibitor payloads suitable for use in ADC technology. In response, the molecular docking software Maestro (Schrödinger Inc) allowed in the next chapter a computationally aided lead optimisation process that afforded new optimised NAMPT inhibitors suitable for use in ADC technology.

3.2. Computationally aided design of NAMPT inhibitors

As concluded in the previous chapter, lead optimisation of NAMPT inhibitors by means of a synthetic-driven exploratory approach was not efficient. As the biological differences in the cellular metabolism of free NAMTP inhibitors against ADC-loaded linker-payloads are significantly different, the selection of chemical modifications with the intention of assuring cytotoxic active molecules when delivered by ADC technology was not trivial.

Since the 1980s, molecular docking approaches have been continuously developed, now allowing competitive and cheap alternatives to the classical synthetic driven, high throughput screening as strategies for discovering new inhibitors. Additionally, the development of imaging techniques such as X-ray diffraction and the analysis of protein-inhibitor co-crystals have allowed high-fidelity atomic-coordinates maps of the catalytic pocket to be obtained. This has opened up an effective and very reliable structure-based form of lead optimisation using the available hardware.[156,157] Access to computational methods allowed the explication of the biological results from section **3.1.4.5**, observed with carboxylic acid **92**. Carboxylic acid **92** was the last analogue, where modification was solely driven by a synthetic exploratory rationale based on biochemical knowledge and literature research but without incorporating computationally aided docking methods, as observed in section **3.1.3.2.**

Therefore, new generations of free NAMPT inhibitor families were designed by *in silico*-driven molecular docking, and promising candidates were synthesised. The new compounds primarily aim to improve the hydrophilic character by using modifications of aniline **36** at the "linker anchor point" and "core ring" levels. Free inhibitor **36** was chosen as the lead candidate for computational docking optimisation by means of Maestro software (Schrödinger. Inc). As compared to the analogues synthesised in the previous sections', aniline inhibitor **36** showed ease synthesis and high potency as free inhibitor. Additionally, a new *in vitro* model with the L540 $CD30^+$ cell line was explored, which showed outstanding performance for free and ADC-loaded NAMPT inhibitors, leading to subcutaneous and disseminated *in vivo* mouse xenograft model testing of the ADCs. The *in vitro* and *in vivo* data demonstrated improved performance for the newly generated inhibitor **94** compared to the inhibitor **36**. Additionally, new lead optimisation campaigns based on inhibitor **94** were performed, seeking to improve the lysosomal stability of the NAMPT inhibitors in order to improve the lysosomal resistance of the inhibitors released from ADCs.

3.2.1. In silico-driven optimisation to reduce passive diffusion of NAMPT inhibitors through cellular membranes

Starting with inhibitor **36** as a template for lead optimisation, two molecular analogues obtained from docking were synthesised based on their significantly more hydrophilic character compared to inhibitor **36** and their ability to not be ionised in the cellular medium. Briefly, the structures of NAMPT inhibitors were studied using molecular dynamics methods to determine conformers with minimal energy in a pH range between 2 and 8. Then, docking of the minimised conformers to five pre-calculated NAMPT catalytic pocket grids was performed using the molecular dynamics-based glide docking strategy. The pocket grids were obtained from experimental X-ray diffraction data for five PDB published inhibitor-NAMPT cocrystals. The resulting docking scores were compared with the docking scores of the parental compounds **36**.

Inhibitors **94** and **105** were selected for their favourable docking abilities and hydrophilicity (Figure **25A**). Based on theoretical calculations of the LogP-value, the hydrophilicity of **94** and **105** was 14 and 35 times higher, respectively, than that of aniline inhibitor **36**. The docking scores for the tertiary alcohols **94** and oxime **105** (-7 and -8, respectively) were close to the calculated score of -8.1 for reference inhibitor **36**, suggesting promising binding to NAMPT. Considering both docking scores and the previously reported advantageous physicochemical properties of the new payloads **94** and **105**, they were leading candidates for the *in-silico* optimisation campaign.

In the case of inhibitor **94**, docking results showed that the introduced hydroxy group modification interacts with a polar groove of NAMPT catalytic pocket where stabilisation by hydrogen bond with the histidine 191 of the enzyme was observed, as shown in Figures **25B** (3D model showing the polar groove) and **25C** (top view of inhibitor **94** showing all the favourable interactions between inhibitor and NAMPT). However, the measured length of 2.3 Å for this intermolecular interaction is shorter than the average length interval of 2.7–3.3 Å reported for stable H-bond formation,[158] suggesting that the variation of free energy associated with H-bond formation may be lower than expected. In the case of oxime inhibitor **105**, the π-π stacking interaction between the pyridyl moiety and Phe193 and Tyr18 of NAMPT as well as the hydrogen bond between the aniline unit of the inhibitor and amino acid Glu376 of the enzyme are preserved (Figure **25D**). Both interactions are reported as key interactions between inhibitor and NAMPT.[122]

In addition, these computational studies showed that to increase the hydrophilicity of the molecule, it was important to select not only the polar group as a modifier but also its position in the molecule. In the case of designed tertiary alcohol **94** and oxime **105** inhibitors, modifications at the "core ring" level of the molecule resulted in their being particularly effective for increasing hydrophilicity. This may be due to the fact that the "core ring" separates the solvent-exposed section of the molecule from the more hydrophobic aliphatic spacer. Accordingly, increasing the hydrophilicity at this point of the NAMPT inhibitor extended the more hydrophilic character through the molecule, while modifications at any of the two ends of the inhibitor were expected to have a lower effect in terms of hydrophilic character.

A)

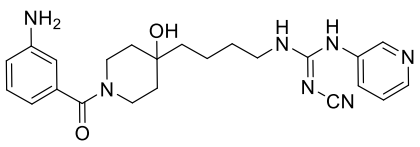

Chemical Formula: $C_{23}H_{29}N_7O_2$
Molecular Weight: 435.53
LogP = 0.71
Inhibitor 94

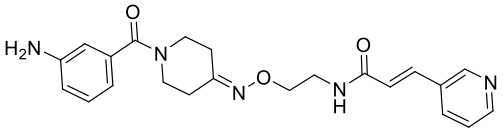

Chemical Formula: $C_{22}H_{25}N_5O_3$
Molecular Weight: 407.47
LogP = 0.29
Inhibitor 105

B)

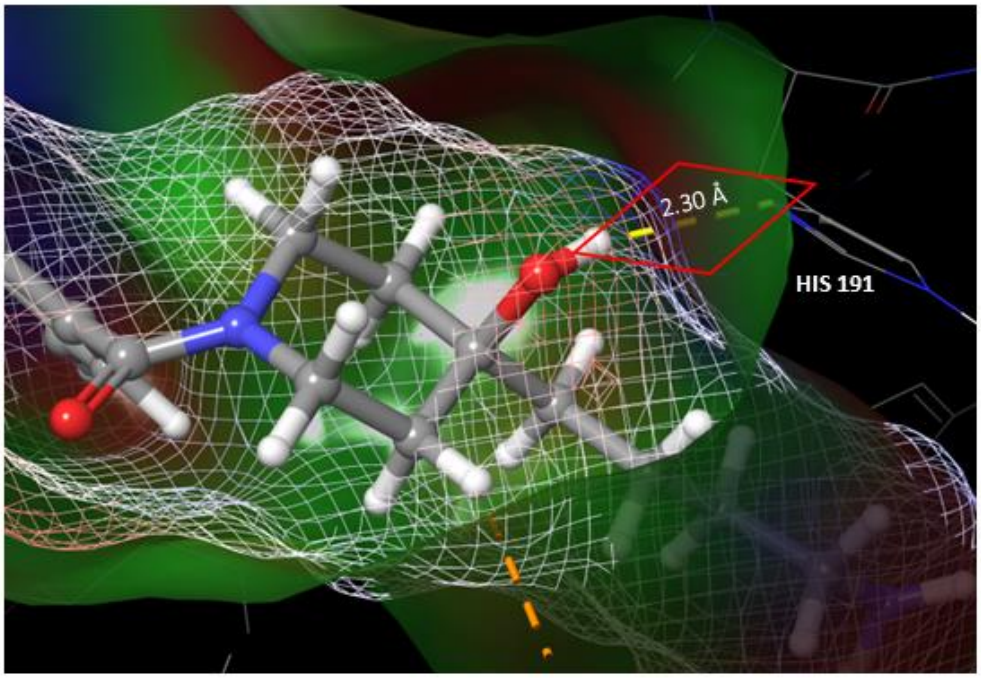
2.30 Å
HIS 191

C)

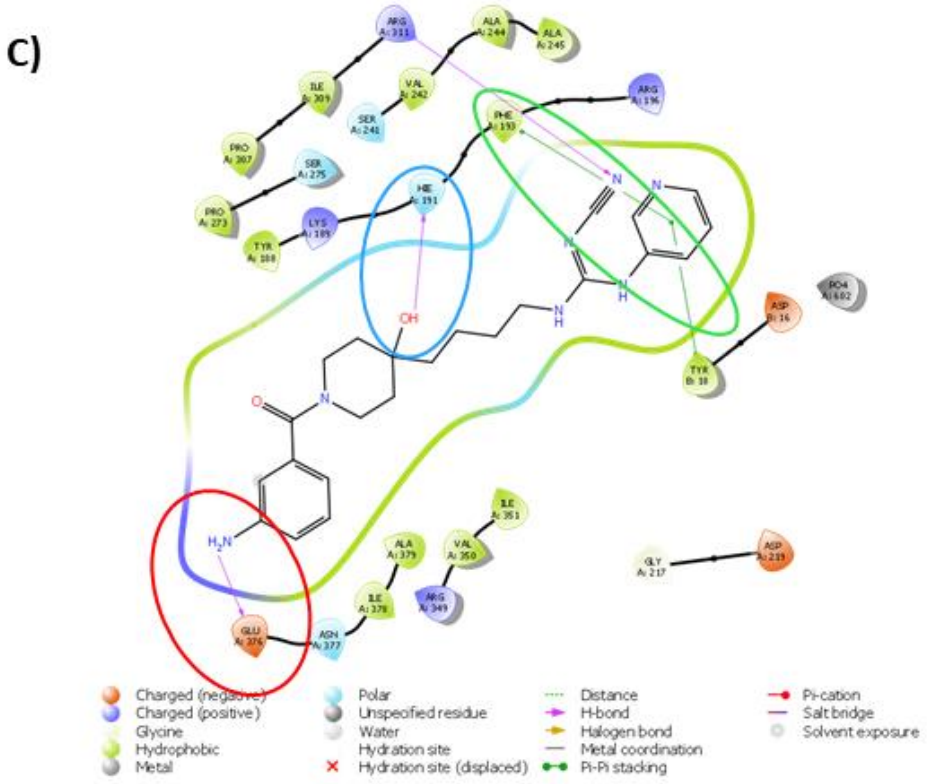
Charged (negative)
Charged (positive)
Glycine
Hydrophobic
Metal
Polar
Unspecified residue
Water
Hydration site
Hydration site (displaced)
Distance
H-bond
Halogen bond
Metal coordination
Pi-Pi stacking
Pi-cation
Salt bridge
Solvent exposure

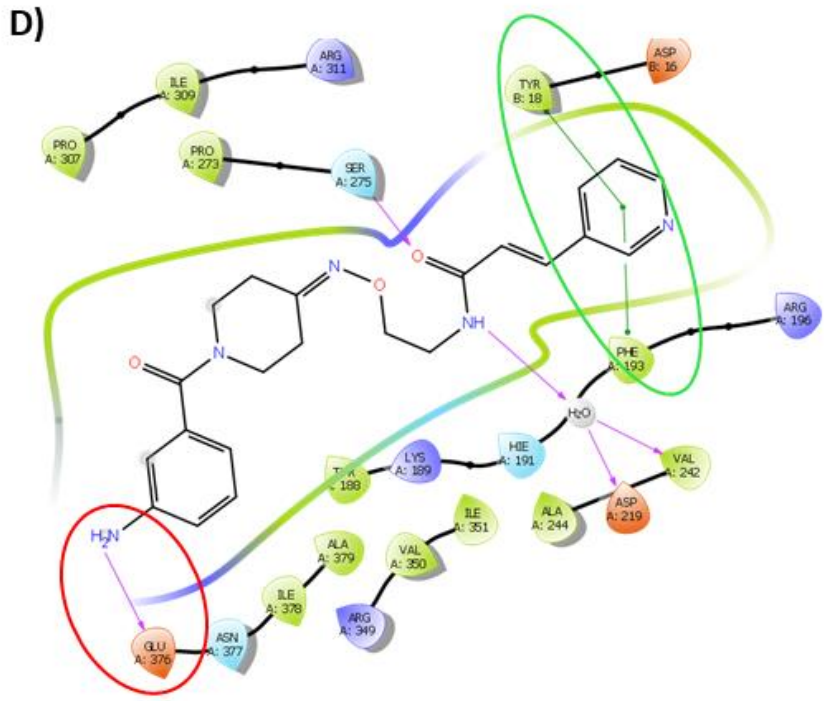

Figure 25. A) Inhibitors **94** and **105** with LogP values; B) 3D model of tertiary alcohol payload **94** docked in NAMPT (structure PDB 4O13); red diamond encloses hydroxy modification in polar cave of the catalytic pocket, establishing H-bond with His191, length 2.3Å. Grid surface corresponds to space occupied by NAMPT inhibitor Van der Walls atomic radius representation. Blurred surfaces represent the catalytic pocket silhouette as a result of representing the atomic radius of NAMPT catalytic pocket residues; C) Interaction diagram of tertiary alcohol payload **94** with NAMPT; D) Interaction diagram of oxime payload **105** with NAMPT. Figures C and D maintain the already described key interactions of inhibitors with NAMPT, π-π stacking between "NAD^+ mimicking moiety" of the inhibitor and Phe 193 and Tyr 18 of NAMPT circled in green, as well as H-bond at the "linker anchor point" level of the inhibitor and Glu376 of the enzyme, circled in red.[122] Additionally, tertiary alcohol payload **94** features at the "core ring" level a new stabilising H-bond interaction between the tertiary alcohol and His 191 of the enzyme, circled in blue.

3.2.2. Synthesis of payloads **94** and **105** and linker-payloads **97** and **110**

From a synthetic point of view, inhibitor **94** was obtained in an eight-step synthesis (Scheme **10a**). The initial approach involved a Wittig reaction (not shown) that was changed by a successful synthetic process involving a Grignard reaction. Despite initial problems in the Grignard reaction related to side reactions leading to the generation of the desired intermediate **53** at only a very low yield (≤ 5%), a good compromise between reaction time and yield was ultimately found. In this approach, the reaction temperature was lowered to 8 °C, and the intermediate complex of the easily enolisable 4-piperidone with the magnesian was stabilised by $LaCl_3$ as reported in the work of Knochel *et al.*,[159] resulting in an increased yield of 47 % (Scheme **10A**).[160] Amine **71** as intermediate was formed by reductive amination of aldehyde **55**. The reductive amination to generate amine **71** was tested under various conditions, including reaction with concentrated ammonia and different pH conditions. Finally, the reaction conditions promoted by ammonium acetate and $NaCNBH_4$ at pH 6 were deemed optimal since amine **71** was produced faster and with higher conversion under such conditions. A possible explanation is that the protonation at pH 6 of the intermediate imine leads to the formation of the iminium ion, which is very reactive to mild reducing agents as $NaCNBH_4$.[161] Synthesis of inhibitor **94** was continued by an addition-elimination reaction between amine **71**

and phenyl *N*-cyano-*N*'-3-pyridinylcarbamimidate, yielding intermediate **75** in a moderate yield of 40 %. Next, after benzyloxycarbonyl deprotection by Pd-catalysed hydrogenation, amide **78** was afforded by DCC/HOBt-mediated coupling of piperidine **77** and benzoic acid **30** at a moderate yield of 37 %. Inhibitor **94** was then accessed by Pd catalysed hydrogenation of the benzyloxycarbamate group in a high yield of 80 %.

The synthesis of inhibitor **105** followed an eight-step approach (cf. Scheme **10b**). Starting from commercially available *tert*-butyl-*N*-hydroxycarbamate and *N*-(2-bromoethyl)phthalimide, intermediate **95** was afforded by an SN_2 reaction in an acceptable yield of 55 %. Then, amine intermediate **96** was afforded from intermediate **95** by hydrazinolysis in an acceptable yield of 50 %. Next, intermediate **98** was synthesised at moderate yield of 35 % by condensation between amine **95** and *E*-3-pyridil acrylic acid in a reaction assisted by DCC/HOBt followed by Boc deprotection in diluted TFA/DCM solution to afford hydroxylamine **99** in a very good yield of 83 %. Next, Oxime bond is synthetised between commercially available Boc-4-piperidone and hydroxylamine **99** under sodium acetate mild basic conditions, affording with a good 70% yield Boc-protected oxime **100**, that followed Boc deprotection under TFA acid conditions in order to afford in good 71% yield oxime **101**. Then, DCC/HOBt-assisted condensation of piperidine **101** and commercially available Boc-3-aminobenzoic acid resulted in intermediate **102** at an acceptable yield of 35 %, which was Boc deprotected in diluted TFA/DCM solution to yield with excellent yield oxime **105**. Next, the corresponding linker-payloads **97** and **110** with cathepsin B-cleavable Val-Ala-PAB linkers, respectively, were synthesised by carbamate formation between the nitrophenyl carbonate-activated Mal-Val-Ala-PAB linker and NAMPT inhibitors **94** and **105**, respectively (Schemes **10A** and **10B**).

A)

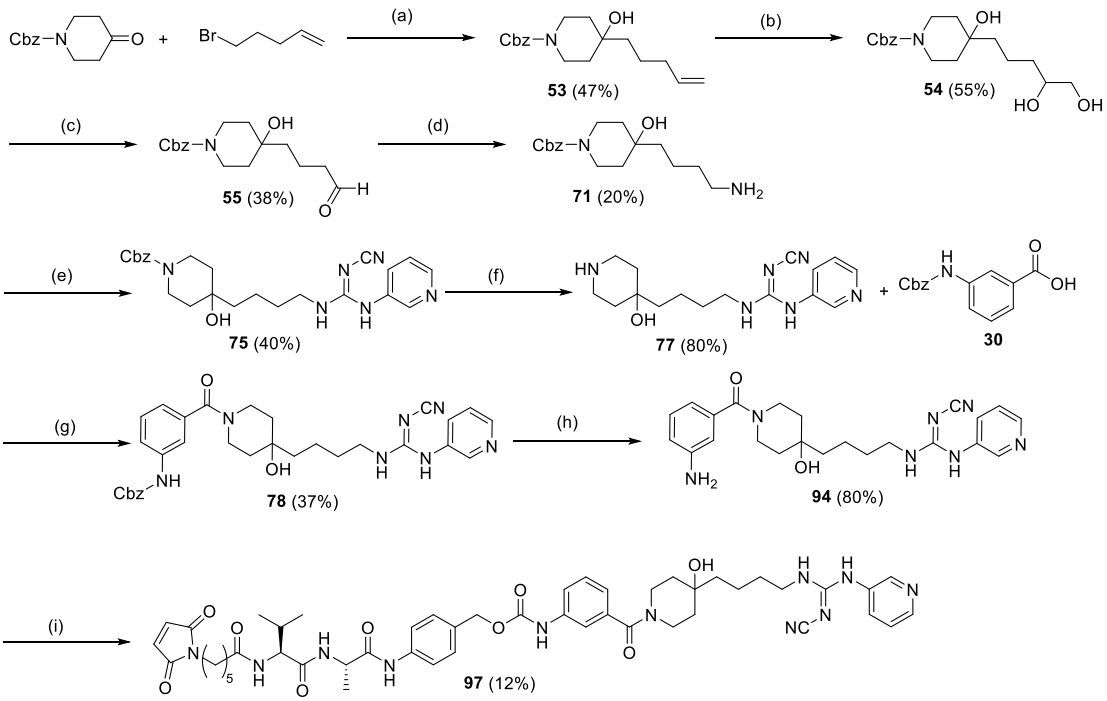

B)

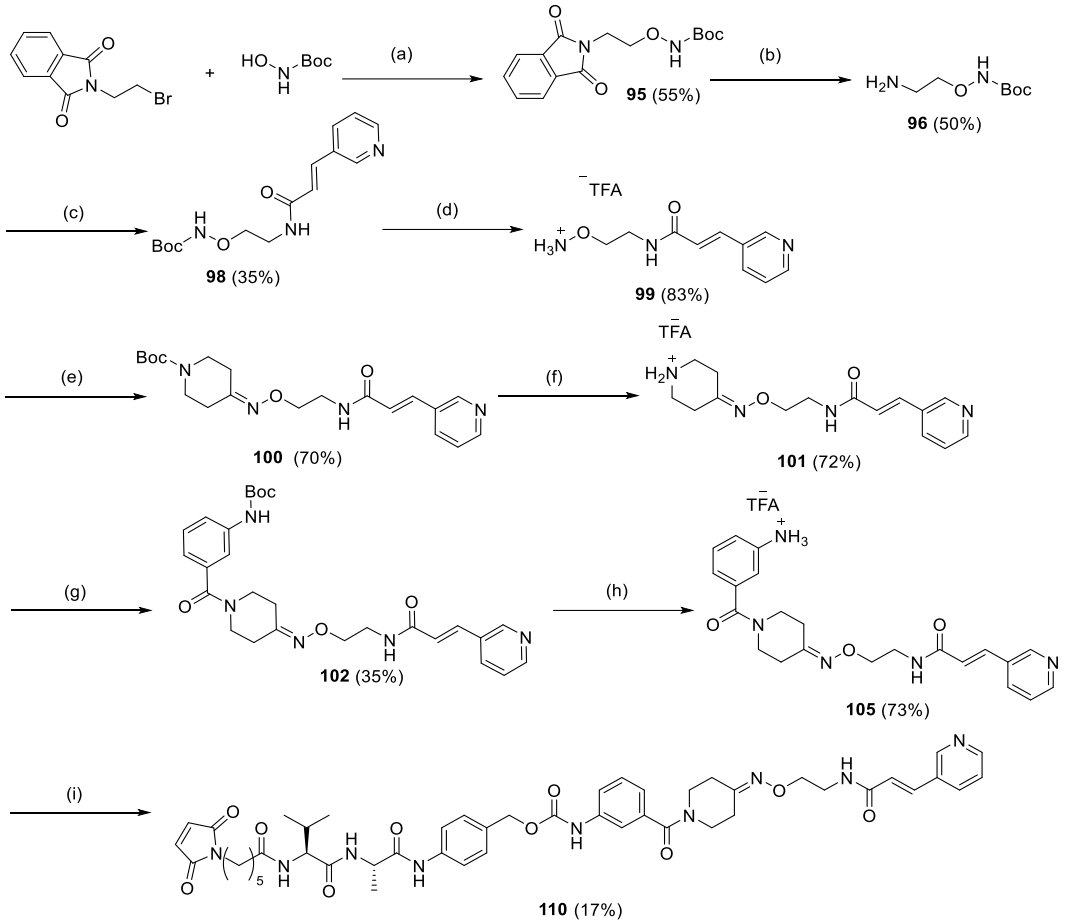

Scheme 10. Synthesis scheme (**correct also position in scheme**) of **A)** Tertiary alcohol payload **94** and linker-payload **97**. Reagents and conditions: (a) Mg, $LaCl_3$-LiCl, THF (abs.), 8 °C, overnight; (b) OsO_4 (cat), *N*-methyl morpholine *N*-oxide (NMO), H_2O, acetone, r.t, overnight; (c) $NaIO_4$, THF/H_2O (2:1), 0 °C, 30 min; (d) ammonium acetate (pH = 6), $NaCNBH_4$, MeOH (abs.), r.t, 4.5 h; (e) Phenyl *N*-cyano-*N*'-3-pyridinylcarbamimidate; Et_3N; 1,4-dioxane; r.t., overnight; (f) H_2, Pd/C, EtOH/EtOAc (1:1), r.t., overnight; (g) DCC/HOBt, DIPEA, DCM (abs.); r.t., overnight; (h) H_2, Pd/C, EtOH/EtOAc (1:1), r.t., 4 h; (i) Mal-Val-Ala-PAB-PNP, PyAOP, DIPEA, DMF (abs.), r.t., overnight. **B)** Oxime containing payload **105** and linker-payload **110**. Reagents and conditions: (a) tert-butyl *N*-hydroxycarbamate, K_2CO_3, *N*-(2-bromoethyl)phthalimide, DMF, r.t., 3 h; (b) Hydrazine monohydrate, EtOH, r.t., 5 h; (c) (*E*)-3-piridyl-acrylic acid, DCC/HOBt, DIPEA, DCM (abs.); r.t., overnight; (d) 15% TFA in DCM, r.t., 2 h; (e) Boc-piperid-4-one, NaOAc, EtOH, r.t., 6 h; (f) 15% TFA in DCM, r.t., 2 h; (g) Boc-3-aminobenzoic acid, DCC/HOBt, DIPEA, DCM (abs.), r.t., overnight; (h) 15% TFA in DCM, r.t., 2 h; (i) Mal-Val-Ala-PAB-PNP, PyAOP, DIPEA, DMF (abs.); r.t., overnight.

3.2.3. Comparative study of glucuronic acid-containing linkers against cathepsin B-cleavable linkers and synthesis of linker-payloads **108** and **109**

Dipeptide linkers cleaved by cathepsin B are widely used in the ADC field. However, a drawback of this linker is that it does not significantly increase the hydrophilicity of the linker-payload when hydrophobic payloads are used. Hence, other families of cleavable linkers have been developed, highlighting sugar-containing linkers such as glucuronic acid. These linkers significantly increase the hydrophilic character of the linker-payload and improve the conjugation process to antibodies by a drastic reduction of aggregations.[162] Moreover, they are used to explore new enzymatic cleavage mechanisms since glucuronide-containing linkers are selectively cleaved by glucuronidases, as reported in the introductory chapter.[162]

Therefore, two new linker-payloads containing NAMPT inhibitors **36** and **94** as payloads and glucuronidase-cleavable linkers were synthesised and conjugated to a Brentuximab-based antibody. Next, a comparative cytotoxicity study compared the new payloads against the performance of ADCs loaded with cathepsin B cleavable linker payloads **37** and **97**.

The glucuronide-containing linker-payloads were synthesised starting from a purchased *N*-Fmoc-*O*-Ac-glucuronic acid-PAB-PNP as the final intermediate of the linker.[153]

The synthesis involved the condensation of the inhibitor with the linker, helped by PyAOP, followed by acetyl and Fmoc deprotection, which was achieved by treating the intermediates with a LiOH/MeOH solution at excellent yields. Afterwards, the maleimide head was incorporated by direct condensation with N-ε-malemidocaproyl-oxysuccinimide ester (EMCS); this yielded linker-payloads **108** and **109** (bearing inhibitors **36** and **94,** respectively) at good yields (cf. Scheme **11**).

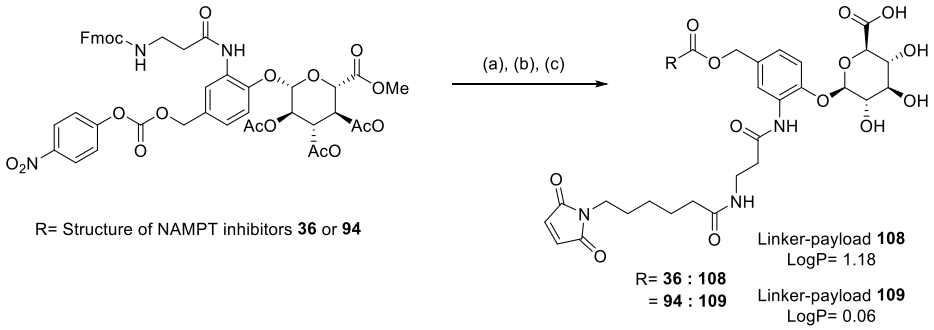

Scheme 11. Reaction scheme of glucuronic acid containing linker-payloads **108** and **109**, including LogP values. Reagents and conditions: (a) **36** or **94**, *N-Fmoc-O-Ac-glucuronic acid-PAB-PNP*, PyAOP, DIPEA, DMF, r.t., overnight leading to intermediates **103** (10 %) and **104** (11 %), respectively; (b) (I) LiOH, MeOH, r.t., 15 min; II) Piperidine absolute, r.t., 30 min leading to intermediates **106** (60 %)and **107** (58 %), respectively; (c) EMCS, DIPEA, DMF, r.t., 15 min leading to linker payloads **108** (50 %) and **109** (51 %), respectively.

3.2.4. Assessing the chemical stability of cyanoguanidine-containing inhibitors: Isolation and identification of the main degradation compound

This section focuses on the chemical synthesis of possible degradation compounds of the inhibitor cyanoguanidine **36** as a first step towards understanding the mechanisms of lysosomal degradation of NAMPT inhibitors containing cyanoguanidines. Chemical approaches were faster and less expensive than biological assays for this purpose, and they allowed the production of a sufficient amount of degradation products for characterisation, testing in cells, and use as a reference compound in analytical techniques.

Previous studies have shown that the cyanoguanidine group contained in NAMPT inhibitors such as **36** and **94** tend towards hydration and degradation at pH values below 2, leading to the formation of guanylurea intermediates.[129] Since the lysosomal pH is acidic and contains numerous hydrolases, NAMPT inhibitors bearing cyanoguanidines may therefore be degraded in the lysosome. Hence, the guanylurea **113** as hydration product of inhibitor **36** was chemically synthetised as a reference standard. The acid hydration reaction involving TFA was performed (Scheme **12**). At pH values above 2 (after 48 hours at 37°C), the reaction did not occur. However, at pH values below 2, the expected guanylurea **113** was obtained in excellent yield and with minimal side products within 24 hours at 37°C when TFA was used as the acid.

3. Results and Discussion

The product was confirmed by mass spectrometry and NMR analysis. Due to the high activation energy required for the generation of the postulated rate-limiting intermediate *O*-trifluoroacyl isourea, a low pH was likeliest required based on the fact that the intermediate carbodiimide loses the resonance stabilisation typical of the guanidine group. Consequently, the equilibrium of the rate-limiting step **A** must shift towards the *O*-trifluoroacyl isourea formation to make the reaction kinetically favourable (Scheme **12**). In addition, the second protonation in step **C** was not favoured, supporting the experimental results of the low pH required for the reaction to proceed. *In silico* docking studies of guanylurea **113** showed significantly poorer performance compared to the parental compound inhibitor **36** (cf. Figure **26**). The major interactions between the NAMPT inhibitor and the enzyme's catalytic pocket were completely absent, indicating that the inhibitor exposes the NAD-mimicking component to the solvent. Therefore, the guanylurea **113** would likely exhibit significantly poorer docking with NAMPT. Aiming to measure the binding capacity of the guanylurea inhibitor to the enzyme by BLI measurements, the guanylurea **113** was condensed with biotin by activation with HATU under basic conditions to synthesise the biotinylated guanylurea **121** at excellent yield.

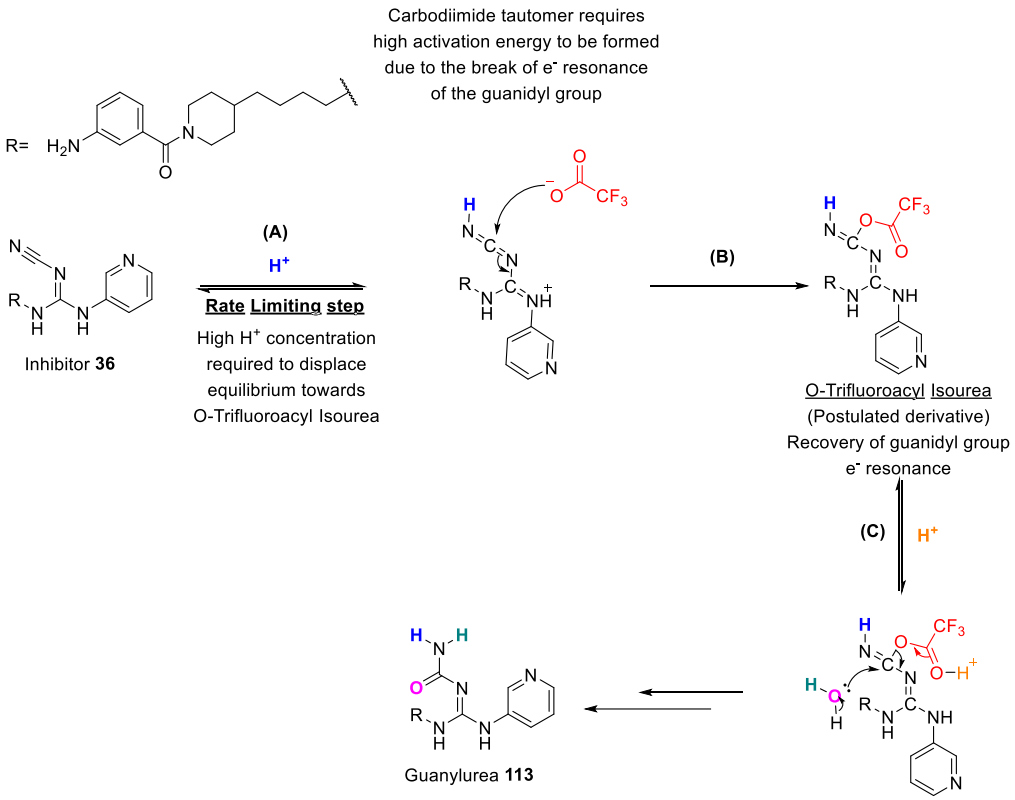

Scheme 12. Mechanistic approach to the hydration of inhibitor **36** to inhibitor **113**, aiming to explain why a significantly lower pH is required for the reaction, including postulated intermediate compounds.

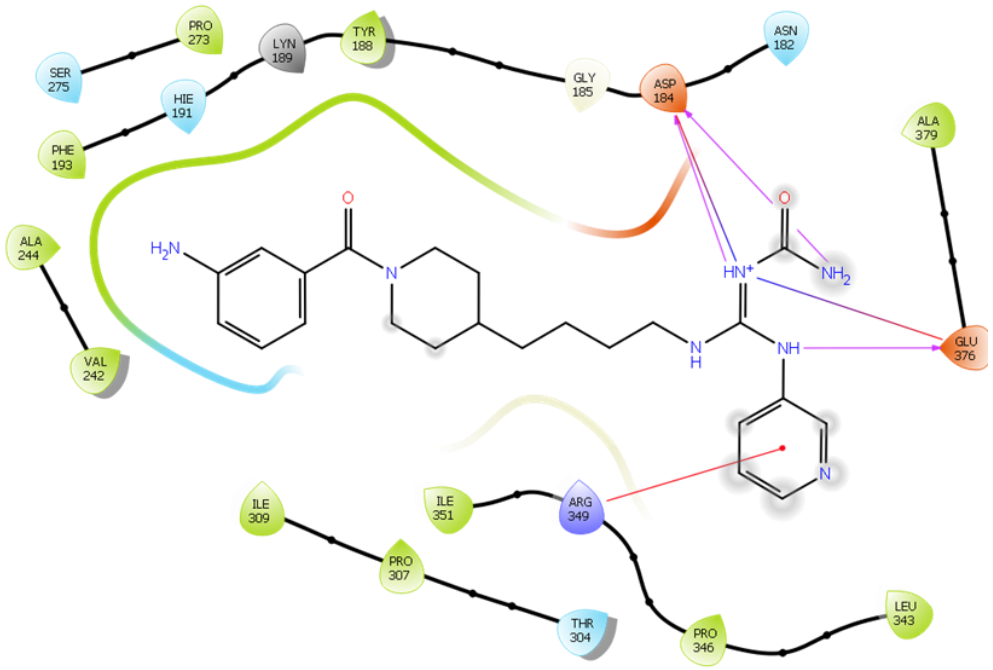

Figure 26. In silico study of cyanoguanidine **113** as a putative lysosomal degradation product of NAMPT inhibitor **36** showed no docking. Interaction diagram with NAMPT enzyme (PDB: 6E68). The lack of π-π stacking can be seen at the pyridine level.

3.2.5. Development of lysosome-resistant NAMPT inhibitors for ADC applications

3.2.5.1 Lysosome-resistant NAMPT inhibitor design: *In silico* approaches

To obtain lysosomal-proof NAMPT inhibitors, a computationally aided database of molecules followed by virtual screening of the database to NAMPT catalytic pocket generated grids were used to identify a suitable substitution for the cyanoguanidine group that was resistant to lysosomal degradation while maintaining significant binding to NAMPT. Initially, it was considered to replace the cyanoguanidine group with an urea or a thiourea group, since both are theoretically resistant to the lysosomal hydration process described in Section **3.2.13** and have been used as NAMPT inhibitors in the literature.[163,164] However, during the first docking, it was found that the urea moiety gave better results than the thiourea (data not shown).

Despite the docking results of the initial urea-containing hit shown in Figure **27A**, using a pyridine-based NAD-mimetic moiety showed similar scores to those of cyanoguanidine **36**. The goal of the new NAMPT inhibitors was to achieve stronger binding to the enzyme and, at the same time increased stability in cellular compartments. Therefore, further optimisation was pursued. Interestingly, the 3D docking diagrams showed that a replacement of the cyanoguanidine group with a urea moiety resulted in bending in a slight shift of the molecule in the catalytic pocket compared to the reference docking of cyanoguanidine **36**. [122] In light of the previous results, it was hypothesised that the driving force to improve binding to the NAMPT enzyme relied on optimising docking interactions at the level of the "NAD^+ mimicking moiety", since this part of the molecule is reported to be one of the major binding contributors.[122]

To optimise the binding of the inhibitor to NAMPT, replacement of the pyridine moiety with an isoindoline group was considered. Previous studies have shown that incorporation of an isoindoline moiety into NAMPT inhibitors could improve their efficacy.[164] It was expected that this change would improve the stabilisation of the π-π stacking interaction between the enzyme and the inhibitor because the aromatic systems of the inhibitor and the enzyme (Tyr18 and Phe191) would be offset from each other. This offset is advantageous since it allows the negative π-cloud over the C atoms of the aromatic rings to be stabilised by the positive density region around the hydrogen atoms of the isoindolin aromatic system. [165] After docking, the isoindoline modification demonstrated a more pronounced offset with the NAMPT amino acids than their pyridine counterparts. This was indicated by the smaller angle between the centroids, which are virtual centres of the aromatic system symbolised as cyan dots in Figure **27A** and **B**. A 180-degree angle would indicate perfect alignment between the aromatic systems and thus repulsive stacking; the smaller angle reflects less repulsive stacking and thus a better docking score. Nevertheless, it was still believed that the molecule could be further optimised because the measured lengths for the π-π interaction of the isoindoline inhibitor were too long to ensure effective stabilisation (≥ 4 Å). As mentioned earlier, π-π stacking is a low-energy, intermolecular, non-covalent interaction that occurs only at very short distances of around 2 Van der Waals radii of the larger atom involved in the interaction. In this case, the largest atom involved is a carbon with a Van der Waals radius of 1.7 Å. Hence, the ideal distance would be around 3.4 Å.[166] Since manual fine-tuning of the molecule to achieve a shorter distance in the π-π stacking was beyond capabilities, a 3000-compound database was created by automated compound enumeration with the Maestro software. Here, the isoindoline-urea hit was used as the initial molecule, and the urea and isoindoline moieties were locked to prevent modifications by the software. The database was then virtually docked to the previously generated grids, and the five highest scoring molecules were selected (cf. Figure **27C**). Among them, isoindoline-urea **124** as hit number one was selected due to its better docking score compared to the other five hit molecules selected. This was consistent with the shorter distance between centroids calculated for isoindoline-urea **124**. In addition, inhibitor **124** was selected due to its simpler synthetic access, which was a necessary consideration due to time constraints.

A) Docking inhibitor **36** and NAMPT (PDB: 6E68)

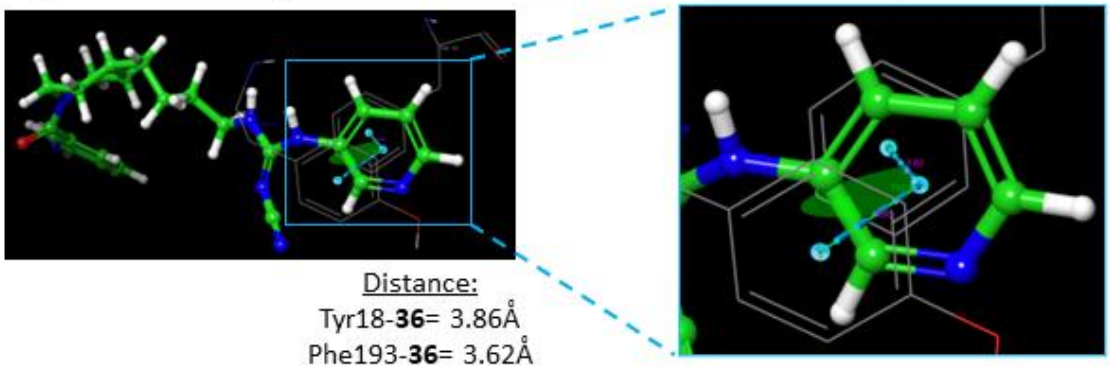

Distance:
Tyr18-**36**= 3.86Å
Phe193-**36**= 3.62Å
Angle between centroids: 150.5°
Docking score: -8.2

Docking Urea-pyridine hit and NAMPT (PDB: 6E68)

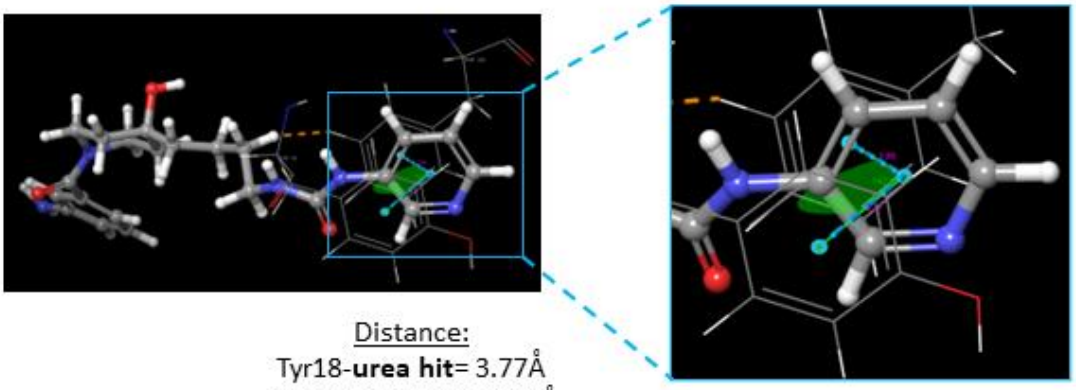

Distance:
Tyr18-**urea hit**= 3.77Å
Phe193-**urea hit**= 3.86Å
Angle between centroids: 142.5°
Docking score: -8.3

B) Docking isoindoline-aniline and NAMPT (PDB: 6E68)

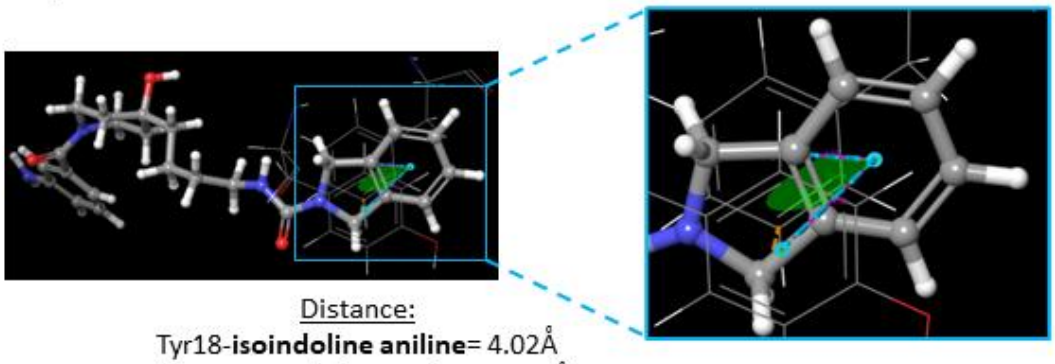

Distance:
Tyr18-**isoindoline aniline**= 4.02Å
Phe193-**isoindoline aniline**= 4.07Å
Angle between centroids: 126.8°
Docking score: -9.9

C)

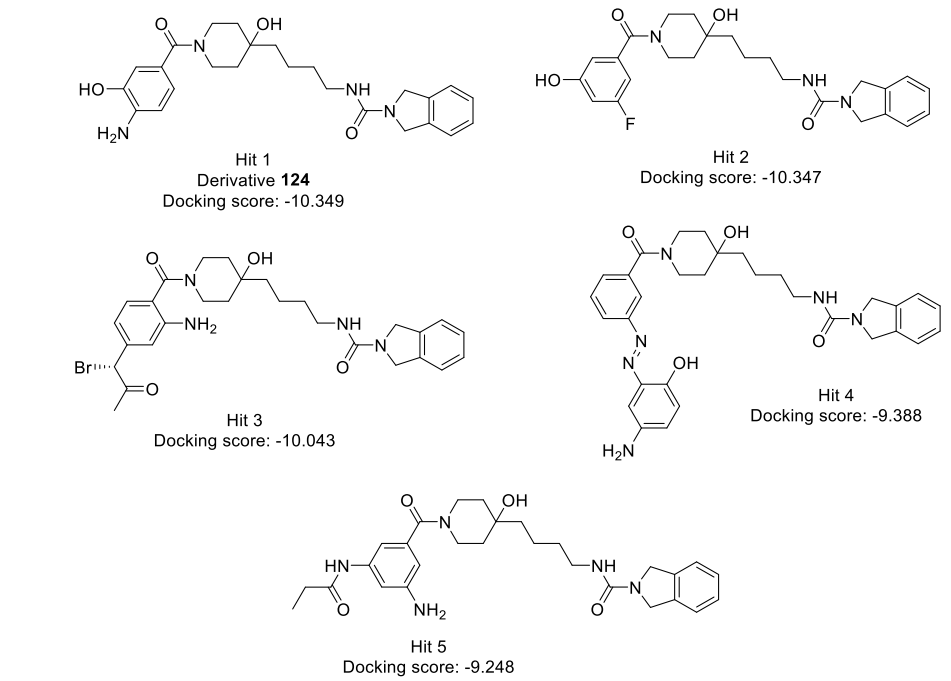

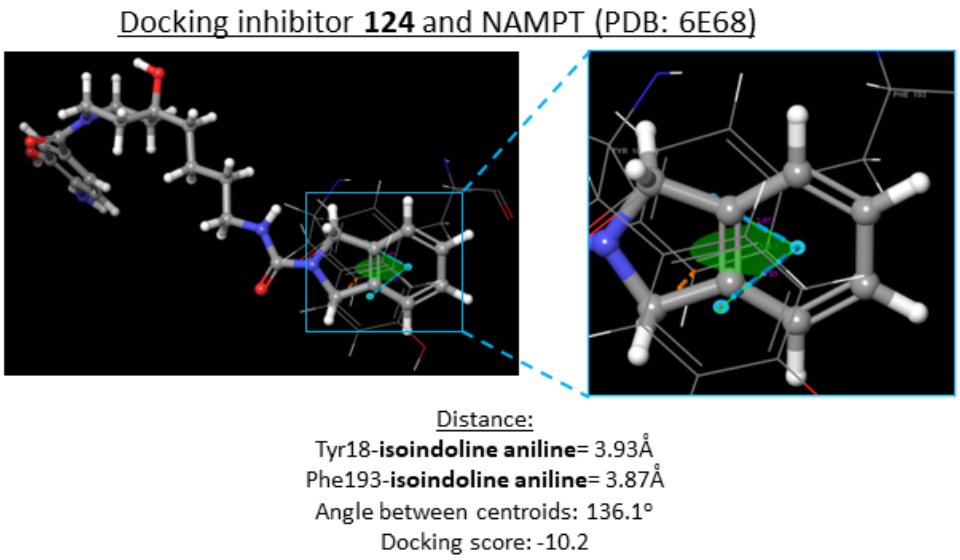

Figure 27. *In silico* optimisation for the lysosomal proof inhibitor: A) Initial urea hit molecule compared with cyanoguanidine **36**; B) Isoindoline-aniline initial hit used as starting molecule for the database generation by means of modifications guided by compound enumeration algorithms. This hit showed improved docking due to a more acute angle between centroids but still a long distance between π-π stacking implicated groups; C) Database screening of the five best hits and inhibitor **124** (hit 1) π-π stacking interaction close up, showing better docking due to reduced interaction distance and improved acute angle between centroids. Inhibitor **124** was chosen to be synthesised.

3.2.5.2 Synthesis of inhibitor **124**

Isoindoline-urea **124** was a promising inhibitor obtained by molecular docking (cf. Section **3.2.5.1**). The synthesis of this inhibitor **124** started with the formation of amine **117.** Starting from commercially available *N*-Boc-piperidone and 5-Br-1-pentene, the Grignard synthesis yields tertiary alcohol intermediate **114** in an acceptable yield of 50 % (Scheme **13B**, step (a)). The alkene moiety of intermediate **114** was further derivatised by osmium tetroxide-catalysed diol formation, obtaining intermediate **115** in good yield of 66 %. Aldehyde **116** was then afforded by mild metaperiodate oxidative cleavage of the diol. The aldehyde **116** was further transformed to amine **117** at a low 12% yield under sodium cyanoborohydride/ammonium acetate reductive amination conditions (cf. Scheme **13B**, step (d)). Next, urea **119** was synthetised from nitrophenyl-activated carbamate **118** (Scheme **13B**, step (e)), which in turn was obtained by direct carbamate formation between the commercially available reagents isoindoline and bis-*p*-nitrophenyl carbonate at an excellent yield 90 % (S. The formation of urea **119** takes place by an addition-elimination mechanism similar to the one described by Kim *et al* in their approach to synthetise asymmetric urea using trichloroethyl carbamates, aliphatic amines and catalytic amounts of DBU.[167] Although the nitrophenyl-carbamate **118** was successfully obtained, the synthesis of the mixed urea **119** showed low reactivity, probably due to the high stability of the carbamate precursor **118**. In this precursor **118**, the nitrogen from the carbamate bond reduces the electrophilic character of the carbonyl moiety due to its electron-donating effect. The reactivity was improved using *N*-methyl-imidazole (NMI), which allowed for the synthesis of mixed urea **119** in a low yield of 8 %. Then the final inhibitor **124** was obtained as a results of Boc deprotection of urea **119**, affording intermediate **122** in 80% good yield, then, DCC/HOBt assisted coupling with intermediate **120**, afforded Boc protected amino alcohol **123** in acceptable 30% yield. Finally, Boc deprotection under acidic conditions led to inhibitor **124** in good 65% yield.

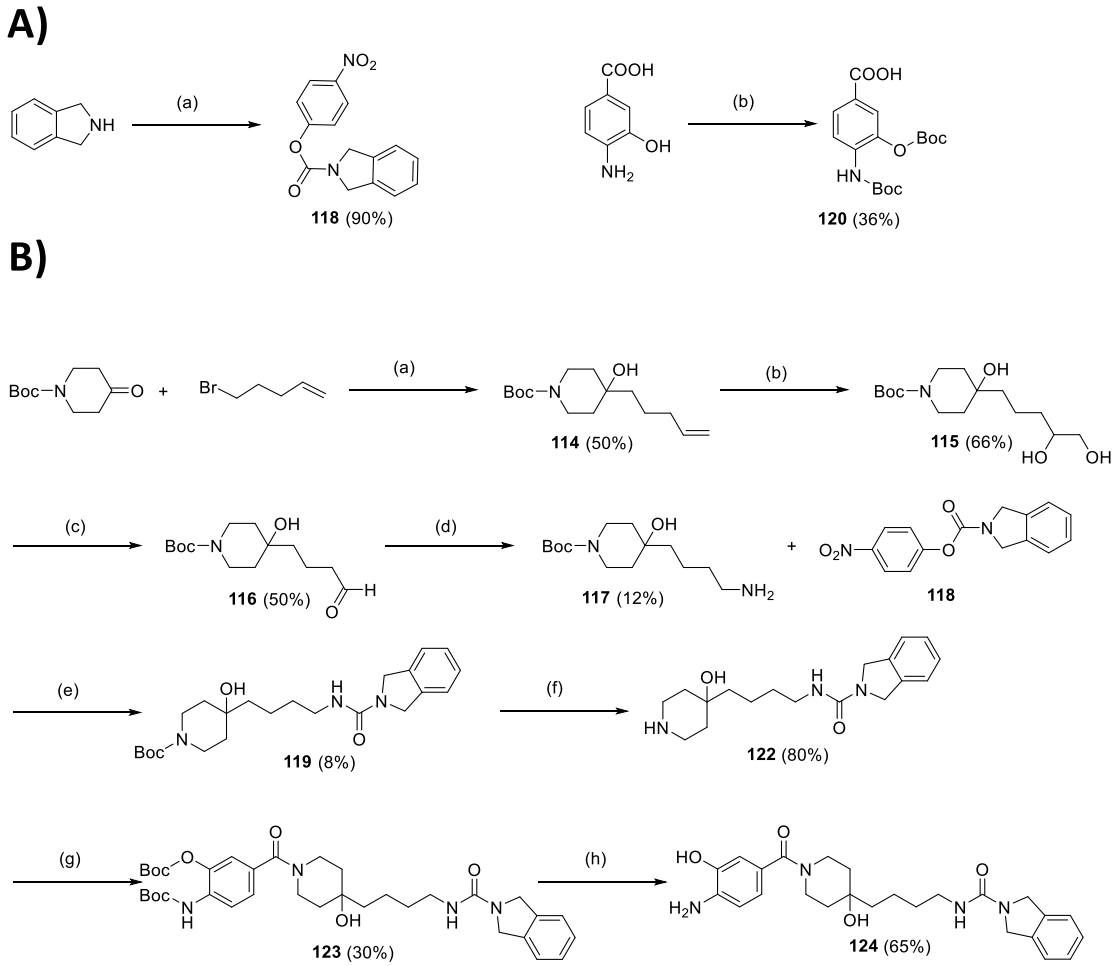

Scheme 13. A) Synthetic scheme of precursors of payload **124**. PNP-activated isoindoline intermediate **118** and Boc-protected 3-hydroxy-4-aminobenzoic acid **120**. Reagents and conditions: Synthesis of intermediate **118**: (a) bis-*p*-nitrophenyl carbonate, DIPEA, DMF (abs.), r.t., 30 min. Synthesis of intermediate **120**: (b) Boc anhydride, Et_3N, DCM (abs.), r.t., overnight. **B)** Synthetic scheme of urea-isoindoline payload **124**. Reagents and conditions: (a) Mg, $LaCl_3$-LiCl, THF (abs.), 8 °C, overnight; (b) OsO_4 (cat), NMO, H_2O, acetone, r.t., overnight; (c) $NaIO_4$, THF/H_2O (2:1), 0 °C, 30 min; (d) ammonium acetate, $NaCNBH_4$, MeOH (abs.), r.t., 4.5 h; (e) DIPEA, *N*-methylimidazole, DMF (abs.), r.t., 3 weeks; (f) 20% TFA in DCM, r.t., 40 min; (g) **120**, DCC, HOBt, DIPEA, DMF (abs.), r.t., 1 h; (h) 20% TFA in DCM, r.t., 20 min.

It is worth mentioning that the optimised results obtained with NMI (cf. Table **6**) may be related to its pKa of 6.95, meaning that the reagent may simultaneously act as an acid and base catalyst. Considering that the reaction to form the mixed urea **119** is classified as an addition-elimination mechanism involving the elimination of *p*-nitrophenolate in a basic medium as a good leaving group, the mechanism of the reaction was proposed as described in Scheme **14**. In this case, NMI may be superior to stronger bases such as DBU (pKa 13.5) due to its acid-base properties, which allows NMI to transfer the proton removed from the amine to the *p*-nitro phenol leaving group. In the studied case, the reaction was particularly slow due to the electron-donating effect of the isoindoline-nitrogen of carbamate **118**, slowing down the addition as the rate-determining step (Scheme **14**).[161]

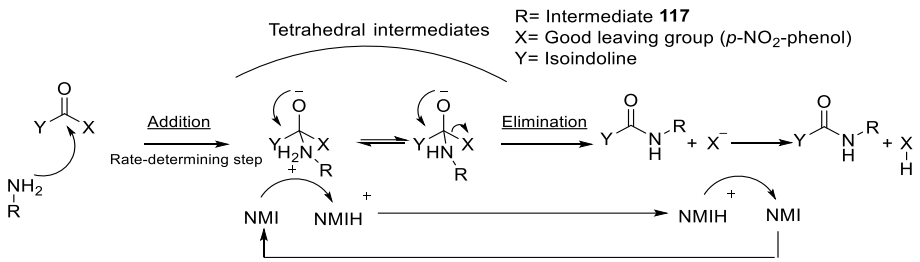

Scheme 14. Base catalysed (using NMI as base) addition-elimination mechanism.[161]

It is believed that an alternative synthetic approach to form the mixed urea **119** may involve the direct attack of isoindoline on a corresponding isocyanate or trifluoroethyl carbamate of amine **117**. These methods, which are commonly used and provide good yields for the synthesis of asymmetric ureas, were not initially pursued due to time constraints and the potential loss of intermediate **117** in the process.[168,169] In the future, these strategies will be explored to improve the synthetic access. Despite the lack of optimisation, sufficient intermediate **119** was obtained after three weeks of reaction time to continue the process and yield isoindoline-urea **124**.

Table 6. Test reaction conditions for the synthesis of intermediate **119**. The bases was the only parameter, which was changed. Abbreviations: NMI = *N*-methyl-imidazole, DMAP = 4-(dimethylamino)pyridine, DBU = 1,8-Diazabicyclo[5.4.0]undec-7-en, DIPEA = *N*,*N*-diisopropylethylamine.

Reaction conditions	Yield
NMI + DIPEA, 45°C	8%
DMAP+0.5eq pyridine, 45°C	3%
DBU, 45°C	5%
DIPEA, 45°C	0%

As expected from *in silico* studies, isoindoline-urea **124** showed activity *in vitro* (cf. Section **3.2.8.5**). However, the attachment of the linker was not successful. For simplification of the synthesis, the phenolic hydroxy-group and the aniline amine-group of precursors **120** were both Boc-protected, resulting in a simultaneous deprotection of both groups during the formation of isoindoline-urea **124**. It is assumed that the presence of both unprotected groups may be problematic for the reaction with the Mal-Val-Ala-PAB-PNP linker to obtain linker-payload **125**. When the pKa for the deprotonation of the phenolic hydroxy-group of inhibitor **124** was calculated *in silico*, a value of 7.86 was obtained (cf. Figure **28**). This means that at a reaction pH of around 10, most of the molecules are deprotonated, resulting in a significantly higher negative charge around the phenol compared to the aniline amine-group. In turn, the resulting phenolate is the most reactive group and may attacks faster the carbonate-activated linker, possibly resulting in an unstable carbonate that cannot be isolated. In the future, it will be necessary to protect the phenolic hydroxy-group and aniline amine-group with different protecting groups to achieve selective deprotection. Alternatively, a modification of the structure by molecular docking, avoiding a reactive phenol, may be considered.

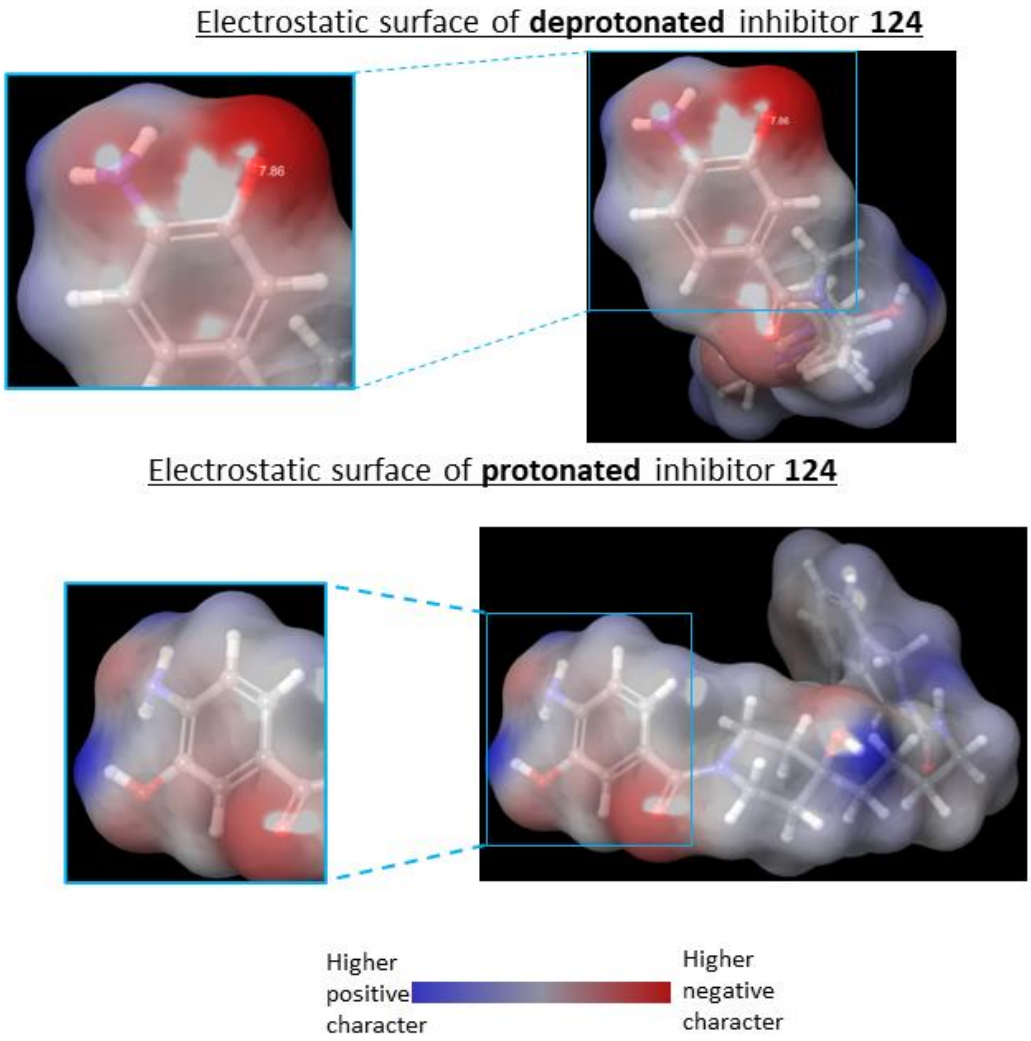

Figure 28. Inhibitor **124** quantum mechanics optimisation (DFT: B3LYP) of urea-isoindoline inhibitor **124** in DMF for PhOH pKa determination (pKa = 7.86) and electrostatic surface representation of deprotonated and protonated inhibitors.

3.2.6. Biological results from computational aided chapter

3.2.6.1 Multiple dosing treatment with NAMPT inhibitor loaded ADCs of NAMPT sensitive cell lines, seeking to maintain a constant extracellular ADC concentration

This experiment is in connection between chapters **3.1** and **3.2** and aims to test if the differences on [NAD^+] diminishing performance observed in Ramos, where [NAD^+] recovery after 24h was observed (Section **3.1.6.1**), and L540, where full [NAD^+] depletion for 72h was observed (Section **3.2.10.2**), were related to a significant faster internalisation of CD19 surface receptor in Ramos or Raji cells, or Her2 receptor in BT-474 against CD30 internalisation in L540 that potentially could led to an insufficient extracellular ADC concentration to maintain a sustained NAMPT inhibition in those cases where Ramos, Raji or BT-474 cells were single dosed with ADC. This idea connects with the fact that the rate of internalisation varies greatly depending on the target as well as the ADC.[170,171] Additionally, a constant inhibition of NAMPT for at least 72h is necessary to achieve successful cytotoxicity with NAMPT inhibitors.[125,146].

3. Results and Discussion

Briefly, a multidosing experiments with daily dosing of fresh DAR10 ADC solutions of the respective anti CD19 or anti-Her2 mAb conjugated with acrylamide or cyanoguanidine linker-payloads **58** and **37** respectively, in Ramos, Raji and BT-474 cells were performed, aiming to maintain during the 96h of the experiment extracellular high concentration of ADC that could potentially compensate a fast internalisation/recycling turnover of ADC-receptor complex in $CD19^+$ and/or $Her2^+$ cell lines against $CD30^+$ L540 cell line. Additionally, this idea would be independent of the NAMPT inhibitor containing ADC used since it was related to the receptor targeted and therefore linker-payload **37** was selected instead of the more synthetically costly linker-payload **97.**

Nevertheless, the cell viability results from the multidosing treatment (Figure **29**) did not show significant better performance of the ADC treated groups against unconjugated mAb treated control groups, discarding the idea of insufficient NAMPT inhibition related to insufficient supply of ADC in a single dose regime in Ramos, Raji or BT-474 cells, and directing the focus of the research in the next sections to the new more hydrophilic linker payloads **97** and **105** as well as understanding the specific biological characteristics of CD30 as receptor and L540 cell line.

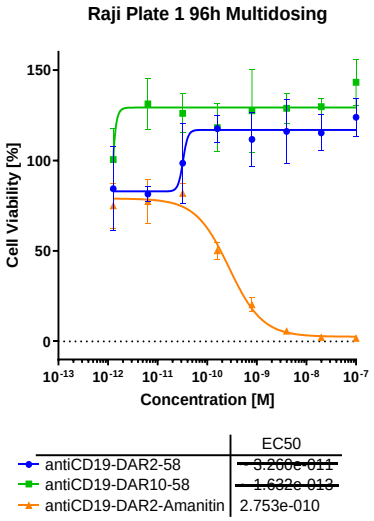

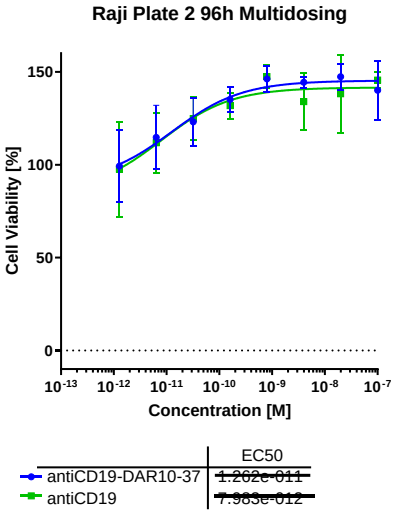

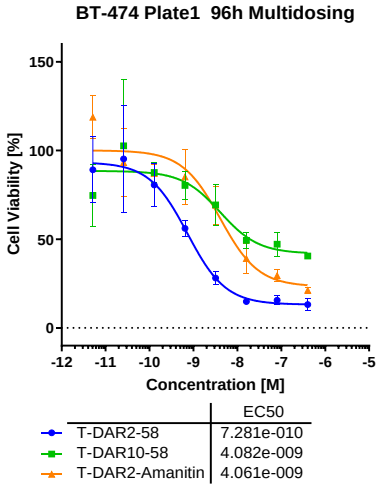

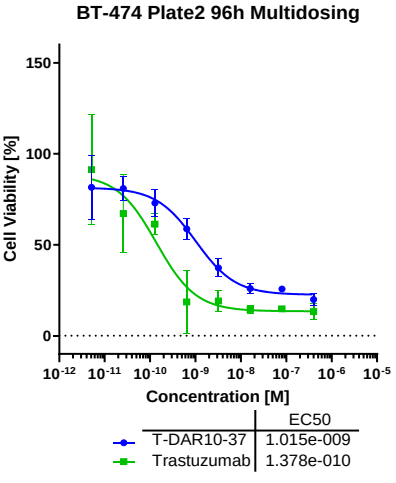

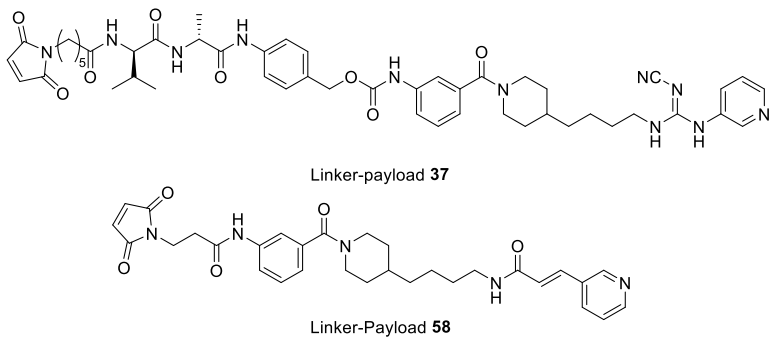

Figure 29. Multiple dosing cytotoxicity experiments on Ramos, Raji, and BT474 cells.

3.2.6.2 New-generation hydrophilic NAMPT inhibitors: *In vitro* test of tertiary alcohol payload **94** and oxime payload **105**

The *in vitro* cytotoxicity of the new NAMPT inhibitors (tertiary alcohol payload **94** and oxime- payload **105**) was investigated in L540 cells, which are reported to be highly sensitive to NAMPT inhibition.[122] As reference controls, aniline-inhibitor **36** (NAMPT inhibitor control) as well as α-amanitin (assay control) were used.

As seen in Figure **30A**, L540 cells showed high sensitivity to NAMPT inhibitor **36** with a cytotoxicity in the nM range. Furthermore, as expected due to its higher hydrophilic character, tertiary alcohol-payload **94**showed significantly lower cytotoxicity than aniline payload **36** as a free inhibitor (140 times less cytotoxicity) most likely due to lower membrane permeability. Oxime-containing payload **105** showed similar activity as payload **94**, with an EC_{50} as a free inhibitor in the µM range in L540 cells (Figure **30B**).

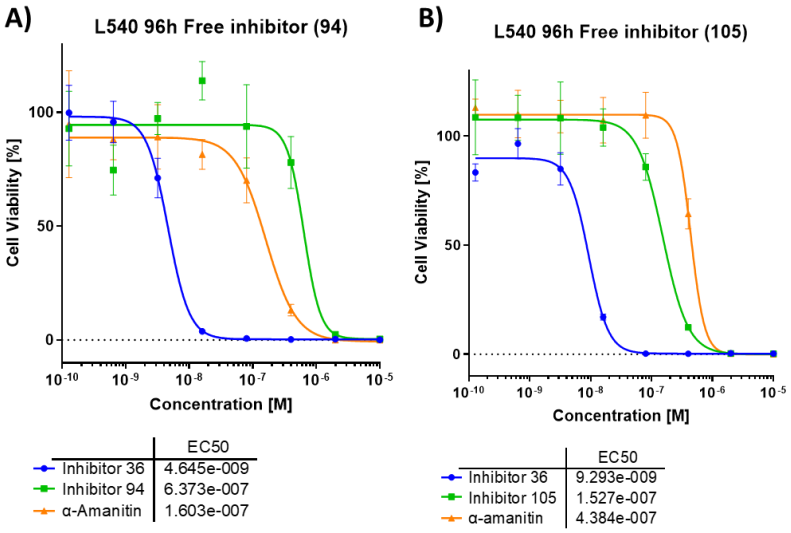

Figure 30. Cytotoxicity assay of free payloads A) **94** and B) **105** compared with free payload **36** and α-amanitin on L540 cells (EC_{50} in M). The chemical schemes of payloads **94** and **105** are also included as a reminder of their structures.

3.2.7. Production of brentuximab-like single thiomab™ anti-CD30 mAb for ADC production with NAMPT inhibitor linker-payloads **97** and **110** and cell viability *in vitro* testing in L540 cells

The anti-CD30 antibody Brentuximab was produced using HDPs proprietary IgG1 expression plasmids for heavy chain (HC) and light chain (LC) as scaffold. The HC includes the mutations Leu234Ala, Leu235Ala (LALA mutation), and Asp265Cys to generate thiomabs™ with diminished effector functions.[172]

Briefly, the sequences of the variable regions of Brentuximab were obtained from the literature and synthetised using the GeneArt service.[173] After amplification by PCR, the PCR fragment and expression plasmids were digested using site-specific endonucleases to prepare the fragment ends for subsequent ligation. Finally, the plasmid integrity, size and sequence of the Brentuximab HC and LC were verified using agarose gel electrophoresis (Figure **31A**) and Sanger sequencing. The mAb was expressed by transfection of HC and LC plasmids in Expi293 cells. On the sixth day after transfection, the mAb was purified from the cell supernatant by protein A affinity chromatography, and aggregates and endotoxin were removed by preparative gel filtration. The mAb was produced with a yield of approx. 120 mg/L Expi293 cell culture.

For conjugation to the Brentuximab-like mAb, the cysteines of the mAb were fully reduced, and the linker payloads **97** and **110** with reactive maleimide moieties were conjugated to the cysteines, affording ADCs with a DAR of approx. 10. Additionally, the linker-payloads **37** and **58** were conjugated in the same way to the Brentuximab-like mAb to generate controls for the *in vitro* testing.

The newly produced ADCs were tested on L540 cells in a cell viability assay. The unconjugated mAb did not show cytotoxicity in L540 cells, whereas the control ADC loaded with linker-payload **37** (cleavable linker) showed higher cell-killing activity than the ADC loaded with linker-payload **58** (non-cleavable linker) (Figure **31B**).

The ADC loaded with tertiary alcohol linker-payload **97** performed better than the aniline- linker-payload **37**-based ADC, both in terms of EC_{50} values, which reached pM values, and in terms of the ability to kill cell populations, as nearly full-blown cytotoxicity was achieved (Figure **31C**). In case of the oxime-inhibitor **105**, the ADC loaded with the corresponding linker payload **110** showed no cytotoxicity in L540 cells (Figure **31D**).

A)

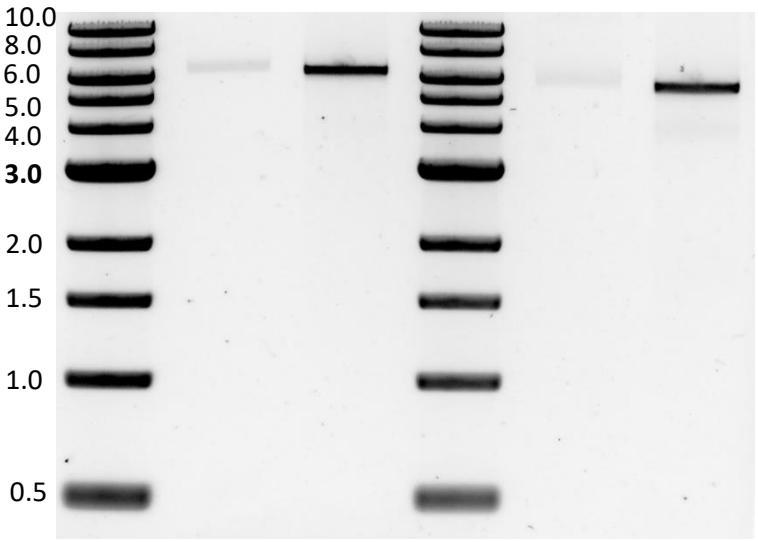

Lane	Sample
1	1kB Ladder
2	Ligation product HC plasmid (HDP+brentuximab)
3	HC HDP original plasmid
4	1kB Ladder
5	Ligation product LC plasmid (HDP+brentuximab)
6	LC HDP original plasmid

B)

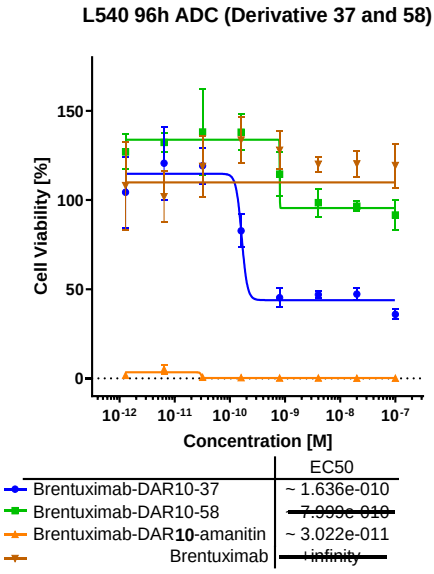

C)

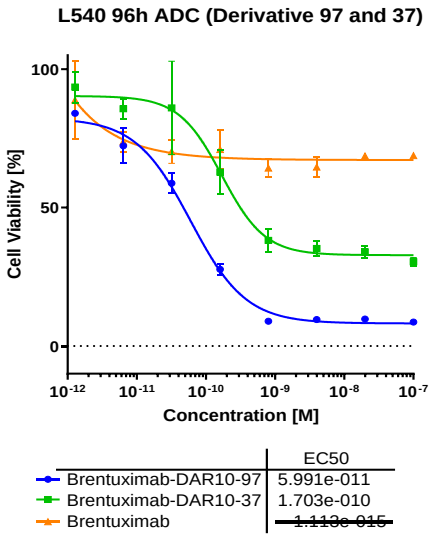

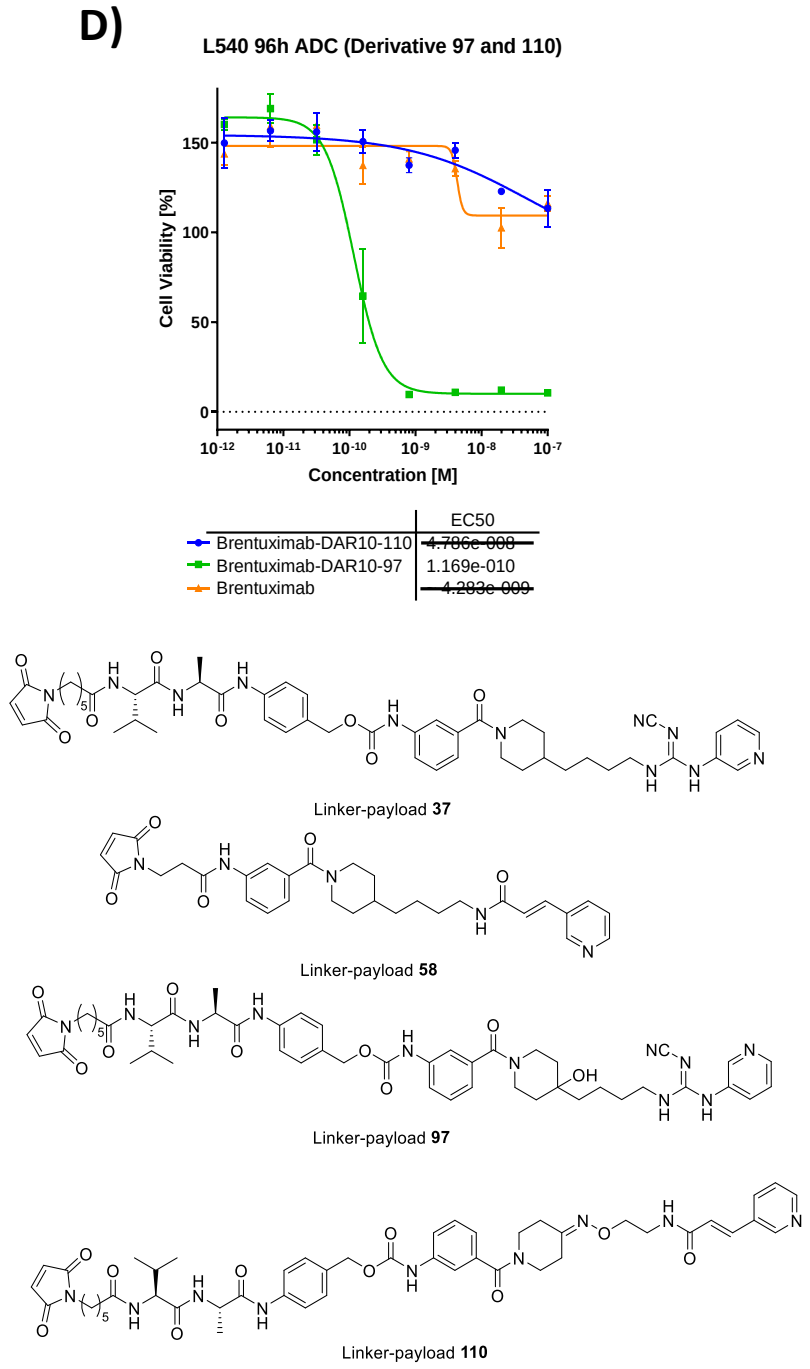

Figure 31. A) Diagnostic digestion of the Brentuximab expression plasmid. Note the higher molecular weight of the construct in lane 2 compared with lane 3 for HC and that in lane 5 compared with lane 6 for LC in both cases, demonstrating successful ligation of the HC and LC backbones with Brentuximab variable regions coding sequences; B) Cytotoxicity assay of the NAMPT inhibitor-loaded control ADCs (cleavable linker payload **37** vs. non-cleavable linker-payload **58**), the unconjugated mAb as a negative control, and the DAR10 amanitin-loaded ADC as a positive control on L540 cells. Linker payload **37** shows better performance both in EC_{50} viability concentration and cell depletion percentage; C) Cytotoxicity assay of the tertiary alcohol linker-payload **97**-based ADC compared with aniline linker-payload **37**-based ADC and unconjugated antibody as a negative control. Linker-payload **97** shows significantly better performance both in EC_{50} viability concentration and cell depletion percentage than linker-payload **37**; D) Cytotoxicity assay of linker-payload **110**-based ADC (oxime) compared with **97**-based ADC (tertiary alcohol) and unconjugated antibody as a negative control. No cytotoxic activity reported for linker payload **110**. All EC_{50} values are determined in M.

3.2.7.1 Site-specific conjugation of linker-payload **97** to Brentuximab-like single and double thiomab™, lowering DAR in NAMPT inhibitor-loaded ADCs below 10: Conjugation and cell viability *in vitro* testing

The potent pM cytotoxicity observed in L540 cells with DAR10 ADCs loaded with NAMPT inhibitor linker-payload **97** (Section **3.2.7**, Figure **31C**) led to the assumption that sufficient cell killing could also be achieved with a lower DAR and a site-specifically conjugated ADC.

To lower the DAR of the Brentuximab-based ADCs loaded with linker-payload **97**, a site-specific conjugation to the additionally engineered cysteine at position 265 (D265C) was performed, affording an ADC with a DAR of 2. After reduction of the thiomab™, the interchain cysteines were re-oxidised by DHAA treatment to induce re-bridging of the disulphide bonds. Under these conditions, the additionally engineered cysteines maintain their reduced state and can be used for conjugation. This ADC was tested *in vitro* for cytotoxicity in L540 cells, but only low cytotoxicity with an EC_{50} in the nM range and high residual cell viability was achieved (Figure **32A**). Therefore, an ADC with a DAR of 4, the double thiomab™ construct Brentuximab-A118C-D265C, was produced by site-specific mutagenesis of Ala118 to Cys in the original HC plasmid using PCR. For PCR-driven site-directed mutagenesis, the mutation was introduced using a primer complementary to a region in the original plasmid, spanning 10 nucleotides upstream and downstream of position A118. The codon annealing to position A118 on the HC was mutated in the primer to a codon coding cysteine. After PCR amplification, the parental (methylated) and therefore non-mutated fragments were degraded by digestion with DpnI. The insertion of the mutation was confirmed by Sanger sequencing, and the double-thiomab™ was expressed in Expi293 cells with a yield of approx. 200 mg mAb per litre Expi293 cell culture, following an analogue procedure like the one described for the single thiomab™ Brentuximab-like mAb (see Section **3.2.7**).

Next, tertiary alcohol linker-payload **97** was site-specifically conjugated to the new double thiomab™ mAb to produce a DAR4 ADC. A cytotoxicity assay in L540 cells showed a cytotoxic potential with an EC_{50} value in the nM range (Figure **32B**), this was a very promising results because as reported up to date, only few examples from Bayer`s NAMPT inhibitors loaded ADCs have been successful in exert cytotoxic effect in cancer cells with ADC harnessing DAR lower than 8.[55]

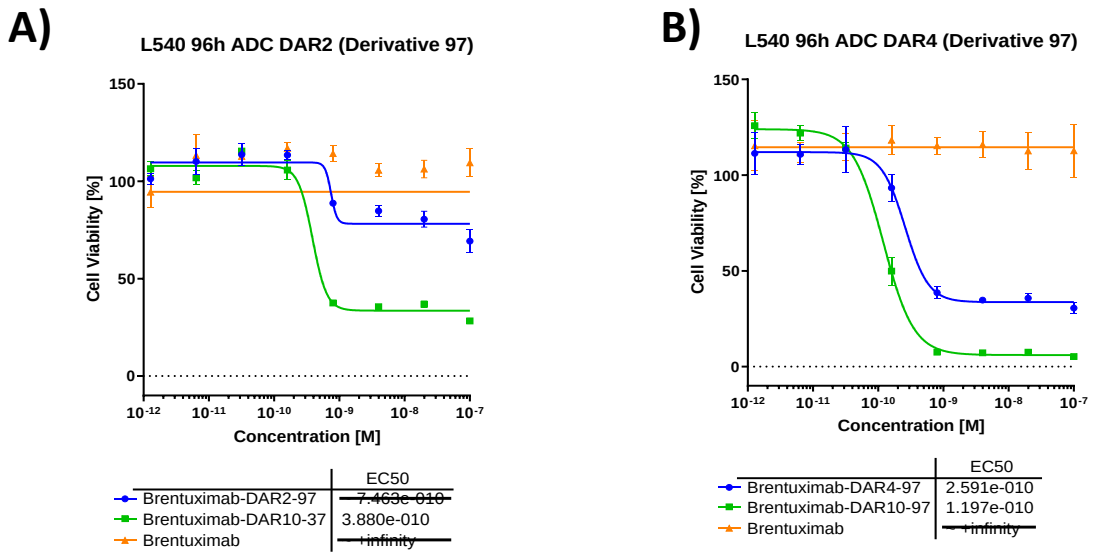

Figure 32. Cytotoxicity assay of A) Brentuximab-DAR2-**97** compared with Brentuximab-DAR10-**37**, and B) Brentuximab-DAR4-**97** compared with Brentuximab-DAR10-**97** on L540 cells (EC_{50} in M).

3.2.8. Comparative study of glucuronic acid-containing linkers against cathepsin B-cleavable linkers: *In vitro* cytotoxicity test of linker-payloads **108** and **109** in L540 cells

In addition to the modifications of the ADC at inhibitor's level reported in the previous sections, the effect on linker modification may have a major effect in the ADC performance as reported in introductory chapters. For this purpose, the work of Neumann, *et al.*[122] Was used as guidance. There glucuronidase cleavable linkers were used preferentially over cathepsin B cleavable linkers in ADCs loaded with aniline inhibitor **36**, reporting good results *in vitro* and *in vivo*. In this section glucuronidase cleavable linker-payloads **108** and **109** were evaluated and compared to their cathepsin B cleavable linker counterparts, linker payloads: **37** and **97** respectively.

Before arriving to the cytotoxic results, it is important to mention that biologically glucuronidase cleavable linkers are significantly different to cathepsin B cleavable linkers. The first ones have a major effect in linker-payload hydrophilicity, increasing it several order of magnitude. This as already mentioned in introduction chapter have a major role in conjugation to the mAb as aggregation and subsequent precipitation is reduced and grants a better biocompatibility of the synthesized ADC as the surface of the antibody remains more hydrophilic, mimicking the unconjugated surface of the mAb. In terms of linker cleavage there are also major differences between both linkers, while cathepsin B proteases are located in the lysosomes, glucuronidases are also reported to be present in the extracellular matrix of the tumour microenvironment, leading to cleavage and release of the potent cytotoxic payloads outside of the target cells what could have an impact on *in vivo* safety.[153]

As expected and based on the LogP calculations, linker payloads **108** and **109** were significantly more hydrophilic than their counterparts with cathepsin B-cleavable linkers (linker payloads **37** and **97**, respectively). Conjugation of linker-payloads **108** and **109** led to DAR-10

brentuximab-based ADCs with remarkably good yield and no payload precipitation during the conjugation process.

In the cytotoxicity assays, a significant improvement in cell population depletion was observed in L540 cells, as well as a slightly lower EC_{50} value for the ADC Brentuximab-DAR10-**108** compared to the ADC loaded with linker-payload **37** (Figure **33a**). In contrast, the ADC Brentuximab-DAR10-**109** did not significantly improve the performance compared to the ADC loaded with the linker-payload **97**, (Figure **33B**).

A)

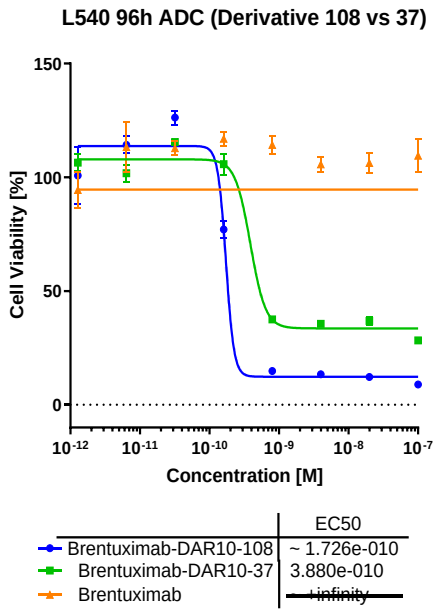

B)

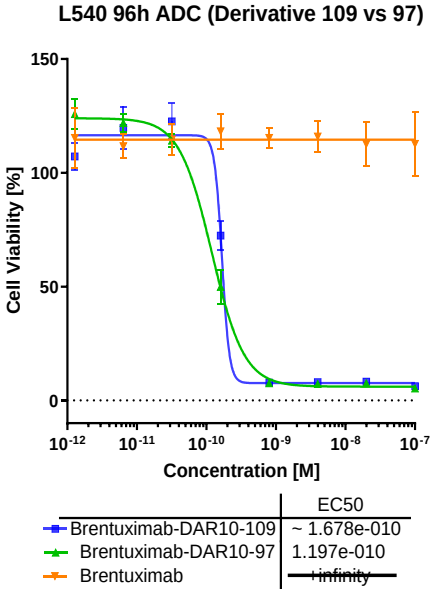

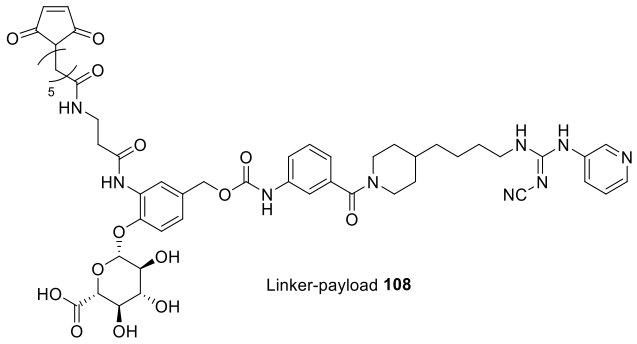

Linker-payload **108**

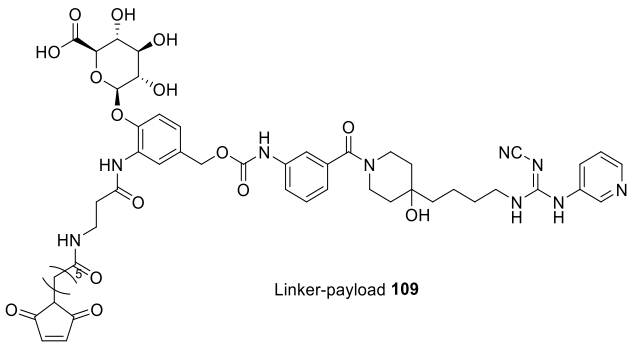

Figure 33. 96h cytotoxicity assays in L540 cells A) Brentuximab-DAR10-**108** compared with Brentuximab-DAR10-**37**, and B) Brentuximab-DAR10-**109** compared with Brentuximab-DAR10-**97** on L540 cells (EC50 in M).

3.2.8.1 Exploring targets to determine the applicability of linker-payload **97** beyond CD30

Next, the applicability and range of action of the new linker-payload **97**, which reports the best cytotoxic results, compared with linker-payload **37** was investigated, aiming to achieve cytotoxic activity in models different from CD30 (L540 cells) in which ADCs bearing linker-payload **37** have not performed well. Hence, ADCs loaded with the linker-payloads **97** and **37**, as control, were prepared, obtaining DAR values close to 10 and using mAbs against CD19, CD20, CD37, and CD123.

Surprisingly, none of the tested ADCs loaded with linker-payload **97** showed activity against their respective receptor-positive cell lines, as summarised in Table **7.** Amanitin-based DAR2 ADCs (ATACs), which were used as positive controls, showed cytotoxicity in most cases in the nM range.

Table 7. Screening of new surface receptors for use with NAMPT inhibitor-loaded ADCs and EC_{50} values of efficacy in different cell lines

CD19, Raji EC_{50} (M)	
AntiCD19-DAR10-**97**	> 10^{-5}
AntiCD19-DAR2-amanitin	2.9 *10^{-10}
CD19, Ramos EC_{50} (M)	
AntiCD19-DAR10-**97**	> 10^{-5}
AntiCD19-DAR2-amanitin	7.9 * 10^{-10}
CD20, Raji EC_{50} (M)	
AntiCD20-DAR10-**97**	> 10^{-5}
AntiCD20-DAR10-**37**	> 10^{-5}
AntiCD20-DAR2-amanitin	3.7 * 10^{-10}
CD37, Raji EC_{50} (M)	
AntiCD37-DAR10-**97**	> 10^{-5}
AntiCD37-DAR10-**37**	> 10^{-5}
AntiCD37-DAR2-amanitin	1.1 * 10^{-9}
CD37, Ramos EC_{50} (M)	
AntiCD37-DAR10-**97**	> 10^{-5}
AntiCD37-DAR10-**37**	> 10^{-5}
AntiCD37-DAR2-amanitin	> 10^{-5}
CD123, MOLM-3 EC_{50} (M)	
AntiCD123-DAR10-**97**	> 10^{-5}
AntiCD123-DAR10-**37**	> 10^{-5}

3.2.8.2 Screening of HDP cell line bank for CD30⁺ cell line as comparative model to L540 cells: Bioinformatic driven CD30⁺ cell line selection and determination of sensitivity to NAMPT inhibitors

The next goal was to find a cell line that had CD30 surface expression comparable to L540 cells and was able to internalise the ADC-receptor complex. Such a cell line was expected to be a comparative model for L540 cells to determine whether the different behaviour of Brentuximab-based ADCs versus CD19- or Erbb2-targeting ADCs was related to the target or the cell line.

In the first screening phase, a bioinformatic approach was followed using the European Bioinformatics Institute's Expression Atlas, in which all cell lines from HDP's internal cell bank were screened for CD30 mRNA expression and/or protein expression and compared with the expression levels of L540 cells.[174] Subsequently, three promising cell lines, namely RPMI-8226, PC-3, and SKOV-3, were selected, and NAMPT sensitivity was evaluated by determining cell viability after treatment with aniline compound **36** and the control compound FK866 compared to the amanitin positive control. The results in Figure **34** showed that only RPMI-8226 and PC-3 cells were sensitive to NAMPT inhibitors.

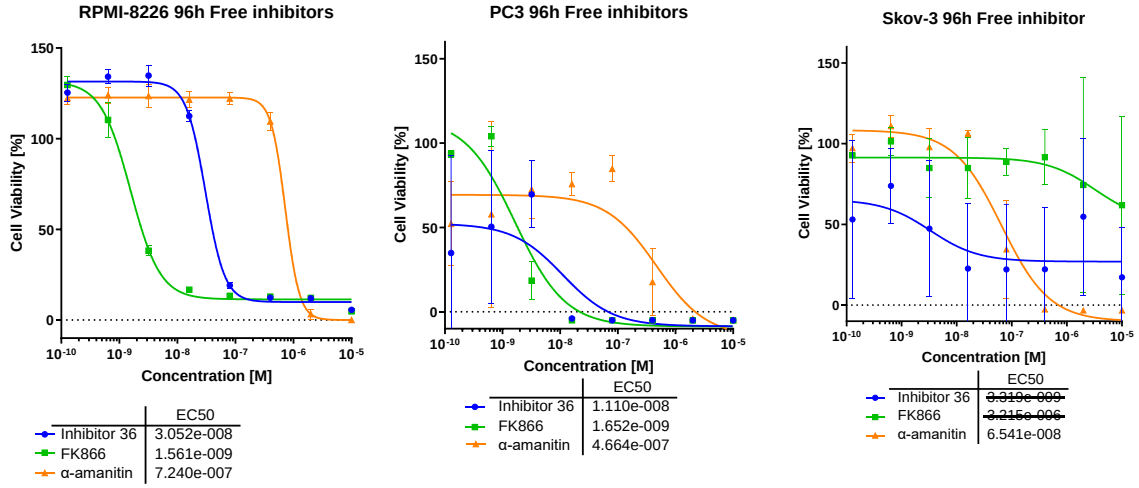

Figure 34. Screening of CD30⁺ cell lines for sensitivity towards NAMPT inhibitors. Cytotoxicity assay of derivative **36** compared with FK866 and alpha amanitin on RPMI-8226, PC-3, and Skov-3 cells.

3.2.8.3 Comparative model to L540 cells: ADC-surface receptor complex internalisation

The ability of RPMI-8226 cells to internalise the receptor-ADC complex was tested by a cytotoxicity assay (Figure **35**). The internalisation and/or release of the payload in the cytoplasm was very low, as only a slight effect was observed with a DAR10 amanitin control ADC, and this control was estimated to induce full-blown cytotoxicity due to the high dose of amanitin at all concentrations tested, therefore, RPMI-8226 it was not a suitable candidate for anti-CD30 ADC treatment, as internalisation and / or lysosomal release of the inhibitor was minimal.

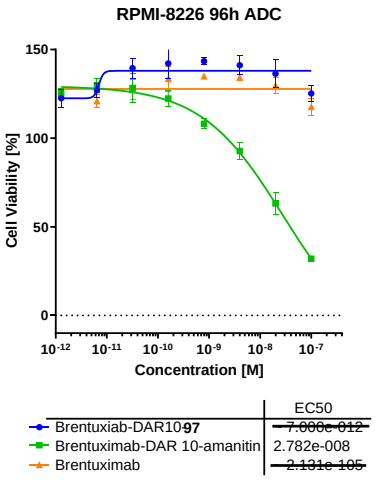

Figure 35. Screening of cell lines for CD30⁺ surface expression. Cytotoxicity assay of antiCD30-ADCs on RPMI-8226 cells.

3.2.8.4 Determining the cytotoxic potential of inhibitor **113**, degradation product of aniline **36**, in L540 cells

The main goal was to determine the remaining *in vitro* cytotoxic activity of the guanylurea-inhibitor **113**, which is the expected acid catalysed hydration compound derived from cyanoguanidine-inhibitor **36**, as demonstrated in section **3.2.4.** The lack of *in vitro* binding to the NAMPT enzyme reported in Section **3.2.9.2** was confirmed by the cytotoxic results of guanylurea **113** compared to cyanoguanidine **36** (Figure **36).** The hydrated metabolite of cyanoguanidine **36** showed no cytotoxicity in L540 cells in the measured concentration range.

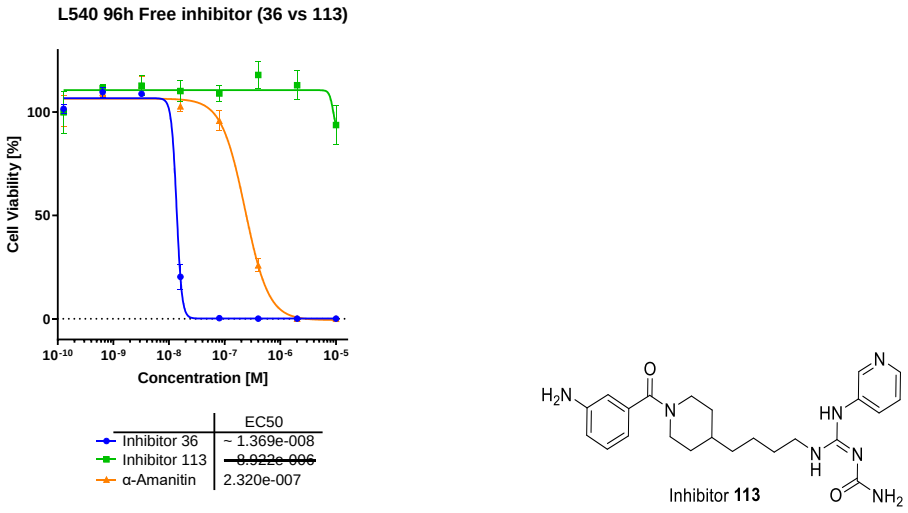

Figure 36. *In vitro* test for inhibitor **113**. Cytotoxicity assay of inhibitor **113** compared with **36**, and α-amanitin as assay control in L540 cells EC_{50} (M).

3.2.8.5 *In vitro* test of isoindoline-urea inhibitor **124**

In this section the urea inhibitor **124** was tested against L540 cells as free inhibitor to determine the cytotoxic activity of the inhibitor **124** compared to standard aniline cyanoguanidine inhibitor **36** and tertiary alcohol cyanoguanidine inhibitor **94**. As expected from

the computational simulation results of section **3.2.5.1**, inhibitor **124** maintained the cytotoxicity towards L540 cells in a range similar (µM) to tertiary alcohol payload **94** when tested as a free inhibitor and lower than highly hydrophobic standard **36** (see Figure **37**).

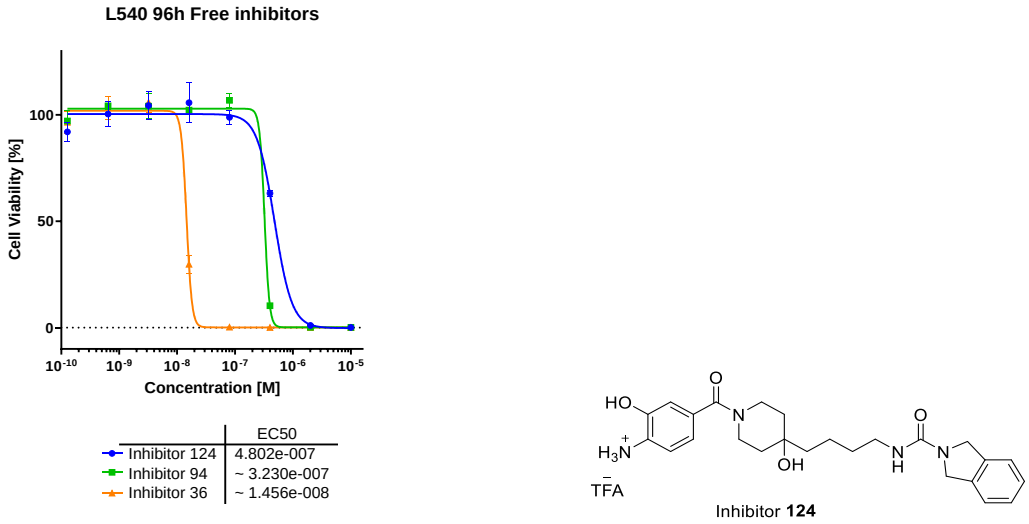

Figure 37. Cytotoxicity of free urea-isoindoline inhibitor **124** compared with cyanoguanidines **94** and **36** in L540 cells (EC_{50} (M)).

3.2.9. Biochemical evaluation of *in silico* lead optimised NAMPT inhibitors: Cellular extract NAD measurement, NAMPT binding affinity by BLI, CD30 surface receptor expression levels by FACS, and determination of NAMPT expression across NAMPT inhibitor sensitive cell lines

3.2.9.1 Quantitation of binding of biotinylated NAMPT inhibitors to NAMPT enzyme in vitro through BLI measurement

The principle behind the enzyme-inhibitor binding kinetics was the measurement of the change in thickness in the biolayer generated over Octet® optic sensors by light interferometry. The sensors were coated with streptavidin, so that they have selective and strong binding to biotinylated molecules as biotinylated NAMPT inhibitors. After binding the inhibitors to the sensor, the binding of the bound inhibitors to the recombinant NAMPT enzyme was assessed over time through changes in the thickness of the biolayer.

First, evaluation of the inhibitory activity of inhibitor **36** by direct binding to NAMPT was accomplished with the biotinylated version **46**. The measurement revealed that the biotinylated inhibitor **46** binds NAMPT with a K_D in the nM range, showing a linear dependency on the enzyme concentration (Figure **22**). The BLI measurement of the biotinylated analogue **111** of inhibitor **94** (Figure **38**) showed a similar binding profile and K_D as for biotinylated inhibitor **46** (Figure **22**), suggesting a similar affinity to NAMPT.

In contrast to the cytotoxicity results of ADCs loaded with oxime linker-payload **110** (parent compound is inhibitor **105** (Figure **31D**), the biotinylated analogue **112** of inhibitor **105** binds with high affinity (nM) to NAMPT (Figure **39**).

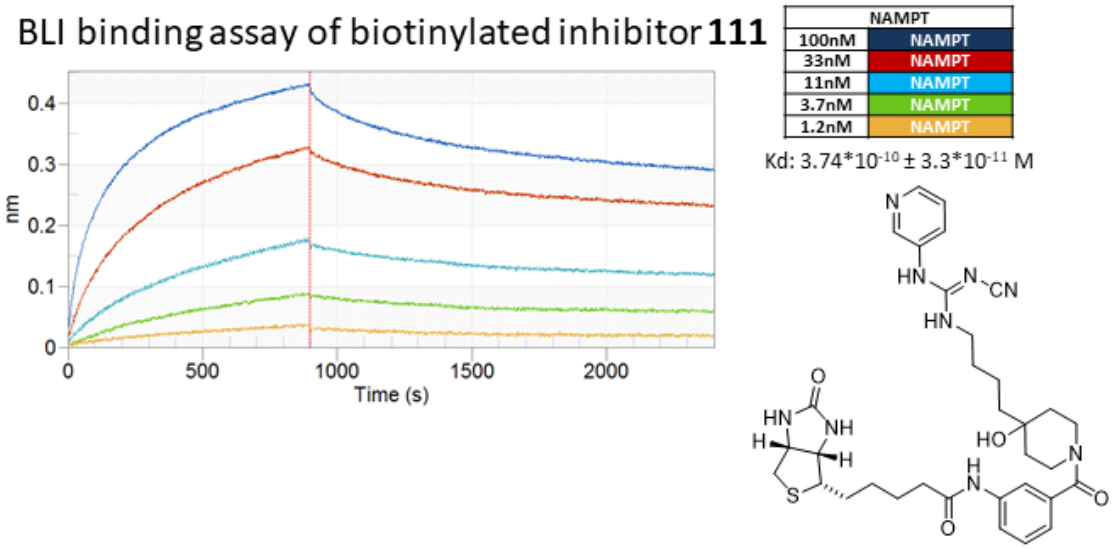

Figure 38. BLI experiment of binding of biotinylated inhibitor **111** (parent compound is tertiary alcohol **94**) to NAMPT. Note the lineal dependency as enzyme concentrations increase, highlighting a potent binding even at lower concentrations.

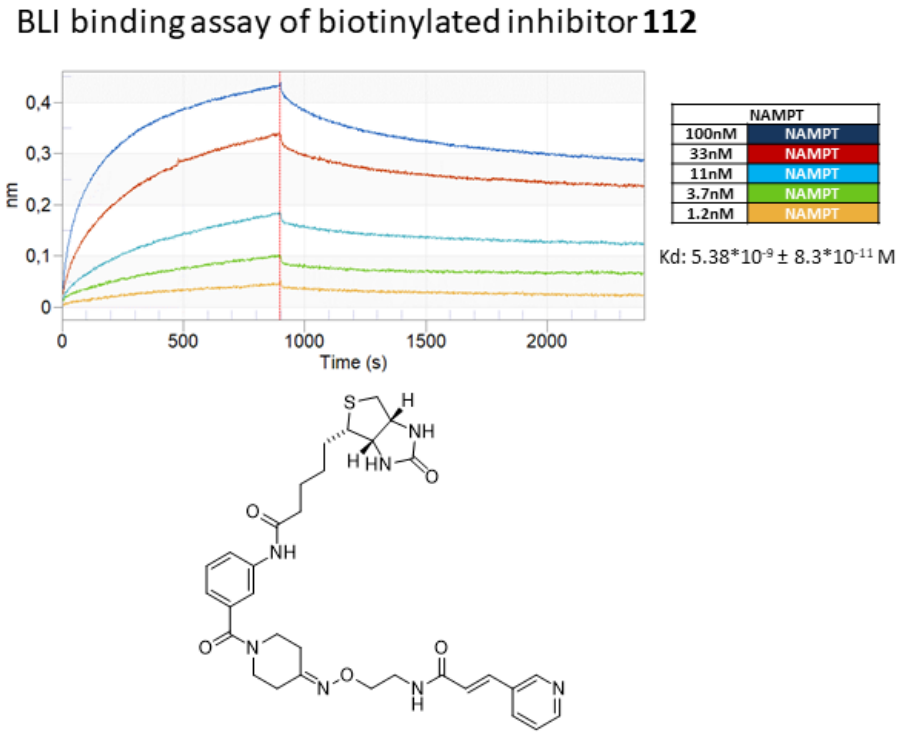

Figure 39. BLI experiment of binding of biotinylated inhibitor **112** (parent compound is oxime **105**) to NAMPT. Note the lineal dependency as enzyme concentrations increase, highlighting a potent binding even at lower concentrations.

3.2.9.2 Determining binding of biotinylated inhibitor **121** as an indirect measurement of the activity of inhibitor **113**, degradation product of aniline **36**, in BLI

BLI measurement of inhibitor 121 (biotinylated version of guanylurea **113**, degradation product of aniline **36)** showed two clear binding trends (Figure **40**, indicated by the red and blue ovals). In the red oval, the three lowest NAMPT concentrations tested were included. The binding to the enzyme was negligible, suggesting that the biotinylated guanylurea **121** had a significantly lower affinity for the enzyme than the biotinylated cyanoguanidine **46** (see Figure **22**). In the blue oval, binding was observed, but to a lesser extent than for cyanoguanidine **46**, as indicated by the significantly thinner diffraction layer. Therefore, guanylurea **121** binds significantly less specifically to NAMPT than the standard control **46** (biotinylated version of **36**) due to the significantly lower effect in the thickness change of the diffraction layer and despite of the similar K_D values.

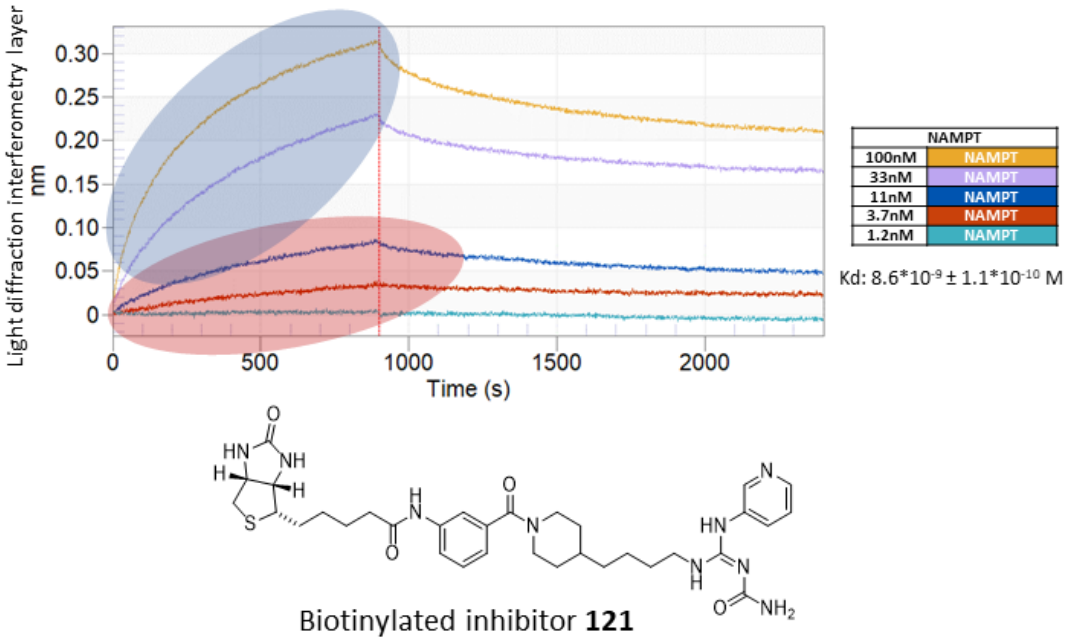

Figure 40. *In vitro* test for inhibitor **113**. BLI measurement of enzyme binding kinetics for guanylurea **121** (biotinylated version of guanylurea **113**, degradation product of aniline **36**).

3.2.10. [NAD^+] determination in cell extracts by colorimetric enzymatic assay: Assessing effects of NAMPT inhibitor loaded ADCs beyond cellular viability

The colorimetric enzymatic assay was intended to complement the *in vitro* cytotoxicity results while at the same time detecting partial NAD^+ depletion in situations where the threshold depletion required to induce cell death was not reached.[125,146] The results are based on total NAD^+ content determination on cells treated with NAMPT inhibitor loaded ADCs or free NAMPT inhibitors, measured at three time points (24 h, 48 h, 72 h) by colorimetric enzymatic assay based on alcohol dehydrogenase (ADH), and normalised to cell extract total protein concentration measured with commercial BCA kit.[86,147]

3.2.10.1 [NAD⁺] cellular extract determination after multiple dosing with NAMPT inhibitor loaded ADCs

To determine whether a sustained ADC concentration in the extracellular medium could have an effect on sustaining NAD⁺ depletion beyond the single dosing treatment, explaining the lack of cytotoxic activity in cell lines different to L540, Ramos cells were treated every 24 hours with a fresh ADC solution diluted in complete cell growth medium. The old medium was removed, and the cells were washed with fresh PBS before every new ADC dosing. However, no significant difference in [NAD⁺] concentration was evident compared with the single-dose treatment (see Figure **24**), as observed in the cellular extract of cells treated multiple times (Figure **41**). In relation to the selected linker-payload **37** against the new and more potent linker-payload **97** chemical supply reasons of the linker-payload molecule were taken into account. While **97** is more potent, also **37** showed good cytotoxic activity in nM range on L540 cells and from a chemical point of view was more available than **97**.

Additionally, the bar plot highlights that after 96h of the multiple-dose ADC treatment, the concentration of intracellular [NAD⁺] was reported to be higher than in the control untreated cell group, while the free inhibitor treated groups remain in undetectable [NAD⁺] concentrations, what supports the idea of a low cytoplasmic concentration of NAMPT inhibitor that is not sufficient to maintain a sustained NAMPT inhibition even after stable extracellular supply of ADC ensured by the multidosing treatment regime.

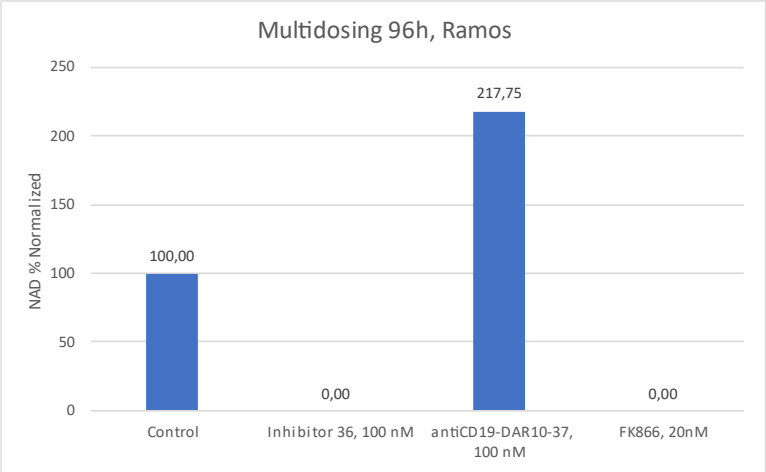

Figure 41. [NAD⁺] determination after multiple-dose treatment in Ramos cells (concentration of ADC or free NAMPT inhibitor in nM).

3.2.10.2 L540 cells: A molecular approach to unveiling high sensitivity to NAMPT inhibitor ADCs

The previous chapters have noted a different behaviour of ADCs loaded with NAMPT inhibitors in an L540 model, where surprisingly high potency was observed, in contrast to the complete lack of activity in all other models tested. The molecular reasons that distinguish L540 cells from other models were of key importance as they were needed to drive the research towards an optimised NAMPT inhibitor able to perform well in any NAMPT inhibition-sensitive cell line.

Initially, the efficacy of ADCs loaded with NAMPT inhibitors was demonstrated through an alternative approach to the cytotoxicity assay, in which the total NAD levels in the cellular extract were determined directly. As depicted in Figure **42A**, ADCs loaded with NAMPT

inhibitors (grey line) showed comparable behaviour with free NAMPT inhibitors (orange and yellow lines), leading to a total depletion of NAD levels in cells after 48h of single-dose treatment. This was in line with the cytotoxicity observed for anti-NAMPT-loaded ADCs in the L540 model.

The differing behaviour of ADCs in the L540 model led to the determination of the NAMPT mRNA expression in L540 cells compared to Ramos and Raji cells. Ramos and Raji cells are two cell lines that are sensitive to NAMPT inhibitors and in which ADCs loaded with NAMPT inhibitors showed no activity. Briefly, cDNA was prepared by retro-transcription of cell lysate mRNA extracts; real-time quantitative PCR (q-RT-PCR) was then performed using a specific primer pair that anneals to the coding region of NAMPT cDNA. For housekeeping, the GAPDH c-DNA was targeted with its respective specific primer pair. The detection was performed using the reporter DNA double-strand binding fluorochrome SYBR-green. After quantification, the results were normalised to Ramos expression levels. This showed that L540 cells had significantly lower NAMPT expression levels than Ramos and Raji cells (Figure **42B**), which renders this cell line more sensitive to NAMPT inhibition than the other two cell lines and as a consequence requires a significantly lower inhibitor concentration in the cytoplasm to achieve critical NAMPT inhibition.

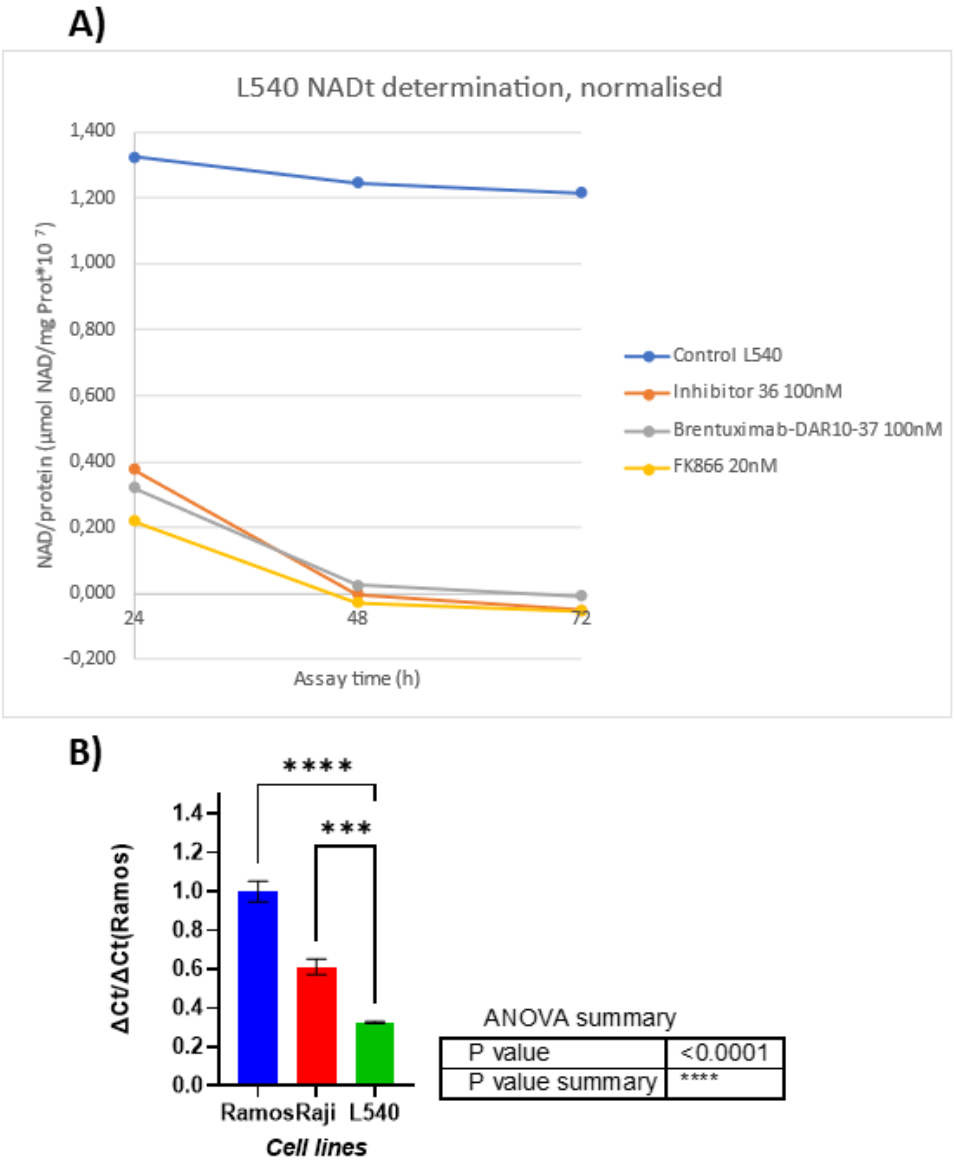

Figure 42. Differential behaviour of L540 cells in NAMPT inhibition: A) Total NAD levels after treatment with ADC and naked inhibitor; B) Normalised NAMPT cDNA expression levels between Ramos, Raji, and L540 cells.

3.2.11. Surface receptor expression determination by FACS

3.2.11.1 Screening of HDP cell line bank for CD30⁺ cell line as comparative model to L540 cells: FACS determination of surface CD30 receptor expression

The CD30 surface expression of RPMI-8226, cell line sensitive to NAMPT inhibition was determined by a FACS binding assay. Briefly, cells were stained with the naked brentuximab-based mAb or with a brentuximab-based DAR10 ADC, before the non-specifically bound mAb/ADC was washed with PBS, and cells were stained with an anti-hFc Alexa 488 reporter secondary mAb. As a negative nonspecific signal control, cells that were not stained with primary mAb/ADC were stained with a secondary reporter mAb, and cells that were not stained with either primary or secondary Ab were used for the negative autofluorescence control. Subsequently, cells from all groups were fixated with formalin, and FACS was performed.

Among all screened cell lines, only RPMI-8226 cells showed CD30 expression on the surface (Figure **43**).

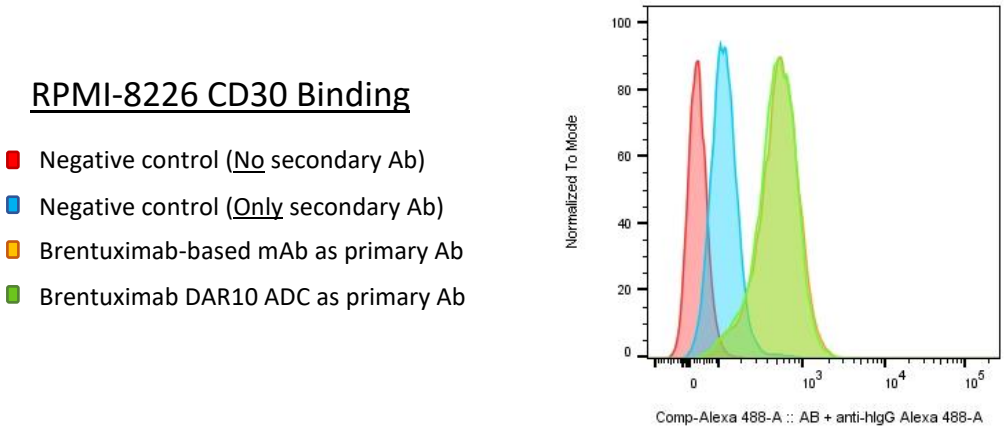

Figure 43. Screening of cell lines for CD30⁺ surface expression. Surface-binding of brentuximab-based mAb and ADC on RPMI-8226 cells.

3.2.12. Metabolic effect in NAMPT inhibitor-sensitive cell lines induced by NAD depletion

3.2.12.1 Effects on the recyclability and internalisation of cell surface receptors

To determine whether NAMPT inhibitors affect not only cellular energy but also receptor recyclability and/or internalisation, FACS quantification of the cell surface receptor CD19 of Ramos cells was performed 24h after ADC treatment.

In brief, two groups of cells were pre-treated for 24 h with DAR10 and DAR2 anti-CD19 ADCs loaded with linker-payload **37**, respectively. Linker-payload **37** was selected due to NAD^+ measurements that reported reduction of NAD^+ concentration in Ramos cell line after 24 h of treatment with ADC, compared with untreated control NAD^+ levels as reported in Section **3.1.6.1**. Additionally, in the experiments performed in this section an untreated group as a control was also considered. Considering the experiment outline, after 24 h of pretreatment, the ADC-containing medium was removed, and the unbound ADC was washed off with dPBS buffer. Cells from each group were then divided into two experimental groups: one was pre-stained with anti-CD19 linker-payload unconjugated monoclonal antibody in order to saturate all free remaining CD19 receptors on the cell surface, while the other experimental group remains untreated with anti-CD19 unconjugated mAb. Next, CD19 receptor bounded monoclonal antibody, or ADC complexes, were stained with an Alexa 488-labelled anti-human IgG Fc secondary antibody (commercially available) in order to generate the fluorescence signal detected by the cytometer.

First, the use of an anti-CD19 antibody or ADC as the primary antibody to bind CD19 receptor in cells showed no significant difference in detectability by the secondary anti-Fc Alexa 488 antibody, as observed in the identical histogram response (Figure **44A**), meaning that the different results reported in the next lines are not related to a different affinity of the secondary reporter antibody for mAb against ADC. Second, a 24-hour pre-treatment with DAR2 ADC of Ramos cells showed no differences compared to the untreated control group, as shown in Figure **44B** (orange curve and grey curve, respectively), meaning that the receptors targeted by

the ADC were not occupied by residual ADC, probably because lysosomal recycling of the receptors remained unaffected. Leading to conclude that the DAR2 ADC do not affected receptor internalisation or the concentration of NAMPT inhibitor inside the cell provided by the DAR2 ADC was not enough to induce a significant effect. Next, the experimental group treated with unconjugated anti-CD19 mAb for accomplish full CD19 receptor saturation, after DAR2 ADC pretreatment, showed that all CD19 receptors were free, as inferred by the equivalent signals from the DAR2 ADC-pretreated cells compared to the control stained with primary unconjugated anti-CD19 antibody (Figure **44C**, orange and blue curves). Thus, the CD19 cellular surface receptor population between the pretreated group and the no pretreated control group were the same meaning that the recycling of receptor to the cellular surface after ADC processing was not affected, then the DAR2 ADC pretreatment for 24h did not induce significant changes in CD19 receptor recycling and/or internalisation.

In contrast, 24 h of pre-treatment with anti-CD19-**DAR10-37** ADC (green curves) lead to significant differences. First, the ADC remained bound to the receptor, as a signal was observed in the absence of anti-CD19 pre-staining of the receptor (Figure **44B**, green and grey curves, respectively), meaning that the reporter secondary antibody was targeting the ADC not internalised after the pretreatment. Second, after staining to saturate all surface receptors with unconjugated anti-CD19 mAb, the cells pre-treated for 24h with DAR10 ADC showed a significant lower signal than the untreated control (Figure **44C**, green and blue curves, respectively), albeit comparable with the signal in the absence of anti-CD19 pre-staining (Figure **44B**, comparison between green curves). Meaning that the number of CD19 receptors in the surface of Ramos cells after pretreatment for 24h with the DAR10 ADC was significantly lower than in the untreated control, blue curves. Therefore, recycling of the internalised receptor was affected by the intracellularly released NAMPT inhibitor. In addition, the fact of observe that some of the ADC-receptor complexes where not cellularly internalised after 24h means that also internalisation pathways were affected by the NAMPT inhibitor.

These results had a major impact on the understanding of the dynamics of the ADCs loaded with NAMPT inhibitors and aware of the importance of new NAMPT inhibitors with enhanced cellular accumulation as a measurement to possibly counteracts the blockages of recycling and/or internalisation of the receptor what potentially could block the sustained influx of inhibitor in the cells.

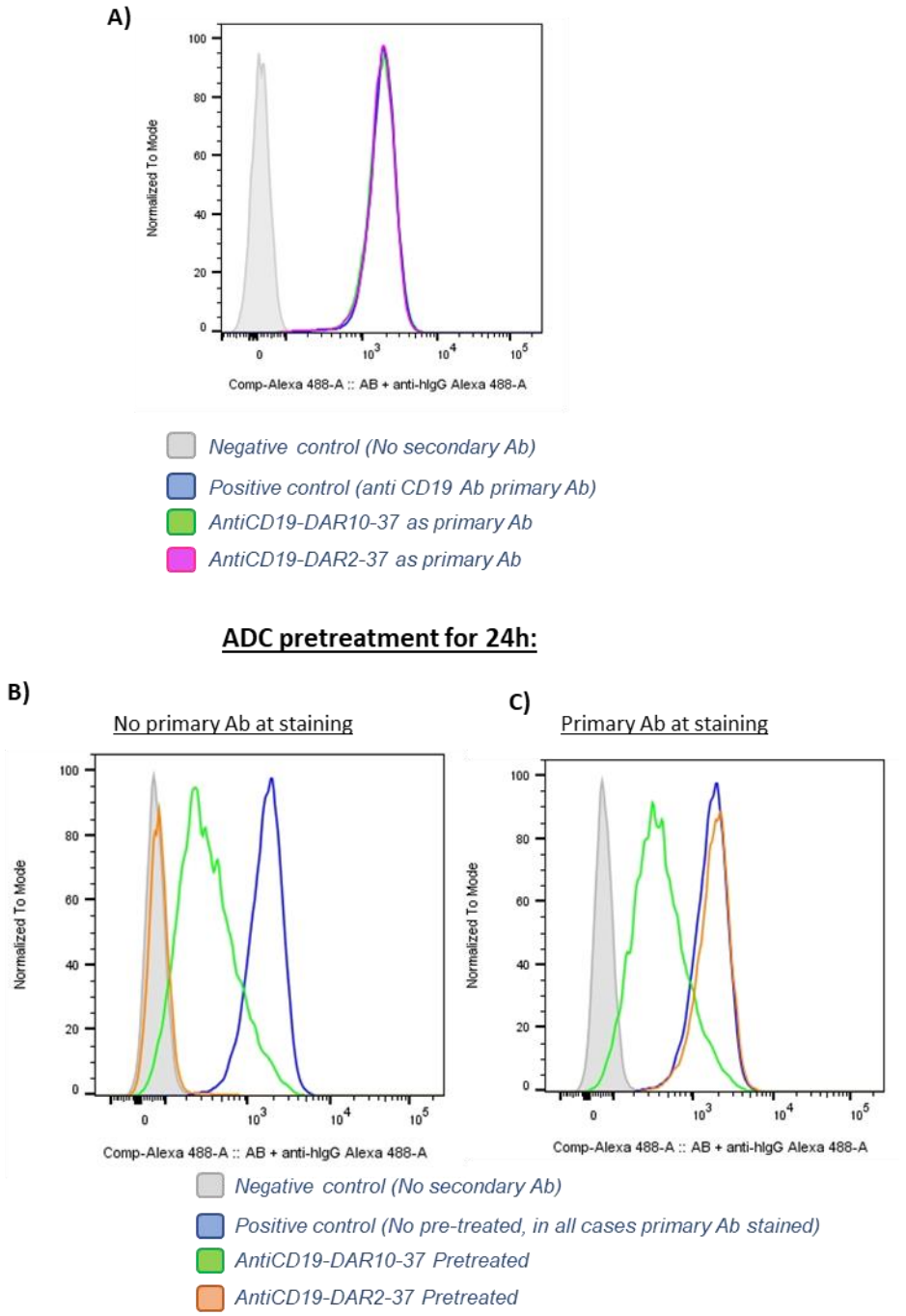

Figure 44. FACS study of Ramos cells: A) Control of affinity of secondary Ab for naked Ab (and ADCs thereof) as primary Ab; B) Cells pre-treated with ADC and directly stained with secondary Ab; C) Cells pre-treated with ADC followed by primary and secondary Ab staining.

However, the metabolic effects on receptor internalisation and/or recycling induced by NAMPT inhibitor loaded ADCs reported above did not carry over to Erbb2^{+} in BT474 cells, as no significant differences were observed between recycling and internalisation of the receptor compared to the control (Figure **45**). Overall, internalisation of the ADC/antibody-receptor complex seemed to be slower than in CD19^{+} cells, as shown in Figures **45B** and **C** (green curve), where a positive signal occurs without using primary antibodies. Meaning that after pre-treatment the receptors still present the ADC bound to them. However, could also be considered that in case of Erbb2 the lysosomal processing of the mAb do not induce the release

of the ADC from the surface receptor. To precise clearly the answer to this question new experiments would be needed in the future.

For the sake of accuracy, all measurements were performed in duplicate.

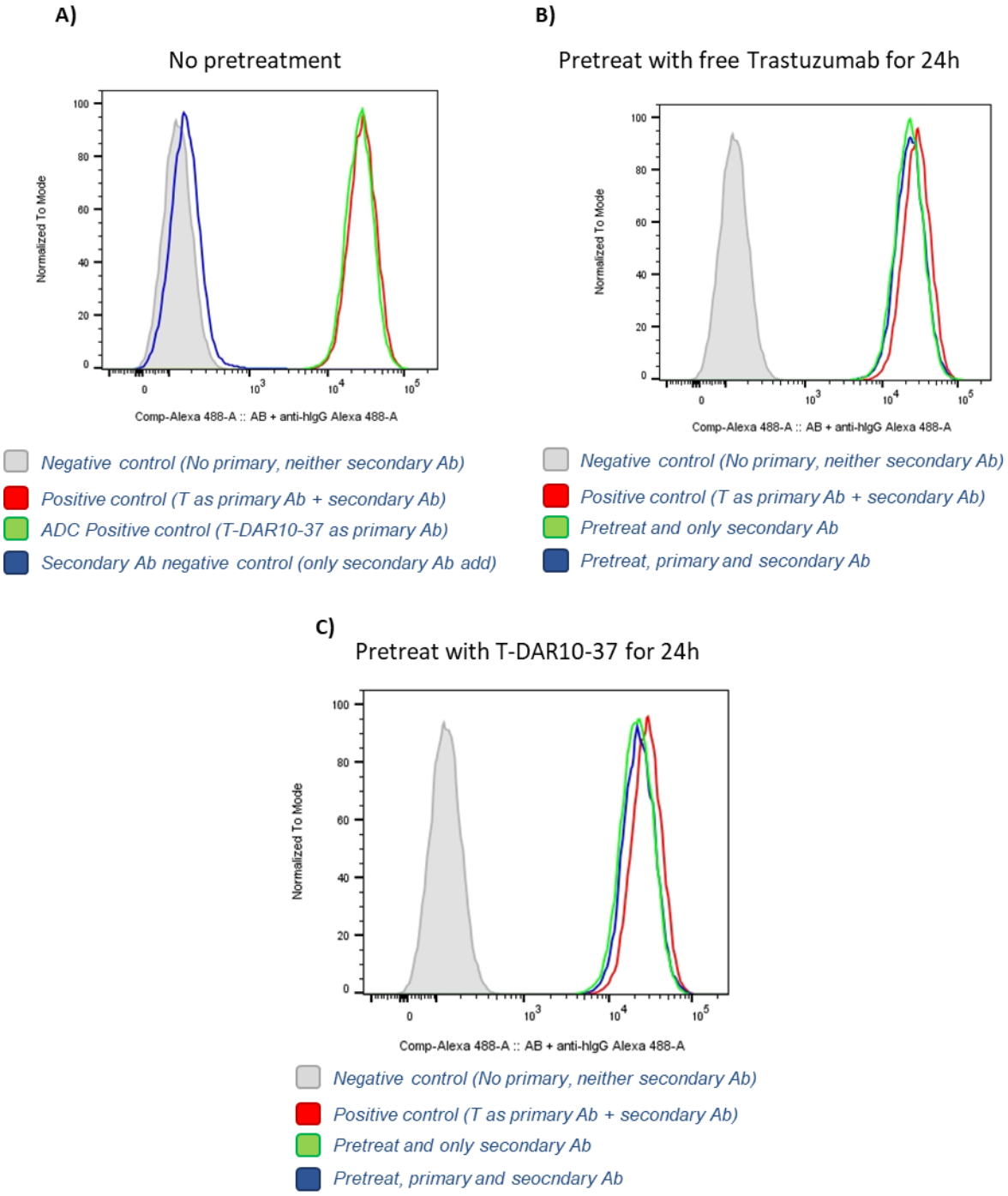

Figure 45. Study of the effect of NAMPT inhibitor-loaded ADCs on Erbb2 receptor internalisation and recycling in BT474 cells: A) Control histogram; B) Pre-treatment of cells with free antibody (control); C) Pre-treatment of cells with ADC.

3.2.13. *In vitro* determination of the lysosomal stability of cyanoguanidine **36** upon incubation in human lysosomal extracts and detection of the main degradation product

The presumed degradation of cyanoguanidine-containing inhibitors in cells was tested by performing a lysosomal stability assay with cyanoguanidine **36** as a reference compound. (LC-MS analyses performed by the Bioanalytic Department of HDP).

Briefly, three groups were incubated for 168 hours at 37°C with gentle agitation. At specific time points (0, 2, 4, 24, 48, 72, 120, and 168h), samples were quenched with an internal standard solution diluted in ACN and measured using HPLC-mass spectrometry to determine the degradation of cyanoguanidine **36** and to verify the formation of guanylurea **113**. Data acquisition was made following a multiple reaction monitoring (MRM) approach, where single monitoring over time for selected masses (of inhibitor **36** and inhibitor **113**) was recorded. Each sample and time point were measured in duplicate. The groups were as follows:

- Test group – 1µg/mL solution of cyanoguanidine **36** was diluted in catabolism buffer (composed of commercial 10X catabolism buffer at pH 5.5 diluted in water) and mixed with commercial human liver lysosomal extracts.
- Catabolism buffer control group – this group aimed to determine the stability of cyanoguanidine **36** in catabolism buffer without the addition of lysosomal extracts.
- Lysosomal extract control group – this group consisted of only lysosomal extracts mixed with a solution of cyanoguanidine **36**.

After 24 hours of incubation with lysosomal enzymes cyanoguanidine **36** was already 10% degraded to guanylurea **113**. This degradation was confirmed to be triggered by the lysosomal environment, most probably by lysosomal enzymes such as hydrolases, as no degradation of cyanoguanidine **36** was found in the control group incubated with catabolism buffer alone, data not shown. As reported in Figure **46A**, after 144 hours, 55% of the initial cyanoguanidine **36** was degraded to guanylurea **113**, which could significantly affect the efficacy of NAMPT inhibitors in cells. The reaction in the lysosome was almost clean, with only an unknown peak detected at 1.6 min of retention time in the chromatogram for guanylurea **113** mass fragments (= 437.55 g/mol). After 72h this peak decreased, and it was neither present in the lysosomal matrix nor in the chromatograms selecting fragments with the mass of inhibitor **36** (Figure **46C**). Therefore, it was considered that the unknown peak may be a possible kinetic tautomer of inhibitor **113**, as the mass and retention times were similar to the peak identified as inhibitor **113**, which was the thermodynamically stable molecule. The observed chromatogram of the lysosomal matrix in the absence of inhibitor **36**, data not shown, proved that the peak at 2.1 min of retention time belongs to the lysosomal matrix as it was present on it, with the same elution time, the absence of the peak at 1.8 min of retention time in the chromatogram of the lysosomal matrix without test compound **36** means that the presence of this peak in the chromatogram of the test group of Figure **46B** was related to the lysosomal degradation of inhibitor **36**.

3. Results and Discussion

A)

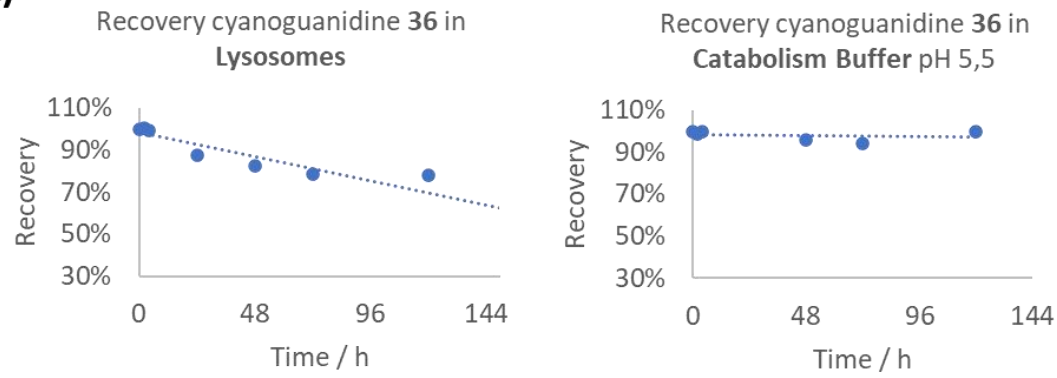

55% degradation of **36** after 144h

B)

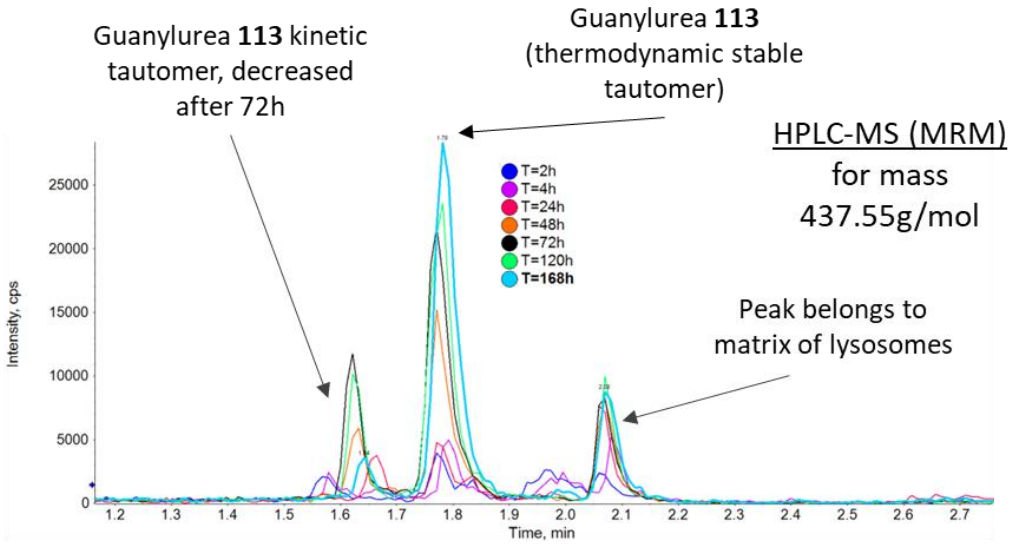

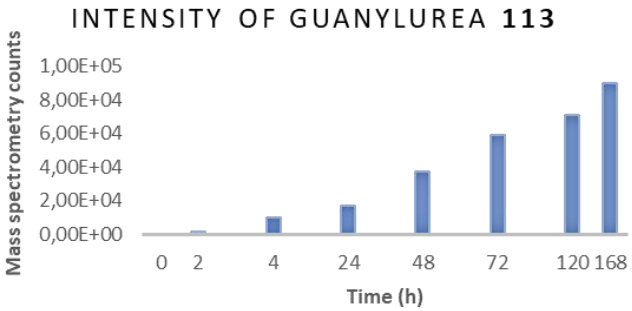

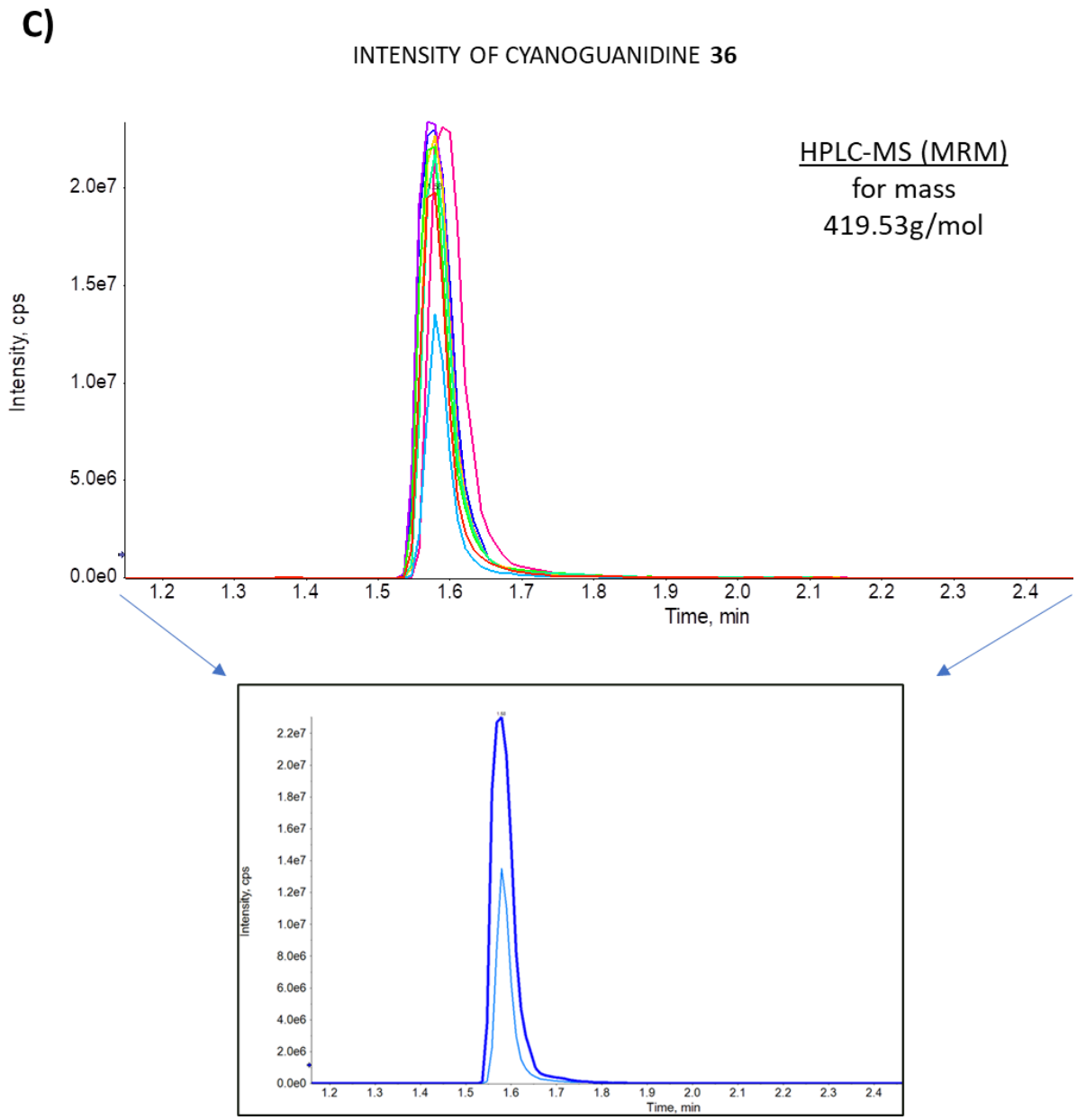

Figure 46. *In vitro* lysosomal stability assay: A) Comparison of cyanoguanidine 36 recovery vs. time with and without lysosomal extract, normalised to T0 value; B) Multiple reaction monitoring (MRM) with different time point chromatograms of products with mass = 437.55 g/mol merged to show guanylurea 113 kinetic and thermodynamic tautomer production while time increases; note how the abundance of kinetic tautomer decreases after 72 h; also included is a bar plot of guanylurea 113 abundance over time; C) MRM with different time point chromatograms of products with mass = 419.53 g/mol merged to show how cyanoguanidine 36 decreases with time; initial and last time point chromatograms are also included for a clearer determination of cyanoguanidine 36 degradation.

3.2.14. *In vivo* efficacy studies

3.2.14.1 *In vivo* performance of NAMPT inhibitor loaded Brentuximab ADC in subcutaneous L540 xenograft

Pursuing the promising *in vitro* results for the new Brentuximab-based DAR10-**97** ADCs, a single- and multiple-dose treatment *in vivo* efficacy experiment in CB17 SCID mice using a subcutaneous L540 Hodgkin lymphoma xenograft model (conducted at Pharmacology Department of Heidelberg Pharma). Dosing concentrations were based on a maximal tolerated dose (MTD) study at HDP and data reported by Seattle Genetics.[122,124]

Briefly, 10 mice per group were inoculated subcutaneously with L540 cells (suspended in 50% volume of Matrigel® and cell culture medium) in the right flank. Tumour growth was detected twice per week by palpation, and tumour volume was measured with a calliper. When tumour volume reached approx. 150 mm^3, the animals were randomised into seven groups. One day after allocation, the animals were intravenously treated with a single dose or multiple doses once per week for four weeks, of ADC solutions as described in Figure **47**. As controls, one group was treated with PBS as an untreated control, one group was treated with anti-Digoxigenin ADC as isotype control, and a third group was treated with unconjugated brentuximab mAb. Tumour volume and animal weight were measured twice per week.

The NAMPT inhibitor ADCs showed concentration- and dose-dependent antitumor activity in this CD30 expressing xenograft mouse model. As shown in the Kaplan-Meier survival plot in Figure **47B**, substantial efficacy was apparent, translated into longer survival in all groups treated with unconjugated Brentuximab and Brentuximab based ADCs compared with PBS and isotype control groups. Observing the potent efficacy of the unconjugated Brentuximab mAb that kept full survival of the group for 50 days compared with the 20 days on average in the PBS or isotype control made difficult to statistically differentiate the efficacy related to the mAb compared with the effect of the intracellularly released NAMPT inhibitor from the ADC. This reduced the significance of the test and avoided the possibility of assessing a statistically significant effect in the ADC treated groups except for the group treated with multiple doses of 12.5 mg/kg of DAR10 ADC which maintain more than 75% of survival after 85 days of study, while all other groups drop their survival percentage to a maximum of 25 %. Hence, the multiple doses treated group with the DAR10 ADC at a dosage of 12.5 mg/kg showed significant survival compared with the controls.

Additionally, a direct relationship was observed between single- and multiple-dose treatments where the multiple doses treated group with doses of 12.5 mg/kg (blue squares) compared with the single dose treated group at a dose of 12.5 mg/kg (inverted blue triangles) showed significant better survival presenting a 75% group survival after 85 days for the multiple dose treated group against the 25 % survival for the single dose group. Also, in terms of dosage was observed a direct relationship between single- and multiple-dose treatments when compared the 6.25 mg/kg multiple dose DAR10 treated group in light blue squared and the 12.5 mg/kg multiple doses treated group in dark blue squares. Showing substantial better survival for the group treated with the higher concentrations.

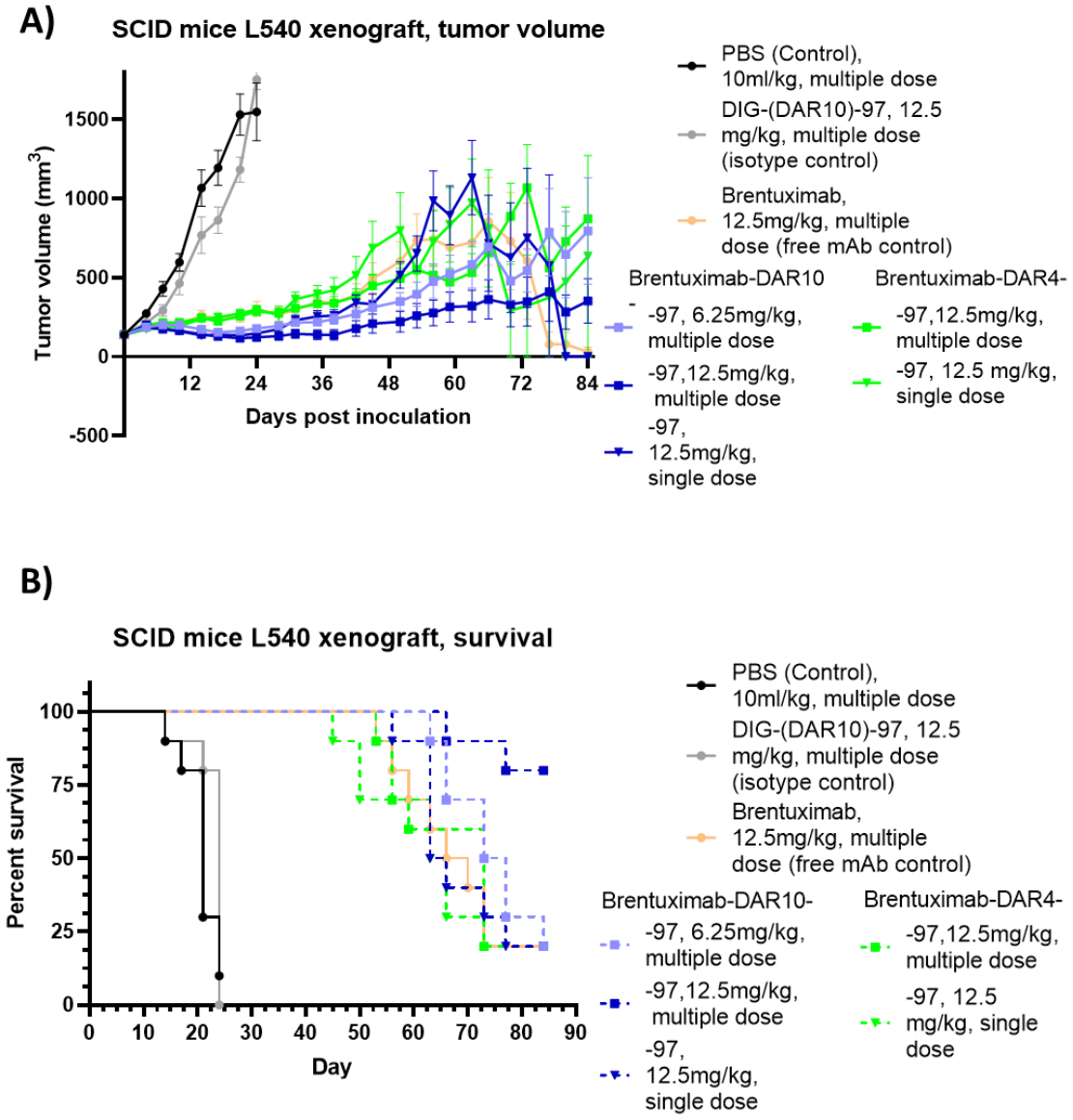

Figure 47. In vivo efficacy study of L540 subcutaneous xenograft model in CB17 SCID, 10 mice per group: A) Tumour volume, B) Survival. Control groups are plotted in circles, black for vehicle (PBS), grey for isotype DAR10 Dig ADC and salmon for free Brentuximab-LALA-D265C mAb. Test groups are divided in two categories, in blue DAR10 ADC using Brentuximab-LALA-D265C as mAb. In green DAR4 ADC using Brentuximab-A118C-LALA-D265C mAb. Additionally multiple dose groups are represented in squares while 1 day post allocation single dose treated groups with inverted triangles.

3.2.14.2 In vivo NXG L540 disseminated model with single- and multiple- dose treatment with Brentuximab-based ADCs loaded with linker-payload **97**

As reported in different studies with L540 cell line *in vivo* models, using ADC or free mAb, the outcomes obtained from subcutaneous xenograft models did not totally resemble reality. L540 is a cell line derived from a Hodgkin lymphoma, a haematological malignancy for which disseminating xenograft models are usually a better choice than subcutaneous models. Therefore, a disseminated model of i.v. injected L540 cells in NXG mice was studied.[175,176]

Briefly, 10 female NXG mice per group were inoculated intravenously with L540 cells. Three days after inoculation, treatment was initiated. Animals were intravenously treated with a single dose or multiple doses once per week for four weeks as described in Figure **48**. As controls, one group was treated with PBS as an untreated control, one group was treated with anti-Digoxigenin ADC as an isotype control, and a third group was treated with unconjugated brentuximab-based mAb. Body weight was measured twice per week.

In Figure **48B**, the Kaplan-Meier plot showed that treating mice with the DAR10 Brentuximab-**97** ADC, either in single or multiple doses, and at a dose of 6.25 mg/kg, resulted in a significant improvement in survival compared to control groups including the group treated with the unconjugated Brentuximab mAb. Mice in ADC treated groups survived more than 80 days after treatment, whereas the control animals survived only until day 30. Furthermore, a payload dose dependency was observed between the DAR4 ADC (green) and DAR10 ADC (blue) treated groups. Mice treated with lower DAR ADCs showed improved survival compared to the mice in the control groups; however, after 50 days, the disease worsened in the DAR4 treated groups, leading to the sacrifice of the mice. It is worth noting that a difference was also evident between the groups treated with low DAR ADC, with the multiple dose-treated groups showing slightly better outcomes when multiple dosed. In line with the results of the subcutaneous xenograft study (Section **3.2.14.1**), an effect of the naked mAb control (salmon solid line) was observed in the disseminated study as well. However, this effect was not as pronounced as in the subcutaneous xenograft model, allowing for a higher significance of the effect in the ADC-treated groups. Nevertheless, this was an unexpected effect of the naked mAb, as effector activities such as ADCC and ADCP were avoided by choosing a highly immunocompromised mouse model as well as by the genetic engineering of the mAb, which minimises FCγ receptor recognition. In summary, the NAMPT inhibitor ADCs showed high *in vivo* antitumor efficacy in CD30 antigen expressing L540 disseminated mouse model.

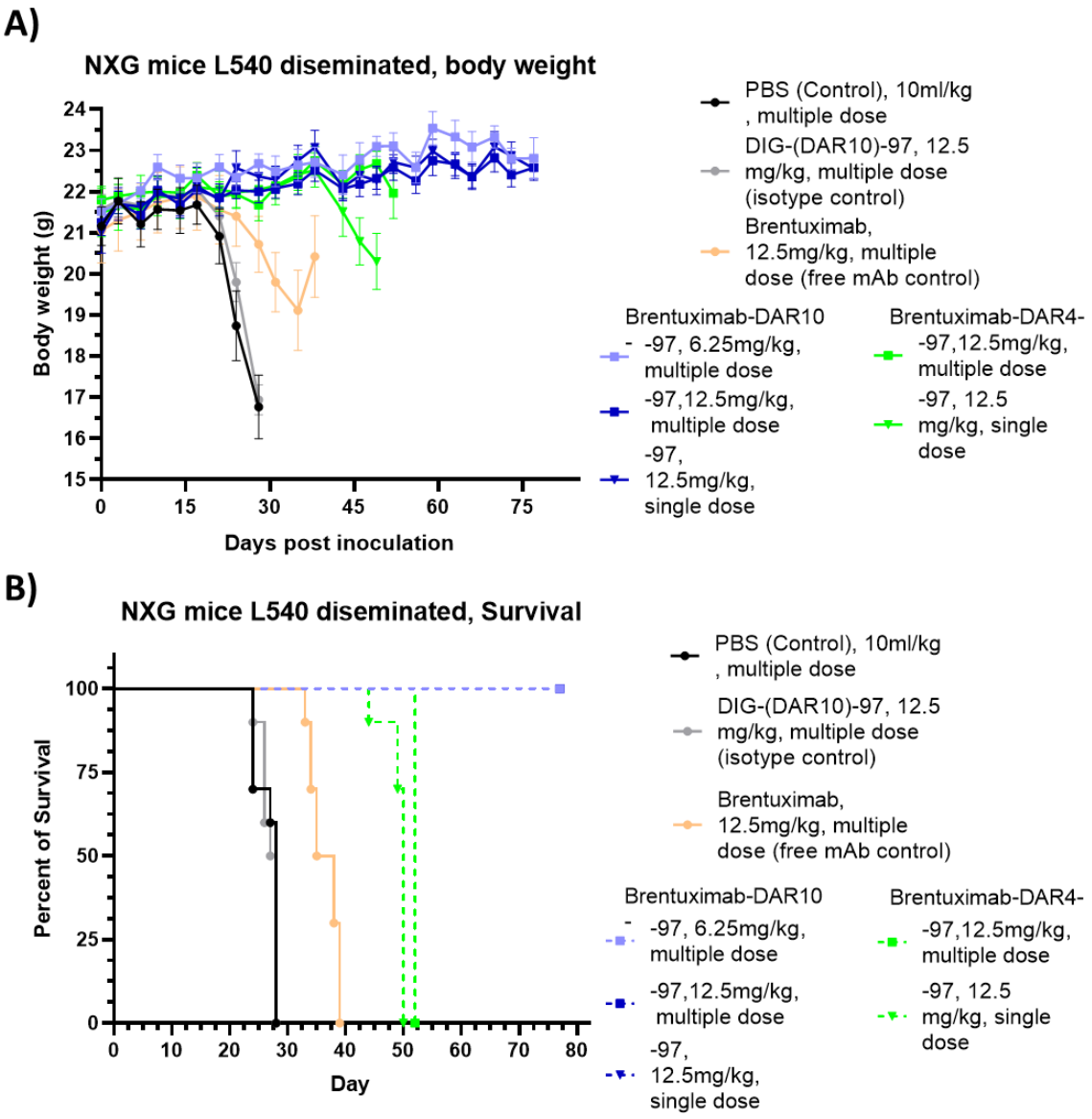

Figure 48. *In vivo* efficacy study of L540 disseminated model in NXG mice, 10 mice per group: A) Body weight; B) Survival. Control groups are plotted in circles, black for vehicle (PBS), grey for isotype DAR10 DIG ADC and salmon for free Brentuximab-LALA-D265C mAb. Test groups are divided into two categories: blue DAR10 ADC using Brentuximab-LALA-D265C as mAb and green DAR4 ADC using Brentuximab-A118C-LALA-D265C mAb. Additionally, multiple-dose groups are represented in squares, while 1-day post-inoculation single-dose treated groups are represented with inverted triangles.

3.2.15. Discussion of computationally aided chapter

The computationally aided design to enhance hydrophilicity for an optimised cellular accumulation profile of ADC-delivered NAMPT inhibitors led to the synthesis of the novel NAMPT inhibitors **94** and **105**, which showed promising *in vitro* cytotoxicity in the µM range. In comparison to the parent inhibitor **36** with EC_{50} in the nM range, the lower EC_{50} values for **94** and **105** resulted not from poorer NAMPT binding but from low passive diffusion into the cells. However, a lower passive diffusion through membranes may also lead to improved cellular retention if the inhibitor was delivered through an ADC platform. This could be highly advantageous since it could increase the therapeutic window of ADCs by avoiding unintended toxic effects in the event of a premature release of the inhibitor into the circulation.

Once the optimised inhibitors were generated, a pressing need still remained to generate efficient targeting ADCs loaded with NAMPT inhibitors. In general, the ADC technology relies on three key components: payload, linker, and target-specific mAb. To understand and further develop the potential of new inhibitors (payloads), it is crucial to choose suitable targets. Based on the data obtained, CD19 or Her-2 did not seem to be a suitable target for cyanoguanidine or acrylamide containing NAMPT inhibitor-based ADCs as no cell line sensitive to NAMPT inhibitor loaded ADCs was detected during the experimental work of this dissertation. CD30 (also called TNFRSF8) was re-emerging as a possible target candidate, reinforced by its reported use as an efficacious target for ADC with the FDA-approved ADC Adcetris.[125, 177] It is usually overexpressed in the blood cancer types leukaemia and lymphomas,[178] and it is beneficial for ADC treatment as blood cancer cells are easier to access than solid tumour cells. Due to the good *in vitro* results reported by Neumann *et al*.,[122] L540 (Hodgkin lymphoma) was selected as $CD30^+$ cell line for *in vitro* and *in vivo* testing of the new ADCs.

Having selected CD30 as the target, the linker-payloads **97** and **110** bearing the new inhibitors (tertiary alcohol **94** and oxime **105**, respectively) were conjugated through Michael addition to the fully reduced Brentuximab-D265C-based thiomab™ mAb. When evaluated for cytotoxicity, the linker payload **97** proved successful in the $CD30^+$ cell line L540 while remaining inactive as payload in $CD19^+$ and $Her2^+$ targeting ADCs.

Unfortunately, no cytotoxicity was observed with any of the ADCs loaded with linker-payload **110**. One explanation could be the instability of the oxime bond, since its formation is subject to a chemical equilibrium in which the oxime bond can be hydrolysed.[161] Moreover, some hydrolases reportedly catalyse the hydrolysis of oxime bonds in cells.[179,180] Additionally, this hypothesis was indirectly confirmed by the results of the BLI experiment for the biotinylated analogue **112** of inhibitor **105**, where good nM binding to NAMPT was observed.

Further studies related to the cleavable or non-cleavable nature of the linker led to the conclusion that the use of a cleavable linker such as Mal-Val-Ala-PAB (linker-payload **37**) is more advantageous than a non-cleavable linker (linker-payload **58**), as higher efficacy was found in terms of EC_{50} and percentage depletion in the cell population. This may be related to the poor stability of NAMPT inhibitors in the lysosome. It is known that non-cleavable linkers require complete degradation of the mAb in the lysosome to allow inhibitor release. This implies a much longer residence time in the lysosome and thus a greater risk for the inhibitor to be hydrolysed.[181]

The linker-payload **37**-loaded Brentuximab-based DAR10 ADC compared with DAR10 brentuximab linker-payload **97**-loaded ADC performed significantly worse. Despite cytotoxicity in the nM range, only partial cell depletion of about 50% (compared with the untreated cell population) was observed for linker-payload **37**. A possible explanation for the insufficient cytotoxicity of the ADC could be the escape of the released inhibitor from the cell by passive diffusion through the cell membrane into the extracellular medium. Consequently, the inhibitor is at least partially cleared from the cell leading to an insufficient inhibition of NAMPT. The hypothesis can be supported by the fact that an ADC loaded with the tertiary alcohol-bearing linker-payload **97** demonstrated almost complete cytotoxicity with pM EC_{50} values, indicating effective cytoplasmic accumulation of the released inhibitor. In that case, the released NAMPT inhibitor is less hydrophobic due to the presence of the tertiary alcohol, and the slightly enhanced hydrophilicity might be sufficient to decrease efflux from the cytoplasm. At the same time, the release from the lysosome might be still maintained due to the differences between the lysosomal and the cytoplasmic membranes. A special difference is that the lysosomal membrane is heavily glycosylated on its luminal side.[182,183] This characteristic of lysosomal membranes may enable more hydrophilic inhibitors like inhibitor **94** to experience prolonged membrane contact times, facilitating efficient crossing of the lysosomal membrane, which results in a substantial release of inhibitor **94** into the cytoplasm. Consequently, such inhibitors maintained enhanced cellular accumulation compared to the more hydrophobic inhibitor **36**. The cytoplasmic membrane on the contrary has a lower glycosylation level on the luminal side leading to a more hydrophobic nature in comparison to luminal side of the lysosomal membrane. As a result, the interaction time of inhibitor **94** with the luminal side of cytoplasmic membrane might be reduced, mainly due to its higher hydrophilicity. In contrast, the more hydrophobic inhibitor **36** was expected to demonstrate enhanced passive diffusion through the cytoplasmic barrier. Therefore, inhibitor **94** exhibits enhanced cytoplasmic accumulation compared to inhibitor **36**. Moreover, this hypothesis is in line with the observed lower cytotoxicity of the free inhibitor **94** compared to inhibitor **36**, as the latter should feature increased passive diffusion through the cytoplasmic membrane due to its more hydrophobic nature. Nevertheless, to fully understand and prove this hypothesis as well as study possible membrane transport mechanisms involved in the cytoplasmic release of NAMPT inhibitors, further investigations are required. The picomolar EC_{50} value suggested that a lower DAR of the ADCs with linker-payload **97** could be to achieve cell killing. This idea was supported by the BLI results for the binding of the biotinylated analogue **111** of **94** (the underlying inhibitor of linker-payload **97**), which showed comparable values of NAMPT affinity to those for inhibitor **46**, the biotinylated analogue of aniline **36** (the underlying inhibitor of linker-payload **37)**. It can be concluded that the increase in the cytotoxic potential of linker-payload **97** against **37** was not related to a higher affinity of the inhibitor to NAMPT but instead to a higher cytoplasmic accumulation. In addition, the ADC conjugated to linker-payload **97** showed four orders of magnitude higher cytotoxicity than the corresponding free inhibitor **94**, suggesting improved *in vivo* tolerability with a broader therapeutical window than the published aniline inhibitor **36**. Overall, the obtained results made the new NAMPTi- loaded ADCs promising candidates for *in vivo* testing.

The high cytotoxic potential of the DAR 10 ADCs loaded with linker-payload **97** led to consider lowering the DAR of the constructs by thiomab™ site-specific conjugation, which is advantageous over the interchain conjugation required for high DAR ADCs. First, site-specific conjugation with a lower DAR can save payload material since a lower amount is needed than

for the high DAR conjugation to the mAb. Second, site-specific conjugation leads to a more homogeneous product, so that ideally only the target DAR is reached, resulting in less aggregation and better PK properties of the ADCs. Moreover, it may eventually lead to an increase in the therapeutic index, as the ADCs are better tolerated *in vivo.*[184]

Initially, a Brentuximab-based DAR2 ADC loaded with linker-payload **97** was tested, which showed EC_{50} values in the nM range. However, the residual cell viability after ADC treatment was too high to assume a full-blown cytotoxicity. This led to the production of a DAR4 ADC with the Brentuximab-based double thiomab™ mutant, particularly created for this purpose. The new DAR4 construct showed significant cell depletion in the cytotoxicity assays, presenting the first low-DAR site-specific ADC loaded with an NAMPT inhibitor that showed promising cytotoxic activity *in vitro.*[55]

In vivo, maximum tolerated dose (MTD) safety studies were conducted in CB17 SCID mice and NXG mice using a single intravenous dose of the DAR10 anti-CD30 brentuximab ADC loaded with NAMPT linker-payload **37** or **97**. The study ended at a dose of 80 mg/kg without any observed toxicity *in vivo*. The dose was not increased beyond 80 mg/kg because the efficacy studies were planned to be carried out at a maximum concentration of 12.5 mg/kg, which is more than six times lower than the dosage used in the MTD study. The *in vivo* testing has revealed significant tumour-suppressing effects in mice treated with NAMPT inhibitor-based ADCs, although the effect was weaker in the subcutaneous xenograft model than in the disseminating model. This is likely due to the fact that macromolecules have a poor penetration into solid tumours, resulting in a lower concentration of ADC in the tumoral stroma of a subcutaneous xenograft and a lower correlation between the administered dose and pharmacodynamics than in a liquid malignancy. To address this, ADCs aimed at treating solid malignancies often incorporate cytotoxic payloads that can passively diffuse from target cells to surrounding tumour stroma cells, resulting in bystander killing. However, linker-payload **97** has been designed to minimise cellular passive diffusion, to improve target cell accumulation and the therapeutic window. This makes ADCs loaded with linker-payload **97** more effective in liquid malignancies, as demonstrated in the disseminated model.[185] In terms of activity, it was evident that a multiple-dose regimen is the preferred and superior option, as the good tolerability observed in the MTD study suggests that it can be selected as the first treatment strategy in future studies. Furthermore, the existing literature only shows one example in which NAMPT inhibitor loaded ADCs with a DAR lower than 8 have an *in vivo* effect. [55] As demonstrated in the L540 disseminated efficacy study (see Section **3.2.14.2**), the site-specific conjugated DAR4 Brentuximab-A118C-LALA-D265C-**97** ADC showed a significant increase in survival compared to controls. However, due to lower tumour penetration and the high activity of the free mAb control, this was not observed in the subcutaneous xenograft study (Section **3.2.14.1**).

Additionally, the potent antitumour activity exerted by the unconjugated mAb Brentuximab-LALA-D265C in L540 cells was surprising, as due to the immunocompromised animal models and the modified mAb used, with FCγ receptor interaction blocking mutations (LALA and D265C), the classical effector responses of the mAb were expected to be minimal. However, as shown in Sections **3.2.14.1** and **3.2.14.2**, the antitumoral effect of the naked antibody was very potent. Yet, no attempt was made to quantify the antitumoral effect of the unconjugated mAb in the parent paper published by Neumann *et al*.,[122] making it difficult to assess.[36–38,122]

The activity of Brentuximab in L540 cells *in vivo* is thought to be the same as for other anti-CD30 mouse-human chimeric mAb as SGN-30 due to their ability to induce G_1 phase cell cycle arrest and death through DNA fragmentation.[176] This effect is dependent on the type of anti-CD30 mouse-human chimeric mAb used and the required dosage for the effect to occur. For example, multiple doses of SGN-30 administered every four days for a total of five injections showed activity at only 1 mg/kg in a L540 SCID mouse disseminated model, with the mice surviving for more than 120 days.[176] The study presented in this dissertation showed lower efficacy results, but in the subcutaneous xenograft model, the effect of ADC treated groups compared to the mAb treated group were not significantly different, with the exception of the multiple-doses treated group with high DAR ADC, which significantly outperformed the mAb treated group. The exact mechanism behind the antibody -CD30 receptor complex mediating intracellular signalling leading to cell death is still unclear, but it has been observed that mAb crosslinking potentiates this effect, which is easier to achieve *in vivo* than *in vitro*. According to Wahl et al., for CD30 as for other TNF superfamily members, signalling through TNF-R-associated factor (TRAF) after receptor multimerization is one possible affected pathway, leading to cell death.[176]

Despite the promising profile as ADC payload of tertiary alcohol **94** and its linker-payload counterpart linker-payload **97**, a pressing question remains around the narrow target applicability of the inhibitor, showing only activity against $CD30^+$ cell line L540. This could be explained through two hypotheses.

First, the metabolism of target-ADC complex internalisation was significantly different among different targets, being sufficient in CD30 but not in CD19, as demonstrated in FACS studies (Section **3.2.12.1)**. In this regard it is important to remember that NAD^+ depletion leads to cell death by cellular energy deprivation, since the NAD^+/$NADH+H^+$ pair plays an essential role as electron transfer cofactor in the mitochondrial electron transportation chain.[186] However, cells have an ATP storage as buffer system for energy shortages that, on average, last for three days after NADt depletion. Thus, cytotoxic effects in cells are observed when [NADt] remains under 10% of the basal values for at least 48h.[144,187]As shown in Section **3.1.6.1**, a partial NAD^+ depletion was induced by the ADC treatments, but in all cases except L540, cells recovered after 24h, or even surpassed their initial NADt levels, which explains the lack of cytotoxic activity of ADCs.

Related to cellular metabolism, two possibilities are considered as possible reasons for the observed recovery of the [NADt] level. First, ADC internalisation is highly dependent on the cell line and the target, with rapid internalisation reported in some cases.[188] Therefore, during the initial 24h after single-dose treatment, ADC levels in the extracellular medium may decrease to a concentration too low to maintain a stable uptake of linker-payload by the $CD19^+$ Ramos cell line and thus a stable NAMPT inhibition. This was related to the fact that published NAMPT inhibitors are hydrophobic, allowing a putative free (bi-directional) passing through cell membranes. Considering that cells treated with ADC contain a low concentration of free NAMPT inhibitor in the extracellular medium, efflux of the intracellularly released inhibitor was expected due to the concentration gradient.[46,189,190] The second possibility relied on cellular adaptation to initial [NADt] depletion, triggering metabolic survival adaptations in cells and resulting in the blocking of non-essential processes, such as endocytosis and/or recycling of ADC-target complexes. This complements the passive efflux of free inhibitor and can explain the recovery of NADt levels.[191–193] However, the first possibility was rejected as no significant

improvement in cytotoxicity was reported with ADC multiple dosing, (Section **3.2.6.1)**. This indicates that the expected reduction of extracellular ADC concentration due to fast internalisation is negligible, allowing persistent ADC internalisation in cells after a single treatment.

For the second possibility, the binding of an ADC or antibody to CD19 was tested in Ramos cells. It could be shown that the ADC was still bound to the receptor after 24h of pre-treatment of cells with DAR10 ADC, pointing to a very slow or no internalisation of the whole complex (Section **3.2.12.1)**. Moreover, a significant depletion of the cell receptor population after treatment compared to untreated control cells was observed, indicating a possible reduction or complete blockade of receptor recycling.

In comparison with the untreated control, DAR2 ADCs were not able to induce any significant changes in cell surface receptor abundance, occupancy by ADCs, or recycling of the receptor. This was probably related to the low DAR leading to a facile release of NAMPT inhibitors in the cytoplasm and the inability to induce noticeable metabolic changes in cells due to a NAMPT inhibitor concentration below threshold. In contrast, DAR10 ADCs showed remaining ADC bound to the receptor, suggesting a stop in ADC internalisation. Additionally, the idea of slow internalisation of the receptor was rejected because the DAR2 ADC did not remain bound to the cell receptor, which would be expected in a case of slow complex internalisation. In terms of receptor recyclability, pre-treatment with the DAR10 ADC showed a significantly lower population of receptors on the cell surface, implying a possible blockade of receptor recycling in addition to impaired receptor internalisation. Hence, the results suggest that targeting CD19 in Ramos cells with DAR10 ADCs induced metabolic changes based on the putative adaptation of the cells to the energy deficiency induced by NAMPT inhibitors. This adds to the reasons behind the lack of cytotoxic efficiency of NAMPT inhibitor-loaded ADCs.

However, CD19-related data should be interpreted cautiously, because when the same experiments were performed with a different target (Her2), the results were inconclusive. A possible explanation lies in a different intracellular pathway for the endocytosed vesicles in $Her2^+$ cells. As suggested, the trastuzumab-Her2 complex may follow slow internalisation and processing in endosomes that release the receptor to the cell surface for recycling. This may differ from the internalisation process of CD19, which has been shown to be faster than Her2.[194] This leads to a gradual decrease in NADt levels in case of trastuzumab-based ADCs, which do not trigger the described cellular adaptation mechanism, unlike the previously reported acute effect in CD19. Additionally, recent results address the complexity of the signalling pathways leading to cellular internalisation, suggesting the RAB family of GTPases as the key director group of proteins. However, the specific mechanism and effector members depend greatly on the antibody as well as the linker-payload and the target, suggesting that the different results with Her2 targeting ADCs may be related to a different internalisation process, one probably controlled by significant different regulators that may not be affected by the effect of NAMPT inhibition.[195]

The second hypothesis related to the narrow scope of applicability of the ADCs, focused on the heterogeneous NAMPT expression levels between cancer cell lines. It was notable that in contrast $CD19^+$ or $HER2^+$ cell lines, L540 cells showed a steady depletion of total NAD^+ levels throughout the 96h after ADC treatment, eventually leading to apoptosis. The reason for this different behaviour currently remains unclear. However, it was demonstrated that L540 cells

had significantly lower concentrations of NAMPT mRNA than other tested cell lines like Raji or Ramos, suggesting a lower concentration of the enzyme in the cytoplasm. Therefore, it was expected that L540 cells showed higher sensitivity to NAMPT inhibitors than other cell lines, in accordance with the results reported by Xiao *et al*. and Böhnke *et al*.,[55,196] where NAMPT mRNA and protein levels inversely correlate with sensitivity to NAMPT inhibitors. While the genetic or epigenetic reasons for this different behaviour were not investigated as they are beyond the scope of this study, the low concentration of NAMPT inhibitor in the cytoplasm was suggested to be the main reason for NAD^+ recovery after 24h in all other ADC-treated cells apart from L540, which showed total depletion after 48h of ADC single-dose treatment (see Section **3.2.10.2**, Figure **42A**).

It can be concluded that the significant better performance of the NAMPT inhibitor-loaded ADC on L540 cells against the other cell lines tested related not only to differences in recyclability and internalisation of the receptor or excessive passive diffusion, although reducing passive diffusion with optimised compounds like tertiary alcohol **94** gave better results *in vitro* (Section **3.2.7**, Figure **32C)**, but also to the significantly lower concentration of NAMPT in L540 cells compared to the other tested cell lines like Ramos or Raji (Section **3.2.10.2**, Figure **42B)**.

Thus far, it has been found that brentuximab-based ADCs loaded with NAMPT inhibitors show promising results in L540 cells when a cathepsin B-cleavable linker was used. However, it was not clear whether this was related solely to the receptor or the cell line or whether another reason was involved.

Unfortunately, none of the ADCs loaded with the new linker-payload **97** showed significant cytotoxicity *in vitro* when tested against targets other than CD30 or in cell lines other than L540. These results imply that despite the improved performance of linker-payload **97** in L540 cells compared to linker-payload **37**, increased hydrophilicity is not the only optimisation required to make NAMPT inhibitors suitable for use in ADC technology across a broad spectrum of tumours.

To shed light on this question, a representative selection of cell lines available at Heidelberg Pharma with the potential to express and internalise CD30 was examined by means of the bioinformatic tool Expression Atlas from EBI, letting to select three cell lines (SKOV-3, RPMI-8226, and PC-3 cells) as potential candidates for CD30-targeted drug delivery with ADCs.[174] The cut-off criteria were based on the Expression Atlas classification of the results, and only cell lines with high or medium expression were selected. These three cell lines were then tested against the free NAMPT inhibitors **36** and FK866. Based on the sensitivity towards the free inhibitors, RPMI-8226 and PC-3 cells were selected for the determination of cell surface CD30 expression by FACS. Upon analysis, only RPMI-8226 cells were found to express CD30 on the surface.

Unfortunately, as described, RPMI-8226 cells showed only minimal sensitivity to a Brentuximab-based ADC, indicating that internalisation was too slow and/or negligible (Section **3.2.8.3)**. Unfortunately, due to the COVID-19 pandemic, it was not possible to purchase other possibly suitable cell lines, and efforts to find a suitable comparison model for L540 cells have been discontinued.

Additionally, it was considered that a suboptimal release of payload from the cathepsin B cleavable linker may underlie the narrow scope of applicability. Thus, the possibility was explored to improve the cytotoxic performance of the ADCs by modifying the cleavage mechanism of the linker while maintaining or increasing the hydrophilicity of the linker-payload.

One solution involved the use of glucuronide cleavable linkers, which significantly improve the hydrophilicity of the linker-payload, resulting in a dramatic reduction of aggregates during the conjugation process while opening the door to a completely different release mechanism.[162] However, glucuronide-containing linkers present two major problems. First, their synthesis is chemically more demanding than that of cathepsin B linkers, and thereby making the process more time-consuming and expensive. Second, glucuronidases are known to be present in the extracellular medium, resulting in extracellular release of payloads.[153] This prevents the inhibitor from entering the lysosome, which would help to avoid chemical hydrolysis of unstable payloads in the lysosome. At the same time, however, the target specificity of the ADC is partially lost, since very potent cytotoxic payloads are released in the extracellular medium, which could lead to nonspecific toxicity and thus reduce the therapeutical window.

Consequently, the use of glucuronidase linkers should be studied on a case-by-case basis to determine their effects on conjugation, cytotoxicity and tolerability. In the work of Neumann *et al.*,[122] a glucuronide-containing linker was chosen for inhibitor **36**. Accordingly, both inhibitor **36** and inhibitor **94** with a glucuronide-containing linker were produced to test whether the newly optimised compound showed a significant improvement in performance compared to linker-payload **97** with a protease-cleavable linker.

The results of this study confirmed those of Neumann *et al*.[122] The inhibitor **36** performed better with the glucuronide-containing linker (linker-payload **108**) compared to the protease-cleavable linker (linker-payload **37**) in both the conjugation process and the *in vitro* cytotoxicity assay. This could be explained by two phenomena. First, inhibitor **36** is highly hydrophobic, so when released in the surroundings of the cells, passive diffusion of the compound into the cytoplasm should be favourable. Second, lysosomal internalisation is avoided, eliminating a potential problem of reduced inhibitor concentration in the cytoplasm due to lysosomal degradation.

However, no improvement was observed in the case of linker-payload **109**. The compound was designed to have lower passive cellular diffusion and therefore penetrates cells less efficiently. At the same time, inhibitor **94** accumulates in cells when administered through ADCs, which increases its cytotoxic effect. Therefore, the use of glucuronic acid-containing linkers was not considered appropriate for the newly prepared inhibitor because they were not an improvement over cathepsin B-cleavable linkers from the standpoint of synthesis, efficacy or biosafety. They are also costlier and have a higher risk of causing nonspecific toxicity.[153]

The above-mentioned concerns suggest that even with the lead optimised tertiary alcohol payload **94**, the concentration of NAMPT inhibitor delivered by ADCs in cells, apart from L540, was not sufficient to maintain a sustained inhibition of the enzyme to induce cytotoxic effects, leading to the hypotesis that the NAMPT inhibitors were degraded in the lysosome.

As shown in Section **3.2.4.1**, inhibitor **36**, which contains a cyanoguanidine group, could get hydrated under highly acidic conditions to guanylurea inhibitor **113** that, showed no activity in L540 cells *in vitro*. This was supported by the results of *in vitro* binding to NAMPT of biotinylated inhibitor **121** (biotinylated version of guanylurea inhibitor **113**); where biotinylated inhibitor **121** showed a higher K_D than the cyanoguanidine **46** (biotinylated version of cyanoguanidine inhibitor **36**)**.** This was depicted by two distinct regimes in the binding to NAMPT. The biotinylated inhibitor **46**showed a homogeneous, concentration-dependent binding, whereas for compound **121** almost no binding was observed at low concentrations of NAMPT. Only at higher concentrations, binding of compound **121** to NAMPT was observed, but the diffraction layer remained thinner than that of biotinylated cyanoguanidine **46**, indicating less binding. These results suggest that guanylurea **113**, even if migration from the lysosome to the cytoplasm occurs, would not be able to maintain stable NAMPT inhibition. This supports the hypothesis that the lack of activity of NAMPT inhibitors delivered by ADCs was due to their degradation to a compound with significantly less activity than the parental inhibitor. This conclusion likely also applies to linker-payload **97** consisting of a cathepsin B-cleavable linker and cyanoguanidine **94**.

Notably, the pH of lysosomes is generally reported to be 5.5, which is significantly higher than the pH in the chemical synthesis of guanylurea **113**. However, NAMPT inhibitors can become substrates for lysosomal hydrolases due to their similarity to NAD^+, catalysing their degradation (even at lysosomal pH) by some of the more than 50 described lysosomal acid hydrolases, including nucleases.[197,198]

The lysosomal hydration of the cyanoguanidine -containing inhibitors was indeed demonstrated through the lysosomal stability assay (Section **3.2.13)**, which showed that cyanoguanidine **36** was degraded to guanylurea inhibitor **113** as confirmed by HPLC-mass spectrometry. The degradation to guanylurea inhibitor **113** reached 55% of the initial cyanoguanidine **36** within 144 hours. These results indicate that the lack of activity of ADCs loaded with NAMPT inhibitors is most likely due to the significant degradation of the cyanoguanidine-containing inhibitors in the lysosome. This explains the promising results in L540 cells, which are more sensitive to NAMPT inhibition because of their lower NAMPT concentration and thus their exhibition of cytotoxic effects even if lower concentrations of active NAMPT inhibitors reach the cellular cytoplasm.

The data on the instability of cyanoguanidine-containing inhibitors led to a computationally assisted lead optimisation campaign of cyanoguanidine **94**, to generate new payloads resistant to lysosomal conditions. After several optimisation steps, inhibitor **124** was chosen as the lead candidate due to its putative ease of synthetic procedure, which was adapted from the synthesising of inhibitor **94**. However, the strategy for synthesising the asymmetric urea led to significantly lower yields than expected and resulted in only minimal quantities of inhibitor **124**. Thus, the molecule was only analysed by mass spectrometry, not NMR. Furthermore, linker conjugation was unsuccessful due to side reactivity between simultaneously deprotected phenol and aniline groups (Section **3.2.5.2)**, leading to the cancellation of the test of linker-payload **125** as an ADC. Nonetheless, the cytotoxic values of payload **124** as a free inhibitor were encouraging, leaving the project open until a new synthetic strategy is developed that can produce payload **124** or an analogue thereof in sufficient quantities for linker attachment

4. Conclusions

Cancer is a pressing challenge for society, and current treatments have greatly improved our understanding to approach this complex polygenic and multifactorial group of diseases. However, many patients still experience negative effects from these treatments, such as severe side effects that seriously impact their quality of life. Targeted therapies, such as antibody-drug conjugates (ADCs), offer a ray of hope by precisely targeting cancer cells, leading to long-term, effective results. Currently, patients can benefit from the 11 FDA-approved ADCs, but there is still much room for improvement, such as increasing the diversity in the mode of action of the ADC payloads. Currently, 70% of the approved payloads target microtubule formation, leaving out the majority of cancer cells responsible for metastatic events.[1,9,40]

Recently, new modes of action in cancer therapy have been gaining attention, particularly those that disrupt cell energy metabolism, such as NAMPT inhibitors. These inhibitors target a key feature of cancer cells, namely their altered and accelerated cell metabolism, which gives them additional selectivity. The first attempts in the use of NAMPT inhibitors, such as FK866, to treat cancer were promising. However, challenges were faced due to their high potency, causing retinal, cardiac, and haematological side effects. The use of NAMPT inhibitors as payloads in ADCs has shown potential by reducing such off-target toxicity events. Companies such as Novartis, Seattle Genetics and Bayer have filed examples of this approach. Nevertheless, ongoing issues with toxicity and selectivity persist.[55,94,121,122]

This thesis is comprised of two distinct parts. The first part examines the use of previously described NAMPT inhibitors and chemically modified inhibitors, such as inhibitor **36**. These inhibitors, modified with chemical handles suitable for linker conjugation, were used to manufacture ADCs targeting cellular surface proteins such as CD19 and HER2. The resulting conjugates showed neither cytotoxicity nor significant depletion of [NAD^+] beyond 24 hours after treatment in all tested cell lines, leading to the conclusion that previously described NAMPT inhibitors may not be the best option for effective ADC payloads. Hence, new derivatives need to be optimized for payload function.

The aim was to develop new NAMPT inhibitors by establishing a chemical structure-biological effect prediction based on synthetically guided screening of NAMPT inhibitor pharmacophore modifications, with the final goal of improving the biological performance of NAMPT inhibitors as payloads in ADC technology. The chemical modifications made to the original inhibitors including benzoic acid **92** did not result in improved performance, highlighting the complexity of the cellular environment and biomolecules like NAMPT.

Considering these initial conclusions, other hypotheses were developed. The second part of the thesis aimed to delve into the biochemical reasons behind the lack of efficacy of the potent published NAMPT inhibitors when used as ADC payloads. The conclusion was that the hydrophobic nature of these free NAMPT inhibitors has a significant impact on their efficacy. The hydrophobicity allows for free diffusion into cellular compartments but also increases the risk of potential side effects due to non-selective passive diffusion out of the cell. Additionally, it was discovered that the complex role of ADC cellular dynamics may have a major effect on their efficacy, depending on the cell surface antigen targeted. The observed metabolic changes

induced by the released NAMPT inhibitors in $CD19^+$ cell lines likely led to the blockage of ADC-receptor complex internalisation and/or recycling. Moreover, the insufficient inhibition of NAMPT by these ADCs was probably enhanced by the expected high cellular permeability due to the high hydrophobicity of the first generations of NAMPTP inhibitors.

Hence, aiming to improve the hydrophilicity without losing affinity for the enzyme, a computational lead optimisation campaign based on published co-crystal structures as templates for docking of the new *in silico*-produced hits led to the synthesis of the tertiary alcohol **94** as an optimised version of aniline **36**. The results showed a significant improvement in cellular accumulation of this new inhibitor when deployed as ADC payload, due to reduced passive cellular diffusion is most likely reduced. This highlights the importance of incorporating biological considerations during the drug discovery phase through the use of *in-silico* techniques, not only for efficiency purposes but also for optimising the final product.

However, the new inhibitor had limited applicability since the activity was influenced by the expression of NAMPT. Due to the lower expression levels of NAMPT, the Hodgkin lymphoma cell line L540 showed high sensitivity towards NAMPT inhibition compared to other tested cell lines. This supports the idea of an inverse relationship between NAMPT inhibitor sensitivity of a cell and intracellular NAMPT levels.[55] The study also provided an explanation for the activity of NAMPT inhibitors as ADC payloads being limited to highly NAMPT sensitive cell lines due to the lysosomal instability of cyanoguanidine-containing NAMPT inhibitors. These results reinforce the importance of considering the cellular biology when developing new NAMPT inhibitors aiming to use them as ADC payloads, as lysosomal stability may not necessarily be a drawback when the inhibitors are used in their free forms.

NAMPT inhibitors shows great potential for the application in the ADC technology as they are payloads with a new mode of action. However, further research is needed to fully comprehend the cellular dynamics and to guide the drug development process as well as target selection. As a conclusion from the obtained results, the development of inhibitors with improved resistance to the lysosomal environment and enhanced cellular accumulation profiles is essential to achieve a broader tumour coverage with NAMPT inhibitor loaded ADCs.

4. Conclusions

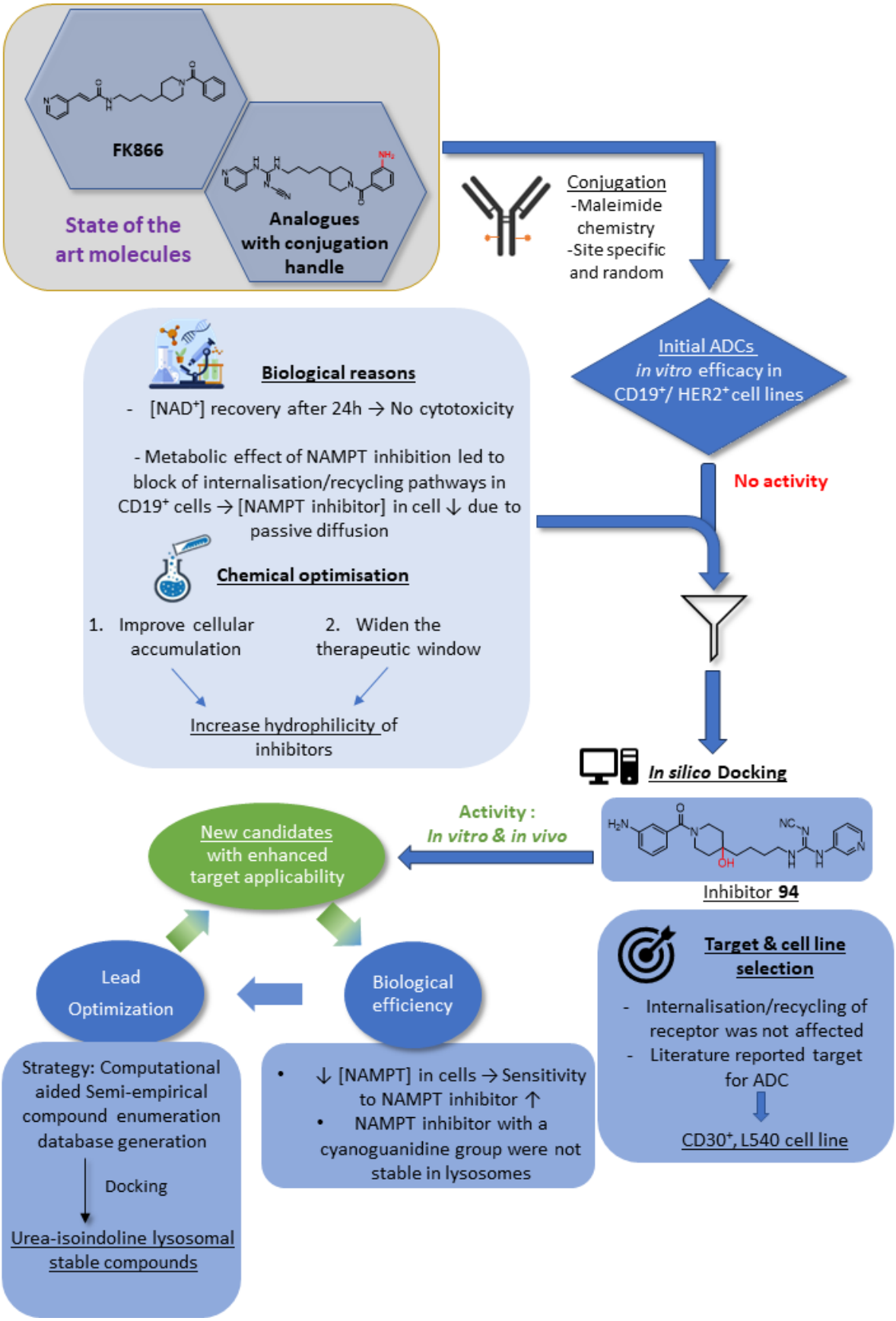

Figure 49. Graphic overview of the project.

5. Summary

Cancer is a complex, multifactorial group of diseases characterised by the uncontrolled growth of tumour cells, resulting in the loss of biological functions in patients. Unlike diseases caused by external agents, such as bacteria or viruses, most cancers are driven by the accumulation of mutations in the healthy cells of patients. Consequently, targeting and eliminating malignant cells while sparing healthy ones poses a significant challenge. Initial approaches to cancer treatment involved chemotherapy and radiotherapy, which targeted actively dividing cells, including healthy cells, but they lacked against non-dividing, dormant tumour cells. Furthermore, these therapies often had teratogenic side effects, leading to the emergence of new cancer variants and tumour escape in non-dividing cell populations.

To overcome the limitations of conventional therapeutic approaches, targeted therapies like antibody-drug conjugates (ADCs) have been developed. ADCs use the specificity and selectivity of monoclonal antibodies (mAbs) to target cell surface receptors and deliver potent cytotoxic compounds conjugated to the mAb framework to targeted cells. However, more than 50% of FDA-approved ADCs currently in clinical use primarily disrupt microtubule metabolism, making them as well only effective against actively dividing cells. Inhibition of NAMPT, the rate-limiting enzyme in the salvage biosynthetic pathway of NAD^+ starting from nicotinamide, induces cell death due to energy shortage in both dividing and non-dividing cell populations. Encouraging *in vitro* and *in vivo* results have been reported for free NAMPT inhibitors, highlighting the potential of NAMPT inhibition as an emerging mode of action in ADC technology.

In the first part of this work, the syntheses of literature presented NAMPT inhibitors and the efficacy limitations in single dose cell viability *in vitro* studies of the obtained inhibitors when used as ADC payloads are described. Then, based on the acquired knowledge, the project aimed to develop and adapt new families of NAMPT inhibitors for use in ADC technology. Initially, analogues of FK866 and CHS828, namely inhibitors **19**, **36** and **57**, were synthesised (Figure **50**). Here, the inhibitors **19** and **36** exhibit a pyridyl residue mimicking NAM and a cyanoguanidine moiety as connecting functional group with capability to hydrogen bonding. Inhibitor **57** on the contrary also contains a pyridyl residue as the NAM mimicking group but an acrylic spacer as connecting functional group with capability to hydrogen bonding. As free small molecules, all three inhibitors **19**, **36** and **57** showed cytotoxicity in nanomolar range in different cell lines such as the human B lymphocyte cell lines Ramos and Raji. Moreover, a strong enzyme binding was determined by bio-layer-interferometry with the biotinylated analogues. Next, a Cathepsin B-cleavable linker was attached to the inhibitors **19** and **36** resulting in the linker-payloads **27** and **37**, respectively, and $Her2^+$- and $CD19^+$-targeting ADCs with a DAR of 10 were generated. However, the results of the cell viability studies in $Her2^+$ and $CD19^+$ cell lines with these DAR10-ADCs demonstrated a lack of activity.[122,127] To unravel possible reasons for the lack in activity of the DAR10-ADCs, the total NAD^+ concentration was determined by a colorimetric assay in the $CD19^+$ Ramos cell line with the CD19-targeting DAR-10 ADC conjugated to linker-payload **37**. Notably, a slight drop in NAD^+ levels was revealed during the initial 24 hours of the treatment with this DAR10-ADC. However, NAD+ levels

recovered after 48 hours indicating a transient effect on NAMPT inhibition and explaining the observed lack of cytotoxic activity.

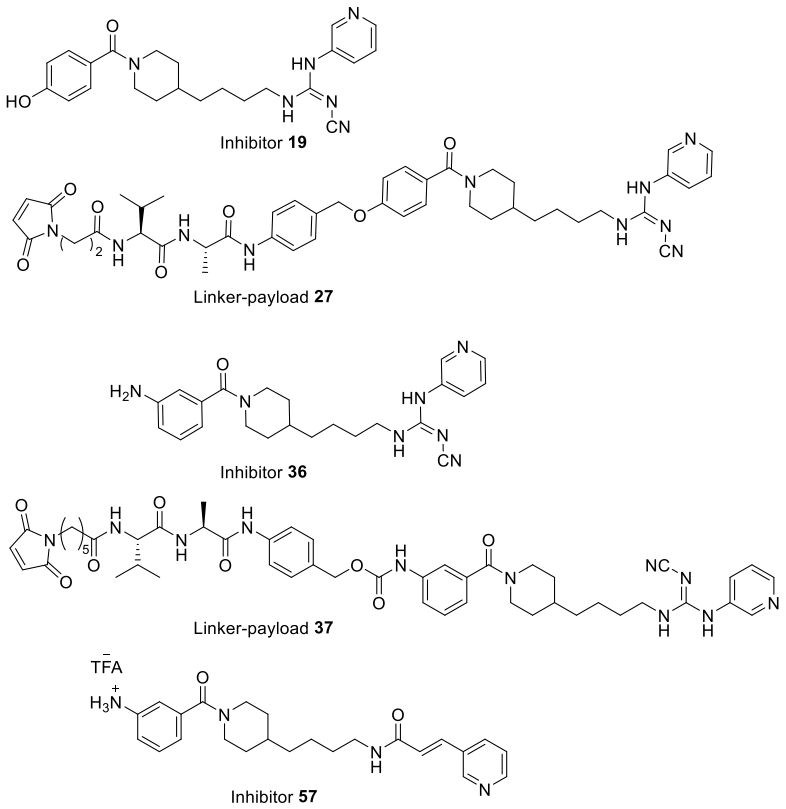

Figure 50. Described NAMPT inhibitors harnessing conjugatable chemical handles and their linker payloads.

To develop more potent and long-lasting NAMPT inhibitors, a small library of five inhibitors (cf. Figure **51A**) was synthesised based on two key criteria: 1.) ease of synthetic approach and linker conjugation, and 2.) modification of the inhibitors according to a proposed structural division of the pharmacophore in five parts (see Figure **51B**), defining pharmacophore as "an ensemble of steric and electronic features that is necessary to ensure the optimal supramolecular interactions with a specific biological target and to trigger (or block) its biological response".[199] Each of these parts of the pharmacophore has a specific role in the interaction with NAMPT namely NAM mimicking group, hydrogen bonding-capable polar group, aliphatic spacer, core ring and the linker anchor point. Different derivatives of the lead structure **36** were synthesized featuring variations in the five mentioned parts of the molecule. In total, five new inhibitors were synthesised: 1.) Inhibitor **43** differs from **36** in a less flexible aliphatic spacer, 2.) **62** in an acryl spacer as different H-bond capable polar group, 3.) **68** in an acryl spacer as different H-bond capable polar group and a piperazyl-moiety as the linker anchor point, 4.) **85** in an elongated aliphatic spacer and 5.) **92** in a benzoic acid residue as linker anchor point (Figure **51A**). From a biochemical standpoint, the various modifications of the five free inhibitors **43**, **62**, **68**, **85**, **92** showed different effects on the cytotoxic performance. No significant effects were found in the exchange of the hydrogen bond capable polar group (cyanoguanidine vs. acryl spacer) as there were comparable cytotoxicity found for inhibitor **62**, **68** and the lead structure **36**. However, modifications at the linker anchor point had the most

significant effects, with inhibitors bearing the 3-aniline moiety exhibiting the highest toxicities due to intermolecular interactions via hydrogen bonding with Glu-376 of NAMPT. [122] In contrast, inhibitor **92** has a benzoic acid at the linker anchor point, which is expected to be ionised at cytoplasmic pH. This interferes with its interaction with NAMPT as demonstrated in the computer simulations and explained its lack of cytotoxicity.

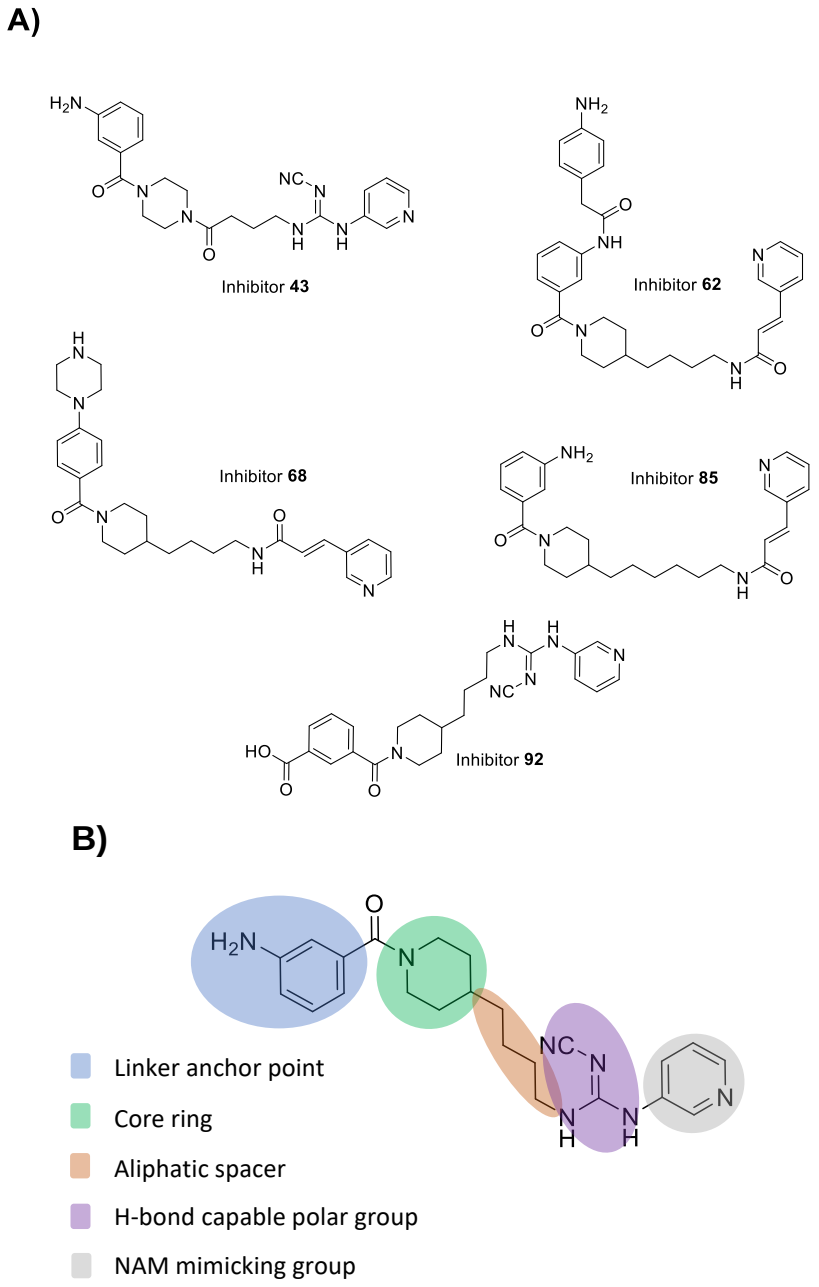

Figure 51. A) Library of chemical screened five NAMPT inhibitors synthesised. B) Structural division of the NAMPT inhibitor (pharmacophore) in five parts using inhibitor **36** as template.

Although the cytotoxicity of the inhibitors was maintained when only the hydrogen bond capable group was changed from a cyanoguanidine moiety to an acryl spacer, a remarkable effect related to the hydrophilicity of the inhibitors was observed. The affinity of acrylamide **57** and cyanoguanidine **36** to NAMPT was evaluated using an *in vitro* bio-layer-interferometry. Despite similar binding affinities, cyanoguanidine **36**, which is 12-fold more hydrophilic than

acrylamide **57** with regard to the logP value, exhibited 11 times lower toxicity. This finding supports the hypothesis that passive diffusion across cellular membranes is the main mechanism for the internalisation of free NAMPT inhibitors, what may result in higher cytoplasmic concentrations for more hydrophobic inhibitors. Thus, the increased hydrophobic character of free NAMPT inhibitors is correlated with higher cytotoxicity.

This discovery also contributed to the understanding of the observed lack of *in vitro* activity of NAMPT ADCs loaded with more hydrophobic NAMPT inhibitors. More hydrophilic NAMPT inhibitors on the contrary have a higher potential as payloads for ADCs, as they may exhibit lower cellular efflux when delivered intracellularly, while allowing an enhanced interaction with the highly glycosylated lysosomal luminal membrane that potentially would grant better travers of ADC's released payloads towards cytoplasm. This idea was supported by the significant loss of ADC internalisation after 24 hours of single-dose treatment of Ramos cells with a DAR10 ADC loaded with hydrophobic NAMPT inhibitors, with the internalisation determined by FACS. Therefore, the use of more hydrophilic inhibitors is necessary to allow cellular accumulation of the ADC-released inhibitor during the initial 24 hours. This proposed accumulation might aim to achieve stable NAMPT inhibition for at least 72 hours, which is a prerequisite for inducing cell death according to literature reports.[122,146] However, it is still unclear how the release from the lysosome takes place if not by passive diffusion via the highly glycosylated lysosomal membrane.[182,183] Another release mechanism from the lysosome than passive diffusion might be present. An attempt to increase ADC toxicity by improving the hydrophilicity of the linker-payload using PEG 4 or PEG 8 chains was unsuccessful. Hence, a new alternative for tackling an increased hydrophilicity on the linker-payloads was explored with inhibitor **92**, which harnessed a carboxylic acid moiety at the linker anchor point. However, inhibitor **92** exhibited a significant lack of activity. Hence, *in silico* docking simulations were performed and showed unfavourable interactions between inhibitor **92** and the enzyme due to the solvation of the carboxylate moiety in the catalytic pocket of NAMPT. This forces the aromatic hydrophobic residues of the inhibitor to get into contact with the solvent, resulting in a thermodynamically unfavourable interaction.

Due to the lack of cytotoxicity of the ADCs generated with these inhibitors, it became evident that an iterative synthetic-based approach for lead optimisation as used for inhibitors **43**, **62**, **68**, **85**, and **92** is not suitable for optimising NAMPT inhibitors for the ADC technology.

In the second chapter, the main objective was the *in silico* design and synthesis of new NAMPT inhibitors followed by biological evaluation of ADCs loaded with this new generation of NAMPT inhibitors. The new generation of NAMPT inhibitors were designed by means of computational assisted lead optimisation using the software Maestro with grids derived from PDB data of NAMPT-inhibitors co-crystals. The main goal of the inhibitor design was to achieve a more hydrophilic and highly potent NAMPT inhibitor as previous observations gave reason to believe the cellular accumulation of a more hydrophilic inhibitor. The computational optimisation of the NAMPT inhibitor used inhibitor **36** as lead structure that upon an iterative process involving molecular modifications and docking led to inhibitor **94** as the best candidate (Figure **52**). In comparison to lead structure **36**, inhibitor **94** only contains an additional tertiary alcohol functionality leading to a major improvement in docking as it interacts with the NAMPT enzyme in a hydrophilic groove of the catalytic pocket through hydrogen bonding. These findings suggested enhanced cytotoxic potential, while at the same logP calculations showed

approximately 300 times improved hydrophilicity of the new inhibitor **94** in comparison to inhibitor **36**.

Inhibitor **94** was synthesised and as expected for non-targeted delivery, the cytotoxicity of free inhibitor **94** was significantly lower (136-fold) compared to the lead structure **36** (Figure **52**) due to the higher hydrophilicity of inhibitor **94**. Due to the higher hydrophilicity, the ability of inhibitor **94** to cross the cell membrane by passive diffusion is most likely reduced in comparison to lead structure **36**. Hence, the intracellular inhibitor concentration differs significantly resulting in the observed reduced cytotoxicity of the free inhibitor **94**.

In relation to ADC targeting, the focus in this second part of the work shifted from CD19 and Her2 to CD30 as target. The aim behind this decision was to broaden the range of targets for the ADCs and to identify a highly sensitive cell lines to NAMPT inhibition. CD30 was chosen as the cellular target for ADCs based on positive results reported in the literature.[122] To target CD30, an anti-CD30 brentuximab-like mAb was designed. The generation of the brentuximab-like mAb involved the production of recombinant vectors containing HDP's proprietary heavy chain (HC) and light chain (LC) DNA expression scaffolds, in which sequences of anti-CD30 brentuximab-based variable regions were incorporated.[173] To enable site-specific conjugation of the NAMPT inhibitors to the antibody and to reduce Fc receptor mediated uptake, engineered cysteines at position D265 (thiomab™) and Fcγ receptor interaction-silencing mutations (LALA) were also added to the Fc region-encoding sequences on the mAb expression vectors. The anti-CD30 thiomab™ was then produced in Expi 293 cells and purified using protein A affinity and gel filtration chromatography. Additionally, a PCR-driven single-point mutation was incorporated in the D265C thiomab™ mAb at position A118C, resulting in the double anti-CD30 thiomab mAb used to produce site specific DAR4 ADCs. The D265C single thiomab™ anti-CD30 mAb was then used to generate DAR10 anti-CD30 ADCs loaded with linker-payloads **37** and **97**, followed by a single-dose, 96-hour cytotoxicity test using the $CD30^+$ L540 cell line. Linker-payload **37** is the corresponding linker-payload of lead structure **36** and the results of the obtained DAR10 anti-CD30-**37** ADC indicated nM IC_{50} values, but still 40% residual cell viability was observed (Figure **52**). In contrast, an anti-CD30 DAR10 ADC loaded with linker-payload **97**, which is the corresponding linker-payload to inhibitor **94**, exhibited improved cytotoxicity with picomolar IC_{50} values and full-blown cytotoxicity in L540 cells. Additionally, the four orders of magnitude lower cytotoxicity of the free inhibitor **94** compared to the anti-CD30 DAR10-**97** ADC is likely favourable for an optimised therapeutical window (Figure **52**).

5. Summary

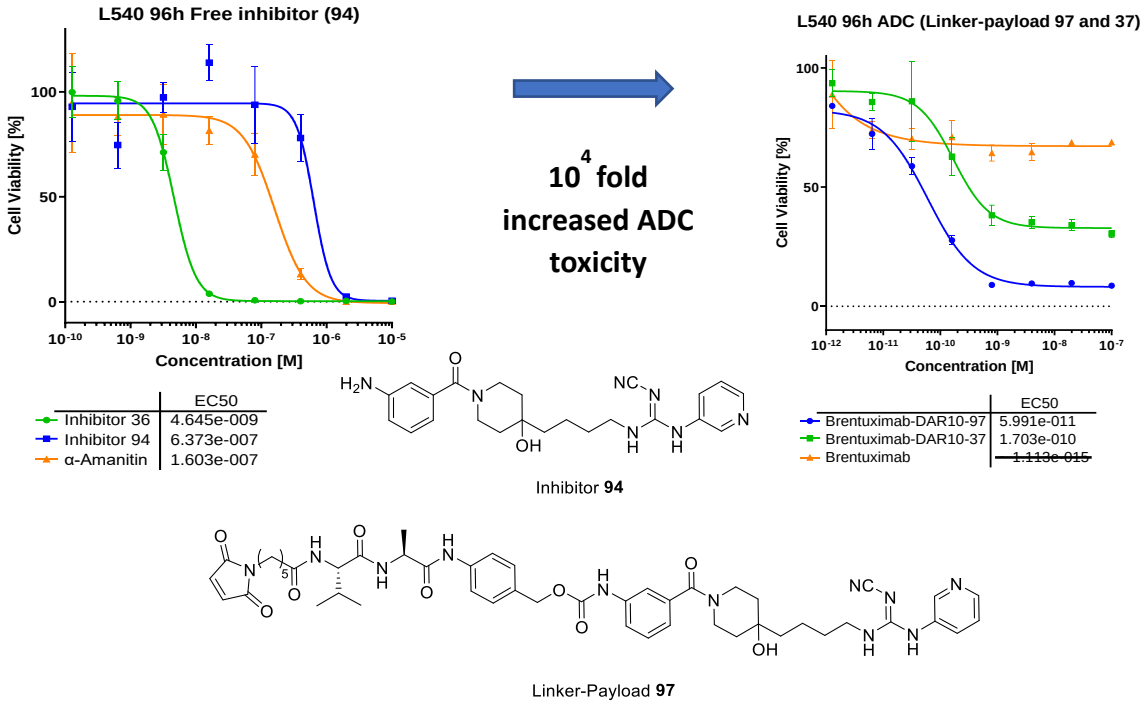

Figure 52. Cytotoxic profile of free inhibitor **94** compared with anti-CD30 mAb (Brentuximab)-**97** ADC showing a 10^4 fold higher toxicity of the ADC in comparison to the free inhibitor.

Furthermore, the new anti-CD30 ADCs loaded with linker-payload **97** enabled nM IC_{50} cytotoxicity even as site-specific DAR4 ADC. The promising antitumoral effects of the new linker-payload tertiary alcohol **97** were not limited to *in vitro* testing; they also demonstrated an 80-day survival advantage in the L540 xenograft disseminated *in vivo* model in NXG mice, as reported in Figure **53**.

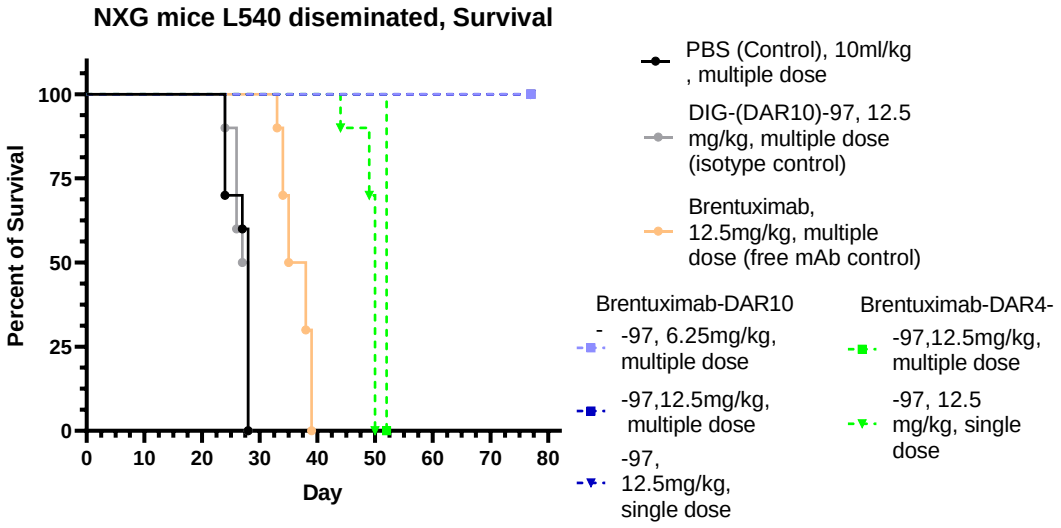

Figure 53. *In vivo efficacy study of L540 disseminated model in NXG mice, 10 mice per group. Control groups are plotted in circles, black for vehicle (PBS), grey for isotype DAR10 DIG ADC and salmon for free Brentuximab-LALA-D265C mAb. Test groups are divided into two categories: blue DAR10 ADC using Brentuximab-LALA-D265C as mAb and green DAR4 ADC using Brentuximab-A118C-LALA-D265C mAb. Additionally, multiple-dose groups are represented in squares, while 1-day post-inoculation single-dose treated groups are represented with inverted triangles.*

5. Summary

However, ADCs loaded with linker-payload **97** were not able to induce cytotoxicity in combination with other targets than CD30. There a several reasons, mechanisms or combinations of mechanisms explaining these findings, and two reasons are mentioned in more detail. On the one hand, it was observed that the target density was reduced after NAMPT inhibitor loaded ADC treatment of cells for 24h, which can result in lower ADC internalisation over time. On the other hand, different NAMPT expression levels could be the reason for the different sensitivity of ADC-treated cell lines. The cytotoxicity of the anti-CD30 ADC loaded with linker-payload **97** for instance was only tested against L540 cells, and this cell line shows significant lower expression of NAMPT compared with other cell lines like Ramos and Raji tested with anti-CD19 ADCs (Figure **54A**). Due to the significant lower expression of NAMPT in L540 cells, the higher sensitivity for treatment with NAMPT inhibitor-loaded ADCs can be explained. Furthermore, it was discovered, that the cyanoguanidine group present in the released NAMPT inhibitors **36** and **94** is chemically instable in the lysosomes. Hence, the stability was examined with inhibitor **36** as model. First, it was chemically demonstrated that the cyanoguanidine moiety on inhibitor **36** undergoes fast hydrolysis to the corresponding guanylurea **113** at pH values below 2. Guanylurea **113** exhibited 655-fold lower cytotoxicity compared to inhibitor **36** due to inefficient binding to NAMPT, as calculated in the *in silico* simulations and confirmed by bio-layer-interferometry measurements with the NAMPT enzyme. Second, an *in vitro* stability assay of inhibitor **36** in human lysosomal extracts at pH 5.5 and 37°C demonstrated, that lysosomal hydrolases could also catalyse the degradation to the corresponding guanylurea even at lysosomal pH, which was confirmed by LC-MS (Figure **54B**). As a consequence, a lower concentration of active inhibitor in the cytosol is expected, which is in accordance with the fact, that only the cell line L540 with lower NAMPT expression levels is sensitive to the treatment with ADCs loaded with cyanoguanidine-containing NAMPT inhibitors.

5. Summary

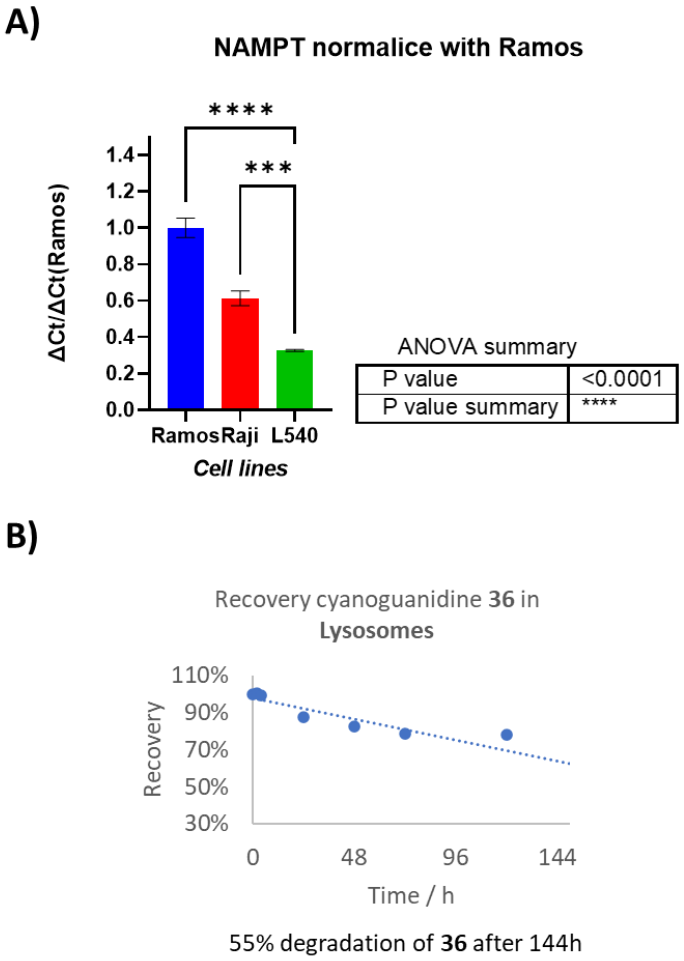

Figure 54. A) Normalised NAMPT mRNA expression levels between Ramos, Raji, and L540 cells. B) *In vitro* lysosomal stability assay, comparison of cyanoguanidine 36 recovery vs. time with lysosomal extracts.

Motivated by the finding, that cyanoguanidine-containing inhibitors are degraded in the lysosome, a virtual screening of a 3000-compound database containing NAMPT inhibitors led to the identification of inhibitor **124** as a promising lysosomal-proof NAMPT inhibitor. In contrast to inhibitor **94**, the cyanoguanidine group was exchanged against a mixed urea and moreover, the NAM mimicking group was switched from a pyridyl- to an isoindoline moiety. Remarkably, the cytotoxicity of the free inhibitor **124** was identical to the one of inhibitor **94** (Figure **55**) demonstrating the power of the *in silico* inhibitor design. However, initial synthetic efforts did not yield inhibitor **124** in sufficient amounts to proceed the next steps of linker-attachment and conjugation to the mAb. Hence, further studies will be required to validate this hypothesis.

5. Summary

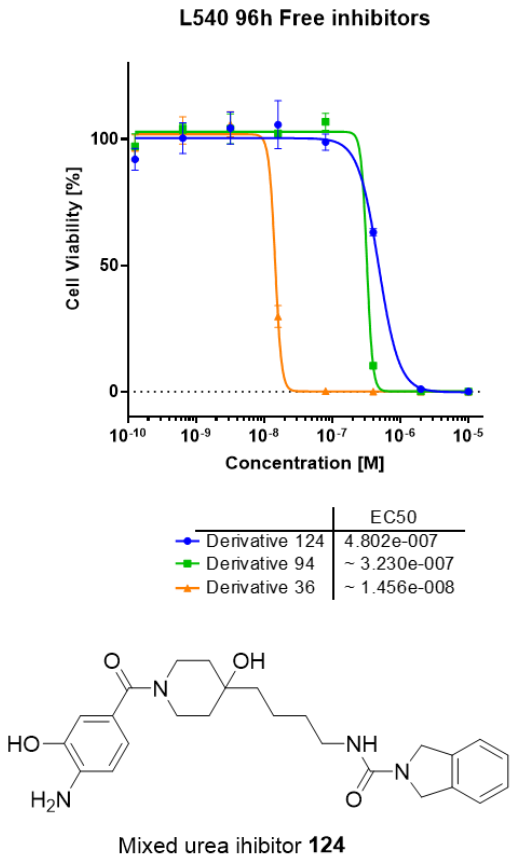

Figure 55. Cytotoxicity of free urea-isoindoline inhibitor **124** compared with cyanoguanidines **94** and **36** in L540 cells (EC_{50} (M)).

In summary, the results of this works demonstrate, that the hydrophobic NAMPT inhibitors described in the literature were not suitable as ADC payloads. *In silico* lead optimisation led to next-generation NAMPT inhibitors with enhanced hydrophilicity exhibiting remarkable antitumoral effects in cellular and *in vivo* models. Additionally, this study highlights that acid-labile groups are not effective in NAMPT inhibitors used as ADC payloads. In response, future studies should explore non-hydrolysable inhibitors to broaden the applicability of NAMPT inhibitor-loaded ADCs.

5. Summary

Zusammenfassung auf Deutsch

Krebs ist eine komplexe, multifaktorielle Gruppe von Krankheiten, die durch das unkontrollierte Wachstum von Tumorzellen gekennzeichnet sind und zum Verlust biologischer Funktionen bei den Patienten führen. Im Gegensatz zu Krankheiten, die durch äußere Einflüsse wie Bakterien oder Viren verursacht werden, entstehen die meisten Krebserkrankungen durch die Anhäufung von Mutationen in den gesunden Zellen der Patienten. Folglich ist es eine große Herausforderung, die bösartigen Zellen gezielt zu bekämpfen und zu eliminieren und gleichzeitig die gesunden Zellen zu schonen. Die ersten Ansätze zur Krebsbehandlung umfassten Chemo- und Strahlentherapie, die auf sich aktiv teilende Zellen, einschließlich gesunder Zellen, abzielten, aber nicht gegen sich nicht teilende, ruhende Tumorzellen wirkten. Darüber hinaus hatten diese Therapien häufig teratogene Nebenwirkungen, was zur Entstehung neuer Krebsvarianten und zum Entweichen von Tumoren in sich nicht teilenden Zellpopulationen führte.

Um die Grenzen herkömmlicher therapeutischer Ansätze zu überwinden, wurden zielgerichtete Therapien wie Antikörper-Wirkstoff-Konjugate (ADCs) entwickelt. ADCs nutzen die Spezifität und Selektivität monoklonaler Antikörper (mAbs), um auf Zelloberflächenrezeptoren zu zielen und wirksame zytotoxische Verbindungen, die mit dem mAb-Gerüst konjugiert sind, an die Zielzellen abzugeben. Mehr als 50 % der von der FDA zugelassenen ADCs, die derzeit in der klinischen Anwendung sind, stören jedoch in erster Linie den Mikrotubuli-Stoffwechsel, so dass auch sie nur gegen sich aktiv teilende Zellen wirksam sind. Die Hemmung von NAMPT, dem geschwindigkeitsbeschränkenden Enzym des NAD^+-Biosynthesewegs ausgehend von Nicotinamid, führt zum Zelltod aufgrund von Energiemangel sowohl in sich teilenden als auch in sich nicht teilenden Zellpopulationen. Es wurden ermutigende *In-vitro*- und *In-vivo*-Ergebnisse für freie NAMPT-Inhibitoren berichtet, die das Potenzial der NAMPT-Inhibition als neue Wirkungsweise in der ADC-Technologie hervorheben.

Im ersten Teil dieser Arbeit werden die Synthesen der in der Literatur vorgestellten NAMPT-Inhibitoren und die Wirksamkeitsbeschränkungen der erhaltenen Inhibitoren in Einzeldosis-Zellviabilitätsstudien in vitro bei Verwendung als ADC-Nutzlast beschrieben. Auf der Grundlage der gewonnenen Erkenntnisse zielte das Projekt darauf ab, neue Familien von NAMPT-Inhibitoren für den Einsatz in der ADC-Technologie zu entwickeln und anzupassen. Zunächst wurden Analoga von FK866 und CHS828, nämlich die Inhibitoren **19**, **36** und **57**, synthetisiert (Abbildung **56**). Dabei weisen die Inhibitoren **19** und **36** einen Pyridylrest auf, der NAM imitiert, und eine Cyanoguanidineinheit als verbindende funktionelle Gruppe mit der Fähigkeit zur Wasserstoffbrückenbindung. Der Inhibitor **57** dagegen enthält ebenfalls einen Pyridylrest als NAM-nachahmende Gruppe, aber einen Acrylspacer als verbindende funktionelle Gruppe mit der Fähigkeit zur Wasserstoffbrückenbindung. Als freie kleine Moleküle zeigten alle drei Inhibitoren **19**, **36** und **57** Zytotoxizität im nanomolaren Bereich in verschiedenen Zelllinien wie den menschlichen B-Lymphozyten-Zelllinien Ramos und Raji. Darüber hinaus wurde mittels Bio-Layer-Interferometrie eine starke Enzymbindung mit den biotinylierten Analoga festgestellt. Anschließend wurde an die Inhibitoren **19** und **36** ein durch Cathepsin B spaltbarer Linker angehängt, was zu den Linker-Payloads **27** bzw. **37** führte, und es wurden $Her2^+$- und $CD19^+$-gerichtete ADCs mit einem DAR von 10 hergestellt. Die Ergebnisse der Zelllebensfähigkeitsstudien in $Her2^+$- und $CD19^+$-Zelllinien mit diesen DAR10-ADCs zeigten jedoch einen Mangel an Aktivität.[122,127] Um mögliche Gründe für die mangelnde Aktivität der

5. Summary

DAR10-ADCs zu entschlüsseln, wurde die Gesamt-NAD^+-Konzentration in der $CD19^+$ Ramos-Zelllinie mit dem CD19-gerichteten DAR-10-ADC, der mit der Linker-Payload **37** konjugiert war, mittels eines kolorimetrischen Assays bestimmt. In den ersten 24 Stunden der Behandlung mit diesem DAR10-ADC wurde ein leichter Abfall der NAD^+-Konzentration festgestellt. Der NAD^+-Spiegel erholte sich jedoch nach 48 Stunden, was auf eine vorübergehende Wirkung der NAMPT-Hemmung hindeutet und das beobachtete Fehlen einer zytotoxischen Aktivität erklärt.

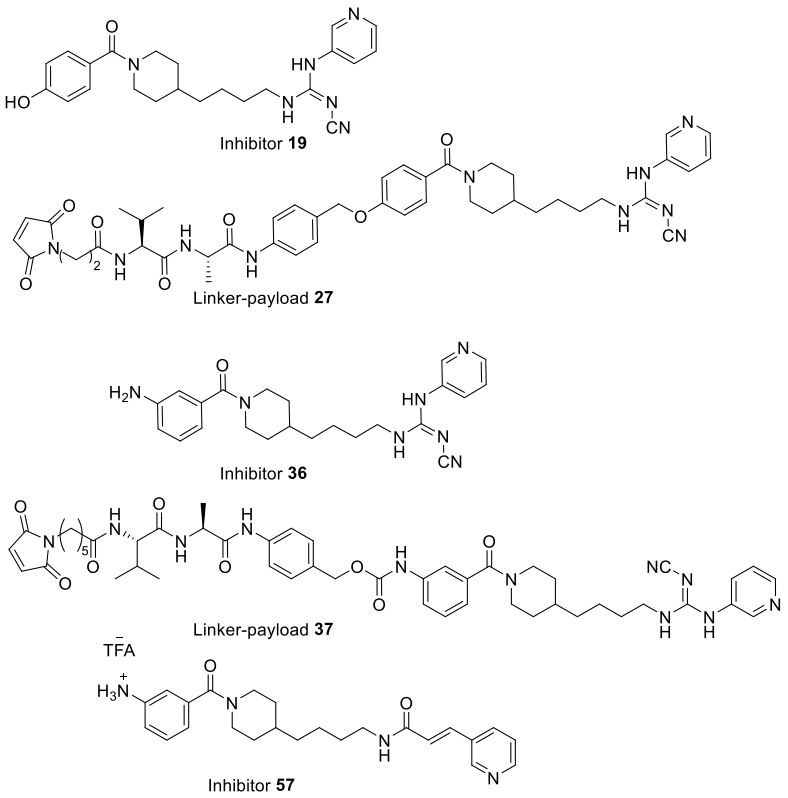

Abbildung 56. Beschriebene NAMPT-Inhibitoren, die konjugierbare chemische Griffe und ihre Linker-Nutzlasten nutzen .

Um wirksamere und langlebigere NAMPT-Inhibitoren zu entwickeln, wurde eine kleine Bibliothek von fünf Inhibitoren (siehe Abbildung **57A**) auf der Grundlage von zwei Schlüsselkriterien synthetisiert: 1.) Einfachheit des synthetischen Ansatzes und der Linker-Konjugation und 2.) Modifizierung der Inhibitoren gemäß einer vorgeschlagenen strukturellen Aufteilung des Pharmakophores in fünf Teile (siehe Abbildung **57B**), wobei das Pharmakophor definiert wird als "ein Ensemble sterischer und elektronischer Merkmale, die notwendig sind, um die optimalen supramolekularen Wechselwirkungen mit einem spezifischen biologischen Ziel zu gewährleisten und dessen biologische Reaktion auszulösen (oder zu blockieren)".[199] Jeder dieser Teile des Pharmakophores spielt eine spezifische Rolle bei der Interaktion mit NAMPT, nämlich die NAM-nachahmende Gruppe, die polare Gruppe, die für Wasserstoffbrückenbindungen geeignet ist, der aliphatische Spacer, der Kernring und der Linker-Ankerpunkt. Es wurden verschiedene Derivate der Leitstruktur **36** synthetisiert, die sich durch Variationen in den fünf genannten Teilen des Moleküls auszeichnen. Insgesamt wurden fünf neue Inhibitoren synthetisiert: 1.) Inhibitor **43** unterscheidet sich von **36** durch einen weniger flexiblen aliphatischen Spacer, 2.) **62** durch einen Acrylspacer als andere H-bindungsfähige polare Gruppe, 3.) **68** durch einen Acrylspacer als andere H-bindungsfähige

polare Gruppe und einen Piperazylrest als Linker-Ankerpunkt, 4.) **85** durch einen verlängerten aliphatischen Spacer und 5.) **92** in einem Benzoesäurerest als Linker-Ankerpunkt (Abbildung **57A**). Aus biochemischer Sicht zeigten die verschiedenen Modifikationen der fünf freien Inhibitoren **43**, **62**, **68**, **85**, **92** unterschiedliche Auswirkungen auf die zytotoxische Leistung. Es wurden keine signifikanten Auswirkungen beim Austausch der wasserstoffbindungsfähigen polaren Gruppe (Cyanoguanidin vs. Acrylspacer) festgestellt, da für die Inhibitoren **62**, **68** und die Leitstruktur **36** eine vergleichbare Zytotoxizität gefunden wurde. Allerdings hatten Modifikationen am Linker-Ankerpunkt die deutlichsten Auswirkungen, wobei die Inhibitoren mit dem 3-Anilin-Anteil die höchsten Toxizitäten aufwiesen, was auf intermolekulare Wechselwirkungen über Wasserstoffbrückenbindungen mit Glu-376 von NAMPT zurückzuführen ist.[122] Im Gegensatz dazu enthält der Inhibitor **92** eine Benzoesäure am Linker-Ankerpunkt, die bei zytoplasmatischem pH-Wert ionisiert sein dürfte. Dies beeinträchtigt seine Interaktion mit NAMPT, wie in den Computersimulationen gezeigt wurde, und erklärt seine mangelnde Zytotoxizität.

5. Summary

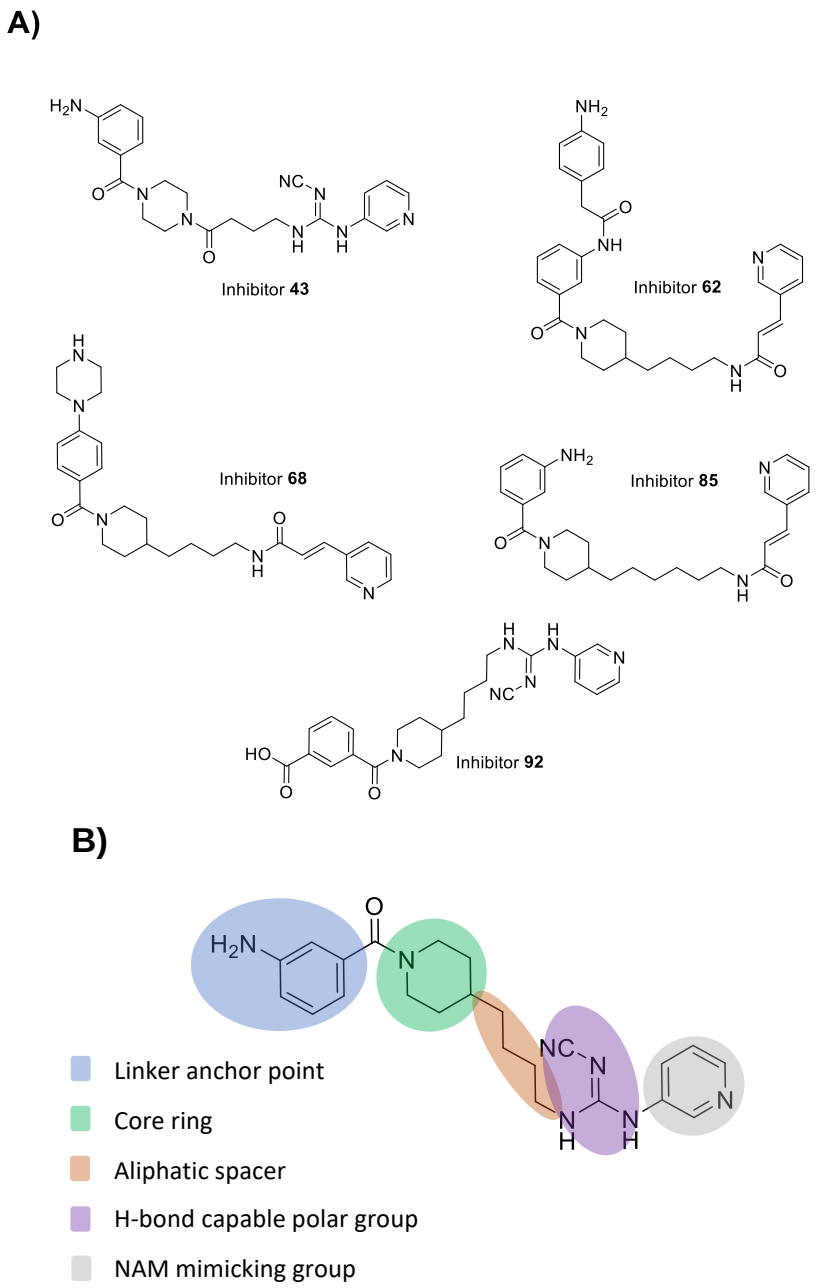

Abbildung 57. A) Bibliothek mit fünf synthetisch hergestellten NAMPT-Inhibitoren. B) Strukturelle Aufteilung des NAMPT-Inhibitors (Pharmakophor) in fünf Teile unter Verwendung des Inhibitors **36** als Vorlage.

Obwohl die Zytotoxizität der Inhibitoren beibehalten wurde, wenn nur die zu Wasserstoffbrückenbindungen fähige Gruppe von einer Cyanoguanidin-Einheit zu einem Acryl-Spacer ausgetauscht wurde, wurde ein bemerkenswerter Effekt im Zusammenhang mit der Hydrophilie der Inhibitoren beobachtet. Die Affinität von Acrylamid **57** und Cyanoguanidin **36** zu NAMPT wurde mit Hilfe einer In-vitro-Bio-Layer-Interferometrie untersucht. Trotz ähnlicher Bindungsaffinitäten wies Cyanoguanidin **36**, das im Hinblick auf den logP-Wert 12-mal hydrophiler als Acrylamid **57** ist, eine 11-mal geringere Toxizität auf. Dieses Ergebnis stützt die Hypothese, dass die passive Diffusion durch die Zellmembranen der Hauptmechanismus für die Internalisierung freier NAMPT-Inhibitoren ist, was zu höheren zytoplasmatischen

Konzentrationen für hydrophobere Inhibitoren führen kann. Der erhöhte hydrophobe Charakter der freien NAMPT-Inhibitoren korreliert also mit einer höheren Zytotoxizität.

Diese Entdeckung trug auch zum Verständnis der beobachteten mangelnden *In-vitro*-Aktivität von NAMPT-ADCs bei, die mit hydrophoberen NAMPT-Inhibitoren beladen sind. Hydrophilere NAMPT-Inhibitoren haben im Gegenteil ein größeres Potenzial als Nutzlast für ADCs, da sie bei intrazellulärer Verabreichung einen geringeren zellulären Efflux aufweisen und gleichzeitig eine bessere Interaktion mit der hoch glykosylierten lysosomalen Luminalmembran ermöglichen, die möglicherweise einen besseren Transport der freigesetzten ADC-Nutzlast in Richtung Zytoplasma gewährleisten würde. Diese Idee wurde durch den signifikanten Verlust der ADC-Internalisierung nach einer 24-stündigen Einzeldosis-Behandlung von Ramos-Zellen mit einem DAR10-ADC, das mit hydrophoben NAMPT-Inhibitoren beladen war, unterstützt, wobei die Internalisierung mittels FACS bestimmt wurde. Daher ist die Verwendung hydrophilerer Inhibitoren erforderlich, um eine zelluläre Akkumulation des freigesetzten ADC-Inhibitors während der ersten 24 Stunden zu ermöglichen. Diese vorgeschlagene Akkumulation könnte darauf abzielen, eine stabile NAMPT-Hemmung für mindestens 72 Stunden zu erreichen, was laut Literaturberichten eine Voraussetzung für die Herbeiführung des Zelltods ist.[122,146] Es ist jedoch noch unklar, wie die Freisetzung aus dem Lysosom erfolgt, wenn nicht durch passive Diffusion über die stark glykosylierte lysosomale Membran.[182,183] Möglicherweise gibt es einen anderen Freisetzungsmechanismus aus dem Lysosom als die passive Diffusion. Ein Versuch, die ADC-Toxizität durch Verbesserung der Hydrophilie der Linker-Payloads mit Hilfe von PEG 4- oder PEG 8-Ketten zu erhöhen, war nicht erfolgreich. Daher wurde mit dem Inhibitor **92** eine neue Alternative zur Erhöhung der Hydrophilie der Linker-Payloads erprobt, bei der eine Carbonsäuregruppe am Linker-Ankerpunkt zum Einsatz kam. Der Inhibitor **92** zeigte jedoch einen erheblichen Mangel an Aktivität. Daher wurden *in silico* Docking-Simulationen durchgeführt, die ungünstige Wechselwirkungen zwischen dem Inhibitor **92** und dem Enzym ergaben, die auf die Solvatisierung des Carboxylatanteils in der katalytischen Tasche von NAMPT zurückzuführen sind. Dadurch werden die aromatischen hydrophoben Reste des Inhibitors gezwungen, mit dem Lösungsmittel in Kontakt zu kommen, was zu einer thermodynamisch ungünstigen Wechselwirkung führt.

Aufgrund der mangelnden Zytotoxizität der mit diesen Inhibitoren hergestellten ADCs wurde deutlich, dass ein auf iterativer Synthese basierender Ansatz zur Leitstrukturoptimierung, wie er für die Inhibitoren **43**, **62**, **68**, **85** und **92** verwendet wurde, nicht für die Optimierung von NAMPT-Inhibitoren für die ADC-Technologie geeignet ist.

Im zweiten Kapitel war das Hauptziel das *In-silico*-Design und die Synthese neuer NAMPT-Inhibitoren, gefolgt von der biologischen Bewertung von ADCs, die mit dieser neuen Generation von NAMPT-Inhibitoren beladen sind. Die neue Generation von NAMPT-Inhibitoren wurde mittels computergestützter Leitstrukturoptimierung unter Verwendung der Software Maestro mit Gittern entworfen, die aus PDB-Daten von NAMPT-Inhibitor-Kokristallen abgeleitet wurden. Das Hauptziel des Inhibitor-Designs war es, einen hydrophileren und hochwirksamen NAMPT-Inhibitor zu entwickeln, da frühere Beobachtungen auf eine zelluläre Akkumulation eines hydrophileren Inhibitors hindeuteten. Bei der rechnerischen Optimierung des NAMPT-Inhibitors wurde Inhibitor **36** als Leitstruktur verwendet, die nach einem iterativen Prozess mit molekularen Modifikationen und Docking zu Inhibitor **94** als dem besten Kandidaten führte (Abbildung **58**). Im Vergleich zur Leitstruktur **36** enthält der Inhibitor **94** nur eine zusätzliche tertiäre Alkoholfunktionalität, was zu einer wesentlichen Verbesserung des

Dockings führt, da er mit dem NAMPT-Enzym in einer hydrophilen Furche der katalytischen Tasche durch Wasserstoffbrückenbindungen interagiert. Diese Ergebnisse deuten auf ein verbessertes zytotoxisches Potenzial hin, während gleichzeitig logP-Berechnungen eine etwa 300-fach verbesserte Hydrophilie des neuen Inhibitors **94** im Vergleich zu Inhibitor **36** zeigten.

Der Inhibitor **94** wurde synthetisiert, und wie für eine nicht zielgerichtete Verabreichung erwartet, war die Zytotoxizität des freien Inhibitors **94** im Vergleich zur Leitstruktur **36** (Abbildung **58**) aufgrund der höheren Hydrophilie des Inhibitors **94** deutlich geringer (136-fach). Aufgrund der höheren Hydrophilie ist die Fähigkeit des Inhibitors **94**, die Zellmembran durch passive Diffusion zu passieren, im Vergleich zur Leitstruktur **36** höchstwahrscheinlich reduziert. Daher unterscheidet sich die intrazelluläre Inhibitorkonzentration erheblich, was zu der beobachteten geringeren Zytotoxizität des freien Inhibitors **94**.

In Bezug auf das ADC-Targeting verlagerte sich der Schwerpunkt in diesem zweiten Teil der Arbeit von CD19 und Her2 auf CD30 als Target. Ziel dieser Entscheidung war es, das Spektrum der Targets für die ADCs zu erweitern und eine hochempfindliche Zelllinie für die NAMPT-Hemmung zu identifizieren. CD30 wurde aufgrund positiver Ergebnisse in der Literatur als zelluläres Ziel für ADCs ausgewählt.[122] Als Zielmolekül für CD30 wurde ein Brentuximab-ähnliches mAb gegen CD30 entwickelt. Zur Herstellung des Brentuximab-ähnlichen mAb wurden rekombinante Vektoren hergestellt, die HDP-eigene DNA-Expressionsgerüste für die schwere Kette (HC) und die leichte Kette (LC) enthielten, in die Sequenzen von Anti-CD30-Brentuximab-basierten variablen Regionen eingebaut wurden.[173] Um eine ortsspezifische Konjugation der NAMPT-Inhibitoren an den Antikörper zu ermöglichen und die durch den Fc-Rezeptor vermittelte Aufnahme zu verringern, wurden den für die Fc-Region kodierenden Sequenzen auf den mAb-Expressionsvektoren auch künstliche Cysteine an Position D265 (thiomab™) und Mutationen zur Unterdrückung der Fcγ-Rezeptor-Interaktion (LALA) hinzugefügt. Das Anti-CD30-Thiomab™ wurde dann in Expi 293-Zellen produziert und mit Protein-A-Affinitäts- und Gelfiltrationschromatographie gereinigt. Zusätzlich wurde eine PCR-gesteuerte Ein-Punkt-Mutation in das D265C thiomab™ mAb an der Position A118C eingebaut, was zu dem doppelten anti-CD30 thiomab mAb führte, das zur Herstellung von ortsspezifischen DAR4 ADCs verwendet wurde. Der einzelne D265C thiomab™ anti-CD30 mAb wurde dann zur Herstellung von DAR10 anti-CD30 ADCs verwendet, die mit den Linker-Payloads **37** und **97** beladen waren, gefolgt von einem 96-stündigen Zytotoxizitätstest mit einer Einzeldosis unter Verwendung der $CD30^+$ L540 Zelllinie. Die Linker-Payload **37** ist die entsprechende Linker-Payload der Leitstruktur **36**, und die Ergebnisse des erhaltenen DAR10-Anti-CD30-**37**-ADC zeigten nM-IC_{50}-Werte, aber es wurde immer noch eine 40%ige Rest-Zellviabilität beobachtet (Abbildung **58**). Im Gegensatz dazu zeigte ein Anti-CD30-DAR10-ADC, der mit der Linker-Payload **97**, der entsprechenden Linker-Payload des Inhibitors **94**, beladen war, eine verbesserte Zytotoxizität mit picomolaren IC_{50}-Werten und eine voll ausgeprägte Zytotoxizität in L540-Zellen. Darüber hinaus ist die um vier Größenordnungen geringere Zytotoxizität des freien Inhibitors **94** im Vergleich zum Anti-CD30 DAR10-**97** ADC wahrscheinlich günstig für ein optimiertes therapeutisches Fenster (Abbildung **58**).

5. Summary

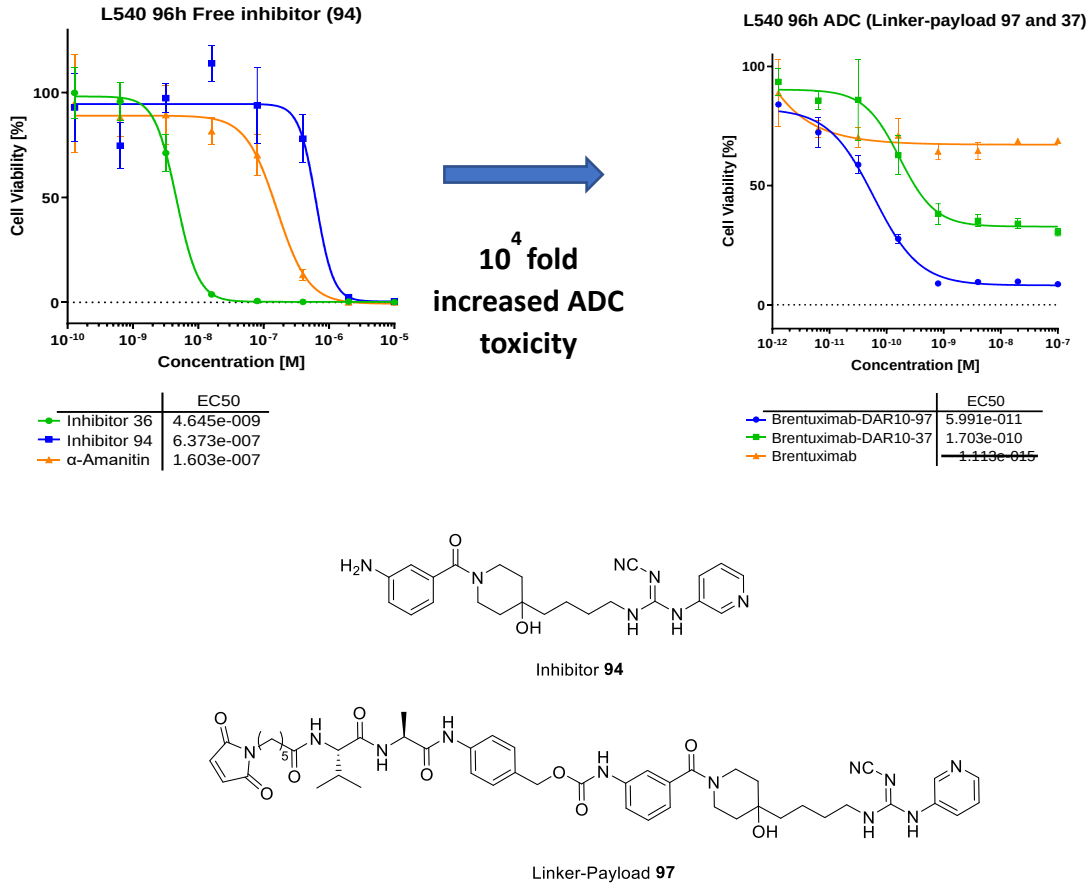

Abbildung 58. Zytotoxisches Profil des freien Inhibitors **94** im Vergleich zum Anti-CD30 mAb (Brentuximab)-**97** ADC, das eine 10^4-fach höhere Toxizität des ADC im Vergleich zum freien Inhibitor zeigt.

Darüber hinaus ermöglichten die neuen Anti-CD30-ADCs, die mit der Linker-Zahllast **97** beladen waren, sogar als ortsspezifische DAR4-ADCs eine nM-IC_{50}-Zytotoxizität. Die vielversprechenden antitumoralen Wirkungen des neuen tertiären Alkohols **97** mit Linker-Payload beschränkten sich nicht auf *In-vitro*-Tests; sie zeigten auch einen 80-Tage-Überlebensvorteil im L540-Xenotransplantat, das *in vivo* in NXG-Mäusen verbreitet wurde, wie in Abbildung **59** dargestellt.

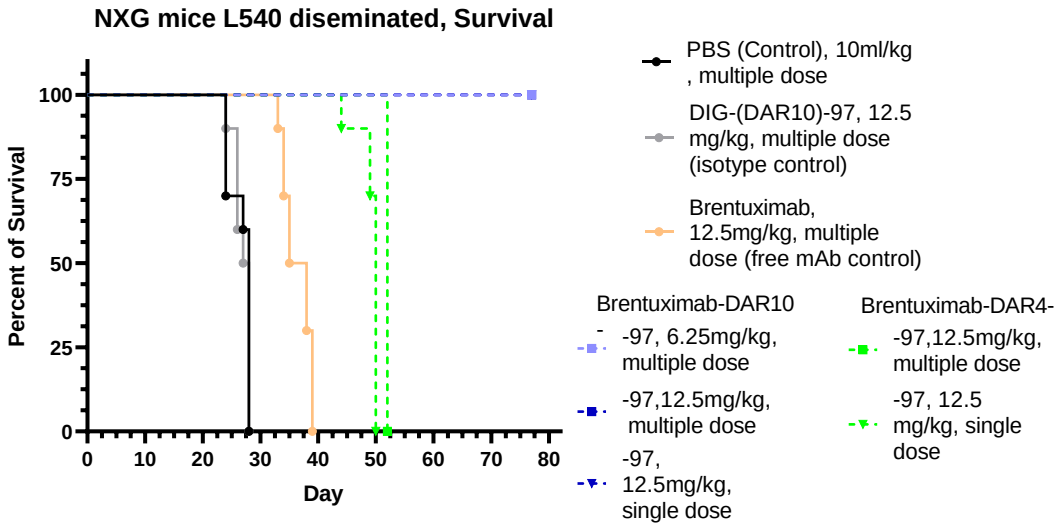

Abbildung 59. *In-vivo*-Wirksamkeitsstudie des L540-Verbreitungsmodells bei NXG-Mäusen, 10 Mäuse pro Gruppe. Kontrollgruppen sind in Kreisen dargestellt, schwarz für Vehikel (PBS), grau für isotypisches DAR10 DIG ADC und lachsfarben für freien Brentuximab-LALA-D265C mAb. Die Testgruppen sind in zwei Kategorien unterteilt: blau DAR10 ADC mit Brentuximab-LALA-D265C als mAb und grün DAR4 ADC mit Brentuximab-A118C-LALA-D265C mAb. Darüber hinaus sind die Gruppen mit Mehrfachdosen in Quadraten dargestellt, während die Gruppen, die 1 Tag nach der Inokulation mit einer Einzeldosis behandelt wurden, mit umgekehrten Dreiecken dargestellt sind.

Mit Linker-Payload **97** beladene ADCs waren jedoch nicht in der Lage, in Kombination mit anderen Targets als CD30 Zytotoxizität zu induzieren. Es gibt mehrere Gründe, Mechanismen oder Kombinationen von Mechanismen, die diese Ergebnisse erklären, und zwei Gründe werden ausführlicher erwähnt. Zum einen wurde beobachtet, dass die Targetdichte nach einer 24-stündigen Behandlung der Zellen mit NAMPT-Inhibitor-beladenem ADC abnahm, was zu einer geringeren Internalisierung des ADC im Laufe der Zeit führen kann. Andererseits könnten unterschiedliche NAMPT-Expressionsniveaus der Grund für die unterschiedliche Empfindlichkeit der mit ADC behandelten Zelllinien sein. Die Zytotoxizität des mit Linker-Payload **97** beladenen Anti-CD30-ADCs wurde beispielsweise nur gegen L540-Zellen getestet, und diese Zelllinie weist im Vergleich zu anderen Zelllinien wie Ramos und Raji, die mit Anti-CD19-ADCs getestet wurden, eine deutlich geringere Expression von NAMPT auf (Abbildung **60A**). Aufgrund der deutlich geringeren Expression von NAMPT in L540-Zellen lässt sich die höhere Empfindlichkeit für die Behandlung mit NAMPT-Inhibitor-beladenen ADCs erklären. Darüber hinaus wurde festgestellt, dass die Cyanoguanidin-Gruppe der freigesetzten NAMPT-Inhibitoren **36** und 94 in den Lysosomen chemisch instabil ist. Daher wurde die Stabilität mit dem Inhibitor **36** als Modell untersucht. Zunächst wurde chemisch nachgewiesen, dass der Cyanoguanidin-Anteil des Inhibitors **36** bei pH-Werten unter 2 schnell zum entsprechenden Guanylharnstoff **113** hydrolysiert wird. Guanylharnstoff **113** wies im Vergleich zu Inhibitor **36** eine 655-fach geringere Zytotoxizität auf, die auf eine ineffiziente Bindung an NAMPT zurückzuführen war, wie in den *in silico*-Simulationen berechnet und durch Bio-Layer-Interferometrie-Messungen mit dem NAMPT-Enzym bestätigt wurde. Zweitens zeigte ein In-vitro-Stabilitätsassay von Inhibitor **36** in menschlichen lysosomalen Extrakten bei pH 5,5 und 37°C, dass lysosomale Hydrolasen den Abbau zum entsprechenden Guanylharnstoff auch bei lysosomalem pH katalysieren können, was durch LC-MS bestätigt wurde (Abbildung **60B**). Infolgedessen wird eine geringere Konzentration des aktiven Inhibitors im Zytosol erwartet,

was mit der Tatsache übereinstimmt, dass nur die Zelllinie L540 mit geringerer NAMPT-Expression empfindlich auf die Behandlung mit ADCs reagiert, die mit Cyanoguanidin-haltigen NAMPT-Inhibitoren beladen sind.

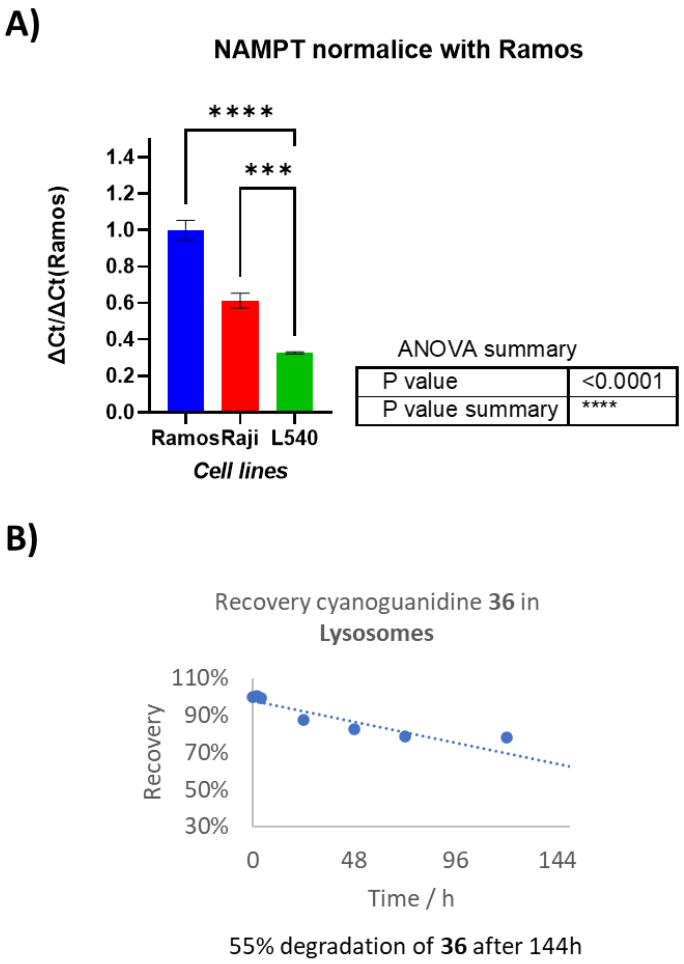

Abbildung 60. A) Normalisierte NAMPT-mRNA-Expressionswerte zwischen Ramos-, Raji- und L540-Zellen. B) *In-vitro*-Test der lysosomalen Stabilität, Vergleich der Wiederfindung von Cyanoguanidin **36** gegen die Zeit mit lysosomalen Extrakten.

Motiviert durch die Erkenntnis, dass Cyanoguanidin-haltige Inhibitoren im Lysosom abgebaut werden, führte ein virtuelles Screening einer 3000 Substanzen umfassenden Datenbank mit NAMPT-Inhibitoren zur Identifizierung von Inhibitor **124** als vielversprechendem lysosomal-sicherem NAMPT-Inhibitor. Im Gegensatz zum Inhibitor **94** wurde die Cyanoguanidin-Gruppe gegen einen gemischten Harnstoff ausgetauscht und die NAM-nachahmende Gruppe von einer Pyridyl- zu einer Isoindolin-Einheit gewechselt. Bemerkenswerterweise war die Zytotoxizität des freien Inhibitors **124** identisch mit der des Inhibitors **94** (Abbildung **61**), was die Leistungsfähigkeit des *In-silico*-Inhibitor-Designs zeigt. Bei den ersten synthetischen Versuchen konnte der Inhibitor **124** jedoch nicht in ausreichenden Mengen hergestellt werden, um die nächsten Schritte der Linker-Bindung und Konjugation an das mAb durchzuführen. Daher sind weitere Studien erforderlich, um diese Hypothese zu bestätigen.

5. Summary

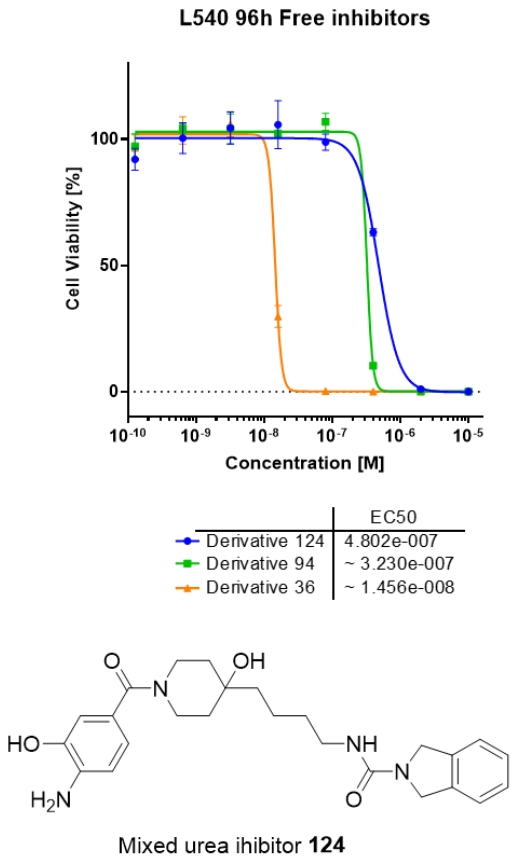

Abbildung 61. Zytotoxizität des freien Harnstoff-Isoindolin-Inhibitors **124** im Vergleich zu den Cyanoguanidinen **94** und **36** in L540-Zellen (EC_{50} (M)).

Zusammenfassend zeigen die Ergebnisse dieser Arbeit, dass die in der Literatur beschriebenen hydrophoben NAMPT-Inhibitoren nicht als ADC-Nutzlasten geeignet waren. Die *In-silico*-Leitstrukturoptimierung führte zu NAMPT-Inhibitoren der nächsten Generation mit erhöhter Hydrophilie, die in zellulären und *In-vivo*-Modellen bemerkenswerte antitumorale Wirkungen zeigen. Darüber hinaus zeigt diese Studie, dass säurelabile Gruppen in NAMPT-Inhibitoren, die als ADC-Nutzlasten verwendet werden, nicht wirksam sind. Zukünftige Studien sollten daher nicht-hydrolysierbare Inhibitoren erforschen, um die Anwendbarkeit von mit NAMPT-Inhibitoren beladenen ADCs zu erweitern.

6. Materials and Methods

6.1. Cell lines

All cell lines are of human origin and are maintained at 37°C, 95% humidity and 5% CO_2. Cells were cultured in cell culture bottles of 75 cm^2 with Hepa filter equipped lid (Greiner Bio-one, Ref: 658175). All mediums used were labelled as "complete", meaning: enriched with 2 mM L-Glutamine (PAN biotech, Ref: P04-80100), 1% Penicillin-Streptomycin antibiotic mix (PAN Biotech, Ref: P06-07100), and 10% heat inactivated FCS (Capricorn scientific, Ref: FBS-11A).

Cell lines were divided into two groups: adherent and non-adherent.

Adherent cell lines

For subculture, when cell culture achieves approximately 70% confluence, cell medium was removed, and cells were washed once with dPBS (PAN biotech, Ref: P04-36500), followed by trypsinisation with 5% trypsin (PAN biotech, Ref: P10-024100) diluted in dPBS. Trypsinisation time was in all cases 5 min at 37 °C. Cell detachment was assessed by sight using a phase contrast optical microscope (Primovert, Zeiss). Trypsinisation was ended by the addition of a similar volume of cell medium with FCS. Cells were then pelleted by centrifugation at 300 G for 5 min (Thermo Scientific, Heraeus, multifuge X3R). The medium with trypsin was removed, and the pellets were resuspended in fresh cell medium (prewarmed to 37°C).

Table 8. Adherent cell lines.

Cell line	Origin (malignancy)	Surface receptor/use	Culture conditions
BT474	Invasive breast carcinoma	$Erbb2^+$	RPMI (Gibco, Ref: 12633-012) complete with extra 10% inactivated FCS and 10 µg Insulin (Sigma, Ref: I9278-5mL)
JIMT1	Pleural effusion metastasis of a breast ductal carcinoma	$Erbb2^+$	Complete DMEM (PAN biotech, Ref: P04-01500)
SKOV-3	Ovarian serous cystadenocarcinoma	$Erbb2^+$ & (CD30 test)	Complete McCoy's 5a (PAN biotech, Ref: P04-05610)
SK-BR-3	Pleural effusion metastasis of a breast adenocarcinoma	$Erbb2^+$	Complete McCoy's 5a Advance
HCC-38	Breast ductal carcinoma	$Erbb2^+$	Complete RPMI
NCI-N87	Liver metastasis of a gastric tubular adenocarcinoma	$Erbb2^+$	Complete RPMI with 1 mM sodium pyruvate, 10 mM Hepes, 4.5 g/L

			glucose, 1.5 g/L $NaHCO_3$. (PAN biotech, Ref: P04-18047)
PC3	Bone metastasis of a prostate carcinoma	CD30 (test)	Ham's F12 (PAN biotech, Ref: P04-15500) and complete RPMI 1:1 mix
HCC-1806	Breast squamous cell carcinoma	CD30 (test)	Complete RPMI with 1 mM sodium pyruvate, 10mM Hepes, 4.5 g/L glucose, 1.5 g/L $NaHCO_3$.

Non-adherent cell lines

For subculture, cells were pelleted by centrifugation at 300 G for 5 min. The old medium was removed, and the pellet was resuspended in fresh dPBS to wash out cellular debris. Cells were pelleted again, dPBS was removed, and the pellet was resuspended in fresh complete medium.

Table 9. Non-adherent cell lines.

Cell line	Origin (malignancy)	Surface receptor/use	Culture conditions
Ramos	Burkitt lymphoma	CD19 and CD37	RPMI advance complete with extra 10% inactivated FCS
Raji	Burkitt lymphoma	CD19, CD20, and CD37	RPMI advance complete
Mec1	B-cell chronic lymphocytic leukaemia	CD19 (CD30 test)	IMDM (PAN Biotech, Ref: P04-20250) complete
Mec2	B-cell chronic lymphocytic leukaemia	CD19	IMDM complete
Nalm6	Adult B acute lymphoblastic leukaemia	CD19	RPMI advance complete
L540	Hodgkin lymphoma	CD30	RPMI advance complete with extra 10% inactivated FCS
RPMI 8226	Multiple myeloma	CD30 test	RPMI advance complete
Molm-13	Acute myeloid leukaemia	CD123	RPMI advance complete
Expi293F	Human embryonic kidney	Ab production upon transfection with Ab	Expi293 expression medium (Gibco, Ref:

		encoding DNA plasmid	A14351-01) without antibiotic supplementation and **8% CO_2**

6.2. Cytotoxicity assays for free inhibitors and ADCs

Cytotoxicity assays were divided into three steps: cell seeding, treatment, and cell viability evaluation:

	1	2	3	4	5	6	7	8	9	10	11	12
		Compound 1			Compound 2			Compound 3				
A	Blank	1A	1B	1C	1A	1B	1C	1A	1B	1C	100%	Background
B	Blank	2A	2B	2C	2A	2B	2C	2A	2B	2C	100%	Background
C	Blank	3A	3B	3C	3A	3B	3C	3A	3B	3C	100%	Background
D	Blank	4A	4B	4C	4A	4B	4C	4A	4B	4C	100%	Background
E	Blank	5A	5B	5C	5A	5B	5C	5A	5B	5C	100%	Background
F	Blank	6A	6B	6C	6A	6B	6C	6A	6B	6C	100%	Background
G	Blank	7A	7B	7C	7A	7B	7C	7A	7B	7C	100%	Background
H	Blank	8A	8B	8C	8A	8B	8C	8A	8B	8C	100%	Background

Scheme 15. BrdU 96-well cell filling scheme. Plates for Celltiter-Glo assay use background wells as second 100% control.

Initially, the assay plates were set, and cell lines were hence counted by means of a Neubauer chamber by diluting 1:10 cells in Trypan blue selection staining solution (Sigma, ref: T8154). The 2 x 10^3 cells were seeded per well in a total volume of 90 µL, following **Scheme 15**, in black 96-well plates with a clear-bottom (Perkin Elmer, Ref: 6005182). A blank control row remained only with 100 µL/well of medium, without cells, while the 100% and background wells contained 2 x 10^3 cells/well in 100 µL medium.

Second, cell treatment was performed in different concentration ranges, depending on whether free inhibitor or Ab/ADC was tested.

For **free inhibitors**, a stock solution (1 x 10^{-2} M in DMSO) was diluted 1:100 in the respective cell culture medium. Afterwards, the working solution (1 x 10^{-4} M) was 1:5 serial diluted seven times, achieving 1.2 x 10^{-9} M as more diluted solution; then, 10 µl of each serial diluted solution were added to the corresponding well triplicates, achieving 100 µL as final well volume.

For **Ab/ADC** treatment, the same procedure was followed, but the initial stock solution (3.4 x 10^{-5} M) was diluted 1:34 to afford the initial working solution. After seven-time serial dilution, the final concentration was 1.2 x 10^{-11} M.

Third, cell viability determination was performed with two types of cytotoxicity assays. The selection of the assay was determined by the classification of the cell line as adherent or non-adherent.

BrdU based assay (BrdU-ELISA kit, Roche, ref: 11669915001) for **adherent** cell lines:

Rationale of the assay:

This assay was based on an ELISA immunochemiluminescent detection of BrdU incorporated into cellular DNA during a 4 h incubation. A higher signal means higher cellular replicative activity; when normalised with an untreated control, the assay gives a direct qualitative measurement of cell population/viability.

The assay was performed as reported by the manufacturer, and chemiluminescence was measured using a CLARIOStar plate reader (BMG Labtech).

Analysis:

After removing the blank signal, the data were processed in GraphPad 9 as follows: transformation using x = log(x), normalisation to the average signal of 100% control wells, and sigmoidal dose-response analysis. The obtained readouts were EC_{50} values.

CellTiter-Glo 2.0 (Promega, ref: G9242) for **non-adherent** cell lines:

Rationale of the assay:

This assay measures by chemiluminescence enzymatic reaction the ATP content in cells, giving a direct qualitative measurement of cell population when normalising data with 100% and blank controls.

The assay was performed as reported by the manufacturer, and chemiluminescence was measured using a CLARIOStar plate reader (BMG Labtech).

Analysis:

After removing the blank signal, the data were processed in GraphPad 9 as follows: transformation using x = log(x), normalisation to the average signal of 100% control wells, and sigmoidal dose-response analysis. The obtained readouts are EC_{50} values.

6.3. Quantification of NAMPT gene expression levels by qRT-PCR

RNA was harvested from L540, Raji, and Ramos cells using the RNeasy Plus Micro kit (Qiagen, ref: 74034). The reverse transcription reaction was performed using the SuperScript II Reverse Transcriptase Kit (ThermoFischer, ref: 18064022) in a C1000 Touch thermal cycler (BioRad). The quantification was conducted through qRT-PCR. Hence, cDNA samples were mixed with specific primers designed within the coding region of NAMPT or Gapdh (housekeeping gene for normalisation). The enzyme, buffers, and SYBR intercalating

fluorochrome were pre-mixed in the Power SYBR Green PCR Master Mix (Thermo Fisher Scientific, ref: 4344463). The PCR reaction was performed on CFX Connect Real-Time System PCR equipment (BioRad). The primer sequences were as follows:

Table 10. qRT-PCR primer sequences synthesised by Thermo Fischer custom DNA oligo services

Gene	Sequence
NAMPT	**Fwd** 5'- CCAGCAGCAGAACACAGTACC -3'
	Re 5'- TCGCTGACCACAGATACAGGC -3'
GAPDH	**Fwd** 5' – GTCTCCTCTGACTTCAACAGCG -3'
	Re 5' – ACCACCCTGTTGCTGTAGCCAA -3'

6.4. Brentuximab-LALA-D265C expression plasmid cloning (HC and LC plasmids)

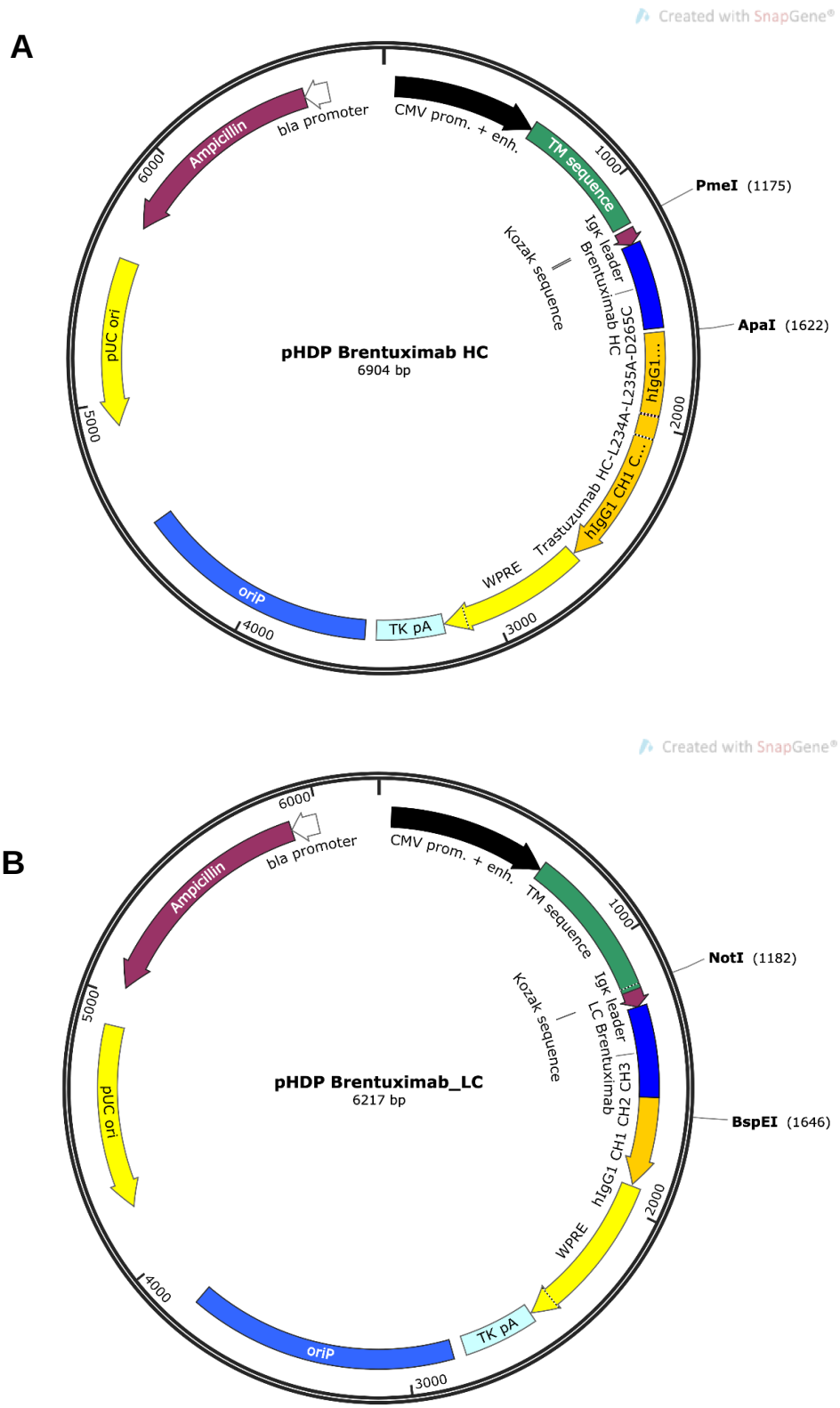

Scheme 16. A) Brentuximab HC expression plasmid; B) Brentuximab LC expression plasmid.

Brentuximab variable region (VR) heavy chain (HC) and light chain (LC) sequences were obtained from the literature and synthetised into carry vector using Gene-Art service (Thermo Fischer). The final plasmid map can be seen in Scheme **16 A** and **B**.[173]

Then, HC and LC sequences were extracted and amplified from the gene-Art vector by PCR (Phusion high-fidelity PCR Master Mix [NEB, Ref: M0531S] in C1000 Touch thermal cycler [BioRad]) following manufacturer indications. Afterwards, the PCR product was purified with the QIAquick PCR purification kit (Quiagen, Ref: 28104).

Table 10. Primers for Gene-Art sequences extraction

Fwd primer	5'-GCGCGACGTAATACGACTCAC-3'
Rv primer	5'-AGGTTTCCCGACTGGAAAGCG-3'

To clone DNA into Ab expression plasmids, the end preparation of PCR-amplified DNA sequences and expression plasmid linearisation was performed by enzymatic digestion, as observed in Scheme **16**. For HC end preparation and expression vector linearisation, PmeI (NEB, Ref: R0189S) and ApaI (NEB, Ref: R0114S) endonucleases were used. For LC, NotI and BspEI (NEB, Ref: R3189S and R0540S, respectively) endonucleases were used. All digested products were then loaded in 1% agarose gel for purification; imaging of gels is performed in the Intas Gelstick Imager (Intas), as observed in Scheme **16**. Afterwards, gel fragment purification was performed using the Qiaquick gel extraction kit (Quiagen, ref: 28704).

Analyze restriction digestion by analytical 1.0% agarose gel electrophoresis.

1: Original HC-LALA-D265C
PmeI + ApaI
1. 6457 bp
2. 456 bp

2: Ori gene Brentuxima-HC
PmeI + ApaI
1. 2356 bp
2. 447 bp

3: HC insert after PCR amplification PCR
PmeI + ApaI
1. 447 bp
2. 67 bp
3. 57 bp

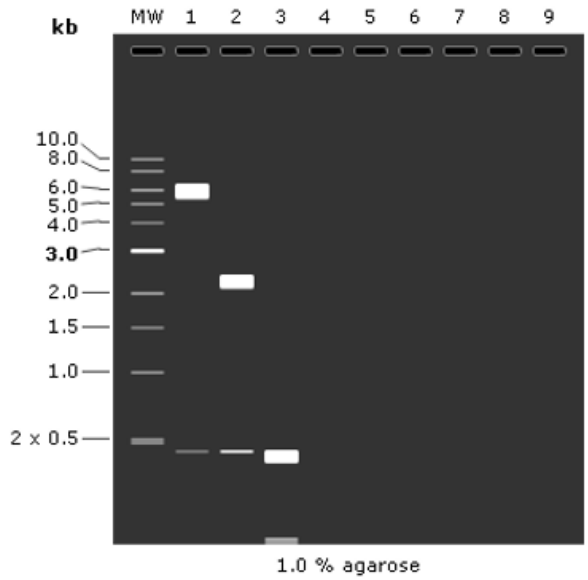

Scheme 17. Theoretical separation of digestion products in 1% agarose gel (HC example).

Then, the ligation reaction of HC and LC inserts in linearised expression plasmids was performed with T4-DNA ligase (NEB, Ref: M0202S) following instructions from the manufacturer (performing the ligation in C1000 Touch thermal cycler O.N. at 16°C) and using an insert:plasmid molar ratio of 3:1.

Next, the ligation reaction product was used to transform chemically competent bacteria using NEB5α *E. coli* (NEB, Ref: C29871) and plated overnight in LB agar plates, supplemented

with ampicillin as a restriction antibiotic (final concentration: 100 µg/mL; Invivogen, Ref: fas-am-s) at 37ºC. Single colonies were picked and amplified overnight in 5 mL of Terrific Broth medium (Sigma, Ref: T0918) supplemented with ampicillin (Serva, Ref: 13399) at 37ºC in a rotating incubator. The plasmid was isolated and purified using the AllPrep DNA/RNA Mini Kit (Qiagen, Ref: 80204) for four colonies. For check positive colonies as well as plasmid integrity, Sanger sequencing was performed at GATC/Eurofins genomics.

Finally, amplification and plasmid isolation of the positive colonies were performed using megaprep with the EndoFree Plasmid Mega kit (Quiagen, Ref: 12381), and the final plasmid concentration was set to 1 mg/mL with NanoDrop One C (Thermo Scientific).

6.5. HC Brentuximab-LALA-A118C-LALA-D265C plasmid generation by PCR single amino acid mutation of HC Brentuximab-LALA-D265C

A single amino acid mutation for the generation of the double thiomab Ab was performed by PCR amplification of the original plasmid (HC Brt-LALA-D265C) using a PCR primer containing the mutation site (in blue): 5'-ggtcactgtctctgca**TGC**AGCACCAAGGGCC-3'. The PCR reaction was carried out with Phusion High-Fidelity PCR Master Mix (NEB, Ref: M0531S) in a C1000 Touch thermal cycler (BioRad) using manufacturer indications. The PCR product was purified with the QIAquick PCR purification kit (Quiagen, Ref: 28104). The remaining original HC plasmid was removed by enzymatic digestion with DpnI (NEB, Ref: C29871).

The PCR product was then transformed into chemically competent bacteria using NEB5α *E. coli* (NEB, Ref: C29871) and plated overnight in LB agar plates supplemented with ampicillin (final concentration: 100 µg/mL; Invivogen, Ref: fas-am-s). Afterwards, single colonies were picked and amplified overnight in 5 mL of Terrific Broth medium (Sigma, Ref: T0918) supplemented with ampicillin (Serva, Ref: 13399) at 37°C in a rotating incubator. The plasmid was isolated and purified using the AllPrep DNA/RNA Mini Kit (Qiagen, Ref: 80204) for four colonies. For check-positive colonies as well as plasmid integrity, Sanger sequencing was performed at GATC/Eurofins Genomics.

Amplification and plasmid isolation of the positive colonies were performed using megaprep with the EndoFree Plasmid Mega kit (Quiagen, Ref: 12381). The final plasmid concentration was set to 1 mg/mL with NanoDrop One C (Thermo Scientific).

6.6. Ab production

Using the plasmids generated in Sections **5.4** and **5.5**, Brentuximab Ab was expressed in Expi293F cells by means of transient transfection with PEI.

Transfection extend was measured in the number of culture flasks (Corning® Erlenmeyer cell culture flasks w/ vent cap; 2 L; polycarbonate [Corning; Ref: 431255-1EA]). For each flask, 1.25×10^9 cells in 425 mL of Expi 293 expression medium were seeded, and cells were counted by means of an automatic optical counter, cytoSMART (Corning). Subsequently, a transfection mix was prepared by mixing 300 µg of HC plasmid DNA and 450 µg of light chain with 25 mL of Opti-MEM medium (Gibco, Ref: 31985-062). Separately, 1.5 mL of PEI reagent (1 mg/mL PEI in H_2O) were mixed in 25 mL of Opti-MEM medium. Pouring PEI into DNA solution yields 50 mL of transfection mix that was directly poured into an Expi293 flask.

After one night of incubation, cells were pelleted by centrifugation at 460 g for 15 at R.T. and medium was exchanged.

After five days, cell supernatant containing desired Ab was harvested. Cell and cell detritus were removed from supernatant by means of diatomaceous earth mix and filtering under vacuum with the 0.2 µM filter provided in the Sartoclear Dynamics® Lab V kit (500 ml, 20 g; Sartorius; Ref: SDLV-0500-20C—E).

Then, Ab was purified from the supernatant by Protein A chromatography, using TOYOSCREEN® AF-rProtein A HC-650F 5ml columns (Tosoh Bioscience; Ref: 0023432) in ÄKTA Pure chromatography system (Cytivia Healthcare) using manufacturer indications.

Finally, aggregates and endotoxin removal were performed by gel filtration low pressure chromatography in HiLoad 26/600 Superdex 200 pg; prepacked XK26-column (Cytiva Healthcare; Ref: 28-9893-36) in ÄKTA Start chromatography system (Cytiva Healthcare) following an isocratic method and using PBS as mobile phase. The detection and automatic fractionation of proteins were assessed by UV absorption at 280 nm.

Subsequently, Ab was set in PBS at a concentration of 5 mg/mL using Amicon Ultra Centrifugal Filters 50,000 MWCO (Millipore, Ref: UFC805024 and Ref: UFC905024). The concentration was determined by absorbance measurement at 280 nm (background 390 nm) in Nano-drop One C. Concentration was calculated afterwards by applying Beer-Lambert law using measured absorbance and calculated extinction factor for each Ab in the Expasy, ProtParam tool.[200] Finally, the product was sterile filtered with a 0.22 µm MillexGV syringe filter (Sigma, Ref: SLGV013SL).

Ab quality control was performed by means of aggregate percentage determination by SEC-HPLC in the Agilent 1260 Infinity HPLC system (Agilent) using a Tosoh UP SW 3000 4.6 mm x 15 cm, 2 µm gel filtration column (Tosoh Bioscience, Ref: 0023449) and isocratic method during 8 min at 0.357 mL/min. UV detection of signals was performed at 280 nm. Running buffer: 0.05% NaN_3 + 0.1 mol/l Na_2SO_4 in 0.1 mol/l $NaPO_4$, pH 6.7.

Endotoxin was determined by means of commercial kit, EndoZyme® II Recombinant Factor C (rFC) Assay (Hyglos, Ref: 890030), following manufacturer indications.

6.7. Ab/ADC cell binding assay: Fluorescence labeled flow cytometry

This assay aims to determine whether a specific Ab/ADC was able to recognise and bind its target receptor on the surface of cells and, additionally, to qualitatively determine the amount of Ab or ADC bonded.

The assay was based on a two-step recognition of the target.

Initially, 1 x 10^6 cells were harvested per condition and centrifuged at 300 G in a 4°C-cooled centrifuge to pellet the cells. The cells were then washed with ice-cold dPBS and resuspended in staining medium (consisting of RPMI 1640 [PAN biotech, Ref: P04-17500], 25 mM HEPES [PAN biotech, Ref: P05-01100], 3% FCS, and 0.02% Na-azide, without antibiotic supplementation) in a 96-well U-bottom cell culture plate (Greiner-bio-one, Ref: 650 180). The cells were resuspended in 200 µL per condition.

	1	2	3	4	5	6	7	8	9	10	11	12
A	1	2	3	4	5	6	7	8				
B												
C												
D												
E												
F												
G												
H												

1) Negative control (no Primary antibody, no Secondary antibody)
2) Negative treatment and primary Ab control (No primary antibody, added secondary antibody)

3) Cells treated with (Primary) ADC A +No Ab
4) Cells treated with (Primary) ADC A + Secondary Ab

5) Cells treated with (Primary) ADC B + No Ab
6) Cells treated with (Primary) ADC B + Secondary Ab

7) Cells treated with (Primary) Free Ab use for ADC + No Ab
8) Cells treated with (Primary) Free Ab use for ADC + Secondary Ab

Scheme 18. Filling scheme for binding assay testing 2 ADCs.

Cells were then seeded in a 96-well U-bottom plate at a density of 50 µL/well in duplicate. Scheme **18** was followed to determine which wells received 2 x 10^{-7} M of a primary Ab/ADC solution and which received staining medium. After 30 min of incubation on ice, the wells were washed with dPBS, and 100 µL of a diluted (1:100) Goat anti-Human IgG (Fc)-AlexaFluor488 F(ab')2 (Dianova, Ref: 109-546-008) reporter secondary Ab was added to the experimental wells. The negative control wells received 100 µL of staining medium. Cells were incubated on ice for 30 min. Following another wash with dPBS, the cells were then transferred to flow cytometry tubes (Corning/BD, Ref: 352054) and fixed with a 2% paraformaldehyde solution (Polyscience, Ref: 18814) in dPBS for a minimum of 2 h. They were then analysed on a FACSLyric flow cytometer (BD) (20,000 cells counted per measurement) using FlowJo software for analysis and plotting (FlowJo, LLC, Ashland, Ore).

6.8. Flow cytometry determination of recycling and internalisation of ADC-targeted cell receptor

This study was conducted to determine the effect of an ADC-delivering NAMPT inhibitor on cell receptor internalisation and recycling.

Hence, 2 x 10^6 cells in 1.25 mL of medium were seeded in a 6-well plate (VWR, Ref: 734-2323) for each ADC/Ab treatment condition, as well as an additional group as an untreated control: 1.25 mL of Ab or ADC (at a concentration of 2 x 10^{-7}M) was added to the treatment conditions, while the control group received 1.25 mL of fresh medium. The cells were incubated for 24 h at 37°C and 5% CO_2 and then assayed to determine binding according to the methods described in Section **6.7**.

6.9. NAMPT inhibitor payload conjugation to Ab; ADC production

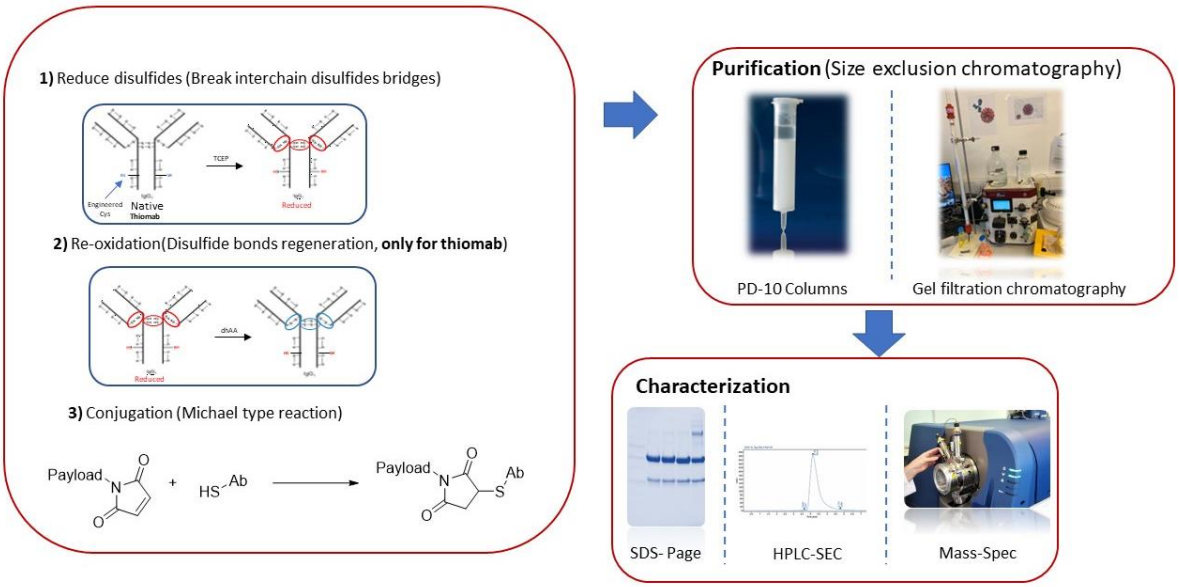

Scheme 19. ADC production workflow.

In this section, two methods for conjugation of maleimide-containing payloads to mAb-reducing cysteines were explained. A graphic explanation of the process can be observed in Scheme **19**.

High DAR conjugation: Conjugation of maleimide-containing payloads to fully reduce mAb

1) Reduction of native interchain cysteines and additionally engineered cysteines (thiomab)

For this study, a 5 mg/mL solution of mAb in PBS was used. The pH and EDTA concentration were adjusted to 7.4 and 1 mM, respectively, using a 100X 100 mM EDTA PBS solution at pH 8.0. The mAb solution was then reduced by adding 40 eq of TCEP from a freshly made 50 mM TCEP solution (with 1mM EDTA, pH 7.4), and incubated for 2 h at 37°C. The solution was then dialysed twice at 4°C in a Slide-A-Lyzer Dialysis Cassette with a 20,000 MWCO (Thermo Scientific, different capacity cassettes were used depending on the sample volume: 3, 12, 30 mL; Ref: 66003, 66012, 66030, respectively), first for 4 h and then overnight. The dialysis was performed in 500 times the volume of the sample in 1x PBS, 1 mM EDTA, and pH 7.4.

2) Conjugation with maleimide containing payload

In this study, the NAMPT inhibitor payload or amanitin payload (as a control, synthesised by HDP chemistry team) was conjugated to the working solution by adding 20 eq of the respective payload (diluted to 10 µg/µL in DMSO) and incubated for 2 h at room temperature on a shaking platform. For hydrophobic payloads, fresh DMSO was added to the solution to a final concentration of 10% V/V, taking into account the DMSO from the payload solution. The remaining thiols were capped by incubating the solution with 12 eq of a freshly prepared 100 mM solution of N-ethylmaleimide in DMSO for 1 hour on a shaking platform. Unreacted maleimide-containing molecules were quenched by incubating the solution with 40 eq of a

freshly prepared 100 mM solution of N-acetyl-L-cysteine in water for 15 min on a shaking platform at room temperature.

Site-specific conjugation of maleimide-containing payloads to reduced thiomab cysteines

1) Reduction of native interchain cysteines and thiomab

For this study, a 5 mg/mL solution of mAb in PBS was used. The pH and EDTA concentrations were adjusted to 7.4 and 1 mM, respectively, using a 100X 100 mM EDTA PBS solution at pH 8.0. The mAb solution was then reduced by adding 40 eq of TCEP from a freshly made 50 mM TCEP solution (with 1 mM EDTA, pH 7.4) and incubated for 2 h at 37°C. The solution was then dialysed twice at 4°C in a Slide-A-Lyzer Dialysis Cassette with a 20,000 MWCO (Thermo Scientific); different capacity cassettes were used depending on the sample volume: 3, 12, 30 mL; Ref: 66003, 66012, 66030, respectively), first for 4 h and then overnight. The dialysis was performed in 500 times the volume of the sample in 1x PBS, 1 mM EDTA, and pH 7.4.

2) Reoxidation of interchain cysteines and disulfide bonds regeneration

To conjugate the payload only to the thiomab cysteines, an oxidation reaction of the interchain cysteines was performed by adding 20 eq of dhAA (a freshly made 50 mM solution in DMSO) and incubating for 3 h at room temperature on a shaking platform.

3) Conjugation with maleimide containing payload

In this study, the NAMPT inhibitor payload or amanitin payload (as a control, synthesised by the HDP chemistry team) was conjugated to the working solution by adding 8 eq of the respective payload (diluted to 10 µg/µL in DMSO) and incubating for 2 h at room temperature on a shaking platform. For hydrophobic payloads, fresh DMSO was added to the solution to a final concentration of 10% V/V, taking into account the DMSO from the payload solution. Unreacted maleimide-containing molecules were quenched by incubating the solution with 25 eq of a freshly prepared 100 mM solution of N-acetyl-L-cysteine in water for 15 min on a shaking platform at room temperature.

Purification and aggregate removal are performed by two means:

1) PD-10 column (GE Healthcare Life Sciences; Ref: 17-0851-01) purification:

This method can only be used for up to 2 mL of ADC reaction mix and does not remove endotoxins.

To purify the ADC reaction mix, PD-10 columns were equilibrated with PBS, pH 7.4 by filling the column completely with the buffer and allowing it to enter the packed bed, then the process was repeated for four times and the flow-through was discarded. Afterwards, the sample was added, up to a maximum volume of 2.0 mL, to the column. Once the sample had entered the packed bed completely, 2.5 mL of PBS, pH7.4 was added and the flow-through was discarded. For sample collection 1.5 mL tubes were prepared and 3.5 mL of PBS was added to the column to elute the 500 µL sample fractions. Then, Bradford reagent (5 µL sample + 5 µL Bradford reagent) was placed on parafilm to identify protein-containing fractions. In order to accurately determine the protein containing fractions, those fractions that were weakly stained

with Bradford reagent were measured in NanoDrop at 280 nm and all the fractions with a protein content of ≥ 0.1 mg/mL were combined.

2) Purification by gel filtration in FPLC ÄKTA Start, using HiLoad 16/600 (Cytiva Healthcare; Ref: 28-9893-35) or 26/600 Superdex 200 pg; prepacked XK26-column

To remove endotoxins and aggregates from the ADC/Ab solution, the method described in Section **6.6** was used with a 16/600 mm size column for up to 50 mg of ADC/Ab, and a 26/600 mm size column for larger amounts. After purification, the ADC solution was dialysed at 4°C overnight using 500 times the sample volume of 1 x PBS, pH 7.4, and Slide-A-Lyzer Dialysis Cassettes with a 20,000 MWCO. Afterwards, the concentration was adjusted to 5 mg/mL using Amicon Ultra Centrifugal Filters with a 50,000 MWCO. Then, the concentration was determined by measuring absorbance at 280 nm (background 390 nm) with a Nanodrop One C and calculating the extinction factor using the amino acid sequence with the ProtParam tool on Expasy. Finally, the solution was sterile filtered with a MillexGV syringe filter with a 0.22 µm pore size.

Quality analysis:

1) Aggregates quantification was performed by HPLC-SEC as described in Section **6.6**.

2) ADC integrity and qualitative determination of conjugation by SDS-Page.

The sample were loaded along with a protein ladder standard and two controls (a positive control of a pre-determined ADC of known DAR and a negative control of free Ab used for conjugation) onto Mini-PROTEAN TGX Stain-Free Gels with a 4–20% gradient and a 12-well comb (BioRad, Ref: 456-8095) to analyse. In all cases, the first lane was loaded with Precision Plus Protein Unstained Standard (BioRad, Ref 161-0363). The samples and controls were both measured in reduced and non-reduced conditions.

the samples we diluted to 1.5 mg/mL in order to be loaded in the gel. For reducing conditions, 4 µL of 4x Roti Load (Carl Roth GmbH, Ref: K929.1) was added to 12 µL of the 1.5 mg/mL sample, then, the mix was heated for 5 minutes at 95°C, and 13.33 µL were loaded onto the gel. For non-reducing conditions, 12 µL of 2x loading buffer without mercaptoethanol (composition of loading buffer without mercaptoethanol: 5526.6 µL H_2O, 657.9 µL 1M Tris-HCl pH 6.8, 1052.6 µL glycerol, 2105.3 µL 10% SDS, and 657.9 µL 0.05% bromophenol blue) were added to 12 µL of the 1.5 mg/mL sample, then, the mix was incubated for 60 min at 37°C, and 20 µL were loaded onto the gel. The electrophoresis was run in a Mini-PROTEAN Tetra system (BioRad, Ref: 165-8000) at 85 V for 10 min until the samples passes the stacking gel, then the voltage was raised to 140 V for 45 min. After electrophoresis, protein signals were monitored in a Azure C400 Imaging System (Azure biosystems) with UV-light. The signal was generated thanks to the trihalo compounds in Mini-PROTEAN TGX Stain-Free Gels that reacts with tryptophan residues in the proteins in a UV-induced 1-min reaction to produce fluorescence signals.

3) DAR analysis by mass spectrometry

The samples were first deglycosylate by incubation at 50°C for 5 min using Rapid PNGase F (NEB, Ref: P0711S). Then, a UPLC-MS tandem device consisting of an ACQUITY UPLC I Class Plus (Waters) and a BioACCord with RDa detector (Waters) as mass spectrometers was used. The

samples were ionised by ESI and measured in positive mode in and by the bioanalytic department of HDP.

6.10. Colorimetric NAD^+ determination by enzymatic assay.[86,147]

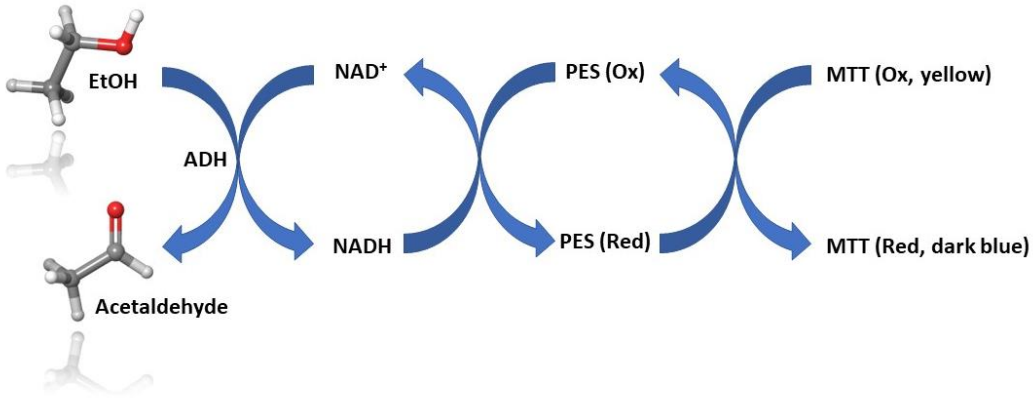

Scheme 20. Colorimetric enzymatic cycle for NAD determination. Reagent or enzyme abbreviations in scheme stand for: Alcohol dehydrogenase (ADH), Phenanzine ethosulfate (PES), and Methylthiazolyldiphenyl-tetrazolium bromide (MTT). Other abbreviations used: Oxidised (Ox), reduced (Red).

To measure the NAD^+ concentration in cell lysates, the enzymatic assay described in Scheme **20** was used. This assay involves reducing NAD^+ to NADH; the signal was detected by quantifying the reduced MTT in a CLARIOStar plate reader at 570 nm at various time points. The results were normalised by the total protein concentration in the lysate, which was determined using a BCA assay kit (Sigma, Ref: 71285-3) following the manufacturer's instructions.

To perform the assay, at least 8 x 10^5 cells on 2 mL of medium per assay condition and an untreated control were seeded in 6-well plates. The cells were then treated with the specified concentration of ADC, mAb, or free inhibitor and incubated at 37°C and 5% CO_2 for 24, 48, or 72 h. After removing the medium, the treated cells were washed with ice-cold dPBS and, if adherent, scraped from the plate (VWR, Ref: 734-2602). Afterwards, the washed cell pool was split for each condition into two aliquots: one for total protein determination and the other for NAD^+ determination.

To obtain total protein extracts, cells were lysed with a protein lysis buffer containing RIPA buffer, 0.5 mM PMSF, and a protease inhibitor cocktail (Sigma, Ref: 11697498001). For NAD^+ determination, cells were pelleted by centrifugation at 300 G in a 4°C cooled centrifuge and lysed in an NAD^+ lysis buffer (20 mM $NaHCO_3$ and 100 mM Na_2CO_3 in water). The lysate was then frozen and thawed (-80°C for 2 h, followed by thawing and vortexing for 20 sec), and the supernatant (containing NAD^+) was separated into a new microcentrifuge tube.

The assay was performed in a 96-well plate (Falcon, Ref: 353072), with 20 µL of each sample added in duplicate. To quantify NAD^+, a 12-point standard curve spanning from 500 µM to 0.0085 µM (0 µM was used as a blank) was also measured in duplicate using β-NAD (Sigma, Ref: N0632). Cycling buffer (freshly prepared without EtOH and containing 100 mM Tris-HCl pH 8, 1 mM PES, 0.5 mM MTT, 0.2 mg/mL ADH [≥ 60 units/mL], and 1% BSA) was added to each well (160 µL/well), and the plate was incubated for 5 min at 37°C. Afterwards, 20 µL of 37°C

pre-warmed 6 M EtOH solution in water was then added to each well using a multichannel pipet to avoid time delays. The first measurement was immediately taken in the plate reader, with further measurements taken at 5, 10, 15, 20, and 30 min.

The data were analysed by calculating the first derivative of each measurement vs. time and interpolating the test values into the NAD^+ standard curve. The results were then normalised with the total protein concentration.

6.11. *In vitro* kinetic quantitation of NAMPT inhibitor binding to NAMPT

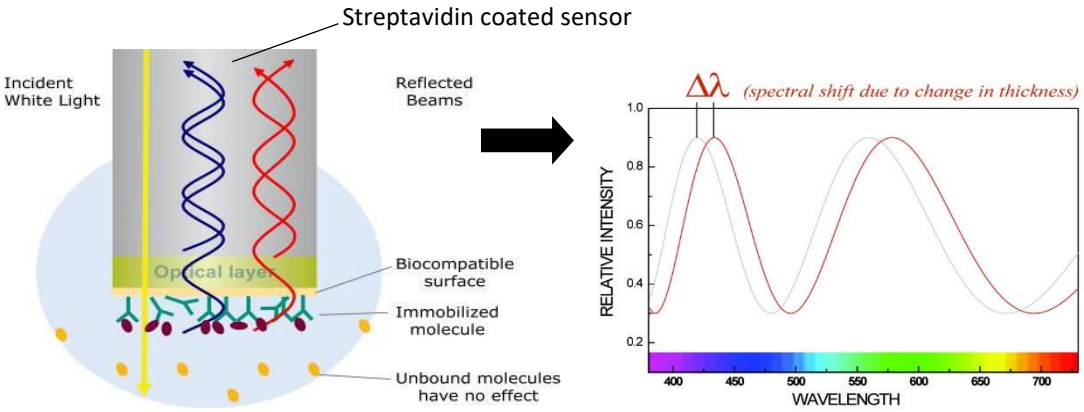

Scheme 21. Biolayer interferometry assay principle, scheme adapted from Octet user manual.

To measure the binding of biotinylated NAMPT inhibitors to the enzyme, an Octet device (Octet K2, Forté Bio) was used, and the assay is based on light biolayer interferometry (as described in Scheme **21**).

The biotinylated inhibitors were loaded on streptavidin-coated sensors (Sartorius, 18-0009), and the loaded sensors were exposed to solutions of different concentrations of the NAMPT enzyme. The kinetic constants k_{on} (association rate constant) and k_{off} (dissociation rate constant) were analysed using the Data Analysis 10.0 software (Forté Bio). These constants measure the speed at which the inhibitor binds to the enzyme and is released, respectively. The equilibrium dissociation constant (Kd) was calculated by the software using these two parameters. The kinetic parameters provide information on the dynamics of the system.

	1	2	3	4	5	6	7	8	9	10	11	12
A		0.1µM		100nM								
B		0.1µM		33nM								
C		0.1µM		11nM								
D		0.1µM		3.7nM								
E		0.1µM		1.2nM								
F		0.1µM		blank								
G												
H												

Buffer (10x Kinetics Buffer)
Ligands [µM] (HDP 40.0146)
Analyte [nM] **NAMPT**
Blank = 10x kinetic buffer

Volume per well = 200µL

Scheme 22. Octet experiment plate design.

Before each experiment, sensors were hydrated in kinetic buffer 10 times for at least 10 min at 30°C. During this time, the biotinylated inhibitor (called the "ligand" in this assay) was diluted from a stock solution of 1.62 x 10^{-2} M in DMSO to 0.1 µM and placed in a black F-bottom 96-well plate (Greiner, Ref: 655209), as described in Scheme **22**. The NAMPT enzyme (recombinant human active NAMPT, My bio source, Ref: MBS142195), called the "analyte" in this assay, was reconstituted to 0.1 mg/mL in 20 mM HCl following the manufacturer's instructions and aliquoted in the 96-well plate as described in Scheme **22**.

In the Experiment software 10.0 (Forté Bio), the analysis parameters and steps were set as described in Table **12**.

Table 11. Experimental steps for biotinylated Inhibitor-NAMPT in vitro biolayer interferometry (BLI) binding assay

Step #	Step Name	Time (sec)	Flow (RPM)	Sample Plate Column	Used Biosensors
1	Baseline	120	1000	1	A + B
2	Loading	300	1000	2	A + B
3	Baseline	60	1000	1	A + B
4	Baseline	120	1000	3	A + B
5	Association	900	1000	4	A + B
6	Dissociation	1500	1000	3	A + B
7	Baseline	120	1000	1	C + D
8	Loading	300	1000	2	C + D
9	Baseline	60	1000	1	C + D
10	Baseline	120	1000	3	C + D
11	Association	900	1000	4	C + D
12	Dissociation	1500	1000	3	C + D
13	Baseline	120	1000	1	E + F
14	Loading	300	1000	2	E + F
15	Baseline	60	1000	1	E + F
16	Baseline	120	1000	3	E + F
17	Association	900	1000	4	E + F
18	Dissociation	1500	1000	3	E + F

6.12. Lysosome stability assay

The aim of this assay was to determine whether NAMPT inhibitors containing cyanoguanidine groups are degraded in lysosomes after release from the ADC.

The test compound was incubated at a concentration of 17.7 µM in a mixture of human liver lysosomal extract (tebu-bio, Seikisui Xenotech, Ref: H0610.L) and 1x catabolism buffer (tebu-bio, Seikisui Xenotech, Ref: K5200) for five days at 37°C. Samples were taken at 0, 2, 4, 24, 48, 72, 120, and 168 hours. Control samples without lysosomal extract were also set up under the same conditions as the test sample. All measurements and samples were taken in duplicate.

To measure the reaction, the compound was quenched by adding 380 µL of internal standard buffer (30 ng/mL of internal standard in ACN) to 20 µL of the sample. An amanitin-stable isotope-labelled analogue was used as the internal standard.

22 µL of the quenched sample was analysed using UPLC-MS-MS QTrap 5500 (Column: Waters ACQUITY UPLC BEH Amide, 1.7 µm, 2.1 x 100 mm, product code: 186004801), the UPLC method described in the HPLC method section. This assay was related to compound **113** (see the "Product synthesis and purification" section). Compound **113** was expected to be the main degradation compound after lysosomal enzymatic digestion and was used as a reference for the detection of catabolites after digestion in the HPLC-MS analysis.

The ion fragments detection method was multiple reaction monitoring (MRM). In this method, the mass is measured by a tandem mass spectrometer where the initial molecular ion is selected as initial mass. Subsequently, the fragmentation of this molecular ion in the second stage of the tandem mass spectrometer is followed by selection of an ion product of the fragmentation reaction of the precursor ions. This method assures significantly more accurate detection and quantitation of molecules in complex matrices.[201]

This study was conducted by the **Bioanalytic Department of HDP**.

6.13. *In vivo* studies MTD

All animals were obtained from Janvier (Le Genest St Isle, France) and kept in the HDP *in vivo* facility for 15 days of quarantine and acclimatisation before the *in vivo* experiments began.

The maximum tolerated dose (MTD) was determined in tumour-free CB17 Scid and NXG female mice.

CB17 Scid mice are derived from BALB/c mice bearing the Scid mutation, a recessive autosomal mutation characterised by an absence of functional T and B cells. Most homozygotes have no detectable IgG, IgM, or IgA immunoglobulins. NXG mice bear the SCID mutation together with the IL2rgTm1 (γc mutation), which blocks the production of various interleukins needed for the development of NK cells. This combination of mutations leads to a severe immunodeficiency with an absence of T, B, and NK lymphocyte compartments.[202]

The tested compounds were administered as sterile solutions in PBS at pH 7.4 containing a maximum of 5% DMSO. Survival and clinical signs were determined daily, and body weight was determined twice a week. Three animals per group were injected with doses of ADC ranging from 5–80 mg/kg and were monitored for clinical signs, such as net body weight loss greater than 20%, lack of recovery, and/or one of the following symptoms: lack of motility, hind leg paralysis, cachexia, poor general health condition, or general signs of pain. The next dosage level was only administered after a minimum seven-day follow-up period. The animals were monitored for approximately two weeks after the administration of the dose. These studies were conducted by and in the ***In Vivo* Biology Department of HDP**.

6.14. *In vivo* efficacy studies

Two types of studies were performed, one using NXG female mice in a disseminated tumour model of L540 cells and the other using CB17 Scid female mice in a subcutaneous tumour model of L540 cells embedded in matrigel.

The study in NXG mice consisted of eight experimental groups with 10 animals per group, each bearing intravenously inoculated L540 tumours. Each animal was inoculated intravenously with 5 x 10^6 L540 tumour cells in 200 µL RPMI w/o Phenol Red into their tail vein on day -3. On day 0, mouse therapy was initiated. The mice were treated with PBS (vehicle

control group) or single or repeated doses (1x/week for 4 weeks) of anti-CD30 ADCs loaded with NAMPT inhibitors at doses of 6.25 and 12.5 mg/kg. Body weight was measured twice per week, and animals were sacrificed and necropsied when one or more termination criteria were met.

The study in CB17 Scid mice consisted of 10 experimental groups with 10 animals each bearing subcutaneous L540 tumours. The animals were inoculated subcutaneously with 1 x 10^7 L540 tumour cells in 200 µL RPMI w/o Phenol Red containing 50% growth factor-reduced Matrigel into their right flank. Once a mean tumour volume of approximately 150 mm^3 was reached, the animals were randomised into 10 groups according to tumour size. Therapy was initiated one day after group allocation. The mice were treated with PBS, unconjugated brentuximab mAb, or single or repeated doses of anti-CD30 ADCs loaded with NAMPT inhibitors, as well as with one anti-Dig ADC loaded with NAMPT inhibitor as isotype control at doses of 12.5 mg/kg for single doses and 6.25 and 12.5 mg/kg 1x/week for 4 weeks. Mice treated 1x/week for 4 weeks at 12.5 mg/kg with the isotype control ADC DIG-LALA-D265C-105 (DAR10) and the unconjugated antibody Brentuximab-LALA-D256C served as controls. Tumour volumes were measured twice per week using calipers, and body weight was determined in parallel. The animals were sacrificed either when tumour volumes were > 1,600 mm^3 or for ethical reasons. Animal experiments were approved by the local ethics committee (G-64/21 and G-157/17, Regierungspräsidium Karlsruhe, Germany).

6.15. Statistical analysis

Statistical analysis was performed using Graph Pad Prism 9 for Windows (GraphPad Software, La Jolla California USA). To study differences in gene expression, *in vitro* cell viability and *in vivo* survival, data were analysed by parametric test (ANOVA) or non-parametric Kruskal-Wallis test depending on the data distribution. Multiple comparisons were studied with t-student test adjusted by Bonferroni test for parametric distributions and U Mann Whitney for non-parametric. Statistical significance was defined as $p < .05$ (*), $p < .01$(**), and $p < .001$ (***).

6.16. Materials and technical equipment: Chemistry

The reaction progression and endpoint were performed by means of thin-layer chromatography (TLC) and reverse-phase HPLC.

For TLC analysis, chromate sheets of silica gel type POLYGRAM® SIL G/UV_{254}, of 0.2 mm thick (Macherey-Nagel) were used. Visualisation of the TLCs is performed by irradiation (254/365 nm) or staining using solutions of chemical developers made of phosphomolybdic acid or Cerium (IV) ammonium (Vaughn's reagent), or 0.3% ninhydrin in EtOH. Mobile phase composition was specified in each reaction.

If required for the reaction, glassware was dried under vacuum and 100 °C for at least 1 h.

For analytical reverse phase HPLC analysis, a Hitachi Chromaster HPLC system equipped with a pump was used (pump, Hitachi 5160; auto sampler, Hitachi 5260; column oven, Hitachi 5310; diode array detector, Hitachi 5430), along with a Phenomenex Luna C18(2) column (100 Å, 10 µm, 4.6 x 250mm [product code 00G-4253-E0]). Data evaluation was accomplished using

OpenLab and Agilent technologies. The methods used were described in the "HPLC methods" subsection.

The separation and purification of every crude product were accomplished by two means:

First, for purification by liquid chromatography (flash chromatography), a Teledyne ISCO combi flash nextgen 300+ equipped with UV/Vis and scattering detectors was used to apply pre-packed silica gel columns in a range of 4 to 330 g of silica with a pore size of 60 Å and a particle size of 40–63 µM (Redi Sep Rf, Teledyne ISCO) as the stationary phase. The eluent was specified in each case as well as the solvent's proportion (volume/volume).

Second, for purification by reversed phase (RP) preparative HPLC, either an ACCQ Prep HP150 (Teledyne ISCO) or a LaPrep Σ (VWR) was used, applying a mobile phase as described under "HPLC methods" and as a column, a Phenomenex Luna C18(2) (100Å, 10µm, 250x21.2 mm and 250x30mm) (Product codes: H18-206477 and H21-201758, respectively) and pre-column Phenomenex (Product code: AJ0-8223).

The ^{1}H nuclear resonance spectroscopy (NMR) spectra were performed by Deutero GmbH with magnets achieving Larmor frequencies of 500 MHz for ^{1}H and 126 MHz for ^{13}C. Every experiment was performed at room temperature using $CDCl_3$, D_6-DMSO, or MeOD as solvents. The chemical shifts δ (ppm) were reported relative to residual solvent signals ($CDCl_3$ 7.26 ppm ^{1}H or 77.0 ppm ^{13}C, D_6-DMSO 2.5 ppm ^{1}H or 39.5 ppm ^{13}C, MeOD 4.87 and 3.31 ppm ^{1}H and 49.1 ppm ^{13}C, D_6-Acetone 2.05 ppm ^{1}H and 206.0 and 29.8 ppm ^{13}C). The coupling constants for ^{1}H spectra were specified in Hertz, and the multiplicity and integrals were provided. The multiplicity code used is as follows: s (singlet), brs (broad singlet), d (doublet), t (triplet), q (quartet), quint (quintuplet), m (multiplet). Data evaluation was accomplished using MestReNova (version 14.1.2-25024, Mestrelab Research S.L. Santiago de Compostela, Spain), and nuclide elucidation from experimental spectra was assisted by the published manual.[203]

ESI-MS studies were performed using a Thermo LTQ OrbitrapXL MS 2.5.5 (Thermo Scientific™) equipped with an ESI source. Samples were dissolved in acetonitrile and introduced by static ESI, aided by HPLC for injection (Agilent 1200 Series HPLC). Nitrogen served both as a nebuliser gas and a dry gas. Helium served as a cooling gas for the ion trap. The mass axis was externally calibrated with Pierce™ LTQ ESI Positive Ion calibration solution (Pierce™, Thermofischer) as a calibration standard. The spectra were recorded and analysed with the XCalibur 2.1.0 (Thermo Scientific™) software by the accumulation and averaging of several single spectra.

All reagents used in the chemistry and biochemistry sections were of the best grade needed, supplied by Sigma-Aldrich, Fluorochem, Alfa Aesar, AmBeed, and VWR, and used without further purification.

Solvents were bought from VWR, Sigma-Aldrich, or Bernd Kraft GmbH and used without further purification; solvent concentrations in reactions were referred to the limiting reagent.

LogP determinations were performed in the Mol inspiration calculator web service,[204] and they were expressed in base 10 logarithmic scale.

6.17. Computational analysis and docking

Computational analysis was performed on a Lenovo P350 workstation equipped with Maestro Release 2021-4 (Schrödinger, LLC, New York, NY, 2021). The descriptions of the methods performed in this section were taken from the Maestro 2021-4 user manual; specific conditions used by calculations are described as performed in our experiments.

6.17.1. NAMPT inhibitor lead optimisation

Compound optimisation was approached in a multistep process, as outlined below.

First, PDB was explored to find suitable co-crystal structures of NAMPT with different inhibitors; among those available, 6E68, 2GVJ, 4O13, 5UPE, and 5U2M were chosen due to the good resolution of the x-ray diffraction data (≤ 2.1Å) and the variation of co-crystallised inhibitors covered.

Grid generation:

PDB diffractograms usually lack the ability to represent side chains on the surface of the structure or to do so inaccurately – or even for whole chains that are solvent-exposed, as these are usually more mobile, and it can be difficult to determine their coordinates from the X-ray data. Additionally, the PDB provided data usually lack some hydrogen atoms (depending on the resolution achieved and the quality of the crystal used) and have incorrect bond order assignments, charge states, or orientations of various groups. For this reason, it was very convenient to make a pre-optimisation of the protein structure before the grid was generated. In this study the automated protein preparation workflow from Maestro's Bioluminate Suite was used, capping peptide termini at their N- and C- ends with acetyl and N-methyl groups, respectively. Default parameters under an OPLS4 force-field for the final optimisation were used for minimising the energy of the protein conformer.

The next step consisted of generating the receptor grid; for this, the Glide suite of Maestro was used, and in all cases, the calculations were made using the original inhibitor bonded in the cocrystal as an initial estimate. The computation parameters were that the size of the docking box was 20% larger than the defined box for the initial ligand. Any constraints for the method were considered.

The next steps were performed with each of the five generated grids using equal parameters and conditions.

Docking of single molecules:

In those cases of manual docking of a limited number of molecules (< 10), the process was started using the automated ligand optimisation process that was based on the OPLS4 force field theory. This method makes an initial guess of the minimum energy for undocked ligands. Additionally, the possibility of ionic species due to pH changes were explored using Epik and the pH range between 5 and 8. The software was limited to generating a maximum of 30 stereoisomers (those of minimum energy) in order to make the computational process less resource-demanding. With the optimised ligand, docking to the generated grids was performed using the Glide flexible ligand docking protocol. Using the extra-precision option and processing the data with Monte Carlo optimisation for flexible ligands, no constraints were considered. From this process, a docking score was obtained, which was used to compare the best hits.

Database generation:

From an initial given molecule provided to the software as an initial seed, the automated reaction-based enumeration from the Pathfinder suite of Maestro was used, which, in short, starts with a PathFinder analysis of the input compound with a default depth of 2 steps and as constraints was input that in the enumeration process was not allowed to modify the NAM mimicking moiety and H-bond capable moiety; reaction paths were chosen at random from the results of the analysis, up to the maximum set; and the default reactant sets from the distribution were used for the enumeration. The similarity for compound picking was evaluated as the Tanimoto similarity between the topological fingerprints generated by RDKit with default settings. The fragments (reactants) used in the enumeration come from the eMolecules building block library.

Once a set of molecules was generated, they were incorporated into a Phase database to make analysis easier. In the database generation, was set as constraints for molecule selection that they must not present charged atoms, and the maximum number of molecules in the database was limited to 3,000 (the best scored ones).

Virtual docking of databases:

This stage was performed under the virtual screening workflow of Glide, where generated phase databases of compounds were screened against the five receptor grids. As filtering criteria, any ionised compound was considered since in analogy to the compounds described in the literature, ionised NAMPT inhibitors were not going to be able to allocate them in the catalytic pocket.

Before docking, a preparation process was introduced for the selected ligands using the same strategy as described before with the ligand optimisation process. Docking was performed in a multistep process based on an optimised MM approach. Initially, a fast, low-accuracy MM optimisation called HTVS was made; 10% of the top hits were kept, which were screened again using the more precise SP method. After scoring, another 10% of inhibitors were kept, and finally, a last round of docking with the high-precision MM XP process was performed, limiting the output to the 10 best-scored ligands. The last step optimisation to obtain more accurate scoring of ligands was carried out by a MM-GBSA (generalised born surface area); this is an end-point binding free energy determination that is much more computationally efficient than alchemical free energy methods like the free energy perturbation (FEP) method.[205] From the list of results, ligands were selected depending on their synthetic complexity in terms of biological stability and docking score.

6.17.2. pKa calculations:

The pKa analysis of selected ionisable groups in the molecule was performed by quantum mechanics approximation of the real energy minimum conformer of given molecules by means of quantum mechanics-based DFT (in all cases the calculation base chosen was B3LYP). For calculation, Jaguar suit of Maestro was used, where pKa was calculated in a multistep approach that involves geometry optimisation of the ionic and neutral species, single-point energy and frequency calculations (with B3LYP DFT), and an empirical correction. The accuracy of the prediction was in the range 0.2–0.5 pKa units for bases and 0.2–1.0 pKa units for acids, depending on the functional group. For the initial guess molecular orbital generation, the atomic overlap was used, and the convergence criteria were used under default parameters,

increasing the number of iterations made by the software to reach the convergence criteria to 500. Additionally, as a solvation model, a polarisable continuum model (PCM) with the dielectric constant of water was used. As a final result, the software reports all the calculated conformers (protonated and de-protonated), ranks them in terms of minimum free energy, and reports pKa for the minimum energy conformer.

6.18. HPLC methods

The machines and column used are described in **6.16**. In all HPLC methods, the detector recorded wavelengths from 200 to 400 nm. The flow rate for the analytical HPLC column is 1.4 mL/min. For preparative HPLC, the column dimensions were either 250 x 21.2 mm with a flow rate of 30 mL/min or 250 x 30 mm with 60 mL/min.

Table 12. HPLC method 1

Time (min)	Solvent 1: H_2O 0.05% TFA	Solvent 2: ACN
0	95	5
14.8	0	100
18	0	100
18.5	95	5
22	95	5

Table 13. HPLC method 2

Time (min)	Solvent 1: H_2O 0.05% TFA	Solvent 2: ACN
0	95	5
14.8	50	50
15	0	100
18	0	100
18.5	95	5
22	95	5

Table 14. HPLC method 3

Time (min)	Solvent 1: H_2O 0.05% TFA	Solvent 2: ACN
0	95	5
10.8	30	70
15	20	80
33.5	0	100
34.5	95	5
35	95	5

Table 15. HPLC method 4

Time (min)	Solvent 1: H_2O 0.05% TFA	Solvent 2: ACN
0	95	5
10.8	30	70
15	20	80
26	0	100
27.5	95	5
28	95	5

Table 16. HPLC method 5

Time (min)	Solvent 1: H_2O 0.05% TFA	Solvent 2: ACN
0	95	5
15	30	70
15.1	0	100
18	0	100
18.5	95	5
22	95	5

Table 17. HPLC method 6

Time (min)	Solvent 1: H_2O 0.05% TFA	Solvent 2: MeOH
0	95	5
14.8	20	80
15	0	100
18	0	100
18.5	95	5
22	95	5

Table 18. HPLC method 7

Time (min)	Solvent 1: H_2O 0.05% TFA	Solvent 2: ACN
0	95	5
2	75	25
35	66.3	33.7
36	0	100
41	0	100
41.5	95	5
43	95	5

Table 19. HPLC method 8

Time (min)	Solvent 1: H_2O	Solvent 2: ACN
0	95	5
2	50	50
15	35	65
15.2	0	100
18	0	100
18.5	95	5
22	95	5

Table 20. HPLC method 9

Time (min)	Solvent 1: H_2O 0.05% TFA	Solvent 2: ACN
0	95	5
2	50	50
13	0	100
18	0	100
18.5	95	5
22	95	5

Table 21. HPLC method 10

Time (min)	Solvent 1: H_2O 0.05% TFA	Solvent 2: ACN
0	95	5
14.8	35	65
15	0	100
18	0	100
18.5	95	5
22	95	5

Table 22. HPLC method 11

Time (min)	Solvent 1: H_2O 0.05% TFA	Solvent 2: ACN
0	95	5
14.8	50	50
21	0	100
24	0	100
24.5	95	5
28	95	5

Table 23. UPLC method for Lysosome assay (flow 0.3 mL/min). The UPLC used is described in **6.12**.

Time (min)	Solvent 1: H_2O + 0.1% Formic acid	Solvent 2: ACN + 0.1% Formic acid
0	5	95
2	50	50
3	50	50
3.1	5	95
5.6	5	95
6.1	5	95

6.19. **General Procedure A.** Synthesis of Boc-protected amine intermediates

Procedure:

The amine intermediate (1eq) was dissolved in DCM (resulting concentration = 0.1 M), triethylamine (1-2 eq) was added, and the reaction mixture was set to 0 °C. A solution of di-*tert*-butyl dicarbonate (1-2 eq) dissolved in DCM at a concentration of 0.67 M was added dropwise. The reaction mixture was stirred at 20 °C for 3 h. The reaction progress was followed by TLC (Hex/EtOAc). The proportion was indicated in each case.

Work up:

After completion, the volatiles were evaporated under reduced pressure, and the crude product was adsorbed on diatomaceous earth and purified by flash chromatography using an isocratic method (Hex/EtOAc).

6.20. **General Procedure B**. Coupling of butyl-amine with phenyl-carboimmidate for N-cyano-3-pyridin-guanidin intermediates

Procedure:

The amine intermediate (1eq) and phenyl (*Z*)-*N*'-cyano-*N*-(pyridin-3-yl)carbamimidate (**1**, 1-1.5eq) were dissolved in 1,4-dioxane or DCM (resulting concentration = 47mM). The reaction mixture was set under argon, and Et_3N (1-3eq) was added. The progress of the reaction was followed by TLC ($CHCl_3$/MeOH).

Work up:

After completion, the volatiles are evaporated under reduced pressure, and the crude product was adsorbed on diatomaceous earth and purified by flash chromatography using an isocratic method (DCM/MeOH).

6.21. **General Procedure C**. Boc deprotection of primary and secondary amines

For Boc-deprotection, two variations were applied depending on the stability of the intermediates against acid.

Variation 1 (Acid-resistant intermediates):

Procedure:

The Boc-protected intermediate was dissolved in pure TFA and the solution was rotated for 5 min at 400 mbar, followed by TFA evaporation lowering pressure to 80 mbar.

Work up:

After completion, the crude product was three times co-evaporated with MeOH. If required, the crude product was purified after co-evaporation.

Variation 2 (Acid-labile intermediates):

Procedure:

Boc-protected intermediates were dissolved in a solution of 10-20% TFA in DCM or DMF. The reaction mixture was stirred at R.T. for 2 h. The reaction progress was followed by TLC and/or HPLC, as specified for each molecule.

Work up:

After completion, the crude product was three times co-evaporated with MeOH. If required, the crude product was purified after co-evaporation.

6.22. **General Procedure D**. Cbz-protection of amines

Procedure:

The amine intermediate (1 eq) was dissolved in THF (resulting concentration = 0.33 M), benzyl chloroformate (1-2 eq) was added, followed by base (NaOH or $NaHCO_3$, 2 eq). The reaction mixture was stirred at r.t. for 3 h. The progress of the reaction was followed by TLC ($CHCl_3$/MeOH).

Work up:

After completion, the reaction mixture was acidified until a pH-value of 2 and extracted with EtOAc (3x). The organic layers were combined and washed with brine. The volatiles were evaporated under reduced pressure, and the crude product was adsorbed on diatomaceous earth and purified by flash chromatography applying a 15-min linear method gradient from 100% $CHCl_3$ to $CHCl_3$/MeOH.

6.23. **General Procedure E**. Cbz-deprotection by hydrogenation

Procedure:

In a three-neck flask equipped with an argon balloon, a hydrogen balloon and an adaptor for connection to a vacuum pump, the Cbz-protected intermediate was dissolved in EtOAc (resulting concentration = 80 mM), followed by the addition of EtOH (same volume as EtOAc) and Pd/C (10-12 mol-%). Five cycles of vacuum/argon, followed by five cycles of vacuum/hydrogen were applied, and the reaction mixture vigorously stirred under hydrogen at r.t. for 3 h.

Work up:

After completion, the system was degassed from hydrogen by applying five vacuum/argon cycles. The reaction crude was filtered through celite, and volatiles were evaporated under reduced pressure. The reaction endpoint was determined by TLC or HPLC. Methods for detection and purification requirements (if needed) are specified for each molecule.

6.24. **General Procedure F**. DCC promoted amide bond formation

Procedure:

The carboxylic acid intermediate (1-2 eq) and amine intermediate (1 eq) were dissolved DCM (abs.) or DMF (abs., resulting concentration = 80 mM). In the following order, DIPEA (1-2.2 eq), HOBt (1-2 eq) and DCC (1-2 eq) were added. The reaction mixture was stirred at r.t. overnight. The reaction progress was followed by TLC and/or HPLC. The exact conditions and methods are described for each individual compound.

Work up:

After completion, the precipitated urea was removed from the reaction crude by filtration through celite, and the liquid layer was collected and washed with an aqueous 5% citric acid solution. The organic layer was collected and washed with water and brine. The organic layer was dried over $MgSO_4$, and volatiles were removed under reduced pressure. The crude product was adsorbed on diatomaceous earth and purified by flash chromatography using a linear solvent gradient specified for each molecule.

6.25. **General Procedure G**. Synthesis of mesylate

Procedure:

An alcohol intermediate (1 eq) was dissolved in DCM (abs., resulting concentration = 0.14 M). The reaction mixture was then cooled down to 0 °C, and methanesulfonyl chloride (1.5 eq) was added, followed by triethylamine (2 eq). The reaction mixture was stirred at r.t. for 1-2 h. The reaction progress was followed by TLC and/or HPLC. The individual conditions and methods applied are described for each intermediate.

Work up:

After completion, the crude product was dissolved in $CHCl_3$, neutralised with an aqueous 5% citric acid solution, dried over $MgSO_4$ and the volatiles evaporated under reduced pressure. Purification conditions were described for each molecule.

6.26. **General Procedure H**. Gabriel synthesis of primary amines (2-steps)

Step 1:

Procedure:

The mesylate intermediate (1 eq) was dissolved in DMF (abs., resulting concentration = 96 mM), potassium phthalimide (1.2 eq) was added, and the reaction mixture was stirred at 50

°C overnight. The reaction progress was followed by TLC and/or HPLC. The exact conditions and methods are described for each individual compound.

Work up:

After completion, reaction crude was dissolved in DCM (10x volume of DMF used in the reaction), and the organic layer was washed 2x with same volume of H_2O. The organic layer was collected and dried over $MgSO_4$. The volatiles were evaporated under reduced pressure. The exact purification conditions were described for each molecule.

Step 2:

Procedure:

The phthalimide from step 1 (1 eq) was dissolved in EtOH (resulting concentration = 90mM). After setting the system under an argon atmosphere, hydrazine monohydrate (4-6 eq) was added. The reaction mixture was stirred at r.t. for 6 h-O.N. The reaction progress was followed by TLC and/or HPLC. The exact conditions and methods are described for each individual compound.

Work up:

After completion, the crude product was filtered to remove precipitates, and the volatiles were evaporated under reduced pressure. The crude product was dried *in vacuo* overnight to remove traces of hydrazine. The exact purification conditions were described for each molecule.

6.27. **General Procedure I**. Coupling of NHS-activated carboxylic acids containing maleimides to amino groups:

Procedure:

The amine intermediate (1-1.2 eq) was dissolved in DMF (abs., resulting concentration = 10 mM), EMCS, BMPS or Mal-d-PEG4-NHS (1-1.5 eq) was added, followed by DIPEA (2-3.3 eq). The reaction progress was followed by TLC and/or HPLC. The exact conditions and methods are described for each individual compound.

Work up:

After completion, volatiles were evaporated under reduced pressure. The exact purification conditions are described for each molecule.

6.28. **General Procedure J**. Coupling of aniline-containing NAMPT inhibitor to PNP-activated linkers

Procedure:

The PNP-activated Linker or free carboxylic acid linker (1-2 eq) was dissolved in DMF (resulting concentration = 25 mM), then PyAOP (1.5-2 eq) or HATU (1.1 eq) was added, followed by DIPEA (5-6 eq, 4eq in case of use HATU) until a pH-value of 10 was reached. The linker was activated for 30 min, then an aniline-containing intermediate (1 eq) was added. The reaction mixture was stirred at r.t. overnight. The reaction progress was followed by TLC and/or HPLC. The exact conditions and methods are described for each individual compound.

Work up:

After completion, the solvent was evaporated under reduced pressure and purified by RP-HPLC, the method is specified for each molecule.

6.29. **General Procedure K**. Biotinylation of aniline-containing free NAMPT inhibitors

Procedure:

Biotin (1 eq), DIPEA (2 eq) and HATU (1.1 eq) were dissolved together in DMF (abs., resulting concentration referred to biotin = 35.5 mM). After 15 min for biotin activation, a solution of the aniline-containing in DMF (abs.) was added to the reaction mixture, followed by DMF (abs.) until the limiting reagent final concentration of 14.2 mM was reached. The reaction progress was followed by TLC and/or HPLC. The exact conditions and methods are described for each individual compound.

Work up:

After completion, volatiles were evaporated under reduced pressure. The crude product was purified by HPLC using a method specified for each molecule.

6.30. **General Procedure L**. Activation of PAB alcohols with bis(*p*-nitrophenyl) carbonate

Procedure:

The linker containing PAB alcohol (1 eq) was dissolved in DMF (abs., resulting concentration = 43.5 mM), bis(*p*-nitrophenyl) carbonate (2 eq) was added, and after dissolution, DIPEA (1.5-3 eq) was added. The reaction progress was followed by TLC and/or HPLC. The exact conditions and methods are described for each individual compound.

Work up:

After completion, the crude product was cooled on ice for 10 min. Then, a solution of 1:1 hexane/MTBE (20x the initial volume of DMF used in the reaction) was added; the reaction mixture was shaken until a solid was formed and centrifuged at 4,500 RPM for 5 min in a precooled (0°C) centrifuge. The generated pellet was washed twice with pure MTBE. The pellet obtained was dried under vacuum and purified by HPLC, using the method specified for each molecule.

6.31. **General Procedure M**. Synthesis of 1-Boc or 1-Cbz- 4-hydroxy-4(pent-4-en-1-yl)piperidine

Procedure (Part 1, Grignard-formation):

Magnesium (solid, turnings; 2 eq) and I_2 (tip of a spatula) were added to a dried three-neck flask equipped with a reflux condenser. An inert atmosphere was set up by flushing the system with argon. Then, THF (abs., resulting concentration = 0.43 M) was added, and the temperature was raised to 70 °C (reflux) for 20 min. The mixture was cooled down to r.t. and afterwards, 5-bromo-1-pentene (1.5 eq) was added dropwise over a period of 10 min. The reaction mixture was kept at r.t. until it got cloudy and the formation of bubbles were observed.

The reaction mixture was then set at 70 °C for 30 min and then cooled to r.t. and kept under argon atmosphere until it was used in the next step.

Procedure (Part 2, alcohol synthesis):

A solution of $LaCl_3$*2LiCl in THF (1 eq) was added to a dried two-neck flask, followed by piperidone (1 eq). The reaction mixture was stirred at r.t. for 1 h, and then, the system was cooled to 8 °C with a chiller, and the Grignard from step 1 was added dropwise. The reaction mixture was kept at 8 °C. The reaction progress was followed by TLC and/or HPLC. The exact conditions and methods are described for each individual compound.

Work up:

After completion, the reaction was quenched with NH_4Cl (sat.), washed once with H_2O and once with brine, and dried over $MgSO_4$. Purification was performed by flash chromatography and the solvent(gradient) is specified for each intermediate.

6.32. **General Procedure N**. OsO_4-catalysed dihydroxylation of alkenes

Procedure:

The alkene (1 eq) was dissolved in acetone (resulting concentration = 0.17 M). Then, NMO (1.2 eq), water (16 eq), and a 2.5 wt.% solution of OsO_4 in *tert*-butanol (0.47 mol-%) were added. The reaction progress was followed by TLC and/or HPLC. The exact conditions and methods are described for each individual compound.

Work up:

After completion, the reaction mixture was quenched with saturated aqueous Na_2SO_3 solution and extracted with $CHCl_3$ (3x). The organic layers were collected and washed once with water and once with brine. The organic layer was dried over $MgSO_4$, and volatiles were removed under reduced pressure. Purification was performed by flash chromatography and the solvent(gradient) is specified for each intermediate.

6.33. **General Procedure O**. Oxidative cleavage of 1,2-diol intermediates

Procedure:

The diol (1 eq) was dissolved in THF (resulting concentration = 0.16 M). Sodium periodate (2 eq) was pre-dissolved in water (resulting concentration 0.08 M). The THF reaction mixture was cooled to 0 °C, and both solutions were then mixed in a ratio of THF/H_2O: 2/1 v/v. The reaction progress was followed by TLC and/or HPLC. The exact conditions and methods are described for each individual compound.

Work up:

After completion, volatiles were evaporated, the crude product re-dissolved in EtOAc and washed once with water and once with brine. The organic layer was dried over $MgSO_4$ and volatiles were evaporated under reduced pressure. Purification was performed by RP-HPLC, using a method specified for each molecule.

6.34. **General Procedure P**. Amine synthesis by reductive amination of aldehydes

Procedure:

The aldehyde (1 eq) was dissolved in MeOH (abs., resulting concentration = 0.23 M). Ammonium acetate (10 eq) and sodium cyanoborohydride (2 eq) were dissolved in MeOH (abs., 0.7 times volume used to dissolve the aldehyde). Then, the ammonium acetate-sodium cyanoborohydride-solution was added to the aldehyde solution. The pH-value was adjusted to 6 with acetic acid. The reaction progress was followed by TLC and/or HPLC. The exact conditions and methods are described for each individual compound.

Work up:

After completion, the reaction mixture was quenched with an aqueous 5% citric acid solution, followed by neutralisation with a sodium hydroxide-solution (5M) until pH = 12. Then, the quenched crude product was extracted with EtOAc (3x), the organic layers were combined and washed once with brine. The organic layer was then dried over $MgSO_4$, and volatiles were evaporated under reduced pressure. The crude product was purified by RP-HPLC, using a method specified for each molecule.

6.35. **General Procedure Q**. Fmoc and acetyl deprotection of glucuronic acid-containing linkers

Procedure

N-Fmoc-*O*-Ac-β-D-glucuronide-linker-payload-intermediate (1 eq) was dissolved in methanol (resulting concentration = 14mM). The solution was cooled to 0 °C, and then an aqueous solution of LiOH monohydrate (concentration of solution = 0.23M) was added (same volume as MeOH). The reaction mixture was stirred at 0 °C for 15 min. The reaction progress was followed by HPLC. Methods are described for each individual intermediate.

Work up:

After completion, the reaction mixture was neutralised using acetic acid (1.1 eq); volatiles were then evaporated under reduced pressure. Fmoc removal was afforded by dissolving the crude product in piperidine (200 eq) and incubate it for 5 min at r.t. The volatiles were evaporated under reduced pressure, and the crude product was purified by HPLC, using the method specified for each individual molecule.

6.36. **General Procedure R**. Urea bond formation between free aliphatic amine and 4-nitrophenyl isoindoline-2-carbamate

Procedure:

The amine intermediate (1 eq) and carbamate (2 eq) were dissolved in DMF (abs., resulting concentration = 23mM). Then, *N*-methylimidazole (10 eq) and DIPEA (1.5 eq) were added. The reaction progress was followed by TLC and/or HPLC. The exact conditions and methods are described for each individual compound.

Work up:

After completion, the crude product was directly injected into the preparative RP-HPLC machine and purified using method 1.

6.37. Product synthesis and purification: Exact conditions and methods for each individual compound.

Phenyl (*Z*)-*N*'-cyano-*N*-(pyridin-3-yl)carbamimidate (1),[206]

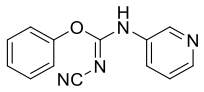

Chemical Formula: $C_{13}H_{10}N_4O$
Molecular Weight: 238.25

Procedure:

3-aminopyridine (1 eq, 34.9 mmol, 3.28 g) and diphenyl *N*-cyanocarbonimidate (1.1 eq, 34.9 mmol, 8.31 g) were charged into a two-neck-flask. Then, DCM (105 mL) was added to the mixture, followed by triethylamine (1 eq, 34.9 mmol, 4.6 mL). The mixture was allowed to react overnight at room temperature and the reaction monitored by TLC (SiO_2, $CHCl_3$/MeOH: 21/1).

After completion, the volatiles were evaporated under reduced pressure, and the crude product was adsorbed on diatomaceous earth. Purification by flash chromatography applying an isocratic method ($CHCl_3$/MeOH: 21/1) afforded carbamimidate (90% yield, 31.4 mmol, 7.48 g) as white to pale yellow crystals. MS (ESI, negative mode): found *m*/*z* = 237.3 $[M-H]^-$, calculated *m*/*z* = 237.1 $[M-H]^-$.

***N*-Boc-4-(4-hydroxy-butyl)-piperidine(2)**[207]

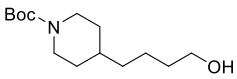

Chemical Formula: $C_{14}H_{27}NO_3$
Molecular Weight: 257.37

Following **General Procedure A**, 4-(4-hydroxy-butyl)piperidine (1 eq, 3.18 mmol, 500 mg) and triethylamine (1.05 eq, 3.34 mmol, 466 µL) were dissolved in DCM (35 mL) and cooled to 0 °C. Then, di-*tert*-butyl dicarbonate (1.05 eq, 3.34 mmol, 729 mg) was added, the reaction mixture temperature allowed to warm to r.t. and was stirred for 3 h. The reaction was monitored by TLC (SiO_2, hexane/EtOAc: 3/1). After completion, the volatiles were evaporated under reduced pressure, and the crude product was adsorbed on diatomaceous earth. Purification by flash chromatography applying an isocratic method (hexane/EtOAc: 4/1) afforded Boc-protected piperidine **2** (82% yield, 2.61 mmol, 671 mg) as clear oil. MS (ESI, negative mode): found *m*/*z* = 256.4 $[M-H]^-$, calculated *m*/*z* = 256.2 $[M-H]^-$.

N-Boc-4-(piperidinyl)butyl-1-azide(3)[208]

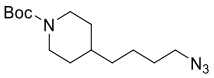

Chemical Formula: $C_{14}H_{26}N_4O_2$
Molecular Weight: 282.39

Procedure:

Intermediate **2** (1 eq, 0.4 mmol, 103 mg) was dissolved in DMF (abs., 5mL, resulting concentration = 77.8 mM) at 0 °C under argon. Then, DPPA (3 eq, 1.17 mmol, 252 µL) and subsequently, DBU (3eq, 1.17 mmol, 174 µL) were added. The reaction mixture was kept for 30 min at 0 °C. Afterwards, it was heated to 100 °C, and sodium azide (3eq, 1.17mmol, 76 mg) was added. The reaction mixture was stirred for 90 min and then cooled to r.t. The reaction was monitored by TLC (SiO_2, hexane/EtOAc: 4/1).

After completion, the crude product was dissolved in DCM and washed with water (2x) and brine (2x). Then, the volatiles were evaporated under reduced pressure and, and the crude product was adsorbed on diatomaceous earth. Purification by flash chromatography, applying an isocratic method (hexane/EtOAc: 4/1) afforded azide **3** (40% yield, 0.16 mmol, 45.2 mg) as yellow oil. MS (ESI, negative mode): found *m/z* = 281.6 $[M-H]^-$, calculated *m/z* = 281.2 $[M-H]^-$.

***N*-Boc-4-(4-piperidinyl)butanoic acid (4)**

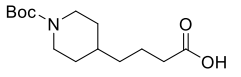

Chemical Formula: $C_{14}H_{25}NO_4$
Molecular Weight: 271.36

Procedure:

4-(4-piperidinyl)butanoic acid hydrochloride (1 eq, 24 mmol, 4.98 g) was dissolved in a mixture of THF/H_2O (17 mL THF and 32 mL H_2O, resulting concentration = 0.75 M). Then, sodium bicarbonate (2.23 eq, 53.6 mmol, 4.5 g) was added slowly, and gas formation was observed. After the gas formation stopped, di-*tert*-butyl dicarbonate (1.12 eq, 27 mmol, 5.9 g) was added, and the reaction mixture was heated to 50 °C for 4 h. The reaction was monitored by TLC (SiO_2, MeOH/DCM/AcOH: 1/20/2%).

After completion, the volatiles were evaporated under reduced pressure until one third of the initial volume was left. EtOAc was added and the pH-value adjusted to 3 by adding an aqueous 20 wt-% potassium bisulfate solution dropwise. The layers were separated, and the aqueous layer was extracted with EtOAc (2x). The combined organic layers were mixed and washed once with water and once with brine. The volatiles were evaporated under reduced pressure. The crude product was adsorbed on diatomaceous earth. Purification by flash chromatography, applying an isocratic method (MeOH/DCM/AcOH 1/20/2%) afforded intermediate **4** (63% yield, 15.12 mmol, 4.1 g) as a turbid white oil. **^{1}H-NMR (500 MHz, $CDCl_3$):** δ/ppm = 4.06 (s, 4H), 2.65 (s, 2H), 2.33 (t, J = 7.5 Hz, 2H), 1.69– 1.59 (m, 2H), 1.44 (s, 14H), 1.06 (qd, J = 12.7, 4.5 Hz, 2H). **^{13}C-NMR (126 MHz, $CDCl_3$):** δ/ppm = 179.37, 154.93, 79.36, 35.77, 35.69, 34.10, 31.95, 28.42, 21.77, 20.82), MS (ESI, positive mode): found *m/z* = 272.2 $[M+H]^+$, calculated *m/z* = 272.2 $[M+H]^+$.

***N*-Boc-4-(piperidinyl)butanamide (5)**

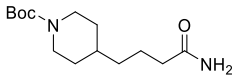

Chemical Formula: $C_{14}H_{26}N_2O_3$
Molecular Weight: 270.37

Procedure:

Under an argon atmosphere, intermediate **4** (1 eq, 0.37 mmol, 100 mg) was charged in a two-neck flask and dissolved in EtOAc (5 mL). Then, *N*-*N*'-carbonyl diimidazole (1.25 eq, 0.46 mmol, 75 mg) was added, and the resulting mixture was stirred for 2.5 h at r.t. Afterwards, the reaction mixture was cooled down to 0 °C, and a concentrated aqueous ammonia solution (1.5 mL) added. The mixture was then allowed to warm to r.t. and was stirred overnight. The reaction was monitored by TLC (SiO_2, $CHCl_3$/MeOH: 15/1).

After completion, the reaction mixture was washed with a saturated, aqueous solution of sodium bicarbonate (3x) and once with brine. Then, the combined organic layers were collected and dried over MgSO4, and the volatiles were evaporated under reduced pressure. Without further purification, intermediate **5** (40% yield, 0.15 mmol, 40 mg) was obtained as oil. MS (ESI, negative mode): found *m*/*z* = 269.6 $[M-H]^-$, calculated *m*/*z* = 269.2 $[M-H]^-$.

N-Boc-4-(piperidinyl)butan-1-amine (6)[209]

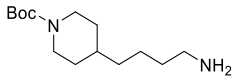

Chemical Formula: $C_{14}H_{28}N_2O_2$
Molecular Weight: 256.39

Procedure:

Intermediate **5** (1 eq, 7.85 mmol, 2.1 g) was dissolved in THF (70 mL, resulting concentration = 0.11 M) and transferred to a three-neck flask equipped with a reflux condenser. Then, the solution was cooled to 0 °C, and a 1M BH_3-THF-solution (7.8 eq, 60 mmol, 60 mL) was added. Next, the system is heated to 73 °C and refluxed overnight. The reaction was monitored by TLC (SiO_2, $CHCl_3$/MeOH/Et_3N: 15/1/1%).

After completion, the mixture was cooled to 0 °C and MeOH (250 mL) was added. Then, the volatiles were evaporated under reduced pressure. The residue was dissolved in methanol (100 mL) and refluxed at 70 °C for 1 h. Afterwards, the volatiles were evaporated under reduced pressure, and crude product was dissolved in EtOAc, and washed once with an aqueous, saturated sodium bicarbonate solution, followed by brine. Next, the combined organic layers were dried over $MgSO_4$ and the obtained crude product was adsorbed on diatomaceous earth. Purification by flash chromatography, applying an isocratic method ($CHCl_3$/MeOH/Et_3N: 15/1/1%) afforded intermediate **6** (10% yield, 0.785 mmol, 200 mg) as a pale-yellow oil. MS (ESI, positive mode): found *m*/*z* = 257.5 $[M+H]^+$, calculated *m*/*z* = 257.2 $[M+H]^+$.

tert-butyl (*E*)-4-(4-(2-cyano-3-(pyridin-3-yl)guanidino)butyl)piperidine-1-carboxylate (7)

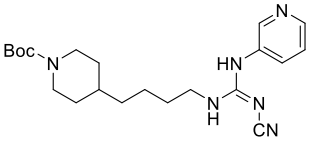

Chemical Formula: $C_{21}H_{32}N_6O_2$
Molecular Weight: 400.53

Following **General Procedure B**, intermediate **6** (1 eq, 0.4 mmol, 102 mg) and intermediate **1** (1 eq, 0.4 mmol, 95.3 mg) were dissolved in dioxane (4 mL), followed by the addition of triethylamine (1.2 eq, 0.4 mmol, 55.8 µL). Then, the reaction mixture was stirred for 36 h. The reaction was monitored by TLC (SiO2, hexane/EtOAc: 1/1 for phenol side product detection and $CHCl_3$/MeOH: 15/1 for product formation). The crude product was adsorbed on diatomaceous earth. Purification by flash chromatography, applying an isocratic method ($CHCl_3$/MeOH: 15/1) afforded intermediate **7** (55% yield, 0.22 mmol, 88.1 mg) as clear sticky oil. MS (ESI, positive mode): found *m*/*z* = 401.4 $[M+H]^+$, calculated *m*/*z* = 401.3 $[M+H]^+$.

(*E*)-2-cyano-1-(4-(piperidin-4-yl)butyl)-3-(pyridin-3-yl)guanidine chloride (8)

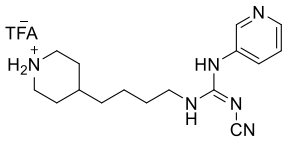

Chemical Formula: $C_{18}H_{26}N_6O_2F_3$
Molecular Weight: 415.42

Following **General Procedure C**, intermediate **7** (1 eq, 0.27 mmol, 108.1 mg) was dissolved in pure TFA as a solvent (4 mL). The reaction mixture was stirred for 15 min at 400 mbar. The reaction was monitored by TLC (SiO_2, $CHCl_3$/MeOH/Et_3N: 10/1/1%). After completion, the crude product was worked up as reported in **General Procedure C,** and intermediate **8** (80% yield, 0.22 mmol, 89.7 mg) was afforded as sticky white crystals and used without further purification in the next reaction step.

(*E*)-4-(4-(4-(2-carbamoyl-3-(pyridin-3-yl)guanidino)butyl)piperidine-1-carbonyl)phenylacetate (9)

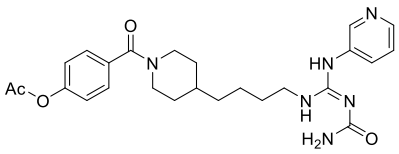

Chemical Formula: $C_{25}H_{32}N_6O_4$
Molecular Weight: 480,57

Procedure:

Intermediate **8** (1 eq, 0.26 mmol, 108 mg) was dissolved under an argon atmosphere in DMF (abs., 7 mL, resulting concentration = 37 mM). Then, *p*-acetoxybenzoic acid succinimide ester premade in HDP (1 eq, 0.35 mmol, 97 mg) was added, followed by DIPEA (4 eq, 1.4 mmol, 244 µL). The reaction was monitored by TLC (SiO_2, hexane/EtOAc/Et_3N: 1/1/1%).

After completion, the crude product was diluted with $CHCl_3$, washed once with H_2O and then rinsed once with brine. The combined organic layers were dried over $MgSO_4$. Then, the

obtained crude oil was adsorbed on diatomaceous earth. Purification by flash chromatography, applying an isocratic method (hexane/EtOAc/Et_3N: 1/1/1%) afforded the guanyl urea intermediate **9** (30% yield, 0.078 mmol, 37 mg) as white crystals. MS (ESI, positive mode): found *m/z* = 481.7 $[M+H]^+$, calculated *m/z* = 481.2 $[M+H]^+$.

Benzyl 4-(4-amino-4-oxobutyl)piperidine-1-carboxylate (10)

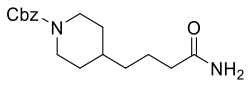

Chemical Formula: $C_{17}H_{24}N_2O_3$
Molecular Weight: 304,39

Following **General Procedure C, variation 1**, intermediate **5** was Boc-deprotected (1 eq, 17.64 mmol, 4.8 g), and the obtained crude product was mixed with a solution of benzyl chloroformate (2 eq, 35.28 mmol, 6.0 g) in THF (53 mL) and an aqueous 2M NaOH (53 mL) solution. The reaction mixture was stirred for 3 h at r.t. The reaction was monitored by TLC (SiO_2, $CHCl_3$/MeOH: 15/1). After completion, the crude product was worked up as reported in **General Procedure D** and was adsorbed on diatomaceous earth. Purification by flash chromatography, applying an isocratic method ($CHCl_3$/MeOH: 15/1), afforded intermediate **10** (40% yield, 7.1 mmol, 2.1 g) as pale-yellow oil. MS (ESI, positive mode): found *m/z* = 305.4 $[M+H]^+$, calculated *m/z* = 305.2 $[M+H]^+$.

N-Cbz-4-(piperidinyl)butan-1-amine (11)

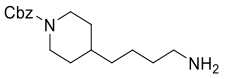

Chemical Formula: $C_{17}H_{26}N_2O_2$
Molecular Weight: 290.41

Procedure:

Intermediate **10** (1 eq, 3.29 mmol, 1 g) was dissolved under argon atmosphere in THF (20 mL). Then, a 1M Borane dimethyl sulphide complex solution in THF (1.5 eq, 4.93 mmol, 4.93 mL) was added to the solution, which is then heated up to reflux and left overnight. The reaction was followed by TLC (SiO_2, $CHCl_3$/MeOH/Et_3N: 5/1/1%).

After completion, the reaction mixture was cooled to 0 °C, and an aqueous 2N NaOH solution (10 mL, 20 mmol) was slowly added. The reaction mixture was maintained under stirring conditions at r.t for 1 h more. The crude product was then diluted with water (10 mL) and extracted with EtOAc (3x). The combined organic layers were washed once with brine and dried over $MgSO_4$. The volatiles were evaporated under reduced pressure and the obtained crude product was adsorbed on diatomaceous earth. Purification by flash chromatography, applying an isocratic method ($CHCl_3$/MeOH/Et_3N: 5/1/1%), afforded intermediate **11** (15% yield, 0.494 mmol, 144 mg) as clear oil. MS (ESI, positive mode): found *m/z* = 291.4 $[M+H]^+$, calculated *m/z* = 291.2 $[M+H]^+$.

benzyl (*E*)-4-(4-(2-cyano-3-(pyridin-3-yl)guanidino)butyl)piperidine-1-carboxylate (12)

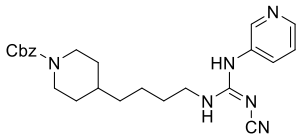

Chemical Formula: $C_{24}H_{30}N_6O_2$
Molecular Weight: 434.54

Following **General Procedure B**, intermediate **11** (1 eq, 1.18 mmol, 343 mg) and intermediate **1** (1.5 eq, 1.76 mmol, 419 mg) were charged in a two-neck flask and dissolved in DCM (30 mL). Then, triethylamine (3 eq, 3.58 mmol, 500 µL) was added, and the reaction mixture was kept stirring for 36 h at r.t. The reaction was monitored by TLC (hexane/EtOAc: 1/1 for phenol side product detection and $CHCl_3$/MeOH: 15/1 for product formation). The crude product was adsorbed on diatomaceous earth. Purification by flash chromatography, applying an isocratic method ($CHCl_3$/MeOH: 15/1), afforded intermediate **12** (40% yield, 0.472 mmol, 205 mg) as sticky oil. **^{1}H-NMR (500 MHz, $CDCl_3$)**: δ/ppm = 8.58 (s, 1H), 8.50 (s, 1H), 7.94 (s, 1H), 7.71 (s, 1H),7.42 – 7.27 (m, 6H), 5.11 (s, 2H), 3.31 (q, J = 6.7 Hz, 2H), 2.74 (s, 2H), 1.57 – 1.50 (m, 2H), 1.37 (s, 1H), 1.30 (s, 2H), 1.30 (d, J = 15.8 Hz, 1H), 1.24 (q, J = 6.7 Hz, 2H), 1.08 (d, J = 12.8Hz, 3H). **^{13}C-NMR (126 MHz, $CDCl_3$):** δ/ppm = 155.14, 136.80, 132.78, 128.32, 127.77, 127.65,66.80, 44.05, 42.05, 35.80, 35.58, 29.29, 23.57). MS (ESI, positive mode): found *m*/*z* = 435.1 $[M+H]^+$, calculated *m*/*z* = 435.2 $[M+H]^+$.

(*E*)-2-cyano-1-(4-(piperidin-4-yl)butyl)-3-(pyridin-3-yl)guanidine (13)

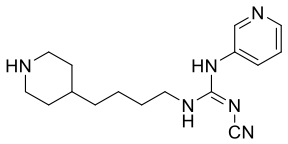

Chemical Formula: $C_{16}H_{24}N_6$
Molecular Weight: 300.41

Following **General Procedure E**, intermediate **12** (1 eq, 0.4 mmol, 174 mg) was dissolved in a solvent mixture of EtOAc (5 mL, resulting concentration in EtOAc = 80mM) and EtOH (5 mL EtOH). Then, a Pd/C catalyst (10% in Pd, 12 mol-%, 50 mg) was added. Afterwards, the system was sealed, and hydrogenation was started according to **General Procedure E**. The reaction takes 3 h, and was monitored by TLC (SiO_2, $CHCl_3$/MeOH/Et_3N: 15/1/1%). After workup, the product is ready to use without further purification, affording intermediate **13** (85% yield, 0.34 mmol, 102 mg) as a white powder. MS (ESI, positive mode): found *m*/*z* = 301.3 $[M+H]^+$, calculated *m*/*z* = 301.2 $[M+H]^+$.

***N*-(4-(4-hydroxy)-butyl)piperinidyl-4-metoxyphenyl-benzamide (14)**

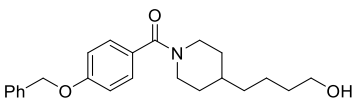

Chemical Formula: $C_{23}H_{29}NO_3$
Molecular Weight: 367.49

Following **General Procedure F**, 4-(4-(hydroxy)-butyl)-piperidine (1 eq, 3.18 mmol, 500 mg) and 4-benzyloxybenzoic acid (1 eq, 3.18 mmol, 726 mg) were dissolved in DCM (abs., 40 mL, resulting concentration = 80mM). Then, DIPEA (1 eq, 3.18 mmol, 554 µL),

HOBt (1 eq, 3.18 mmol, 430 mg) and DCC (1 eq, 3.18 mmol, 656 mg) were sequentially charged to the reaction mixture. The resulting mixture was stirred overnight at r.t., and the reaction monitored by TLC (SiO_2, hexane/EtOAc/MeOH: 10/10/1). After completion, the work-up was performed as described in **General Procedure F,** and the crude product was adsorbed on diatomaceous earth. Purification by flash chromatography, applying an isocratic method (Hex/EtOAc/MeOH: 10/10/1), afforded intermediate **14** (50% yield, 1.59 mmol, 584 mg) as oil. **^{1}H-NMR (500 MHz, $CDCl_3$):** δ/ppm = 7.46 – 7.30 (m, 7H), 6.97 (d, J = 8.7 Hz, 2H), 5.09 (s, 2H), 3.64 (t, J =6.6 Hz, 2H), 1.88 – 0.99 (m, 15H). **^{13}C-NMR (126 MHz, $CDCl_3$):** δ/ppm = 170.18, 159.68, 136.52, 132.04, 128.87, 128.72, 128.60, 128.06, 127.42, 114.49, 114.38, 69.99, 62.77, 36.14, 32.80, 22.79. MS (ESI, positive mode): found *m/z* = 368.1 $[M+H]^+$, calculated *m/z* = 368.2 $[M+H]^+$.

***N*-(4-(4-methanesulfonyl)-butyl)piperinidyl-4-methoxyphenyl-benzamide (15)**

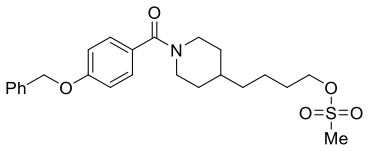

Chemical Formula: $C_{24}H_{31}NO_5S$
Molecular Weight: 445.57

Following **General Procedure G**, intermediate **14** (1 eq, 2.99 mmol, 1 g) was dissolved in DCM (abs., 22 mL). Then, the reaction mixture was cooled to 0 °C and methanesulfonyl chloride (1.5 eq, 4.49 mmol, 347 µL) was added. Triethylamin (2 eq, 6 mmol, 837 µL) was added and the reaction stirred for 2 h at r.t.. The reaction was monitored by TLC (SiO_2, DCM/MeOH: 30/1). After completion, the work-up was performed as described in **General Procedure G,** and the crude product was adsorbed on diatomaceous earth. Purification by flash chromatography, applying an isocratic method (DCM/MeOH: 30/1), afforded intermediate **15** (73% yield, 2.18 mmol, 971 mg) as pale-yellow oil. **^{1}H-NMR (500 MHz, d6-DMSO):** δ/ppm = 7.48 – 7.39 (m, 2H), 7.39 – 7.29 (m, 5H), 7.08 – 7.00 (m, 2H), 5.14 (s, 2H), 4.19 (t, J = 6.4 Hz, 2H), 3.15 (s, 3H), 2.88 – 2.84 (m, 2H), 1.72 – 1.60 (m, 4H), 1.55 – 1.45 (m, 1H), 1.42 – 1.32 (m, 2H), 1.30 – 1.21 (m, 2H), 1.05 (qd, J = 12.4, 4.1 Hz, 2H). **^{13}C-NMR (126 MHz, d6-DMSO):** δ/ppm = 169.05, 159.42, 137.14, 129.04, 128.98, 128.76, 128.20, 128.01, 114.75, 70.65, 69.66, 36.92, 35.56, 35.47, 28.97, 22.28. MS (ESI, positive mode): found *m/z* = 446.1 $[M+H]^+$, calculated *m/z* = 446.2 $[M+H]^+$.

***N*-(4-(4-phtalimido)-butyl)piperinidyl-4-methoxyphenyl-benzamide (16)**

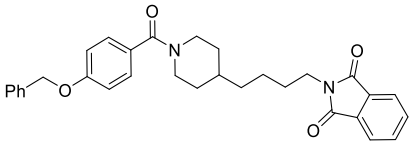

Chemical Formula: $C_{31}H_{32}N_2O_4$
Molecular Weight: 496.61

Following **General Procedure H part 1**, intermediate **15** (1 eq, 1.15 mmol, 512 mg) and potassium phthalimide (1.2 eq, 1.38 mmol, 255 mg) were dissolved in DMF (abs. 12 mL). The reaction mixture was stirred overnight at 50 °C. The reaction was monitored by TLC (SiO_2, hexane/EtOAc/MeOH: 13/7/1). After completion, the work-up was performed as described in **General Procedure H part 1**, and the crude product was adsorbed on

diatomaceous earth. Purification by flash chromatography, applying an isocratic method (Hex/EtOAc/MeOH: 13/7/1), afforded intermediate **16** (60% yield, 0.69 mmol, 343 mg) as pale-yellow oil. **^{1}H-NMR (500 MHz, d6-DMSO):** δ/ppm = 7.92 – 7.79 (m, 6H), 7.49 – 7.42 (m, 1H), 7.46 – 7.36 (m, 1H), 7.40 – 7.28 (m, 3H), 7.07 – 7.00 (m, 2H), 5.14 (s, 2H), 3.57 (t, J = 7.1 Hz, 2H), 2.85 – 2.80 (m, 2H), 1.64 – 1.53 (m, 4H), 1.50 – 1.42 (m, 1H), 1.35 – 1.22 (m, 4H), 1.03 (qd, J = 12.2, 4.1 Hz, 2H). **^{13}C-NMR (126 MHz, d6-DMSO):** δ/ppm = 169.03, 168.24, 159.41, 137.14, 135.03, 134.66, 131.92, 129.03, 128.97, 128.75, 128.19, 128.01, 123.63, 123.28, 114.74, 69.66, 37.64, 35.60, 28.39, 23.62. MS (ESI, negative mode): found *m*/*z* = 495.0 $[M-H]^-$, calculated *m*/*z* = 495.2 $[M-H]^-$.

N-(4-(4-amino)-butyl)piperinidyl-4-metoxyphenyl-benzamide (17)

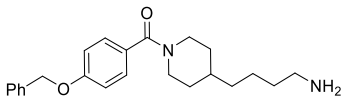

Chemical Formula: $C_{23}H_{30}N_2O_2$
Molecular Weight: 366.51

Following **General Procedure H part 2**, intermediate **16** (1 eq, 0.9 mmol, 447 mg) was dissolved in EtOH (10 mL). Then, hydrazine monohydrate (4 eq, 3.6 mmol, 177 µL) was added, and the reaction stirred for 6 h at r.t. The reaction was monitored by TLC (SiO_2, $CHCl_3$/MeOH/Et_3N: 10/1/1%). After completion, the work-up was performed as described in **General Procedure H part 2**, and the crude product was adsorbed on diatomaceous earth. Purification by flash chromatography, applying an isocratic method ($CHCl_3$/MeOH/Et_3N: 10/1/1%), afforded intermediate **17** (40% yield, 0.36 mmol, 132 mg) as white crystals. **^{1}H-NMR (500 MHz, d6-DMSO):** δ/ppm = 7.45 (d, J = 6.9 Hz, 2H), 7.40 (t, J = 7.3 Hz, 2H), 7.36 – 7.30 (m, 3H), 7.04 (d, J = 8.6 Hz, 2H), 5.14 (s, 2H), 4.17 – 4.13 (m, 2H), 2.57 (t, J = 7.0 Hz, 2H), 1.69 – 1.59 (m, 2H), 1.53 – 1.42 (m, 1H), 1.38 (p, J = 7.1 Hz, 2H), 1.29 (dq, J = 17.6, 5.0, 3.5 Hz, 2H), 1.21 (q, J = 6.4, 5.9 Hz, 2H), 1.05 (qd, J = 12.5, 4.3 Hz, 2H). **^{13}C-NMR (126 MHz, d6-DMSO):** δ/ppm = 168.63, 136.72, 128.65, 128.56, 128.33, 127.77, 127.58, 114.34, 69.26, 40.61, 35.54, 35.27, 31.88, 31.73, 23.51, 23.21. MS (ESI, negative mode): found *m*/*z* = 365.0 $[M-H]^-$, calculated *m*/*z* = 365.2 $[M-H]^-$.

(*E*)-1-(4-(1-(benzyloxycarbonyl)-piperidin-4-yl)butyl)-2-cyano-3-(pyridin-3-yl)guanidine (18)

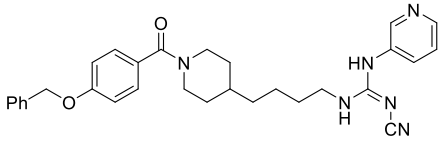

Chemical Formula: $C_{30}H_{34}N_6O_2$
Molecular Weight: 510.64

Following **General Procedure B**, intermediate **17** (1 eq, 0.41 mmol, 209 mg) and intermediate **1** (1 eq, 0.41 mmol, 98 mg) were dissolved in 1,4-dioxane (18 mL). Triethylamine (3 eq, 1.18 mmol, 164 µL) is then added, and the reaction end was determined after 48 h by TLC (SiO_2, $CHCl_3$/MeOH: 15/1). After completion, the work-up was performed as described in **General Procedure B**, and the crude product was adsorbed on diatomaceous earth. Purification by flash chromatography, applying an isocratic method ($CHCl_3$/MeOH: 15/1), afforded intermediate **18** (36% yield, 0.148 mmol, 75 mg) as sticky crystals. **^{1}H-NMR (500 MHz, d6-DMSO):** δ/ppm = 9.02 (s, 1H), 8.46 (d, J

= 2.5 Hz, 1H), 8.32 (dd, J = 4.7, 1.5 Hz, 1H), 7.66 (ddd, J = 8.2, 2.6, 1.5 Hz, 1H), 7.49 – 7.29 (m, 9H), 7.08 – 7.01 (m, 2H), 5.14 (s, 2H), 3.27 (s, 2H), 3.26 – 3.20 (m, 3H), 1.66 (d, J = 11.3 Hz, 2H), 1.51 (p, J = 7.3 Hz, 3H), 1.38 – 1.20 (m, 4H), 1.06 (qd, J = 12.2, 4.2 Hz, 2H). **^{13}C-NMR (126 MHz, d6-DMSO):** δ/ppm 168.64, 159.01, 157.95, 145.27, 144.72, 136.72, 134.60, 130.70, 128.64, 128.56, 128.34, 127.78, 127.59, 123.47, 116.85, 114.34, 69.26, 66.26, 41.44, 35.28, 35.21, 31.86, 28.86, 23.07). MS (ESI, negative mode): found *m*/*z* = 509.7 $[M-H]^-$, calculated *m*/*z* = 509.2 $[M-H]^-$.

(*E*)-2-cyano-1-(4-(1-(4-hydroxybenzoyl)piperidin-4-yl)butyl)-3-(pyridin-3-yl)guanidine (19)

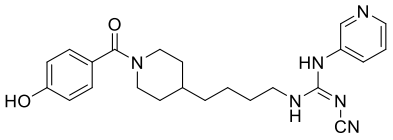

Chemical Formula: $C_{23}H_{28}N_6O_2$
Molecular Weight: 420.52

Following **General Procedure E**, intermediate **18** (1 eq, 0.23 mmol, 117 mg) was dissolved in a solvent mixture of EtOAc (9.6 mL) and EtOH (9.6 mL EtOH). Then, a Pd/C catalyst (10% in Pd, 12 mol-%, 40 mg) was added and the hydrogenation started according to **General Procedure E**. The reaction was performed for 3.5 h and monitored by TLC (SiO_2, $CHCl_3$/MeOH/Et_3N: 15/1/1%). After work-up, the product was ready to use without further purification, affording intermediate **19** (85% yield, 0.20 mmol, 82 mg) as a white powder. **^{1}H-NMR (500 MHz, d6-DMSO):** δ/ppm = 9.37 (s, 1H), 8.66 (d, J = 2.5 Hz, 1H), 8.45 (dd, J = 5.1, 1.4 Hz, 1H), 7.98 (d, J = 8.4 Hz, 1H), 7.68 – 7.60 (m, 2H), 7.25 – 7.17 (m, 2H), 6.82 – 6.75 (m, 2H), 3.28 (q, J = 6.9 Hz, 2H), 1.67 (d, J = 12.9 Hz, 2H), 1.53 (p, J = 7.2 Hz, 3H), 1.38 – 1.21 (m, 4H), 1.05 (qd, J = 12.3, 4.2 Hz, 2H). **^{13}C-NMR (126 MHz, d6-DMSO):** δ/ppm = 169.09, 158.42, 141.61, 140.73, 136.16, 133.61, 128.73, 126.67, 124.98, 114.76, 114.60, 66.28, 41.62, 35.33, 35.28, 31.92, 28.87, 23.09. MS (ESI, negative mode): found *m*/*z* = 419.4 $[M-H]^-$, calculated *m*/*z* = 419.2 $[M-H]^-$.

***tert*-butyl((9*S*,12*S*)-7-(4-((4-(4-(4-((*E*)-2-cyano-3-(pyridin-3-yl)guanidino)butyl)piperidine-1-carbonyl)phenoxy)methyl)phenyl)-2,2,9,13-tetramethyl-8,11-dioxo-5-oxa-7,10-diaza-2-silatetradecan-12-yl)carbamate (20)**

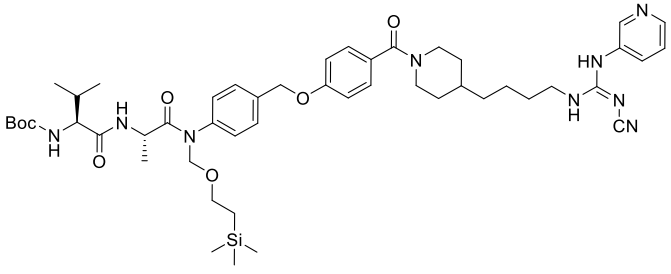

Chemical Formula: $C_{49}H_{71}N_9O_7Si$
Molecular Weight: 926,25

Procedure:

Intermediate **19** (1 eq, 0.12 mmol, 50.46 mg) was dissolved under an argon atmosphere in DMF (abs., 2.5 mL, resulting concentration = 48 mM). Then, caesium carbonate (1 eq, 0.12 mmol, 39.1 mg) was charged to the mixture, and after 30 min, a solution of *tert*-

butyl ((9*R*,12*R*)-7-(4-(bromomethyl)phenyl)-2,2,9,13-tetramethyl-8,11-dioxo-5-oxa-7,10-diaza-2-silatetradecan-12-yl)carbamate (1.7 eq, 0.2 mmol, 118 mg) in DMF (abs., 0.6 mL) was added. The reaction was stirred overnight and monitored by HPLC (method 4). After completion, the reaction was quenched with acetic acid until a pH-value of 5 was reached. The volatiles were evaporated under reduced pressure. The crude product was purified by preparative HPLC (method 4, t_R = 15.5 min), affording intermediate **20** (40% yield, 0.048 mmol, 44.46 mg) as sticky oil. MS (ESI, positive mode): found *m/z* = 927.3 $[M+H]^+$, calculated *m/z* = 927.5 $[M+H]^+$.

(*S*)-2-amino-*N*-((*S*)-1-((4-((4-(4-(4-((*E*)-2-cyano-3-(pyridin-3-yl)guanidino)butyl)piperidine-1-carbonyl)phenoxy)methyl)phenyl)amino)-1-oxopropan-2-yl)-3-methylbutanamide (21)

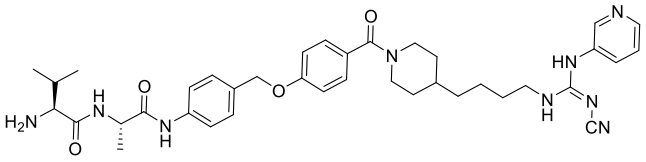

Chemical Formula: $C_{38}H_{49}N_9O_4$
Molecular Weight: 695,87

Following **General Procedure C**, intermediate **20** (1 eq, 0.026 mmol, 24 mg) was dissolved in pure TFA (3 mL). The reaction mixture was stirred under 400 mbar for 5 min. Then, the crude product was worked up as described in **General Procedure C**. Without further purification, the product was used directly in a second deprotection step for SEM-group removal. For this purpose, the crude product was dissolved in ACN (5 mL) and then, an aqueous ammonia solution was added dropwise until a pH-value of 10 was reached. The mixture was stirred for 5 min and the reaction monitored by HPLC (method 4), elution time. After completion, crude is neutralised and used without purification in the production of intermediate **27**. t_R (HPLC) = 9.88 min.

4-(piperidin-4-yl)-1-butanol (22)[210]

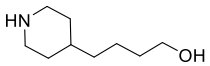

Chemical Formula: $C_9H_{19}NO$
Molecular Weight: 157.26

4-(piperidin-4-yl)-butanoic acid (1 eq, 52.55 mmol, 9 g) was dissolved under an argon atmosphere in THF (abs., 150 mL, resulting concentration = 0.35 M) and cooled down to 0 °C. Lithium aluminium hydride (4 eq, 174 mmol, 6.6 g) was added slowly to the reaction mix, controlling the temperature with a thermometer. Afterwards, the reaction mixture was allowed to warm to r.t. and was kept stirring for 15 min, followed by heating to reflux overnight. The reaction was monitored by TLC (SiO_2, EtOAc/Et_3N/MeOH: 18/2/80). After completion, the reaction mixture was cooled to 0 °C and an aqueous 30 wt-% KOH-solution (30 mL) was added dropwise under argon via dropping funnel. Subsequently, the suspension was warmed to r.t. and stirred for 1 h. Then, the white suspension is filtered through celite, and the remaining solids were washed with fresh THF. The combined liquids were concentrated under reduced pressure. The crude product was dissolved in DCM, filtered, and the volatiles evaporated under reduced pressure, affording intermediate **22** (95% yield, 49.9 mmol, 7.8 g) as a white melting solid ready to

use without further purification. MS (ESI, positive mode): found *m/z* = 158.4 $[M+H]^+$, calculated *m/z* = 158.2 $[M+H]^+$.

4-(*N*-Boc)-*N*-(4-(4-hydroxy)-butyl)-piperidinyl)benzamide (23)

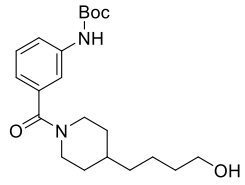

Chemical Formula: $C_{21}H_{32}N_2O_4$
Molecular Weight: 376.50

Following **General Procedure F**, intermediate **22** (1 eq, 18.36 mmol, 3.2 g) and 3-(*N*-Boc)-amino)benzoic acid (1 eq, 18.36 mmol, 4.4 g) were dissolved in DCM (abs., 230 mL). Then, DIPEA (1 eq, 18.36 mmol, 3.2 mL), HOBt (1 eq, 18.36 mmol, 2.5 g) and DCC (1 eq, 18.36 mmol, 3.8 g) were added sequentially and stirred overnight at r.t. The reaction was monitored by TLC (SiO_2, hexane/EtOAc/MeOH: 10/10/1). After completion, the work-up was performed as described in **General Procedure F,** and the crude product was adsorbed on diatomaceous earth. Purification by flash chromatography, applying an isocratic method (Hex/EtOAc/MeOH: 10/10/1), afforded intermediate **23** (57% yield, 10.5 mmol, 3.9 g) as oil. MS (ESI, positive mode): found *m/z* = 377.2 $[M+H]^+$, calculated *m/z* = 377.2 $[M+H]^+$.

4-(*N*-Boc)-*N*-(4-(4-methanesulfonyl)-butyl)-piperidinyl)benzamide (24)

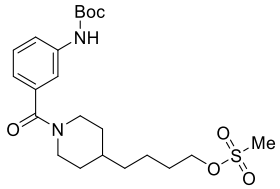

Chemical Formula: $C_{22}H_{34}N_2O_6S$
Molecular Weight: 454.58

Following **General Procedure G**, intermediate **23** (1 eq, 16.08 mmol, 6 g) is dissolved in DCM (abs., 118 mL). The solution was cooled to 0 °C and then, methane sulfonyl chloride (1.5 eq, 24.12 mmol, 2.8g) was added, followed by triethylamine (2 eq, 32.16 mmol, 4.5 mL). The reaction was stirred for 2 h at r.t. and monitored by TLC (SiO_2, DCM/MeOH: 30/1). After completion, the work-up was performed as described in **General Procedure G,** and the crude product was adsorbed on diatomaceous earth. Purification by flash chromatography, applying an isocratic method (DCM/MeOH: 30/1), afforded intermediate **24** (75% yield, 12.06 mmol, 5.5 g) as an oil. MS (ESI, positive mode): found *m/z* = 455.2 $[M+H]^+$, calculated *m/z* = 455.2 $[M+H]^+$.

3-((*N*-Boc)-amino)-*N*-(4-(4-phtalimidyl)-butyl)-piperidinyl)benzamide (25)

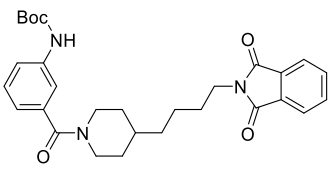

Chemical Formula: $C_{29}H_{35}N_3O_5$
Molecular Weight: 505.62

Following **General Procedure H part 1**, intermediate **24** (1 eq, 14.3 mmol, 6.5 g) and potassium phthalimide (1.2 eq, 17.16 mmol, 3.2 g) were dissolved in DMF (abs. 150 mL) and stirred at 50 °C overnight. The reaction was monitored by TLC (SiO_2, hexane/EtOAc/MeOH: 13/7/1). After completion, the work-up was performed as described in **General Procedure H part 1**, and the crude product was adsorbed on diatomaceous earth. Purification by flash chromatography, applying an isocratic method (hexane/EtOAc/MeOH: 13/7/1), afforded intermediate **25** (96% yield, 13.7 mmol, 6.9 g) as a melting solid. MS (ESI, positive mode): found *m/z* = 506.4 $[M+H]^+$, calculated *m/z* = 506.2 $[M+H]^+$.

3-(*N*-Boc)-*N*-(4-(4-amino)-butyl)-piperidinyl)benzamide (26)

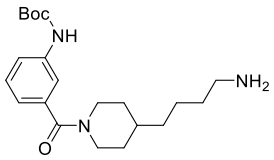

Chemical Formula: $C_{21}H_{33}N_3O_3$
Molecular Weight: 375.51

Following **General Procedure H part 2**, intermediate **25** (1 eq, 13.84 mmol, 7 g) was dissolved in EtOH (180 mL). Then, hydrazine monohydrate (4 eq, 55.38 mmol, 2.7 mL) was added and the reaction mixture stirred for 6 h at r.t. The reaction was monitored by TLC (SiO_2, $CHCl_3$/MeOH/Et_3N: 10/1/1%). After completion, the work-up was performed as described in **General Procedure H part 2**, and the crude product was adsorbed on diatomaceous earth. Purification by flash chromatography, applying an isocratic method ($CHCl_3$/MeOH/Et_3N: 10/1/1%), afforded intermediate **26** (60% yield, 8.3 mmol, 3.1 g) as colourless oil. MS (ESI, positive mode): found *m/z* = 375.9 $[M+H]^+$, calculated *m/z* = 376.2 $[M+H]^+$.

(*S*)-*N*-((*S*)-1-((4-((4-(4-(4-((*E*)-2-cyano-3-(pyridin-3-yl)guanidino)butyl)piperidine-1-carbonyl)phenoxy)methyl)phenyl)amino)-1-oxopropan-2-yl)-2-(3-(2,5-dioxo-2,5-dihydro-1H-pyrrol-1-yl)propanamido)-3-methylbutanamide (27)

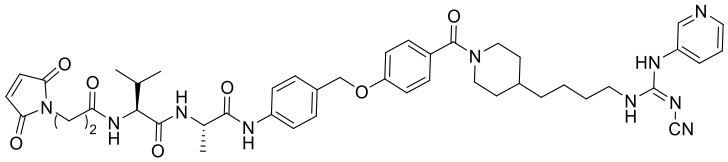

Chemical Formula: $C_{45}H_{54}N_{10}O_7$
Molecular Weight: 846,99

Following **General Procedure I**, intermediate **21** (1 eq, 0.01 mmol, 7 mg) and BMPS (1 eq, 0.01 mmol, 2.66 mg) were dissolved in DMF (1 mL). Then, DIPEA (2 eq, 0.02 mmol, 3.48 µL) was and the reaction was stirred for 4 h at r.t. The reaction was monitored by HPLC (method 2). After completion, the work-up was performed as described in **General Procedure I** and purified by preparative HPLC (method 2, t_R = 12.49min), affording intermediate **27** (40% yield, 0.004 mmol, 3.4 mg) as white powder after lyophilisation. MS (ESI, positive mode): found *m/z* = 848.1 $[M+H]^+$, calculated *m/z* = 846.4 $[M+H]^+$.

tert-butyl(*E*)-(3-(4-(4-(2-cyano-3-(pyridin-3-yl)guanidino)butyl)piperidine-1-carbonyl)phenyl)carbamate (28)

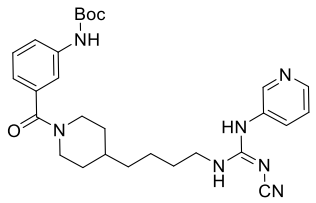

Chemical Formula: $C_{28}H_{37}N_7O_3$
Molecular Weight: 519.65

Following **General Procedure B**, intermediate **26** (1 eq, 6.7 mmol, 2.5 g) and intermediate **1** (1 eq, 6.7 mmol, 1.6 g) were dissolved in 1,4-dioxane (143 mL). Then, triethylamine (1.2 eq, 8.05 mmol, 1.1 mL) was added and the mixture stirred for 36 h at r.t. The reaction was monitored by TLC (SiO_2, $CHCl_3$/MeOH: 15/1). After completion, the work-up was performed as described in **General Procedure B,** and the crude product adsorbed on diatomaceous earth. Purification by flash chromatography, applying an isocratic method ($CHCl_3$/MeOH: 15/1), afforded intermediate **28** (40% yield, 2.68 mmol, 1.4 g) as sticky oil. **^{1}H-NMR (500 MHz, d6-DMSO):** δ/ppm = 9.00 (s, 1H), 8.46 (dd, J = 2.6, 0.8 Hz, 1H), 8.33 (dd, J = 4.7, 1.5 Hz, 1H), 7.69 – 7.62 (m, 1H), 7.47 (dq, J = 4.7, 1.9, 1.5 Hz, 1H), 7.39 – 7.32 (m, 2H), 7.32 – 7.25 (m, 1H), 6.92 (dt, J = 7.6, 1.3 Hz, 1H), 3.28 (s, 2H), 3.23 (q, J = 6.7 Hz, 2H), 1.56 – 1.42 (m, 3H), 1.48 (s, 9H), 1.37 – 1.24 (m, 2H), 1.10 – 1.01 (m, 2H). **^{13}C-NMR (126 MHz, d6-DMSO):** δ/ppm = 168.96, 158.29, 152.98, 145.63, 145.07, 139.83, 137.19, 134.90, 131.07, 128.92, 123.81, 120.28, 118.95, 116.38, 79.51, 79.40, 41.80, 35.64, 35.50, 29.19, 28.34, 23.42, 18.77. MS (ESI, positive mode): found *m/z* = 521.0 $[M+H]^+$, calculated *m/z* = 520.3 $[M+H]^+$.

3-(*N*-Cbz)-amino-benzoic Acid (30)

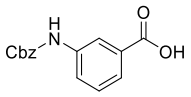

Chemical Formula: $C_{15}H_{13}NO_4$
Molecular Weight: 271.27

Following **General Procedure D**, 3-aminobenzoic acid (1 eq, 4.79 mmol, 657 mg) and benzyl chloroformate (1 eq, 4.79 mmol, 683 µL) were dissolved in THF (150 mL), followed by the addition of sodium bicarbonate (2 eq, 9.6 mmol, 806 mg). The reaction system is stirred for 7 h and was monitored by TLC (SiO_2, $CHCl_3$/MeOH/AcOH: 15/1/1%). After completion, work-up was performed as described in **General Procedure D,** and the crude product was ready to use without further purification. Intermediate **30** (90% yield, 4.3 mmol, 1.2 g) was afforded as pale-orange crystals. **^{1}H-NMR (500 MHz, d6-Acetone):** δ/ppm = 9.09 (s, 1H), 8.43 (t, J = 2.0 Hz, 1H), 7.98 (ddd, J = 8.2, 2.3, 1.1 Hz, 1H), 7.83 (ddd, J = 7.8, 1.7, 1.0 Hz, 1H), 7.56 (t, J = 8.0 Hz, 1H), 7.45 – 7.27 (m, 5H), 5.19 (s, 2H). **^{13}C-NMR (126 MHz, d6-Acetone):** δ/ppm = 162.92, 154.30, 141.06, 137.51, 130.56, 130.27, 129.26, 128.99, 128.91, 125.27, 124.98, 120.51, 67.19. MS (ESI, negative mode): found *m/z* = 270.1 $[M-H]^-$, calculated *m/z* = 270.1 $[M-H]^-$.

3-(*N*-Cbz)-amino-*N'*-(4-(4-hydroxy)-butyl)-piperidinyl-benzamide (31)

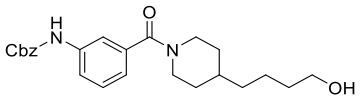

Chemical Formula: $C_{24}H_{30}N_2O_4$
Molecular Weight: 410.51

Following **General Procedure F**, intermediate **22** (1 eq, 3.49 mmol, 549 mg) and intermediate **30** (1 eq, 3.49 mmol, 947 mg) were dissolved in DCM (abs., 43.67 mL). Then, DIPEA (1 eq, 3.49 mmol, 608 µL), HOBt (1 eq, 3.49 mmol, 475 mg) and DCC (1 eq, 3.49 mmol, 722 mg) were added sequentially and the reaction mixture stirred overnight. The reaction was monitored by TLC (SiO_2, hexane/EtOAc/MeOH: 10/10/1). After completion, the work-up was performed as described in **General Procedure F**, and the crude product was adsorbed on diatomaceous earth. Purification by flash chromatography, applying an isocratic method (Hex/EtOAc/MeOH: 10/10/1), afforded intermediate **31** (40% yield, 1.4 mmol, 573 mg) as oil. MS (ESI, positive mode): found *m/z* = 411.2 $[M+H]^+$, calculated *m/z* = 411.2 $[M+H]^+$.

3-(*N*-Cbz)-*N*-(4-(4-methanesulfonyl)-butyl)-piperidinyl)benzamide (32)

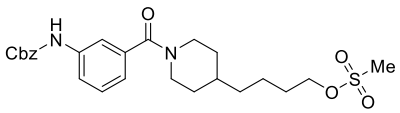

Chemical Formula: $C_{25}H_{32}N_2O_6S$
Molecular Weight: 488.60

Following **General Procedure G**, intermediate **31** (1 eq, 1.04 mmol, 427 mg) was dissolved in DCM (abs. 10 mL). The solution was cooled to 0 °C and methanesulfonyl chloride (1.5 eq, 1.56 mmol, 182 mg) was added. Afterwards, triethylamine (2 eq, 2.08 mmol, 291 µL) was charged into the reaction flask and the reaction stirred for 2 h at r.t. The reaction was monitored by TLC, DCM/MeOH: 30/1. After completion, the work-up was performed as described in **General Procedure G,** and the crude product was adsorbed on diatomaceous earth. Purification by flash chromatography, applying an isocratic method (DCM/MeOH: 30/1), afforded intermediate **32** (75% yield, 0.78 mmol, 381 mg) as an oil. MS (ESI, positive mode): found *m/z* = 489.2 $[M+H]^+$, calculated *m/z* = 489.2 $[M+H]^+$.

3-(*N*-Cbz)-*N*-(4-(4-phtalimidyl)-butyl)-piperidinyl)benzamide (33)

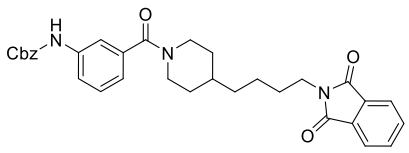

Chemical Formula: $C_{32}H_{33}N_3O_5$
Molecular Weight: 539.63

Following **General Procedure H part 1**, intermediate **32** (1 eq, 13.67 mmol, 6.7 g) and potassium phthalimide (1.2 eq, 16.4 mmol, 3.1 g) were dissolved in dry-DMF (145 mL) and the reaction mixture was stirred overnight at 50 °C. The reaction was monitored by TLC (hexane/EtOAc/MeOH: 13/7/1). After completion, work-up was performed as described in **General Procedure H part 1**, and the crude product was adsorbed on

diatomaceous earth. Purification by flash chromatography, applying an isocratic method (Hex/EtOAc/MeOH: 13/7/1), afforded intermediate **33** (80% yield, 10.9 mmol, 5.9 g) as oil. MS (ESI, positive mode): found *m/z* = 540.4 $[M+H]^+$, calculated *m/z* = 540.2 $[M+H]^+$.

3-(*N*-Cbz)-*N*-(4-(4-phtalimidyl)-butyl)-piperidinyl)benzamide (34)

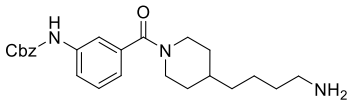

Chemical Formula: $C_{24}H_{31}N_3O_3$
Molecular Weight: 409.53

Following **General Procedure H part 2**, intermediate **33** (1 eq, 10.56 mmol, 5.7 g) was dissolved in EtOH (120 mL). Then, hydrazine monohydrate (4 eq, 42.2 mmol, 2.1 mL) was added and the reaction mixture was stirred overnight at r.t. The reaction was monitored by TLC (SiO_2, $CHCl_3$/MeOH/Et_3N: 10/1/1%). After completion, work-up was performed as described in **General Procedure H part 2**, and the crude product was adsorbed on diatomaceous earth. Purification by flash chromatography, applying an isocratic method ($CHCl_3$/MeOH/Et_3N: 10/1/1%), afforded intermediate **34** (50% yield, 5.28 mmol, 2.2 g) as white crystals. MS (ESI, positive mode): found *m/z* = 410.5 $[M+H]^+$, calculated *m/z* = 410.2 $[M+H]^+$.

benzyl(*E*)-(3-(4-(4-(2-cyano-3-(pyridin-3-yl)guanidino)butyl)piperidine-1-carbonyl)phenyl)carbamate (35)

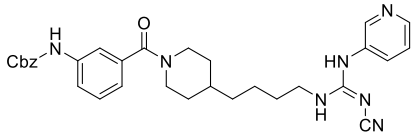

Chemical Formula: $C_{31}H_{35}N_7O_3$
Molecular Weight: 553.67

Following **General Procedure B**, intermediate **34** (1 eq, 8.55 mmol, 3.5 g) and intermediate **1** (1 eq, 8.55 mmol, 2.0 g) were dissolved in 1,4-dioxane (185 mL). Then, triethylamine (2.4 eq, 20.5 mmol, 2.86 mL) was added and the reaction mixture stirred overnight at r.t. The reaction was monitored by TLC (SiO_2, $CHCl_3$/MeOH: 15/1). After completion, the work-up was performed as described in **General Procedure B,** and the crude product was adsorbed on diatomaceous earth. Purification by flash chromatography, applying an isocratic method ($CHCl_3$/MeOH: 15/1), afforded intermediate **35** (41% yield, 3.5 mmol, 1.9 g) as sticky oil. MS (ESI, positive mode): found *m/z* = 554.4 $[M+H]^+$, calculated *m/z* = 554.2 $[M+H]^+$.

(*E*)-1-(4-(1-(3-aminobenzoyl)piperidin-4-yl)butyl)-2-cyano-3-(pyridin-3-yl)guanidine (36)

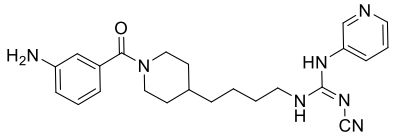

Chemical Formula: $C_{23}H_{29}N_7O$
Molecular Weight: 419.53

Following **General Procedure E**, intermediate **35** (1 eq, 5.06 mmol, 2.8 g) was dissolved in a solvent mixture of EtOAc (50 mL) and EtOH (50 mL). Then, Pd/C (10% in Pd, 12 mol-%) was added, and the hydrogenation was started according to **General Procedure E**.

The reaction mixture was stirred overnight and the progress monitored by TLC (SiO_2, $CHCl_3$/MeOH/Et_3N: 15/1/1%) and HPLC (method 1). After workup, the product is ready to use without further purification, affording intermediate **36** (85% yield, 4.3 mmol, 1.8 g) as white powder. t_R/min (HPLC, method 1) = 8.96 min. **^{1}H-NMR** and **^{13}C-NMR** as described in the literature,[122] MS (ESI, negative mode): found *m/z* = 418.4 $[M-H]^-$, calculated *m/z* = 418.2 $[M-H]^-$.

4-((*S*)-2-((*S*)-2-(6-(2,5-dioxo-2,5-dihydro-1*H*-pyrrol-1-yl)hexanamido)-3-methylbutanamido)propanamido)benzyl (3-(4-(4-((*E*)-2-cyano-3-(pyridin-3-yl)guanidino)butyl) piperidine-1-carbonyl)phenyl)carbamate (37)

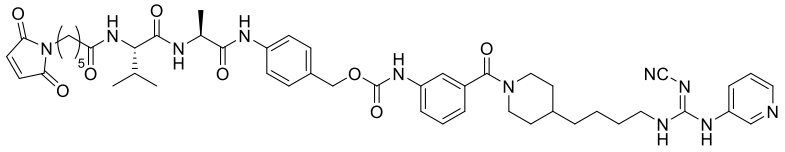

Chemical Formula: $C_{49}H_{61}N_{11}O_8$
Molecular Weight: 932,10

Following **General Procedure J**, mc-Val-Ala-PAB-PNP (CAS-No. 1639939-40-4, 1.5 eq, 0.023 mmol, 15 mg) was dissolved in DMF (612 µL), followed by the addition of PyAOP (1.5 eq, 0.023 mmol, 12 mg) and DIPEA (6 eq, 0.092 mmol, 16 µL). The mixture was stirred for 30 min at r.t. and then, intermediate **36** (1 eq, 0.015 mmol, 6.3 mg) was added. The reaction mixture was stirred overnight at R.T and the reaction progress monitored by RP-HPLC (method 1). After completion, the mixture is directly purified by preparative HPLC (method 1, t_R = 15.09 min), affording intermediate **37** (30% yield, 0.004 mmol, 4.2 mg) as a white solid. MS (ESI, negative mode): found *m/z* = 931.4 $[M-H]^-$, calculated *m/z* = 931.4 $[M-H]^-$.

Benzyl 4-(4-((tert-butoxycarbonyl)amino)butanoyl)piperazine-1-carboxylate (38)

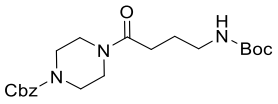

Chemical Formula: $C_{21}H_{31}N_3O_5$
Molecular Weight: 405.50

Following **General Procedure F**, Boc-GABA-OH (1 eq, 24.6 mmol, 5 g) and 1-Cbz-piperazine (1 eq, 24.6 mmol, 5.4 g) were dissolved in DCM (abs., 385 mL). Then, DIPEA (1 eq, 24.6 mmol, 4.3 mL), HOBt (1 eq, 24.6 mmol, 3.3 g) and DCC (1 eq, 24.6 mmol, 5.1 g) were added sequentially and the reaction mixture stirred overnight at r.t. The reaction was monitored by TLC (SiO_2, hexane/EtOAc/MeOH: 13/7/1). After completion, the work-up was performed as described in **General Procedure F,** and the crude product was adsorbed on diatomaceous earth. Purification by flash chromatography, applying an isocratic method (Hex/EtOAc/MeOH: 13/7/1), afforded intermediate **38** (60% yield, 14.8 mmol, 6 g) as oil. MS (ESI, positive mode): found *m/z* = 406.2 $[M+H]^+$, calculated *m/z* = 406.2 $[M+H]^+$.

Benzyl 4-(4-aminobutanoyl)piperazine-1-carboxylate (39)

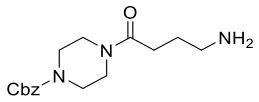

Chemical Formula: $C_{16}H_{23}N_3O_3$
Molecular Weight: 305,38

Following **General Procedure C variation 2**, intermediate **38** (1 eq, 2 mmol, 811 mg) was dissolved in solution of TFA/DCM (50 mL, 1:10). The reaction mixture was stirred for 2 h at r.t. The reaction was monitored by TLC (SiO_2, $CHCl_3$/MeOH/Et_3N: 10/1/1%). After completion, the work-up was performed as described in **General Procedure C** affording intermediate **39** (90% yield, 1.8 mmol, 550 mg) as colourless melting crystals. Without further purification, the product was directly used in the next reaction step.

Benzyl (*E*)-4-(4-(2-cyano-3-(pyridin-3-yl)guanidino)butanoyl)piperazine-1-carboxylate (40)

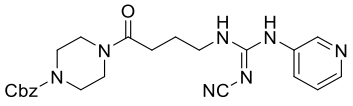

Chemical Formula: $C_{23}H_{27}N_7O_3$
Molecular Weight: 449.52

Following **General Procedure B**, intermediate **39** (1 eq, 6.55 mmol, 2 g) and intermediate **1** (1 eq, 6.55 mmol, 1.5 g) were dissolved in 1,4-dioxane (142 mL). Triethylamine (3 eq, 19.65 mmol, 2.7 mL) was added and the reaction mixture stirred overnight at r.t. The reaction was monitored by TLC (SiO_2, $CHCl_3$/MeOH: 15/1). After completion, the work-up was performed as described in **General Procedure B,** and the crude product was adsorbed on diatomaceous earth. Purification by flash chromatography, applying an isocratic method ($CHCl_3$/MeOH: 15/1), afforded intermediate **40** (50% yield, 3.3 mmol, 1.5 g) as pale-yellow oil. MS (ESI, positive mode): found *m*/*z* = 450.3 $[M+H]^+$, calculated *m*/*z* = 450.2 $[M+H]^+$.

(*E*)-2-cyano-1-(4-oxo-4-(piperazin-1-yl)butyl)-3-(pyridin-3-yl)guanidine (41)

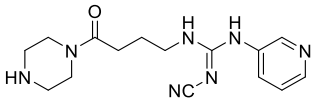

Chemical Formula: $C_{15}H_{21}N_7O$
Molecular Weight: 315.38

Following **General Procedure E**, intermediate **40** (1 eq, 1.69 mmol, 760 mg) was dissolved in a solvent mixture of EtOAc (50 mL) and EtOH (50 mL EtOH). Then, Pd/C (10% in Pd, 12 mol-%) was added (12% mol, 200 mg), and the hydrogenation was started according to **General Procedure E**. The reaction was stirred overnight and monitored by TLC (SiO_2, $CHCl_3$/MeOH/Et_3N: 10/1/1%). The work-up was performed as described in **General Procedure E**, and the product was ready to use without further purification. Intermediate **41** (90% yield, 1.52 mmol, 480 mg) was obtained as a white powder. MS (ESI, positive mode): found *m*/*z* = 316.0 $[M+H]^+$, calculated *m*/*z* = 316.2 $[M+H]^+$.

Benzyl(*E*)-(3-(4-(4-(2-cyano-3-(pyridin-3-yl)guanidino)butanoyl)piperazine-1carbonyl)phenyl)carbamate (42)

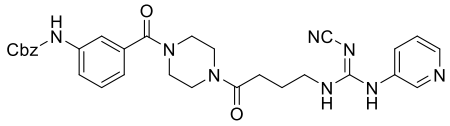

Chemical Formula: $C_{30}H_{32}N_8O_4$
Molecular Weight: 568,64

Following **General Procedure F**, intermediate **41** (1 eq, 1.78 mmol, 561 mg) and intermediate **30** (1 eq, 1.78 mmol, 483 mg) were dissolved in DCM (abs., 30 mL). Then, DIPEA (1 eq, 1.78 mmol, 311 µL), HOBt (1 eq, 1.78 mmol, 239 mg) and DCC (1 eq, 1.78 mmol, 369 mg) were sequentially added and stirred overnight at room temperature. The reaction progress was monitored TLC (SiO_2, $CHCl_3$/MeOH: 15/1). After completion, the work-up was performed as described in **General Procedure F,** and the crude product was adsorbed on diatomaceous earth. Purification by flash chromatography, applying an isocratic method ($CHCl_3$/MeOH: 15/1), afforded intermediate **42** (40% yield, 0.71 mmol, 405 mg) as oil. MS (ESI, positive mode): found *m*/*z* = 569.7 $[M+H]^+$, calculated *m*/*z* =569.2 $[M+H]^+$.

(*E*)-1-(4-(4-(3-aminobenzoyl)piperazin-1-yl)-4-oxobutyl)-2-cyano-3-(pyridin-3-yl)guanidine (43)

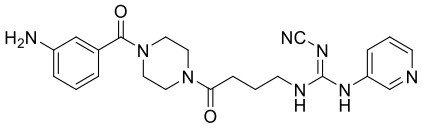

Chemical Formula: $C_{22}H_{26}N_8O_2$
Molecular Weight: 434,50

Following **General Procedure E**, intermediate **42** (1 eq, 0.98 mmol, 557 mg) was dissolved in a solvent mixture of EtOAc (50 mL) and EtOH (50 mL). Then, Pd/C (10% in Pd, 12% mol, 350 mg) was added, and the hydrogenation was started according to **General Procedure E**. The reaction was stirred overnight and monitored by TLC (SiO_2, $CHCl_3$/MeOH/Et_3N: 10/1/1%). The work-up was performed as described in **General Procedure E**, and the product is ready to use without further purification. Intermediate **43** (80% yield, 0.78 mmol, 341 mg) was obtained as a white powder. **^{1}H-NMR (500 MHz, d6-DMSO):** δ/ppm = 9.17 (s, 1H), 8.51 (d, J = 2.7 Hz, 1H), 8.32 (dd, J = 4.7, 1.5 Hz, 1H), 7.72 (d, J = 8.2 Hz, 1H), 7.36 (ddd, J = 8.3, 4.7, 0.8 Hz, 1H), 7.10 – 7.02 (m, 1H), 6.62 (ddd, J = 8.1, 2.4, 1.0 Hz, 1H), 6.59 – 6.53 (m, 1H), 6.49 (ddd, J = 7.4, 1.6, 1.0 Hz, 1H), 5.21 (s, 2H), 3.48 (s, 2H), 3.30 – 3.20 (m, 6H), 2.39 (s, 2H), 1.77 (p, J = 7.0 Hz, 2H). **^{13}C-NMR (126 MHz, d6-DMSO):** δ/ppm = 170.65, 169.80, 158.07, 148.65, 145.23, 144.59, 136.24, 134.63, 130.55, 128.73, 123.45, 116.83, 114.78, 113.78, 111.99, 41.12, 29.23, 24.21. MS (ESI, positive mode): found *m*/*z* = 435.2 $[M+H]^+$, calculated *m*/*z* =435.2 $[M+H]^+$.

4-((*S*)-2-((S)-2-(6-(2,5-dioxo-2,5-dihydro-1*H*-pyrrol-1-yl)hexanamido)-3-methylbutanamido) propanamido)benzyl (3-(4-(4-((*E*)-2-cyano-3-(pyridin-3-yl)guanidino)butanoyl)piperazine-1-carbonyl)phenyl)carbamate (44)

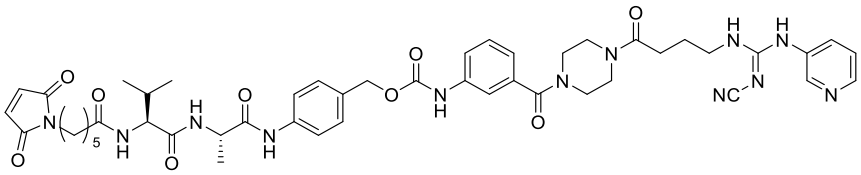

Chemical Formula: $C_{48}H_{58}N_{12}O_9$
Molecular Weight: 947,07

Following **General Procedure J**, mc-Val-Ala-PAB-PNP (CAS-No. 1639939-40-4, 1.5 eq, 0.005 mmol, 3.26 mg) was dissolved in DMF (200 µL) and then, PyAOP (1.5 eq, 0.005 mmol, 2.6 mg) and DIPEA (6 eq, 0.021 mmol, 3.7µL) were added. The mixture was stirred for 30 min at r.t. and next, intermediate **43** (1 eq, 0.0035 mmol, 1.5 mg) was added, and the reaction mix was stirred overnight at r.t. After completion, reaction mixture is directly purified by preparative HPLC (method 1, t_R = 13.77 min), affording intermediate **44** (30% yield, 0.001 mmol, 1 mg) as a white solid. MS (ESI, positive mode): found *m/z* = 948.1 $[M+H]^+$, calculated *m/z* =947.4 $[M+H]^+$. MS (ESI, negative mode): found *m/z* = 946.8 $[M-H]^-$, calculated *m/z* = 946.4 $[M-H]^-$.

(*E*)-*N*-(3-(4-(4-(2-cyano-3-(pyridin-3-yl)guanidino)butanoyl)piperazine-1-carbonyl)phenyl)-3-(2,5-dioxo-2,5-dihydro-1*H*-pyrrol-1-yl)propenamide (45)

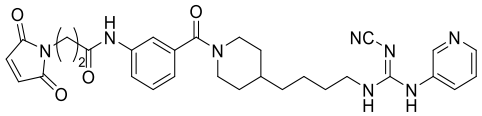

Chemical Formula: $C_{30}H_{34}N_8O_4$
Molecular Weight: 570,65

Following **General Procedure, I**, intermediate **36** (1 eq, 0.024 mmol, 10 mg) and BMPS (1 eq, 0.05 mmol, 13.3 mg) were dissolved in DMF (abs., 2.4 mL). Then, DIPEA (2 eq, 0.05 mmol, 8.7 µL) was added and the reaction stirred for 4 h at r.t. The reaction was monitored by HPLC (method 2). After completion, the work-up was performed as described in **General Procedure I** and purified by preparative HPLC using (method 2, t_R = 9.00 min). Intermediate **45** (38% yield, 0.009 mmol, 5.2 mg) was afforded as white powder after lyophilisation. MS (ESI, positive mode): found *m/z* = 571.4 $[M+H]^+$, calculated *m/z* =571.2 $[M+H]^+$.

(*E*)-*N*-(3-(4-(4-(2-cyano-3-(pyridin-3-yl)guanidino)butanoyl)piperazine-1-carbonyl)phenyl) biotinamide (46)

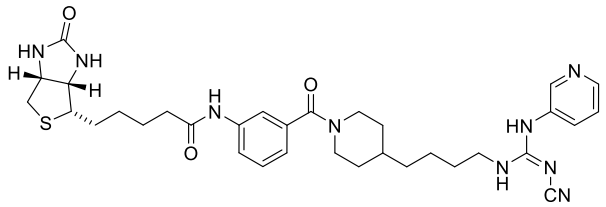

Chemical Formula: $C_{33}H_{43}N_9O_3S$
Molecular Weight: 645,83

Following **General Procedure K**, biotin (1 eq, 0.071 mmol, 17.3 mg) and HATU (1.1 eq, 0.08 mmol, 30.4 mg) were dissolved in DMF (abs., 5 mL) and stirred at r.t. After 20 min, DIPEA (2 eq, 0.14 mmol, 24 µL) and intermediate **36** (1 eq, 0.071 mmol, 30 mg) were added, and the reaction mixture was stirred over the weekend. The reaction was monitored by TLC (SiO_2, $CHCl_3$/MeOH 10/1) and HPLC (method 2). After completion, the work-up is performed as described in **General Procedure K** and purification by preparative HPLC (method 2, t_R = 12.05 min) afforded intermediate **46** (45% yield, 0.03 mmol, 22 mg) as a white solid after lyophilisation. **^{1}H-NMR (500 MHz, d6-DMSO):** δ/ppm = 9.95 (s, 1H), 9.25 (s, 1H), 8.61 (d, J = 2.5 Hz, 1H), 8.42 (dd, J = 5.0, 1.4 Hz, 1H), 7.91 (d, J = 8.4 Hz, 1H), 7.66 (t, J = 1.9 Hz, 1H), 7.62 – 7.53 (m, 2H), 7.33 (t, J = 7.9 Hz, 1H), 6.99 (dt, J = 7.6, 1.3 Hz, 1H), 6.31 (s, 2H), 3.26 (q, J = 6.7 Hz, 2H), 2.83 (dd, J = 12.4, 5.1 Hz, 1H), 2.63 – 2.50 (m, 2H), 2.32 (t, J = 7.8 Hz, 2H), 1.78 – 1.19 (m, 17H), 1.05 (d, J = 13.7 Hz, 2H). **^{13}C-NMR (126 MHz, d6-DMSO):** δ/ppm = 171.29, 168.55, 162.59, 157.64, 142.38, 141.57, 139.20, 136.82, 135.80, 133.09, 128.65, 124.67, 120.92, 119.57, 117.05, 116.55, 66.26, 60.97, 59.15, 55.25, 41.57, 39.72, 36.15, 35.30, 35.18, 28.84, 28.09, 27.99, 24.93, 23.09. MS (ESI, positive mode): found *m/z* = 646.3 $[M+H]^+$, calculated *m/z* =646.3 $[M+H]^+$.

Mal-β-Ala-PEG(4)-Val-Ala-PAB-OH (CAS-No. 2417003-93-9) (47)

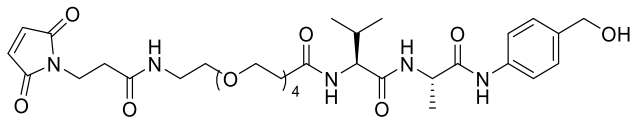

Chemical Formula: $C_{33}H_{49}N_5O_{11}$
Molecular Weight: 691,78

Following **General Procedure I**, H-Val-Ala-PAB-OH (CAS-No. 1343476-44-7, 1 eq, 0.034 mmol, 10 mg) and Mal-dPEG(4)-NHS (CAS-No. 756525-99-2, 1 eq, 0.034 mmol, 17 mg) were dissolved in DMF (abs., 2 mL). Then, DIPEA (2 eq, 0.07 mmol, 12.2 µL) was added and the reaction stirred for for 2.5h at r.t. The reaction was monitored by HPLC (method 5). After completion, the work-up was performed as described in **General Procedure I** and purification by preparative HPLC (method 5, t_R = 11.56 min) afforded intermediate **47** (33% yield, 0.01 mmol, 7.8 mg) as oil. MS (ESI, negative mode): found *m/z* = 690.1 $[M-H]^-$, calculated *m/z* = 690.3 $[M-H]^-$.

Mal-β-Ala-PEG(4)-Val-Ala-PAB-PNP (CAS-No. 2417003-94-0) (48)

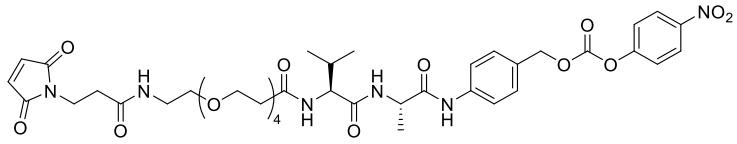

Chemical Formula: $C_{40}H_{52}N_6O_{15}$
Molecular Weight: 856,88

Following **General Procedure L**, Intermediate **47** (1 eq, 0.087 mmol, 60 mg) and bis-(*p*-nitro-phenyl)carbonate (2 eq, 0.17 mmol, 52 mg) were dissolved in DMF (abs., 2 mL). Then, DIPEA (1.5 eq, 0.13 mmol, 23 µL) was added and the reaction mixture stirred for 3 h at r.t. The reaction was monitored by HPLC (method 6). After completion, the work-up was performed following **General Procedure L**, followed by purification by preparative HPLC (method 6, t_R = 12.99 min) affording intermediate **48** (30% yield, 0.03 mmol, 22

mg) as a white solid after lyophilisation. MS (ESI, positive mode): found *m/z* = 857.8 $[M+H]^+$, calculated *m/z* =857.4 $[M+H]^+$.

Mal-β-Ala-PEG(8)-Val-Ala-PAB-OH (CAS-No. 756525-93-6) (49)

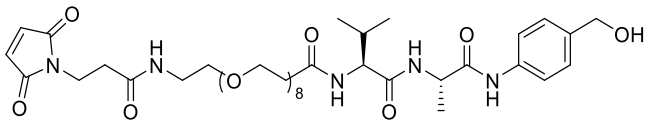

Chemical Formula: $C_{41}H_{65}N_5O_{15}$
Molecular Weight: 867,99

Following **General Procedure I**, H-Val-Ala-PAB-OH (CAS-No. 1343476-44-7, 1.2 eq, 0.087 mmol, 26 mg) and Mal-dPEG(8)-NHS (CAS-No. 756525-93-6, 1 eq, 0.072 mmol, 50 mg) were dissolved in DMF (abs., 4.28 mL). Then, DIPEA (2 eq, 0.15 mmol, 26 µL) was added and the reaction stirred for 3 h at r.t. The reaction was monitored by HPLC (method 5). After completion, the work-up was performed as described in **General Procedure I** and purification by preparative HPLC (method 5, t_R = 15.24 min) afforded intermediate **49** (22% yield, 0.02 mmol, 14 mg) as oil. MS (ESI, positive mode): found *m/z* = 868.7 $[M+H]^+$, calculated *m/z* =868.4 $[M+H]^+$.

4-((2*S*,5*S*)-25-(2,5-dioxo-2,5-dihydro-1*H*-pyrrol-1-yl)-5-isopropyl-2-methyl-4,7,23-trioxo-10,13,16,19-tetraoxa-3,6,22-triazapentacosanamido)benzyl (3-(4-(4-((*E*)-2-cyano-3-(pyridin-3-yl)guanidino)butyl)piperidine-1-carbonyl)phenyl)carbamate (50)

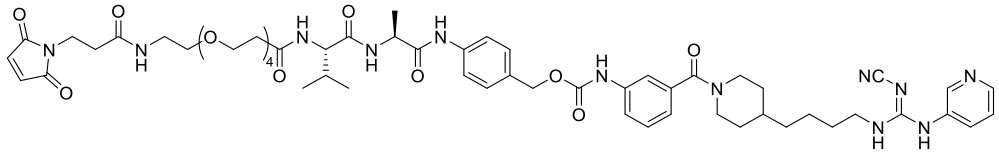

Chemical Formula: $C_{57}H_{76}N_{12}O_{13}$
Molecular Weight: 1137,31

Following **General Procedure J**, Intermediate **48** (1 eq, 0.043 mmol, 37 mg) and HATU (1.1 eq, 0.05 mmol, 19 mg) were dissolved in DMF (abs., 3.03 mL). Then, DIPEA (4 eq, 0.17 mmol, 29 µL) was added and stirred at r.t. After 20 min, intermediate **36** (1 eq, 0.043 mmol, 18 mg) was added and the reaction stirred over the weekend. The reaction was monitored by TLC (SiO_2, $CHCl_3$/MeOH 10/1) and HPLC (method 7). After completion, the work-up was performed as described in **General Procedure J** and purified by preparative HPLC (method 7 t_R = 12.82 min), affording intermediate **50** (20% yield, 0.009 mmol, 10 mg) as a white solid after lyophilisation. **^{1}H-NMR (500 MHz, d6-DMSO):** δ/ppm = 9.90 (s, 1H), 9.82 (s, 1H), 9.06 (s, 1H), 8.35 (s, 2H), 8.11 (d, J = 7.0 Hz, 1H), 7.83 (d, J = 8.6 Hz, 1H), 7.65 – 7.58 (m, 1H), 7.53 – 7.45 (m, 1H), 7.42 – 7.28 (m, 4H), 7.01 – 6.92 (m, 2H), 5.09 (s, 2H), 4.40 (p, J = 6.9 Hz, 2H), 4.20 (dd, J = 8.6, 6.7 Hz, 1H), 3.68 – 3.54 (m, 4H), 3.56 – 3.43 (m, 11H), 3.36 (t, J = 5.9 Hz, 2H), 3.27 – 3.06 (m, 4H), 1.97 (h, J = 6.7 Hz, 1H), 1.68 – 1.62 (m, 1H), 1.39 – 1.12 (m, 15H), 0.86 (dd, J = 17.7, 6.8 Hz, 6H). **^{13}C-NMR (126 MHz, d6-DMSO):** δ/ppm = 170.70, 170.55, 170.22, 169.33, 153.25, 139.01, 138.75, 136.90, 134.39, 131.02, 128.77, 128.73, 120.36, 118.89, 69.64, 69.57, 69.41, 69.34, 68.84, 66.77, 65.50, 57.40, 53.47, 48.88, 43.62, 41.69, 41.43, 35.80, 35.26, 35.12, 33.93, 33.79, 30.37, 30.30, 28.82, 23.05, 17.95, 17.76, 16.61. MS (ESI, negative mode): found *m/z* = 1136.2 $[M-H]^-$, calculated *m/z* = 1136.6 $[M-H]^-$.

Mal-β-Ala-PEG(8)-Val-Ala-PAB-PNP (51)

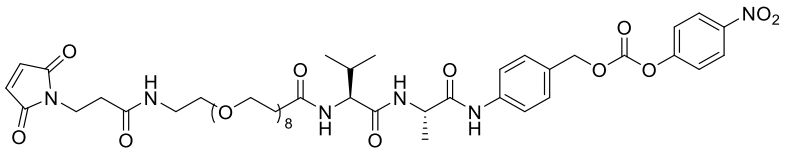

Chemical Formula: $C_{48}H_{68}N_6O_{19}$
Molecular Weight: 1033,10

Following **General Procedure L**, intermediate **49** (1 eq, 0.044 mmol, 38 mg) and bis-(*p*-nitro-phenyl) carbonate (2 eq, 0.09 mmol, 27 mg) were dissolved in DMF (abs., 1 mL). Then, DIPEA (3 eq, 0.13 mmol, 23 µL) was added and the reaction mixture stirred for 3 h at r.t. The reaction progress was monitored by HPLC (method 6). After completion, the work-up was performed following **General Procedure L**, and purification by preparative HPLC (method 6, t_R = 12.89 min) afforded intermediate **51** (10% yield, 0.004 mmol, 4.5 mg) as a white solid after lyophilisation. MS (ESI, positive mode): found *m/z* = 1034.0 $[M+H]^+$, calculated *m/z* =1034.4 $[M+H]^+$.

Mal-Peg(8)-Val-Ala-Pab-36 (52)

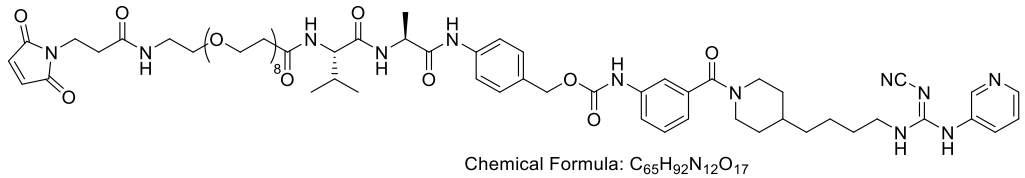

Chemical Formula: $C_{65}H_{92}N_{12}O_{17}$
Molecular Weight: 1313,52

Following **General Procedure J**, Intermediate **51** (1 eq, 0.023 mmol, 24 mg) and HATU (1.1 eq, 0.025 mmol, 9.5 mg) were dissolved in DMF (abs., 1.6 mL). Then, DIPEA (4 eq, 0.09 mmol, 15 µL) was added and the reaction stirred at r.t. After 20 min, intermediate **36** (1 eq, 0.023 mmol, 9.6 mg) was added and the reaction stirred over the weekend. The reaction was monitored by TLC (SiO_2, $CHCl_3$/MeOH 10/1) and HPLC (method 7). After completion, the work-up was performed as described in **General Procedure J** and purified by preparative HPLC (method 7, t_R = 9.03 min), affording intermediate **52** (1% yield, 0.23 µmol, 0.3 mg) as a white solid after lyophilisation. MS (ESI, positive mode): found *m/z* = 1314.5 $[M+H]^+$, calculated *m/z* =1314.7 $[M+H]^+$.

***N*-Cbz-4-(pent-4-(en)-yl)-4-hydroxy-piperidine (53)**

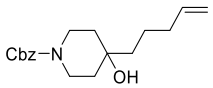

Chemical Formula: $C_{18}H_{25}NO_3$
Molecular Weight: 303.40

Following **General Procedure M**, magnesium (turnings; 2 eq, 13 mmol, 316 mg) and a spatula tip of I_2 were charged into a dried three-neck dried flask under Ar atmosphere, followed by the addition of THF (abs. 15 mL). After the activation of magnesium following the instructions from **General Procedure M**, 5-bromo-1-pentene (1.5 eq, 9.9 mmol, 1.2 mL) was added. In parallel, *N*-Cbz-4-piperidone (1 eq, 6.5 mmol, 1.5 g) was dissolved in a 0.6 M solution of $LaCl_3$*2LiCl in THF (10.8 mL) in a second dried two-neck flask, and the mixture was activated at for 1 h at r.t., followed by cooling down to 8 °C. Next, the Grignard solution is added at 8 °C dropwise to the activated piperidone

solution, and the resulting reaction mixture is stirred overnight at 8 °C. The reaction was monitored by TLC (SiO_2, hexane/EtOAc: 1/1) and HPLC (method 8). After completion, the work-up was performed as described in **General Procedure M,** and the crude product was adsorbed on diatomaceous earth. Purification by flash chromatography, applying an isocratic method (Hex/EtOAc: 1/1), afforded intermediate **53** (47% yield, 3.1 mmol, 927 mg) as oil. t_R/min (HPLC, method 8) = 11.75. **^{1}H-NMR (500 MHz, d6-DMSO):** δ/ppm = 7.40 – 7.28 (m, 5H), 5.80 (ddt, J = 16.9, 10.2, 6.6 Hz, 1H), 5.06 (s, 2H), 5.00 (dq, 1H), 4.94 (ddt, J = 10.2, 2.3, 1.2 Hz, 1H), 4.16 (s, 1H), 3.75 – 3.65 (m, 2H), 1.99 (dtd, J = 7.3, 6.2, 5.8, 1.5 Hz, 2H), 1.48 – 1.29 (m, 8H). **^{13}C-NMR (126 MHz, d6-DMSO):** δ/ppm = 154.30, 138.75, 137.03, 128.26, 127.61, 127.34, 114.48, 67.50, 65.88, 41.88, 33.63, 21.54. MS (ESI, negative mode): found *m/z* = 302.1 $[M-H]^-$, calculated *m/z* = 302.2 $[M-H]^-$.

5-(*N*-Cbz-1-hydroxy-piperinidyl)-1,2-pentandiol (54)

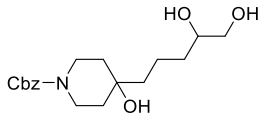

Chemical Formula: $C_{18}H_{27}NO_5$
Molecular Weight: 337.42

Following **General Procedure N**, Intermediate **53** (1 eq, 0.988 mmol, 300 mg) was dissolved in acetone (6 mL). Then, NMO (1.2 eq, 1.19 mmol, 139 mg) was added, followed by H_2O (16 eq, 16.7 mmol, 300 µL). Finally, an OsO_4-solution (0.47% mol, 4.6 µmol, 1 µL) was added and the reaction stirred overnight. The reaction progress was monitored by TLC (SiO_2, hexane/EtOAc: 1/1 for olefine consumption, $CHCl_3$/MeOH: 10/1 for diol formation) and HPLC (method 9). After completion, the work-up was performed as described in **General Procedure M,** and the crude product was adsorbed on diatomaceous earth. Purification by flash chromatography, applying an isocratic method ($CHCl_3$/MeOH: 10/1), afforded intermediate **53** (55% yield, 0.54 mmol, 183 mg) as oil. t_R/min (HPLC, method 8) = 13.50. MS (ESI, positive mode): found *m/z* = 338.17 $[M+H]^+$ 360.25 $[M+Na]^+$, calculated *m/z* =338.4 $[M+H]^+$.

4-(*N*-Cbz-1-hydroxy-piperinidyl)-butanal (55)

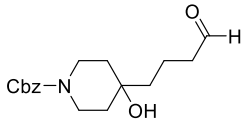

Chemical Formula: $C_{17}H_{23}NO_4$
Molecular Weight: 305.37

Following **General Procedure O**, intermediate **54** (1 eq, 0.377 mmol, 127 mg) was dissolved in THF (2.4 mL). In parallel, sodium periodate (2 eq, 0.754 mmol, 161 mg) is dissolved in H_2O (1.2 mL). Then, both solutions are mixed following instructions from **General Protocol O**. The reaction mixture is stirred for 1 h. The reaction was monitored by HPLC (method 7). After completion, reaction the work-up was performed following **General Procedure O**. Purification by preparative HPLC (method 7, t_R = 6.94 min) afforded intermediate **55** (38% yield, 0.14 mmol, 44 mg) as a white solid after lyophilisation. **^{1}H-NMR (500 MHz, d6-DMSO):** δ/ppm = 9.67 (s, 1H), 7.41 – 7.29 (m, 5H), 5.07 (s, 2H), 4.85 (ddd, J = 8.0, 5.8, 2.3 Hz, 1H), 3.67 (d, J = 13.1 Hz, 2H), 3.28 (s, 1H), 1.73 – 1.52 (m, 4H), 1.49 – 1.14 (m, 6H). **^{13}C-NMR (126 MHz, d6-DMSO):** δ/ppm = 203.38,

154.40, 137.01, 128.29, 127.65, 127.35, 70.83, 65.93, 59.61, 43.38, 41.58, 39.23, 37.62, 34.22, 32.53, 31.47, 30.33, 20.63, 16.86, 15.17, 13.97, 1.83). MS (ESI, positive mode): found *m/z* = 306.25 $[M+H]^+$ 328.25 $[M+Na]^+$, calculated *m/z* =306.2 $[M+H]^+$.

***Tert*-butyl(*E*)-(3-(4-(4-(3-(pyridin-3-yl)acrylamido)butyl)piperidine-1-carbonyl)phenyl)carbamate (56)**

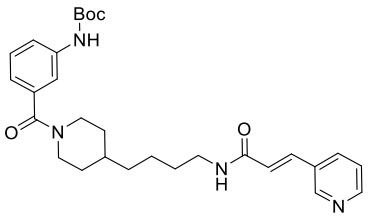

Chemical Formula: $C_{29}H_{38}N_4O_4$
Molecular Weight: 506,65

Following **General Procedure F**, intermediate **26** (1 eq, 2.09 mmol, 785 mg) and (*E*)-3-(3-pyridyl)-acrylic acid (1 eq, 2.09 mmol, 312 mg) were dissolved in DCM (abs., 230 mL). Then, DIPEA (1 eq, 2.09 mmol, 365 µL), HOBt (1 eq, 2.09 mmol, 281 mg) and DCC (1 eq, 2.09 mmol, 433 mg) were added sequentially and the reaction mixture stirred overnight at r.t. The reaction was monitored by TLC (SiO_2, DCM/MeOH: 30/1). After completion, the work-up was performed as described in **General Procedure F**, and the crude product was adsorbed on diatomaceous earth. Purification by flash chromatography, applying an isocratic method (DCM/MeOH: 30/1), afforded intermediate **56** (37% yield, 0.77 mmol, 392 mg) as oil. MS (ESI, positive mode): found *m/z* = 507.3 $[M+H]^+$, calculated *m/z* =507.3 $[M+H]^+$.

(*E*)-*N*-(4-(1-(3-aminobenzoyl)piperidin-4-yl)butyl)-3-(pyridin-3-yl)acrylamide (57)

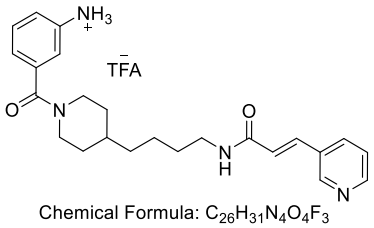

Chemical Formula: $C_{26}H_{31}N_4O_4F_3$
Molecular Weight: 521.54

Following **General Procedure C variation 1**, Intermediate **56** (1 eq, 2.37mmol, 1.2 g) was dissolved in pure TFA (15 mL) as a solvent. The reaction mixture was stirred at 400 mbar for 5 min. The reaction was monitored by HPLC (method 2). After completion, the work-up was performed as as described in **General Procedure C**. The crude product was purified by preparative HPLC (method 2, t_R = 9.06 min), affording intermediate **57** (60% yield, 1.4 mmol, 742 mg) as oil. **^{1}H-NMR (500 MHz, d6-DMSO):** δ/ppm = 9.20 (s, 2H), 8.94 (d, J = 2.1 Hz, 1H), 8.72 (dd, J = 5.2, 1.5 Hz, 1H), 8.36 (dt, J = 8.2, 1.8 Hz, 1H), 8.21 (t, J = 5.6 Hz, 1H), 7.77 (dd, J = 8.1, 5.2 Hz, 1H), 7.51 (d, J = 16.0 Hz, 1H), 7.39 (t, J = 7.7 Hz, 1H), 7.09 (d, J = 8.0 Hz, 2H), 6.84 (d, J = 15.9 Hz, 1H), 3.19 (q, J = 6.6 Hz, 2H), 1.56 – 1.21 (m, 8H), 1.09 – 1.02 (m, 2H). **^{13}C-NMR (126 MHz, d6-DMSO):** δ/ppm = 168.02, 163.95, 145.66, 144.92, 138.44, 137.64, 133.36, 129.54, 126.44, 125.58, 122.10, 120.88, 118.32, 116.61, 114.30, 38.68, 35.42, 35.22, 29.16, 26.78, 23.41. MS (ESI, positive mode): found *m/z* = 407.3 $[M+H]^+$, calculated *m/z* =407.2 $[M+H]^+$.

(*E*)-*N*-(4-(1-(3-(3-(2,5-dioxo-2,5-dihydro-1*H*-pyrrol-1-yl)propanamido)benzoyl)piperidin-4-yl)butyl)-3-(pyridin-3-yl)acrylamide (58)

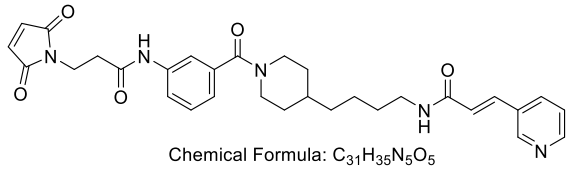

Chemical Formula: $C_{31}H_{35}N_5O_5$
Molecular Weight: 557,65

Following **General Procedure J**, 3-maleimidyl-propionic acid (1.5 eq, 0.07 mmol, 12 mg) was dissolved in DMF (1.6 mL). Then, PyAOP (1.5 eq, 0.07 mmol, 38 mg) and DIPEA (6 eq, 0.3 mmol, 53 µL) were added and stirred for 30 min at r.t. Next, intermediate **57** (1 eq, 0.05 mmol, 26 mg) was added, and the reaction mixture was stirred overnight at r.t. The reaction progress was monitored by HPLC (method 2). After completion, the reaction mixture was directly purified by preparative HPLC (method 2, t_R = 11.83 min), affording intermediate **58** (34% yield, 0.017 mmol, 9.5 mg) as a white solid. **^{1}H-NMR (500 MHz, d6-DMSO):** δ/ppm = 10.07 (s, 1H), 8.85 (d, J = 2.2 Hz, 1H), 8.63 (dd, J = 5.0, 1.5 Hz, 1H), 8.21 – 8.12 (m, 2H), 7.66 – 7.59 (m, 2H), 7.53 (ddd, J = 8.1, 2.2, 1.1 Hz, 1H), 7.48 (d, J = 15.9 Hz, 1H), 7.33 (t, J = 7.9 Hz, 1H), 7.04 – 6.97 (m, 3H), 6.78 (d, J = 15.9 Hz, 1H), 3.72 (t, J = 7.1 Hz, 2H), 3.19 (q, J = 6.8 Hz, 2H), 2.64 – 2.52 (m, 2H), 1.56 – 1.15 (m, 7H), 1.09 – 1.02 (m, 2H). **^{13}C-NMR (126 MHz, d6-DMSO):** δ/ppm 171.20, 169.20, 169.06, 164.65, 148.22, 147.38, 139.43, 136.77, 135.05, 134.66, 129.23, 125.98, 125.28, 121.79, 120.34, 117.82, 39.19, 35.97, 35.79, 35.55, 34.30, 29.70, 23.97. MS (ESI, positive mode): found *m/z* = 558.3 $[M+H]^+$, calculated *m/z* =558.3 $[M+H]^+$.

4-((S)-2-((*S*)-2-(6-(2,5-dioxo-2,5-dihydro-1*H*-pyrrol-1-yl)hexanamido)-3-methylbutanamido)propanamido)benzyl(3-(4-(4-((*E*)-3-(pyridin-3-yl)acrylamido)butyl)piperidine-1-carbonyl)phenyl)carbamate (59)

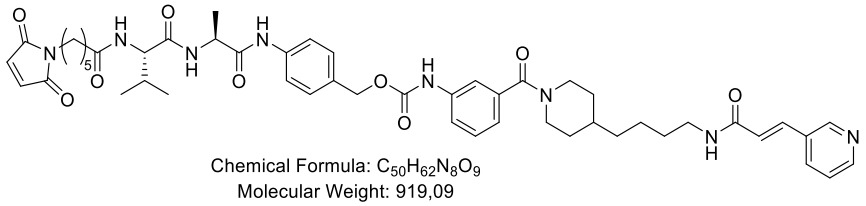

Chemical Formula: $C_{50}H_{62}N_8O_9$
Molecular Weight: 919,09

Following **General Procedure J**, mc-Val-Ala-PAB-PNP (CAS-No. 1639939-40-4, 1.5 eq, 0.037 mmol, 24 mg) was dissolved in DMF (1.5 mL). Then, PyAOP (1.5 eq, 0.037 mmol, 19 mg) and DIPEA (6 eq, 0.15 mmol, 26 µL) were added and stirred for 30 min at r.t. Next, intermediate **57** (1 eq, 0.025 mmol, 13 mg) was added and the reaction mixture stirred overnight at r.t. The reaction progress was monitored by HPLC (method 2). After completion, the reaction mixture was directly purified by preparative HPLC (method 2, t_R = 15.37 min), affording intermediate **59** (20% yield, 0.005 mmol, 4.5 mg) as white solid. **^{1}H-NMR (500 MHz, d6-DMSO):** δ/ppm = 9.91 (s, 1H), 9.83 (s, 1H), 8.75 (d, J = 2.2 Hz, 1H), 8.55 (dd, J = 4.7, 1.7 Hz, 1H), 8.39 – 8.31 (m, 3H), 8.17 – 8.06 (m, 1H), 7.77 (d, J = 8.6 Hz, 1H), 7.68 – 7.58 (m, 5H), 7.53 – 7.39 (m, 4H), 6.74 (d, J = 15.9 Hz, 1H), 5.09 (s, 2H), 4.40 (p, J = 6.9 Hz, 1H), 4.16 (dd, J = 8.6, 6.8 Hz, 1H), 3.37 (t, J = 7.1 Hz, 2H), 3.02 (dtd, J = 6.6, 3.9, 2.4 Hz, 3H), 1.91 – 1.81 (m, 24H), 1.79 – 1.68 (m, 2H), 0.86

(d, J = 6.8 Hz, 3H), 0.83 (d, J = 6.8 Hz, 3H). **^{13}C-NMR (126 MHz, d6-DMSO):** δ/ppm = 172.21, 171.00, 170.90, 170.88, 168.50, 164.25, 153.29, 149.60, 148.63, 139.05, 138.79, 136.95, 134.79, 134.32, 134.07, 131.05, 130.82, 128.79, 126.20, 124.47, 123.93, 122.16, 122.13, 120.39, 118.92, 65.53, 57.51, 48.92, 47.17, 38.59, 36.91, 35.40, 35.21, 34.83, 29.15, 27.63, 25.81, 25.75, 25.69, 25.64, 25.57, 24.76, 17.82. MS (ESI, positive mode): found *m/z* = 920.2 $[M+H]^+$, calculated *m/z* =920.5 $[M+H]^+$.

4-(*N*-Boc-amino)-phenylacetic acid (60)

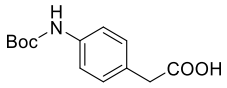

Chemical Formula: $C_{13}H_{17}NO_4$
Molecular Weight: 251.28

Following **General Procedure A**, 4-amino-phenylacetic acid (1 eq, 6.62 mmol, 1 g) and di-*tert*-butyl dicarbonate (2 eq, 3.34 mmol, 3 g) were dissolved in DCM (60 mL) and cooled to 0 °C. Then, triethylamin (2 eq, 3.34 mmol, 1.9 mL) was added, the mixture allowed to warm to r.t. and stirred overnight. The reaction progress was monitored by TLC (SiO_2, $CHCl_3$/MeOH/AcOH: 30/1/1%). After completion, the volatiles were evaporated under reduced pressure, and the crude product was adsorbed on diatomaceous earth. Purification by flash chromatography, applying an isocratic method ($CHCl_3$/MeOH/AcCOOH: 30/1/1%), afforded intermediate **60** (80% yield, 5.3 mmol, 1.3 g) as pale orange crystals. MS (ESI, negative mode): found *m/z* = 250.2 $[M-H]^-$, calculated *m/z* = 250.1 $[M-H]^-$.

***Tert*-butyl(*E*)-(4-(2-oxo-2-((3-(4-(4-(3-(pyridin-3-yl)acrylamido)butyl)piperidine-1-carbonyl)phenyl)amino)ethyl)phenyl)carbamate (61)**

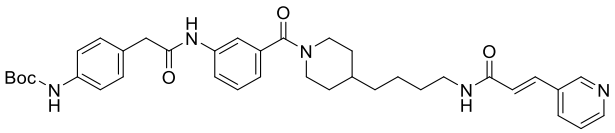

Chemical Formula: $C_{37}H_{45}N_5O_5$
Molecular Weight: 639,80

Following **General Procedure J**, intermediate **60** (1 eq, 0.098 mmol, 24.6 mg) was dissolved in DMF (2 mL). Then, PyAOP (1.5 eq, 0.15 mmol, 77mg) and DIPEA (5 eq, 0.49 mmol, 85µL) were added and stirred for 30 min at r.t. Next, intermediate **57** (1.5 eq, 0.15 mmol, 78 mg) was added, and the reaction mix is stirred overnight at R.T. The reaction progress was monitored by HPLC (method 10). After completion, the reaction mixture was directly purified by preparative HPLC (method 10, t_R = 13.07 min), affording intermediate **61** (20% yield, 0.02 mmol, 13 mg) as a white solid. MS (ESI, positive mode): found *m/z* = 640.3 $[M+H]^+$, calculated *m/z* =640.3 $[M+H]^+$.

(*E*)-*N*-(4-(1-(3-(2-(4-aminophenyl)acetamido)benzoyl)piperidin-4-yl)butyl)-3-(pyridin-3-yl)acrylamide (62)

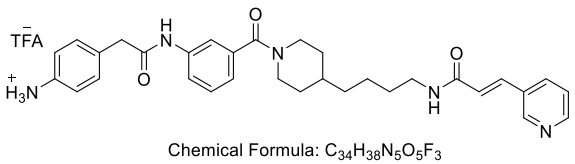

Chemical Formula: $C_{34}H_{38}N_5O_5F_3$
Molecular Weight: 654.69

Following **General Procedure C variation 1**, Intermediate **57** (1 eq, 0.011 mmol, 5.73 mg) was dissolved in pure TFA (2 mL). The reaction mixture was stirred at 400 mbar for 5 min the progress monitored by HPLC (method 2). After completion, the work-up was performed as described in **General Procedure C**. Purification by preparative HPLC (method 2, t_R = 7.40 min) afforded intermediate **62** (55% yield, 0.006 mmol, 4 mg) as oil. MS (ESI, positive mode): found *m*/*z* = 540.3 $[M+H]^+$, calculated *m*/*z* =540.3 $[M+H]^+$.

***Tert*-butyl4-(4-(4-(4-hydroxybutyl)piperidine-1-carbonyl)phenyl)piperazine-1-carboxylate (63)**

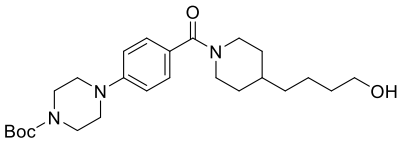

Chemical Formula: $C_{25}H_{39}N_3O_4$
Molecular Weight: 445.60

Following **General Procedure F**, intermediate **22** (1 eq, 1.63 mmol, 256 mg) and 4-(4-carboxy-phenyl)-piperazine-1-carboxylic acid *tert*-butyl ester (1 eq, 1.63 mmol, 500 mg) were dissolved in DCM (abs., 20.5 mL). Then, DIPEA (1 eq, 1.63 mmol, 285 µL), HOBt (1 eq, 1.63 mmol, 219 mg), and DCC (1 eq, 1.63 mmol, 338 mg) were added sequentially and the reactions mixture was stirred overnight at r.t. The reaction was monitored by TLC (SiO_2, hexane/EtOAc/MeOH: 10/10/1). After completion, the work-up was performed as described in **General Procedure F,** and the crude product was adsorbed on diatomaceous earth. Purification by flash chromatography, applying an isocratic method (hexane/EtOAc/MeOH: 10/10/1), afforded intermediate **63** (40% yield, 0.65 mmol, 290 mg) as orange oil. MS (ESI, positive mode): found *m*/*z* = 446.4 $[M+H]^+$, calculated *m*/*z* =446.3 $[M+H]^+$.

***Tert*-butyl-4-(4-(4-(4-methanesulfonylbutyl)piperidine-1-carbonyl)phenyl)piperazine-1-carboxylate (64)**

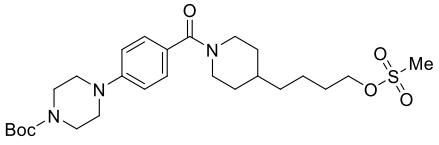

Chemical Formula: $C_{26}H_{41}N_3O_6S$
Molecular Weight: 523.69

Following **General Procedure G**, intermediate **63** (1 eq, 1.29 mmol, 575 mg) was dissolved in DCM (abs., 10 mL) and cooled to 0 °C. Then, methanesulfonyl chloride (1.5 eq, 1.93 mmol, 152 µL) and DIPEA (2 eq, 2.57 mmol, 448 µL) were added and stirred for 2 h at r.t. The reaction progress was monitored by TLC (SiO_2, DCM/MeOH: 30/1). After

completion, the work-up was performed as described in **General Procedure G,** and the crude product was adsorbed on diatomaceous earth. Purification by flash chromatography, applying an isocratic method (DCM/MeOH: 30/1), afforded intermediate **64** (73% yield, 0.94 mmol, 493 mg) as an orange oil. MS (ESI, positive mode): found *m/z* = 524.4 $[M+H]^+$, calculated *m/z* =524.3 $[M+H]^+$.

***Tert*-butyl-4-(4-(4-(4-phtalimidylbutyl)piperidine-1-carbonyl)phenyl)piperazine-1-carboxylate (65)**

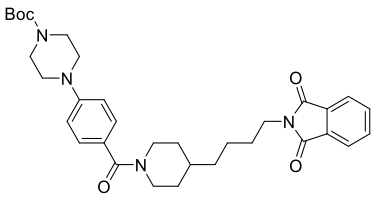

Chemical Formula: $C_{33}H_{42}N_4O_5$
Molecular Weight: 574,72

Following **General Procedure H part 1**, intermediate **64** (1 eq, 0.83 mmol, 434 mg) and potassium phthalimide (1.2 eq, 0.997 mmol, 188 mg) were dissolved in DMF (abs. 9 mL). Following the temperature conditions described in **General Procedure H part 1**, the reaction mixture was stirred overnight. The reaction was monitored by TLC (SiO_2, hexane/EtOAc/MeOH: 13/7/1). After completion, the work-up was performed as described in **General Procedure H part 1**, and the crude product was adsorbed on diatomaceous earth. Purification by flash chromatography, applying an isocratic method (hexane/EtOAc/MeOH: 13/7/1), afforded intermediate **65** (81% yield, 0.67 mmol, 386 mg) as brown oil. MS (ESI, positive mode): found *m/z* = 575.6 $[M+H]^+$, calculated *m/z* =575.3 $[M+H]^+$.

***Tert*-butyl-4-(4-(4-(4-aminobutyl)piperidine-1-carbonyl)phenyl)piperazine-1-carboxylate (66)**

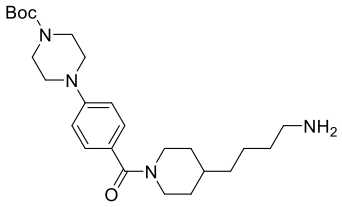

Chemical Formula: $C_{25}H_{40}N_4O_3$
Molecular Weight: 444.62

Following **General Procedure H part 2**, intermediate **65** (1 eq, 0.7 mmol, 402 mg) was dissolved in EtOH (13 mL). Then, hydrazine monohydrate (4 eq, 4.18 mmol, 208 µL) was added and the reaction mixture stirred overnight at r.t. The reaction progress was monitored by TLC (SiO_2, $CHCl_3$/MeOH/Et_3N: 10/1/1%). After completion, the work-up was performed as described in **General Procedure H part 2**, and the crude product was adsorbed on diatomaceous earth. Purification by flash chromatography, applying an isocratic method ($CHCl_3$/MeOH/Et_3N: 10/1/1%), afforded intermediate **66** (52% yield, 0.36 mmol, 162 mg) as pale-yellow crystals. MS (ESI, positive mode): found *m/z* = 445.4 $[M+H]^+$, calculated *m/z* =445.2 $[M+H]^+$.

***Tert*-butyl(*E*)-4-(4-(4-(4-(3-(pyridin-3-yl)acrylamido)butyl)piperidine-1-carbonyl)phenyl)piperazine-1-carboxylate (67)**

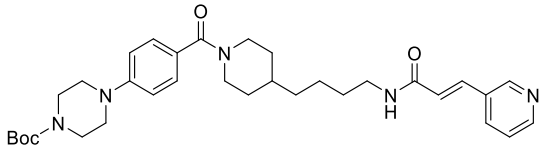

Chemical Formula: $C_{33}H_{45}N_5O_4$
Molecular Weight: 575,75

Following **General Procedure F**, intermediate **66** (1 eq, 0.373 mmol, 166 mg) and (*E*)-3-(3-pyridyl)-acrylic acid (1 eq, 0.37 mmol, 56 mg) were dissolved in DCM (abs., 5 mL). Then, DIPEA (1 eq, 0.37 mmol, 65 µL), HOBt (1 eq, 0.37 mmol, 50 mg) and DCC (1 eq, 0.37 mmol, 77 mg) were added sequentially, and the resulting reaction mixture was stirred overnight at r.t. The reaction progress was monitored by TLC (SiO_2, DCM/MeOH: 10/1). After completion, the work-up was performed as described in **General Procedure F**, and the crude product was adsorbed on diatomaceous earth. Purification by flash chromatography, applying an isocratic method (DCM/MeOH: 10/1), afforded intermediate **67** (35% yield, 0.13 mmol, 75 mg) as oil. MS (ESI, positive mode): found *m/z* = 577.1 $[M+H]^+$, calculated *m/z* =576.4 $[M+H]^+$.

(*E*)-N-(4-(1-(4-(piperazin-1-yl)benzoyl)piperidin-4-yl)butyl)-3-(pyridin-3-yl)acrylamide (68)

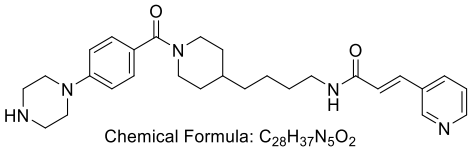

Chemical Formula: $C_{28}H_{37}N_5O_2$
Molecular Weight: 475,64

Following **General Procedure C variation**, intermediate **67** (1 eq, 0.13 mmol, 75 mg) was dissolved in pure TFA (2 mL). The solution was stirred at 400 mbar for 5 min. The reaction progress was monitored by HPLC (method 2). After completion, the work-up was performed as described in **General Procedure C**. The crude product was purified by preparative HPLC using (method 2, t_R = 9.12 min), affording intermediate **68** (60% yield, 0.078 mmol, 37 mg) as brown oil. **^{1}H-NMR (500 MHz, d6-DMSO):** δ/ppm = 8.87 (s, 1H), 8.83 (d, J = 2.2 Hz, 1H), 8.62 (dd, J = 5.0, 1.6 Hz, 1H), 8.14 (dt, J = 8.0, 1.9 Hz, 1H), 7.58 (dd, J = 8.0, 5.0 Hz, 1H), 7.47 (d, J = 15.9 Hz, 1H), 7.29 (d, J = 8.8 Hz, 2H), 7.00 (d, J = 8.8 Hz, 2H), 6.78 (d, J = 15.9 Hz, 1H), 3.42 (dd, J = 6.6, 4.0 Hz, 4H), 3.26 – 3.15 (m, 8H), 2.86 (s, 2H), 1.67 (d, J = 12.7 Hz, 2H), 1.47 (dq, J = 14.6, 7.4 Hz, 3H), 1.38 – 1.21 (m, 3H), 1.05 (qd, J = 12.4, 4.2 Hz, 2H). **^{13}C-NMR (126 MHz, d6-DMSO):** δ/ppm = 168.96, 164.22, 150.46, 148.10, 147.19, 135.87, 134.31, 131.58, 128.35, 127.06, 125.26, 124.63, 114.87, 114.80, 44.83, 42.60, 38.67, 35.44, 35.33, 31.98, 29.17, 23.43. MS (ESI, positive mode): found *m/z* = 476.3 $[M+H]^+$, calculated *m/z* =476.3 $[M+H]^+$.

4-((*S*)-2-((S)-2-(6-(2,5-dioxo-2,5-dihydro-1*H*-pyrrol-1-yl)hexanamido)-3-methylbutanamido)propanamido)benzyl4-(4-(4-(4-((*E*)-3-(pyridin-3-yl)acrylamido)butyl)piperidine-1-carbonyl)phenyl) piperazine-1-carboxylate (69)

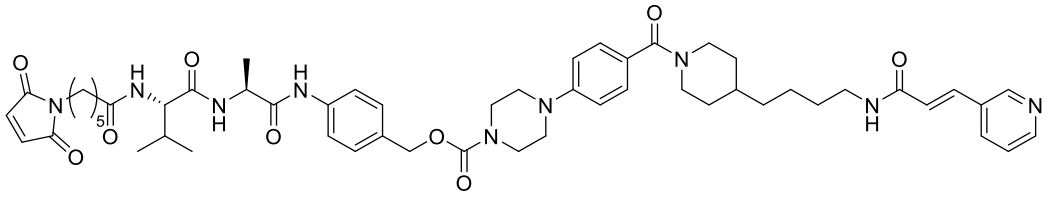

Chemical Formula: $C_{54}H_{69}N_9O_9$
Molecular Weight: 988,20

Following **General Procedure J**, mc-Val-Ala-PAB-PNP (CAS-No. 1639939-40-4, 1.5 eq, 0.023 mmol, 15 mg) was dissolved in DMF (1 mL). Then, PyAOP (1.5 eq, 0.032 mmol, 16 mg) and DIPEA (6 eq, 0.13 mmol, 23 µL) were added and at stirred for 30 min at r.t. Next, intermediate **68** (1 eq, 0.05 mmol, 24 mg) was added, and the resulting mixture was stirred overnight at r.t. The reaction was monitored by HPLC (method 2). After completion, the reaction mixture was directly purified by preparative HPLC (method 2, t_R = 15.37 min), affording intermediate **69** (12% yield, 0.006 mmol, 6 mg) as white solid. **^{1}H-NMR (500 MHz, d6-DMSO):** δ/ppm 9.88 (s, 1H), 8.78 (d, J = 2.2 Hz, 1H), 8.58 (dd, J = 4.9, 1.6 Hz, 1H), 8.10 (t, J = 5.7 Hz, 1H), 8.10 – 8.01 (m, 2H), 7.74 (d, J = 8.5 Hz, 1H), 7.59 (d, J = 8.5 Hz, 2H), 7.51 (dd, J = 8.0, 4.9 Hz, 1H), 7.45 (d, J = 15.9 Hz, 1H), 7.32 (d, J = 8.6 Hz, 2H), 7.25 (d, J = 8.7 Hz, 2H), 6.98 (s, 2H), 6.94 (d, J = 8.8 Hz, 2H), 6.74 (d, J = 15.9 Hz, 1H), 5.04 (s, 2H), 4.16 (dd, J = 8.6, 6.7 Hz, 1H), 3.37 (t, J = 7.1 Hz, 2H), 3.30 (h, J = 3.7 Hz, 4H), 3.24 – 3.14 (m, 7H), 2.84 (s, 2H), 2.24 – 2.06 (m, 2H), 1.97 (h, J = 6.8 Hz, 1H), 1.87 (td, J = 6.2, 3.3 Hz, 4H), 1.66 (d, J = 12.8 Hz, 2H), 1.48 (ddd, J = 21.1, 11.7, 5.3 Hz, 8H), 1.39 – 1.14 (m, 13H), 1.05 (q, J = 10.3 Hz, 2H), 0.85 (dd, J = 16.5, 6.8 Hz, 6H). **^{13}C-NMR (126 MHz, d6-DMSO):** δ/ppm = 172.19, 170.96, 170.88, 169.00, 164.16, 154.36, 148.93, 147.98, 138.59, 134.80, 134.54, 134.30, 131.42, 131.10, 128.34, 128.28, 126.18, 126.11, 124.77, 124.18, 118.99, 114.37, 66.03, 57.49, 48.89, 47.32, 47.21, 47.17, 43.03, 38.57, 36.91, 35.39, 35.30, 34.82, 31.93, 30.32, 30.19, 29.14, 27.61, 25.67, 25.62, 25.55, 24.74, 23.37, 19.06, 18.03, 17.81. MS (ESI, positive mode): found *m/z* = 989.5 $[M+H]^+$, calculated *m/z* =989.5 $[M+H]^+$.

(*E*)-*N*-(4-(1-(4-(4-(3-(2,5-dioxo-2,5-dihydro-1*H*-pyrrol-1-yl)propanoyl)piperazin-1-yl)benzoyl)piperidin-4-yl)butyl)-3-(pyridin-3-yl)acrylamide (70)

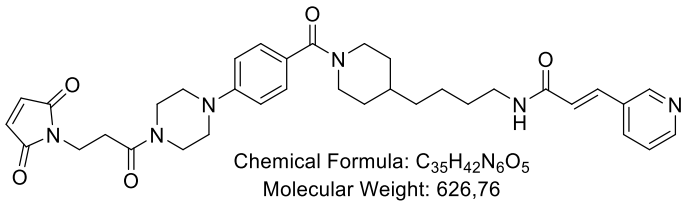

Chemical Formula: $C_{35}H_{42}N_6O_5$
Molecular Weight: 626,76

Following **General Procedure J**, 3-maleimidopropionic acid (1.5 eq, 0.08 mmol, 13.5mg) was dissolved in DMF (1 mL). Then, PyAOP (1.5 eq, 0.032 mmol, 16 mg) and DIPEA (6 eq, 0.13 mmol, 23 µL) were added and stirred for 30 min at r.t. Next, intermediate **68** (1 eq, 0.05 mmol, 24 mg) was added and the reaction mixture stirred overnight at r.t. The reaction progress was monitored by HPLC (method 2). After completion, reaction mixture was directly purified by preparative HPLC (method 2, t_R = 12.18 min), affording intermediate **70** (34% yield, 0.017 mmol, 10.6 mg) as a white solid. **^{1}H-NMR (500 MHz, d6-DMSO):** δ/ppm = 8.81 (s, 1H), 8.60 (d, J = 4.0 Hz, 1H), 8.15 – 8.06 (m, 2H), 7.54 (dd, J = 8.0, 4.9 Hz, 1H), 7.46 (d, J = 15.9 Hz, 1H), 7.26 (d, J = 8.7 Hz, 2H), 7.00 (s, 2H), 6.95 (d, J = 8.9 Hz, 2H), 6.75 (d, J = 15.9 Hz, 1H), 4.05 (s, 8H), 3.69 – 3.61 (m, 2H), 3.56 (t, J = 5.2 Hz, 4H), 3.27 – 3.16 (m, 2H), 2.69 – 2.61 (m, 2H), 1.70 – 1.63 (m, 2H), 1.46 (q, J = 6.9 Hz, 3H), 1.35 – 1.20 (m, 4H), 1.11 – 0.99 (m, 2H). **^{13}C-NMR (126 MHz, d6-DMSO):** δ/ppm 170.67, 169.02, 168.14, 164.13, 151.11, 148.51, 147.61, 135.25, 134.51, 134.39, 131.30, 128.30, 126.03, 124.98, 124.36, 114.25, 47.55, 47.14, 44.37, 40.53, 38.58, 35.40, 35.31, 33.55, 31.94, 30.91, 29.14, 23.37. MS (ESI, positive mode): found *m/z* = 627.5 $[M+H]^+$, calculated *m/z* =627.3 $[M+H]^+$.

Benzyl 4-(4-aminobutyl)-4-hydroxypiperidine-1-carboxylate (71)

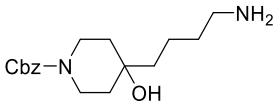

Chemical Formula: $C_{17}H_{26}N_2O_3$
Molecular Weight: 306.41

Following **General Procedure P**, intermediate **55** (1 eq, 4.27 mmol, 1.3 g) was dissolved in MeOH (abs., 18.24 mL). In parallel, ammonium acetate (10 eq, 42.66 mmol, 3.3 g) and sodium cyanoborohydride (2 eq, 8.53 mmol, 536 mg) were charged in a two-neck flask and dissolved in MeOH (abs. 13 mL). Then, following the conditions described in **General Procedure P**, ammonium acetate / cyanoborohydride solution was added to the intermediate **55**-solution and stirred for 8 h at r.t. The reaction progress was monitored by TLC (SiO_2, $CHCl_3$/MeOH/Et_3N: 10/1/1%) and HPLC (method 11). After completion, the work-up was performed as described in **General Procedure P**. The crude product was purified by preparative HPLC (method 11, t_R = 15.57 min), affording intermediate **71** (20% yield, 0.854 mmol, 262 mg) as a white solid. **^{1}H-NMR (500 MHz, d6-DMSO):** δ/ppm = 7.41 – 7.27 (m, 5H), 5.06 (s, 2H), 3.71 (dt, J = 13.2, 4.0 Hz, 2H), 2.82 – 2.75 (m, 2H), 1.56 – 1.32 (m, 10H). **^{13}C-NMR (126 MHz, d6-DMSO):** δ/ppm = 154.33, 137.05, 128.29, 127.65, 127.36, 67.55, 66.28, 65.92, 41.66, 39.78,

38.84, 35.97, 27.57, 19.35. MS (ESI, positive mode): found *m/z* = 307.33 $[M+H]^+$, calculated *m/z* =306.2 $[M+H]^+$.

6-(Pyridin-4-yl)hex-5-yn-1-ol (72)

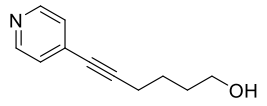

Chemical Formula: $C_{11}H_{13}NO$
Molecular Weight: 175,23

Step 1:

4-Bromopyridine hydrochloride (1 eq, 10.28 mmol, 2g) was dissolved in an aqueous 2 M NaOH-solution (8 mL). The reaction mixture was then stirred for 5 min. The aqueous solution was extracted with EtOAc (3x), and the combined organic layers were washed once with H_2O and once with brine and dried over MgSO4. The volatiles were evaporated under reduced pressure.

Step 2:

The product from step 1 was charged into a three-neck flask equipped with a reflux condenser, dissolved in triethylamine (2.8 eq, 28.7 mmol, 4 mL) and the solution degassed with argon. Next, Hex-5-yn-1-ol (1 eq, 10.28 mmol, 1.13 mL), Bis(triphenylphosphine)palladium chloride (1.1 mol-%, 0.114 mmol, 80 mg) and copper(I) iodide (2.04% mol, 0.21 mmol, 40 mg) were added sequentially. The reaction mixture was heated to reflux for 30 min and the reaction progress was monitored by TLC (SiO_2, EtOAc 100%). After completion, the reaction mixture was cooled to r.t. and extracted with EtOAc (100 mL) and the organic layer washed with H_2O (25 mL). Next, the organic layer was collected and washed once with H_2O and once with brine, dried over $MgSO_4$, and the volatiles were evaporated under reduced pressure. The crude product was adsorbed on diatomaceous earth. Purification by flash chromatography, applying an isocratic method (EtOAC = 100%), afforded intermediate **72** (30% yield, 3.1 mmol, 540 mg) as a white solid. MS (ESI, positive mode): found *m/z* = 176.2 $[M+H]^+$, calculated *m/z* =176.1 $[M+H]^+$.

6-(Piperidin-4-yl)hexan-1-ol (73)

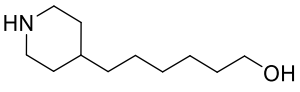

Chemical Formula: $C_{11}H_{23}NO$
Molecular Weight: 185,31

Intermediate **72** (1 eq, 3.32 mmol, 582 mg) was charged in a three-neck flask and dissolved in acetic acid (15 mL). Two of the three necks were then equipped with a balloon filled with argon and a balloon filled with hydrogen, respectively. Afterwards, PtO_2 (20% mol, 0.664 mmol, 81 mg) was added through the central neck, and the system connected to a vacuum pump. Without stirring, the system was degassed with five cycles comprising evacuation and flushing with argon followed by five evacuation/flushing cycles with hydrogen in the same manner as for argon. Then, vigorous stirring was started, and the reaction mixture was kept at r.t. for 3 h. The reaction progress was

monitored by TLC (SiO_2, $CHCl_3$/MeOH/Et_3N: 10/1/1%). After completion, the work-up was performed as described in **General Procedure E**, affording intermediate **73** (85% yield, 2.8 mmol, 523 mg) as a white solid. MS (ESI, positive mode): found *m/z* = 186.5 $[M+H]^+$, calculated *m/z* =187.1 $[M+H]^+$.

6-(*N*-Boc-piperidin-4-yl)hexan-1-ol (74)

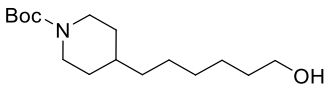

Chemical Formula: $C_{16}H_{31}NO_3$
Molecular Weight: 285,43

Following **General Procedure A**, intermediate **73** (1 eq, 3.48 mmol, 645 mg) and di-*tert*-butyl dicarbonate (2 eq, 6.97 mmol, 6.3 g) were dissolved in DCM (90 mL) and cooled to 0 °C. Then, triethylamine (2 eq, 6.97 mmol, 4 mL) was added and the mixture allowed to warm to r.t. The mixture was stirred overnight at r.t. and the progress monitored by TLC (SiO_2, hexane/EtOAc: 4/1). After completion, the volatiles are evaporated under reduced pressure, and the crude product was adsorbed on diatomaceous earth. Purification by flash chromatography, applying an isocratic method (Hex/EtOAc: 4/1), afforded intermediate **74** (70% yield, 2.44 mmol, 695 mg) as clear oil. MS (ESI, positive mode): found *m/z* = 308.33 $[M+Na]^+$, calculated *m/z* = 286.2 $[M+H]^+$.

Benzyl (*E*)-4-(4-(2-cyano-3-(pyridin-3-yl)guanidino)butyl)-4-hydroxypiperidine-1-carboxylate (75)

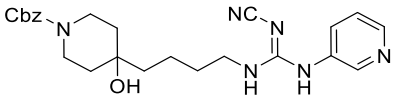

Chemical Formula: $C_{24}H_{30}N_6O_3$
Molecular Weight: 450,54

Following **General Procedure B**, intermediate **71** (1 eq, 0.161 mmol, 49 mg) and intermediate **1** (1.1 eq, 0.178 mmol, 41 mg) were dissolved in 1,4-dioxane (3.8 mL). Triethylamine (2.4 eq, 19.65 mmol, 54 µL) was added and the resulting mixture stirred overnight at r.t. The reaction progress was monitored by TLC (SiO_2, $CHCl_3$/MeOH: 15/1). After completion, the work-up was performed as described in **General Procedure B**, and purification by preparative HPLC (method 2, t_R = 12.94 min), afforded intermediate **75** (40% yield, 0.06 mmol, 29 mg) as sticky oil. MS (ESI, positive mode): found *m/z* = 451.4 $[M+H]^+$, calculated *m/z* =451.2 $[M+H]^+$.

***N*-Boc-4-(6-methanesulfonyl-hexyl)-piperidine (76)**

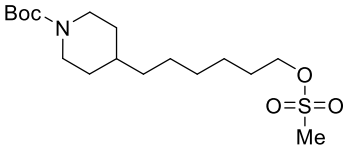

Chemical Formula: $C_{17}H_{33}NO_5S$
Molecular Weight: 363,51

Following **General Procedure G**, intermediate **74** (1 eq, 1.52 mmol, 434 mg) was dissolved in DCM (abs., 11.3 mL). The solution was cooled to 0 °C and methanesulfonyl chloride (1.5 eq, 2.28 mmol, 180 µL) was added, followed by triethylamine (2 eq, 3.04

mmol, 424 µL). The reaction was stirred for 1.5 h at r.t. The reaction was monitored by TLC (SiO_2, DCM/MeOH: 30/1) and after completion, the work-up was performed as described in **General Procedure G.** The crude product was adsorbed on diatomaceous earth, and purification by flash chromatography, applying an isocratic method (DCM/MeOH: 30/1), afforded intermediate **76** (70% yield, 1.1 mmol, 387 mg) as an oil. MS (ESI, positive mode): found *m/z* = 364.1 $[M+H]^+$, calculated *m/z* =364.2 $[M+H]^+$.

(*E*)-2-cyano-1-(4-(4-hydroxypiperidin-4-yl)butyl)-3-(pyridin-3-yl)guanidine (77)

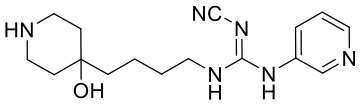

Chemical Formula: $C_{16}H_{24}N_6O$
Molecular Weight: 316,41

Following **General Procedure E**, intermediate **75** (1 eq, 0.07 mmol, 32 mg) was dissolved in a solvent mixture of EtOAc (5 mL) and EtOH (5 mL). Then, a Pd/C (10% in Pd, 12 mol-%, 80 mg) was added and the hydrogenation started according to **General Procedure E**. The reaction mixture was stirred overnight at r.t and the progress monitored by TLC (SiO_2, $CHCl_3$/MeOH/Et_3N: 15/1/1%). After work-up according to **General Procedure E**, the product was ready to use without further purification. Intermediate **77** (73% yield, 0.05 mmol, 16 mg) was afforded as a white powder. MS (ESI, positive mode): found *m/z* = 317.2 $[M+H]^+$, calculated *m/z* =317.2 $[M+H]^+$.

benzyl(*E*)-(3-(4-(4-(2-cyano-3-(pyridin-3-yl)guanidino)butyl)-4-hydroxypiperidine-1-carbonyl)phenyl)carbamate (78)

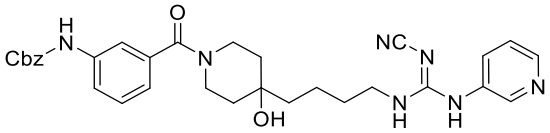

Chemical Formula: $C_{31}H_{35}N_7O_4$
Molecular Weight: 569,67

Following **General Procedure F**, intermediate **77** (1 eq, 1.78 mmol, 563 mg) and intermediate **30** (1 eq, 1.78 mmol, 483 mg) were dissolved in DCM (abs., 30 mL). Then, DIPEA (1 eq, 1.78 mmol, 313 µL), HOBt (1 eq, 1.78 mmol, 241 mg) and DCC (1 eq, 1.78 mmol, 370 mg) were sequentially added and the resulting mixture stirred overnight at r.t. The reaction progress was monitored by TLC (SiO_2, $CHCl_3$/MeOH: 15/1) and HPLC (method 11). After completion, the work-up was performed as described in **General Procedure F** and the crude product purified by preparative HPLC (method 11, t_R = 13.74 min), affording intermediate **78** (37% yield, 0.66 mmol, 375 mg) as oil. MS (ESI, positive mode): found *m/z* = 570.3 $[M+H]^+$, calculated *m/z* =570.3 $[M+H]^+$.

***N-Boc*-4-(6-phtalimidyl-hexyl)-piperidine (79)**

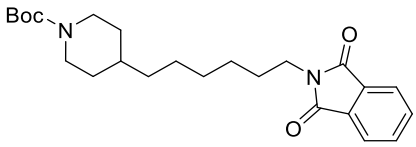

Chemical Formula: $C_{24}H_{34}N_2O_4$
Molecular Weight: 414,55

Following **General Procedure H part 1**, intermediate **76** (1 eq, 0.998 mmol, 363 mg) and potassium phthalimide (1.2 eq, 1.2 mmol, 226 mg) were dissolved in DMF (abs., 10.7 mL). Following the temperature conditions described in **General Procedure H part 1**, the reaction mixture was stirred overnight. The reaction progress was monitored by TLC (SiO_2, hexane/EtOAc/MeOH: 13/7/1). After completion, the work-up was performed as described in **General Procedure H part 1**, and the crude product is adsorbed on diatomaceous earth. Purification by flash chromatography, applying an isocratic method (Hex/EtOAc/MeOH: 13/7/1), afforded intermediate **79** (75% yield, 0.75 mmol, 310 mg) as oil. MS (ESI, positive mode): found *m/z* = 415.2 $[M+H]^+$, calculated *m/z* =415.2 $[M+H]^+$.

N-*Boc*-4-(6-amino-hexyl)-piperidine (80)

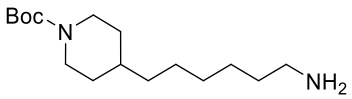

Chemical Formula: $C_{16}H_{32}N_2O_2$
Molecular Weight: 284,44

Following **General Procedure H part 2**, Intermediate **79** (1 eq, 0.81 mmol, 336 mg) was dissolved in EtOH (12 mL). Then, hydrazine monohydrate (4 eq, 3.25 mmol, 162 µL) was added and the reaction mixture stirred overnight at r.t. The reaction progress was monitored by TLC (SiO_2, $CHCl_3$/MeOH/Et_3N: 10/1/1%). After completion, the work-up was performed as described in **General Procedure H part 2**, and the crude product was adsorbed on diatomaceous earth. Purification by flash chromatography, applying an isocratic method ($CHCl_3$/MeOH/Et_3N: 10/1/1%), afforded intermediate **80** (50% yield, 0.4 mmol, 115 mg) as oil. MS (ESI, positive mode): found *m/z* = 285.3 $[M+H]^+$, calculated *m/z* =285.2 $[M+H]^+$.

3-((Benzyloxy)carbonyl)benzoic acid (81)

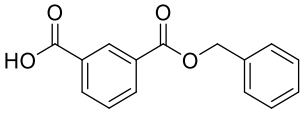

Chemical Formula: $C_{15}H_{12}O_4$
Molecular Weight: 256,26

Part 1:

Isophthalic acid (1 eq, 20 mmol, 3.3 g) was dissolved in MeOH (resulting concentration = 0.66 M, 30 mL). Then, H_2O (2 mL) and Et_3N (1 eq, 20 mmol, 2.8 mL) were added, and the reaction mixture was stirred overnight at r.t. After completion, the volatiles were evaporated under reduced pressure.

Part 2:

The residue from Part 1 was dissolved in DMF (resulting concentration = 0.66 M, 30 mL) and set under an argon atmosphere. Then, benzyl bromide (1.1 eq, 22 mmol, 2.62 mL) was added slowly added to the reaction mixture. The reaction was stirred for 2 h at 100 °C. The reaction progress was monitored by TLC (SiO_2, $CHCl_3$/MeOH/AcOH: 15/1/1%). After completion, the reaction was stopped by dropping the temperature to 0 °C. After the formation of a precipitate, an aqueous 5% $NaHCO_3$ solution (100 mL) was added and extracted EtOAc (3x 60 mL). The aqueous layer was acidified with 2M HCl until a pH-value of 3 was reached, followed by an extraction with EtOAc (3x). The combined organic layers were dried over MgSO4, and the volatiles were evaporated under reduced pressure. The crude product was adsorbed on diatomaceous earth and purification by flash chromatography, applying an isocratic method ($CHCl_3$/MeOH/AcOH: 18/1/1%), afforded intermediate **81** (40% yield, 8 mmol, 2 g) as pale brown crystals. **^{1}H-NMR (500 MHz, $CDCl_3$):** δ/ppm = 8.80 (s, 1H), 8.31 (d, J = 7.7 Hz, 1H), 8.29 (d, J = 7.7 Hz, 1H), 7.57 (td, J = 7.7, 0.5 Hz, 1H), 7.51 – 7.44 (m, 2H), 7.44 – 7.32 (m, 3H), 5.41 (s, 2H). **^{13}C-NMR (126 MHz, $CDCl_3$):** δ/ppm = 171.12, 165.49, 135.69, 134.78, 134.44, 131.45, 130.79, 129.84, 128.80, 128.67, 128.43, 128.34, 67.15. MS (ESI, negative mode): found *m/z* = 255.1 $[M-H]^-$, calculated *m/z* = 253.2 $[M-H]^-$.

***Tert*-butyl (*E*)-4-(6-(3-(pyridin-3-yl)acrylamido)hexyl)piperidine-1-carboxylate (82)**

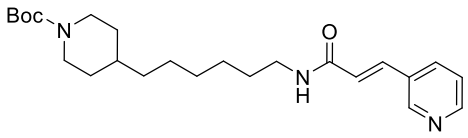

Chemical Formula: $C_{24}H_{37}N_3O_3$
Molecular Weight: 415,58

Following **General Procedure F**, intermediate **80** (1 eq, 2.09 mmol, 594 mg) and *trans*-3-(3-pyridyl)acrylic acid (1 eq, 2.09 mmol, 312 mg) were dissolved in DCM (abs. 1.7 mL). Then, DIPEA (1 eq, 2.09 mmol, 368 µL), HOBt (1 eq, 2.09 mmol, 283 mg) and DCC (1 eq, 2.09 mmol, 434 mg) were added sequentially and the resulting mixture stirred overnight at r.t. The reaction progress was monitored by (SiO_2, TLC DCM/MeOH: 10/1) and HPLC (method 11). After completion, the work-up was performed as described in **General Procedure F** and the crude product purified by preparative HPLC (method 11, t_R = 17.34

min) affording intermediate **82** (35% yield, 0.73 mmol, 304 mg) as oil. MS (ESI, positive mode): found *m/z* = 416.33 $[M+H]^+$, calculated *m/z* =416.2 $[M+H]^+$.

(*E*)-*N*-(6-(piperidin-4-yl)hexyl)-3-(pyridin-3-yl)acrylamide (83)

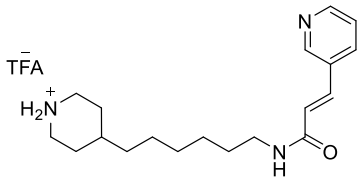

Chemical Formula: $C_{21}H_{30}N_3O_2F_3$
Molecular Weight: 429,47

Following **General Procedure C variation 1**, intermediate **82** (1 eq, 0.73 mmol, 303 mg) was dissolved in pure TFA (2 mL) and the solution stirred at 400 mbar for 5 min. The reaction was monitored by TLC (SiO_2, $CHCl_3$/MeOH/Et_3N: 10/1/1%). After completion, the work-up was performed as described in **General Procedure C** affording intermediate **83** (80% yield, 0.584 mmol, 251 mg) as oil without further purification. MS (ESI, positive mode): found *m/z* = 316.4 $[M+H]^+$, calculated *m/z* =316.2 $[M+H]^+$.

***Tert*-butyl(*E*)-(3-(4-(6-(3-(pyridin-3-yl)acrylamido)hexyl)piperidine-1-carbonyl)phenyl)carbamate (84)**

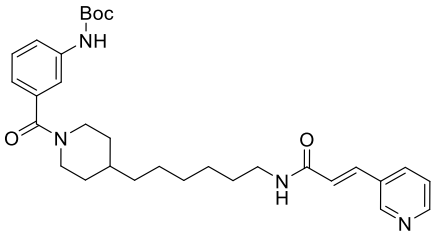

Chemical Formula: $C_{31}H_{42}N_4O_4$
Molecular Weight: 534,70

Following **General Procedure F**, intermediate **83** (1 eq, 0.132 mmol, 57 mg) and Boc-3-aminobenzoic acid (1 eq, 0.132 mmol, 31.3 mg) were dissolved in DCM (abs., 1.7 mL). Then, DIPEA (1 eq, 0.132 mmol, 23.2 µL), HOBt (1 eq, 0.132 mmol, 18 mg) and DCC (1 eq, 0.132 mmol, 27 mg) were added sequentially, and the resulting reaction mixture was stirred overnight at r.t. The reaction progress was monitored by TLC (SiO_2, hexane/EtOAc/MeOH: 10/10/1) and HPLC (method 2). After completion, the work-up was performed as described in **General Procedure F** and the crude product purified by preparative HPLC (method 2, t_R = 16.76 min) affording intermediate **84** (40% yield, 0.05 mmol, 28 mg) as oil. MS (ESI, positive mode): found *m/z* = 535.5 $[M+H]^+$, calculated *m/z* =535.2 $[M+H]^+$.

(*E*)-*N*-(6-(1-(3-aminobenzoyl)piperidin-4-yl)hexyl)-3-(pyridin-3-yl)acrylamide (85)

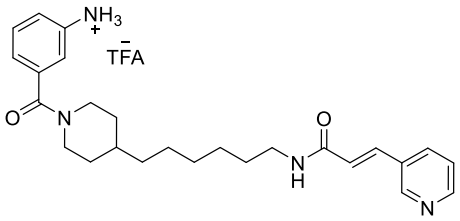

Chemical Formula: $C_{28}H_{35}N_4O_4F_3$
Molecular Weight: 548,59

Following **General Procedure C variation 1**, intermediate **84** (1 eq, 0.73 mmol, 390 mg) was dissolved in pure TFA (2 mL) and the reaction stirred at 400 mbar for 5 min. The reaction was monitored by TLC (SiO_2, $CHCl_3$/MeOH/Et_3N: 10/1/1%). After completion, the work-up was performed as described in **General Procedure C** affording intermediate **85** (80% yield, 0.584 mmol, 320 mg) as oil without further purification. MS (ESI, positive mode): found *m/z* = 435.4 $[M+H]^+$, calculated *m/z* =435.2 $[M+H]^+$.

Benzyl 3-(4-(4-hydroxybutyl)piperidine-1-carbonyl)benzoate (86)

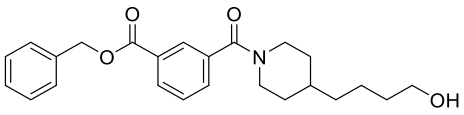

Chemical Formula: $C_{24}H_{29}NO_4$
Molecular Weight: 395,50

Following **General Procedure F**, intermediate **81** (1 eq, 3.38 mmol, 866 mg) and intermediate **22** (1 eq, 3.38 mmol, 532 mg) were dissolved in DCM (abs., 43 mL). Then, DIPEA (1 eq, 3.38 mmol, 594 µL), HOBt (1 eq, 3.38 mmol, 461 mg) and DCC (1 eq, 3.38 mmol, 691 mg) were added sequentially and the resulting reaction mixture stirred overnight at r.t. The reaction progress was monitored by TLC (hexane/EtOAc/MeOH: 10/10/1). After completion, the work-up was performed as described in **General Procedure F** and the crude product adsorbed on diatomaceous earth. Purification by flash chromatography, applying an isocratic method (hexane/EtOAc/MeOH: 10/10/1), afforded intermediate **86** (38% yield, 1.28 mmol, 508 mg) as oil. MS (ESI, positive mode): found *m/z* = 396.2 $[M+H]^+$, calculated *m/z* =396.4 $[M+H]^+$.

Benzyl 3-(4-(4-((methylsulfonyl)oxy)butyl)piperidine-1-carbonyl)benzoate (87)

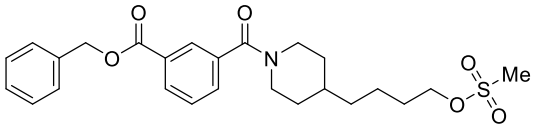

Chemical Formula: $C_{25}H_{31}NO_6S$
Molecular Weight: 473,58

Following **General Procedure G**, intermediate **86** (1 eq, 2.05 mmol, 811 mg) was dissolved in DCM (abs., 15 mL). The solution was cooled to 0 °C and methanesulfonyl chloride (1.5 eq, 3.1 mmol, 245 µL) was added followed by triethylamine (2 eq, 4.1 mmol, 572 µL). The reaction mixture was stirred for 1.5h at r.t and the progress monitored by TLC (SiO_2, DCM/MeOH: 30/1). After completion, the work-up was performed as

described in **General Procedure G,** and the crude product adsorbed on diatomaceous earth. Purification by flash chromatography, applying an isocratic method (DCM/MeOH: 30/1), afforded intermediate **87** (80% yield, 1.64 mmol, 777 mg) as an oil. MS (ESI, positive mode): found *m/z* = 475.1 $[M+H]^+$, calculated *m/z* = 474.8 $[M+H]^+$.

Benzyl 3-(4-(4-((phtalimidyl)oxy)butyl)piperidine-1-carbonyl)benzoate (88)

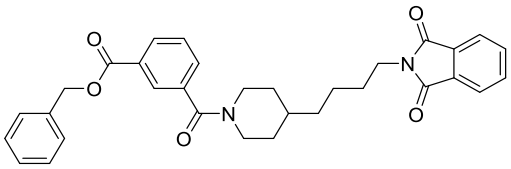

Chemical Formula: $C_{32}H_{32}N_2O_5$
Molecular Weight: 524,62

Following **General Procedure H part 1**, intermediate **87** (1 eq, 1.84 mmol, 871 mg) and potassium phthalimide (1.2 eq, 2.2 mmol, 414 mg) were dissolved in DMF (abs., 20 mL). Following the temperature conditions described in **General Procedure H part 1**, the reaction mixture was stirred overnight. The reaction progress was monitored by TLC (hexane/EtOAc/MeOH: 13/7/1). After completion, the work-up was performed as described in **General Procedure H part 1** and the crude product adsorbed on diatomaceous earth. Purification by flash chromatography, applying an isocratic method (Hex/EtOAc/MeOH: 13/7/1), afforded intermediate **88** (65% yield, 1.2 mmol, 630 mg) as oil. **^{1}H-NMR (500 MHz, d6-DMSO):** δ/ppm = 8.05 (dt, J = 7.7, 1.5 Hz, 1H), 7.92 (t, J = 1.7 Hz, 1H), 7.92 – 7.77 (m, 5H), 7.60 (t, J = 7.6 Hz, 1H), 7.53 – 7.32 (m, 5H), 5.37 (s, 2H), 3.57 (t, J = 7.1 Hz, 2H), 1.78 – 0.97 (m, 14H). **^{13}C-NMR (126 MHz, d6-DMSO):** δ/ppm = 167.80, 167.58, 164.90, 136.89, 135.85, 134.22, 131.50, 131.33, 129.84, 129.71, 128.97, 128.40, 128.04, 127.91, 127.20, 122.84, 66.33, 37.22, 35.13, 35.06, 27.97, 23.21. MS (ESI, positive mode): found *m/z* = 525.5 $[M+H]^+$, calculated *m/z* = 525.2 $[M+H]^+$.

Benzyl 3-(4-(4-((amino)oxy)butyl)piperidine-1-carbonyl)benzoate (89)

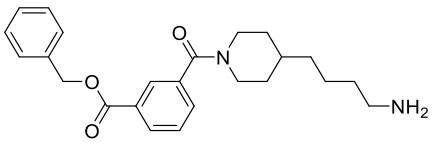

Chemical Formula: $C_{24}H_{30}N_2O_3$
Molecular Weight: 394,52

Following **General Procedure H part 2**, Intermediate **88** (1 eq, 1.72 mmol, 902 mg) was dissolved in EtOH (32 mL). Then, hydrazine monohydrate (6 eq, 10.3 mmol, 513 µL) was added and the resulting reaction mixture stirred overnight at r.t. The reaction progress was monitored by TLC (SiO_2, $CHCl_3$/MeOH/Et_3N: 10/1/1%). After completion, the work-up was performed as described in **General Procedure H part 2** and the crude product adsorbed on diatomaceous earth. Purification by flash chromatography, applying an isocratic method ($CHCl_3$/MeOH/Et_3N: 10/1/1%), afforded intermediate **89** (55% yield, 0.95 mmol, 373 mg) as pale-yellow crystals. **^{1}H-NMR (500 MHz, d6-DMSO):** δ/ppm = 8.05 (dt, J = 7.7, 1.5 Hz, 1H), 7.93 – 7.91 (m, 1H), 7.66 (dt, J = 7.6, 1.5 Hz, 1H), 7.60 (td, J = 7.6, 0.6 Hz, 1H), 7.45 – 7.27 (m, 5H), 5.37 (s, 2H), 2.90 – 2.58 (m, 4H), 2.42 (q, J = 7.1 Hz, 2H), 1.41 – 1.14 (m, 11H). **^{13}C-NMR (126 MHz, d6-DMSO):** δ/ppm = 167.61, 164.92, 131.33, 129.85, 128.99, 128.41, 128.06, 127.92, 127.88, 127.86, 127.20, 66.34, 41.39, 35.60,

35.36, 35.19, 35.12, 33.16, 29.06, 23.39, 23.29, 11.69. MS (ESI, positive mode): found *m/z* = 395.4 $[M+H]^+$, calculated *m/z* = 395.4 $[M+H]^+$.

Benzyl(*E*)-3-(4-(4-(2-cyano-3-(pyridin-3-yl)guanidino)butyl)piperidine-1-carbonyl)benzoate (90)

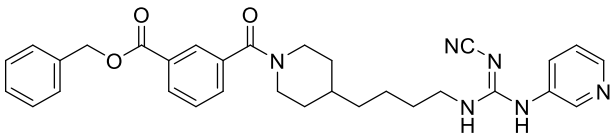

Chemical Formula: $C_{31}H_{34}N_6O_3$
Molecular Weight: 538,65

Following **General Procedure B**, intermediate **89** (1 eq, 0.51 mmol, 201 mg) and intermediate **1** (1.1 eq, 0.56 mmol, 135 mg) were dissolved in 1,4-dioxane (12 mL). Triethylamine (2.4 eq, 1.22 mmol, 3.3 µL) was added and the resulting reaction mixture stirred overnight at r.t. The reaction progress was monitored by TLC (SiO_2, $CHCl_3$/MeOH: 15/1). After completion, the work-up was performed as described in **General Procedure B** and the crude product adsorbed on diatomaceous earth. Purification by flash chromatography, applying an isocratic method (DCM/MeOH: 9/1), afforded intermediate **90** (40% yield, 0.2 mmol, 110 mg) as sticky oil. **^{1}H-NMR (500 MHz, d6-DMSO):** δ/ppm = 9.01 (s, 1H), 8.46 (dd, J = 2.6, 0.8 Hz, 1H), 8.33 (dd, J = 4.7, 1.5 Hz, 1H), 8.05 (dt, J = 7.7, 1.5 Hz, 1H), 7.92 (td, J = 1.8, 0.6 Hz, 1H), 7.66 (dt, J = 7.6, 1.5 Hz, 2H), 7.60 (td, J = 7.7, 0.6 Hz, 1H), 7.48 (d, J = 6.7 Hz, 1H), 7.44 – 7.32 (m, 5H), 5.37 (s, 2H), 3.45 (qd, J = 7.0, 5.1 Hz, 2H), 3.23 (q, J = 7.0 Hz, 2H), 1.51 (p, J = 7.1 Hz, 3H), 1.36 – 1.23 (m, 5H), 1.06 (t, J = 7.0 Hz, 5H). **^{13}C-NMR (126 MHz, d6-DMSO):** δ/ppm = 167.62, 164.92, 157.95, 145.29, 144.72, 136.91, 135.86, 134.56, 131.33, 130.72, 129.86, 129.74, 128.99, 128.41, 128.07, 127.92, 127.21, 123.47, 116.83, 66.35, 55.92, 41.45, 35.23, 35.09, 28.85, 23.07, 18.42. MS (ESI, positive mode): found *m/z* = 539.5 $[M+H]^+$, calculated *m/z* = 539.4 $[M+H]^+$.

***N*-(3-(4-(4-((*E*)-3-(pyridin-3-yl)acrylamido)butyl)piperidine-1-carbonyl)phenyl)biotinamide (91)**

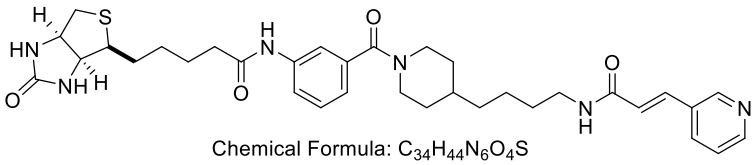

Chemical Formula: $C_{34}H_{44}N_6O_4S$
Molecular Weight: 632,82

Following **General Procedure K**, biotin (1 eq, 0.071 mmol, 17.3 mg) and HATU (1.1 eq, 0.08 mmol, 30.4 mg) were dissolved in DMF (abs., 5 mL). DIPEA (2 eq, 0.14 mmol, 24 µL) was added and the resulting reaction mixture stirred for 20 min at r.t. Then, intermediate **57** (1 eq, 0.071 mmol, 37 mg) was added and the reaction stirred for 48h. The reaction progress was monitored by TLC (SiO_2, $CHCl_3$/MeOH 10/1) and HPLC (method 2). After completion, the work-up was performed as described in **General Procedure K** and purified by preparative HPLC (method 2, t_R = 12.86 min), affording intermediate **91** (42% yield, 0.03 mmol, 20 mg) as a white solid after lyophilisation. **^{1}H-NMR (500 MHz, d6-**

DMSO): δ/ppm = 10.16 (s, 1H), 9.77 (s, 1H), 8.73 (d, J = 2.2 Hz, 1H), 8.53 (d, J = 4.6 Hz, 1H), 8.07 (s, 1H), 7.95 (d, J = 8.1 Hz, 1H), 7.64 (s, 1H), 7.57 (d, J = 8.0 Hz, 1H), 7.51 (d, J = 8.3 Hz, 2H), 7.47 – 7.38 (m, 2H), 7.33 (t, J = 7.8 Hz, 1H), 7.22 (d, J = 8.3 Hz, 2H), 7.00 (d, J = 7.5 Hz, 1H), 6.70 (d, J = 15.9 Hz, 1H), 6.35 (s, 1H), 6.29 (s, 1H), 3.57 (s, 2H), 3.18 – 2.52 (m, 11H), 1.72 – 0.82 (m, 28H). MS (ESI, positive mode): found *m/z* = 633.7 $[M+H]^+$, calculated *m/z* = 633.4 $[M+H]^+$.

(*E*)-3-(4-(4-(2-cyano-3-(pyridin-3-yl)guanidino)butyl)piperidine-1-carbonyl)benzoic acid (92)

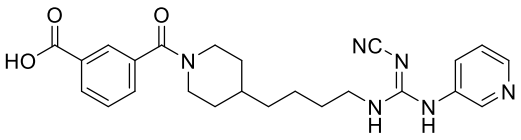

Chemical Formula: $C_{24}H_{28}N_6O_3$
Molecular Weight: 448,53

Following **General Procedure E**, intermediate **90** (1 eq, 0.18 mmol, 97 mg) was dissolved in a solvent mixture of EtOAc (5 mL) and EtOH (5 mL). Then, Pd/C (10% in Pd, 12 mol-%, 50 mg) was added and the hydrogenation process started according to **General Procedure E**. The reaction proceeds overnight and the progress was monitored by (SiO_2, TLC $CHCl_3$/MeOH: 10/1). The work-up was performed as described in **General Procedure E.** Without further purification, intermediate **92** (80% yield, 0.14 mmol, 65 mg) was afforded as a white powder. MS (ESI, positive mode): found *m/z* = 449.3 $[M+H]^+$, calculated *m/z* = 449.4 $[M+H]^+$.

4-((*S*)-2-((*S*)-2-(6-(2,5-dioxo-2,5-dihydro-1*H*-pyrrol-1-yl)hexanamido)-3-methylbutanamido) propanamido)benzyl 3-(4-(4-((*E*)-2-cyano-3-(pyridin-3-yl)guanidino)butyl)piperidine-1-carbonyl) benzoate (93)

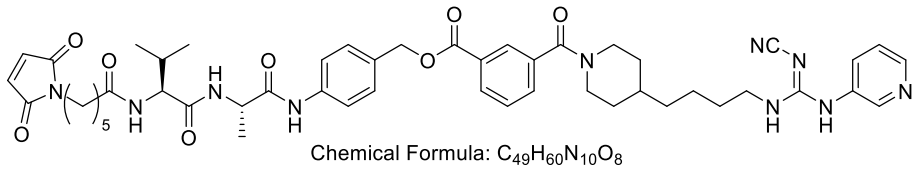

Chemical Formula: $C_{49}H_{60}N_{10}O_8$
Molecular Weight: 917,08

Intermediate **92** (1 eq, 10 µmol, 4.5 mg) was dissolved in DMF (resulting concentration = 50 mM, 0.2 mL), followed by the addition of 0.1 mL of a stock solution containing 1.1 M DIC and 1.1 M HOBt in DMF (10 eq each, 0.111 mmol). The reaction mixture was pre-activated for 40 min. Next, mc-Val-Ala-PAB-OH (CAS-No. 1870916-87-2, 81.26 mg, 0.17 mmol) and DIPEA (48.34 µL, 0.28 mmol) were dissolved in 1 mL DMF (= master mix two). Master mix two (0.2 mL containing 0.03 mmol = 3 eq mc-Val-Ala-PAB-OH and 0.055 mmol = 5 eq DIPEA) was added to the reaction mixture containing intermediate **92**, DIC and HOBt. The reaction mixture was stirred for 24 h and the progress was monitored by TLC (SiO_2, DCM/MeOH 9/1) and HPLC (method 11). After completion, the volatiles were evaporated under reduced pressure, and the crude product was purified by preparative HPLC (method 11, t_R = 13.43 min) affording intermediate **93** (20% yield, 0.002 mmol, 1.83 mg) as white solid. MS (ESI, positive mode): found *m/z* = 917.7 $[M+H]^+$, calculated *m/z* = 917.4 $[M+H]^+$.

(*E*)-1-(4-(1-(3-aminobenzoyl)-4-hydroxypiperidin-4-yl)butyl)-2-cyano-3-(pyridin-3-yl)guanidine (94)

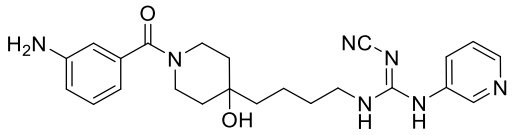

Chemical Formula: $C_{23}H_{29}N_7O_2$
Molecular Weight: 435,53

Following **General Procedure E**, intermediate **78** (1 eq, 0.02 mmol, 11.4 mg) was dissolved in a solvent mixture of EtOAc (1 mL) and EtOH (1 mL). Then, Pd/C (10% in Pd, 12 mol-%, 15 mg) was added and the hydrogenation process was started according to **General Procedure E**. The reaction proceeded for 4 h and the progress was monitored by TLC (SiO_2, $CHCl_3$/MeOH/Et_3N: 15/1/1%). The work-up was performed as described in **General Procedure E.** Without further purification, intermediate **94** (80% yield, 0.016 mmol, 7 mg) was afforded as a white powder. **^{1}H-NMR (500 MHz, d6-DMSO):** δ/ppm = 8.38 (d, J = 2.6 Hz, 1H), 8.28 (dd, J = 4.8, 1.5 Hz, 1H), 7.64 (dt, J = 8.1, 2.1 Hz, 1H), 7.44 – 7.30 (m, 1H), 7.05 (t, J = 7.8 Hz, 1H), 6.62 (ddd, J = 8.1, 2.3, 1.0 Hz, 1H), 6.51 (t, J = 1.9 Hz, 1H), 6.46 (dt, J = 7.5, 1.3 Hz, 1H), 3.98 – 3.93 (m, 4H), 3.56 – 3.52 (m, 6H), 1.57 – 1.14 (m, 10H). **^{13}C-NMR (126 MHz, d6-DMSO):** δ/ppm = 169.36, 157.91, 148.51, 145.24, 144.68, 137.13, 134.59, 130.66, 128.63, 123.45, 118.45, 116.83, 114.37, 113.52, 111.68, 66.25, 41.95, 41.55, 29.40, 19.53. MS (ESI, positive mode): found *m*/*z* = 436.33 $[M+H]^+$, calculated *m*/*z* = 436.4 $[M+H]^+$.

***tert*-butyl (2-(1,3-dioxoisoindolin-2-yl)ethoxy)carbamate (95)** [211]

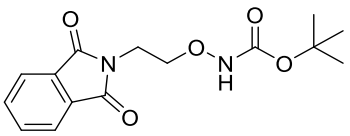

Chemical Formula: $C_{15}H_{18}N_2O_5$
Molecular Weight: 306,32

Following patent WO2006069246, potassium carbonate (2.33 eq, 87.6 mmol, 12g) and *N*-(2-bromoethyl)phthalimide (1.05 eq, 39.7 mmol, 10g) were added to a solution of *tert*-butyl *N*-hydroxycarbamate (1 eq, 37.6 mmol, 5 g) in DMF (resulting concentration = 1.2 M, 30 mL) at 0 °C. The reaction mixture was stirred for 3 h at r.t and the progress was monitored by TLC (SiO_2, hexane/EtOAc 1:1). After completion, the mixture was diluted in H_2O (200mL) and extracted with EtOAC (200 mL). The organic layer was collected and washed once with H_2O and once with brine. The organic layer was dried over $MgSO_4$, and the volatiles were evaporated under reduced pressure. The crude product was adsorbed on diatomaceous earth, and purification by flash chromatography, applying a gradient (20:1 - 1:1 hexane:EtOAc, 30 min), afforded intermediate **95** (55% yield, 21 mmol, 6.3 g) as white solid. MS (ESI, positive mode): found *m*/*z* = 307.0 $[M+H]^+$ and 324.2 $[M+NH_4$, calculated *m*/*z* = 307.4 $[M+H]^+$.

***tert*-Butyl (2-aminoethoxy)carbamate (96)**

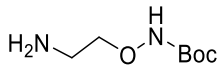

Chemical Formula: $C_7H_{16}N_2O_3$
Molecular Weight: 176,22

Following **General Procedure H part 2**, Intermediate **95** (1 eq, 3.69 mmol, 1.1 g) was dissolved in EtOH (23 mL). Then, hydrazine monohydrate (5 eq, 10.3 mmol, 921 µL) was added and the reaction mixture stirred for 5 h at r.t. The progress was monitored by TLC (SiO_2, $CHCl_3$/MeOH/Et_3N: 10/1/1%). After completion, the work-up was performed as described in **General Procedure H part 2**, and the crude product adsorbed on diatomaceous earth. Purification by flash chromatography, applying an isocratic method ($CHCl_3$/MeOH/Et_3N: 9/1/1%), afforded intermediate **96** (50% yield, 1.8 mmol, 325 mg) as crystals. MS (ESI, positive mode): found *m/z* = 177.2 $[M+H]^+$, calculated *m/z* = 177.4 $[M+H]^+$.

4-((*S*)-2-((*S*)-2-(6-(2,5-dioxo-2,5-dihydro-1H-pyrrol-1-yl)hexanamido)-3-methylbutanamido)propanamido)benzyl(3-(4-(4-((*E*)-2-cyano-3-(pyridin-3-yl)guanidino)butyl)-4-hydroxypiperidine-1-carbonyl)phenyl)carbamate (97)

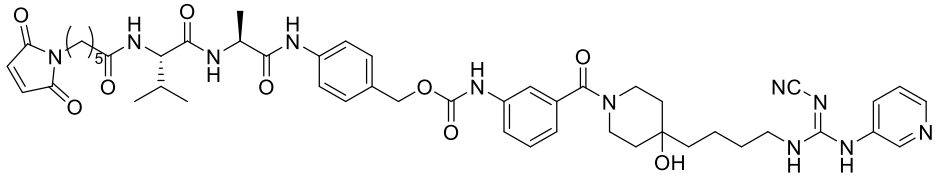

Chemical Formula: $C_{49}H_{61}N_{11}O_9$
Molecular Weight: 948,10

Following **General Procedure J**, mc-Val-Ala-PAB-PNP (CAS-No. 1639939-40-4, 2 eq, 0.014 mmol, 9 mg) was dissolved in DMF (0.5 mL). Then, PyAOP (2 eq, 0.014 mmol, 7 mg) and DIPEA (4 eq, 0.028 mmol, 5 µL) were added and stirred for 30 min at r.t. Then, intermediate **94** (1 eq, 0.007 mmol, 3 mg) was added and the resulting reaction mixture stirred overnight at r.t. The reaction progress was monitored by HPLC (method 2). After completion, reaction mixture is directly purified by preparative HPLC (method 2, t_R = 14.57 min) affording intermediate **97** (12% yield, 0.8 µmol, 0.8 mg) as a white solid. MS (ESI, negative mode): found *m/z* = 946.5 $[M-H]^-$, calculated *m/z* = 946.4 $[M-H]^-$.

***tert*-butyl (*E*)-(2-(3-(pyridin-3-yl)acrylamido)ethoxy)carbamate (98)**

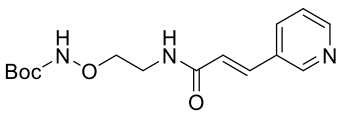

Chemical Formula: $C_{15}H_{21}N_3O_4$
Molecular Weight: 307,35

Following **General Procedure F**, intermediate **96** (1 eq, 1.95 mmol, 344 mg) and *trans*-3-(3-pyridyl)acrylic acid (1 eq, 1.95 mmol, 291mg) were dissolved in DCM (abs., 25 mL). Then, DIPEA (1 eq, 1.95 mmol, 340 µL), HOBt (1 eq, 1.95 mmol, 263 mg) and DCC (1 eq,

1.95 mmol, 402 mg) were sequentially added and the resulting reaction mixture stirred overnight at r.t. The reaction progress was monitored by TLC (SiO_2, DCM/MeOH: 10/1). After completion, the work-up was performed as described in **General Procedure F**, and the crude product adsorbed on diatomaceous earth. Purification by flash chromatography, applying an isocratic method (DCM/MeOH: 10/1), afforded intermediate **98** (35% yield, 0.68 mmol, 210 mg) as oil. MS (ESI, positive mode): found m/z = 308.2 $[M+H]^+$, calculated m/z = 308.4 $[M+H]^+$.

(*E*)-*N*-(2-(aminooxy)ethyl)-3-(pyridin-3-yl)acrylamide (99)

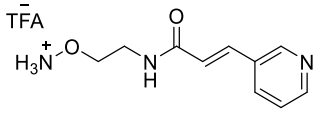

Chemical Formula: $C_{12}H_{14}N_3O_4F_3$
Molecular Weight: 321,24

Following **General Procedure C variation 2**, Intermediate **98** (1 eq, 0.52 mmol, 160 mg) was dissolved in a 15% TFA solution in DCM (15 mL). The reaction mixture was stirred for 2 h at r.t. and the progress monitored by TLC (SiO_2, $CHCl_3$/MeOH/Et_3N: 10/1/1%). After completion, the work-up was performed as described in **General Procedure C**, and without further purification, intermediate **99** (83 % yield, 0.43 mmol, 139 mg) was afforded as oil.

***tert*-butyl (*E*)-4-((2-(3-(pyridin-3-yl)acrylamido)ethoxy)imino)piperidine-1-carboxylate (100)**

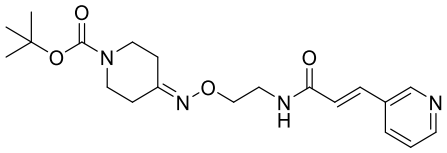

Chemical Formula: $C_{20}H_{28}N_4O_4$
Molecular Weight: 388,47

Intermediate **99** (1 eq, 0.52 mmol, 167 mg) and *N*-Boc-piperid-4-one (1 eq, 0.52 mmol, 104 mg) were dissolved in ethanol (resulting concentration = 0.13 M, 4 mL). After solubilisation, sodium acetate (2 eq, 1.04 mmol, 85 mg) was added and the resulting reaction mixture stirred for 6 h at r.t. The reaction was monitored by TLC (SiO_2, DCM/MeOH: 10/1). After completion, the volatiles were evaporated under reduced pressure. The residue was then redissolved in chloroform (100 mL) and the organic layer once washed with an aqueous, saturated sodium bicarbonate solution (50 mL) and once with water (50 mL). Then, the combined organic layers were dried over $MgSO_4$ and the volatiles evaporated under reduced pressure. The crude product was adsorbed on diatomaceous earth, and purification by flash chromatography, applying a gradient method (100% DCM to 100% DCM/MeOH: 9/1 in 15 min), afforded intermediate **100** (70% yield, 0.43 mmol, 168 mg) as oil. MS (ESI, positive mode): found m/z = 389.2 $[M+H]^+$, calculated m/z = 389.4 $[M+H]^+$.

(*E*)-*N*-(2-((piperidin-4-ylideneamino)oxy)ethyl)-3-(pyridin-3-yl)acrylamide, TFA salt (101)

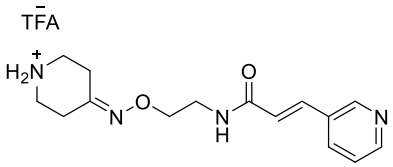

Chemical Formula: $C_{17}H_{21}N_4O_4F_3$
Molecular Weight: 402,36

Following **General Procedure C variation 2**, intermediate **100** (1 eq, 0.31 mmol, 120 mg) was dissolved in a 15 % TFA solution in DCM (15 mL). The reaction mixture was stirred at r.t. for 2 h. The progress was monitored by TLC (SiO_2, $CHCl_3$/MeOH/Et_3N: 10/1/1%). After completion, the work-up was performed as described in **General Procedure C**, and without further purification, intermediate **101** (72% yield, 0.22 mmol, 90 mg) was afforded as oil.

***tert*-butyl(*E*)-(3-(4-((2-(3-(pyridin-3-yl)acrylamido)ethoxy)imino)piperidine-1-carbonyl)phenyl)carbamate (102)**

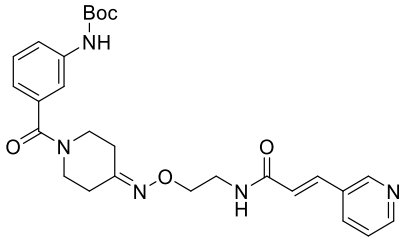

Chemical Formula: $C_{27}H_{33}N_5O_5$
Molecular Weight: 507,59

Following **General Procedure F**, intermediate **101** (1 eq, 0.33 mmol, 133 mg) and Boc-3-aminobenzoic acid (2 eq, 0.66 mmol, 157 mg) were dissolved in dry-DCM (5.5 mL). Then, DIPEA (2.2 eq, 0.73 mmol, 127 µL), HOBt (2 eq, 0.66 mmol, 89 mg) and DCC (2 eq, 0.66 mmol, 136 mg) were added sequentially and the resulting reaction mixture stirred overnight at r.t. The reaction progress was monitored by TLC (SiO_2, DCM/MeOH: 9/1). After completion, the work-up was performed as described in **General Procedure F** and the crude product adsorbed on diatomaceous earth. Purification by flash chromatography, applying an isocratic method (DCM/MeOH: 10/1), afforded intermediate **102** (35% yield, 0.12 mmol, 59 mg) as oil. MS (ESI, positive mode): found m/z = 508.2 $[M+H]^+$, calculated m/z = 508.4 $[M+H]^+$.

(2*S*,3*R*,4*S*,5*S*,6*S*)-2-(2-(3-((((9*H*-fluoren-9-yl)methoxy)carbonyl)amino)propanamido)-4-((((3-(4-(4-((*E*)-2-cyano-3-(pyridin-3-yl)guanidino)butyl)piperidine-1-carbonyl)phenyl)carbamoyl)oxy)methyl)phenoxy)-6-(methoxycarbonyl)tetrahydro-2*H*-pyran-3,4,5-triyl triacetate (103)

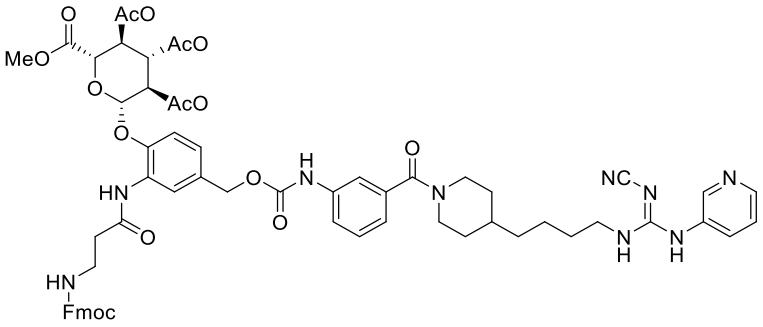

Chemical Formula: $C_{62}H_{67}N_9O_{16}$
Molecular Weight: 1194,26

Following **General Procedure J**, *N*-Fmoc-*O*-Ac-β-D-glucuronide-PNP-carbonate (CAS-Nr. 894095-98-8, 1.5 eq, 0.036 mmol, 33 mg) was dissolved in DMF (1.5 mL). Then, PyAOP (1.5 eq, 0.036 mmol, 18 mg) and DIPEA (6 eq, 0.14 mmol, 25µL) were added and stirred for 30 min at r.t. Next, intermediate **36** (1 eq, 0.024 mmol, 10 mg) was added, and the reaction mixture was stirred overnight at r.t. The reaction progress was monitored by HPLC (method 11). After completion, the reaction mixture was directly purified by preparative HPLC (method 11, t_R = 18.32 min), affording intermediate **103** (10% yield, 0.0024 mmol, 3 mg) as a white solid. MS (ESI, positive mode): found *m/z* = 1194.4 $[M+H]^+$, calculated *m/z* = 1194.5 $[M+H]^+$.

(2*S*,3*R*,4*S*,5*S*,6*S*)-2-(2-(3-((((9*H*-fluoren-9-yl)methoxy)carbonyl)amino)propanamido)-4-((((3-(4-(4-(€-2-cyano-3-(yridine-3-yl)guanidino)butyl)-4-hydroxypiperidine-1-carbonyl)phenyl)carbamoyl)oxy)methyl)phenoxy)-6-(methoxycarbonyl)tetrahydro-2*H*-pyran-3,4,5-triyl triacetate (104)

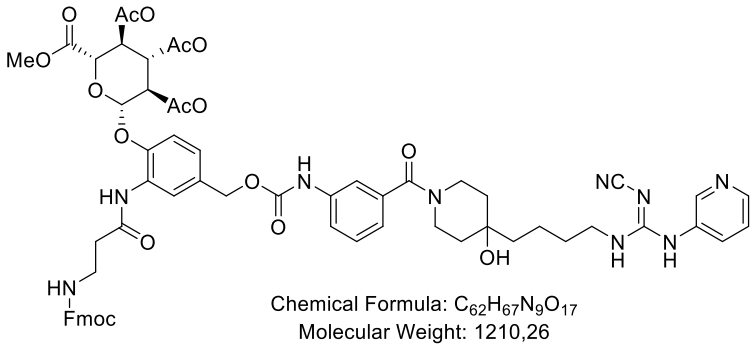

Chemical Formula: $C_{62}H_{67}N_9O_{17}$
Molecular Weight: 1210,26

Following **General Procedure J**, *N*-Fmoc-*O*-Ac-β-D-glucuronide-PNP-carbonate (CAS-Nr. 894095-98-8, 1.5 eq, 0.036 mmol, 31 mg) was dissolved in DMF (1.4 mL). PyAOP (1.5 eq, 0.036 mmol, 17 mg) and DIPEA (6 eq, 0.13 mmol, 23 µL) were added and stirred for 30 min at r.t. Next, intermediate **94** (1 eq, 0.023 mmol, 10 mg) was added and the reaction mixture stirred overnight at r.t. The reaction end point was followed by HPLC (method 11). After completion, the reaction mixture was directly purified by preparative HPLC (method 11, t_R = 18.54 min), affording intermediate **104** (11% yield,

0.0025 mmol, 3 mg) as a white solid. MS (ESI, positive mode): found *m/z* = 1210.4 $[M+H]^+$, calculated *m/z* = 1210.5 $[M+H]^+$.

(E)-N-(2-(((1-(3-aminobenzoyl)piperidin-4-ylidene)amino)oxy)ethyl)-3-(pyridin-3-yl)acrylamide, TFA salt (105)

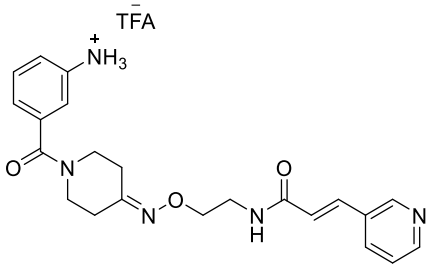

Chemical Formula: $C_{24}H_{26}N_5O_5F_3$
Molecular Weight: 521,48

Following **General Procedure C variation 2**, Intermediate **102** (1 eq, 0.04 mmol, 20 mg) was dissolved in a solution of 15% TFA in DCM (15 mL). The reaction mixture was stirred at r.t. for 1.5 h. The reaction progress was monitored by TLC (SiO_2, $CHCl_3$/MeOH/Et_3N: 10/1/1%). After completion, the work-up was performed as described in **General Procedure C**, affording intermediate **105** (73% yield, 0.03 mmol, 15 mg) as oil without further purification. MS (ESI, positive mode): found *m/z* = 408.3 $[M+H]^+$, calculated *m/z* = 408.4 $[M+H]^+$.

(2*S*,3*S*,4*S*,5*R*,6*S*)-6-(2-(3-aminopropanamido)-4-((((3-(4-(4-((*E*)-2-cyano-3-(pyridin-3-yl)guanidino)butyl)piperidine-1-carbonyl)phenyl)carbamoyl)oxy)methyl)phenoxy)-3,4,5-trihydroxytetrahydro-2*H*-pyran-2-carboxylic acid (106)

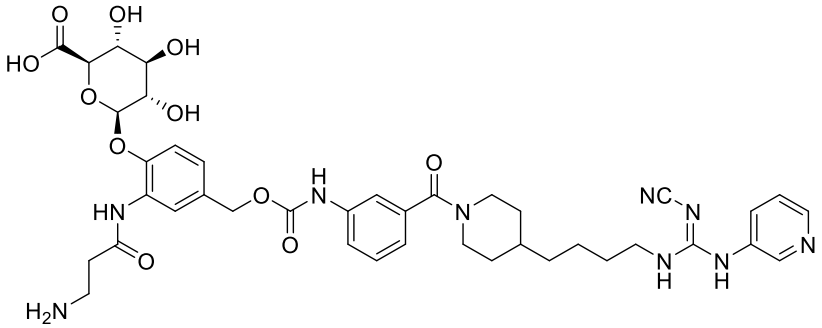

Chemical Formula: $C_{40}H_{49}N_9O_{11}$
Molecular Weight: 831,88

Following **General Procedure Q**, intermediate **103** (1 eq, 0.01 mmol, 12 mg) was dissolved in MeOH (0.67 mL) followed by the addition of an aqueous 0.23 M LiOH solution (0.67 mL). The solution was stirred for 15 min and the reaction progress monitored by HPLC (method 2). After completion, the work-up was performed as described in **General Procedure Q**. Purification by RP-HPLC (method 2, t_R = 9.12 min) afforded intermediate **106** (60% yield, 0.006 mmol, 5 mg) as an oil.

(2*S*,3*S*,4*S*,5*R*,6*S*)-6-(2-(3-aminopropanamido)-4-((((3-(4-(4-((*E*)-2-cyano-3-(pyridin-3-yl)guanidino)butyl)-4-hydroxypiperidine-1-carbonyl)phenyl)carbamoyl)oxy)methyl)phenoxy) -3,4,5-trihydroxytetrahydro-2*H*-pyran-2-carboxylic acid (107)

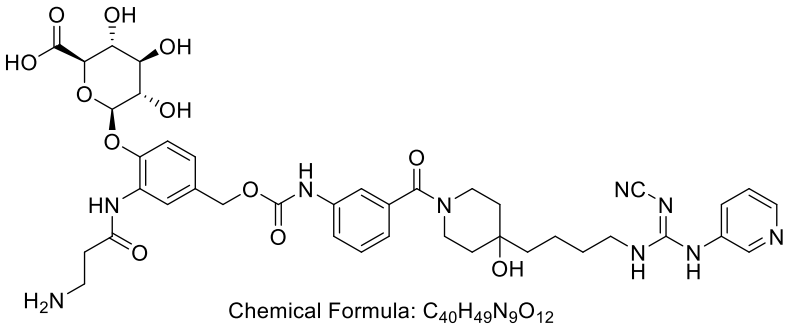

Chemical Formula: $C_{40}H_{49}N_9O_{12}$
Molecular Weight: 847,88

Following **General Procedure Q**, Intermediate **104** (1 eq, 0.007 mmol, 8.5 mg) was dissolved in MeOH (0.5 mL) followed by the addition of an aqueous 0.23 M LiOH solution (0.5 mL). The solution was stirred for 15 min at r.t. and the reaction progress was monitored by HPLC (method 2). After completion, the work-up was performed as described in **General Procedure Q**. Purification by HPLC (method 2, t_R = 8.50 min) afforded intermediate **107** (58% yield, 4 µmol, 3 mg) as an oil.

(2*S*,3*S*,4*S*,5*R*,6*S*)-6-(4-((((3-(4-(4-((*E*)-2-cyano-3-(pyridin-3-yl)guanidino)butyl)piperidine-1-carbonyl)phenyl)carbamoyl)oxy)methyl)-2-(3-(6-(2,5-dioxo-2,5-dihydro-1*H*-pyrrol-1-yl)hexanamido)propanamido)phenoxy)-3,4,5-trihydroxytetrahydro-2*H*-pyran-2-carboxylic acid (108)

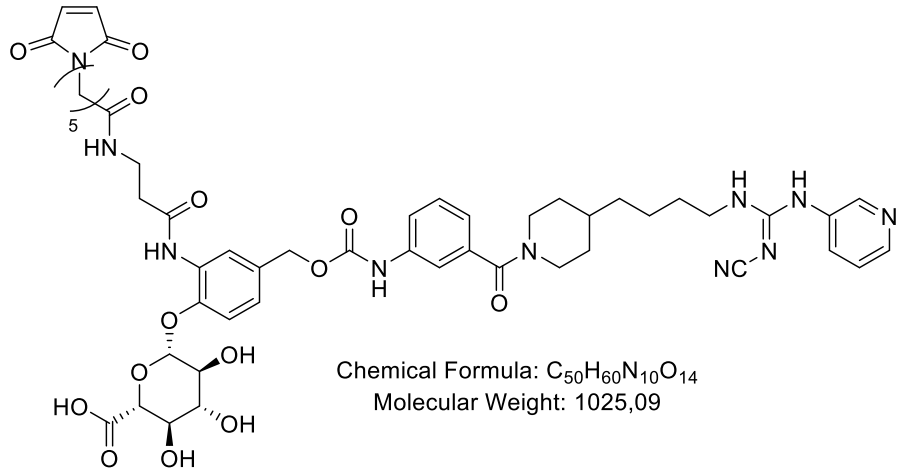

Chemical Formula: $C_{50}H_{60}N_{10}O_{14}$
Molecular Weight: 1025,09

Following **General Procedure I**, intermediate **106** (1.2 eq, 0.001 mmol, 0.83 mg) and EMCS (1.5 eq, 0.015 mmol, 4.6 mg) were dissolved in DMF (abs., 0.8 mL). DIPEA (3.3 eq, 0.033 mmol, 5.7 µL) was added and the reaction stirred for 15 min at r.t. The reaction progress was monitored by HPLC (method 2). After completion, the work-up was performed as described in **General Procedure I** and purification by preparative HPLC (method 2, t_R = 7.10 min) afforded intermediate **108** (50% yield, 5 x 10^{-4} mmol, 0.51 mg)

as a white solid. MS (ESI, positive mode): found *m/z* = 1025.3 $[M+H]^+$, calculated *m/z* = 1025.4 $[M+H]^+$.

(2*S*,3*S*,4*S*,5*R*,6*S*)-6-(4-((((3-(4-(4-((*E*)-2-cyano-3-(pyridin-3-yl)guanidino)butyl)-4-hydroxypiperidine-1-carbonyl)phenyl)carbamoyl)oxy)methyl)-2-(3-(6-(2,5-dioxo-2,5-dihydro-1*H*-pyrrol-1-yl)hexanamido)propanamido)phenoxy)-3,4,5-trihydroxytetrahydro-2*H*-pyran-2-carboxylic acid (109)

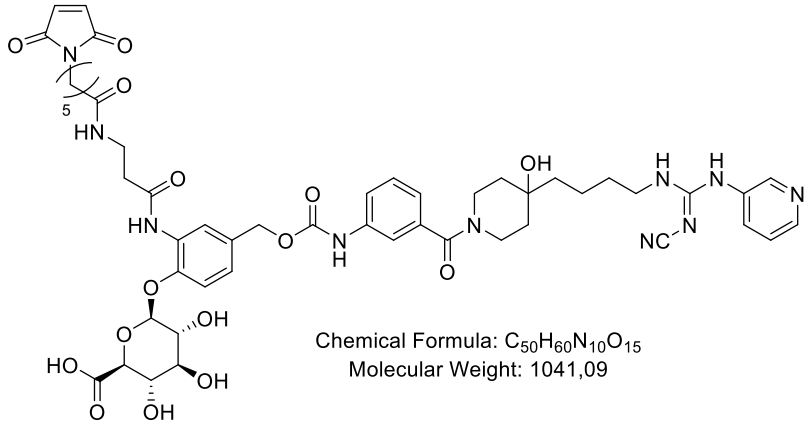

Chemical Formula: $C_{50}H_{60}N_{10}O_{15}$
Molecular Weight: 1041,09

Following **General Procedure I**, intermediate **107** (1 eq, 0.007 mmol, 6 mg) and EMCS (1.5 eq, 0.011 mmol, 3.37 mg) were dissolved in DMF (abs., 0.6 mL). Then, DIPEA (3.3 eq, 0.025 mmol, 4.3 µL) was added and the reaction mixture stirred for 30 min at r.t. The reaction progress was monitored by HPLC (method 2). After completion, the work-up was performed as described in **General Procedure I** and purification by preparative HPLC (method 2, t_R = 5.40 min) afforded intermediate **109** (51% yield, 4 µmol, 3.7 mg) as a white solid. MS (ESI, positive mode): found *m/z* = 1041.4 $[M+H]^+$, calculated *m/z* = 1041.4 $[M+H]^+$.

4-((*S*)-2-((*S*)-2-(6-(2,5-dioxo-2,5-dihydro-1*H*-pyrrol-1-yl)hexanamido)-3-methylbutanamido)propanamido)benzyl(3-(4-((2-((*E*)-3-(pyridin-3-yl)acrylamido)ethoxy)imino) piperidine-1-carbonyl)phenyl)carbamate (110)

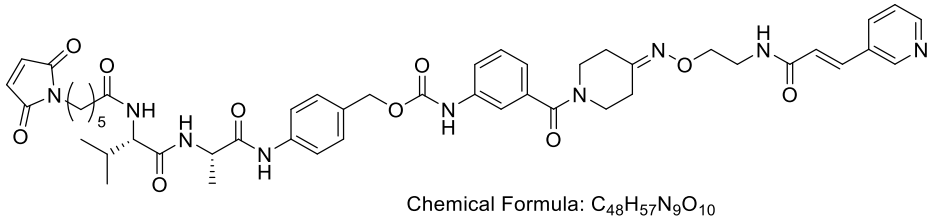

Chemical Formula: $C_{48}H_{57}N_9O_{10}$
Molecular Weight: 920,04

Following **General Procedure J**, mc-Val-Ala-PAB-PNP (CAS-No. 1639939-40-4, 2 eq, 40 µmol, 26 mg) was dissolved in DMF (1.4 mL). PyAOP (2 eq, 0.039 mmol, 18 mg) and DIPEA (5 eq, 0.1 mmol, 18 µL) were added and stirred for 30 min at r.t. Next, intermediate **105** (1 eq, 0.02 mmol, 10.4 mg) was added, and the reaction mixture was stirred overnight at r.t. The reaction progress was monitored by HPLC (method 2). After completion, the reaction mixture was directly purified by preparative HPLC (method 2, t_R = 16.97 min), affording intermediate **110** (17% yield, 0.003 mmol, 3 mg) as a white solid. MS (ESI, positive mode): found *m/z* = 920.4 $[M+H]^+$, calculated *m/z* = 920.4 $[M+H]^+$.

(*E*)-*N*-(3-(4-(4-(2-cyano-3-(pyridin-3-yl)guanidino)butyl)-4-hydroxypiperidine-1-carbonyl)phenyl)biotinamide (111)

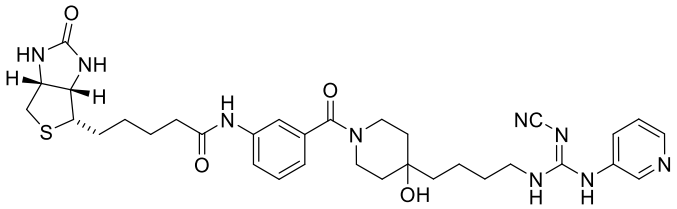

Chemical Formula: $C_{33}H_{43}N_9O_4S$
Molecular Weight: 661,83

Following **General Procedure K**, biotin (1 eq, 20 µmol, 4.9 mg) and HATU (1.1 eq, 0.02 mmol, 7.6 mg) were dissolved in DMF (abs., 2 mL). Then, DIPEA (2 eq, 40 µmol, 7 µL) was added and stirred for 20 min at r.t. Then, intermediate **94** (1 eq, 0.02 mmol, 8.7 mg) was added and stirred overnight at r.t. The reaction progress was monitored by HPLC (method 11). After completion, the work-up was performed as described in **General Procedure K** and purified by preparative HPLC (method 11, t_R = 12.32 min), affording intermediate **111** (38% yield, 0.008 mmol, 5.24 mg) as a white solid after lyophilisation. MS (ESI, positive mode): found *m/z* = 662.3 $[M+H]^+$, calculated *m/z* = 662.4 $[M+H]^+$.

(*E*)-*N*-(3-(4-((2-(3-(pyridin-3-yl)acrylamido)ethoxy)imino)piperidine-1-carbonyl)phenyl)biotinamide (112)

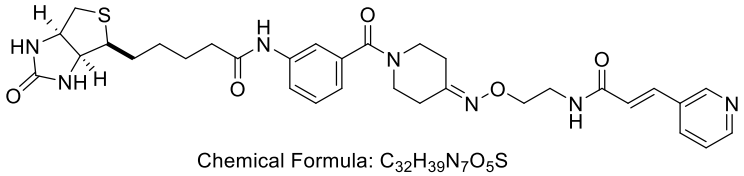

Chemical Formula: $C_{32}H_{39}N_7O_5S$
Molecular Weight: 633,77

Following **General Procedure K**, biotin (1 eq, 20 µmol, 2.45 mg) and HATU (1.1 eq, 0.01 mmol, 3.8 mg) were dissolved in DMF (abs., 1 mL) followed by the addition of DIPEA (2 eq, 0.02 mmol, 3.5 µL) and the resulting solution stirred for 20 min at r.t. Then, intermediate **105** (1 eq, 0.01 mmol, 5.2 mg) was added and and the resulting mixture stirred overnight at r.t. The reaction progress was monitored by HPLC (method 11). After completion, the work-up was performed as described in **General Procedure K** and purification by preparative HPLC (method 11, t_R = 10.32 min) afforded intermediate **111** (40% yield, 0.008 mmol, 5.3 mg) as a white solid after lyophilisation. MS (ESI, positive mode): found *m/z* = 634.4 $[M+H]^+$, calculated *m/z* = 634.4 $[M+H]^+$.

(*E*)-1-(((4-(1-(3-aminobenzoyl)piperidin-4-yl)butyl)amino)(pyridin-3-ylamino)methylene)urea (113)

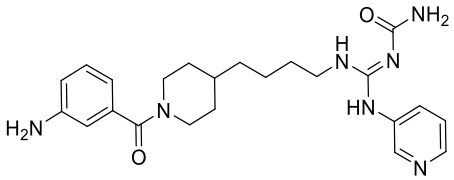

Chemical Formula: $C_{23}H_{31}N_7O_2$
Molecular Weight: 437,55

Intermediate **36** (1 eq, 0.01 mmol, 4.2 mg) was dissolved in a premixed solution of MeOH/H_2O (4/1) and TFA (until pH=1) (5 mL). The reaction mixture was stirred overnight at 37°C and the progress monitored by HPLC (method 2). After completion, the reaction mixture is directly purified by preparative HPLC (method 2, t_R = 9.76 min), affording intermediate **113** (95% yield, 0.009 mmol, 4.2 mg) as a white solid. **^{1}H-NMR (500 MHz, CD_3OD):** δ/ppm = 8.66 – 8.58 (m, 2H), 7.90 (ddd, J = 8.2, 2.6, 1.5 Hz, 1H), 7.62 (ddd, J = 8.2, 4.9, 0.8 Hz, 1H), 7.47 (t, J = 7.8 Hz, 1H), 7.26 (ddd, J = 8.1, 2.3, 1.0 Hz, 1H), 7.22 (dt, J = 7.6, 1.3 Hz, 1H), 7.18 (t, J = 1.9 Hz, 1H), 4.61 (d, J = 13.0 Hz, 1H), 3.75 – 3.41 (m, 4H), 3.34 (s, 1H), 1.93 – 1.07 (m, 11H). **^{13}C-NMR (126 MHz, CD_3OD):** δ/ppm = 171.15, 162.44, 162.15, 156.54, 149.68, 148.12, 138.93, 137.06, 131.25, 126.57, 124.28, 122.71, 119.72, 118.99, 43.72, 43.32, 33.88, 32.98, 29.58, 24.73, 18.36. MS (ESI, positive mode): found *m/z* = 438.3 $[M+H]^+$, calculated *m/z* = 438.4 $[M+H]^+$.

***N-Boc*-4-(pent-4-(en)-yl)-4-hydroxy-piperidine (114)**

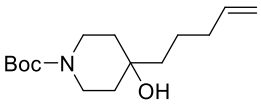

Chemical Formula: $C_{15}H_{27}NO_3$
Molecular Weight: 269,39

Following **General Procedure M**, magnesium (turnings; 2eq, 46.6 mmol, 1.1 g) and the tip of a spatula of I_2 were charged in a dried three-neck flask under an argon atmosphere. THF (abs., 46.3 mL) was added and activation of magnesium performed as described in **General Procedure M**. Then, 5-bromopentene (1.5 eq, 34.9 mmol, 4.2 mL) was added as described in **General Procedure M** (solution A). In parallel, *N*-Boc-4-piperidone (1 eq, 23.3 mmol, 4.6 g) was dissolved in a $LaCl_3$*2LiCl solution in THF (0.6 M, 38.7 mL) in a dried two-neck flask. The mixture was activated for 1 h at r.t. followed by cooling to 8 °C (solution B). Next, solution A is added dropwise to solution B at 0 °C, and the resulting reaction mixture was stirred overnight at 8 °C. The reaction end point was monitored by TLC (SiO_2, hexane/EtOAc: 1/1). After completion, the work-up was performed as described in **General Procedure M** and the crude product adsorbed on diatomaceous earth. Purification by flash chromatography, applying an isocratic method (hexane/EtOAc: 1/1), afforded intermediate **114** (50% yield, 11.65 mmol, 3.1 g) as oil. MS (ESI, positive mode): found *m/z* = 270.0 $[M+H]^+$, calculated *m/z* = 270.0 $[M+H]^+$.

***tert*-Butyl 4-(4,5-dihydroxypentyl)-4-hydroxypiperidine-1-carboxylate (115)**

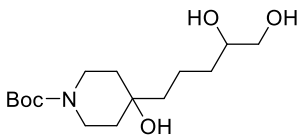

Chemical Formula: $C_{15}H_{29}NO_5$
Molecular Weight: 303,40

Following **General Procedure N**, intermediate **114** (1 eq, 7.8 mmol, 2.1 g) was dissolved in acetone (47.4 mL). Then, NMO (1.2 eq, 9.35 mmol, 1.1 g) was added followed by water (16 eq, 124.8 mmol, 2.2 mL). Finally, OsO_4-solution in *tert*-butanol (0.47% mol, 468.8 µmol, 102 µL) was added and the resulting reaction mixture stirred overnight at r.t. The reaction progress was monitored by TLC (SiO_2, hexane/EtOAc: 1/1 for olefine

consumption, $CHCl_3$/MeOH: 10/1 for diol formation). After completion, the work-up was performed as described in **General Procedure M** and the crude product adsorbed on diatomaceous earth. Purification by flash chromatography, applying an isocratic method ($CHCl_3$/MeOH: 10/1), afforded intermediate **115** (66% yield, 5.1 mmol, 1.6 mg) as oil. MS (ESI, positive mode): found *m/z* = 304.1 $[M+H]^+$, calculated *m/z* = 304.4 $[M+H]^+$.

***tert*-Butyl 4-hydroxy-4-(4-oxobutyl)piperidine-1-carboxylate (116)**

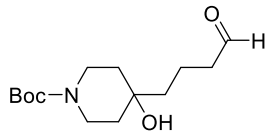

Chemical Formula: $C_{14}H_{25}NO_4$
Molecular Weight: 271,36

Following **General Procedure O**, Intermediate **115** (1 eq, 5.83 mmol, 1.8 g) was dissolved in THF (36.8 mL). In parallel, sodium periodate (2 eq, 11.7 mmol, 2.5 g) was dissolved in water (18.4 mL). Then, both solutions were mixed following instructions from **General procedure O**. The reaction mixture was stirred for 1 h and the progress monitored by TLC (SiO_2, DCM/MeOH: 9/1). After completion, the work-up was performed as described in **General Procedure O**, and without further purification, intermediate **116** (50% yield, 2.9 mmol, 791 mg) was afforded as a white solid after lyophilisation. **^{1}H-NMR (500 MHz, d6-DMSO).** δ/ppm = 9.66 (t, J = 1.7 Hz, 1H), 3.64 – 3.51 (m, 2H), 1.69 – 1.08 (m, 17H). **^{13}C-NMR (126 MHz, d6-DMSO):** δ/ppm = 203.35, 153.96, 89.72, 78.26, 70.89, 40.25, 34.18, 32.55, 31.50, 28.00, 16.90. MS (ESI, positive mode): found *m/z* = 272.0 $[M+H]^+$, calculated *m/z* = 272.4 $[M+H]^+$.

tert-butyl 4-(4-aminobutyl)-4-hydroxypiperidine-1-carboxylate (117)

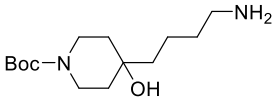

Chemical Formula: $C_{14}H_{28}N_2O_3$
Molecular Weight: 272,39

Following **General Procedure P**, intermediate **116** (1 eq, 3.28 mmol, 890 mg) was dissolved in MeOH (abs., 14.02 mL). In parallel, ammonium acetate (10 eq, 32.8 mmol, 2.5 g) and sodium cyanoborohydride (2 eq, 6.56 mmol, 412 mg) were added into a two-neck flask and dissolved in MeOH (abs., 10 mL). Then, following the conditions described in **General Procedure P**, the ammonium acetate / sodium cyanoborohydride solution is poured into the intermediate **116** solution and stirred for 8 h at r.t. The reaction was monitored by TLC (SiO_2, $CHCl_3$/MeOH/Et_3N: 10/1/1%). After completion, the work-up was performed as described in **General Procedure P**. Purification by preparative HPLC (method 11) afforded intermediate **117** (12% yield, 0.39 mmol, 107 mg) as an oil. MS (ESI, positive mode): found *m/z* = 273.2 $[M+H]^+$, calculated *m/z* = 273.4 $[M+H]^+$.

4-nitrophenyl isoindoline-2-carboxylate (118)

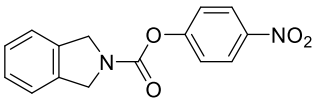

Chemical Formula: $C_{15}H_{12}N_2O_4$
Molecular Weight: 284,27

Isoindoline (1 eq, 0.42 mmol, 48 µL) was dissolved in DMF (abs. resulting concentration = 0.11 M, 3.7 mL). Then, *bis*-*p*-nitrophenyl carbonate (1.1 eq, 0.462 mmol, 141 mg) was added. After solubilisation, DIPEA (1.5 eq, 0.63 mmol, 110 µL) was added and the resulting reaction mixture stirred for 30 min at r.t. The reaction progress was monitored by HPLC (method 1). After completion, the reaction mixture was directly purified by preparative HPLC system (method 1, t_R = 13.78 min), affording intermediate **118** (90% yield, 0.38 mmol, 107 mg) as white crystals. **^{1}H-NMR (500 MHz, $CDCl_3$):** δ/ppm = 8.27 (d, J = 9.1 Hz, 2H), 7.39 (d, J = 9.1 Hz, 2H), 7.35 – 7.28 (m, 4H), 4.96 (s, 2H), 4.85 (s, 2H). **^{13}C-NMR (126 MHz, $CDCl_3$)** δ/ppm = 156.09, 151.65, 144.81, 136.06, 135.83, 127.84, 127.78, 125.10, 122.81, 122.66, 122.15, 52.81, 52.66. MS (ESI, negative mode): found *m*/*z* = 283.3 $[M-H]^-$, calculated *m*/*z* = 283.4 $[M-H]^-$.

***tert*-butyl 4-hydroxy-4-(4-(isoindoline-2-carboxamido)butyl)piperidine-1-carboxylate (119)**

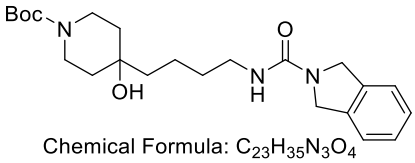

Chemical Formula: $C_{23}H_{35}N_3O_4$
Molecular Weight: 417,55

Following **General Procedure R**, intermediate **118** (2 eq, 0.84 mmol, 239 mg) and intermediate **117** (1 eq, 0.42 mmol, 114 mg) were dissolved in DMF (abs., resulting concentration = 26.7 mmol, 18.4 mL). Then, *N*-methylimidazole (10 eq, 4.22 mmol, 336 µL) were as added and the resulting reaction mixture was stirred for three weeks at 45 °C. The reaction end point was followed by HPLC (method 19. After completion, the work-up was performed as described in **General Procedure R**. Purification by preparative HPLC (method 1, t_R = 14.01 min) afforded intermediate **119** (8% yield, 30 µmol, 14 mg) as an oil. MS (ESI, positive mode): found *m*/*z* = 418.3 $[M+H]^+$, calculated *m*/*z* = 418.4 $[M+H]^+$.

3-(*Boc*-hydroxy)-4-(*Boc*-amino)benzoic Acid (120)

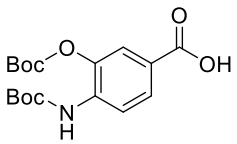

Chemical Formula: $C_{17}H_{23}NO_7$
Molecular Weight: 353,37

44-amino-3-hydroxybenzoic acid (1 eq, 6.53 mmol, 1 g) and triethylamine (3.5 eq, 22.9 mmol, 3.19 mL) were dissolved in DCM (abs., resulting concentration = 0.17 M, 39.2 mL) at 0 °C. Then, a solution of di-*tert*-butyl dicarbonate (3.5 eq, 22.9 mmol, 5 g) in DCM

(abs., resulting concentration = 0.33 M, 20 mL) and was added dropwise at 0 °C. The reaction mixture was stirred overnight at 20 °C. The reaction progress was monitored by TLC (SiO_2, hexane/EtOAc: 2/1). After completion, the volatiles were evaporated under reduced pressure. Then, the crude product was adsorbed on diatomaceous earth. Purification by flash chromatography, applying an isocratic method (hexane/EtOAc: 2/1) afforded intermediate **120** (36% yield, 2.35 mmol, 831 mg) as a white solid. **^{1}H-NMR (500 MHz, d6-DMSO):** δ/ppm = 10.51 (s, 1H), 8.29 (s, 1H), 7.59 (dd, J = 8.6, 2.0 Hz, 1H), 7.51 (d, J = 2.1 Hz, 1H), 6.81 (d, J = 8.6 Hz, 1H), 1.50 (d, J = 1.2 Hz, 18H). **^{13}C-NMR (126 MHz, d6-DMSO):** δ/ppm = 160.64, 150.79, 147.25 (d, J = 6.2 Hz), 135.74, 129.59, 124.63, 114.77, 112.34, 84.92, 83.24, 27.16, 26.91. MS (ESI, negative mode): found *m/z* = 352.1 $[M-H]^-$, calculated *m/z* = 352.4 $[M-H]^-$.

(E)-N-(3-(4-(4-(2-carbamoyl-3-(pyridin-3-yl)guanidino)butyl)piperidine-1-carbonyl)phenyl)biotinamide (121)

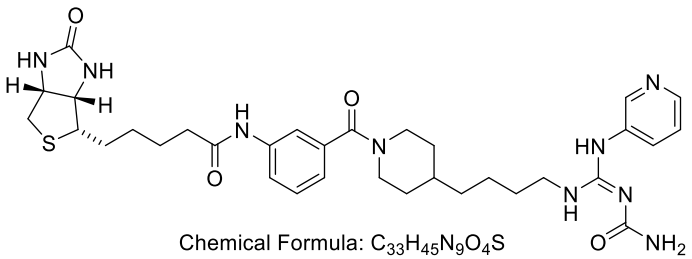

Chemical Formula: $C_{33}H_{45}N_9O_4S$
Molecular Weight: 663,84

Following **General Procedure K**, biotin (1 eq, 30 µmol, 3.7 mg) and HATU (1.1 eq, 30 µmol, 11.4 mg) were dissolved in DMF (abs., 2.4 mL). DIPEA (2 eq, 50 µmol, 8.8 µL) was added and the resulting mixture stirred for 20 min at r.t. Then, intermediate **113** (1 eq, 0.03 mmol, 13 mg) was added and the resulting mixture stirred overnight at r.t. The reaction progress was monitored by HPLC (method 11). After completion, the work-up was performed as described in **General Procedure K**, and purification by preparative HPLC (method 11, t_R = 11.20 min) afforded intermediate **121** (44% yield, 0.01 mmol, 9.1 mg) as a white solid after lyophilisation. MS (ESI, positive mode): found *m/z* = 664.4 $[M+H]^+$, calculated *m/z* = 664.4 $[M+H]^+$.

***N*-(4-(4-hydroxypiperidin-4-yl)butyl)isoindoline-2-carboxamide, TFA salt (122)**

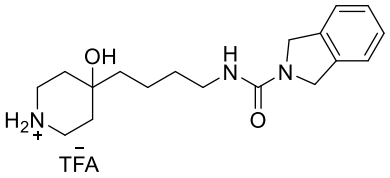

Chemical Formula: $C_{20}H_{28}N_3O_4F_3$
Molecular Weight: 431,44

Following **General Procedure C variation 2**, intermediate **119** (1 eq, 0.05 mmol, 21 mg) was dissolved in a solution of 20 % TFA in DCM (6 mL). The reaction mixture was stirred at r.t. for 30 min. The reaction progress was monitored by TLC (SiO_2, DCM/MeOH: 10/1) and HPLC (method 2). After completion, the work-up was performed as described in **General Procedure C**, and without further purification, intermediate **122** (80% yield, 0.04 mmol, 17.3 mg) was afforded as oil. **HPLC:** t_R/min = 9.89 min.

***tert*-butyl(2-((*tert*-butoxycarbonyl)oxy)-4-(4-hydroxy-4-(4-(isoindoline-2-carboxamido)butyl)piperidine-1-carbonyl)phenyl)carbamate (123)**

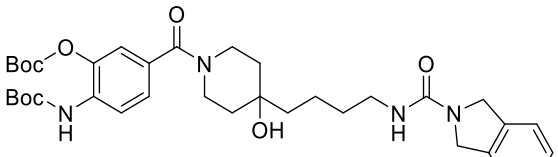

Chemical Formula: $C_{35}H_{48}N_4O_8$
Molecular Weight: 652,79

Following **General Procedure F**, intermediate **122** (1 eq, 0.05 mmol, 22 mg) and intermediate **120** (2 eq, 0.1 mmol, 35 mg) were dissolved in DCM (abs., 1 mL). Then, DIPEA (2.2 eq, 0.11 mmol, 19 µL), HOBt (2 eq, 0.1 mmol, 13 mg) and DCC (2 eq, 0.1 mmol, 21 mg) were added sequentially to the reaction mixture and stirred overnight at r.t. The reaction progress was monitored by TLC (SiO_2, DCM/MeOH: 9/1). After completion, the work-up was performed as described in **General Procedure F,** and purification by preparative HPLC (method 1, t_R = 13.82 min) afforded intermediate **123** (30 % yield, 0.02 mmol, 9.8 mg) as white powder after lyophilisation. MS (ESI, positive mode): found *m/z* = 653.2 $[M+H]^+$, calculated *m/z* = 653.4 $[M+H]^+$.

***N*-(4-(1-(4-amino-3-hydroxybenzoyl)-4-hydroxypiperidin-4-yl)butyl)isoindoline-2-carboxamide TFA salt (124)**

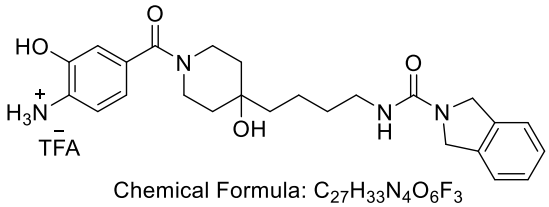

Chemical Formula: $C_{27}H_{33}N_4O_6F_3$
Molecular Weight: 566,56

Following **General Procedure C variation 2**, Intermediate **123** (1 eq, 0.02 mmol, 13 mg) was dissolved in a solution of 20 % TFA in DCM (4 mL). The reaction mixture was stirred for 20 min at r.t. The reaction progress was monitored by TLC (SiO_2, DCM/MeOH: 10/1) and HPLC (method 2). After completion, the work-up was performed as described in **General Procedure C**, and without further purification intermediate **124** (65 % yield, 0.01 mmol, 7.4 mg) was afforded as a white solid. **^{1}H-NMR (500 MHz, d6-DMSO):** δ/ppm = 7.33 – 7.23 (m, 4H), 6.73 (d, J = 1.8 Hz, 1H), 6.68 – 6.58 (m, 2H), 6.23 (d, J = 5.6 Hz, 1H), 4.56 (s, 4H), 1.48 – 1.33 (m, 10H). **HPLC:** t_R/min = 8.14. MS (ESI, positive mode): found *m/z* = 453.3 $[M+H]^+$, calculated *m/z* = 453.4 $[M+H]^+$.

7. Bibliography

(1) *Cancer*. https://www.who.int/news-room/fact-sheets/detail/cancer (accessed 2023-01-03).

(2) Senga, S. S.; Grose, R. P. Hallmarks of Cancer—the New Testament. *Open Biol* **2021**, *11* (1). https://doi.org/10.1098/RSOB.200358/.

(3) Watson, J. D.; Crick, F. H. C. Molecular Structure of Nucleic Acids: A Structure for Deoxyribose Nucleic Acid. *Nature 1953 171:4356* **1953**, *171* (4356), 737–738. https://doi.org/10.1038/171737a0.

(4) Smith, A. E.; Smith, R.; Paucha, E. Characterization of Different Tumor Antigens Present in Cells Transformed by Simian Virus 40. *Cell* **1979**, *18* (2), 335–346. https://doi.org/10.1016/0092-8674(79)90053-9.

(5) Melero, J. A.; Stitt, D. T.; Mangel, W. F.; Carroll, R. B. Identification of New Polypeptide Species (48-55K) Immunoprecipitable by Antiserum to Purified Large T Antigen and Present in SV40-Infected and -Transformed Cells. *Virology* **1979**, *93* (2), 466–480. https://doi.org/10.1016/0042-6822(79)90250-2.

(6) M, K.; E, M.; R, C.; P, M. Simian Virus 40-Transformed Cells Express New Species of Proteins Precipitable by Anti-Simian Virus 40 Tumor Serum. *J Virol* **1979**, *31* (2), 472–483. https://doi.org/10.1128/JVI.31.2.472-483.1979.

(7) Mullis, K.; Faloona, F.; Scharf, S.; Saiki, R.; Horn, G.; Erlich, H. Specific Enzymatic Amplification of DNA in Vitro: The Polymerase Chain Reaction. *Cold Spring Harb Symp Quant Biol* **1986**, *51 Pt 1* (1), 263–273. https://doi.org/10.1101/SQB.1986.051.01.032.

(8) Hanahan, D.; Weinberg, R. A. *The Hallmarks of Cancer Review Evolve Progressively from Normalcy via a Series of Pre*; 2000; Vol. 100.

(9) Hanahan, D. Hallmarks of Cancer: New Dimensions. *Cancer Discovery*. American Association for Cancer Research Inc. January 1, 2022, pp 31–46. https://doi.org/10.1158/2159-8290.CD-21-1059.

(10) Weinberg, R. A. (Robert A. *The Biology of Cancer*, second.; 2014.

(11) Liu, J. K. H.; Irvine, A. F.; Jones, R. L.; Samson, A. Immunotherapies for Hepatocellular Carcinoma. *Cancer Medicine*. John Wiley and Sons Inc February 1, 2022, pp 571–591. https://doi.org/10.1002/cam4.4468.

(12) Lowenstein, P. R.; Castro, M. G. Evolutionary Basis of a New Gene- and Immune-Therapeutic Approach for the Treatment of Malignant Brain Tumors: From Mice to Clinical Trials for Glioma Patients. *Clinical Immunology* **2018**, *189*, 43–51. https://doi.org/10.1016/j.clim.2017.07.006.

(13) Ketabat, F.; Pundir, M.; Mohabatpour, F.; Lobanova, L.; Koutsopoulos, S.; Hadjiiski, L.; Chen, X.; Papagerakis, P.; Papagerakis, S. Controlled Drug Delivery Systems for Oral Cancer Treatment—Current Status and Future Perspectives. *Pharmaceutics*. MDPI AG July 1, 2019. https://doi.org/10.3390/pharmaceutics11070302.

(14) Gomis, R. R.; Gawrzak, S. Tumor Cell Dormancy. *Mol Oncol* **2017**, *11* (1), 62–78. https://doi.org/10.1016/j.molonc.2016.09.009.

(15) Zhong, L.; Li, Y.; Xiong, L.; Wang, W.; Wu, M.; Yuan, T.; Yang, W.; Tian, C.; Miao, Z.; Wang, T.; Yang, S. Small Molecules in Targeted Cancer Therapy: Advances, Challenges, and Future Perspectives. *Signal Transduction and Targeted Therapy*. Springer Nature December 1, 2021. https://doi.org/10.1038/s41392-021-00572-w.

6. Bibliography

(16) Kurzrock, R.; Markman, M. *Targeted Cancer Therapy*, 1st ed.; Humana Press, 2008.

(17) Soverini, S.; Bassan, R.; Lion, T. Treatment and Monitoring of Philadelphia Chromosome-Positive Leukemia Patients: Recent Advances and Remaining Challenges. *Journal of Hematology & Oncology 2019 12:1* **2019**, *12* (1), 1–14. https://doi.org/10.1186/S13045-019-0729-2.

(18) Cromm, P. M.; Crews, C. M. The Proteasome in Modern Drug Discovery: Second Life of a Highly Valuable Drug Target. *ACS Cent Sci* **2017**, *3* (8), 830. https://doi.org/10.1021/ACSCENTSCI.7B00252.

(19) Meehan, R. S.; Chen, A. P. New Treatment Option for Ovarian Cancer: PARP Inhibitors. *Gynecol Oncol Res Pract* **2016**, *3* (1). https://doi.org/10.1186/S40661-016-0024-7.

(20) Zahavi, D.; Weiner, L. Monoclonal Antibodies in Cancer Therapy. *Antibodies* **2020**, *9* (3), 34. https://doi.org/10.3390/antib9030034.

(21) Kunert, R.; Reinhart, D. Advances in Recombinant Antibody Manufacturing. *Appl Microbiol Biotechnol* **2016**, *100* (8), 3451–3461. https://doi.org/10.1007/S00253-016-7388-9/FIGURES/3.

(22) Kennedy, L. B.; Salama, A. K. S. A Review of Cancer Immunotherapy Toxicity. *CA Cancer J Clin* **2020**, *70* (2), 86–104. https://doi.org/10.3322/caac.21596.

(23) Heeke, A. L.; Tan, A. R. Checkpoint Inhibitor Therapy for Metastatic Triple-Negative Breast Cancer. *Cancer and Metastasis Reviews* **2021**, *40* (2), 537–547. https://doi.org/10.1007/S10555-021-09972-4/TABLES/2.

(24) Tolcher, A. W. The Evolution of Antibody-Drug Conjugates: A Positive Inflexion Point. *American Society of Clinical Oncology Educational Book* **2020**, No. 40, 127–134. https://doi.org/10.1200/edbk_281103.

(25) Ryan, D.; Bodei, L. Radioimmunotherapy in Oncology. *Curr Radiol Rep* **2017**, *5* (12), 1–9. https://doi.org/10.1007/S40134-017-0258-0/METRICS.

(26) Sharma, S. K.; Bagshawe, K. D. Translating Antibody Directed Enzyme Prodrug Therapy (ADEPT) and Prospects for Combination. *http://dx.doi.org/10.1080/14712598.2017.1247802* **2016**, *17* (1), 1–13. https://doi.org/10.1080/14712598.2017.1247802.

(27) Domínguez-Escrig, J. L.; Ramón-Borja, J. C. [Focal Laser Ablation and Photodynamic Vascular Therapy with Soluble TOOKAD® in the Treatment of Low Risk Prostate Cancer]. *Arch Esp Urol* **2016**, *69* (6), 327–336.

(28) Rück, A.; Böhmler, A.; Steiner, R. PDT with TOOKAD(®) Studied in the Chorioallantoic Membrane of Fertilized Eggs. *Photodiagnosis Photodyn Ther* **2005**, *2* (1), 79–90. https://doi.org/10.1016/S1572-1000(05)00006-2.

(29) Chu, B. C. F.; Whiteley, J. M. High Molecular Weight Derivatives of Methotrexate as Chemotherapeutic Agents. *Mol Pharmacol* **1977**, *13* (1).

(30) Szekerke, M.; Wade, R.; Whisson, M. E. The Use of Macromolecules as Carriers of Cytotoxic Groups (Part I) Conjugates of Nitrogen Mustards with Proteins, Polypeptidyl Proteins and Polypeptides. *Neoplasma* **1972**, *19* (3), 199–209.

(31) Yu, J.; Song, Y.; Tian, W. How to Select IgG Subclasses in Developing Anti-Tumor Therapeutic Antibodies. *Journal of Hematology and Oncology*. BioMed Central Ltd. May 5, 2020. https://doi.org/10.1186/s13045-020-00876-4.

6. Bibliography

(32) Leung, D.; Wurst, J. M.; Liu, T.; Martinez, R. M.; Datta-Mannan, A.; Feng, Y. Antibody Conjugates-Recent Advances and Future Innovations. *Antibodies*. MDPI March 1, 2020. https://doi.org/10.3390/antib9010002.

(33) Liu, H.; May, K. Disulfide Bond Structures of IgG Molecules. *https://doi.org/10.4161/mabs.4.1.18347* **2012**, *4* (1), 17–23. https://doi.org/10.4161/MABS.4.1.18347.

(34) Evans, R.; Thurber, G. M. Design of High Avidity and Low Affinity Antibodies for in Situ Control of Antibody Drug Conjugate Targeting. *Scientific Reports 2022 12:1* **2022**, *12* (1), 1–11. https://doi.org/10.1038/s41598-022-11648-0.

(35) *Bioconjugation*; Massa, S., Devoogdt, N., Eds.; Humana Press, 2019.

(36) Wilkinson, I.; Anderson, S.; Fry, J.; Julien, L. A.; Neville, D.; Qureshi, O.; Watts, G.; Hale, G. Fc-Engineered Antibodies with Immune Effector Functions Completely Abolished. *PLoS One* **2021**, *16* (12 December). https://doi.org/10.1371/journal.pone.0260954.

(37) Aoyama, M.; Tada, M.; Yokoo, H.; Demizu, Y.; Ishii-Watabe, A. Fcγ Receptor-Dependent Internalization and Off-Target Cytotoxicity of Antibody-Drug Conjugate Aggregates. *Pharm Res* **2022**, *39* (1), 89–103. https://doi.org/10.1007/s11095-021-03158-x.

(38) Saunders, K. O. Conceptual Approaches to Modulating Antibody Effector Functions and Circulation Half-Life. *Frontiers in Immunology*. Frontiers Media S.A. 2019. https://doi.org/10.3389/fimmu.2019.01296.

(39) Lahnsteiner, M.; Kastner, A.; Mayr, J.; Roller, A.; Keppler, B. K.; Kowol, C. R. Improving the Stability of Maleimide–Thiol Conjugation for Drug Targeting. *Chemistry - A European Journal* **2020**, *26* (68), 15867–15870. https://doi.org/10.1002/chem.202003951.

(40) Sheyi, R.; de la Torre, B. G.; Albericio, F. Linkers: An Assurance for Controlled Delivery of Antibody-Drug Conjugate. *Pharmaceutics*. MDPI February 1, 2022. https://doi.org/10.3390/pharmaceutics14020396.

(41) Lu, J.; Jiang, F.; Lu, A.; Zhang, G. Linkers Having a Crucial Role in Antibody–Drug Conjugates. *Int J Mol Sci* **2016**, *17* (4). https://doi.org/10.3390/IJMS17040561.

(42) Pettinato, M. C. Introduction to Antibody-Drug Conjugates. *Antibodies*. MDPI December 1, 2021. https://doi.org/10.3390/antib10040042.

(43) Wang, Y.; Fan, S.; Zhong, W.; Zhou, X.; Li, S. Development and Properties of Valine-Alanine Based Antibody-Drug Conjugates with Monomethyl Auristatin E as the Potent Payload. *Int J Mol Sci* **2017**, *18* (9). https://doi.org/10.3390/IJMS18091860.

(44) Dorywalska, M.; Dushin, R.; Moine, L.; Farias, S. E.; Zhou, D.; Navaratnam, T.; Lui, V.; Hasa-Moreno, A.; Casas, M. G.; Tran, T. T.; Delaria, K.; Liu, S. H.; Foletti, D.; O'Donnell, C. J.; Pons, J.; Shelton, D. L.; Rajpal, A.; Strop, P. Molecular Basis of Valine-Citrulline-PABC Linker Instability in Site-Specific ADCs and Its Mitigation by Linker Design. *Mol Cancer Ther* **2016**, *15* (5), 958–970. https://doi.org/10.1158/1535-7163.MCT-15-1004.

(45) Biniossek, M. L.; Nägler, D. K.; Becker-Pauly, C.; Schilling, O. Proteomic Identification of Protease Cleavage Sites Characterizes Prime and Non-Prime Specificity of Cysteine Cathepsins B, L, and S. *J Proteome Res* **2011**, *10* (12), 5363–5373. https://doi.org/10.1021/PR200621Z.

6. Bibliography

(46) Beck, A.; Goetsch, L.; Dumontet, C.; Corvaïa, N. Strategies and Challenges for the next Generation of Antibody-Drug Conjugates. *Nat Rev Drug Discov* **2017**, *16* (5), 315–337. https://doi.org/10.1038/NRD.2016.268.

(47) Birrer, M. J.; Moore, K. N.; Betella, I.; Bates, R. C. Antibody-Drug Conjugate-Based Therapeutics: State of the Science. *JNCI: Journal of the National Cancer Institute* **2019**, *111* (6), 538–549. https://doi.org/10.1093/JNCI/DJZ035.

(48) Figueroa-Vazquez, V.; Ko, J.; Breunig, C.; Baumann, A.; Giesen, N.; Palfi, A.; Muller, C.; Lutz, C.; Hechler, T.; Kulke, M.; Muller-Tidow, C.; Kramer, A.; Goldschmidt, H.; Pahl, A.; Raab, M. S. HDP-101, an Anti-Bcma Antibody–Drug Conjugate, Safely Delivers Amanitin to Induce Cell Death in Proliferating and Resting Multiple Myeloma Cells. *Mol Cancer Ther* **2021**, *20* (2), 367–378. https://doi.org/10.1158/1535-7163.MCT-20-0287.

(49) Doronina, S. O.; Toki, B. E.; Torgov, M. Y.; Mendelsohn, B. A.; Cerveny, C. G.; Chace, D. F.; DeBlanc, R. L.; Gearing, R. P.; Bovee, T. D.; Siegall, C. B.; Francisco, J. A.; Wahl, A. F.; Meyer, D. L.; Senter, P. D. Development of Potent Monoclonal Antibody Auristatin Conjugates for Cancer Therapy. *Nature Biotechnology 2003 21:7* **2003**, *21* (7), 778–784. https://doi.org/10.1038/nbt832.

(50) Liu, C.; Tadayoni, B. M.; Bourret, L. A.; Mattocks, K. M.; Derr, S. M.; Widdison, W. C.; Kedersha, N. L.; Ariniello, P. D.; Goldmacher, V. S.; Lambert, J. M.; Blättler, W. A.; Chari, R. V. J. Eradication of Large Colon Tumor Xenografts by Targeted Delivery of Maytansinoids. *Proc Natl Acad Sci U S A* **1996**, *93* (16), 8618–8623. https://doi.org/10.1073/PNAS.93.16.8618.

(51) Tsugaya, M.; Washida, H.; Hirao, N.; Hachisuka, Y.; Sakagami, H.; Iwase, Y. The Treatment of Bladder Cancer by Neothramycin. 泌尿器科紀要 **1986**, *32* (10), 1443–1448.

(52) Kamal, A.; Rao, M. V.; Laxman, N.; Ramesh, G.; Reddy, G. S. K. Recent Developments in the Design, Synthesis and Structure-Activity Relationship Studies of Pyrrolo[2,1-c][1,4]Benzodiazepines as DNA-Interactive Antitumour Antibiotics. *Curr Med Chem Anticancer Agents* **2002**, *2* (2), 215–254. https://doi.org/10.2174/1568011023354119.

(53) Yasuzawa, T.; Iida, T.; Muroi, K.; Ichimura, M.; Takahashi, K.; Sano, H. Structures of duocarmycins, novel antitumor antibiotics produced by streptomyces sp. *Chem Pharm Bull (Tokyo)* **1988**, *36* (9), 3728–3731. https://doi.org/10.1248/CPB.36.3728.

(54) Lutz, C.; Simon, W.; Werner-Simon, S.; Pahl, A.; Müller, C. Total Synthesis of α- and β-Amanitin. *Angew Chem Int Ed Engl* **2020**, *59* (28), 11390–11393. https://doi.org/10.1002/ANIE.201914935.

(55) Böhnke, N.; Berger, M.; Griebenow, N.; Rottmann, A.; Erkelenz, M.; Hammer, S.; Berndt, S.; Günther, J.; Wengner, A. M.; Stelte-Ludwig, B.; Mahlert, C.; Greven, S.; Dietz, L.; Jörißen, H.; Barak, N.; Bömer, U.; Hillig, R. C.; Eberspaecher, U.; Weiske, J.; Giese, A.; Mumberg, D.; Nising, C. F.; Weinmann, H.; Sommer, A. A Novel NAMPT Inhibitor-Based Antibody-Drug Conjugate Payload Class for Cancer Therapy. *Bioconjug Chem* **2022**, *33* (6), 1210–1221. https://doi.org/10.1021/ACS.BIOCONJCHEM.2C00178/ASSET/IMAGES/LARGE/BC2C00178_0005.JPEG.

(56) Lahnsteiner, M.; Alexanderk Astner +,]; Josefmayr,]; Roller, A.; Keppler, B. K.; Kowol, C. R.; Lahnsteiner,] M; Kastner, + A; Mayr, J.; Keppler, B. K.; Owol, C. R. K. Improving the Stability of Maleimide–Thiol Conjugation for Drug Targeting. *Chemistry – A European Journal* **2020**, *26* (68), 15867–15870. https://doi.org/10.1002/CHEM.202003951.

(57) Szijj, P. A.; Bahou, C.; Chudasama, V. Minireview: Addressing the Retro-Michael Instability of Maleimide Bioconjugates. *Drug Discov Today Technol* **2018**, *30*, 27–34. https://doi.org/10.1016/J.DDTEC.2018.07.002.

(58) Tumey, L. N.; Charati, M.; He, T.; Sousa, E.; Ma, D.; Han, X.; Clark, T.; Casavant, J.; Loganzo, F.; Barletta, F.; Lucas, J.; Graziani, E. I. Mild Method for Succinimide Hydrolysis on ADCs: Impact on ADC Potency, Stability, Exposure, and Efficacy. *Bioconjug Chem* **2014**, *25* (10), 1871–1880. https://doi.org/10.1021/BC500357N/SUPPL_FILE/BC500357N_SI_001.PDF.

(59) Lyon, R. P.; Setter, J. R.; Bovee, T. D.; Doronina, S. O.; Hunter, J. H.; Anderson, M. E.; Balasubramanian, C. L.; Duniho, S. M.; Leiske, C. I.; Li, F.; Senter, P. D. Self-Hydrolyzing Maleimides Improve the Stability and Pharmacological Properties of Antibody-Drug Conjugates. *Nature Biotechnology 2014 32:10* **2014**, *32* (10), 1059–1062. https://doi.org/10.1038/nbt.2968.

(60) Fontaine, S. D.; Reid, R.; Robinson, L.; Ashley, G. W.; Santi, D. V. Long-Term Stabilization of Maleimide-Thiol Conjugates. *Bioconjug Chem* **2015**, *26* (1), 145–152. https://doi.org/10.1021/BC5005262/SUPPL_FILE/BC5005262_SI_001.PDF.

(61) Kalia, D.; Malekar, P. V.; Parthasarathy, M. Exocyclic Olefinic Maleimides: Synthesis and Application for Stable and Thiol-Selective Bioconjugation. *Angewandte Chemie International Edition* **2016**, *55* (4), 1432–1435. https://doi.org/10.1002/ANIE.201508118.

(62) Bernardes, G. J. L.; Chalker, J. M.; Errey, J. C.; Davis, B. G. Facile Conversion of Cysteine and Alkyl Cysteines to Dehydroalanine on Protein Surfaces: Versatile and Switchable Access to Functionalized Proteins. *J Am Chem Soc* **2008**, *130* (15), 5052–5053. https://doi.org/10.1021/JA800800P/SUPPL_FILE/JA800800P-FILE003.PDF.

(63) Badescu, G.; Bryant, P.; Bird, M.; Henseleit, K.; Swierkosz, J.; Parekh, V.; Tommasi, R.; Pawlisz, E.; Jurlewicz, K.; Farys, M.; Camper, N.; Sheng, X.; Fisher, M.; Grygorash, R.; Kyle, A.; Abhilash, A.; Frigerio, M.; Edwards, J.; Godwin, A. Bridging Disulfides for Stable and Defined Antibody Drug Conjugates. *Bioconjug Chem* **2014**, *25* (6), 1124–1136. https://doi.org/10.1021/BC500148X/ASSET/IMAGES/MEDIUM/BC-2014-00148X_0016.GIF.

(64) Junutula, J. R.; Raab, H.; Clark, S.; Bhakta, S.; Leipold, D. D.; Weir, S.; Chen, Y.; Simpson, M.; Tsai, S. P.; Dennis, M. S.; Lu, Y.; Meng, Y. G.; Ng, C.; Yang, J.; Lee, C. C.; Duenas, E.; Gorrell, J.; Katta, V.; Kim, A.; McDorman, K.; Flagella, K.; Venook, R.; Ross, S.; Spencer, S. D.; Lee Wong, W.; Lowman, H. B.; Vandlen, R.; Sliwkowski, M. X.; Scheller, R. H.; Polakis, P.; Mallet, W. Site-Specific Conjugation of a Cytotoxic Drug to an Antibody Improves the Therapeutic Index. *Nature Biotechnology 2008 26:8* **2008**, *26* (8), 925–932. https://doi.org/10.1038/nbt.1480.

(65) Hallam, T. J.; Wold, E.; Wahl, A.; Smider, V. V. Antibody Conjugates with Unnatural Amino Acids. *Mol Pharm* **2015**, *12* (6), 1848–1862. https://doi.org/10.1021/acs.molpharmaceut.5b00082.

(66) Peters, C.; Brown, S. Antibody-Drug Conjugates as Novel Anti-Cancer Chemotherapeutics. *Biosci Rep* **2015**, *35* (4). https://doi.org/10.1042/BSR20150089.

(67) Study of Single Agent Belantamab Mafodotin Versus Pomalidomide Plus Low-dose Dexamethasone (Pom/Dex) in Participants With Relapsed/Refractory Multiple Myeloma (RRMM) - Full Text View - *ClinicalTrials.gov*. https://clinicaltrials.gov/ct2/show/NCT04162210 (accessed 2023-04-14).

(68) Chelariu-Raicu, A.; Mahner, S.; Moore, K. N.; Lorusso, D.; Coleman, R. L. Integrating Antibody Drug Conjugates in the Management of Gynecologic Cancers. *International Journal of Gynecologic Cancer* **2023**, *33* (3), 420–429. https://doi.org/10.1136/IJGC-2022-003701.

6. Bibliography

(69) Teicher, B. A.; Chari, R. V. J. Antibody Conjugate Therapeutics: Challenges and Potential. *Clinical Cancer Research*. October 15, 2011, pp 6389–6397. https://doi.org/10.1158/1078-0432.CCR-11-1417.

(70) Staudacher, A. H.; Brown, M. P. Antibody Drug Conjugates and Bystander Killing: Is Antigen-Dependent Internalisation Required? *British Journal of Cancer 2017 117:12* **2017**, *117* (12), 1736–1742. https://doi.org/10.1038/bjc.2017.367.

(71) Deonarain, M. P.; Xue, Q. Tackling Solid Tumour Therapy with Small-Format Drug Conjugates. *Antibody Therapeutics*. Oxford University Press December 1, 2020, pp 237–245. https://doi.org/10.1093/abt/tbaa024.

(72) Tolcher, A. W.; Carneiro, B. A.; Dowlati, A.; Razak, A. R. A.; Chae, Y. K.; Villella, J. A.; Coppola, S.; Englert, S.; Phillips, A. C.; Souers, A. J.; Salman, Z.; Penugonda, S.; Powderly, J. D.; LoRusso, P. A First-in-Human Study of Mirzotamab Clezutoclax as Monotherapy and in Combination with Taxane Therapy in Relapsed/Refractory Solid Tumors: Dose Escalation Results. *https://doi.org/10.1200/JCO.2021.39.15_suppl.3015* **2021**, *39* (15_suppl), 3015–3015. https://doi.org/10.1200/JCO.2021.39.15_SUPPL.3015.

(73) Zhang, X.; Liu, X.; Zhou, D.; Zheng, G. Targeting Anti-Apoptotic BCL-2 Family Proteins for Cancer Treatment. *https://doi.org/10.4155/fmc-2020-0004* **2020**, *12* (7), 563–565. https://doi.org/10.4155/FMC-2020-0004.

(74) Kostova, V.; Désos, P.; Starck, J. B.; Kotschy, A. The Chemistry behind Adcs. *Pharmaceuticals*. MDPI May 1, 2021. https://doi.org/10.3390/ph14050442.

(75) Lee, J.; Kim, H.; Lee, J. E.; Shin, S. J.; Oh, S.; Kwon, G.; Kim, H.; Choi, Y. Y.; White, M. A.; Paik, S.; Cheong, J. H.; Kim, H. S. Selective Cytotoxicity of the NAMPT Inhibitor FK866 Toward Gastric Cancer Cells With Markers of the Epithelial-Mesenchymal Transition, Due to Loss of NAPRT. *Gastroenterology* **2018**, *155* (3), 799-814.e13. https://doi.org/10.1053/j.gastro.2018.05.024.

(76) Cambronne, X. A.; Kraus, W. L. Location, Location, Location: Compartmentalization of NAD+ Synthesis and Functions in Mammalian Cells. *Trends in Biochemical Sciences*. Elsevier Ltd October 1, 2020, pp 858–873. https://doi.org/10.1016/j.tibs.2020.05.010.

(77) Garten, A.; Petzold, S.; Körner, A.; Imai, S. ichiro; Kiess, W. Nampt: Linking NAD Biology, Metabolism and Cancer. *Trends in Endocrinology and Metabolism*. April 2009, pp 130–138. https://doi.org/10.1016/j.tem.2008.10.004.

(78) Cambronne, X. A.; Kraus, W. L. Location, Location, Location: Compartmentalization of NAD+ Synthesis and Functions in Mammalian Cells. *Trends in Biochemical Sciences*. Elsevier Ltd October 1, 2020, pp 858–873. https://doi.org/10.1016/j.tibs.2020.05.010.

(79) Wei, Y.; Xiang, H.; Zhang, W. Review of Various NAMPT Inhibitors for the Treatment of Cancer. *Front Pharmacol* **2022**, *13*, 3385. https://doi.org/10.3389/FPHAR.2022.970553/BIBTEX.

(80) Morales, J. C.; Li, L.; Fattah, F. J.; Dong, Y.; Bey, E. A.; Patel, M.; Gao, J.; Boothman, D. A. Review of Poly (ADP-Ribose) Polymerase (PARP) Mechanisms of Action and Rationale for Targeting in Cancer and Other Diseases. *Critical Reviews™ in Eukaryotic Gene Expression* **2014**, *24* (1), 15–28. https://doi.org/10.1615/CRITREVEUKARYOTGENEEXPR.2013006875.

(81) Nakagawa, T.; Guarente, L. Sirtuins at a Glance. *Journal of Cell Science*. March 15, 2011, pp 833–838. https://doi.org/10.1242/jcs.081067.

(82) Ramsey, K. M.; Yoshino, J.; Brace, C. S.; Abrassart, D.; Kobayashi, Y.; Marcheva, B.; Hong, H. K.; Chong, J. L.; Buhr, E. D.; Lee, C.; Takahashi, J. S.; Imai, S. I.; Bass, J.

Circadian Clock Feedback Cycle through NAMPT-Mediated NAD+ Biosynthesis. *Science (1979)* **2009**, *324* (5927), 651–654. https://doi.org/10.1126/SCIENCE.1171641/SUPPL_FILE/RAMSEY.SOM.PDF.

(83) Kiledjian, M. Eukaryotic RNA 5′-End NAD+ Capping and DeNADding. *Trends in Cell Biology*. Elsevier Ltd June 1, 2018, pp 454–464. https://doi.org/10.1016/j.tcb.2018.02.005.

(84) Burgos, E. S.; Ho, M. C.; Almo, S. C.; Schramm, V. L. A Phosphoenzyme Mimic, Overlapping Catalytic Sites and Reaction Coordinate Motion for Human NAMPT. *Proc Natl Acad Sci U S A* **2009**, *106* (33), 13748–13753. https://doi.org/10.1073/PNAS.0903898106/SUPPL_FILE/0903898106SI.PDF.

(85) Carbone, F.; Liberale, L.; Bonaventura, A.; Vecchié, A.; Casula, M.; Cea, M.; Monacelli, F.; Caffa, I.; Bruzzone, S.; Montecucco, F.; Nencioni, A. Regulation and Function of Extracellular Nicotinamide Phosphoribosyltransferase/Visfatin. *Compr Physiol* **2017**, *7* (2), 603–621. https://doi.org/10.1002/CPHY.C160029.

(86) Nahimana, A.; Attinger, A.; Aubry, D.; Greaney, P.; Ireson, C.; Thougaard, A. V.; Tjørnelund, J.; Dawson, K. M.; Dupuis, M.; Duchosal, M. A. The NAD Biosynthesis Inhibitor APO866 Has Potent Antitumor Activity against Hematologic Malignancies. *Blood* **2009**, *113* (14), 3276–3286. https://doi.org/10.1182/BLOOD-2008-08-173369.

(87) Lee, J.; Kim, H.; Lee, J. E.; Shin, S. J.; Oh, S.; Kwon, G.; Kim, H.; Choi, Y. Y.; White, M. A.; Paik, S.; Cheong, J. H.; Kim, H. S. Selective Cytotoxicity of the NAMPT Inhibitor FK866 Toward Gastric Cancer Cells With Markers of the Epithelial-Mesenchymal Transition, Due to Loss of NAPRT. *Gastroenterology* **2018**, *155* (3), 799-814.e13. https://doi.org/10.1053/J.GASTRO.2018.05.024.

(88) Peterse, E. F. P.; Van Den Akker, B. E. W. M.; Niessen, B.; Oosting, J.; Suijker, J.; De Jong, Y.; Danen, E. H. J.; Cleton-Jansen, A. M.; Bovée, J. V. M. G. NAD Synthesis Pathway Interference Is a Viable Therapeutic Strategy for Chondrosarcoma. *Mol Cancer Res* **2017**, *15* (12), 1714–1721. https://doi.org/10.1158/1541-7786.MCR-17-0293.

(89) Tateishi, K.; Wakimoto, H.; Iafrate, A. J.; Tanaka, S.; Loebel, F.; Lelic, N.; Wiederschain, D.; Bedel, O.; Deng, G.; Zhang, B.; He, T.; Shi, X.; Gerszten, R. E.; Zhang, Y.; Yeh, J. R. J.; Curry, W. T.; Zhao, D.; Sundaram, S.; Nigim, F.; Koerner, M. V. A.; Ho, Q.; Fisher, D. E.; Roider, E. M.; Kemeny, L. V.; Samuels, Y.; Flaherty, K. T.; Batchelor, T. T.; Chi, A. S.; Cahill, D. P. Extreme Vulnerability of IDH1 Mutant Cancers to NAD+ Depletion. *Cancer Cell* **2015**, *28* (6), 773–784. https://doi.org/10.1016/J.CCELL.2015.11.006.

(90) Pour, Z. B.; Nourbakhsh, M.; Mousavizadeh, K.; Madjd, Z.; Ghorbanhosseini, S. S.; Abdolvahabi, Z.; Hesari, Z.; Mobaser, S. E. Up-Regulation of MiR-381 Inhibits NAD+ Salvage Pathway and Promotes Apoptosis in Breast Cancer Cells. *EXCLI J* **2019**, *18*, 683. https://doi.org/10.17179/EXCLI2019-1431.

(91) Galli, U.; Colombo, G.; Travelli, C.; Tron, G. C.; Genazzani, A. A.; Grolla, A. A. Recent Advances in NAMPT Inhibitors: A Novel Immunotherapic Strategy. *Frontiers in Pharmacology*. Frontiers Media S.A. May 12, 2020. https://doi.org/10.3389/fphar.2020.00656.

(92) Ravaud, A.; Cerny, T.; Terret, C.; Wanders, J.; Bui, B. N.; Hess, D.; Droz, J. P.; Fumoleau, P.; Twelves, C. Phase I Study and Pharmacokinetic of CHS-828, a Guanidino-Containing Compound, Administered Orally as a Single Dose Every 3 Weeks in Solid Tumours: An ECSG/EORTC Study. *Eur J Cancer* **2005**, *41* (5), 702–707. https://doi.org/10.1016/J.EJCA.2004.12.023.

(93) Watson, M.; Roulston, A.; Bélec, L.; Billot, X.; Marcellus, R.; Bédard, D.; Bernier, C.; Branchaud, S.; Chan, H.; Dairi, K.; Gilbert, K.; Goulet, D.; Gratton, M.-O.; Isakau, H.; Jang, A.; Khadir, A.; Koch, E.; Lavoie, M.; Lawless, M.; Nguyen, M.; Paquette, D.; Turcotte, É.; Berger, A.; Mitchell, M.; Shore, G. C.; Beauparlant, P. The Small Molecule GMX1778 Is a Potent Inhibitor of NAD+ Biosynthesis: Strategy for Enhanced Therapy in Nicotinic Acid Phosphoribosyltransferase 1-Deficient Tumors. *Mol Cell Biol* **2009**, *29* (21), 5872–5888. https://doi.org/10.1128/MCB.00112-09.

(94) Hasmann, M.; Schemainda, I. FK866, a Highly Specific Noncompetitive Inhibitor of Nicotinamide Phosphoribosyltransferase, Represents a Novel Mechanism for Induction of Tumor Cell Apoptosis; 2003; Vol. 63. http://aacrjournals.org/cancerres/article-pdf/63/21/7436/2509899/7436.pdf.

(95) Bair, K. W.; Baumeister, T.; Buckmelter, A. J.; Clodfelter, K. H.; Dragovich, P.; Gosselin, F.; Han, B.; Lin, J.; Reynolds, D. J.; Roth, B.; Smith, C. C.; Wang, Z.; Yuen, P.-W.; Zheng, X. N-(Sulfonylbenzyl)Heteroarylcarboxamide Derivatives as Nicotinamide Phosphoribosyltransferase (NAMPT) Inhibitors and Their Preparation and Use for the Treatment of Diseases, March 8, 2012.

(96) Burkholder, T. P.; Del Prado, M. F.; Fernandez, M. C.; Heinz II, L. J.; Prieto, L.; Zhao, G. Preparation of Novel Pyridyloxyacetyl Tetrahydroisoquinoline Compounds Useful as NAMPT Inhibitors, April 16, 2015.

(97) Curtin, M. L.; Sorensen, B. K.; Heyman, H. R.; Clark, R. F.; Woller, K. R.; Shah, O. J.; Michaelides, M.; Tse, C.; Vasudevan, A.; Mack, H.; Hansen, T. M.; Sweis, R.; Pliushchev, M. A. Dihydroisoindolecarboxamide Derivatives as NAMPT and ROCK Inhibitors and Their Preparation, May 17, 2012.

(98) Polinsky, A.; Korotchkina, L.; Vujcic, S.; Chernova, O. Preparation of Benzamide and Nicotinamide Compounds for the Treatment of Cancer, July 2, 2015.

(99) Olesen, U. H.; Christensen, M. K.; Björkling, F.; Jäättelä, M.; Jensen, P. B.; Sehested, M.; Nielsen, S. J. Anticancer Agent CHS-828 Inhibits Cellular Synthesis of NAD. *Biochem Biophys Res Commun* **2008**, *367* (4), 799–804. https://doi.org/10.1016/J.BBRC.2008.01.019.

(100) *A Phase I/II Study of GMX1777 in Combination With Temozolomide for the Treatment of Metastatic Melanoma - Full Text View - ClinicalTrials.gov*. https://clinicaltrials.gov/ct2/show/NCT00724841?term=GMX1777&draw=2&rank=1 (accessed 2023-01-23).

(101) *Safety and Efficacy of GMX1777 in the Treatment of Refractory Solid Tumors or Lymphomas - Full Text View - ClinicalTrials.gov*. https://clinicaltrials.gov/ct2/show/NCT00457574?term=GMX1777&draw=2&rank=2 (accessed 2023-01-23).

(102) Von Heideman, A.; Berglund, Å.; Larsson, R.; Nygren, P.; Larsson, R. Safety and Efficacy of NAD Depleting Cancer Drugs: Results of a Phase i Clinical Trial of CHS 828 and Overview of Published Data. *Cancer Chemother Pharmacol* **2010**, *65* (6), 1165–1172. https://doi.org/10.1007/S00280-009-1125-3/METRICS.

(103) *FK866, a Highly Specific Noncompetitive Inhibitor of Nicotinamide Phosphoribosyltransferase, Represents a Novel Mechanism for Induction of Tumor Cell Apoptosis | Cancer Research | American Association for Cancer Research*. https://aacrjournals.org/cancerres/article/63/21/7436/510728/FK866-a-Highly-Specific-Noncompetitive-Inhibitor (accessed 2023-01-24).

(104) Nacarelli, T.; Fukumoto, T.; Zundell, J. A.; Fatkhutdinov, N.; Jean, S.; Cadungog, M. G.; Borowsky, M. E.; Zhang, R. NAMPT Inhibition Suppresses Cancer Stem-like Cells

Associated with Therapy-Induced Senescence in Ovarian Cancer. *Cancer Res* **2020**, *80* (4), 890–900. https://doi.org/10.1158/0008-5472.CAN-19-2830.

(105) Sauer, H.; Kampmann, H.; Khosravi, F.; Sharifpanah, F.; Wartenberg, M. The Nicotinamide Phosphoribosyltransferase Antagonist FK866 Inhibits Growth of Prostate Tumour Spheroids and Increases Doxorubicin Retention without Changes in Drug Transporter and Cancer Stem Cell Protein Expression. *Clin Exp Pharmacol Physiol* **2021**, *48* (3), 422–434. https://doi.org/10.1111/1440-1681.13452.

(106) Xie, H.; Lei, Y.; Mao, Y.; Lan, J.; Yang, J.; Quan, H.; Zhang, T. FK866 Inhibits Colorectal Cancer Metastasis by Reducing NAD+ Levels in Cancer-Associated Fibroblasts. *Genes Genomics* **2022**, *44* (12). https://doi.org/10.1007/S13258-022-01318-W.

(107) Kozako, T.; Aikawa, A.; Ohsugi, T.; Uchida, Y. ichiro; Kato, N.; Sato, K.; Ishitsuka, K.; Yoshimitsu, M.; Honda, S. ichiro. High Expression of NAMPT in Adult T-Cell Leukemia/Lymphoma and Anti-Tumor Activity of a NAMPT Inhibitor. *Eur J Pharmacol* **2019**, *865*. https://doi.org/10.1016/j.ejphar.2019.172738.

(108) Schuster, S.; Penke, M.; Gorski, T.; Gebhardt, R.; Weiss, T. S.; Kiess, W.; Garten, A. FK866-Induced NAMPT Inhibition Activates AMPK and Downregulates MTOR Signaling in Hepatocarcinoma Cells. *Biochem Biophys Res Commun* **2015**, *458* (2), 334–340. https://doi.org/10.1016/J.BBRC.2015.01.111.

(109) Holen, K.; Saltz, L. B.; Hollywood, E.; Burk, K.; Hanauske, A. R. The Pharmacokinetics, Toxicities, and Biologic Effects of FK866, a Nicotinamide Adenine Dinucleotide Biosynthesis Inhibitor. *Invest New Drugs* **2008**, *26* (1), 45–51. https://doi.org/10.1007/S10637-007-9083-2.

(110) Ginet, V.; Puyal, J.; Rummel, C.; Aubry, D.; Breton, C.; Cloux, A. J.; Majjigapu, S. R.; Sordat, B.; Vogel, P.; Bruzzone, S.; Nencioni, A.; Duchosal, M. A.; Nahimana, A. A Critical Role of Autophagy in Antileukemia/Lymphoma Effects of APO866, an Inhibitor of NAD Biosynthesis. *Autophagy* **2014**, *10* (4), 603–617. https://doi.org/10.4161/auto.27722.

(111) Zabka, T. S.; Singh, J.; Dhawan, P.; Liederer, B. M.; Oeh, J.; Kauss, M. A.; Xiao, Y.; Zak, M.; Lin, T.; McCray, B.; La, N.; Nguyen, T.; Beyer, J.; Farman, C.; Uppal, H.; Dragovich, P. S.; O'Brien, T.; Sampath, D.; Misner, D. L. Retinal Toxicity, in Vivo and in Vitro, Associated with Inhibition of Nicotinamide Phosphoribosyltransferase. *Toxicol Sci* **2015**, *144* (1), 163–172. https://doi.org/10.1093/TOXSCI/KFU268.

(112) Zheng, X.; Bauer, P.; Baumeister, T.; Buckmelter, A. J.; Caligiuri, M.; Clodfelter, K. H.; Han, B.; Ho, Y. C.; Kley, N.; Lin, J.; Reynolds, D. J.; Sharma, G.; Smith, C. C.; Wang, Z.; Dragovich, P. S.; Gunzner-Toste, J.; Liederer, B. M.; Ly, J.; O'Brien, T.; Oh, A.; Wang, L.; Wang, W.; Xiao, Y.; Zak, M.; Zhao, G.; Yuen, P. W.; Bair, K. W. Structure-Based Discovery of Novel Amide-Containing Nicotinamide Phosphoribosyltransferase (Nampt) Inhibitors. *J Med Chem* **2013**, *56* (16), 6413–6433. https://doi.org/10.1021/JM4008664/SUPPL_FILE/JM4008664_SI_001.PDF.

(113) Zhao, G.; Green, C. F.; Hui, Y. H.; Prieto, L.; Shepard, R.; Dong, S.; Wang, T.; Tan, B.; Gong, X.; Kays, L.; Johnson, R. L.; Wu, W.; Bhattachar, S.; Prado, M. Del; Gillig, J. R.; Fernandez, M. C.; Roth, K. D.; Buchanan, S.; Kuo, M. S.; Geeganage, S.; Burkholder, T. P. Discovery of a Highly Selective NAMPT Inhibitor That Demonstrates Robust Efficacy and Improved Retinal Toxicity with Nicotinic Acid Coadministration. *Mol Cancer Ther* **2017**, *16* (12), 2677–2688. https://doi.org/10.1158/1535-7163.MCT-16-0674.

(114) Curtin, M. L.; Heyman, H. R.; Clark, R. F.; Sorensen, B. K.; Doherty, G. A.; Hansen, T. M.; Frey, R. R.; Sarris, K. A.; Aguirre, A. L.; Shrestha, A.; Tu, N.; Woller, K.; Pliushchev, M. A.; Sweis, R. F.; Cheng, M.; Wilsbacher, J. L.; Kovar, P. J.; Guo, J.; Cheng, D.;

Longenecker, K. L.; Raich, D.; Korepanova, A. V.; Soni, N. B.; Algire, M. A.; Richardson, P. L.; Marin, V. L.; Badagnani, I.; Vasudevan, A.; Buchanan, F. G.; Maag, D.; Chiang, G. G.; Tse, C.; Michaelides, M. R. SAR and Characterization of Non-Substrate Isoindoline Urea Inhibitors of Nicotinamide Phosphoribosyltransferase (NAMPT). *Bioorg Med Chem Lett* **2017**, *27* (15), 3317–3325. https://doi.org/10.1016/J.BMCL.2017.06.018.

(115) Wilsbacher, J. L.; Cheng, M.; Cheng, D.; Trammell, S. A. J.; Shi, Y.; Guo, J.; Koeniger, S. L.; Kovar, P. J.; He, Y.; Selvaraju, S.; Heyman, H. R.; Sorensen, B. K.; Clark, R. F.; Hansen, T. M.; Longenecker, K. L.; Raich, D.; Korepanova, A. V.; Cepa, S.; Towne, D. L.; Abraham, V. C.; Tang, H.; Richardson, P. L.; McLoughlin, S. M.; Badagnani, I.; Curtin, M. L.; Michaelides, M. R.; Maag, D.; Buchanan, F. G.; Chiang, G. G.; Gao, W.; Rosenberg, S. H.; Brenner, C.; Tse, C. Discovery and Characterization of Novel Nonsubstrate and Substrate NAMPT Inhibitors. *Mol Cancer Ther* **2017**, *16* (7), 1236–1245. https://doi.org/10.1158/1535-7163.MCT-16-0819/86868/AM/DISCOVERY-AND-CHARACTERIZATION-OF-NOVEL-NON.

(116) Cassar, S.; Dunn, C.; Olson, A.; Buck, W.; Fossey, S.; Ramos, M. F.; Sancheti, P.; Stolarik, D. A.; Britton, H.; Cole, T.; Bratcher, N.; Huang, X.; Peterson, R.; Longenecker, K.; LeRoy, B. From the Cover: Inhibitors of Nicotinamide Phosphoribosyltransferase Cause Retinal Damage in Larval Zebrafish. *Toxicol Sci* **2018**, *161* (2), 300–309. https://doi.org/10.1093/TOXSCI/KFX212.

(117) Gudkov, A.; Polinsky, A.; Balan, V.; Chernova, O.; Hall, B. M.; Komarob, P. G.; Kazyulkin, D. N. Removal of Senescence-Associated Macrophages for Treating Age-Related Diseases Using Pharmaceutical Compositions, November 2, 2017.

(118) Somers, K.; Evans, K.; Cheung, L.; Karsa, M.; Pritchard, T.; Kosciolek, A.; Bongers, A.; El-Ayoubi, A.; Forgham, H.; Middlemiss, S.; Mayoh, C.; Jones, L.; Gupta, M.; Kees, U. R.; Chernova, O.; Korotchkina, L.; Gudkov, A. V.; Erickson, S. W.; Teicher, B.; Smith, M. A.; Norris, M. D.; Haber, M.; Lock, R. B.; Henderson, M. J. Effective Targeting of NAMPT in Patient-Derived Xenograft Models of High-Risk Pediatric Acute Lymphoblastic Leukemia. *Leukemia 2019 34:6* **2019**, *34* (6), 1524–1539. https://doi.org/10.1038/s41375-019-0683-6.

(119) Gibson, A. E.; Yeung, C.; Issaq, S. H.; Collins, V. J.; Gouzoulis, M.; Zhang, Y.; Ji, J.; Mendoza, A.; Heske, C. M. Inhibition of Nicotinamide Phosphoribosyltransferase (NAMPT) with OT-82 Induces DNA Damage, Cell Death, and Suppression of Tumor Growth in Preclinical Models of Ewing Sarcoma. *Oncogenesis* **2020**, *9* (9). https://doi.org/10.1038/S41389-020-00264-0.

(120) Korotchkina, L.; Kazyulkin, D.; Komarov, P. G.; Polinsky, A.; Andrianova, E. L.; Joshi, S.; Gupta, M.; Vujcic, S.; Kononov, E.; Toshkov, I.; Tian, Y.; Krasnov, P.; Chernov, M. V.; Veith, J.; Antoch, M. P.; Middlemiss, S.; Somers, K.; Lock, R. B.; Norris, M. D.; Henderson, M. J.; Haber, M.; Chernova, O. B.; Gudkov, A. V. OT-82, a Novel Anticancer Drug Candidate That Targets the Strong Dependence of Hematological Malignancies on NAD Biosynthesis. *Leukemia* **2020**, *34* (7), 1828–1839. https://doi.org/10.1038/S41375-019-0692-5.

(121) Karpov, A. S.; Abrams, T.; Clark, S.; Raikar, A.; D'Alessio, J. A.; Dillon, M. P.; Gesner, T. G.; Jones, D.; Lacaud, M.; Mallet, W.; Martyniuk, P.; Meredith, E.; Mohseni, M.; Nieto-Oberhuber, C. M.; Palacios, D.; Perruccio, F.; Piizzi, G.; Zurini, M.; Bialucha, C. U. Nicotinamide Phosphoribosyltransferase Inhibitor as a Novel Payload for Antibody-Drug Conjugates. *ACS Med Chem Lett* **2018**, *9* (8), 838–842. https://doi.org/10.1021/ACSMEDCHEMLETT.8B00254/ASSET/IMAGES/LARGE/ML-2018-00254Q_0005.JPEG.

(122) Neumann, C. S.; Olivas, K. C.; Anderson, M. E.; Cochran, J. H.; Jin, S.; Li, F.; Loftus, L. V.; Meyer, D. W.; Neale, J.; Nix, J. C.; Pittman, P. G.; Simmons, J. K.; Ulrich, M. L.;

Waight, A. B.; Wong, A.; Zaval, M. C.; Zeng, W.; Lyon, R. P.; Senter, P. D. Targeted Delivery of Cytotoxic NAMPT Inhibitors Using Antibody–Drug Conjugates. *Mol Cancer Ther* **2018**, *17* (12), 2633–2642. https://doi.org/10.1158/1535-7163.MCT-18-0643.

(123) Palacios, D. S.; Meredith, E.; Kawanami, T.; Adams, C.; Chen, X.; Darsigny, V.; Geno, E.; Palermo, M.; Baird, D.; Boynton, G.; Busby, S. A.; George, E. L.; Guy, C.; Hewett, J.; Tierney, L.; Thigale, S.; Weihofen, W.; Wang, L.; White, N.; Yin, M.; Argikar, U. A. Structure Based Design of Nicotinamide Phosphoribosyltransferase (NAMPT) Inhibitors from a Phenotypic Screen. *Bioorg Med Chem Lett* **2018**, *28* (3), 365–370. https://doi.org/10.1016/J.BMCL.2017.12.037.

(124) Neumann, C. S.; Olivas, K. Ligand Drug Conjugates for Targeted Delivery of Nicotinamide Adenine Dinucleotide Salvage Pathway Inhibitors for Treatment of Cancer and Autoimmune Diseases, April 26, 2018.

(125) Neumann, C. S.; Olivas, K. C.; Anderson, M. E.; Cochran, J. H.; Jin, S.; Li, F.; Loftus, L. v.; Meyer, D. W.; Neale, J.; Nix, J. C.; Pittman, P. G.; Simmons, J. K.; Ulrich, M. L.; Waight, A. B.; Wong, A.; Zaval, M. C.; Zeng, W.; Lyon, R. P.; Senter, P. D. Targeted Delivery of Cytotoxic NAMPT Inhibitors Using Antibody–Drug Conjugates. *Mol Cancer Ther* **2018**, *17* (12), 2633–2642. https://doi.org/10.1158/1535-7163.MCT-18-0643.

(126) Boehnke, N.; Griebenow, N.; Sommer, A.; Hammer, S.; Berndt, S.; Stelte-Ludwig, B.; Beier, R.; Mahlert, C.; Greven, S.; Giese, A.; Guenther, J.; Barak, N.; Boemer, U.; Dietz, L.; Joerissen, H.; Erkelenz, M.; Rottmann, A.; Wengner, A. M.; Fernandez-Montalvan, A. E. Antibody Drug Conjugates (ADCS) with NAMPT Inhibitors, January 28, 2021.

(127) Vogel, P.; Duchosal, M.; Aimable, N.; Robina, I.; Mollinedo, F.; Nencioni, A. Preparation of Piperidine Derivatives for the Treatment of Pancreatic Cancer, 2018.

(128) Mitsunobu, O.; Yamada, M. *Preparation of Esters of Carboxylic and Phosphoric Acid via Quaternary Phosphonium Salts*; 1967; Vol. 40.

(129) Hill, S. v; Williams, A.; Longridge, J. L. *Acid-Catalysed Hydrolysis of Cyanamides : Estimates of Carbodi-Imide Basicity and Tautomeric Equilibrium Constant between Carbodi-Imide and Cyanamide*.

(130) Vogel, P.; Duchosal, M.; Aimable, N.; Robina, I.; Mollinedo, F.; Nencioni, A. Preparation of Piperidine Derivatives for the Treatment of Pancreatic Cancer, 2018.

(131) Brown, W. H.; Iverson, B. L.; Anslyn, E. V; Foote, C. S. *Organic Chemistry*, 7th ed.; Wadsworth Cengage learning, 2013.

(132) Gabriel, S. Ueber Eine Darstellungsweise Primärer Amine Aus Den Entsprechenden Halogenverbindungen. *Berichte der deutschen chemischen Gesellschaft* **1887**, *20* (2), 2224–2236. https://doi.org/10.1002/cber.18870200227.

(133) Leo, A.; Hansch, C.; Elkins, D. Partition Coefficients and Their Uses. *Chem Rev* **1971**, *71* (6), 525–616. https://doi.org/10.1021/CR60274A001/ASSET/CR60274A001.FP.PNG_V03.

(134) Nieto-Draghi, C.; Fayet, G.; Creton, B.; Rozanska, X.; Rotureau, P.; De Hemptinne, J. C.; Ungerer, P.; Rousseau, B.; Adamo, C. A General Guidebook for the Theoretical Prediction of Physicochemical Properties of Chemicals for Regulatory Purposes. *Chem Rev* **2015**, *115* (24), 13093–13164. https://doi.org/10.1021/ACS.CHEMREV.5B00215/SUPPL_FILE/CR5B00215_SI_001.PDF.

(135) Sonogashira, K. Development of Pd–Cu Catalyzed Cross-Coupling of Terminal Acetylenes with Sp2-Carbon Halides. *J Organomet Chem* **2002**, *653* (1–2), 46–49. https://doi.org/10.1016/S0022-328X(02)01158-0.

(136) Malesevic, M.; Strijowski, U.; Bächle, D.; Sewald, N. An Improved Method for the Solution Cyclization of Peptides under Pseudo-High Dilution Conditions. *J Biotechnol* **2004**, *112* (1–2), 73–77. https://doi.org/10.1016/J.JBIOTEC.2004.03.015.

(137) *RCSB PDB - 5U2M: Crystal structure of human NAMPT with A-1293201*. https://www.rcsb.org/structure/5U2M (accessed 2022-11-02).

(138) *RCSB PDB - 5UPE: Crystal structure of human NAMPT with isoindoline urea inhibitor compound 5*. https://www.rcsb.org/structure/5UPE (accessed 2022-11-02).

(139) *RCSB PDB - 4O13: The crystal structure of NAMPT in complex with GNE-618*. https://www.rcsb.org/structure/4O13 (accessed 2022-11-02).

(140) *RCSB PDB - 2GVJ: Crystal Structure of Human NMPRTase in complex with FK866*. https://www.rcsb.org/structure/2GVJ (accessed 2022-11-02).

(141) *RCSB PDB - 6E68: NAMPT co-crystal with inhibitor compound 2*. https://www.rcsb.org/structure/6E68 (accessed 2022-11-02).

(142) Rane, C.; Senapedis, W.; Baloglu, E.; Landesman, Y.; Crochiere, M.; Das-Gupta, S.; Minden, A. A Novel Orally Bioavailable Compound KPT-9274 Inhibits PAK4, and Blocks Triple Negative Breast Cancer Tumor Growth. *Sci Rep* **2017**, *7*. https://doi.org/10.1038/srep42555.

(143) DSMZ ACC 64. BT-474.

(144) Nahimana, A.; Attinger, A.; Aubry, D.; Greaney, P.; Ireson, C.; Thougaard, A. V.; Tjørnelund, J.; Dawson, K. M.; Dupuis, M.; Duchosal, M. A. The NAD Biosynthesis Inhibitor APO866 Has Potent Antitumor Activity against Hematologic Malignancies. *Blood* **2009**, *113* (14), 3276–3286. https://doi.org/10.1182/blood-2008-08-173369.

(145) Caimi, P. F.; Ai, W.; Alderuccio, J. P.; Ardeshna, K. M.; Hamadani, M.; Hess, B.; Kahl, B. S.; Radford, J.; Solh, M.; Stathis, A.; Zinzani, P. L.; Havenith, K.; Feingold, J.; He, S.; Qin, Y.; Ungar, D.; Zhang, X.; Carlo-Stella, C. Loncastuximab Tesirine in Relapsed or Refractory Diffuse Large B-Cell Lymphoma (LOTIS-2): A Multicentre, Open-Label, Single-Arm, Phase 2 Trial. *Lancet Oncol* **2021**, *22* (6), 790–800. https://doi.org/10.1016/S1470-2045(21)00139-X.

(146) Nagro, C. Del; Xiao, Y.; Rangell, L.; Reichelt, M.; O'Brien, T. Depletion of the Central Metabolite NAD Leads to Oncosis-Mediated Cell Death. *J Biol Chem* **2014**, *289* (51), 35182–35192. https://doi.org/10.1074/JBC.M114.580159.

(147) Brunnbauer, P.; Leder, A.; Kamali, C.; Kamali, K.; Keshi, E.; Splith, K.; Wabitsch, S.; Haber, P.; Atanasov, G.; Feldbrügge, L.; Sauer, I. M.; Pratschke, J.; Schmelzle, M.; Krenzien, F. The Nanomolar Sensing of Nicotinamide Adenine Dinucleotide in Human Plasma Using a Cycling Assay in Albumin Modified Simulated Body Fluids. *Scientific Reports 2018 8:1* **2018**, *8* (1), 1–15. https://doi.org/10.1038/s41598-018-34350-6.

(148) *al (12) international application published under the patent cooperation treaty (PCT)*; 2018.

(149) Lee, A. Loncastuximab Tesirine: First Approval. *Drugs 2021 81:10* **2021**, *81* (10), 1229–1233. https://doi.org/10.1007/S40265-021-01550-W.

(150) Zammarchi, F.; Corbett, S.; Adams, L.; Tyrer, P. C.; Kiakos, K.; Janghra, N.; Marafioti, T.; Britten, C. E.; Havenith, C. E. G.; Chivers, S.; D'Hooge, F.; Williams, D. G.; Tiberghien, A.; Howard, P. W.; Hartley, J. A.; Van Berkel, P. H. ADCT-402, a PBD

Dimer-Containing Antibody Drug Conjugate Targeting CD19-Expressing Malignancies. *Blood* **2018**, *131* (10), 1094–1105. https://doi.org/10.1182/BLOOD-2017-10-813493.

(151) Rassy, E.; Rached, L.; Pistilli, B. Antibody Drug Conjugates Targeting HER2: Clinical Development in Metastatic Breast Cancer. *The Breast* **2022**, *66*, 217–226. https://doi.org/10.1016/J.BREAST.2022.10.016.

(152) von Arx, C.; De Placido, P.; Caltavituro, A.; Di Rienzo, R.; Buonaiuto, R.; De Laurentiis, M.; Arpino, G.; Puglisi, F.; Giuliano, M.; Del Mastro, L. The Evolving Therapeutic Landscape of Trastuzumab-Drug Conjugates: Future Perspectives beyond HER2-Positive Breast Cancer. *Cancer Treat Rev* **2023**, *113*. https://doi.org/10.1016/J.CTRV.2022.102500.

(153) López Rivas, P.; Müller, C.; Breunig, C.; Hechler, T.; Pahl, A.; Arosio, D.; Belvisi, L.; Pignataro, L.; Dal Corso, A.; Gennari, C. β-Glucuronidase Triggers Extracellular MMAE Release from an Integrin-Targeted Conjugate. *Org Biomol Chem* **2019**, *17* (19), 4705–4710. https://doi.org/10.1039/C9OB00617F.

(154) Dyson, H. J.; Wright, P. E.; Scheraga, H. A. The Role of Hydrophobic Interactions in Initiation and Propagation of Protein Folding. *Proc Natl Acad Sci U S A* **2006**, *103* (35), 13057–13061. https://doi.org/10.1073/PNAS.0605504103/ASSET/A63FAF4F-488D-48DB-A595-78DDBCDF592E/ASSETS/GRAPHIC/ZPQ0340632240005.JPEG.

(155) Tedeschini, T.; Campara, B.; Grigoletto, A.; Bellini, M.; Salvalaio, M.; Matsuno, Y.; Suzuki, A.; Yoshioka, H.; Pasut, G. Polyethylene Glycol-Based Linkers as Hydrophilicity Reservoir for Antibody-Drug Conjugates. *Journal of Controlled Release* **2021**, *337*, 431–447. https://doi.org/10.1016/J.JCONREL.2021.07.041.

(156) Moitessier, N.; Englebienne, P.; Lee, D.; Lawandi, J.; Corbeil, C. R. Towards the Development of Universal, Fast and Highly Accurate Docking/Scoring Methods: A Long Way to Go. *Br J Pharmacol* **2008**, *153 Suppl 1* (Suppl 1). https://doi.org/10.1038/SJ.BJP.0707515.

(157) McConkey, B.; Sobolev, V.; Edelman, M. The Performance of Current Methods in Ligand-Protein Docking. *Curr Sci* **2002**, *83* (7), 845–856.

(158) Harris, T. K.; Mildvan, A. S. High-Precision Measurement of Hydrogen Bond Lengths in Proteins by Nuclear Magnetic Resonance Methods. *Proteins: Structure, Function and Genetics*. May 15, 1999, pp 275–282. https://doi.org/10.1002/(SICI)1097-0134(19990515)35:3<275::AID-PROT1>3.0.CO;2-V.

(159) Krasovskiy, A.; Kopp, F.; Knochel, P. Soluble Lanthanide Salts (LnCl3,·2 LiCl) for the Improved Addition of Organomagnesium Reagents to Carbonyl Compounds. *Angewandte Chemie - International Edition* **2006**, *45* (3), 497–500. https://doi.org/10.1002/anie.200502485.

(160) Grignard. V. Sur Quelques Nouveaux Composés Organo-Métalliques Du Magnésium et Leur Application à La Synthèse d'alcools et d'hydrocarbures. *C R Hebd Seances Acad Sci* **1900**, *130*, 1322.

(161) Clayden, J.; Greeves, N.; Warren, S. *Organic Chemistry*, 2nd ed.; Oxford University press: Oxford, 2012.

(162) Jeffrey, S. C.; Andreyka, J. B.; Bernhardt, S. X.; Kissler, K. M.; Kline, T.; Lenox, J. S.; Moser, R. F.; Nguyen, M. T.; Okeley, N. M.; Stone, I. J.; Zhang, X.; Senter, P. D. Development and Properties of β-Glucuronide Linkers for Monoclonal Antibody-Drug Conjugates. *Bioconjug Chem* **2006**, *17* (3), 831–840. https://doi.org/10.1021/BC0600214/SUPPL_FILE/BC0600214SI20060126_040917.PDF.

(163) Wilsbacher, J. L.; Cheng, M.; Cheng, D.; Trammell, S. A. J.; Shi, Y.; Guo, J.; Koeniger, S. L.; Kovar, P. J.; He, Y.; Selvaraju, S.; Heyman, H. R.; Sorensen, B. K.; Clark, R. F.; Hansen, T. M.; Longenecker, K. L.; Raich, D.; Korepanova, A. V.; Cepa, S.; Towne, D. L.; Abraham, V. C.; Tang, H.; Richardson, P. L.; McLoughlin, S. M.; Badagnani, I.; Curtin, M. L.; Michaelides, M. R.; Maag, D.; Buchanan, F. G.; Chiang, G. G.; Gao, W.; Rosenberg, S. H.; Brenner, C.; Tse, C. Discovery and Characterization of Novel Nonsubstrate and Substrate NAMPT Inhibitors. *Mol Cancer Ther* **2017**, *16* (7), 1236–1245. https://doi.org/10.1158/1535-7163.MCT-16-0819.

(164) Curtin, M. L.; Heyman, H. R.; Clark, R. F.; Sorensen, B. K.; Doherty, G. A.; Hansen, T. M.; Frey, R. R.; Sarris, K. A.; Aguirre, A. L.; Shrestha, A.; Tu, N.; Woller, K.; Pliushchev, M. A.; Sweis, R. F.; Cheng, M.; Wilsbacher, J. L.; Kovar, P. J.; Guo, J.; Cheng, D.; Longenecker, K. L.; Raich, D.; Korepanova, A. V.; Soni, N. B.; Algire, M. A.; Richardson, P. L.; Marin, V. L.; Badagnani, I.; Vasudevan, A.; Buchanan, F. G.; Maag, D.; Chiang, G. G.; Tse, C.; Michaelides, M. R. SAR and Characterization of Non-Substrate Isoindoline Urea Inhibitors of Nicotinamide Phosphoribosyltransferase (NAMPT). *Bioorg Med Chem Lett* **2017**, *27* (15), 3317–3325. https://doi.org/10.1016/J.BMCL.2017.06.018.

(165) Martinez, C. R.; Iverson, B. L. Rethinking the Term “Pi-Stacking.” *Chem Sci* **2012**, *3* (7), 2191–2201. https://doi.org/10.1039/C2SC20045G.

(166) Janiak, C. A Critical Account on π–π Stacking in Metal Complexes with Aromatic Nitrogen-Containing Ligands. *Journal of the Chemical Society, Dalton Transactions* **2000**, No. 21, 3885–3896. https://doi.org/10.1039/B003010O.

(167) Jang, H. S.; Kim, H. K. Novel Direct Synthesis of Asymmetrical Urea Compounds from Trichloroethyl Carbamates Using Catalytic DBU. *Bull Korean Chem Soc* **2017**, *38* (12), 1515–1518. https://doi.org/10.1002/BKCS.11314.

(168) Gastaldi, S.; Weinreb, S. M.; Stien, D. Diiodosilane: A Reagent for Mild, Efficient Conversion of Carbamates to Ureas via Isocyanates. *Journal of Organic Chemistry* **2000**, *65* (10), 3239–3240. https://doi.org/10.1021/JO9919714/SUPPL_FILE/JO9919714_S.PDF.

(169) Bogolubsky, A. V.; Ryabukhin, S. V.; Pipko, S. E.; Lukin, O.; Shivanyuk, A.; Mykytenko, D.; Tolmachev, A. A Facile Synthesis of Unsymmetrical Ureas. *Tetrahedron* **2011**, *67* (20), 3619–3623. https://doi.org/10.1016/J.TET.2011.03.101.

(170) Kuo, W. Y.; Hsu, H. J.; Wu, C. Y.; Chen, H. Sen; Chou, Y. C.; Tsou, Y. L.; Peng, H. P.; Jian, J. W.; Yu, C. M.; Chiu, Y. K.; Chen, I. C.; Tung, C. P.; Hsiao, M.; Lin, C. L.; Wang, Y. A.; Wang, A. H. J.; Yang, A. S. Antibody-Drug Conjugates with HER2-Targeting Antibodies from Synthetic Antibody Libraries Are Highly Potent against HER2-Positive Human Gastric Tumor in Xenograft Models. *MAbs* **2019**, *11* (1), 153–165. https://doi.org/10.1080/19420862.2018.1541370.

(171) Jacobson, O.; Li, Q.; Chen, H.; Niu, G.; Kiesewetter, D. O.; Xu, L.; Cook, K.; Yang, G.; Dall’Acqua, W.; Tsui, P.; Peng, L.; Chen, X. PET-Guided Evaluation and Optimization of Internalized Antibody–Drug Conjugates Targeting Erythropoietin-Producing Hepatoma A2 Receptor. *Journal of Nuclear Medicine* **2017**, *58* (11), 1838–1844. https://doi.org/10.2967/jnumed.117.192245.

(172) Lund, J.; Pound, J. D.; Jones, P. T.; Duncan, A. R.; Bentley, T.; Goodall, M.; Levine, B. A.; Jefferis, R.; Winte, G. Multiple Binding Sites on the CH2 Domain of IgG for Mouse Fc Gamma R11. *Mol Immunol* **1992**, *29* (1), 53–59. https://doi.org/10.1016/0161-5890(92)90156-R.

6. Bibliography

(173) Francisco, J.; Risdon, G.; Wahl, A.; Siegall, C.; Senter, P.; Doronita, S.; Toki, B. RECOMBINANT ANTI-CD30 ANTIBODIES AND USES THEREOF. US 2008/0213289 A1, January 18, 2008.

(174) *Home* < *Expression Atlas* < *EMBL-EBI*. https://www.ebi.ac.uk/gxa/home (accessed 2022-11-09).

(175) Neumann, C. S.; Olivas, K. Ligand Drug Conjugates for Targeted Delivery of Nicotinamide Adenine Dinucleotide Salvage Pathway Inhibitors for Treatment of Cancer and Autoimmune Diseases, April 26, 2018.

(176) Wahl, A. F.; Klussman, K.; Thompson, J. D.; Chen, J. H.; Francisco, L. v; Risdon, G.; Chace, D. F.; Siegall, C. B.; Francisco, J. A. *The Anti-CD30 Monoclonal Antibody SGN-30 Promotes Growth Arrest and DNA Fragmentation in Vitro and Affects Antitumor Activity in Models of Hodgkin's Disease*; 2002; Vol. 62. http://aacrjournals.org/cancerres/article-pdf/62/13/3736/2494985/ch1302003736.pdf.

(177) Okeley, N. M.; Miyamoto, J. B.; Zhang, X.; Sanderson, R. J.; Benjamin, D. R.; Sievers, E. L.; Senter, P. D.; Alley, S. C. Intracellular Activation of SGN-35, a Potent Anti-CD30 Antibody-Drug Conjugate. *Clin Cancer Res* **2010**, *16* (3), 888–897. https://doi.org/10.1158/1078-0432.CCR-09-2069.

(178) *Search results* < *Expression Atlas* < *EMBL-EBI*. https://www.ebi.ac.uk/gxa/search?geneQuery=%5B%7B%22value%22%3A%22TNFRSF8%22%2C%22category%22%3A%22symbol%22%7D%5D&species=homo%20sapiens&conditionQuery=%5B%7B%22value%22%3A%22cancer%22%7D%5D&bs=%7B%22homo%20sapiens%22%3A%5B%22DISEASE%22%5D%7D&ds=%7B%22kingdom%22%3A%5B%22animals%22%5D%2C%22factors%22%3A%5B%22disease%22%5D%2C%22regulation%22%3A%5B%22UP%22%5D%7D#baseline (accessed 2022-10-31).

(179) Kölmel, D. K.; Kool, E. T. Oximes and Hydrazones in Bioconjugation: Mechanism and Catalysis. *Chem Rev* **2017**, *117* (15), 10358. https://doi.org/10.1021/ACS.CHEMREV.7B00090.

(180) Velikogne, S.; Breukelaar, W. B.; Hamm, F.; Glabonjat, R. A.; Kroutil, W. CâC-Ene-Reductases Reduce the CâN Bond of Oximes. *ACS Catal* **2020**, *10* (22), 13377–13382. https://doi.org/10.1021/ACSCATAL.0C03755/ASSET/IMAGES/LARGE/CS0C03755_0005.JPEG.

(181) Kopp, A.; Thurber, G. M. Severing Ties: Quantifying the Payload Release from Antibody Drug Conjugates. *Cell Chem Biol* **2019**, *26* (12), 1631. https://doi.org/10.1016/J.CHEMBIOL.2019.12.001.

(182) Fukuda, M. Lysosomal Membrane Glycoproteins. Structure, Biosynthesis, and Intracellular Trafficking. *J Biol Chem* **1991**, *266* (32), 21327–21330. https://doi.org/10.1016/S0021-9258(18)54636-6.

(183) Schwake, M.; Schröder, B.; Saftig, P. Lysosomal Membrane Proteins and Their Central Role in Physiology. *Traffic* **2013**, *14* (7), 739–748. https://doi.org/10.1111/TRA.12056.

(184) Sadiki, A.; Vaidya, S. R.; Abdollahi, M.; Bhardwaj, G.; Dolan, M. E.; Turna, H.; Arora, V.; Sanjeev, A.; Robinson, T. D.; Koid, A.; Amin, A.; Zhou, Z. S. Site-Specific Conjugation of Native Antibody. *Antib Ther* **2020**, *3* (4), 271–284. https://doi.org/10.1093/ABT/TBAA027.

(185) Staudacher, A. H.; Brown, M. P. Antibody Drug Conjugates and Bystander Killing: Is Antigen-Dependent Internalisation Required. *British Journal of Cancer*. Nature Publishing Group 2017, pp 1736–1742. https://doi.org/10.1038/bjc.2017.367.

6. Bibliography

(186) Lehninger, A. L. *Lehninger Principes of Biochemistry*; 2021.

(187) Wilsbacher, J. L.; Cheng, M.; Cheng, D.; Trammell, S. A. J.; Shi, Y.; Guo, J.; Koeniger, S. L.; Kovar, P. J.; He, Y.; Selvaraju, S.; Heyman, H. R.; Sorensen, B. K.; Clark, R. F.; Hansen, T. M.; Longenecker, K. L.; Raich, D.; Korepanova, A. V.; Cepa, S.; Towne, D. L.; Abraham, V. C.; Tang, H.; Richardson, P. L.; McLoughlin, S. M.; Badagnani, I.; Curtin, M. L.; Michaelides, M. R.; Maag, D.; Buchanan, F. G.; Chiang, G. G.; Gao, W.; Rosenberg, S. H.; Brenner, C.; Tse, C. Discovery and Characterization of Novel Nonsubstrate and Substrate NAMPT Inhibitors. *Mol Cancer Ther* **2017**, *16* (7), 1236–1245. https://doi.org/10.1158/1535-7163.MCT-16-0819.

(188) Khongorzul, P.; Ling, C. J.; Khan, F. U.; Ihsan, A. U.; Zhang, J. Antibody-Drug Conjugates: A Comprehensive Review. *Molecular Cancer Research*. American Association for Cancer Research Inc. 2020, pp 3–19. https://doi.org/10.1158/1541-7786.MCR-19-0582.

(189) Sorkin, M. R.; Walker, J. A.; Kabaria, S. R.; Torosian, N. P.; Alabi, C. A. Responsive Antibody Conjugates Enable Quantitative Determination of Intracellular Bond Degradation Rate. *Cell Chem Biol* **2019**, *26* (12), 1643-1651.e4. https://doi.org/10.1016/J.CHEMBIOL.2019.09.008.

(190) Maass, K. F.; Kulkarni, C.; Betts, A. M.; Wittrup, K. D. Determination of Cellular Processing Rates for a Trastuzumab-Maytansinoid Antibody-Drug Conjugate (ADC) Highlights Key Parameters for ADC Design. *AAPS Journal* **2016**, *18* (3), 635–646. https://doi.org/10.1208/S12248-016-9892-3/FIGURES/10.

(191) Schuster, S.; Penke, M.; Gorski, T.; Gebhardt, R.; Weiss, T. S.; Kiess, W.; Garten, A. FK866-Induced NAMPT Inhibition Activates AMPK and Downregulates MTOR Signaling in Hepatocarcinoma Cells. *Biochem Biophys Res Commun* **2015**, *458* (2), 334–340. https://doi.org/10.1016/J.BBRC.2015.01.111.

(192) Cordover, E.; Wei, J.; Patel, C.; Shan, N. L.; Gionco, J.; Sargsyan, D.; Wu, R.; Cai, L.; Kong, A. N.; Jacinto, E.; Minden, A. KPT-9274, an Inhibitor of PAK4 and NAMPT, Leads to Downregulation of MTORC2 in Triple Negative Breast Cancer Cells. *Chem Res Toxicol* **2020**, *33* (2), 482–491. https://doi.org/10.1021/ACS.CHEMRESTOX.9B00376/ASSET/IMAGES/MEDIUM/TX9B00376_0005.GIF.

(193) López-Hernández, T.; Haucke, V.; Maritzen, T. Endocytosis in the Adaptation to Cellular Stress. *Cell Stress* **2020**, *4* (10), 230. https://doi.org/10.15698/CST2020.10.232.

(194) Cheng, J.; Liang, M.; Carvalho, M. F.; Tigue, N.; Faggioni, R.; Roskos, L. K.; Vainshtein, I. Molecular Mechanism of HER2 Rapid Internalization and Redirected Trafficking Induced by Anti-HER2 Biparatopic Antibody. *Antibodies* **2020**, *9* (3), 1–21. https://doi.org/10.3390/ANTIB9030049.

(195) Engebraaten, O.; Yau, C.; Berg, K.; Borgen, E.; Garred, Ø.; Berstad, M. E. B.; Fremstedal, A. S. V.; DeMichele, A.; Veer, L. van 't; Esserman, L.; Weyergang, A. RAB5A Expression Is a Predictive Biomarker for Trastuzumab Emtansine in Breast Cancer. *Nature Communications 2021 12:1* **2021**, *12* (1), 1–11. https://doi.org/10.1038/s41467-021-26018-z.

(196) Xiao, Y.; Elkins, K.; Durieux, J. K.; Lee, L.; Oeh, J.; Yang, L. X.; Liang, X.; DelNagro, C.; Tremayne, J.; Kwong, M.; Liederer, B. M.; Jackson, P. K.; Belmont, L. D.; Sampath, D.; O'Brien, T. Dependence of Tumor Cell Lines and Patient-Derived Tumors on the NAD Salvage Pathway Renders Them Sensitive to NAMPT Inhibition with GNE-618. *Neoplasia* **2013**, *15* (10), 1151-IN23. https://doi.org/10.1593/NEO.131304.

6. Bibliography

(197) Jaattela, M.; Kallunki, T. *Lysosomes, Biology, Diseases, and Therapeutics*, 1st ed.; Maxfield, F., Willard, J., Lu, S., Eds.; John Wiley & Sons: Hoboken, 2016.

(198) Pisoni, R. *Subcellular Biochemistry, Biology of the Lysosome*, First.; Lloyd, J., Mason, R., Eds.; Springer Science, 1996; Vol. 27.

(199) Wermuth, C. G.; Ganellin, C. R.; Lindberg, P.; Mitscher, L. A. Glossary of Terms Used in Medicinal Chemistry (IUPAC Recommendations 1998). *Pure and Applied Chemistry* **1998**, *70* (5), 1129–1143. https://doi.org/10.1351/PAC199870051129/MACHINEREADABLECITATION/RIS.

(200) *ExPASy - ProtParam tool*. https://web.expasy.org/protparam/ (accessed 2022-10-25).

(201) Lange, V.; Picotti, P.; Domon, B.; Aebersold, R. Selected Reaction Monitoring for Quantitative Proteomics: A Tutorial. *Mol Syst Biol* **2008**, *4* (1), 222. https://doi.org/10.1038/MSB.2008.61.

(202) *Home - Janvier Labs*. https://janvier-labs.com/en/ (accessed 2023-01-02).

(203) Pretsch, E.; Buhlmann, P.; Badertscher, M. *Structure Determination of Organic Compounds (Tables of Spectral Data)*, Fifth.; Springer, 2020.

(204) *Calculation of molecular properties and bioactivity score*. https://www.molinspiration.com/cgi-bin/properties (accessed 2022-10-31).

(205) Wang, E.; Sun, H.; Wang, J.; Wang, Z.; Liu, H.; Zhang, J. Z. H.; Hou, T. End-Point Binding Free Energy Calculation with MM/PBSA and MM/GBSA: Strategies and Applications in Drug Design. *Chemical Reviews*. American Chemical Society August 28, 2019, pp 9478–9508. https://doi.org/10.1021/acs.chemrev.9b00055.

(206) Humphrey, S. J.; Meisheri, K. D.; Ludens, J. H.; Hester Jr., J. B. Preparation of Pyridinylcyanoguanidines as Potassium Channel Blockers., August 3, 1995.

(207) Egbertson, M. S.; Chang, C. T. C.; Duggan, M. E.; Gould, R. J.; Halczenko, W.; Hartman, G. D.; Laswell, W. L.; Lynch, J. J.; Lynch, R. J.; Manno, P. D.; Naylor, A. M.; Prugh, J. D.; Ramjit, D. R.; Sitko, G. R.; Smith, R. S.; Turchi, L. M.; Zhang, G. Non-Peptide Fibrinogen Receptor Antagonists. 2. Optimization of a Tyrosine Template as a Mimic for Arg-Gly-Asp. *J Med Chem* **1994**, *37* (16), 2537–2551. https://doi.org/10.1021/JM00042A007/ASSET/JM00042A007.FP.PNG_V03.

(208) Fratta, S.; Biniecka, P.; Moreno-Vargas, A. J.; Carmona, A. T.; Nahimana, A.; Duchosal, M. A.; Piacente, F.; Bruzzone, S.; Caffa, I.; Nencioni, A.; Robina, I. Synthesis and Structure-Activity Relationship of New Nicotinamide Phosphoribosyltransferase Inhibitors with Antitumor Activity on Solid and Haematological Cancer. *Eur J Med Chem* **2023**, *250*, 115170. https://doi.org/10.1016/J.EJMECH.2023.115170.

(209) Biedermann, E.; Hasmann, M.; Loser, R.; Rattel, B.; Reiter, F.; Schein, B.; Seibel, K.; Vogt, K. Preparation of Pyridyl Alkene- and Pyridyl Alkyne- Acid Amides as Cytostatics and Immunosuppressives, December 24, 1997.

(210) Rice, L. M.; Grogan, C. H. Hypotensive Agents. IX. 3-Azabicyclo[3.3.1]Nonane Derivatives. *Journal of Organic Chemistry* **1958**, *23* (6), 844–846. https://doi.org/10.1021/JO01100A023/ASSET/JO01100A023.FP.PNG_V03.

(211) Miao, Z.; LIU, J.; Norman, T.; Driver, R. Compositions containing, methods involving, and uses of non-natural amino acids and polypeptides. **2006**.